PREDICTION AND EVALUATION OF FLYING QUALITIES IN TURBULENCE

E. D. ONSTOTT
E. P. SALMON
R. L. McCORMICK

FOREWORD

This report was prepared by the Northrop Corporation, Aircraft Division, Hawthorne, California, under USAF Contract No. F33615-71-C-1076. The contract work was performed under Project No. 8219, "Stability and Control for Air Force Missiles, Aerospace Vehicles and Aircraft," Task No. 821904, "Control System Theory Applied to Combat Aircraft Flight Control Design," Work Unit No. 029, "Airplane Flying Characteristics in Atmospheric Turbulence." The program was administered by the Air Force Flight Dynamics Laboratory, Air Force Systems Command, Wright-Patterson Air Force Base, Ohio. The Program Monitor and Project Engineer was Mr. Frank L. George (AFFDL/FGC).

The reporting period extended from 4 December 1970 through 4 October 1971. This report was submitted on 30 October 1971, and the internal Northrop Report is NOR 71-139.

The Principal Investigator, E. D. Onstott, acknowledges his gratitude to E. P. Salmon for assistance in preparing the computer program, and to R. L. McCormick whose ingenuity in developing and operating the simulation was essential to the success of the program. A special gratitude is also extended to the three pilots, J. B. Jordan, W. W. Koepcke, and J. T. Thomas, whose talents and cooperation have been exceptional.

This technical report is presented in the interest of exchanging technical knowledge and data. Publication of this report by the Air Force does not imply acceptance of the conclusions presented.

C. B. WESTBROOK
Chief, Control Criteria Branch
Flight Control Division
Air Force Flight Dynamics Laboratory

ABSTRACT

A method for predicting tracking performance of piloted Class IV airplanes in turbulence has been validated through a moving base simulation of sixteen F-5 and A-7 configurations on the Northrop Large Amplitude Flight Simulator. The method is based on pilot model theory and predicts root mean square tracking errors for piloted tasks in turbulence. Both lateral and longitudinal dynamics are considered and the accuracy of the method is assessed. Specification design criteria are evolved from the simulation data for bank angle and pitch angle attitude-hold tasks in turbulence. Digital programs which perform the prediction calculations accept arbitrary equations of motion and are available on request from the United States Air Force; a user's guide is included in the report along with complete tracking error, gust level, and pilot rating data from the simulation.

TABLE OF CONTENTS

TABLE OF CONTENTS (Continued)

APPENDIXES

LIST OF ILLUSTRATIONS

LIST OF ILLUSTRATIONS (Continued)

LIST OF ILLUSTRATIONS (Continued)

LIST OF ILLUSTRATIONS (Continued)

LIST OF ILLUSTRATIONS (Continued)

LIST OF ILLUSTRATIONS (Continued)

LIST OF ILLUSTRATIONS (Continued)

LIST OF ILLUSTRATIONS (Continued)

LIST OF ILLUSTRATIONS (Continued)

LIST OF ILLUSTRATIONS (Continued)

SYMBOLS

a_{ij}	- Coefficients in equations of motion
b	- Airplane wing span, ft
C_D	= $D/\frac{1}{2}\rho_o V_o^2 S$, Airplane drag coefficient
C_{D_o}	- Drag coefficient at zero angle of attack
C_{D_α}	= $\partial C_D/\partial \alpha$, Nondimensional drag coefficient derivative with respect to angle of attack, 1/rad
$C_{D_\alpha 2}$	= $\partial C_D/\partial \alpha^2$, Nondimensional drag coefficient derivative with respect to angle of attack squared, $1/rad^2$
C_ℓ	= $L/\frac{1}{2}\rho_o V_o^2 S b$, Airplane rolling moment coefficient
C_{ℓ_r}	= $\partial C_\ell / \partial (rb/2V_o)$, Nondimensional rolling moment coefficient derivative with respect to yawing rate, 1/rad
C_{ℓ_β}	= $\partial C_\ell / \partial \beta$, Nondimensional rolling moment coefficient derivative with respect to sideslip, 1/rad
C_L	= $L/\frac{1}{2}\rho_o V_o^2 S$, Airplane lift coefficient
C_{L_o}	- Lift coefficient at zero angle of attack
C_{L_α}	= $\partial C_L/\partial \alpha$, Nondimensional lift coefficient derivative with respect to angle of attack, 1/rad
$C_{L_{\delta_e}}$	= $\partial C_L/\partial \delta_e$ Nondimensional lift coefficient derivative with respect to elevator control, 1/rad
C_n	= $N/\frac{1}{2}\rho_o V_o^2 S b$, Airplane yawing moment coefficient
C_{n_p}	= $\partial C_n/\partial (pb/2 V_o)$, Nondimensional yawing moment coefficient derivative with respect to rolling rate, 1/rad
$C_{n_{\delta_a}}$	= $\partial C_n/\partial \delta_a$, Nondimensional yawing moment coefficient derivative with respect to aileron control 1/rad
D	- Drag, lb

SYMBOLS (Continued)

$D_{q\,1}$ - pilot model delay numerator in q loop

$D_{q\,2}$ - pilot model delay denominator in q loop

$e_i^{-\tau s}$ - ith Padé approximation of $e^{-\tau s}$

F - greatest common denominator

F_{ij} - forcing function coefficients

g - acceleration due to gravity, ft/sec^2

G(s) - transfer function

G_{ij} - feedback transfer function

H(s) - transfer function, tracking command filter

i = 1, 2, 3, 4, 5, a, r

I_n - rms contour integral

I_x - moment of inertia about x-axis, $ft\text{-}lb\text{-}sec^2$

I_y - moment of inertia about y-axis, $ft\text{-}lb\text{-}sec^2$

I_z - moment of inertia about z-axis, $ft\text{-}lb\text{-}sec^2$

I_{xz} - product of inertia, $ft\text{-}lb\text{-}sec^2$

j - imaginary base

K_P - pilot model gain

K_{P_θ} or K_θ - pilot model gain in θ loop closure

K_{P_ϕ} or K_ϕ - pilot model gain in ϕ loop closure

K_{P_ψ} or K_ψ - pilot model gain in ψ loop closure

K_q - pilot model gain in q loop

L - turbulence scale length

L_p = $(1/I_x)\,(\partial L/\partial p)$, rad/sec

L_r = $(1/I_x)\,(\partial L/\partial r)$, rad/sec

L_β = $(1/I_x)\,(\partial L/\partial \beta)$, rad/sec^2

L_{δ_a} = $(1/I_x)\,(\partial L/\partial \delta_a)$, $1/sec^2$ -in

L_{δ_r} = $(1/I_x)\,(\partial L/\partial \delta_r)$, $1/sec^2$ -in

SYMBOLS (Continued)

L_i'	$= \left[L_i + (I_{xz}/I_x)\, N_i\right] / \left[1 - (I_{xz}^2 / I_x I_z)\right]$; $i = \beta, \delta_a, \delta_r, p, r$
m	- W/g, lb-sec^2/ft
M	- Pitching moment, ft-lb
ms	- mean square
M_q	$= (1/I_y)\ (\partial M/\partial q)$, rad/sec
N_p	$= (1/I_z)\ (\partial N/\partial p)$, rad/sec
N_r	$= (1/I_z)\ (\partial N/\partial r)$, rad/sec
N_β	$= (1/I_z)\ (\partial N/\partial \beta)$, rad/sec^2
N_{δ_a}	$= (1/I_z)\ (\partial N/\partial \delta_a)$, 1/sec^2-rad
N_{δ_r}	$= (1/I_z)\ (\partial N/\partial \delta_r)$, 1/sec^2-rad
N_i'	$= \left[N_i + (I_{xz}/I_x) L_i\right] / \left[1-(I_{xz}^2/I_x I_z)\right]$; $i = \beta, \delta_a, \delta_r, p, r$
$N_{q_i\ j}$	- dynamic numerator
$N^{qi\ \ qj}_{k\ \ i}$	- coupling numerator
p	- roll rate, rad/sec
PR	- predicted or reported pilot rating
q	= pitch rate
q_g	- longitudinal correlated q gust
q_o	$= 1/2\rho_o V_o^2$, dynamic pressure, lb/ft^2
r	- yaw rate, rad/sec
r_g	- lateral correlated r gust
rms	- root mean square
s	- Laplace operator
T_I	- pilot model lag in seconds
T_L	- pilot model lead in seconds
T_{L_g}	- correlated L gust filter

SYMBOLS (Continued)

T_{r_g}	- correlated r gust filter
T_{v_g}	- v gust filter
T_{w_g}	- w gust filter
U_o	- V_o ft/sec
v_g	- lateral v gust
V_o	- initial true velocity, ft/sec
ΔV	- perturbation true velocity, ft/sec
W	- airplane weight, lb
w_g	- longitudinal w gust
W.N.	- white noise
x, y, z	- Stability axes (i.e., a right hand orthogonal body-axis system with origin at the center of gravity, the z-axis in the plane of symmetry and the x-axis aligned with the relative wind of zero sideslip trimmed flight)
Y	- side force, lb
Y_q or Y_{p_q}	- pilot transfer function controlling q
$Y^*_{\delta_r}$	= $(1/m\ V_o)\ (\partial Y/\partial_r)$, 1/sec-rad
α	- Angle of attack, rad
β	- sideslip angle, deg
δa	- aileron command, rad
δ_i	- ith control surface
δ_r	- rudder command, rad
Δ	- airframe characteristic polynomial
Δ_{sys}	- system characteristic polynomial
θ	- pitch angle, deg
θ_e	- pitch angle tracking error, deg

SYMBOLS (Concluded)

ϕ	- bank angle , deg
ϕ_c	- bank angle command , deg
ϕ_e	- bank angle tracking error, closed loop deg
ϕ_ϵ	- bank angle system error, open loop deg
Φ_{cc}	- command power spectrum
Φ_{g_β}	- turbulence power spectrum
Φ_{nn}	- remnant power spectrum
ψ	- heading angle , deg
ψ_c	- heading angle command, deg
ψ_e	- heading tracking error, deg
ψ_ϵ	- heading angle system error , deg
ρ	- atmospheric density, lb-sec^2/ft^4
σ, σ_q	- rms system tracking error
σ_v	- rms v gust
σ_w	- rms w gust
σ_m	- minimum tracking error
τ	- pilot model time delay in seconds
ω	- frequency
ω_c	- crossover frequency
$[\ ]^-$	- realizable part of

I. INTRODUCTION

A. SCOPE AND PURPOSE OF THIS REPORT

This study of airplane flying qualities in turbulence is a contribution to the growing research into the dynamics of piloted flight. The development of techniques for analyzing the pilot-vehicle system has taken place over several decades and the success of this work is well known. An essential feature of these methods is the representation of the human pilot as a control system element. The pilot models usually employed, especially in the extensive work of Systems Technology, Inc., are linear approximations to the pilot. They are developed by curve fitting experimental power spectra for actual or simulated flight and include uncorrelated pilot generated noise called pilot remnant. Many researchers have investigated pilot dynamics in terms of human physiology, including the dynamics of neural pathways, muscular response, and vestibular sensing. This has resulted in improved understanding of the pilot's input to the airplane control system and has, further, led to better definitions of desirable airplane characteristics.

The specification of aircraft dynamics desirable to the pilot is usually phrased in terms of parameters such as frequency and damping, as well as other frequency domain quantities, but for the study of flying qualities in turbulence, it is useful to examine the time domain statistics of the piloted system. The object of this is to determine the way and extent that increasing turbulence degrades a time invariant system and increases the workload of the pilot. Root mean square tracking errors for attitude hold tasks in turbulence turn out to be useful measures of performance that are sensitive to changes in airplane dynamics and, experimentally, are nearly independent of the pilot. Pilot models along with spectral turbulence models, such as those of Dryden, or less conveniently, von Karman, can be used to predict these attitude hold tracking errors and forms the basis for the Northrop study of flying qualities in turbulence.

The research reported here is both a continuation and an extension of the Air Force program, "Airplane Flying Characteristics in Turbulence," (Reference 1). This former effort demonstrated that root mean square tracking error of certain airframe designs could be predicted in the above way by pilot-vehicle analysis, and the accuracy of the specific approach immediately suggested the possibility of evolving a validated analysis methodology and specification criteria for flying qualities in turbulence. The

current program has achieved both of these objectives through further development of the prediction methods and by an extensive simulation of the F-5 and A-7 as two representative Class IV airplanes. The results show that the optimism of the former program is fully justified and the prediction method has been extended to include lateral and longitudinal tasks in still air and in turbulence. The simulation was flown by one former Navy and two former Air Force pilots, including two graduates of test pilot schools. The resulting 1326 data flights, each of 100 seconds duration, have been used to validate the prediction methods and are characterized by tight clustering of the tracking error data. Pilot ratings were also taken for the turbulence flights and these also show consistency among the pilots. The simulation data have been included in numerical form (Appendix IV).

B. PREDICTION OF FLYING QUALITIES IN TURBULENCE

The essential features of the prediction method, as presented in Reference 1 and validated in this report, are fixed form gain-lead-time delay pilot models and optimization of the system, with respect to mean square tracking error, by selection of the pilot model gain.

Since the disturbance to the system as measured by tracking errors is the quantity of interest, the various features of flying qualities in turbulence are referred to it. The results of Reference 1 show that not only is the magnitude of the rms error important, but also the sensitivity of the system tracking error to pilot anticipation (lead) and control amplitude (gain). Furthermore, the previous study showed that the predicted error was verifiable by moving base simulation. The models used were of fixed form and, in most cases, a pilot lead of .5 seconds was appropriate. Since the usefulness of an evaluation method depends on standardized and readily available procedures, fixed pilot model lead and time delay were used throughout the study. Perturbations of pilot model lead were made at optimum gain and the .5 second lead was found to be correct in almost all cases.

Digital programs have been developed which greatly simplify the analysis procedure. These have grown out of the program reported in Reference 1 and are available upon request from the United States Air Force. A user's guide is included in Appendix I. The programs are considerably more general than their predecessor, and will accept the user's equations of motion. Furthermore, the programs can be readily modified to include additional feedback loops without having to provide the literal determinant expansions associated with the multiloop analysis.

C. SPECIFICATION CRITERIA AND EVALUATION OF FLYING QUALITITES IN TURBULENCE

There are several recognized limitations to the current Military Specification, "Flying Qualities of Piloted Airplanes," Reference 2, which have prompted the current research into closed loop pilot-vehicle analysis. The correlation between open loop dynamic characteristics of airplanes and the flying qualities during piloted flight is the basis for most items of the Specification. Since closing a feedback loop around a dynamic system may effect gross changes in the system dynamics, such a correlation will be valid only for those airplanes which do not depart too far from conventional design. In addition, the increasing use of flight control augmentation devices means that current flying qualities criteria may not be sufficient for the evaluation of modern high performance airplanes. Thus, a standardized procedure is needed which can directly evaluate an airplane in terms of its closed loop piloted characteristics. In order for this approach to be compatible with the established Air Force evaluation ratings of Levels 1, 2 or 3, numerical performance predictions are needed which account for subjective handling qualities effects including pilot work load.

Another area of concern is the lack of any precise method of establishing flying qualities requirements for performance in atmospheric turbulence. Acceptable representations of gust spectra have been established, and their use has been cited in some paragraphs of the Specification. However, no numerical criteria have been developed for acceptable flying qualities in turbulence and no precise analytical technique for evaluating airplane performance in turbulence has been established. Furthermore, the difficulties attendant with flight testing in turbulence can be avoided by the use of analytical evaluation procedures. This approach not only avoids the problems of searching out suitable turbulence for flight testing, but also supplements the use of pilot ratings as a turbulence performance parameter. Pilot ratings have proved to be insufficient for flying qualities in turbulence evaluations, Reference 1, and a better approach is to develop criteria based on physically measurable performance quantities that can be analytically predicted. This has proved to be successful in terms of the normal mode F-5 and A-7 airplanes,and example criteria,based on the results, are presented in Section IV.

D. A READER'S GUIDE TO THE REPORT

Although this report is a complete account of the simulation and the resulting validation of the prediction method,there are further details of the earlier study that are to be found in Reference 1, and the reader who is interested in using these methods should be familiar with that report as well.

The general reader will find that both Reference 1 and this report can be read quickly, the physical bulk of each report notwithstanding. The following selections from this report will provide a short but complete account of the present and previous programs:

II. PREDICTION METHODS

A. SUMMARY OF EARLIER RESULTS

As stated in the Introduction, the research reported here is an extension and further evaluation of the flying qualities in turbulence analysis methods reported in Reference 1. The essential features of this approach are closed loop pilot-vehicle representations of the linear system, and the optimization of the total system performance by selecting the gain in a fixed form pilot model. Root mean square (rms) performance measures are used and the objective is to study the rms performance of the system rather than to examine in detail the pilot's activity at the controls. The experimental results of Reference 1 show, as well as the results of the current program, that these system models not only are useful for predicting the tracking accuracy of piloted airplanes in turbulence, but also provide a direct means of determining the extent to which a pilot must generate lead for optimum tracking. Another important consideration is the sensitivity of the system to changes in pilot gain. This can also be directly evaluated and several examples of airplane control failures will illustrate the effects of pilot gain sensitivity on tracking performance and pilot opinion.

In order to keep the mathematical models and subsequent analysis as simple as possible, linear system representations are used for both airplane and pilot, and the tracking tasks are based on Gaussian processes. Let the power spectrum of a desired Gaussian command tracking task or Dryden gust disturbance be represented by ϕ_{ii}, then the transfer function H(s) which filters white noise is the physically realizable part

$$H(s) = \left[\phi_{ii}(s)\right]^{-}$$

of the spectral factoring of $\phi_{ii}(s)$

$$\phi_{ii}(s) = \left[\phi_{ii}(s)\right]^{+}\left[\phi_{ii}(s)\right]^{-}.$$

If the pilot-vehicle closed loop transfer function for a particular piloted task of tracking the variable q is represented by G(s), then the system performance σ_q per unit rms input disturbance with spectrum $\phi_{ii}(s)$ is given by

$$\sigma_q^2 = \frac{\frac{1}{2\pi j}\int_{-j\infty}^{j\infty} \phi_{ii}(s) \left| G(s) \right|^2 ds}{\frac{1}{2\pi j}\int_{-j\infty}^{j\infty} \phi_{ii}(s)\, ds}$$

This quotient of integrals is the basic calculation of the prediction method, and is solved with little difficulty, by an exact method in the multiloop performance prediction program discussed in Appendix I. Thus, the performance can be evaluated once $\phi_{ii}(s)$ and G(s) have been determined.

The algebraic methods for deriving the multiloop transfer functions for an airplane with feedback loops closed by augmentation system and the pilot, Figure 1, are fully presented in Appendix I of Reference I. The resulting expressions formerly required the tedious evaluation of many determinants, but are now generated automatically in the lateral and longitudinal programs developed during the current program. Furthermore, the programs are set up to accept a general pilot model.

The simplest form of transfer function that is representative of the pilot's dynamic response includes the features of gain K_p, lead T_L, and time delay τ which model, respectively, the stick amplitude, anticipation, and overall inability of the pilot to react instantly to a change in state of the airplane. The time delay τ is represented by the exponential transfer function $e^{-\tau s}$ and is approximated by means of the Padé formulas $e_i^{-\tau s}$ given for easy reference in Figure 2. In this way, the pilot model Y_p takes the form

$$Y_p = K_p (T_L s + 1) e_i^{-\tau s}$$

This model was used in the research program of Reference 1 to predict the rms excursions of a piloted wings-level task in turbulence. The result was that the prediction and the simulation performance data closely matched over a wide range of gust disturbance susceptibility. Figure 3 shows this agreement where each point represents the average for a T-33 variable stability configuration normalized to a gust level of 10 ft/sec rms.

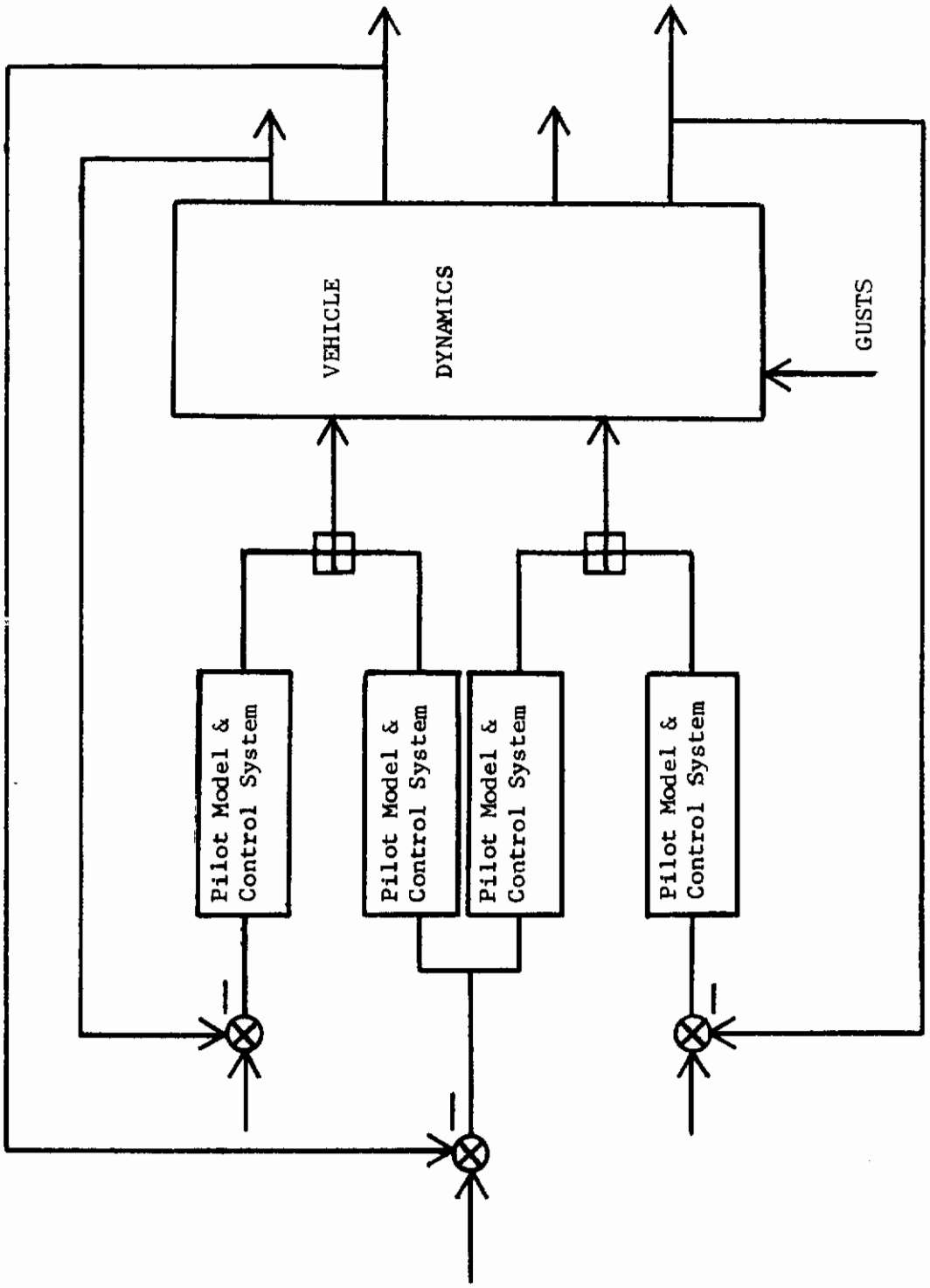

FIGURE 1 PILOT VEHICLE SYSTEM

$$e_1^{-x} \doteq \frac{2 - x}{2 + x}$$

$$e_2^{-x} \doteq \frac{12 - 6x + x^2}{12 + 6x + x^2}$$

$$e_3^{-x} \doteq \frac{120 - 60x + 12x^2 - x^3}{120 + 60x + 12x^2 + x^3}$$

$$e_4^{-x} \doteq \frac{1680 - 840x + 180x^2 - 20x^3 + x^4}{1680 + 840x + 180x^2 + 20x^3 + x^4}$$

$$e_5^{-x} \doteq \frac{30240 - 15120x + 3360x^2 - 420x^3 + 30x^4 - x^5}{30240 + 15120x + 3360x^2 + 420x^3 + 30x^4 + x^5}$$

where $x = \tau s$

FIGURE 2. PADÉ APPROXIMATIONS

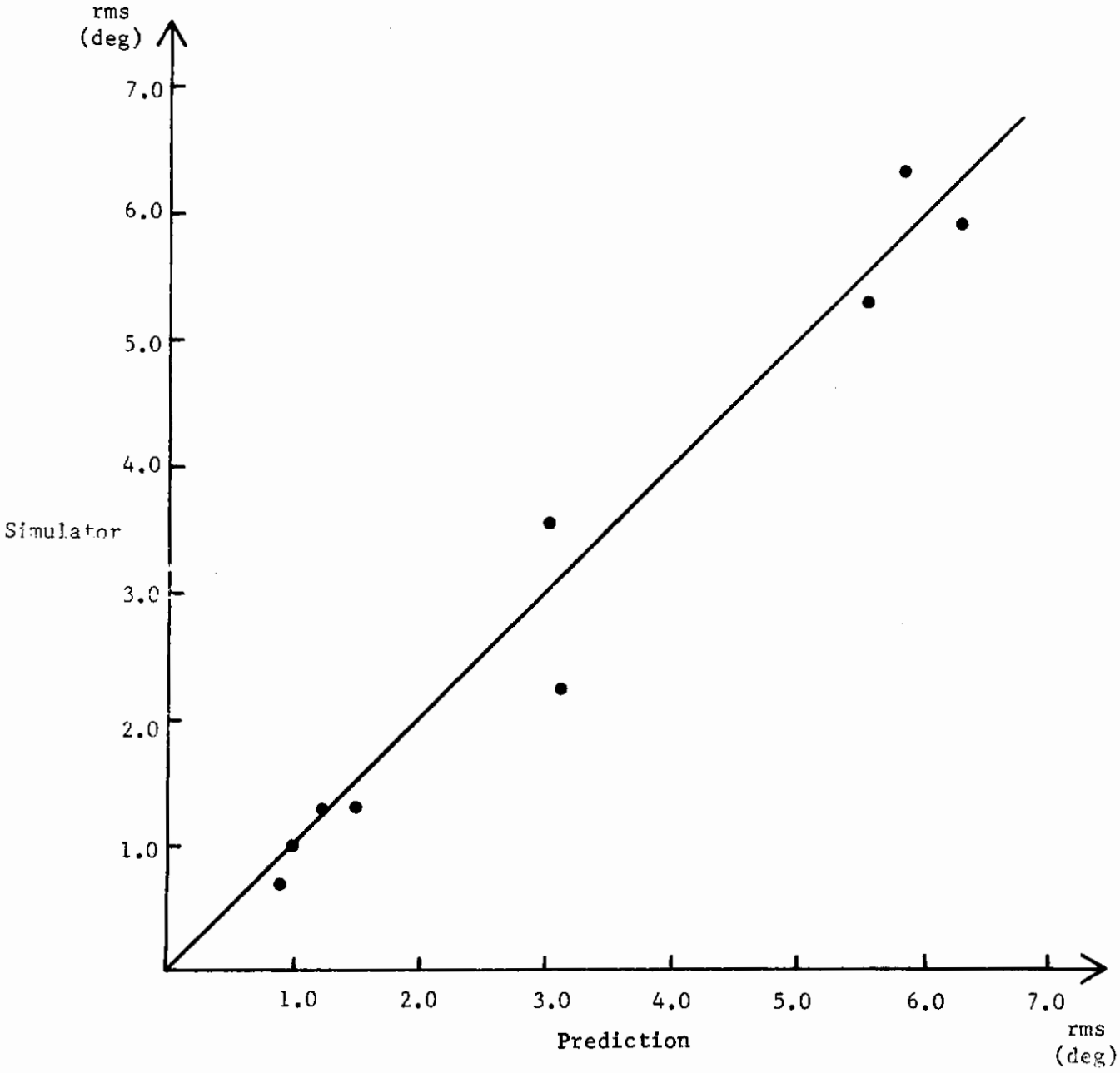

FIGURE 3. BANK ANGLE SIMULATOR VERSUS PREDICTION TRACKING ERRORS (Reference 1)

Other tasks, including heading and command tracking in still and turbulent air, also were studied and reported in Reference 1. A further result was that a pilot lead of .5 sec is near optimum for good or moderately good airplanes, and that a time delay of .45 sec is appropriate for heading and all command tracking tasks. The wings-level task depends heavily on acceleration cues that effectively reduce the pilot time delay to .3 sec, a result that can be understood, theoretically, as shown in Section IV of Reference 1.

The gust disturbance used was the Dryden form representing the v gust with a power spectrum of ϕ_v approximated by

$$\phi_v(\omega) = \sigma_v \frac{L}{V_o} \frac{1 + 3\left(\frac{L\omega}{V_o}\right)^2}{\left[1 + \left(\frac{L\omega}{V_o}\right)^2\right]^2}$$

The command tracking tasks were compensatory tasks deriving from white noise filtered by

$$H(s) = \frac{K}{(s + .5)^2}$$

for the bank angle command tracking task and

$$H(s) = \frac{K}{(s + .2)^2}$$

for the command tracking task in heading. The predictions for still air command tracking correlated well with simulator results, and a further result concerns a cross plot of rms performance in still air bank angle command tracking, and the lateral wings level task in turbulence. Figure 4 shows this cross plot in which each point represents a different T-33 configuration. The horizontal scatter demonstrates the relative independence of tracking errors in turbulence and in still air.

Further considerations concerning pilot gain and lead sensitivity are discussed in Reference 1, where the general shape of predicted rms performance versus pilot model gain graphs are related to important subjective handling characteristics.

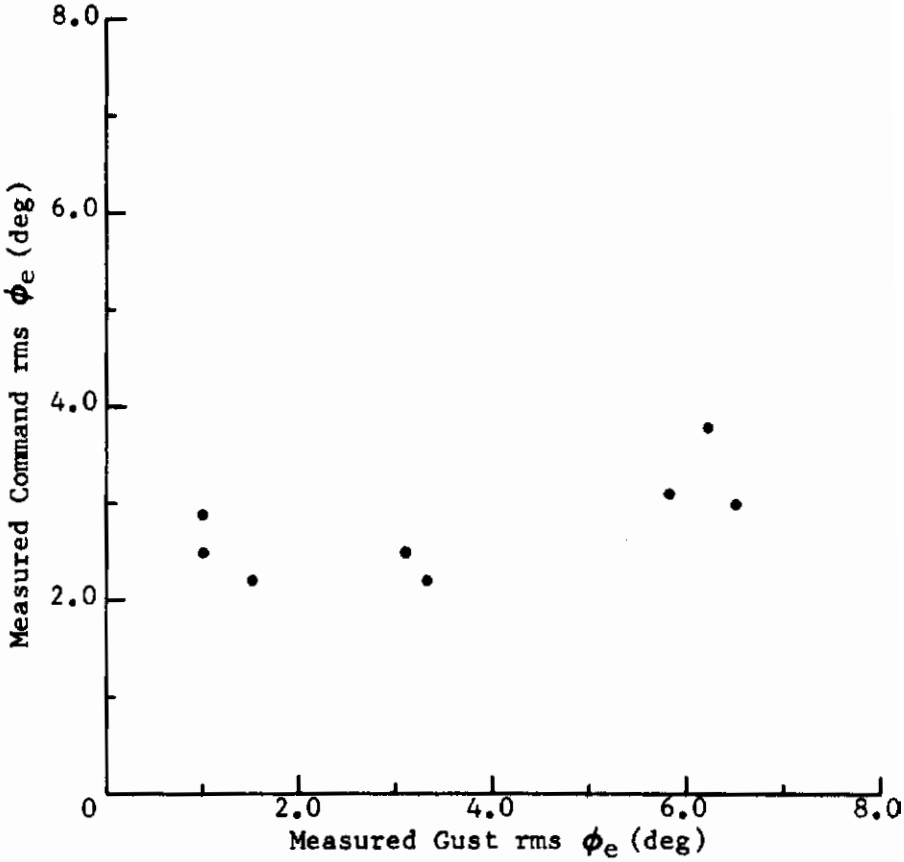

FIGURE 4. INDEPENDENCE OF STILL AIR AND TURBULENCE BANK ANGLE TRACKING ERROR (Ref. 1)

B. ROLL TASK ANALYSIS MODELS

The roll task study is similar to the one reported above from Reference 1. The compensatory model of minimizing bank angle error is equivalent to the piloted task of trying to hold wings level in turbulence, Figure 5, and the pilot task of following a continuous but random commanded bank angle, Figure 6. The transfer functions for these systems are generated automatically by the digital program, along with the rms tracking error, and the equations of motion, used along with the aerodynamic and control data, are given in the appendices. In addition, the command tracking signal, the pilot models and the gust representations must be specified.

The command tracking task was generated by means of the filter

$$H(s) = \frac{K}{(s + .5)^2}$$

Since the white noise source used in the simulation had a bandwidth of 50 Hertz and incorporated a prefilter to provide control over low frequency fluctuations, the prefilter was used in the prediction calculation. Thus, the command tracking task is modeled by white noise filtered by

$$H(s) = \frac{s^2}{(s + .3)^2} \cdot \frac{K}{(s + .5)^2}$$

More will be said about this prefilter in Sections III and IV. The pilot model used for the command tracking calculation was

$$Y_{p_\phi} = K_\phi (.5\, s + 1)\, e_2^{-.45s}$$

in which the second order Padé approximation was used.

The turbulence model for the wings level task included not only the lateral v gust, but also the correlated r gust. The Dryden form filter for these are given in Figure 7 and were also prefiltered in the above manner. The r gust contribution to the error was estimated at between 10 and 20 percent, depending on the aerodynamics of the airplane, and provides enough contribution to warrant its inclusion in both the simulation and the prediction program. The p gust was found to be of little consequence and, hence, was neither simulated nor included in the prediction program. The pilot model used in the turbulence task is

$$Y_{p_\phi} = K_\phi (.5\, s + 1)\, e_3^{-.3s}$$

where the third order Padé approximation was used to provide sufficient high frequency accuracy.

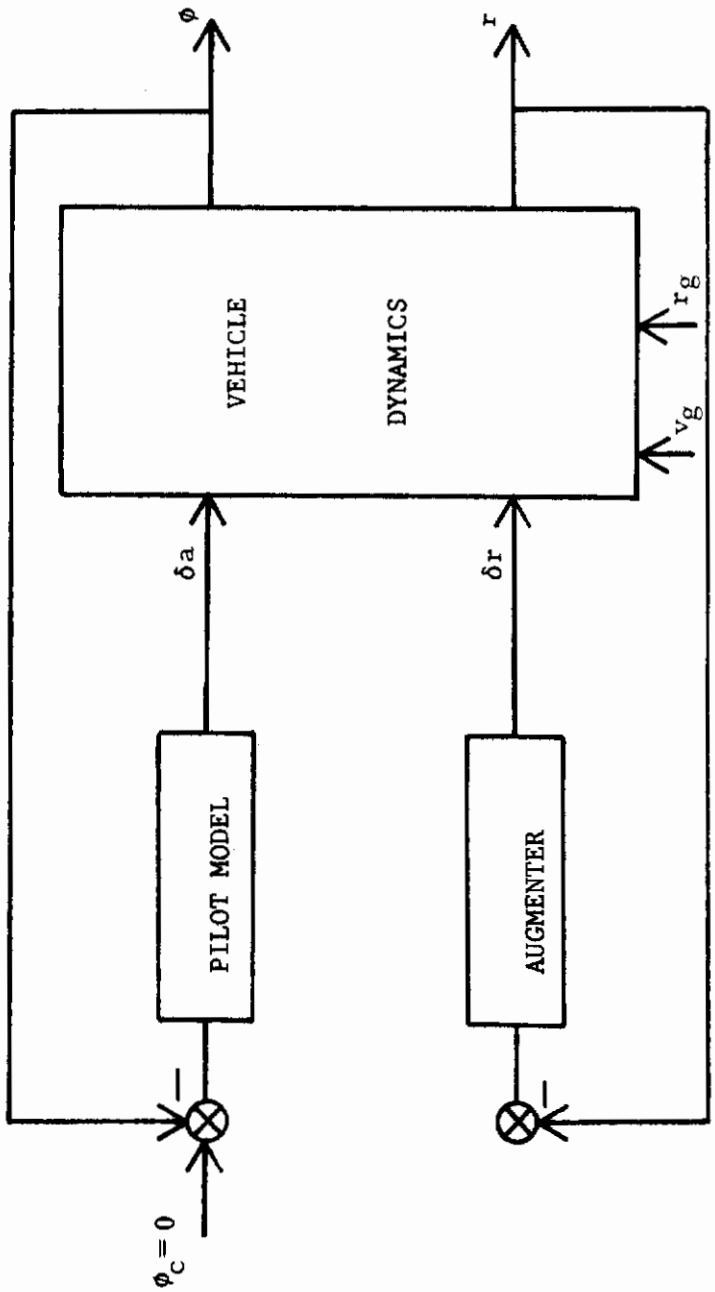

FIGURE 5. SYSTEM DIAGRAM OF BANK ANGLE TURBULENCE TASK

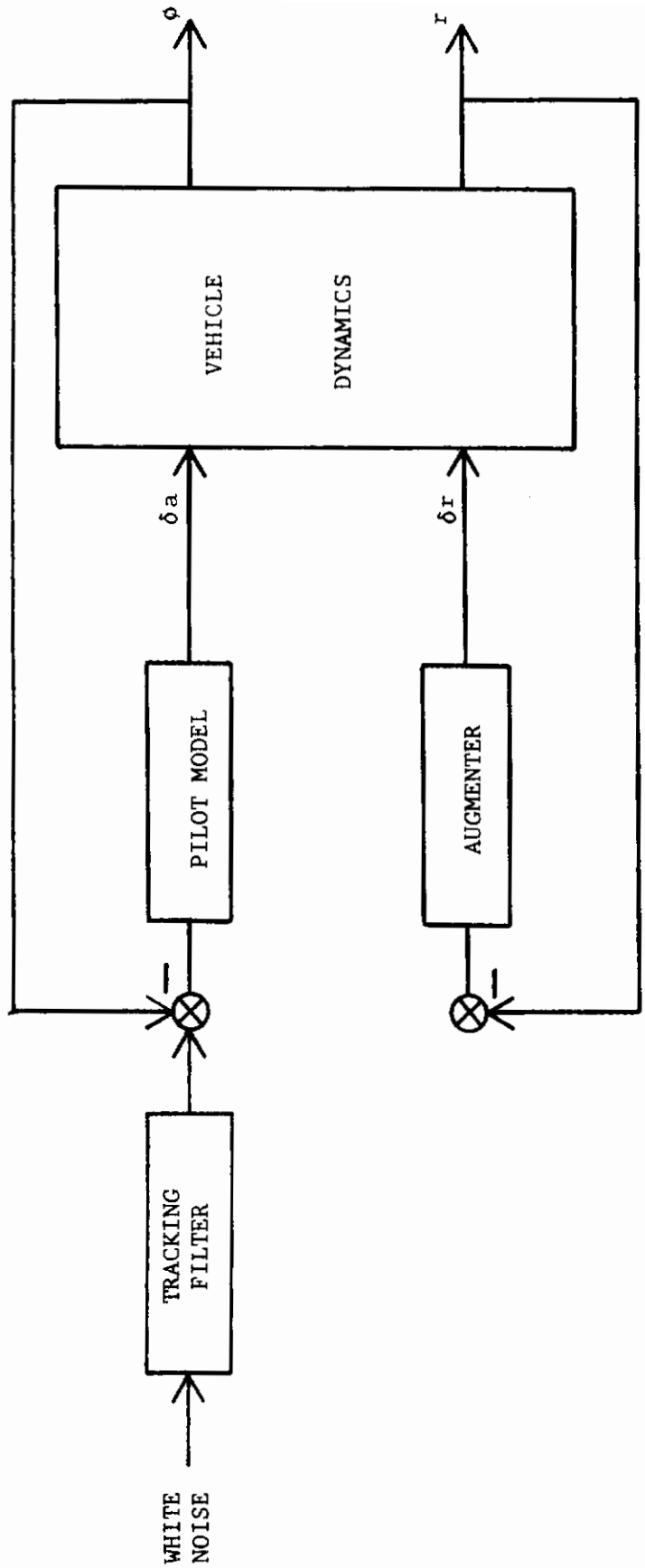

FIGURE 6. SYSTEM DIAGRAM OF BANK ANGLE COMMAND TRACKING TASK

$$T_{v_g}(s) = \sigma_v \sqrt{\frac{L_v}{\pi V_o}} \cdot \frac{1 + \frac{\sqrt{3}\, L_v}{V_o} s}{\left(1 + \frac{L_v}{V_o} s\right)^2}$$

$$T_{r_g}(s) = \frac{-\frac{1}{V_o} s}{1 + \frac{3b}{\pi V_o} s} \cdot T_{v_g}(s)$$

$$T_{w_g}(s) = \sigma_w \sqrt{\frac{L_w}{\pi V_o}} \cdot \frac{1 + \frac{\sqrt{3}\, L_w}{V_o} s}{\left(1 + \frac{L_w}{V_o} s\right)^2}$$

$$T_{q_g}(s) = \frac{\frac{1}{V_o} s}{1 + \frac{4b}{\pi V_o} s} \cdot T_{w_g}(s)$$

FIGURE 7. DRYDEN TURBULENCE MODELS

The prediction procedure (which serves as a model for the other tasks discussed in Sections C and D) requires computing ϕ_e as a function of K_p where: ϕ_e is the rms bank angle error. The minima of this function then are used as performance predictions for the turbulence and still air tasks. In addition, further assessment of the turbulence flying predictions is made by using the optimum gain K_{p_ϕ} and perturbing the pilot model lead from 0.0 to 1.0 seconds. The two graphs, gain and lead variations, have been plotted for all configurations in both normal and failure modes. These are best understood when viewed with the simulation results and are included with the simulation data in Appendix IV. Root locus graphs are also plotted easily since the program prints out these system eigenvalues for each rms computation.

C. HEADING TASK ANALYSIS MODELS

A system diagram of the heading task in turbulence is given in Figure 8. This task requires pilot models in both the bank angle and heading control loops, which are given by:

$$Y_{p_\phi} = K_\phi (.5\, s + 1)\, e_2^{-.45s}$$

$$Y_{p_\psi} = K_\psi (.5\, s + 1)\, e_2^{-.45s}$$

The prediction procedure here involves optimization over variations in K_{p_ϕ} and K_{p_ψ}. These two parameter studies are too voluminous to be included as graphs.

In general, the subject heading of flying qualities in turbulence involves many aspects of handling qualities that have not been considered during this study; for example, the use of rudder control. The minima of rms ψ occur for values of K_{p_ϕ} which are much lower than those required for the wings level task and near optimum performance is often obtained for large variations in K_{p_ϕ}. This is clearly reflected in much of the simulator data in Section III. A recently completed study by Franklin, Reference 3, appears to be an important contribution to the study of heading task, but was received too late to allow comparisons with this study, beyond observing that both investigators coincidently chose the same prefilters for the white noise generators.

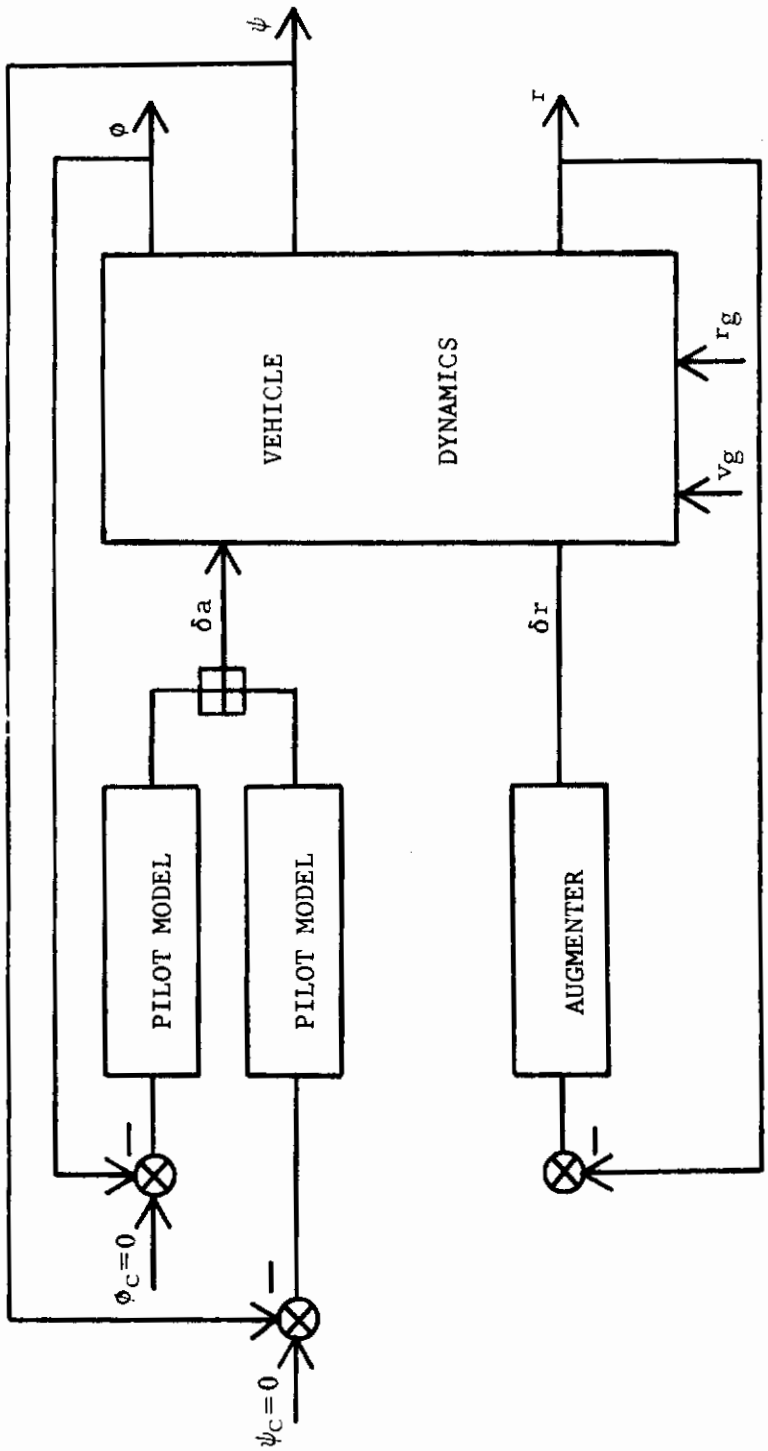

FIGURE 8. SYSTEM DIAGRAM OF HEADING TRACKING TASK IN TURBULENCE

D. PITCH TASK ANALYSIS MODELS

The pitch task study closely resembles the bank angle analysis discussed above. System diagrams for the level attitude task in turbulence and command tracking in still air are shown in Figures 9 and 10, and the pilot model used for both tasks is given by

$$Y_{p_\theta} = K_\theta \, (.5\, s + 1)\, e_2^{-.45s}$$

As with the bank angle study, variations of θ_e are computed with respect to both pilot model gain and lead, and the graphs of these functions are discussed in Section III, along with root locus diagrams as a function of pilot model gain.

The Dryden filters for the w and correlated q gusts are given in Figure 7 and were prefiltered. Again the correlated q gust produced 10 to 20 percent of the tracking error, and the u gust proved to be insignificant for the airplanes and flight conditions studied.

The command tracking task was generated by the filter

$$H(s) = \frac{s^2}{(s + .3)^2} \cdot \frac{K}{(s + .2)^2}$$

As will be seen in the next section, the fixed-form pilot model works well for predicting pitch attitude hold tracking in turbulence although the lower frequency command tracking predictions clearly require more elaborate models.

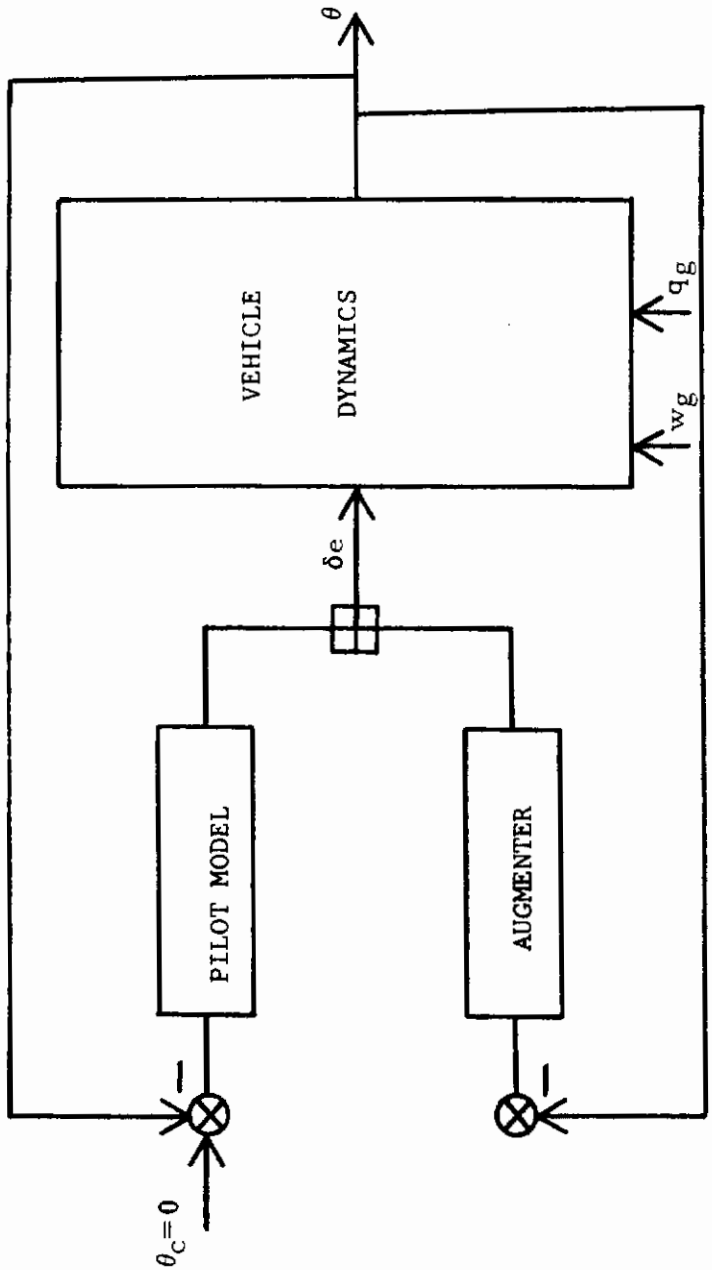

FIGURE 9. SYSTEM DIAGRAM OF PITCH ANGLE TRACKING TASK IN TURBULENCE

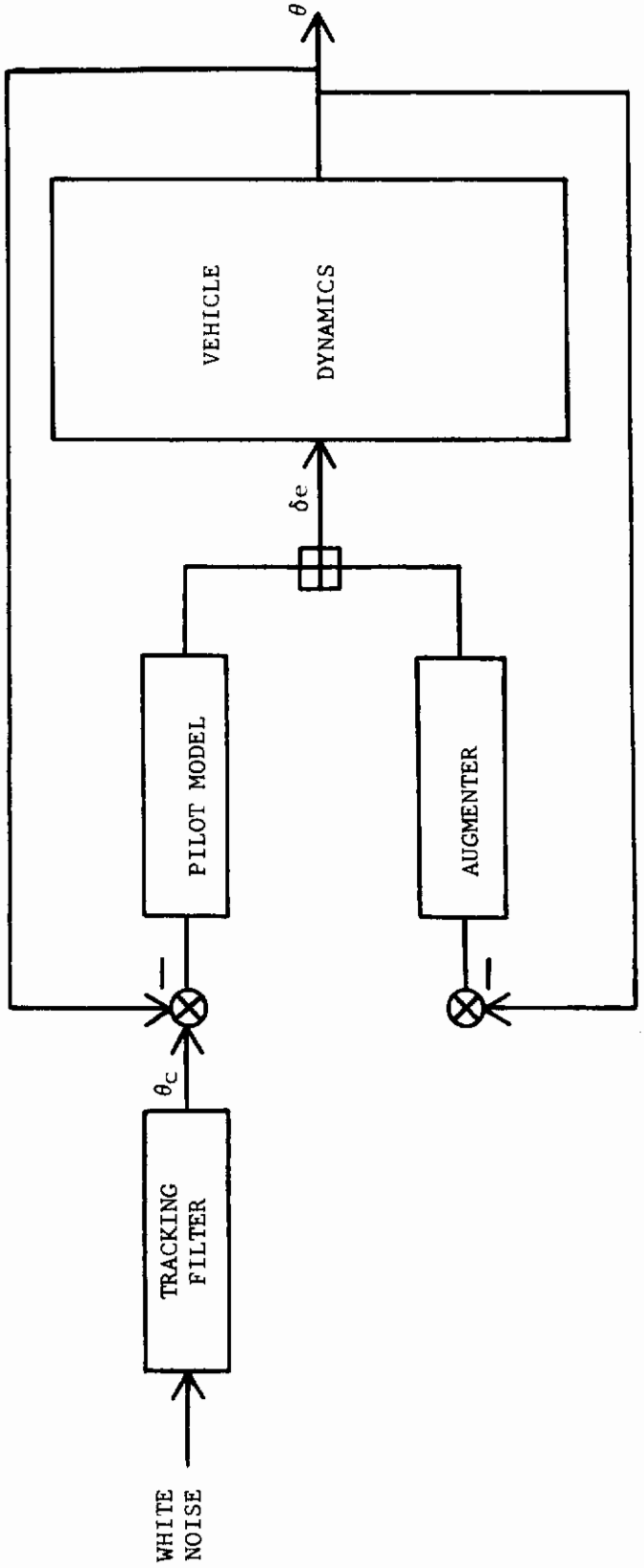

FIGURE 10. SYSTEM DIAGRAM OF PITCH ANGLE COMMAND TRACKING

III. VALIDATION OF THE PREDICTION METHODS BY MOVING BASE SIMULATION

A. EXPERIMENTAL CONSIDERATIONS

One of the most important results of the study reported in Reference 1 is the confirmation that proper acceleration cues to the pilot are necessary for meaningful flying qualities evaluation in turbulence. In order to provide the necessary motion cues for the F-5 and A-7 simulation, the Northrop Large Amplitude Flight Simulator (LAFS) was utilized. The large amplitude capacity of the beam allows the turbulence tasks to be flown with only weak centering washout control of the beam and cab, and the calibration of the frequency response of the simulator showed improvement over that reported in Appendix III of Reference 1. This provided a faithful representation of the acceleration characteristics of turbulence and aircraft response, without pilot concern over reaching the travel limits of the simulator and automatically resetting. The simulator drives were left constant for the entire turbulence simulation. For the lower frequency command tracking tasks, the translational displacement of the beam was reduced.

Since very small errors in the analog computations can distort the mean square quantities measured, three kinds of checks were used for each airplane studied and for each failure mode. Static and dynamic response checks were digitally calculated, and each time a configuration was flown, a pulse initiated time history was matched to the digital check. In addition, the equations were driven with lateral and longitudinal turbulence, and the stick-fixed rms bank angle and pitch errors were measured. These checked closely with the open-loop prediction calculations and provided a test of the gust filter and mean square analog circuits, as well as a check against small biasing voltages that did not affect the fidelity of the simulation, but greatly reduced the accuracy of the mean square data.

In order to eliminate such small biasing voltages and to control skewed statistics from long period components in the noise, a prefilter was used. This filter provided a low-frequency second-order cutoff at .3 radian per second so that sinusoids of periods longer than 20 seconds were suppressed, providing essentially unbiased turbulence and tracking commands over the 100 second recording period of each flight.

Obtaining the above checks proved to be difficult and time consuming. However, the very tight clustering of the simulator data and its agreement with the predictions showed the importance of such care in turbulence research.

The cockpit was a standard Class IV representation with all relevent instruments operating. In order to control the experiment as precisely as possible and eliminate threshold effects, the tasks were all flown IFR in a darkened room. The display utilized the bank and pitch steering bars of the ADI with 10 degrees full deflection on both the roll and pitch tasks. The heading task also used the HSI (Horizontal Situation Indicator). The lateral and longitudinal stick was provided with breakout and force gradients that approximated the reported data for each flight condition. The rudder pedals were not used.

B. DEFINITION OF PILOT TASKS

All tasks, both turbulence and command tracking, were compensatory in nature; the error being presented on the cockpit instruments. The pilot was asked to zero the bank steering bar for the bank angle tasks, the pitch steering bar for the pitch angle tasks, and the HSI for the heading task. At all times, the pilot was flying the complete airplane, although the lateral and longitudinal gusts were not simulated together. Each flight lasted approximately two minutes. After becoming familiar with the configuration, the pilot generally would acquire the task within ten seconds, whereupon data were taken for a 100 second period. Each pilot was instructed to track as tightly as he felt necessary to improve performance; i.e., to minimize rms tracking error, and yet sustain his performance uniformly over each flight during a two hour flying session. When flying lateral turbulence, the pilot was asked to hold approximate altitude; and when flying longitudinal turbulence, he was asked to keep wings approximately level but to pay no attention to heading. Likewise, the pilot was asked not to pay attention to heading during the bank angle task. Similar instructions applied to the command tracking flights without turbulence.

C. DATA TAKING AND PILOT RATINGS

Data were taken from analog mean square circuits as integrated squared voltages and later reduced digitally. Care was taken to scale the circuits so that small voltages as well as overloading were avoided; this required some rescaling during the course of the simulation. The flights were monitored on paper and a close watch was kept for

biasing voltages on the error and turbulence voltages. Occasionally, problems would appear that would require shutting down until the problem was eliminated. This accounts for departures from a standard schedule in the table of simulation data (Appendix IV).

Pilot ratings were requested after turbulence flights only. The pilots were given a rating sheet, Figure 11, and usually flew the same configuration, with approximately the same gust level, at least twice before giving the rating. The pilots were asked to rate the difficulty of the task, but not to rate the roughness of the ride nor to compensate the rating for the turbulence level. The pilots felt some uncertainty about the meaning of such ratings in turbulence, but they were able to assign numbers without difficulty. The consistency of the pilot ratings obtained indicates that the above instructions, though somewhat general, were sufficient for pilots to assign work level ratings for the airplanes in turbulence.

It should be carefully noted that the pilot ratings obtained in the above manner may not correspond to familiar Cooper or Cooper Harper rating scales since these scales reflect the global merit of the airplane in still air tasks or in turbulence. If given accurately, the Cooper or Cooper Harper ratings in turbulence may be only weakly related to turbulence intensity since the pilot might compensate the rating for the turbulence level. In other words, the pilot might reason, after a particular flight in rough air, that the flight was difficult but the gusts were very strong and, therefore, the airplane must be given a good rating since it was controllable in such heavy turbulence. On the other hand, the pilot might have been flying a configuration that was very prone to atmospheric disturbance under conditions of only light to moderate turbulence. This variability in gust susceptibility has been clearly seen during the current simulation as well as in the study of Reference 1. In both simulations, the gust levels were set by asking the pilots to indicate when the intensity of the turbulence was light, moderate, and heavy. Although the gust levels are scattered for statistical reasons, it is clear that the pilots reported differing gust levels as heavy for different configurations. For example, the T-33 configuration BC 2.4 of Reference 1 was impossible to simulate at v gust levels over 10 ft/second rms, whereas AB 3.3 could be flown at well over 20 ft/second rms turbulence. The data in Appendix IV includes further examples. Thus, the pilot is not able to estimate the turbulence intensity reliably, which means that the compensated rating for turbulence flights might be in error. Thus, by asking for the actual workload, a more precise measure of pilot controllability can be obtained. The data obtained shows this to be the case, as discussed in Section IV.

CATEGORY		ADJECTIVE DESCRIPTION WITHIN CATEGORY		NUMERICAL RATING
ACCEPTABLE	SATISFACTORY		EXCELLENT	1
			GOOD	2
			FAIR	3
	UNSATISFACTORY		FAIR	4
			POOR	5
			BAD	6
UNACCEPTABLE	FLYABLE		BAD	7
			VERY BAD	8
			DANGEROUS	9
	UNFLYABLE		UNFLYABLE	10

7 REQUIRED MAJOR PORTION OF PILOT'S ATTENTION

8 CONTROLLABLE ONLY WITH A MINIMUM OF COCK-PIT DUTIES

9 AIRCRAFT JUST CONTROLLABLE WITH COMPLETE ATTENTION

FIGURE 11. PILOT RATING SCALE

D. ROLL TASK SIMULATION

The data included in this report consist of the pilot model gain and lead variation prediction graphs, gust and command tracking simulator data, and root locus diagrams of the dynamics as a function of pilot model gain. These data are located in Appendix IV and will be referred to by figure number. In addition, Appendix IV contains further details about how the data were obtained and plotted. The pilot task and simulation arrangement have been discussed above, and the aerodynamic and control data are to be found in Appendix III for all airplanes, augmenters, and control failure configurations. Since many features of the shape of the variation graphs relate to handling qualities, a case by case discussion of the bank angle data follows.

F-5 Flight Condition #1: Mach .81, Altitude 5135 feet, Figures 63-67.
With augmenter, the variation graphs, Figure 63, indicate that the pilot cannot reduce the tracking error below the open-loop value of 1.19 degrees for 10 ft/second turbulence. However, this open-loop tracking error proves to be among the lowest of the simulated airplanes, and the plateau of the gain variation graph through a gain of .4 deg/deg indicates that the pilot will not experience performance gain sensitivity. The simulator data demonstrate, Figure 64, the linear relationship which exists between tracking error and gust level for good airplanes. The numbers attached to the graphical data are pilot ratings and show that the airplane is acceptable for light and moderately heavy turbulence.

Without augmenter, Figure 65, the tracking error increases rapidly with increased pilot gain. Thus, the pilot has to be careful not to excite the system beyond the open-loop response level. This, in addition to the unacceptable dutch roll damping, Figure 67, accounts for the higher pilot ratings and tracking errors on the simulator data graphs (Figure 66).

F-5 Flight Condition #2: Mach .4, Altitude 4950 feet, Figures 68-72.
As a result of the lower airspeed this airplane is more disturbed by turbulence than #1. The variation graphs show that with augmenter, the pilot can reduce the tracking from the open-loop value with the undemanding lead of $T_L = .5$ sec used in the fixed form prediction pilot models. The simulator data show good agreement with the predictions and with acceptable pilot ratings for light and moderate turbulence.

Without augmenter, the pilot model cannot reduce the tracking errors, and the pilot ratings indicated that the airplane is unsatisfactory in low turbulence and unacceptable in heavy turbulence.

F-5 Flight Condition #3: Mach .9, Altitude 5000 feet, Figures 73-77.
This airplane is much like #1, and the prediction data show features to which the discussion of #1 applies.

F-5 Flight Condition #4: Mach .8, Altitude 32,150 feet, Figures 78-81.
The normal mode augmented airplane is controllable by the pilot, with the undemanding lead of T_L = .5 sec being optimum, and the gain variation graph shows that the pilot gain is not critical. The pilot ratings at low turbulence reflect these characteristics along with the acceptable dutch roll eigenvalue and its associated locus. The airplane is also acceptable though rated unsatisfactory at moderate to heavy gust levels, a result of the large bank angle excursions (probable peaks of 10 degree bank) at the higher turbulence level.

Without augmenter, the gain variation graph on Figure 80 shows a local minimum at a gain of .9 deg/deg. A careful monitoring of the lateral stick showed that the pilots were using large aileron deflections and, therefore, high gain. Thus, the simulation data show that the pilots apparently operate at this gain. Furthermore, Reference 1 includes several examples where the pilots operated at gains at which the gain variation graphs show local minima. This minimum shows greater gain sensitivity than the augmented case. This, along with the too lightly damped dutch roll eigenvalue, accounts for the higher pilot ratings and scatter in the performance data. The high susceptibility of this failure mode to gust disturbance and bad pilot ratings at light to moderate turbulence clearly indicate that this configuration has very poor flying qualities in turbulence.

A-7 Flight Condition #1: Mach .6, Altitude 15,000 feet, Figures 83-92.
With augmenter, this airplane displays sensitivity to both pilot gain and lead. The predicted disturbance level is not unusually high although the open-loop disturbance level is large. The pilot ratings show that in light to moderate turbulence, the airplane rates fair to poor.

Without augmenter, this airplane shows unusually high sensitivity to pilot gain and lead perturbation. This results in poor to bad pilot ratings at light to moderate gust levels, and bad to very bad ratings at moderate turbulence. The scatter in the command tracking data reflects the low frequency of the roll eigenvalues and a tendency for PIO during the tracking task.

A failure mode of the A-7 lateral control system was also simulated for each flight condition of the A-7, with and without augmenter. The exact control system in

all cases is specified in Appendix III.

The control failure mode, with and without augmenter, causes only small departures from the other A-7 flight condition airplanes and the above discussion applies here.

A-7 Flight Condition #2: Mach .9, Altitude 15,000 feet, Figures 93-102. The gain and lead variation graphs show that the augmented normal mode airplane has reasonably good turbulence handling qualities since perturbations in gain and lead do not cause significant increases in tracking error. The performance, which is exactly predicted in this case, is the lowest of the entire bank angle simulation. In spite of this, the pilot ratings are higher than for other airplanes having greater disturbance in gusts. The pilot ratings are fair at light turbulence levels and fair to bad at moderate turbulence levels. The problem appears to be with the control system, although the time histories check with the simulator. The pilot reported that the airplane was sluggish and unpleasant in the turbulence tasks.

Without augmenter, the gain variation graph shows that the pilot model cannot significantly improve upon the open-loop tracking error, and the pilot ratings are deteriorated to fair through very bad in light to moderate gusts.

With the control failure, the airplane is not much different from the normal mode case. However, the tracking errors are larger but the pilot ratings are better, being good to fair in the light turbulence range. This phenomenon occurs with several configurations and is a result of the particular rating system used. Since the pilot rates on workload exclusively, this simply shows that the relationship of tracking accuracy and pilot workload varies from airplane to airplane.

A-7 Flight Condition #3: Mach .6, Altitude 35,000 feet, Figures 103-112. All normal and failure mode airplanes at this flight condition display sensitivity to perturbation in pilot gain and lead. However, the pilot found the augmented and unaugmented airplanes, without failure, relatively easy to fly, and the tracking performance was near median in the simulation data.

The failure mode airplanes, with and without augmenter, were very unpleasant to fly, being rated bad to very bad at moderate to heavy turbulence.

A-7 Flight Condition #4: Mach .9, Altitude 35,000 feet, Figures 113-122. The normal mode airplane has gain and lead variation graphs that indicate good turbulence handling qualities. The simulator data show that although the tracking error is greater than flight condition #2, the pilot ratings are much better.

The same comments apply to the failure mode with augmenter, although the pilot ratings are somewhat worse - fair at light turbulence and bad at moderate turbulence. In the cases without augmenters, the pilot gain variation graphs show more sensitivity to pilot gain perturbations and have higher associated pilot ratings.

E. HEADING TASK SIMULATION

Since the heading study will not figure in the discussion on specification criteria, a less thorough description and interpretation of the data will be given here.

The data for each configuration and mode are presented in four graphs. The first, Heading Error versus Gust Level, also has pilot ratings attached to the data. The second graph shows the amount of bank angle used during the flight. It is significant that for many of the cases where the heading error versus gust level data are tightly clustered about a line through the origin, the rms bank angle data are greatly scattered. (Good examples of this are found in Figures 125, 129, 143, and 145. This substantiates the analytical finding that with respect to the pilot model described in Section II, the heading error surfaces parameterized by bank angle pilot model gain K_ϕ and heading pilot gain K_ψ often resemble the surface shown in Figure 12.) Thus, in these cases, the pilot can select the amount of bank angle during the task from peaks of six degrees ϕ, to cite Figure 145 again, up to 80 degrees with little or no advantage to heading tracking performance gained by the larger excursions. The third graph shows the rms sideslip versus gust level. The performance data here resemble the heading error versus gust level data and shows tight clustering. The fourth graph gives the rms yaw rate versus gust level. Complete data for the heading study are presented in Figures 123 through 170.

F. PITCH TASK SIMULATION

The data presentation format for the pitch task simulation follows that of the bank angle study above. Unlike the bank angle case, there is no great diversity in the qualitative aspect of the different configurations in the pitch task. The data are presented in Figures 171 through 210.

The normal-mode airplanes all have gain and lead variation graphs that show a plateau in the gain variation graph. Thus, the pilot cannot substantially reduce the open-loop performance. However, the normal-mode airplanes are not sensitive to pilot gain perturbations and this, coupled with low lead variation, indicates that little or no lead is required; thus, optimal turbulence tracking is easy for the pilot. As a consequence, the pilot can track close to optimum for a wide range of workload and, since the pilot rating, as defined for this study, reflects the workload, it is expected that some disagreement in pilot ratings should result. This is seen to be the case in the simulator data, particularly at higher gust levels. Figure 177 shows pilot ratings of 3, 5.5 and 7.0 at nearby points. Figure 182 shows two pair of neighboring points, with ratings of 2.5 and 5 for one pair of points and 3.5 and 7.5 for the other. The

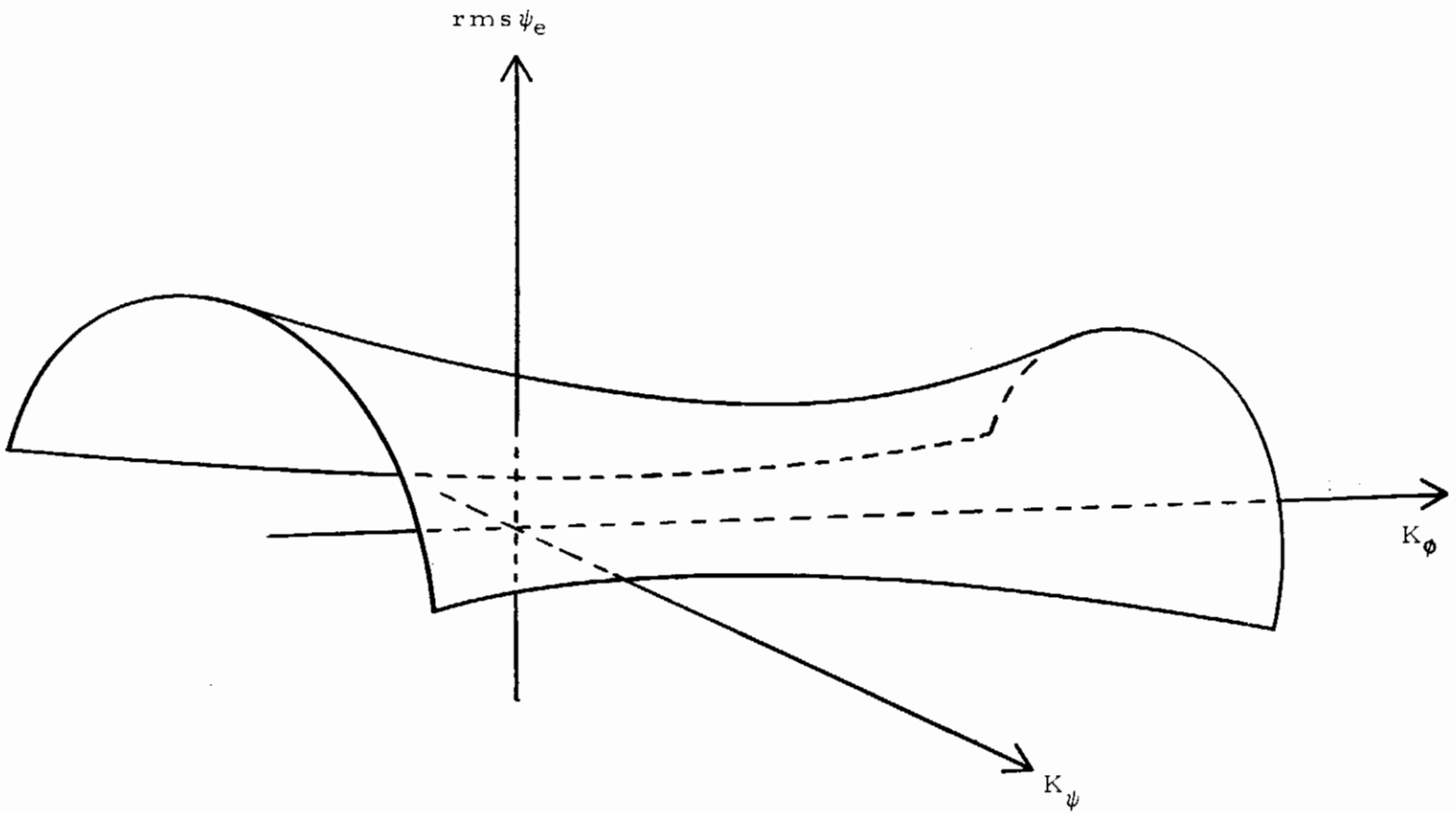

FIGURE 12. HEADING TRACKING ERROR PREDICTION SURFACE PARAMETERIZED BY BANK ANGLE AND HEADING PILOT MODEL GAINS

agreement between the pilots, nevertheless, is good in both ratings and tracking errors for most configurations for which the pilot can reduce the tracking error below the open loop value. The predictions also show good matching with the simulation data although they are less accurate than in the bank angle case.

The unaugmented airplanes show increased sensitivity to pilot gain and sometimes a requirement for large pilot lead (for example, Figure 178).

The command tracking simulator data are tightly clustered and in most cases the tracking errors are lower than the predictions. The cause of this is that the fixed-form pilot model does not have the correct low-frequency characteristics for this task. The longitudinal phugoid mode becomes unstable for low gains in the pilot model, thus resulting in larger tracking error predictions than if the mode were controlled, allowing higher pilot model gains. It has been found that this phugoid mode has little effect on simulator pilot tracking errors, and that predictions can be improved either by adding an altitude feedback loop to the pilot model or by suppressing the forward velocity equation of motion.

A fuselage bending mode is known to be of importance in the handling qualities of the F-5. This was accounted for by normal acceleration to elevator feedback in both the simulation and the prediction computations by incorporating this closure into the equations of motion and, hence, into the aerodynamic data.

G. ASSESSMENT OF THE PREDICTION METHODS

Prediction lines have been shown on the simulation data graphs in Appendix IV. In order to obtain a better view of the accuracy of the prediction techniques, a brief description of the result is included here.

As a means of comparing the simulation and the prediction, the simulation data have been normalized to a standard turbulence level of 10 ft/second and then averaged. These averages and the corresponding predictions are given in Figures 13, 14 and 15. To help visualize these numbers, cross plots of these averages against the predictions have been graphed in two ways; normal mode alone, and normal and control or augmenter failure modes combined.

Figure 16 shows the normal mode bank angle results which illustrate the accuracy of the method for normal mode airplanes, and the entire bank angle study is summarized in Figure 17. Here the data are more scattered since many of the failure mode airplanes introduce piloting effects and techniques not required for the control of normal mode acceptable airplanes and not accounted for by the fixed form pilot model. Figure 18 shows that the prediction and simulation command tracking

Configuration	rms ϕ_e (deg) Computed Average at 10 ft/sec v_g	rms ϕ_e (deg) Prediction	rms ϕ_e (deg) Computed Average at 10 degrees ϕ_c	rms ϕ_e (deg) Prediction
F-5 #1 AUG	1.50	1.19	4.78	4.03
W/O AUG	1.78	1.01	5.06	4.26
F-5 #2 AUG	2.60	2.45	4.38	4.76
W/O AUG	3.04	3.94	4.29	5.22
F-5 #3 AUG	1.45	1.10	4.79	4.03
W/O AUG	1.74	.86	4.41	4.06
F-5 #4 AUG	2.16	2.25	4.76	5.73
W/O AUG	3.76	3.35	4.76	5.90
A-7 #1 AUG	1.77	1.60	5.73	4.19
W/O AUG	2.36	3.53	5.24	5.95
F AUG	2.24	1.45	5.06	3.62
F W/O AUG	3.19	2.81	4.58	4.32
A-7 #2 AUG	1.10	1.10	4.01	3.46
W/O AUG	1.50	1.96	3.99	4.06
F AUG	1.58	1.00	4.04	3.56
F W/O AUG	2.03	1.67	5.18	3.71
A-7 #3 AUG	1.88	1.97	4.85	5.59
W/O AUG	2.12	3.58	5.11	4.87
F AUG	2.45	1.66	4.83	4.39
F W/O AUG	2.82	2.48	4.67	5.99
A-7 #4 AUG	1.57	1.27	3.84	4.11
W/O AUG	1.86	2.48	3.86	5.31
F AUG	2.45	2.12	4.77	3.77
F W/O AUG	2.96	1.97	3.82	4.32

FIGURE 13. AVERAGED BANK ANGLE SIMULATION AND PREDICTION DATA

Configuration	rms ψ_e (deg) Computed Average 10 ft/sec V_g	rms ψ_e (deg) Prediction
F-5 #1 AUG	.93	.66
W/O AUG	1.11	.79
F-5 #2 AUG	1.99	1.28
W/O AUG	2.53	1.73
F-5 #3 AUG	.85	.59
W/O AUG	1.02	.68
F-5 #4 AUG	1.12	.82
W/O AUG	1.66	1.20
A-7 #1 AUG	1.20	.88
W/O AUG	1.62	1.12
F AUG	1.42	.87
F W/O AUG	1.30	1.04
A-7 #2 AUG	.76	.58
W/O AUG	.91	.77
F AUG	.88	.58
F W/O AUG	.84	.76
A-7 #3 AUG	1.86	1.01
W/O AUG	2.27	1.24
F AUG	2.03	1.0
F W/O AUG	2.06	1.22
A-7 #4 AUG	1.08	.69
W/O AUG	1.27	.93
F AUG	1.64	.70
F W/O AUG	1.63	.82

FIGURE 14. AVERAGED HEADING ANGLE SIMULATION AND PREDICTION DATA

Configuration	rms θ_e (deg) Computed Average at 10 ft/sec w_g	rms θ_e (deg) Prediction	rms θ_e (deg) Computed Average rms θ_c = 10°	rms θ_c (deg) Prediction
F-5 #1 AUG	.74	.42	2.87	3.83
W/O AUG	1.03	.71	2.82	4.60
F-5 #2 AUG	1.02	.79	3.53	3.81
W/O AUG	1.38	1.25	3.69	3.95
F-5 #3 AUG	.61	.42	2.70	3.74
W/O AUG	.80	.63	3.61	5.80
F-5 #4 AUG	.66	.51	3.69	4.64
W/O AUG	.72	.82	3.67	5.01
A-7 #1 AUG	.72	.54	3.23	3.24
W/O AUG	1.10	.98	3.63	4.63
A-7 #2 AUG	.63	.42	2.78	6.11
W/O AUG	1.02	.67	2.84	4.39
A-7 #3 AUG	.60	.63	3.07	6.20
W/O AUG	.83	1.23	3.36	5.35
A-7 #4 AUG	.59	.45	3.13	3.83
W/O AUG	.93	.79	3.13	5.77

FIGURE 15. AVERAGED PITCH ANGLE SIMULATION AND PREDICTION DATA

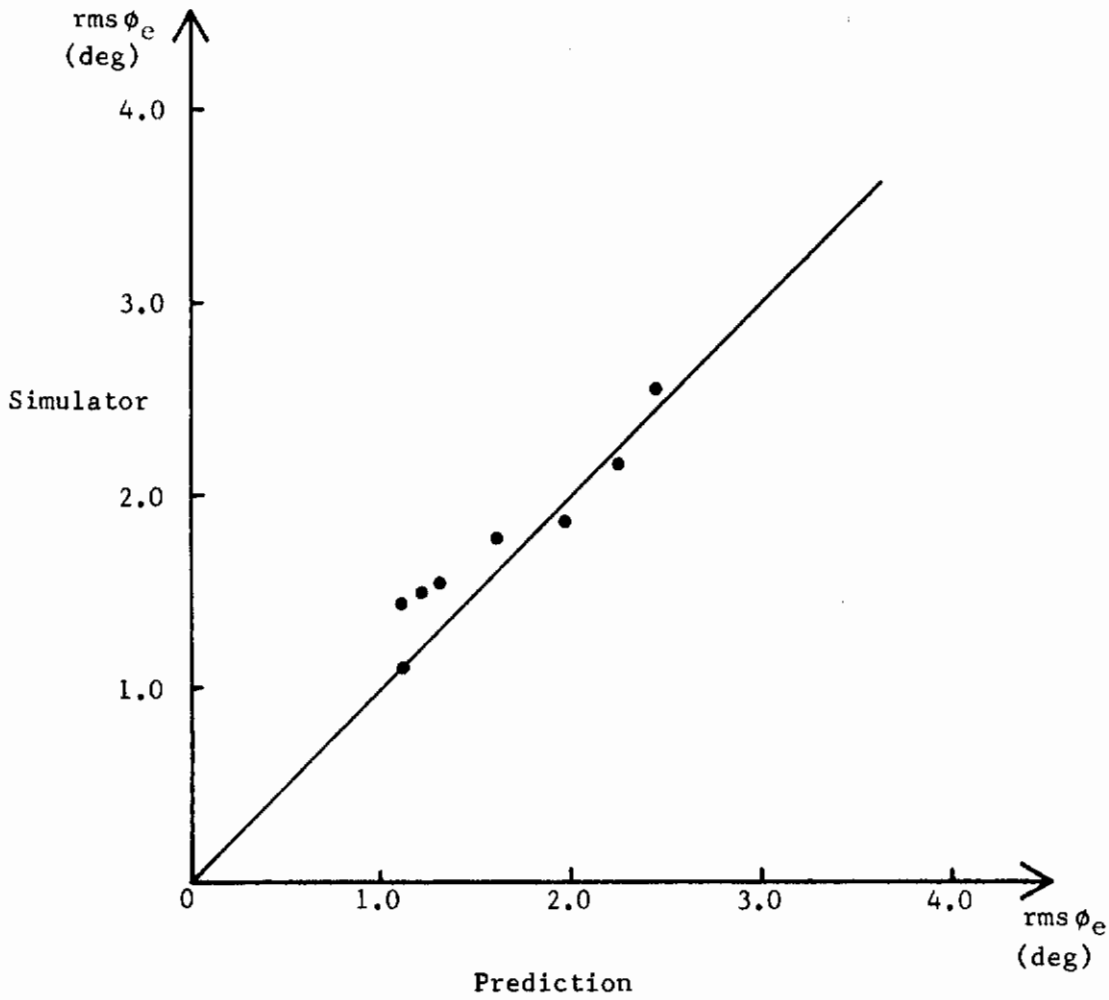

FIGURE 16. BANK ANGLE GUST TRACKING DATA FOR NORMAL MODE F-5 AND A-7 AIRPLANES

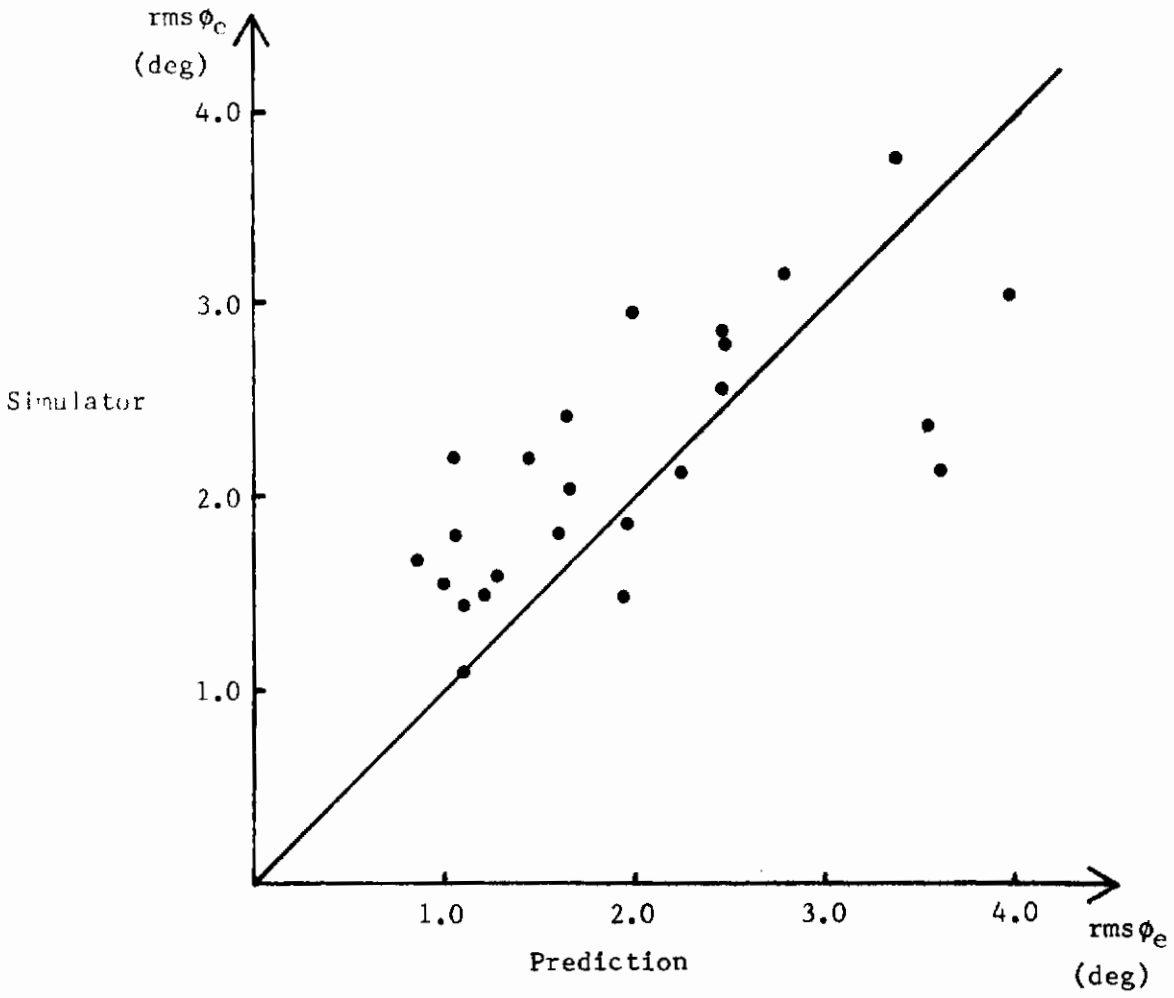

FIGURE 17. BANK ANGLE GUST TRACKING DATA FOR NORMAL AND FAILURE MODE F-5 AND A-7 AIRPLANES

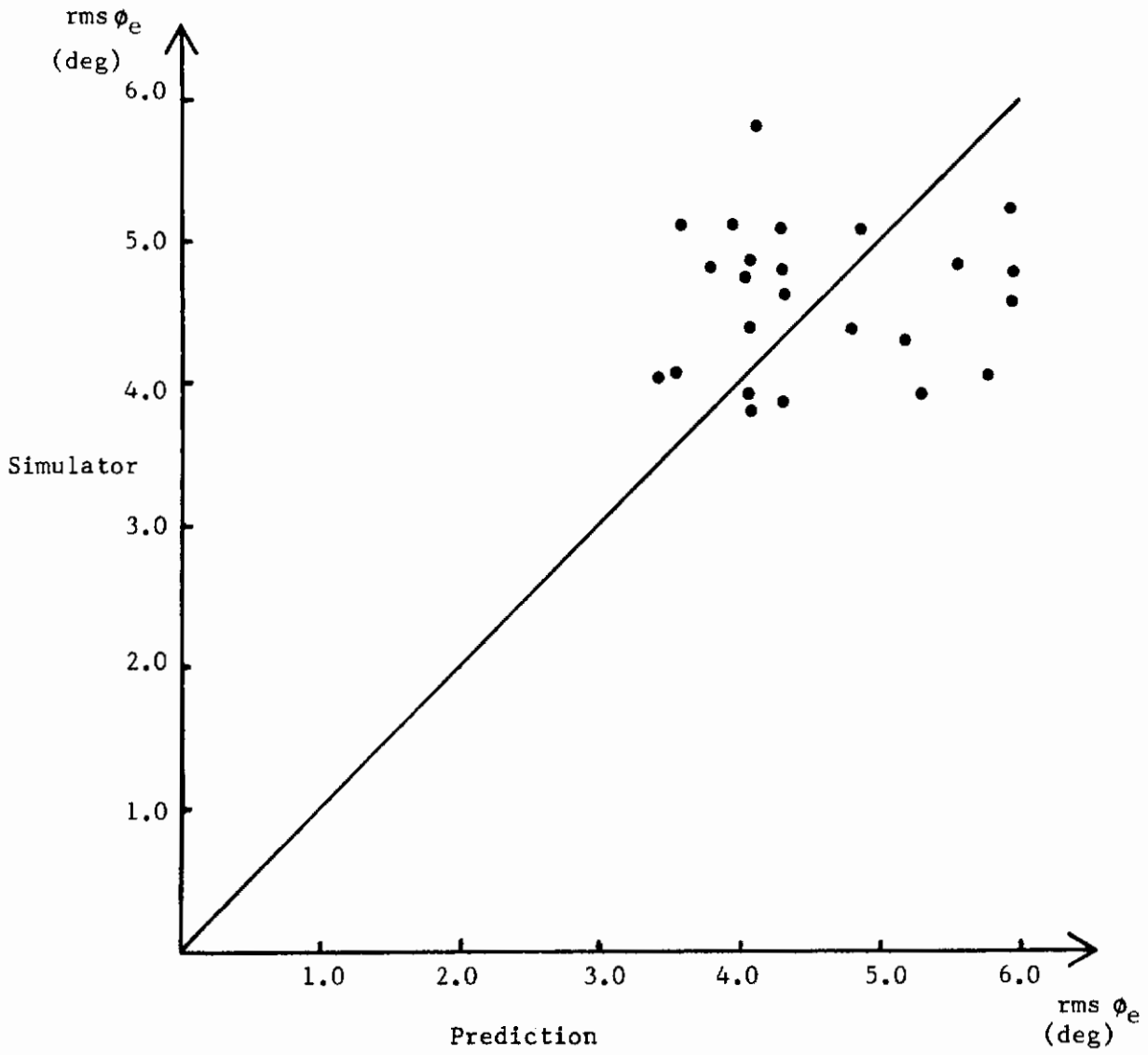

FIGURE 18. BANK ANGLE COMMAND TRACKING DATA FOR NORMAL AND FAILURE MODE F-5 AND A-7 AIRPLANES

results generally match, but that for the tracking task employed, the method is not useful for ranking the performance between configurations.

The normal mode heading data in Figure 19 show close agreement for six of the eight airplanes. Figure 20 shows that for all configurations, even though the method predicts errors somewhat low, the result can still be used to rank performance.

Except for one case, the normal mode airplanes in pitch angle attitude hold tasks have nearly the same performance as shown in Figure 21. However, the failure mode airplanes show a considerable scatter in their responses, Figure 22, and are both evaluated and ranked well by the method. On the other hand, the pitch angle command tracking predictions are mostly too high as a result of the poor low-frequency response of the fixed form pilot model, Figure 23.

In order to assess these results numerically, averages of the percent errors of the predictions were computed for each of the Figures 16 through 22. These analyses and the standard deviations of the prediction error distributions are shown in Figure 24. It should be noted that these figures evaluate only the prediction method's ability to predict the turbulence tracking errors. Accordingly, in the bank angle case, the normal mode average error is 13.35% at predictions of 1.10 degrees to 2.25 degrees, over a range of 205%. For all bank angle cases, the error average is 29.89% over a range of 389%. The average heading prediction error for all airplanes is 54.08% over a range of 298%, which does not take into account the strong correlation along a line displaced upwards from the line of agreement. Thus, the ability of the method to rank cases would be much better than these error averages indicate. The pitch data show an average prediction error of 31.78% for all airplanes over a range of 297%. These relations of prediction error to range of data are shown in Figure 25.

This ability to estimate system performance, and to rank prospective designs in terms of tracking ability, makes it now practical to consider turbulence effects during the design phase, and provides a means of analytically evaluating airplanes against turbulence flying qualitites criteria.

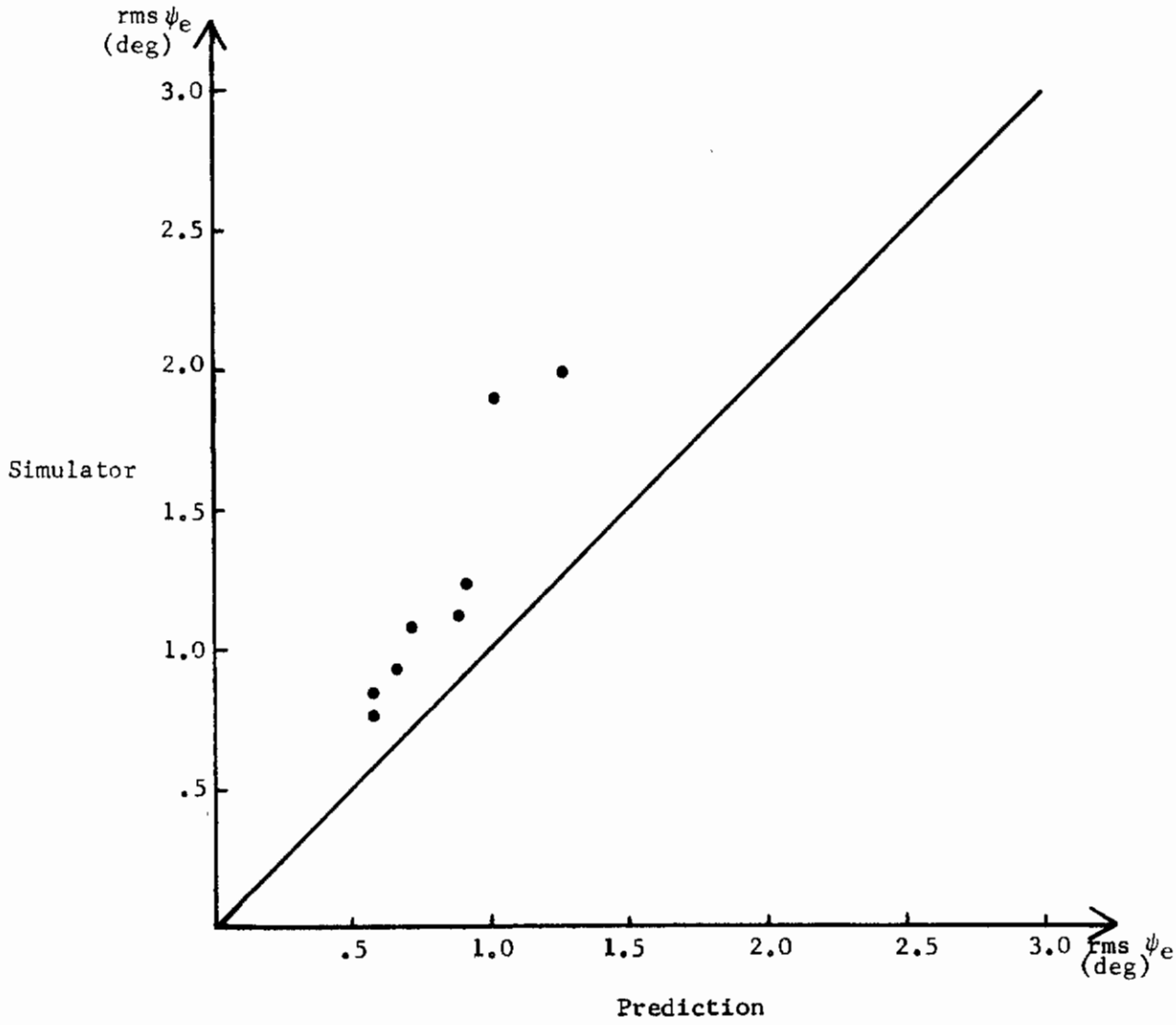

FIGURE 19. HEADING ANGLE GUST TRACKING DATA FOR NORMAL MODE F-5 AND A-7 AIRPLANES

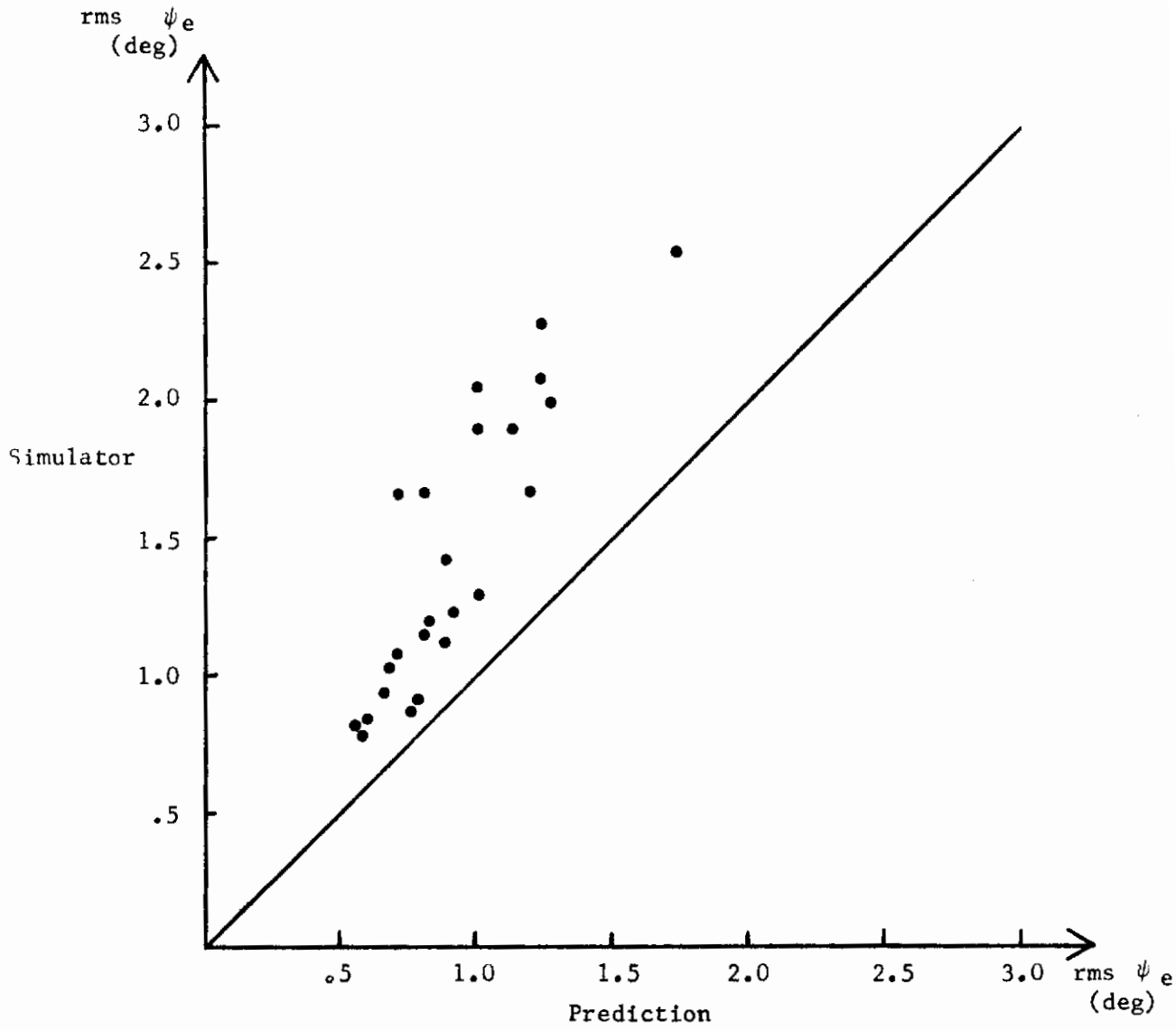

FIGURE 20. HEADING ANGLE GUST TRACKING DATA FOR NORMAL AND FAILURE MODE F-5 AND A-7 AIRPLANES

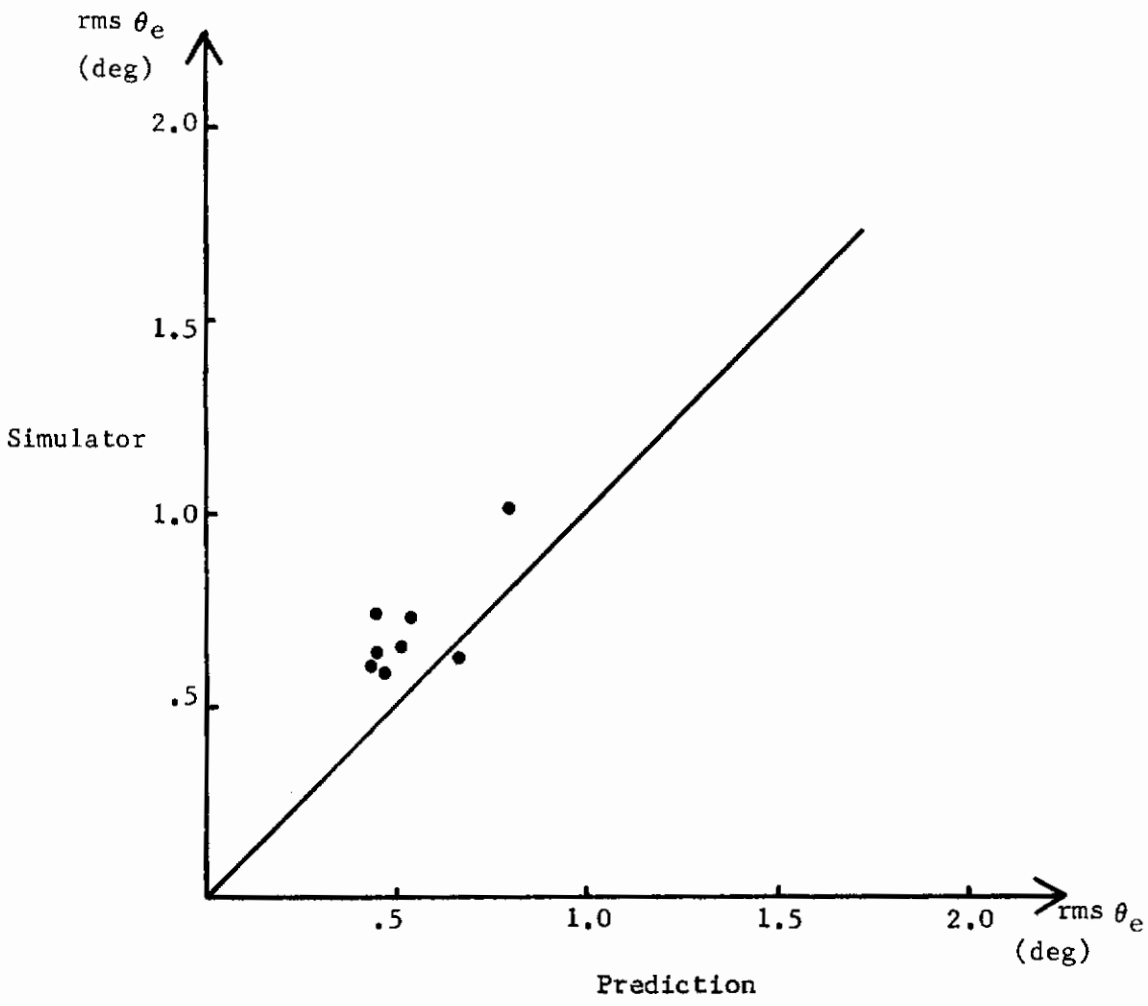

FIGURE 21. PITCH ANGLE GUST TRACKING DATA FOR NORMAL MODE F-5 AND A-7 AIRPLANES

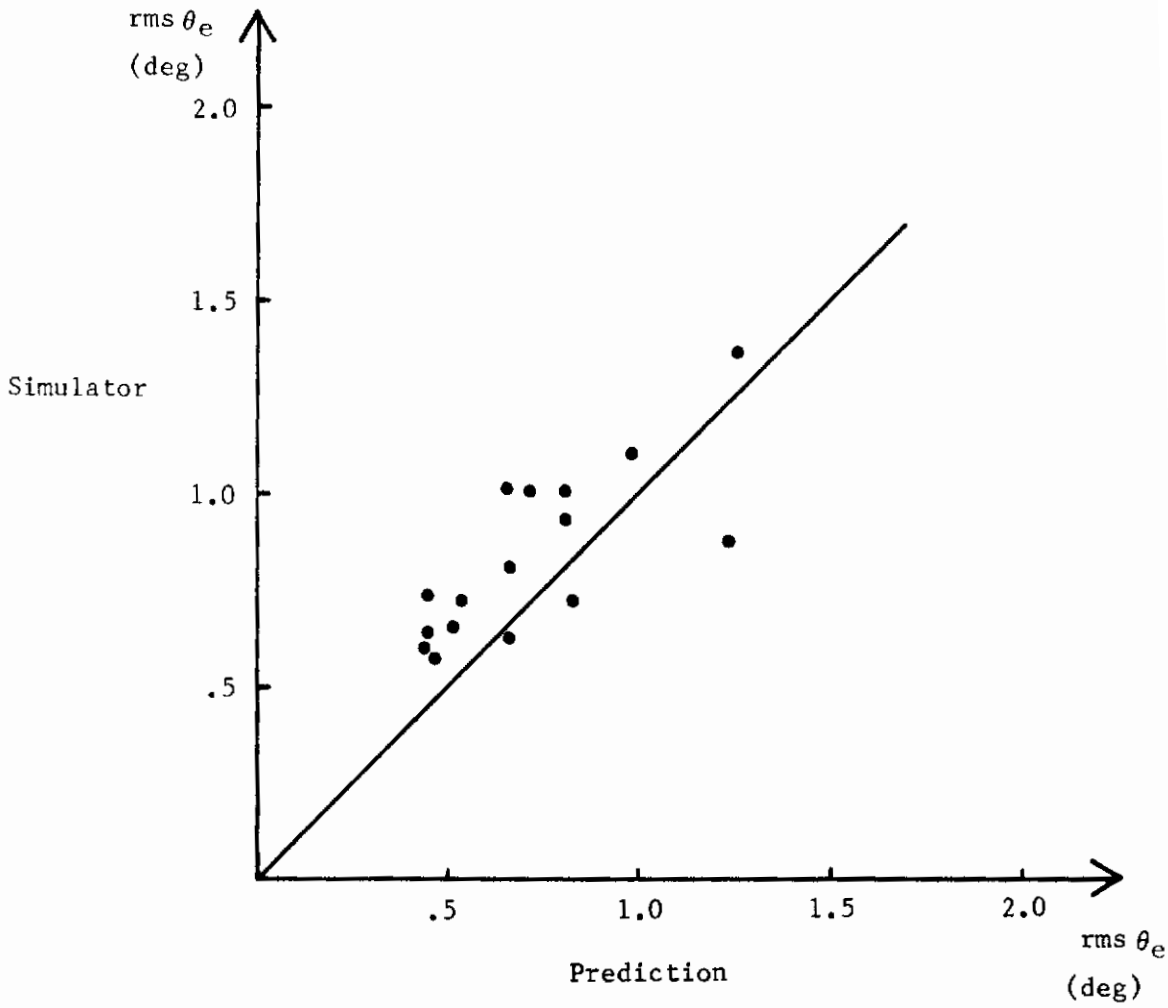

FIGURE 22. PITCH ANGLE GUST TRACKING DATA FOR NORMAL AND FAILURE MODE F-5 AND A-7 AIRPLANES

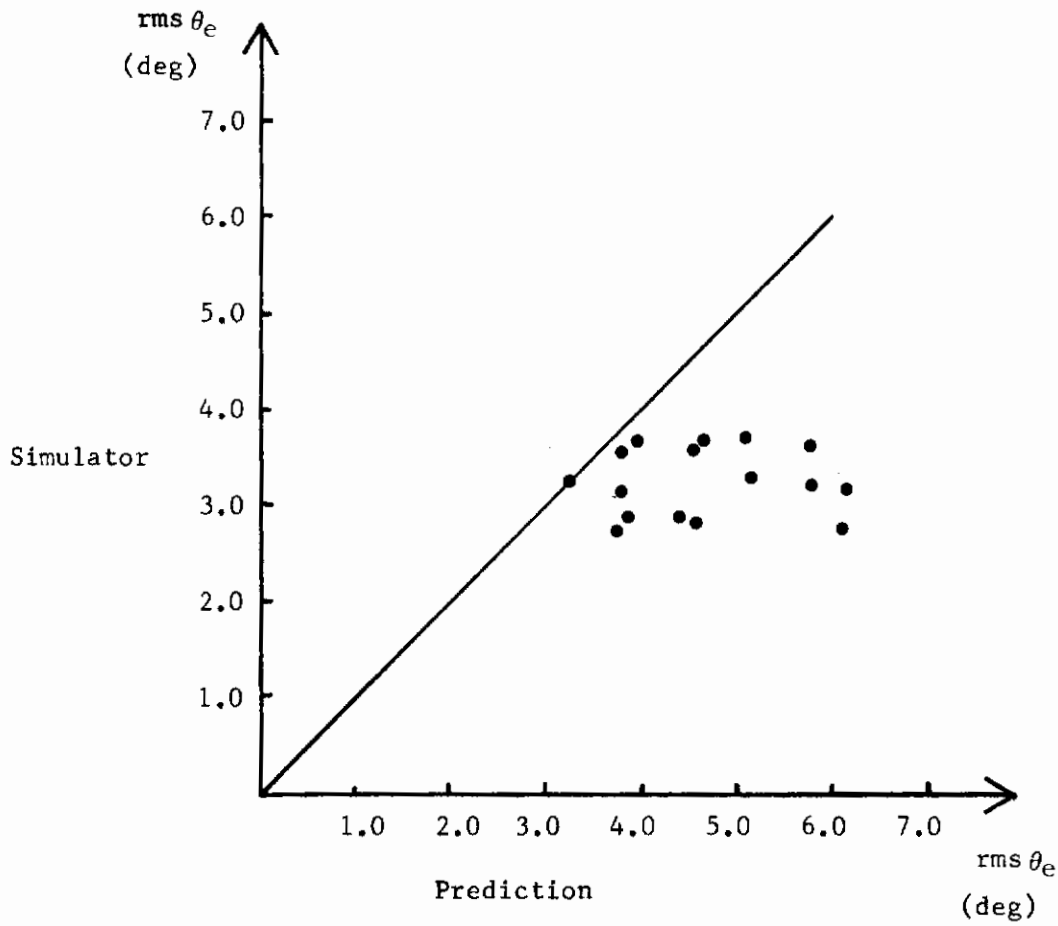

FIGURE 23. PITCH ANGLE COMMAND TRACKING DATA FOR NORMAL AND FAILURE MODE F-5 AND A-7 AIRPLANES

CONFIGURATIONS AVERAGED	AVERAGE % ERROR OF PREDICTIONS	% STANDARD DEVIATION OF PREDICTIONS
Bank Angle Gust Tracking Normal Modes Only	13.35	11.23
Bank Angle Gust Tracking Normal and Failure Modes	29.89	24.22
Heading Angle Gust Tracking Normal Modes Only	48.14	16.03
Heading Angle Gust Tracking Normal and Failure Modes	54.08	29.72
Pitch Angle Gust Tracking Normal Modes Only	37.39	19.29
Pitch Angle Gust Tracking Normal and Failure Modes	31.78	26.13

FIGURE 24. STATISTICS OF PREDICTION ERRORS

CONFIGURATIONS AVERAGED	AVERAGE % ERROR OF PREDICTIONS	% RANGE OF PREDICTIONS
Bank Angle Gust Tracking Normal Modes Only	13.35	205
Bank Angle Gust Tracking Normal and Failure Modes	29.89	389
Heading Angle Gust Tracking Normal Modes Only	48.14	211
Heading Angle Gust Tracking Normal and Failure Modes	54.08	298
Pitch Angle Gust Tracking Normal Modes Only	37.39	189
Pitch Angle Gust Tracking Normal and Failure Modes	31.78	297

FIGURE 25. PREDICTION ERRORS AND PERCENT RANGE OF PREDICTIONS

IV. SPECIFICATION CRITERIA

A. OBJECTIVES OF SPECIFICATION CRITERIA

There are two principal purposes for flying qualities specifications in MIL-F-8785B: to provide a reliable guide to the acceptability of military airplanes, and to provide a standard against which airplanes can be designed. In order to evolve practical criteria, the methods of application must be considered, and compliance with any requirement must be demonstrable by analytical or experimental evaluation, preferably both. This means that such criteria must be developed around existing analysis methodologies that are readily available, easily applied, and unambiguous in outcome.

These requirements, along with sufficient data, have limited the nature of the criteria in MIL-F-8785B, and its predecessor, to considerations of numerical measures of unpiloted dynamic response which have been found to correlate well with pilot opinion. On the other hand, a great amount of research has gone into the development of techniques for analyzing the flying qualities of the pilot-airplane system through frequency domain techniques, such as multiloop analysis of pilot vehicle systems. However, the resulting methods have not lent themselves to rigidly standardized evaluation methods and numerical criteria.

The necessity of developing criteria for flying qualities in turbulence is recognized in MIL-F-8785B, although no criteria or analysis methods are presented. Furthermore, the Background Information and User's Guide for MIL-F-8785B suggests the importance of analyzing the piloted airplane. The work reported in Reference 1, and its continuation reported in Section III of this volume, make it clear that the suggestion for closed-loop analysis is not only appropriate but indispensable; good airplanes in still air can be good or bad in turbulence even at low gust levels of 5 ft/sec rms or less. Furthermore, through use of fixed-form pilot models with a standard linear representation of the airplane and its control system, an analysis method has been validated which has the following features required of a useful evaluation technology:

1. Available computer programs make the method readily available and easily used as shown in Section II and Appendix I.
2. The analysis is a completely standardized procedure.

3. The results in terms of minimum root mean square tracking error are numerical and, therefore, are unambiguous.

4. The accuracy of the prediction method has been ascertained by two moving-base simulations for a total (including the work in Reference 1) of over 1700 simulator flights of 34 configurations of Class IV airplanes flown by 5 pilots.

Thus, a natural criterion for performance of airplanes in turbulence is to specify acceptable rms tracking error in bank and pitch angle for a nominal gust level and fixed-form pilot model. The validation simulation for such a criterion includes many configurations with augmenter or control system failures which have unacceptable characteristics in turbulence. A tentative requirement based on airplanes in turbulence will be presented at the end of this section. It will be seen that the simulator results are largely independent of the pilot so that such a criterion rates the airplane and not the individual pilot.

In addition to specifying tracking accuracy, it is necessary to require pilot acceptance. For some handling qualities parameters, good performance correlates well with good pilot ratings. It is thus necessary to see whether additional kinds of criteria are necessary to guarantee an acceptable pilot rating for attitude-hold tasks in turbulence.

B. PERFORMANCE AND PILOT RATINGS

Any specification criterion evolved from the simulation must necessarily involve the pilot rating data obtained. The simulator data presented in Appendix IV in graphical and tabular form, show that the pilots agree well in terms of tracking error and have general agreement in pilot ratings. In order to obtain a better estimate of this agreement, pilot ratings of the two test pilots, JBJ and WWK, have been cross-plotted for the same airplane and control system state at approximately the same turbulence levels. Figure 26 shows the bank angle task data for which the pilot ratings correlate strongly. A count of the points reveals that 83% of the compared ratings are within ±1 rating unit. The pitch angle task pilot ratings have been cross-plotted in Figure 27. Here, 65% of the compared ratings are within ±1 rating unit. If the lower boundary is extended downwards by one-half unit, 84% of the cross-plotted ratings are encompassed.

Since ratings occur at whole and half rating units, the ±1 boundary line has been slightly expanded to include all points that lie on the boundary. The expanded boundaries do not enclose any points that were originally excluded. Multiple points are indicated by placing them adjacently but pointing away from the origin.

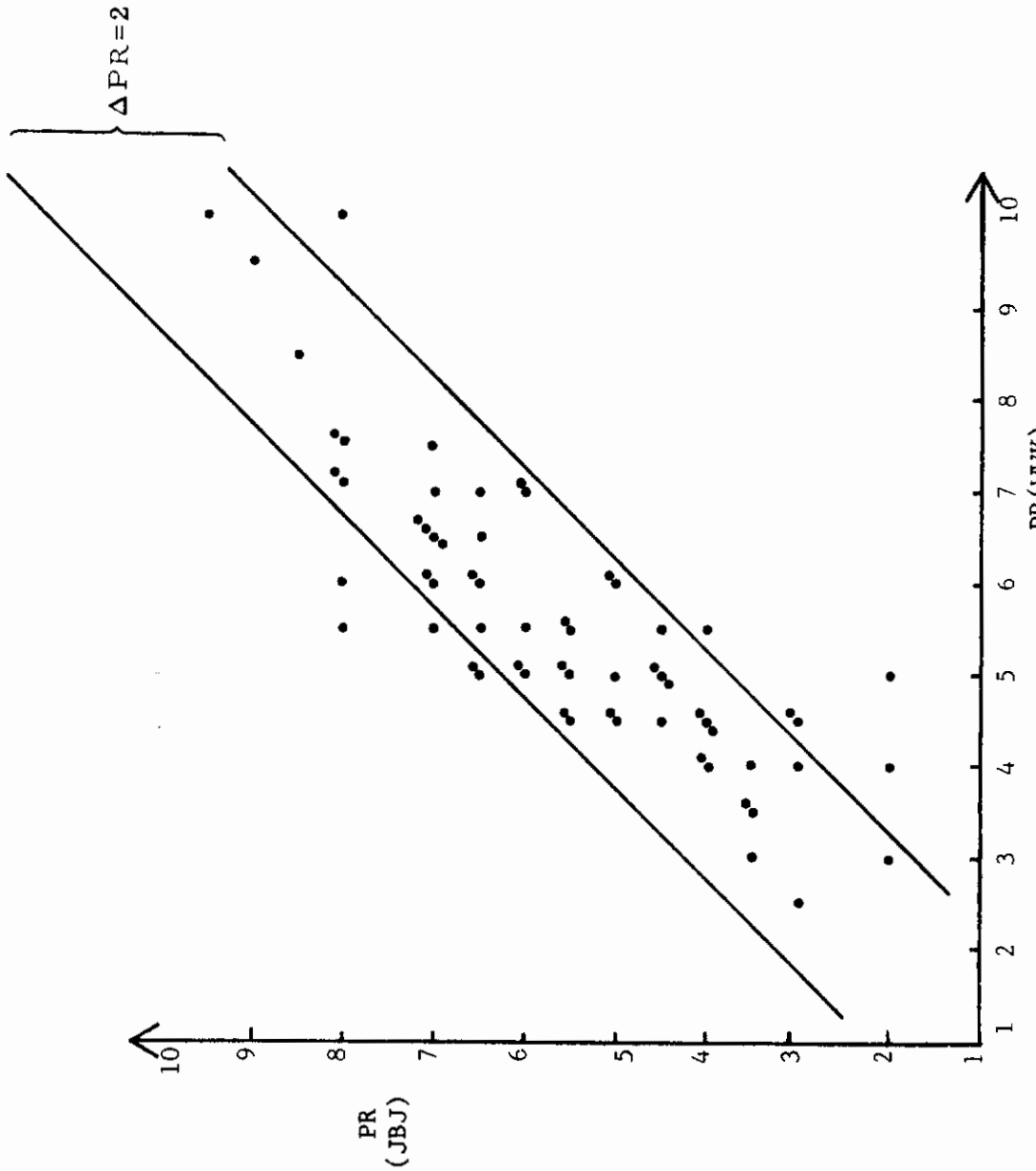

FIGURE 26. AGREEMENT BETWEEN PILOT RATINGS OF TEST PILOTS JBJ AND WWK FOR ALL F-5 AND A-7 AIRPLANES FOR THE BANK ANGLE TASK

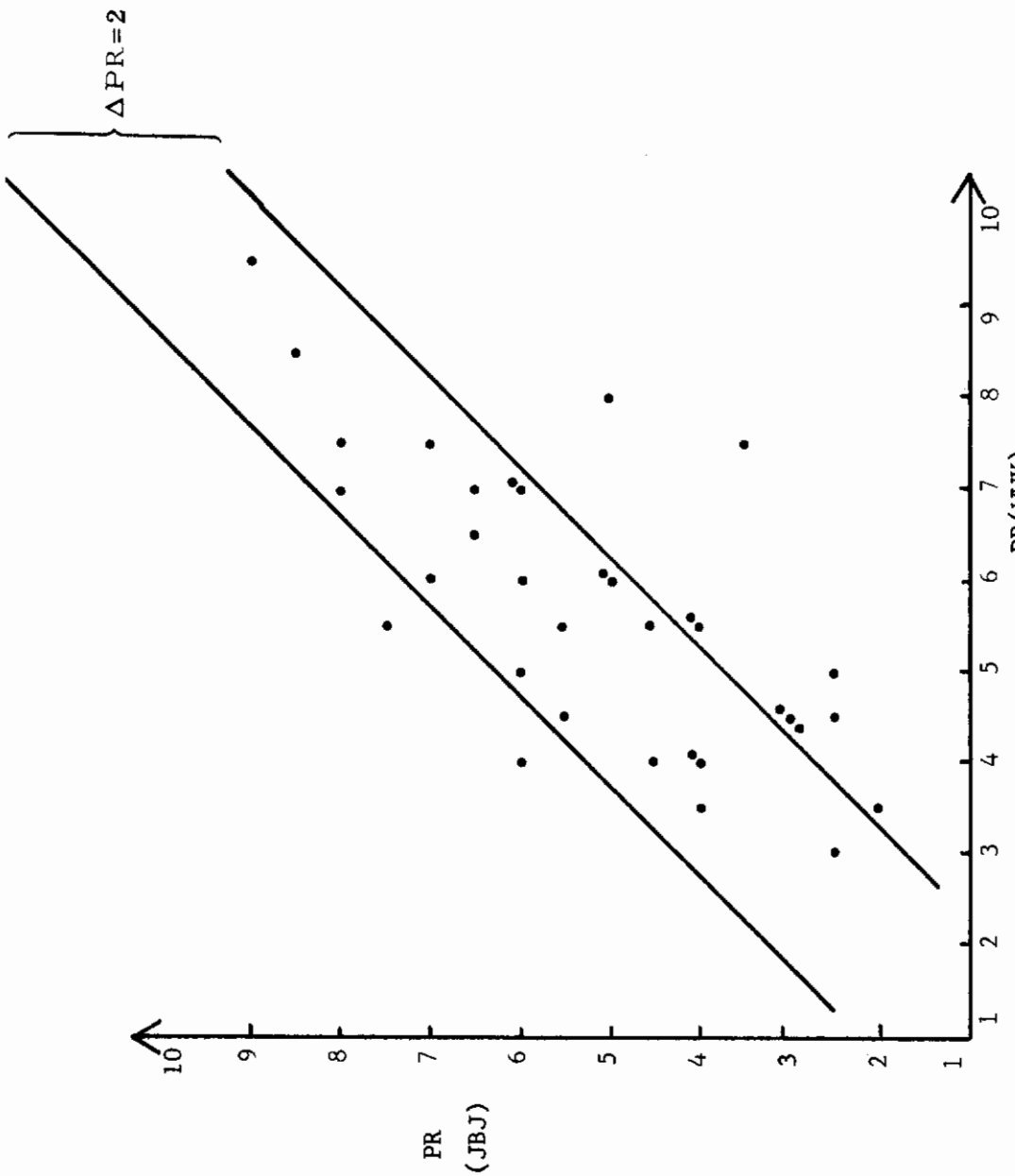

FIGURE 27. AGREEMENT BETWEEN PILOT RATINGS OF TEST PILOTS JBJ AND WWK FOR ALL F-5 AND A-7 AIRPLANES FOR THE PITCH ANGLE TASK

Similar cross-plots can be obtained from the data of Appendix IV which compare pilot JTT with JBJ and WWK. These differ slightly from Figures 26 and 27 and are not presented. Thus, it is clear that both pilot tracking error and pilot ratings are highly correlated between the three pilots. Cross-plots of the gust and still air command tracking simulation data have been made to demonstrate the independence of still air and turbulence flying characteristics. These confirm the earlier results of Figure 4 and are found in Figures 28 and 29.

C. PILOT RATINGS AND FLYING QUALITIES CRITERIA

Since an apparently natural approach to the turbulence flying qualities specification is through restricting the allowed tracking error for a given level of turbulence, it is necessary to see whether such criteria ensure acceptable pilot ratings. Figure 30 shows a graph of pilot ratings versus tracking error for the entire bank angle simulation. Although the data tend to cluster along a line approximately through the origin, the data are very scattered and exhibit a range of pilot ratings from 2 to 9 at a tracking error of 1 degree rms. If the normal mode airplanes only are plotted as in Figure 31, the scatter is nearly as bad. In pitch, a large scattering of the data is obtained for the entire pitch task simulation as shown in Figure 32, and for the normal mode cases only, Figure 33.

Since it has just been demonstrated that the pilots agree on both tracking errors and pilot ratings, this scatter reflects the diversity between the tested configurations. Nonlinear relations between tracking error and pilot rating within the data for each airplane also contribute to the scatter as will be seen next. It must be kept in mind that all of the data of the last four figures range over turbulence levels from 3 ft/sec to nearly 17 ft/sec. Restricting the gust level sharply reduces the scatter. This is the way criteria will be developed in the following sections.

D. PERFORMANCE CRITERIA

Criteria will be proposed for performance in light to moderate turbulence levels of 7 ft/sec or less. The boundaries will be based upon the normal mode F-5 and A-7 airplanes which are presumed to be Level 1 in light turbulence; at worst Level 2 in moderate turbulence of 10 ft/sec rms. Compared to many of the failure mode airplanes and T33 configurations of Reference 1, these airplanes appear to perform well. In order to see the relation between pilot ratings and tracking error for the restricted gust levels, Figures 30 through 33 have been replotted for the light to

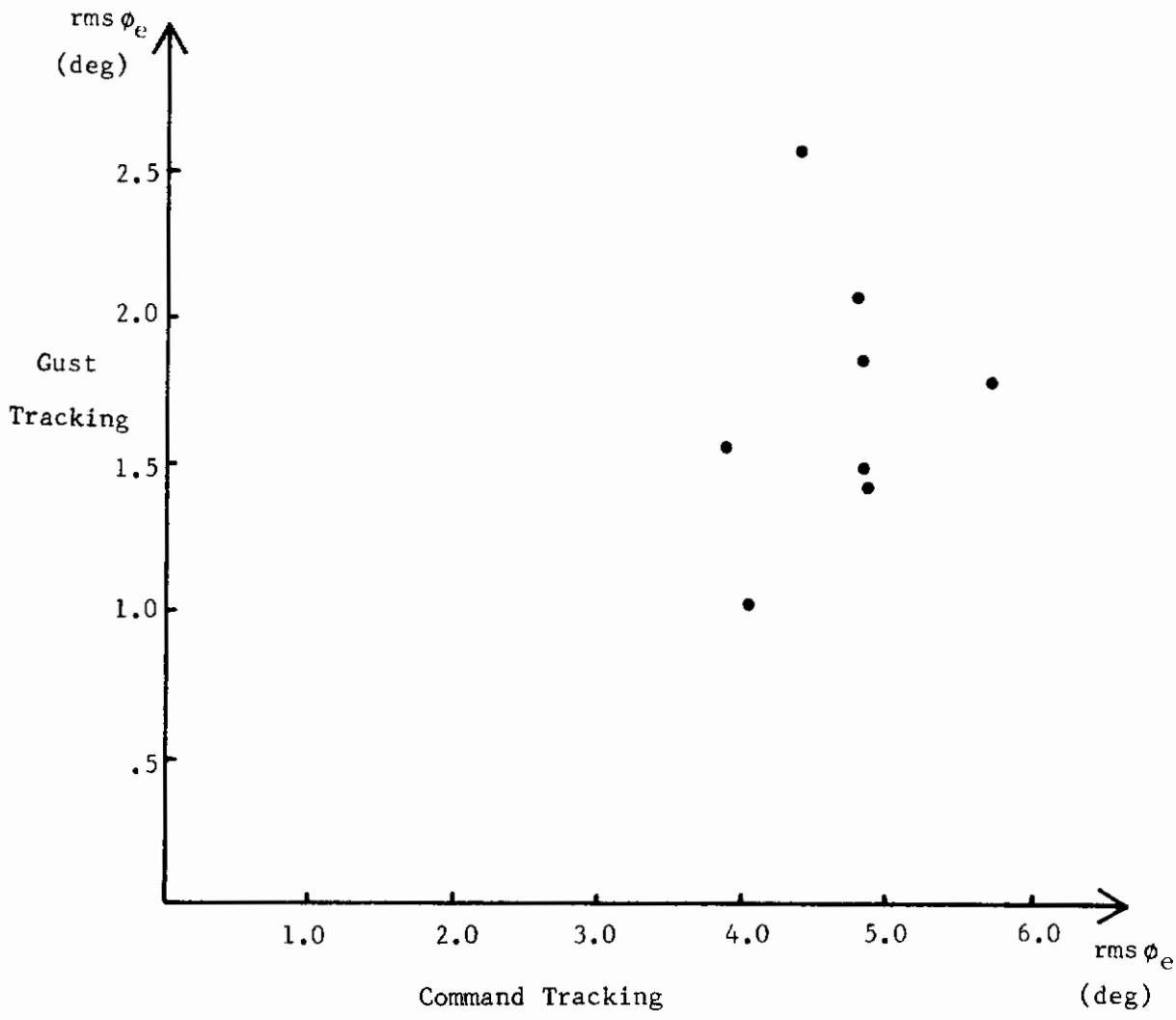

FIGURE 28. BANK ANGLE GUST TRACKING VERSUS BANK ANGLE COMMAND TRACKING FOR NORMAL MODE F-5 AND A-7

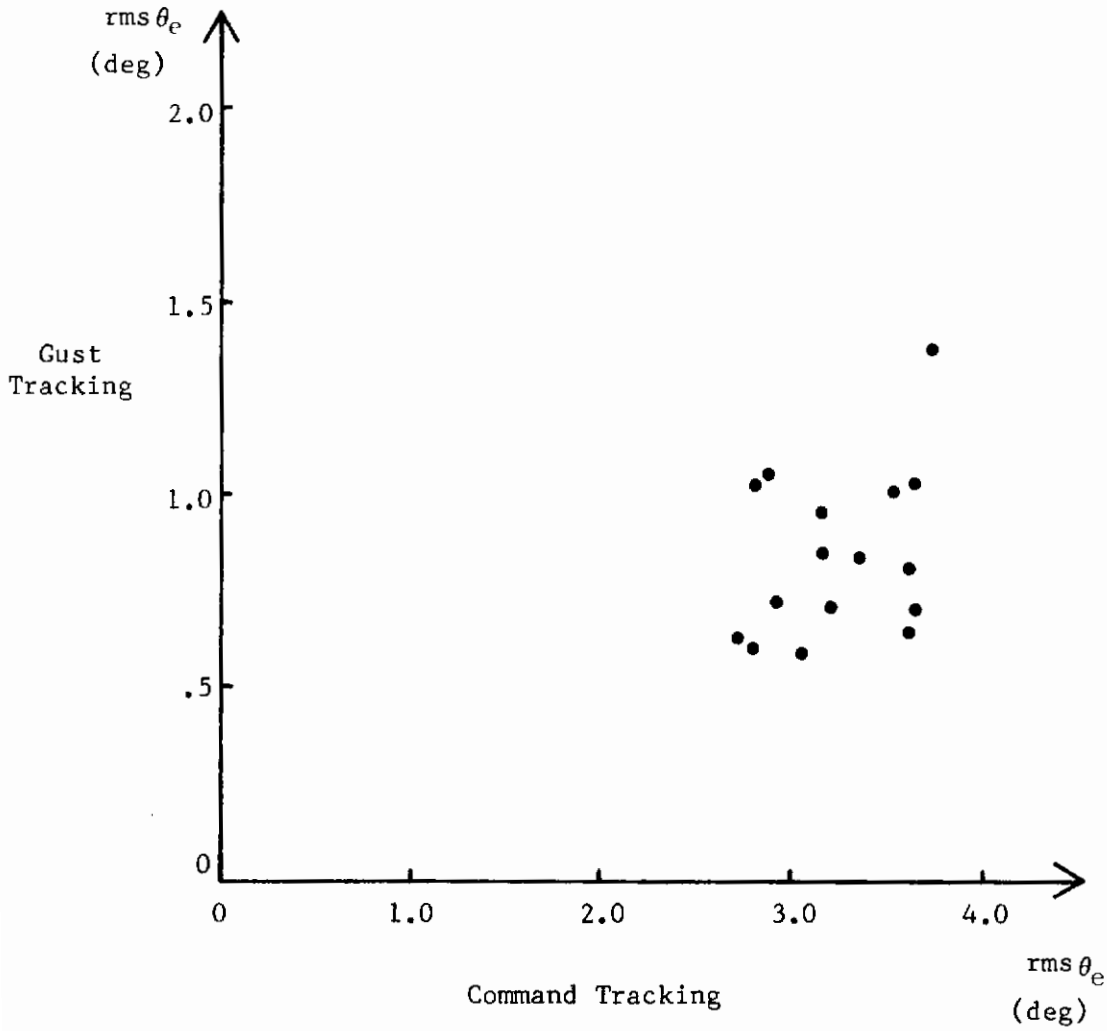

FIGURE 29. PITCH GUST TRACKING VERSUS PITCH COMMAND TRACKING FOR NORMAL AND FAILURE MODE F-5 AND A-7 AIRPLANES

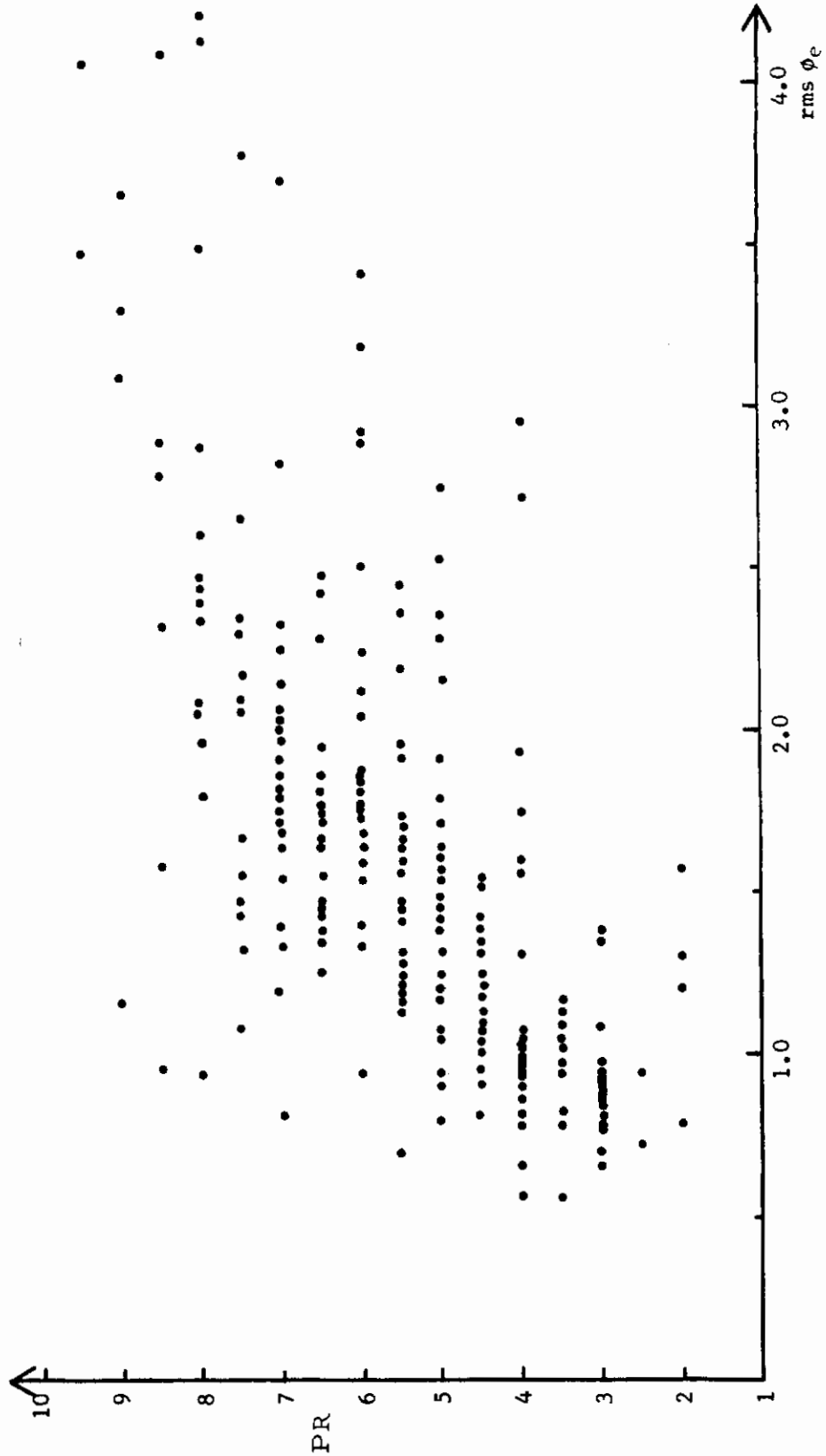

FIGURE 30. BANK ANGLE ERRORS VERSUS PILOT RATING
FOR NORMAL AND FAILURE MODE F-5 AND A-7 AIRPLANES
FOR ALL GUST LEVELS

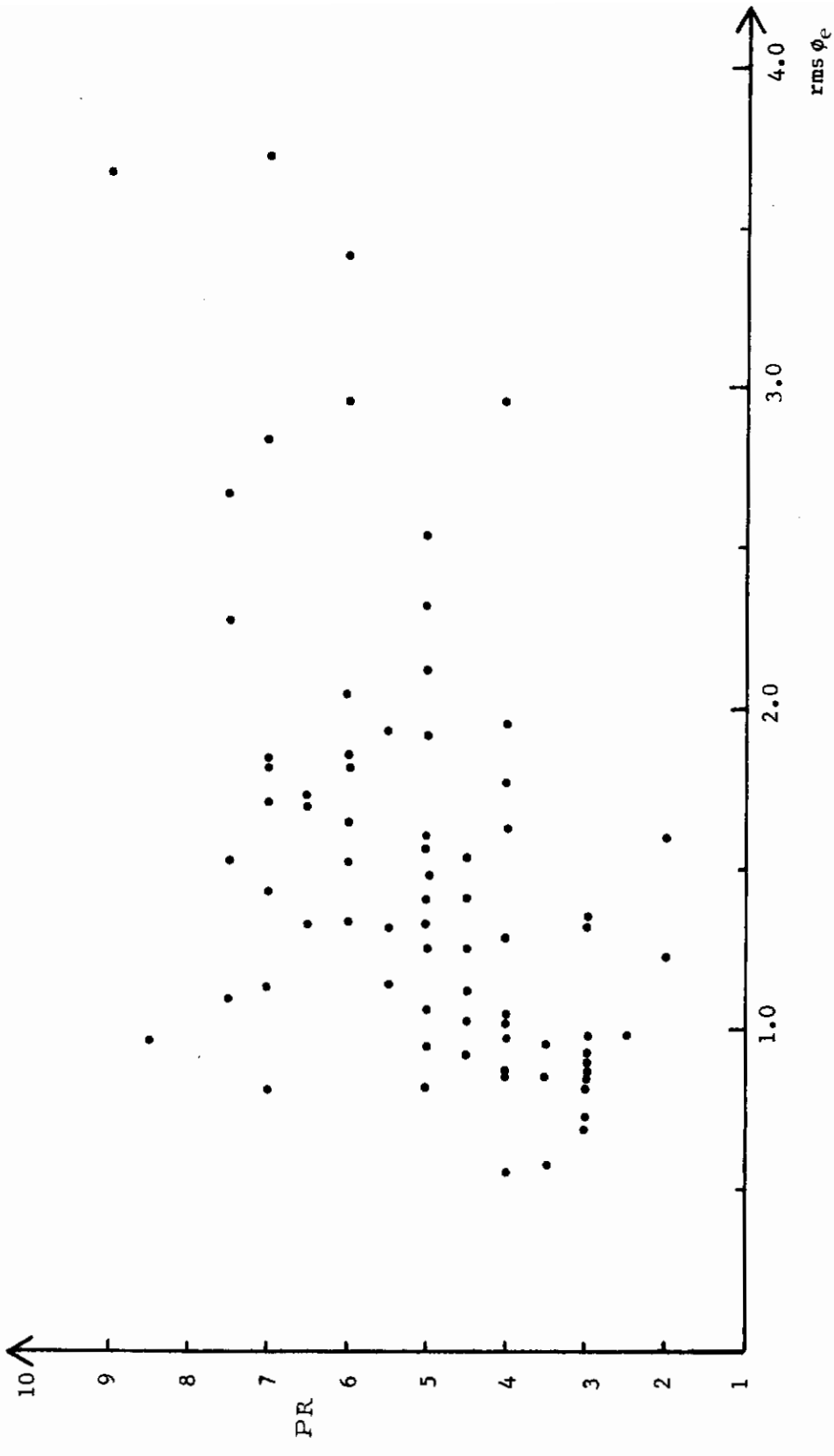

FIGURE 31. BANK ANGLE ERRORS VERSUS PILOT RATING
FOR NORMAL MODE F-5 AND A-7 AIRPLANES FOR
ALL GUST LEVELS

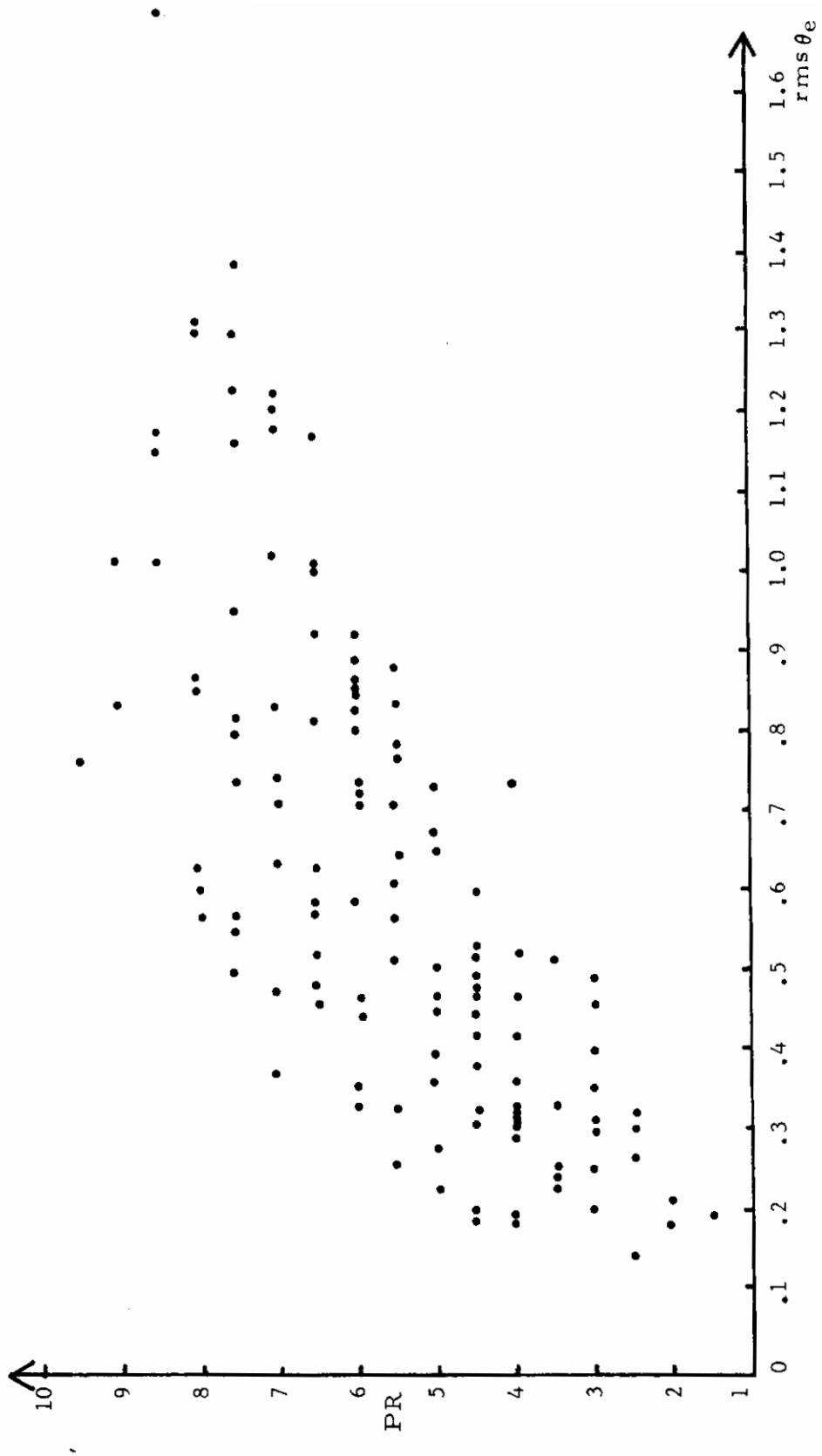

FIGURE 32. PITCH ANGLE ERROR VERSUS PILOT RATING FOR ALL F-5 AND A-7 AIRPLANES AT ALL GUST LEVELS

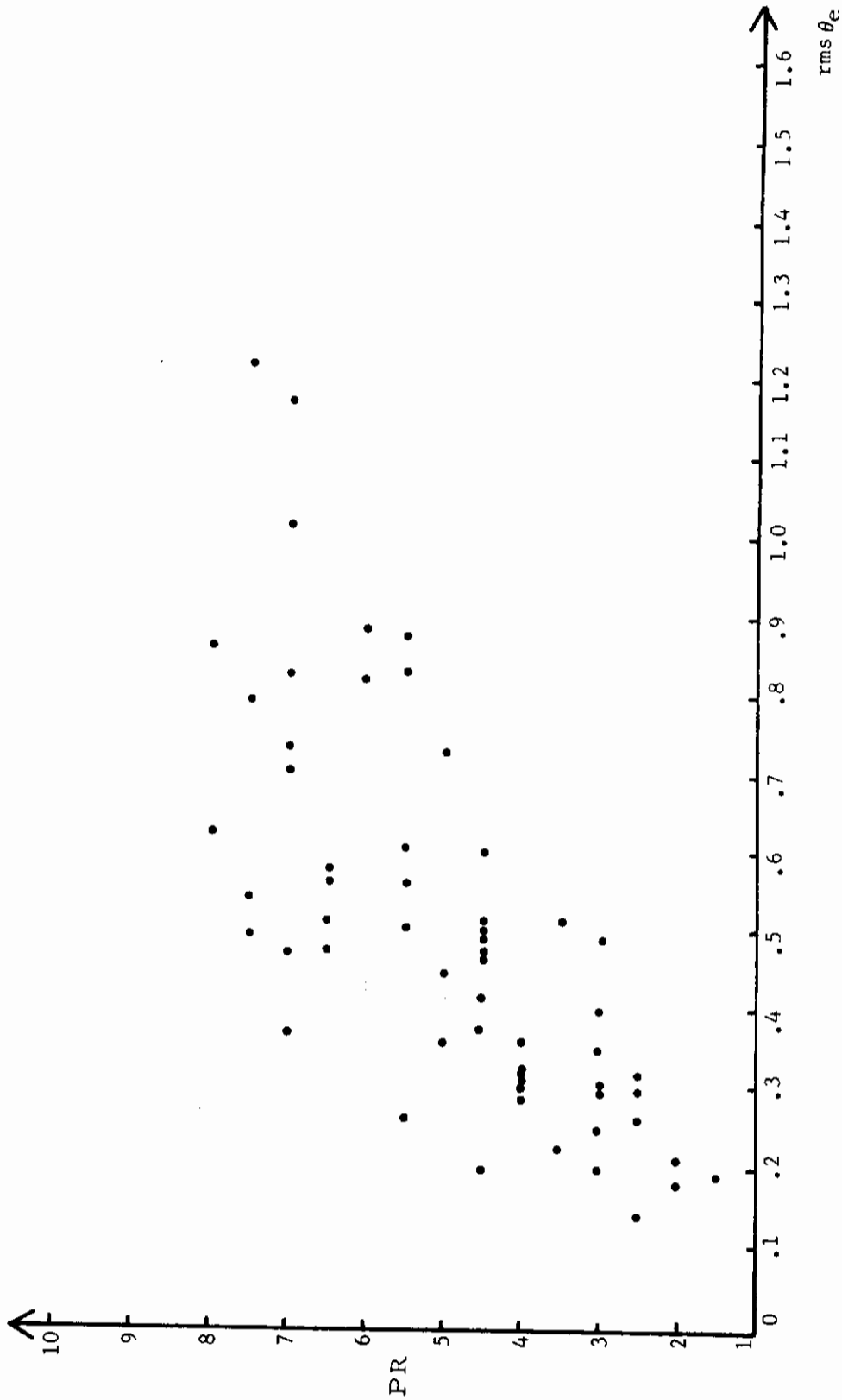

FIGURE 33. PITCH ANGLE ERRORS VERSUS PILOT RATING FOR NORMAL MODE F-5 AND A-7 AIRPLANES AT ALL GUST LEVELS

moderate turbulence flights only.

The normal mode bank angle data are shown in Figure 34. The tracking errors show an empirical boundary at 1.5 degrees, and this is proposed as a boundary for the specification. In addition, all data points lie below the rating line of 6.5. Thus, for the normal mode airplanes in light to moderate turbulence, bounded tracking performance ensures bounded pilot ratings. By taking, as working examples, the normal mode F-5 and A-7 airplane as acceptable standards in both still air and in turbulence, the pilot ratings as designated above in Figure 11 for turbulence tracking define, then, this acceptable performance, which will be referred to as Level 1 through the rest of this report. These pilot ratings are not comparable to ordinary pilot ratings for calm air evaluation, but nevertheless they reflect pilot work level and discomforture. Thus, in turbulence where the pilot must necessarily work harder than in calm air, pilot ratings greater than 3.5 can be expected for Level 1 airplanes. The key point is this: By considering gust levels of 7 ft/sec rms it is found that specifying allowable tracking errors ensures that normal mode airplanes (Level 1 airplanes in calm air) will have bounded pilot ratings; thus, a tracking error specification will also ensure pilot acceptance as defined by the normal mode F-5 and A-7 airplanes taken as representative standards.

In order to see the consequences of the boundary, Figure 35 transfers the boundary to the graph of normal and control or augmenter failure mode airplanes in 7 ft/sec rms or less turbulence. It is seen that approximately 18% of the flights were unsatisfactory with regard to the boundary. Thus, the proposed turbulence level and proposed specification boundary eliminates 16% of the worst flight while ensuring bounded pilot ratings.

The same procedure can be carried out with the pitch data. Figure 36 shows pilot rating versus pitch angle tracking error for normal mode airplanes in gust levels of less than 7 ft/sec rms. A proposed specification boundary has been drawn at .55 degrees. When both normal and failure mode data are plotted, Figure 37, the recommended boundary is seen to exclude 12% of the flights.

E. RECOMMENDED SPECIFICATION CRITERIA FOR FLYING QUALITIES IN TURBULENCE

Since the above boundaries for performance were obtained for data points deriving from simulator flight of 7 ft/sec rms turbulence or less, the data represent an average turbulence level that is less than 7 ft/sec rms (approximately 5.5 ft/sec rms). Thus, the proposed specification boundaries of Figures 32 through 35 must be

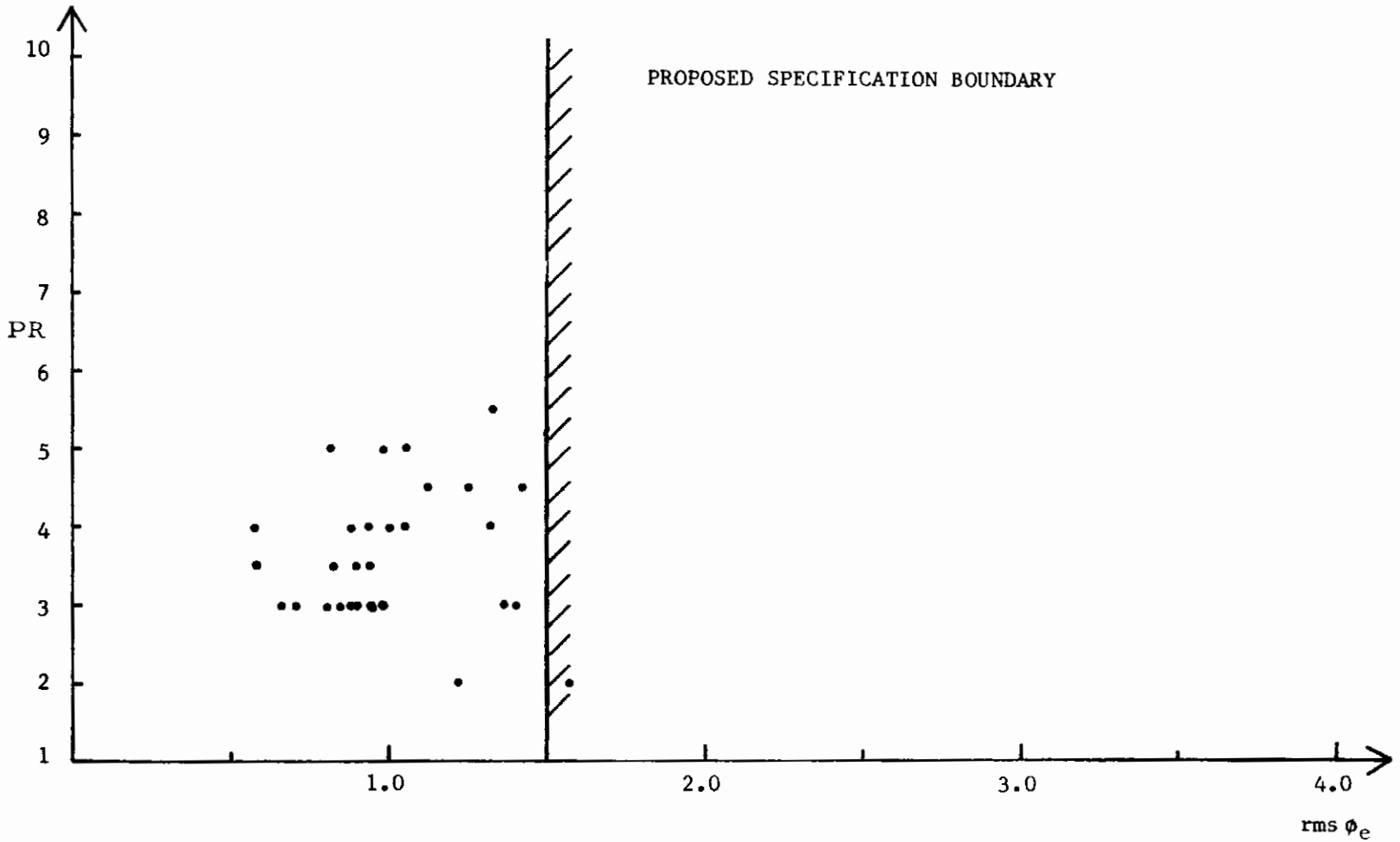

FIGURE 34. BANK ANGLE ERRORS VERSUS PILOT RATING
FOR NORMAL MODE AIRPLANES AT GUST LEVELS BELOW 7 ft/sec

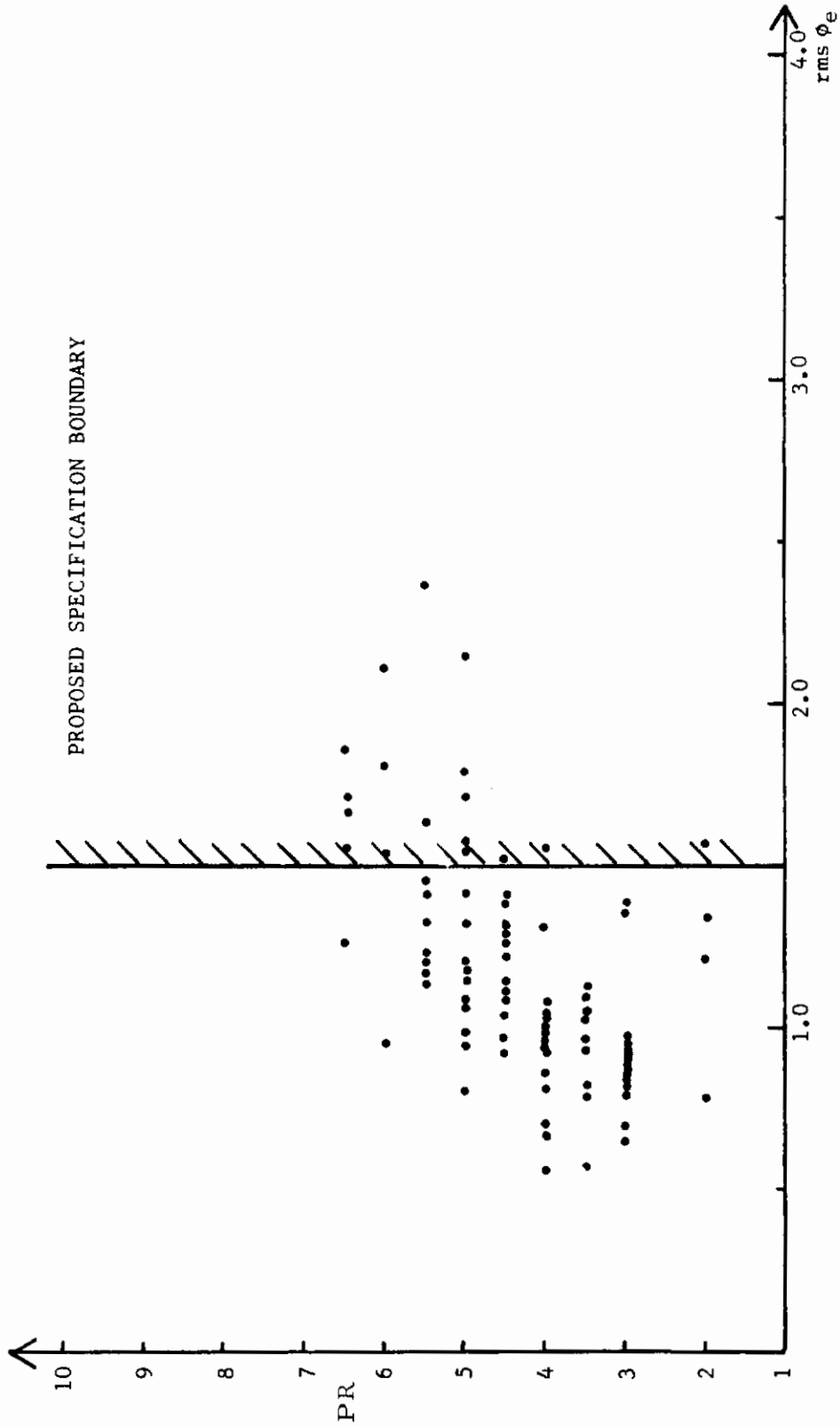

FIGURE 35. BANK ANGLE ERRORS VERSUS PILOT RATING
FOR NORMAL AND FAILURE MODE F-5 AND A-7 AIRPLANES
AT GUST LEVELS BELOW 7 ft/sec

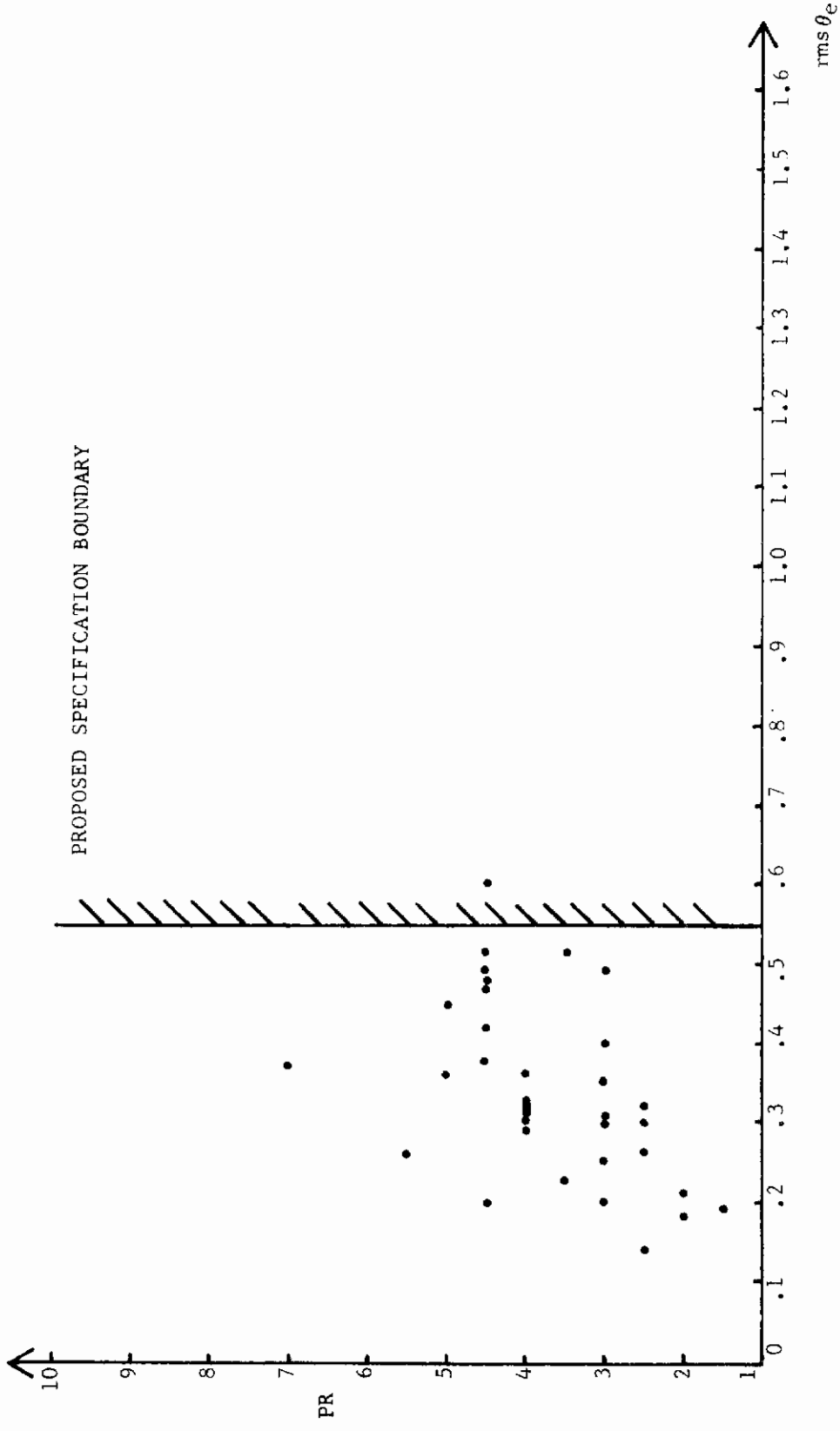

FIGURE 36. PITCH ANGLE ERROR VERSUS PILOT RATING FOR NORMAL MODE F-5 AND A-7 AIRPLANES AT GUST LEVELS LESS THAN 7 ft/sec

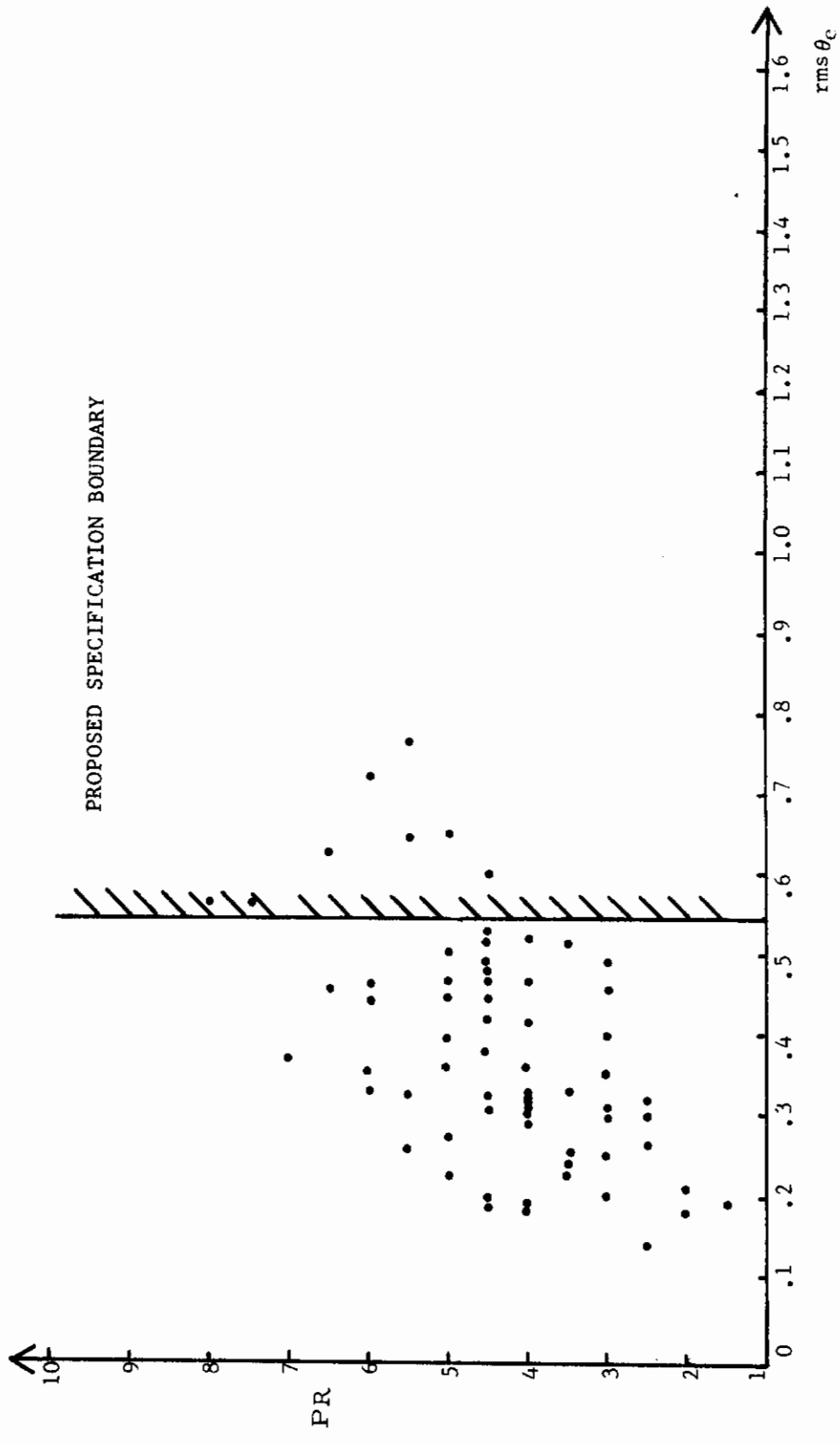

FIGURE 37. PITCH ANGLE ERROR VERSUS PILOT RATING FOR ALL F-5 AND A-7 AIRPLANES AT GUST LEVELS LESS THAN 7 ft/sec rms

multiplied by 10/5.5 in order to correspond to the prediction and to simulator data normalized to 10 ft/sec rms turbulence. This results in an acceptable rms tracking error of 2.7 degrees for bank angle tracking and 1.00 degree for pitch angle tracking. To see how these criteria separate the airplanes on the basis of normalized simulator data averages and the corresponding predictions, the simulator versus prediction graphs for the bank angle and pitch studies are reproduced with the proposed specification boundaries added. Figures 38 and 39 show the normal mode airplanes, all but one of which satisfy the criteria. Figures 40 and 41 show the normal and failure mode data, and it is apparent that the airplanes with worst tracking performance have been excluded.

The proposed specification boundary has been shown on both the simulation and on the prediction axes of these graphs. Since the normal-mode airplanes correlate well and lie within the boundary on both axes, it is reasonable to require compliance with both boundaries whenever simulator or adequate flight test data, including in-flight simulation data, are available. The requirement that the predictions satisfy the criteria ensures that the performance requirement will be met with a low work load for the pilot in terms of lead, even though testing or simulation tracking scores may be lower than the prediction as a result of pilots using greater than .5 second lead.

With these considerations in mind, the following statement is an example of the closed-loop criterion recommended for inclusion as a specification requirement in MIL-F-8785B:

3.7.5.1 Piloted Airplanes in Turbulence

This requirement is to ensure adequate pilot control of pitch and bank angle attitude during Category A missions of Class IV airplanes operating in light and moderate turbulence. Using the Dryden form gust spectra with a scale length of 1750 feet, closed-loop pilot-vehicle root mean square tracking errors for pitch and bank angle attitude hold tasks shall be computed using a turbulence prefilter represented by

$$\frac{s^2}{(s + .3)^2}$$

and the pilot model transfer functions:

bank angle $\qquad K_\phi \; \dfrac{(.5s + 1)(.09s^2 - 1.8s + 12)}{(.09s^2 + 1.8s + 12)}$

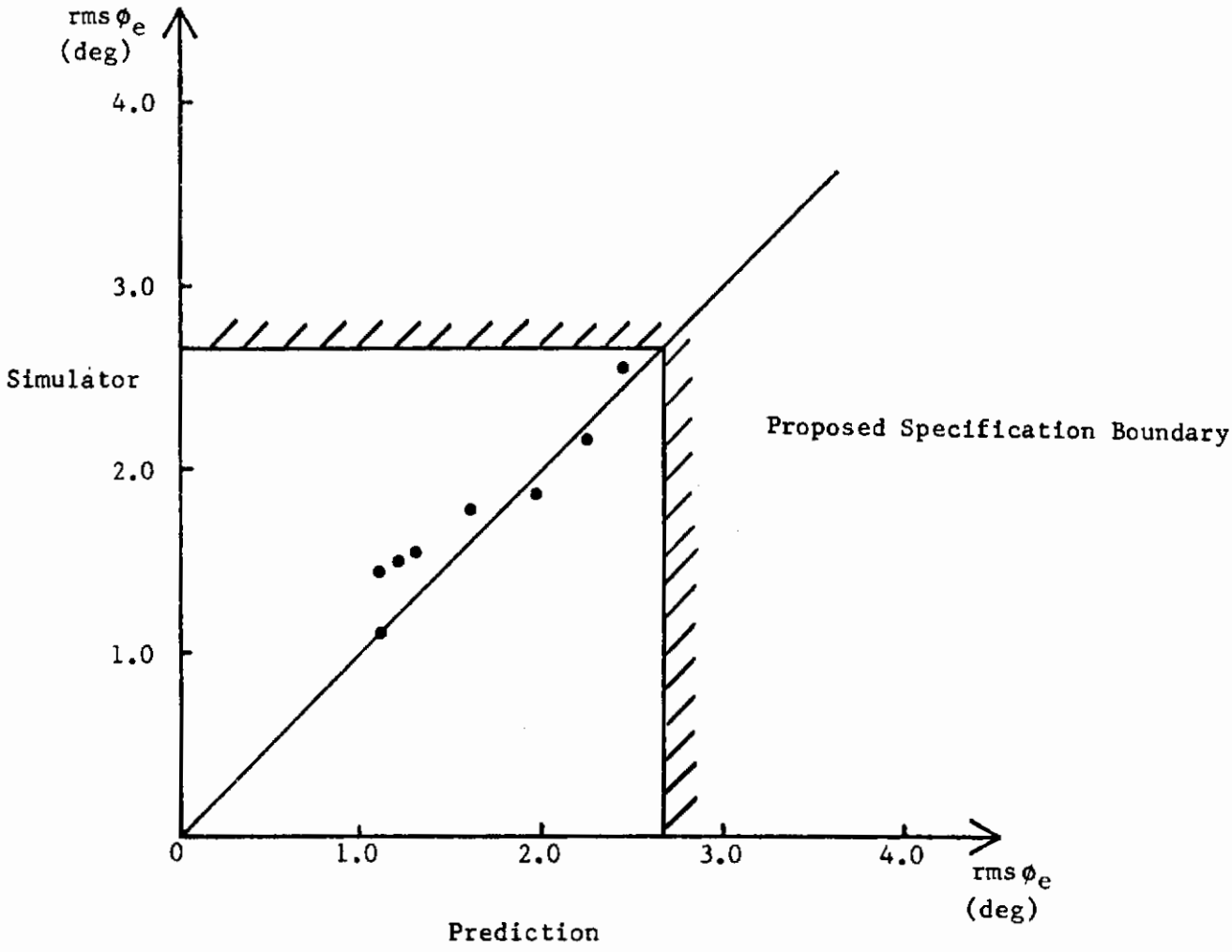

FIGURE 38. BANK ANGLE GUST TRACKING DATA FOR NORMAL MODE F-5 AND A-7 AIRPLANES SHOWING PROPOSED CRITERION

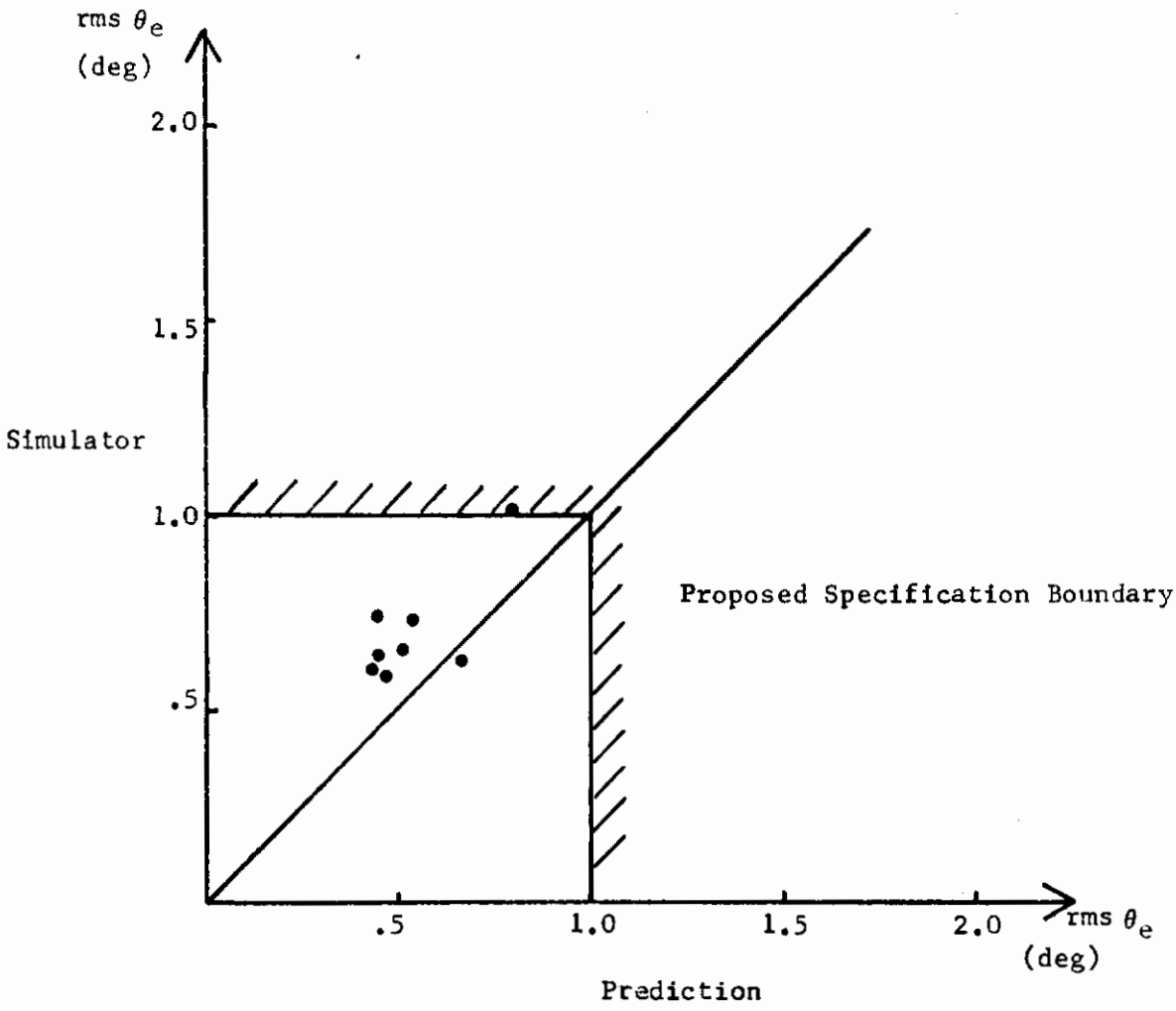

FIGURE 39. PITCH ANGLE GUST TRACKING DATA FOR NORMAL MODE F-5 AND A-7 AIRPLANES SHOWING PROPOSED CRITERION

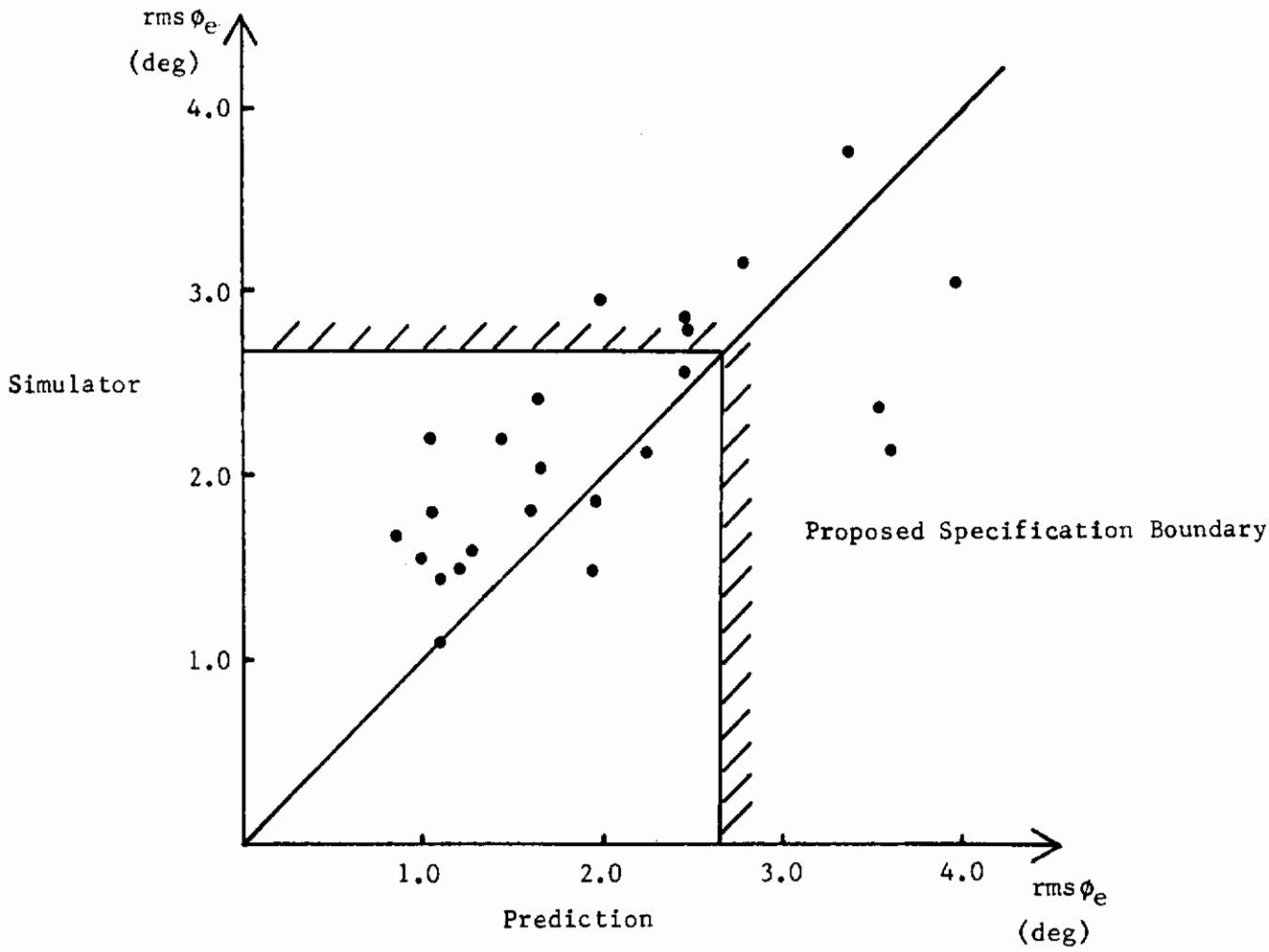

FIGURE 40. BANK ANGLE GUST TRACKING DATA FOR NORMAL AND FAILURE MODE F-5 AND A-7 AIRPLANES SHOWING PROPOSED CRITERION

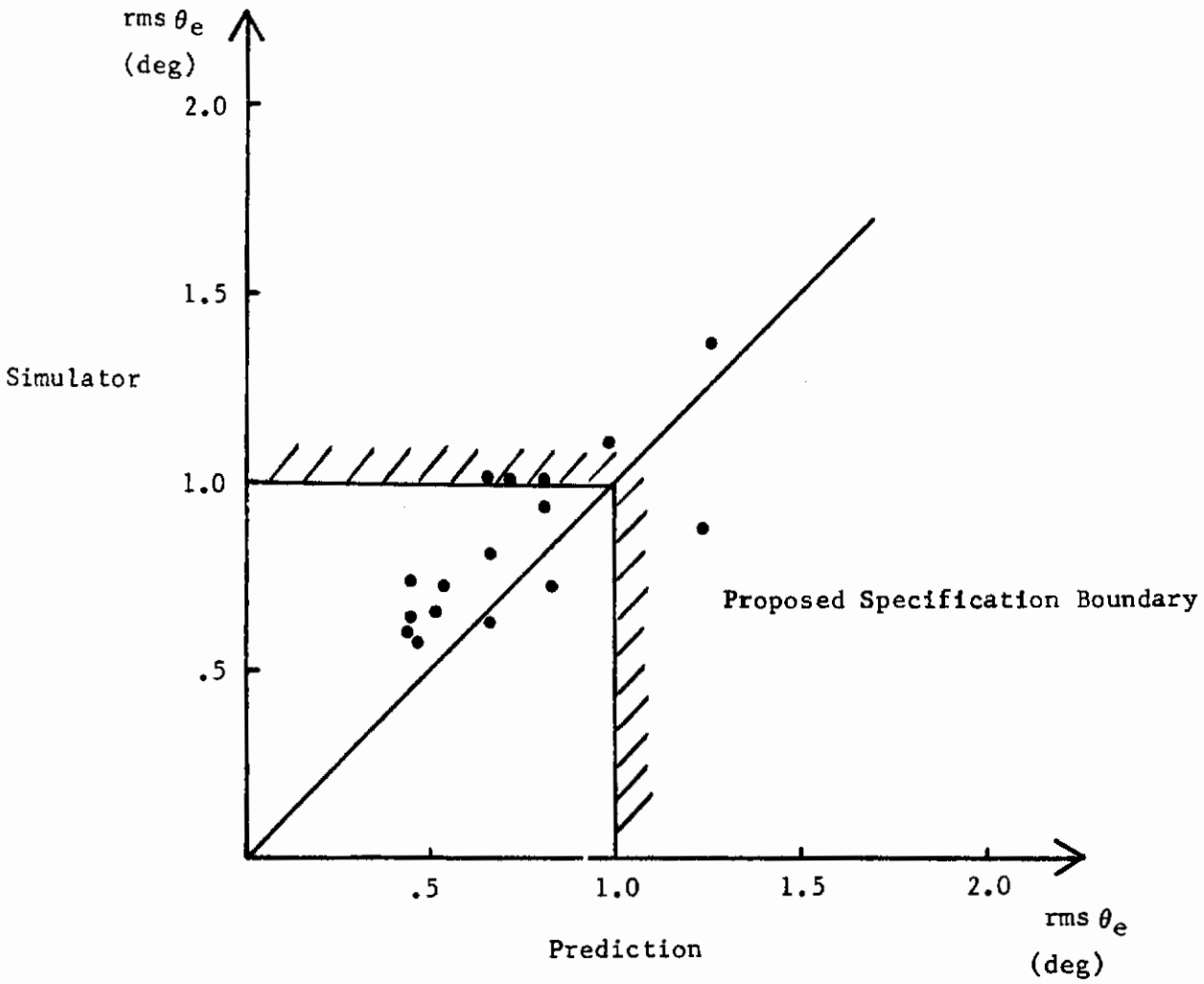

FIGURE 41. PITCH ANGLE GUST TRACKING DATA FOR NORMAL AND FAILURE MODE F-5 AND A-7 AIRPLANES SHOWING PROPOSED CRITERION

pitch angle $K_\theta \dfrac{(.5s + 1)(.2025s^2 - 2.7s + 12)}{(.2025s^2 + 2.7s + 12)}$

The airplane control and augmentation systems shall be represented by a linear representation for each flight condition over Mach .4, and the pilot model gains K_ϕ and K_θ shall be chosen to minimize the root mean square tracking error for 10 ft/sec rms turbulence incorporating v, r, w, and q gusts. Level 1 performance will then be met if the root mean square tracking errors are:

- Less than 2.7 degrees in bank angle;
- Less than 1.0 degree in pitch angle.

In addition, it is required that simulation and flight test data, when available, meet this requirement.

Although this specification is based on normal-mode airplanes that are well behaved in turbulence, there are difficulties to be overcome before it can be included in MIL-F-8785B. The assumption that the F-5 and A-7 airplanes are representative of Level 1 Class IV airplanes must be tested, and further simulation over larger parts of the flight envelop must be completed, especially at low Mach number. Once the simulator results are obtained, a program of flight testing or in-flight simulation must be carried out to verify that pilot acceptability is ensured (in the sense of Subsection D above) by tracking error requirements. With these programs completed, there would be sufficient data to assign margins and recommend final specification criteria, of the kind above, for inclusion in MIL-F-8785B.

The suitability of such criteria is established by the present program since the results of the simulator evaluation are largely independent of the pilot. A review of the simulator data conclusively demonstrates that for normal-mode airplanes, the pilots achieve very nearly the same tracking error, and that the errors scale linearly with gust level from light to heavy turbulence. The pilots reported different techniques. WWK preferred to operate as little as possible and to simply ride it out in cases where there was little promise of tracking improvement. JBJ, on the other hand, generally attempted to track tightly in all cases. In spite of these differences, the agreement in not only tracking error performance but also in pilot ratings illustrates that it is the airplanes that are being rated, not the pilots.

This, coupled with the total system performance prediction methods, completes the requirements for a specification. By avoiding the complexities of the pilot's dynamics at the stick, a simple and standardized total system model has been evolved which demonstrates strong correlation with the simulation data. The availability of the prediction method or a ready-to-operate digital program removes the main difficulties usually associated with a new methodology. The above validation analysis establishes that these prediction techniques have sufficient accuracy for use with the criteria suggested above, thus completing the program as outlined in Subsection A of Section IV.

One further matter that requires some comment is prefilters. Since the turbulence power spectra contain very low frequency energy, which is observed as mean winds during finite data taking flights, it is not possible to simulate or flight test in (unfiltered) turbulence and measure the gust levels accurately since the mean of the turbulence velocity field may not be zero. By filtering out the very low frequency components representing mean winds ($\omega < .3$ rad or a period of approximately 20 sec) a data taking period of 100 seconds becomes a sufficiently long time to obtain a reasonable average value. The simulator data reported here have been obtained from such prefiltered gust spectra and, hence, the turbulence models must include this prefilter.

V. FURTHER CONSIDERATIONS

A. FLIGHT TEST PROGRAMS

A fundamental premise underlying the entire program is that the moving-base simulation provides a suitable representation of the flying characteristics of airplanes in turbulence. Some studies have been carried out which indicate that moving-base simulators provide a reliable instrument for reproducing the subjective aspects of airplane flying qualities, but little is known about the validity of numerical measures, such as attitude hold tracking errors, in turbulence.

The difficulty in carrying out a program of flight tests to measure tracking error is almost entirely one of obtaining suitable turbulence. Even in the simulation with pure Gaussian gust distributions, it was necessary to prefilter the noise in order to remove slowly varying voltages (analogs to mean side winds) that bias the measurement of the gust intensity. Thus, close attention will have to be paid during reduction of data from flight testing to the characteristics of the record used to ensure a reasonably steady and zero-mean cross wind.

A better approach to the validation of the simulator by flight testing is through inflight simulation. Flight testing with the Total In-Flight Simulator, and programs such as reported in Reference 3, will provide useful data through the on-board generation of turbulence and turbulence effects. Since further experimentation is required before the criteria of the kind suggested in Section IV can be adopted, a flight test program should be carried out to test two assumptions:

1. The simulator and the prediction methods rank airplanes correctly in terms of tracking performance.
2. The simulator and prediction methods produce tracking errors and pilot ratings that correspond to flight test data.

Since control of the turbulence environment is essential for accurate evaluation of tracking errors per unit gust, it is recommended that a program of in-flight simulation be carried out. The task should correspond to the attitude hold task as detailed in Section III. Once an assessment of the simulation results has been made with respect to the above two items, several other extensions can be attempted. For example,

non-Gaussian turbulence models have been studied as a way of producing the patchy character of real gusts. Using such models in conjunction with in-flight simulators would be of value in assessing items 1 and 2. Another important study is to fly (and simulate) the turbulence tasks VFR rather than IFR. This will introduce some visual threshold effects and represents another step toward actual flight.

Above all, the prediction methods have worked well for the F-5 and A-7 airplanes, and the suggested criteria rest on the assumption that these airplanes are representative of Class IV airplanes. This should also be tested by both in-flight simulation and ground-based moving-base simulation. Criteria ultimately rest on the experience of many airplanes, and in this new field of research the data are still very limited.

B. RECOMMENDATIONS FOR FURTHER APPLICATIONS

There are numerous ways that the above analysis methods can be developed to provide direct applications in the study of airplane design. Weapons delivery is one area where many applications have been made at Northrop. Both turbulence and command tracking predictions have been used to correlate with simulation of weapons delivery tasks, and improved designs based on this analysis have been verified by moving-base simulation.

A somewhat different extension of the work is the inverse problem: Given one airplane with defects, how can it be improved? Owing to the complexity of the multiloop system transfer functions, improvement often means careful and simultaneous adjustment of several aerodynamic and control parameters along with the control system configuration. Thus, the likelihood of achieving the desired results by cut-and-try methods is poor. The general applicability of the methods applies over all areas of military and civilian flying where tracking tasks are being performed in turbulence. A natural application is to other classes of airplanes in other category tasks; for example, transports in landing approach under turbulent conditions. Another example is the study of large flexible airplanes.

C. LARGE FLEXIBLE AIRPLANES

An important problem of current interest is the handling and ride qualities of large flexible airplane such as the B-1 in low-altitude high-speed penetration and

landing approach. A short preliminary study of the B-1 airplane has provided some insight into this application.

The flexible airplane is represented by a set of rigid mode equations which is coupled to a set of flexibility equations. These are linear, and the gust forcing functions enter into all equations through the aerodynamic coefficient in the rigid equations and through shaping filters for the flexibility mode equations. Since the prediction programs can accept a sufficient number of equations of motion to handle this problem, some calculations can easily be carried out. The primary difficulty associated with this problem is one of representing the control and augmentation systems. The pilot models used have been simple, although it is realized that certain factors of the handling and ride qualities interface may affect the form of the models. The demonstration of the applicability of the basic prediction computation methods and the success of the Class IV validation program reported above suggests that the approach to Class IV flying qualities in turbulence analysis should apply to these Class III airplanes.

Ride qualities evaluation can also be developed from the prediction method. The assessment of the acceleration at the pilot station requires both the root mean square and the power spectrum of the acceleration. It is an easy matter to derive the acceleration to unit gust transfer function for the closed-loop pilot vehicle system. This can be used to calculate the root mean square acceleration, and the power spectrum can be algebraically obtained. Although a study of ride qualities has not been completed, the normal acceleration to gust rms calculation has been included in the longitudinal prediction program.

In short, the following areas appear to be important and promising for future research:

1. Weapons delivery under turbulent conditions.
2. The inverse problem: relating the turbulence handling qualities to the aerodynamics.
3. Large flexible airplanes in terrain-following and landing approach in turbulence.
4. Landing approach of all classes of airplanes in turbulence.
5. In-flight refueling in turbulence accounting for the response in turbulence of both airplanes.

VI. CONCLUSIONS

There were two fundamental objectives of this program: to validate the flying qualities in turbulence prediction methods developed in a previous study (Reference 1); and to evolve design specification criteria for piloted airplanes flying in turbulence. Both of these objectives have been achieved.

The research documented in this report has not only validated the results of the previous program (Reference 1), but has led to a much deeper understanding of the flying qualities of airplanes in turbulence. An experimental program using the Northrop Large Amplitude Flight Simulator studied 16 configurations of normal and failure-mode F-5 and A-7 airplanes. These were flown by three pilots, including former Navy and Air Force test pilots, for a total of 1326 flights of 100 seconds duration. Careful attention was paid to the techniques necessary to obtain faithful representations of the F-5 and A-7 airplanes and accurate measurements of the turbulence intensity, command tracking signal intensity, and tracking error.

This resulted in data which demonstrate several features of the pilot that have not previously been fully realized. For almost all configurations the pilots not only achieved similar tracking errors at similar gust levels, but also agreed closely in pilot ratings for the turbulence tasks. In addition, the tracking error scaled linearly with the gust level from light to heavy so that most of the data appear clustered about a line through the origin on a graph of tracking error versus turbulence level. Thus, the consistency of the tracking error performance, pilot ratings, and linear scaling of tracking error with gust level is one of the major demonstrations of this program. Since these data will undoubtedly yield more information than has been treated in this study, they have been reported in their entirety in numerical form (Appendix IV).

The specific achievements of this program are summarized in the following paragraphs.

A. VALIDATION OF THE PREDICTION METHOD

There were three attitude-hold tasks in turbulence, bank angle, heading angle, and pitch angle. The Dryden turbulence models included v, w, and the correlated r

and q gusts, and fixed-form pilot models were used in a linear pilot-vehicle system from which root mean square tracking errors were calculated. A statistical analysis of the prediction and simulator data has been included (Figures 172 and 173) that shows the method to have an average error of 13% over a range of predicted bank angle error of 205% for normal-mode airplanes. In pitch, the average error is 32% over a range of 297% for all airplanes. The study in heading shows that the prediction method can be usually applied to this multiloop task description. These results are, therefore, much more accurate than open-loop estimates and provide a reliable way to analytically assess the performance of the piloted airplane in turbulence. Moreover, the theoretical graphs of tracking error versus pilot model gain and of tracking error versus pilot model lead yield valuable information about the dynamic characteristics of the pilot-vehicle system. Furthermore, the prediction method consists of a standardized procedure that can be easily carried out using the computer programs developed during this effort. A User's Guide is contained in Appendix I, and the program is available on request from the United States Air Force. These new programs are considerably more general than the one reported in Reference 1, and include both lateral and longitudinal dynamics. The equations of the aircraft dynamics are furnished by the user.

B. SPECIFICATION CRITERIA

The availability of a validated analysis method for evaluating performance in turbulence makes it possible to develop specification criteria. Using the F-5 and A-7 airplanes as representative of acceptable airplanes in normal-mode operation, criteria were developed for both bank angle and pitch angle performance in light to moderate turbulence. An example of a paragraph for inclusion in MIL-F-8785B has been given to illustrate the precise form that turbulence flying qualities criteria can take when based on the validated prediction method.

C. APPLICATION TO AIRPLANE DESIGN AND EVALUATION

Although assessment of an airplane design against a criterion is one important use for the prediction method, in practice the techniques are valuable in ranking competitive designs with respect to tracking performance. Since a superposition principle applies to the pilot-vehicle system, it is possible to evaluate many precision tasks in turbulence. Examples studied at Northrop, in conjunction with several development programs (including the Northrop A-9 airplane), have shown that the best

aerodynamic or control design for still air may not be the best for low-level turbulence. Since the actual mission will likely encounter low-level turbulence, it is, therefore, useful to design about a nominal gust level. In this way, the flying quality prediction methods provide a powerful and accurate guide to the tradeoff analysis of still air and turbulence condition designs.

D. FINAL REMARKS

This program has led to both validated flying qualities prediction methods and specification criteria for Class IV airplanes flying in turbulence. The accuracy of the method has been shown for both qualitative and quantitative characteristics, and the human pilot demonstrates unexpected reliability as a linear operator for both single and multiloop turbulence tracking tasks.

The success of these methods for Category A operation of Class IV airplanes suggests applications to other tasks in different categories and for other classes of airplanes. A preliminary study of a large flexible airplane has been partially carried out and indicates that the prediction techniques apply. Other promising and important continuations of this research have been suggested in Section V, and it is hoped that the achievements of this program will stimulate further effort in these directions.

REFERENCES

1. Onstott, E. D., and Salmon, E. P., Airplane Flying Qualities in Turbulence, AFFDL-TR-70-143, Air Force Flight Dynamics Laboratory, Wright-Patterson Air Force Base, Ohio, February 1971.
2. Chalk, C. R., et al, Background Information and User's Guide for MIL-F 8785B (ASG), Military Specification - Flying Qualities of Piloted Airplane, AFFDL-TR-69-72, Air Force Flight Dynamics Laboratory, Wright-Patterson Air Force Base, Ohio, August 1969.
3. Franklin, James A., Turbulence and Lateral-Directional Flying Qualities, NASA-CR-1718, April 1971.
4. Parrag, Michael L., Pilot Evaluations in a Ground Simulator of the Effects of Elevator Control System Dynamics in Fighter Aircraft, AFFDL-TR-67-19, Air Force Flight Dynamics Laboratory, Wright-Patterson Air Force Base, Ohio, September 1969.

BIBLIOGRAPHY

Anderson, R. O., "A New Approach to the Specification and Evaluation of Flying Qualities," AFFDL-TR-69-120, Air Force Flight Dynamics Laboratory, Wright-Patterson Air Force Base, Ohio, June 1970.

Baron, J., et al, "Application of Optimal Control Theory to the Prediction of Human Performance in a Complex Task," AFFDL-TR-69-81, March 1970.

Dillow, James D., "The Paper Pilot - A Digitial Computer Program to Predict Pilot Rating for the Hover Task," FDCC TM-69-3, December 1969 (to be published as AFFDL-TR-70-40).

Durand, T. S., "Carrier Landing Analysis," STI-TR-137-2, February 1967.

Franklin, James A., "Influence of Turbulence on Lateral-Directional Flying Qualities," AIAA Paper No. 70-998, August 1970.

Heifferon, J. C., and Hannen, R. A., "The Effects of Changes in Input Power Spectra on Human Operator Compensatory Tracking," Proceedings of the Sixth Annual Conference on Manual Control, Air Force Institute of Technology, Wright-Patterson Air Force Base, Ohio, April 1970.

Kensinger, J. T., "A Method to Determine the Allowable Error of a Sensor Used to Display Angle of Attack," AFIT, GE/EE/68-9, Air Force Institute of Technology, March 1968.

Laning, J. H., and Battin, R. H., "Random Processes in Automatic Control," McGraw-Hill, New York, 1956.

McDonnell, John D., "Pilot Rating Techniques for the Estimation and Evaluation of Handling Qualities," Systems Technology, Inc., AFFDL-TR-68-76, December 1968.

McRuer, D. T., "Analysis of Multiloop Vehicular Control Systems," Systems Technology, Inc., ASD-TDR-62-1014, Aeronautical Systems Division, Wright-Patterson Air Force Base, Ohio, March 1964.

McRuer, D. T., et al, "Human Pilot Dynamics in Compensatory Systems," Systems Technology, Inc., AFFDL-TR-65-15, July 1965.

McRuer, D. T., et al, "New Approaches to Human Pilot Vehicle Dynamic Analysis," Systems Technology, Inc., AFFDL-TR-67-150, February 1968.

Meeker, J. I., "Evaluation of Lateral-Directional Handling Qualities of Piloted Re-entry Vehicles Using Fixed-Base and Inflight Evaluation," Cornell Aeronautical Laboratory, Inc., NASA CR-778, May 1967.

Skelton, Grant B., "Investigation of the Effects of Gusts on V/STOL Craft in Transition and Hover," Honeywell, Inc., AFFDL-TR-68-85, October 1968.

Stapelford, R. L., et al, "Experiments and a Model for Pilot Dynamics with Wind and Motion Inputs," Systems Technology, Inc., NASA CR-1325, May 1969.

Tsu, C. N., "A Note About the Effects of Product of Inertia in Lateral Stability," J. Institute of Aeronautical Sciences, Volume 21, No. 7, July 1954.

APPENDIX I

GUIDE TO THE EXTENDED LATERAL AND LONGITUDINAL TURBULENCE PREDICTION PROGRAMS

APPENDIX I

GUIDE TO THE EXTENDED LATERAL AND LONGITUDINAL TURBULENCE PREDICTION PROGRAMS

INTRODUCTION

The methodology documented in this report requires the calculation of closed-loop pilot-vehicle performance. The use of conventional transfer functions for computing pilot-vehicle performance is advantageous from the point of view of the information available from a knowledge of pole-zero locations. Hence, rms performance has been calculated from closed-loop transfer functions. Multiloop analysis techniques allow a systematic development of the required transfer functions from polynomials which are intuitively related to system performance. Unfortunately, the technique is time-consuming; therefore, digital computer programs have been developed to calculate closed-loop pilot-vehicle transfer functions and to generate the rms performance.

Three digital computer programs are documented in this appendix. The programs provide:

1. Lateral command tracking response;
2. Lateral gust response;
3. Longitudinal gust and command tracking response.

The formulation of these three programs has been kept as modular as possible so that the interested user may reformulate the logic to suit his particular needs. In fact, all three programs use a common subroutine package. The elements of the subroutine package will be detailed, following which instructions will be given for use of the Lateral Command Tracking Program, the Lateral Gust Response Program and, finally, the Longitudinal Program.

SUBROUTINES

This collection of subroutines contains 13 programs designed to aid in handling polynomials. Those which could be of use for general operations are described in detail; those subroutines peculiar to the digital programs of this effort are merely summarized.

TPREF (AK, LPN, AL, LPD). This subroutine multiplies the command tracking filter by $\frac{S^2}{(S+.3)^2}$. The resulting transfer function is then scaled to give a command of 10° rms and is returned to the main program as the command tracking filter. The elements of the argument are:

AK — linear array of the coefficients of the numerator polynomial of the command tracking filter, starting with the coefficient of the highest power of s, $[\,AK(1)S^n + AK(2)S^{n-1} + - - - - - + AK(n+1)S^0\,]$.

LPN — number of coefficients in AK.

AL — coefficients of the denominator polynomial of the command tracking filter, starting with the coefficient of the highest power of s.

LPD — number of coefficients in AL.

AK and AL are effectively limited to ten elements.

PREF (AM, LGN, AN, LGD, UO). This subroutine multiplies the gust filter by $\frac{s^2}{(s+.3)^2}$. The resulting transfer function is then scaled to give turbulence of 10 ft/sec rms, and is returned to the main program as the gust filter. The elements of the argument are:

AM — linear array of the coefficients of the numerator polynomial of the gust filter, starting with the coefficient of the highest power of s.

LGN — number of coefficients of AM.

AN — coefficients of the denominator polynomial of the gust filter, starting with the coefficient of the highest power of s.

LGD — number of coefficients of AN.

UO — velocity of the vehicle.

AM and AN are effectively limited to nine elements.

NUM (A, B1, Bs . . . . .). This subroutine is unique to the Longitudinal Program. It is designed to formulate the numerator polynomials of the closed-loop longitudinal transfer function. The input arguments consist of pilot model transfer functions and N-symbols required for the particular numerator.

NSYM (NCA1, NCB1, NCA2, NCB2, DDET, ND). This subroutine calculates the N-symbols required for use of the multiloop analysis technique. The logic of the pro-

gram can be most easily understood by starting with the matrix description of the aircraft equations of motion below:

$$[A]\ [X] = [B]\ [S]$$

A is the matrix of the coefficients of the unknown of the selected equation of motion. For example, in the typical three degree-of-freedom lateral equation, A would contain the coefficient of ϕ, r, and β (see page 262). Thus, the elements of the matrix A would be polynomial in s. Similarly, B gives the coefficients of the control deflection or turbulence inputs. NSYM will replace one or two columns of A by columns of B and calculate the characteristic polynomial of the resulting matrix. This polynomial is simply an N-symbol of the multiloop analysis transfer function.

The elements of the argument of NSYM are defined below:

NCA1 — integer giving the first column of A to be replaced

NCB1 — the column of B to replace NCA1

NCA2 — the second column of A to be replaced

NCB2 — the column of B to replace NCB2

DDET — linear array of the coefficients of the resulting characteristic polynomial, starting with the highest power of s

ND — the number of coefficients in DDET.

If no columns are to be replaced, set the appropriate argument elements to zero.

The user should note that the polynomial elements of the A and B matrices are calculated in the main routine of the supplied programs for a particular set of equations of motion. Thus, only stability derivatives need be input. However, the areas in the program where A and B are defined can be easily discerned, and the user may change the equations to meet his own purposes (i.e., additional terms, change of axis systems, etc.). The elements of A and B are limited to third order polynomials of the form:

$$A(1, I, J)\, S^3 + - - - - + A(4, I, J)$$

I row

J column

The size of A is limited to 16 x 16 of these polynomial elements and the size of B to 16 x 5. If NSYM is used in other programs, the user must include the common block:

COMMON A, B, N

where N is the size of A.

LMPY (A1, A2, A3 . . . . .). This subroutine is unique to the Longitudinal Program. It is designed to multiply seven polynomials together. The argument of the program consists of linear arrays of the coefficients of the seven input polynomials plus the resulting product and the number of coefficients in each polynomial. The size of any polynomial is limited to 30 coefficients.

RMS (X, Y, N1, N2, H). This subroutine will calculate the rms response of a transfer function to a white noise input. It performs checks to determine whether the input function is stable. If the transfer function is unstable, a zero value of the rms is returned. The elements of the argument are defined below:

X - a linear array of the coefficients of the numerator polynomial of the transfer function, starting with the highest power of s

Y — the coefficients of the denominator polynomial of the transfer function, starting with the highest power of s

N1 — the number of coefficients in the numerator

N2 — the number of coefficients in the denominator

H — the rms response to white noise.

INV (C, N, DET). This subroutine calculates the determinant of an arithmetic matrix. The elements of the argument are defined below:

C — an n x n array of the input matrix elements

N — the size of C

DET — the determinant of C that is calculated.

EQUATE (AA, N, BB). This subroutine will equate two arithmetic matrices. The elements of the argument are described below:

AA — a square array of the elements of the input matrix

N — the size of AA

BB — a square array of the elements of the output matrix which the program equates to AA.

ADD (A, B, C, N, M, MAX). This subroutine will add two polynomials and return the sum. The elements of the argument are defined below:

A — a linear array of the coefficients of one input polynomial, starting with the highest power of s

B — the coefficients of the second input polynomial

C — the polynomial sum of A + B, starting with the coefficient of the highest power of s in the first storage location

N — the number of coefficients of A

M — the number of coefficients of B

MAX — the number of coefficients of C.

MPY (A, B, C, N, M, L). This subroutine will multiply two polynomials and return the product. The elements of the argument are described below:

A — a linear array of the coefficients of one input polynomial, starting with the highest power of s

B — the coefficients of the second input polynomial

C — the polynomial product of A x B, starting with the coefficeint of the highest power of s in the first storage location

N — the number of coefficients in A

M — the number of coefficients in B

L — the number of coefficients in C.

MULR (A, N1, X, Y). This subroutine is designed to call a root-finding routine and,thus,return the roots of the polynomial. By calling the root-finder from this subroutine, it is possible for the user to easily substitute a root-finder from his own library without changing the main program. The elements of the argument are defined below:

A — a linear array of the coefficients of the polynomial to be factored, starting with the highest power of s

N1 — the order of A

X — a linear array of the real parts of the roots of A

Y — a linear array of the corresponding imaginary parts of the roots of A.

MMPY (A1, A2 . . . . .). This subroutine is unique to the Lateral Program. It is designed to multiply eight polynomials together and return the product.

POLRT (XCOF . . . . .). This subroutine factors a polynomial. It is called by the subroutine MULR and may be replaced by the user's own root-finding routine.

LONGITUDINAL PROGRAM

A block diagram of the longitudinal pilot-vehicle system is depicted in Figure 42, and a flow chart of the digital computer program to calculate closed-loop pilot-vehicle performance is shown in Figure 43. The input format for the digital computer program is given in Figure 44.

The longitudinal airframe and control system equations of motion are presented in this subsection of Appendix I. These equations are written in a wind-axis system in which the X-axis always points into the relative wind and the lift and drag forces always lie along the Z- and X-axes. Small angle assumptions are made and a level-flight initial condition is chosen. Provision is made for pitch rate feedback, both with and without washout, and for fuselage bending.

It should be noted that while wind axis equations of motion are used in the longitudinal program, body axis equations are used in the lateral program. This was done to match the mechanization of the man-in-the-loop simulation which had been designed to minimize the use of computing equipment. The interested reader may consult Reference 4 for a more complete discussion of this type of mechanization. However, the equation of motion may be readily changed as explained in the discussion of the subroutine NSYM.

Also presented are the transfer functions for the loop closures shown in the block diagram of Figure 42. Pilot transfer functions may be entered into the program as ratios of polynomials.

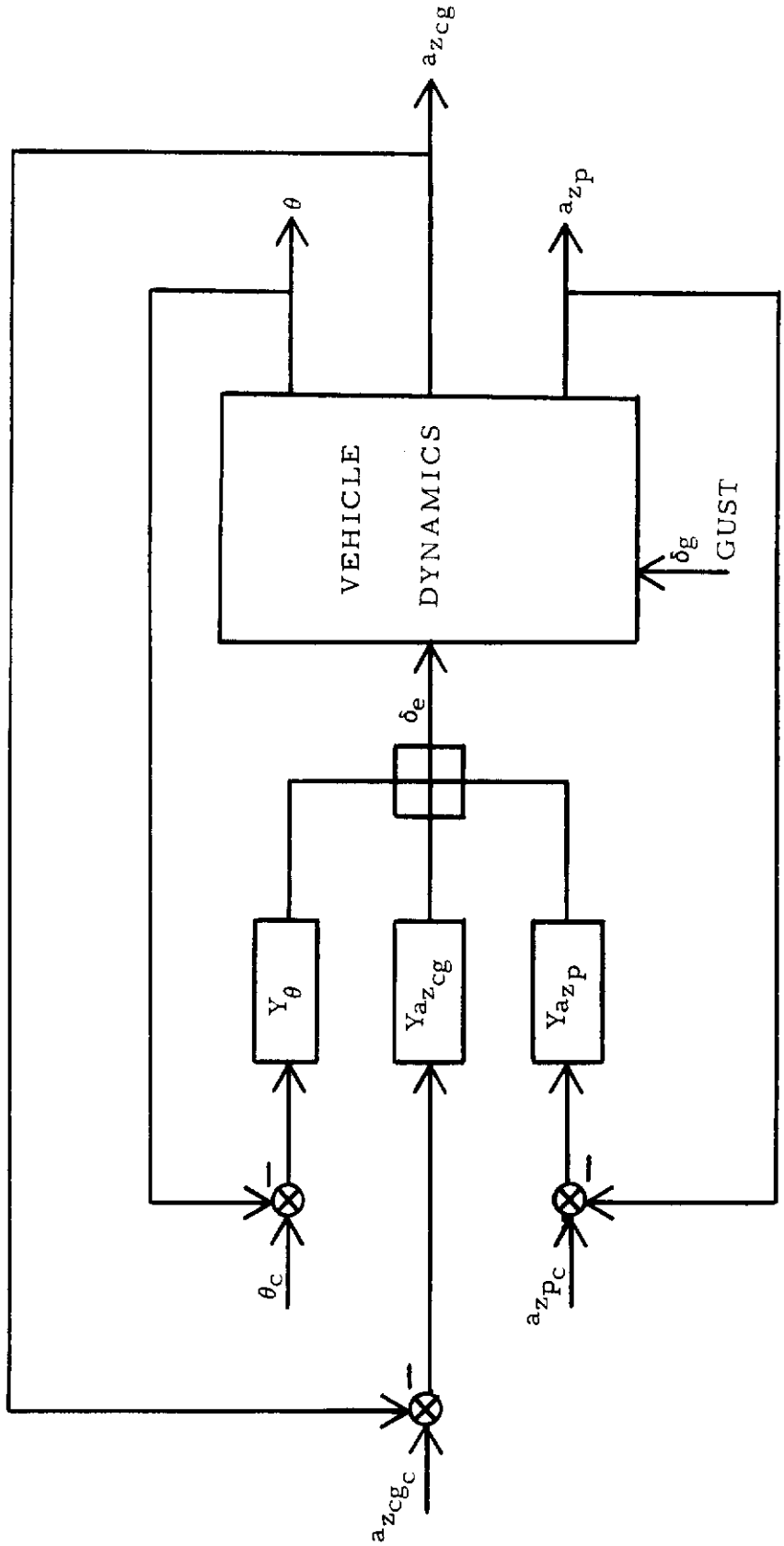

FIGURE 42. LONGITUDINAL BLOCK DIAGRAM

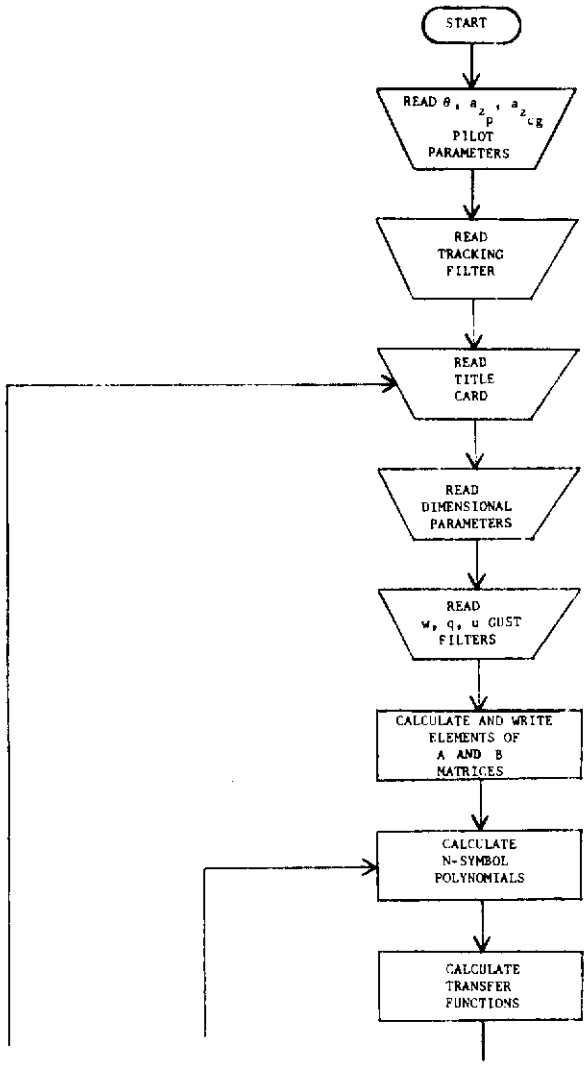

FIGURE 43. LONGITUDINAL FLOW CHART

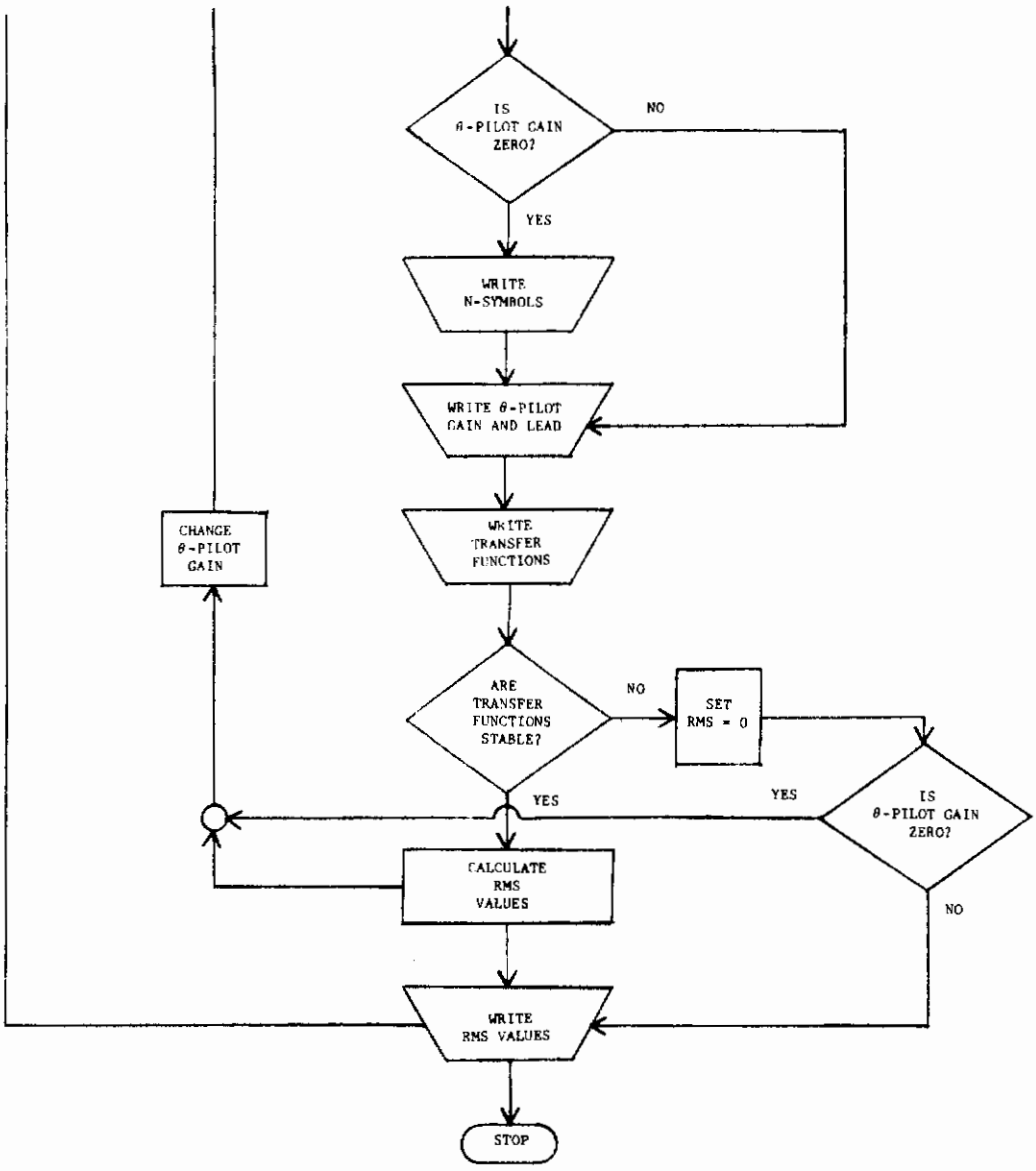

FIGURE 43. (Concluded)

KEY PUNCH FORM - GENERAL PURPOSE

FORM 20-708 (R.1 69)

JOB TITLE					ENGINEER	PAGE 1 OF
DPWA SERIAL NO.	PRE.	NDP JOB NO	DASH	FOR ORGN. NO.	ANALYST	DATE

INPUT FOR LONGITUDINAL MULTILOOP ANALYSIS PROGRAM

The necessary input format for this program is described below, along with required explanations. Note that the symbol * before a line indicates a data card as opposed to explanations.

* N N N N N N

- Integer indicating the number of coefficients in mechanical control denominator
- Integer indicating the number of coefficients in mechanical control numerator
- Integer indicating the number of coefficients in Pade denominator
- Integer indicating the number of coefficients in Pade numerator
- Integer indicating the number of coefficients in θ-pilot compensation denominator
- Integer indicating the number of coefficients in θ-pilot compensation numerator

* | θ_0 | θ_{n-1} | θ_{n-2} | θ_{n-3} | θ_{n-4} | θ_{n-5} |

The above card enters the coefficients of the θ-pilot compensation numerator in decreasing powers of s. Up to 9 coefficients may be entered by using a second card if necessary.

* Coefficients of the θ-pilot compensation denominator are entered in the same manner as above.

* Coefficients of Pade numerator are entered in the same manner as above.

* Coefficients of Pade denominator are entered in the same manner as above.

* Coefficients of mechanical control numerator are entered in the same manner as above.

* Coefficients of mechanical control denominator are entered in the same manner as above.

* GTH

- θ-pilot gain for first computing cycle

FIGURE 44. LONGITUDINAL INPUT FORMAT

KEY PUNCH FORM - GENERAL PURPOSE

FORM 20-708 (R-1 69)

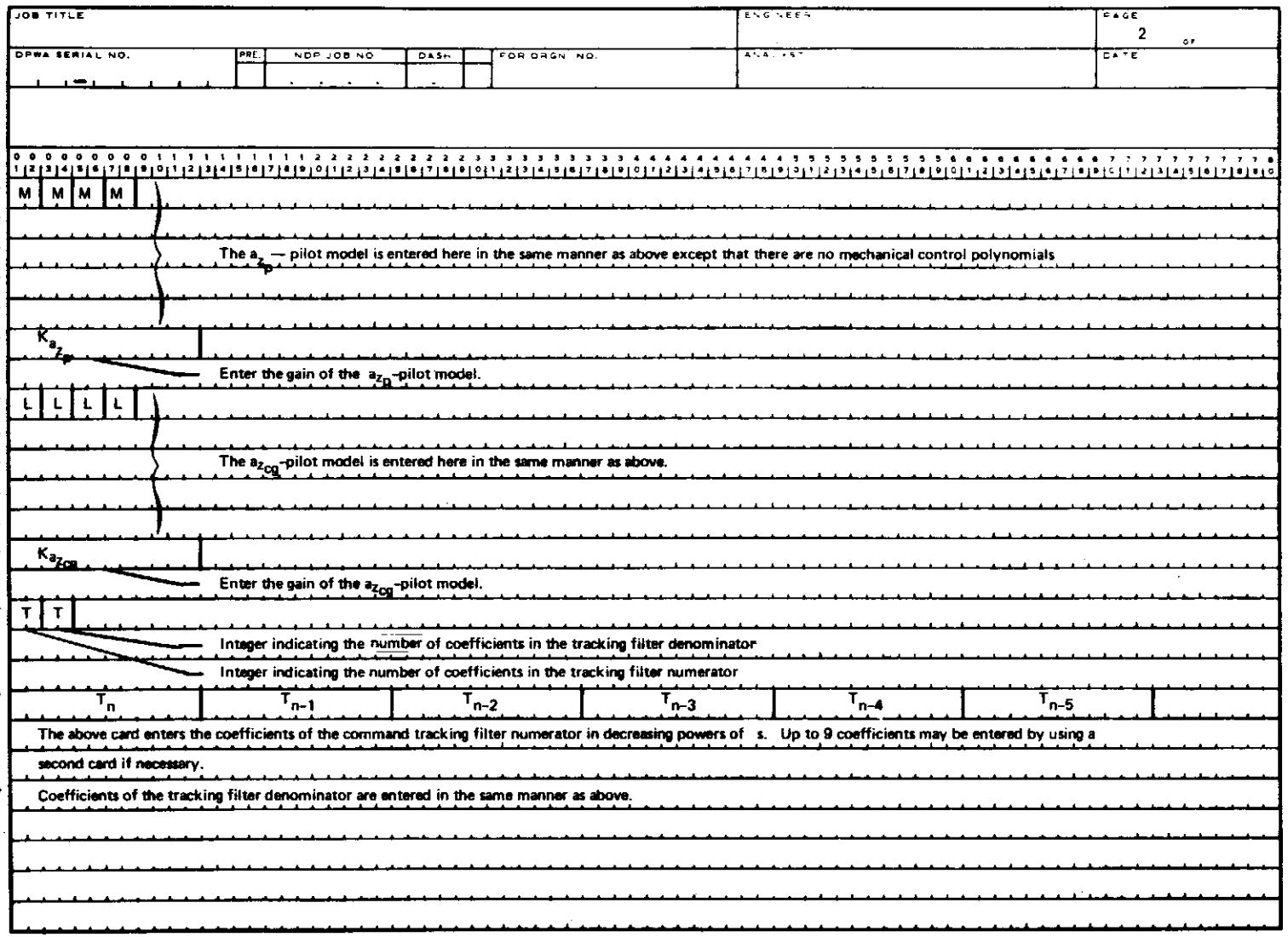

FIGURE 44. (Continued)

KEY PUNCH FORM - GENERAL PURPOSE

FORM 20-708 (R.1-69)

JOB TITLE					ENGINEER	PAGE 3 OF
DPWA SERIAL NO.	PRE.	NDP JOB NO.	DASH	FOR ORGN NO.	ANALYST	DATE

A A						
Integer indicating the number of columns in the A matrix						
Integer indicating the number of rows in the A matrix						
B B						
Integer indicating the number of columns in the B matrix						
Integer indicating the number of rows in the B matrix						
A title of up to 64 characters (including blanks) may be entered here.						
Dimensional input:						
X_v	X_α	Z_v	Z_α	Z_{δ_e}	M_α	
$M_{\dot{\alpha}}$	M_q	M_{δ_e}	L_x	V_o	Q_{aug_1}	
Q_{aug_2}	T_{aug}	K_b				
W W						
Integer indicating the number of coefficients in the w-gust filter denominator						
Integer indicating the number of coefficients in the w- gust filter numerator						
W_n	W_{n-1}	W_{n-2}	W_{n-3}	W_{n-4}	W_{n-5}	
The above card enters the coefficients of the w-gust filter numerator in decreasing powers of s. Up to 9 coefficients may be entered by using a second card if necessary.						
Coefficients of the w-gust filter denominator are entered in the same manner as above.						
The q-gust filter is entered in the same manner as above.						

FIGURE 44. (Continued)

KEY PUNCH FORM - GENERAL PURPOSE

FORM 20-706 (R.1-69)

JOB TITLE					ENGINEER	PAGE 4 OF
DPWA SERIAL NO.	PRE.	NDP JOB NO	DASH	FOR ORGN NO.	ANALYST	DATE

The u-gust filter is entered in the same manner as above.

F — Increment by which θ -pilot gain is changed each computing cycle

G — Integer indicating the number of θ -pilot gains for which computations are desired.

As many data sets may be "stacked" as desired. Following the first set, all succeeding sets must start at the title card.

FIGURE 44. (Concluded)

The theta pilot is expressed as:

$$Y_\theta = (\text{Gain}) \frac{(\text{Pilot Compensation Numerator})}{(\text{Pilot Compensation Denominator})}$$

$$\bullet \frac{(\text{Time Delay Approximation Numerator})}{(\text{Time Delay Approximation Denominator})}$$

$$\bullet \frac{(\text{Mechanical Control System Numerator})}{(\text{Mechanical Control System Denominator})}$$

The normal acceleration pilot models are similar, except that the provision for the mechanical control system polynomials is not included in these models. The acceleration pilot models can, of course, be used for augmenter feedbacks, with the location of the sensor determined by the quantity L_x in the airframe input data for an off-cg sensor location.

The other inputs are given in Figure 44 and are self-explanatory.

AIRFRAME AND CONTROL SYSTEM EQUATIONS

$$\dot{V} - X_V \Delta V - X_\alpha \alpha + g\theta = -X_\alpha \alpha_g - X_V v_g$$

$$-Z_V \Delta V + \dot{\alpha} - Z_\alpha \alpha - \dot{\theta} = Z_{\delta_e} \delta_e - Z_\alpha \alpha_g - Z_V v_g$$

$$-M_{\dot{\alpha}} \dot{\alpha} - M_\alpha \alpha + \ddot{\theta} - M_q \dot{\theta} = M_{\delta_e} \delta_e - M_\alpha \alpha_g - M_q q_g$$

$$\delta_e = \delta_{e_{comm}} + K_b V_o (\dot{\theta} - \dot{\alpha}) + Q_{aug_1} \dot{\theta} + Q_{aug_2} \frac{T_{aug} s}{T_{aug} s + 1} \dot{\theta}$$

δ_e, $\delta_{e_{comm}}$: + T.E. down

K_b = Fuselage bending factor, a positive number expressed as rad/fps

Q_{aug_1}, Q_{aug_2} are positive numbers for stabilizing feedback, sec

T_{aug} : Washout time constant, sec

$X_V = -2q_o S C_{D_o}/mV_o$

$X_\alpha = -(q_o S C_{D_\alpha}/m) + g$

$Z_V = -2q_o S C_L/mV_o^2$

$Z_\alpha = -q_o S C_{L_\alpha}/mV_o$

$Z_{\delta_e} = -q_o S C_{L_{\delta_e}}/mV_o$

(For additional symbol definitions see Appendix II.)

TRANSFER FUNCTIONS

$$\Delta'' = \Delta + Y_\theta N_{\theta_{\delta_e}} + Y_{a_{Z_p}} N_{a_{Z_p}{}_{\delta_e}} + Y_{a_{Z_{cg}}} N_{a_{Z_{cg}}{}_{\delta_e}}$$

Gust Tracking

$$\frac{\theta}{\delta_{g_w}} = \frac{N_{\theta_{\delta_{g_w}}} + Y_{a_{Z_p}} N^{\theta}_{\delta_{g_w}} {}^{a_{Z_p}}_{\delta_e} + Y_{a_{Z_{cg}}} N^{\theta}_{\delta_{g_w}} {}^{a_{Z_{cg}}}_{\delta_e}}{\Delta''}$$

$$\frac{a_{Z_p}}{\delta_{g_w}} = \frac{N_{a_{Z_p}{}_{\delta_{g_w}}} + Y_\theta N^{\theta}_{\delta_e} {}^{a_{Z_p}}_{\delta_{g_w}} + Y_{a_{Z_p}} N^{a_{Z_p}}_{\delta_{g_w}} {}^{a_{Z_{cg}}}_{\delta_e}}{\Delta''}$$

$$\frac{\theta}{\delta_{g_q}} = \frac{N_{\theta_{\delta_{g_q}}} + Y_{a_{Z_p}} N^{\theta}_{\delta_{g_q}} {}^{a_{Z_p}}_{\delta_e} + Y_{a_{Z_{cg}}} N^{\theta}_{\delta_{g_w}} {}^{a_{Z_{cg}}}_{\delta_e}}{\Delta''}$$

$$\frac{a_{Z_p}}{\delta_{g_q}} = \frac{N_{a_{Z_p}{}_{\delta_{g_q}}} + Y_\theta N^{\theta}_{\delta_e} {}^{a_{Z_p}}_{\delta_{g_q}} + Y_{a_{Z_p}} N^{a_{Z_p}}_{\delta_{g_q}} {}^{a_{Z_{cg}}}_{\delta_e}}{\Delta''}$$

$$\frac{\theta}{\delta_{g_u}} = \frac{N_{\theta_{\delta_{g_u}}} + Y_{a_{Z_p}} N^{\theta}_{\delta_{g_u}} {}^{a_{Z_p}}_{\delta_e} + Y_{a_{Z_{cg}}} N^{\theta}_{\delta_{g_w}} {}^{a_{Z_{cg}}}_{\delta_e}}{\Delta''}$$

$$\frac{a_{Z_p}}{\delta_{g_u}} = \frac{N_{a_{Z_p}\delta_{g_u}} + Y_\theta N_{\delta_e \delta_{g_u}} + Y_{a_{Z_p}} N_{\delta q_u \delta_e}}{\Delta''}$$

Inasmuch as q_g is correlated with w_g, θ and a_{Z_p} for the combination of these two gust components are:

$$\theta = w_g \left[\left(\frac{\theta}{\delta g_w}\right) + q_g \left(\frac{\theta}{\delta g_q}\right)\right]$$

$$a_{Z_p} = w_g\left[\left(\frac{a_{Z_p}}{\delta g_w}\right) + q_g \left(\frac{a_{Z_p}}{\delta g_q}\right)\right]$$

For the u_g gust component:

$$\theta = u_g \left(\frac{\theta}{\delta g_u}\right)$$

$$a_{Z_p} = u_g \left(\frac{a_{Z_p}}{\delta g_u}\right)$$

COMMAND TRACKING

$$\frac{\theta_E}{\theta_C} = \frac{\Delta + Y_{a_{Z_p}} N_{a_{Z_p}\delta e} + Y_{a_{Z_{cg}}} N_{a_{Z_{cg}}\delta e}}{\Delta''}$$

$$\frac{a_{Z_p}}{\theta_C} = \frac{Y_\theta N_{a_{Z_p}\delta e}}{\Delta''}$$

EXAMPLE OUTPUTS

The output of the longitudinal program for an example case is given in Figure 45. For this case, pitch rate is fed back through a washout filter. Fuselage bending also is included. Because these feedbacks are incorporated into the equations of motion, the N-symbols include their effects. A second-order Pade approximation is used along with a first-order lead in the θ-pilot model. No mechanical control system is included.

The symbols for the rms values in the program printout are defined below:

THT: Rms theta error in degrees due to a 10-degree rms theta input command.

AZPT: Rms acceleration at the pilot's station in fps^2 due to the above input command.

THW: Rms theta error in degrees due to a 10-fps rms w-gust.

AZPW: Rms acceleration at the pilot's station in fps^2 due to the above gust.

THQ: Rms theta error in degrees due to a 10-fps w-gust and correlated q-gust.

AZPQ: Rms acceleration at the pilot's station in fps^2 due to the above gusts.

THU: Rms theta error in degrees due to a 10-fps V-gust.

AZPU: Rms acceleration at the pilot's station in fps^2 due to the above gust.

CHECK CASE FOR PITCH-ANGLE CLOSURE, GLST AND COMMAND TRACKING

THE A MATRIX COEFFICIENTS ARE LISTED BELOW

I	J	S**3	S**2	S**1	S**0
1	1	0.0	0.0	0.10000000E 01	0.17559998E-01
1	2	0.0	0.0	0.0	-0.63849991E 02
1	3	0.0	0.0	0.0	0.32199997E 02
1	4	0.0	0.0	0.0	0.0
1	5	0.0	0.0	0.0	0.0
2	1	0.0	0.0	0.65423974E-05	0.81779988E-04
2	2	0.0	0.75720906E-01	0.10850716E 01	0.17319994E 01
2	3	0.0	-0.71115553E-01	-0.92608476E 00	0.0
2	4	0.0	0.0	0.0	0.0
2	5	0.0	0.0	0.0	0.0
3	1	0.0	0.0	0.0	0.0
3	2	0.0	-0.54C49653E 00	-0.59002094E 01	0.10700000E 02
3	3	0.79999983E-01	0.22545176E 01	0.10945486E 02	0.0
3	4	0.0	0.0	0.0	0.0
3	5	0.0	0.0	0.0	0.0
4	1	0.0	0.0	0.0	0.0
4	2	0.0	0.0	-0.88900000E 03	0.0
4	3	0.0	0.12000000E 02	0.88900000E 03	0.0
4	4	0.0	0.0	0.0	0.10000000E 01
4	5	0.0	0.0	0.0	0.0
5	1	0.0	0.0	0.0	0.0
5	2	0.0	0.0	-0.88900000E 03	0.0
5	3	0.0	0.0	0.88900000E 03	0.0
5	4	0.0	0.0	0.0	0.0
5	5	0.0	0.0	0.0	0.10000000E 01

THE B MATRIX COEFFICIENTS ARE LISTED BELOW

I	J	S**3	S**2	S**1	S**0
1	1	0.0	0.0	0.0	0.0
1	2	0.0	0.0	0.0	-0.63849991E 02
1	3	0.0	0.0	0.0	0.0
1	4	0.0	0.0	0.0	0.17559998E-01
2	1	0.0	0.0	-0.29711992E-01	-0.37140000E 00
2	2	0.0	0.0	0.0	0.17319994E 01
2	3	0.0	0.0	0.0	0.0
2	4	0.0	0.0	0.0	0.81779988E-04
3	1	0.0	0.0	-0.37887974E 01	-0.47359985E 02
3	2	0.0	0.0	0.0	0.10700000E 02
3	3	0.0	0.0	0.0	0.15199995E 01
3	4	0.0	0.0	0.0	0.0
4	1	0.0	0.0	0.0	0.0
4	2	0.0	0.0	0.0	0.0
4	3	0.0	0.0	0.0	0.0
4	4	0.0	0.0	0.0	0.0
5	1	0.0	0.0	0.0	0.0
5	2	0.0	0.0	0.0	0.0
5	3	0.0	0.0	0.0	0.0
5	4	0.0	0.0	0.0	0.0

FIGURE 45. LONGITUDINAL EXAMPLE OUTPUT

```
      THE N-SYMBOLS ARE LISTED BELOW
   COEFFICIENTS ARE LISTED FROM S**N THRU S**0

N/TH/DE          =  -0.30295E 00 -0.80786E 01 -0.59968E 02 -0.79144E 02 -0.16179E 01
N/AZP/DE         =   0.15223E 01  0.40730E 02  0.74884E 03  0.11530E 05  0.69612E 05  0.13275E 04  0.0
N/TH/WG/AZP/DE   =   0.55526E 04  0.69522E 05  0.14383E 04  0.0
N/TH/QG/AZP/DE   =  -0.40149E 02 -0.50257E 03 -0.88127E 01  0.0
N/TH/UG/AZP/DE   =   0.27507E 00  0.34383E 01  0.0          0.0
N/TH/WG/AZCG/DE  =   0.55526E 04  0.69522E 05  0.14383E 04  0.0
N/TH/QG/AZCG/DE  =  -0.40149E 02 -0.50257E 03 -0.88127E 01  0.0
N/TH/UG/AZCG/DE  =   0.27507E 00  0.34383E 01  0.0          0.0
N/AZCG/DE        =  -0.21131E 01 -0.56213E 02  0.29229E 02  0.10580E 05  0.69593E 05  0.13275E 04  0.0
N/TH/DE/AZP/WG   =  -0.55526E 04 -0.69522E 05 -0.14383E 04  0.0
N/TH/DE/AZP/QG   =   0.40149E 02  0.50257E 03  0.88127E 01  0.0
N/TH/DE/AZP/UG   =  -0.27507E 00 -0.34383E 01  0.0          0.0
N/AZP/WG/AZCG/DE =  -0.66631E 05 -0.83427E 06 -0.17267E 05 -0.25000E 00  0.0          0.0
N/AZP/QG/AZCG/DE =   0.48179E 03  0.60308E 04  0.10575E 03  0.0          0.0          0.0
N/AZP/UG/AZCG/DE =  -0.33008E 01 -0.41260E 02  0.17166E-04  0.0          0.0          0.0
DELTA            =   0.60577E-02  0.21919E 00  0.24974E 01  0.11123E 02  0.29075E 02  0.55077E 00  0.28176E-01
N/TH/WG          =   0.17466E 01  0.21865E 02  0.41415E 00  0.44703E-07
N/TH/QG          =   0.11510E 00  0.16513E 01  0.26622E 01  0.54166E-01
N/TH/UG          =   0.44140E-04  0.48184E-03 -0.87382E-03  0.0
N/AZP/WG         =   0.10225E 03  0.23361E 04  0.63065E 04  0.13527E 03  0.25049E 02  0.0
N/AZP/QG         =  -0.13811E 01 -0.26C39E 02 -0.24689E 03 -0.23451E 04 -0.44595E 02  0.0
N/AZP/UG         =   0.52783E-02  0.11866E 00  0.37677E 00  0.77682E 00  0.0          0.0


THETA GAIN =  0.Q            LEAD =  0.500


THE TRANSFER FUNCTIONS ARE LISTED BELOW.  (THE COEFFICIENT OF THE HIGHEST POWER OF S IS PRINTED FIRST)

    DENOMINATOR
          0.60577E-02          0.29994E 0C          0.57782E 01          0.57403E 02          0.32535E 03          0.10473E 04
          0.17303E 04          0.33014E 02          0.16697E 01
    THETA PER THETA COMMAND NUMERATOR
          0.0                  0.0                  0.0                  0.0                  0.0                  0.0
          0.0                  0.C
    AZP PER AZP COMMAND NUMERATOR
          0.0                  0.0                  0.0                  0.0                  0.0                  0.0
          0.0                  0.0                  0.0
    THETA PER W GUST NUMERATOR
          0.17466E 01          0.45147E 02          0.39538E 03          0.13013E 04          0.24543E 02          0.26491E-05
    THETA PER Q GUST NUMERATOR
          0.11510E 00          0.31856E 01          0.31495E 02          0.13340E 03          0.15849E 03          0.32099E 01
    THETA PER U GUST NUMERATOR
          0.44140E-04          0.10702E-02          0.81648E-02          0.16906E-01         -0.51782E-01          0.0
    AZP PER W GUST NUMERATOR
          0.10225E 03          0.36991E 04          0.43507E 05          0.22264E 06          0.37555E 06          0.83502E 04
          0.14844E 04          0.0
    AZP PER Q GUST NUMERATOR
         -0.13811E 01         -0.44450E 02         -0.67584E 03         -0.71792E 04         -0.45936E 05         -0.13957E 06
         -0.26427E 04          0.0
    AZP PER U GUST NUMERATOR
          0.52783E-02          0.18902E 00          0.22713E 01          0.12831E 02          0.32683E 02          0.46035E 02
          0.0                  0.0
    THE POLES OF THE CLOSED-LOOP TRANSFER FUNCTIONS ARE BELOW IN REAL-IMAGINARY PAIRS
         -0.93531E-02         -0.29810E-01         -0.93531E-02          0.29810E-01         -0.25696E 01         -0.37382E 01
         -0.25696E 01          0.37382E 01         -0.12500E 02          0.0                 -0.18526E 02          0.0
         -0.66650E 01         -0.38520E 01         -0.66650E 01          0.38520E 01
```

FIGURE 45. (Continued)

```
THETA GAIN =  0.200          LEAD =  0.500

THE TRANSFER FUNCTIONS ARE LISTED BELOW.  (THE COEFFICIENT OF THE HIGHEST POWER OF S IS PRINTED FIRST)

    DENOMINATOR
          0.60577E-02          0.33023E 00          0.62428E 01          0.55234E 02          0.29524E 03          0.12490E 04
          0.26973E 04          0.97630E 03          0.20845E 02
    THETA PER THETA COMMAND NUMERATOR
          0.30295E-01          0.46462E 00         -0.21687E 01         -0.30102E 02          0.20174E 03          0.96691E 03
          0.94328E 03          0.19176E 02
    AZP PER AZP COMMAND NUMERATOR
          0.0                  0.0                  0.0                  0.0                  0.0                  0.0
          0.0                  0.0                  0.0
    THETA PER W GUST NUMERATOR
          0.17466E 01          0.45147E 02          0.39538E 03          0.13013E 04          0.24543E 02          0.26491E-05
    THETA PER Q GUST NUMERATOR
          0.11510E 00          0.31856E 01          0.31495E 02          0.13340E 03          0.15849E 03          0.32099E 01
    THETA PER U GUST NUMERATOR
          0.44140E-04          0.10702E-02          0.81648E-02          0.16906E-01         -0.51782E-01          0.0
    AZP PER W GUST NUMERATOR
          0.10225E 03          0.42544E 04          0.44168E 05          0.16212E 06          0.66637E 06          0.83701E 06
          0.18531E 05          0.0
    AZP PER Q GUST NUMERATOR
         -0.13811E 01         -0.48465E 02         -0.68061E 03         -0.67416E 04         -0.48040E 05         -0.14555E 06
         -0.27472E 04          0.0
    AZP PER U GUST NUMERATOR
          0.52783E-02          0.21652E 00          0.23034E 01          0.98319E 01          0.47152E 02          0.86786E 02
          0.0                  0.0
    THE POLES OF THE CLOSED-LOOP TRANSFER FUNCTIONS ARE BELOW IN REAL-IMAGINARY PAIRS
         -0.22769E-01          0.0                 -0.41636E 00          0.0                 -0.37506E 01          0.0
         -0.10809E 02          0.0                 -0.26029E 02          0.0                 -0.12500E 02          0.0
         -0.49391E 00         -0.52228E 01         -0.49391E 00          0.52228E 01

THETA PILOT PARAMETERS AND RMS ERROR OUTPUTS ARE BELOW

  GAIN   LEAD   DELAY     THT          AZPT          THW          AZPW          THQ          AZPQ          THU          AZPU
  0.0    0.500  0.450   0.1000E 02   0.0          0.4627E 00   0.7563E 01   0.5254E 00   0.6633E 01   0.1721E-02   0.1760E 00
  0.200  0.500  0.450   0.5039E 01   0.4638E 02   0.4130E 00   0.8149E 01   0.4817E 00   0.8067E 01   0.2162E-03   0.1775E 00
```

FIGURE 45. (Concluded)

LATERAL PROGRAMS

A block diagram of the lateral pilot-vehicle system is depicted in Figure 46, and flow charts of the digital computer programs to calculate closed-loop pilot-vehicle performance are included as Figure 47 for gust tracking and as Figure 48 for command tracking. The input formats for these digital computer programs are given in Figures 49 and 50.

The lateral airframe and control system equations of motion are presented in this subsection. These equations are small-perturbation equations in a body-axis system. Provision is made for roll-rate feedback and an aileron-to-rudder interconnect. As shown in Figure 46, a separate loop is provided for yaw-rate feedback.

Also presented in this subsection are the transfer functions for the loop closures shown in the block diagram of Figure 46.

Pilot transfer functions may be entered into programs as ratios of polynomials.

The phi-pilot is expressed as:

$$Y_{\phi} = (\text{Gain}) \frac{(\text{Pilot Compensation Numerator})}{(\text{Pilot Compensation Denominator})}$$

$$\bullet \frac{(\text{Time Delay Approximation Numerator})}{(\text{Time Delay Approximation Denominator})}$$

$$\bullet \frac{(\text{Mechanical Control System Numerator})}{(\text{Mechanical Control System Denominator})}$$

The si-pilot and beta-pilot models are similar except that the provision for the mechanical control system polynomials is not included in these models.

The other inputs are given in Figure 49 and are self-explanatory.

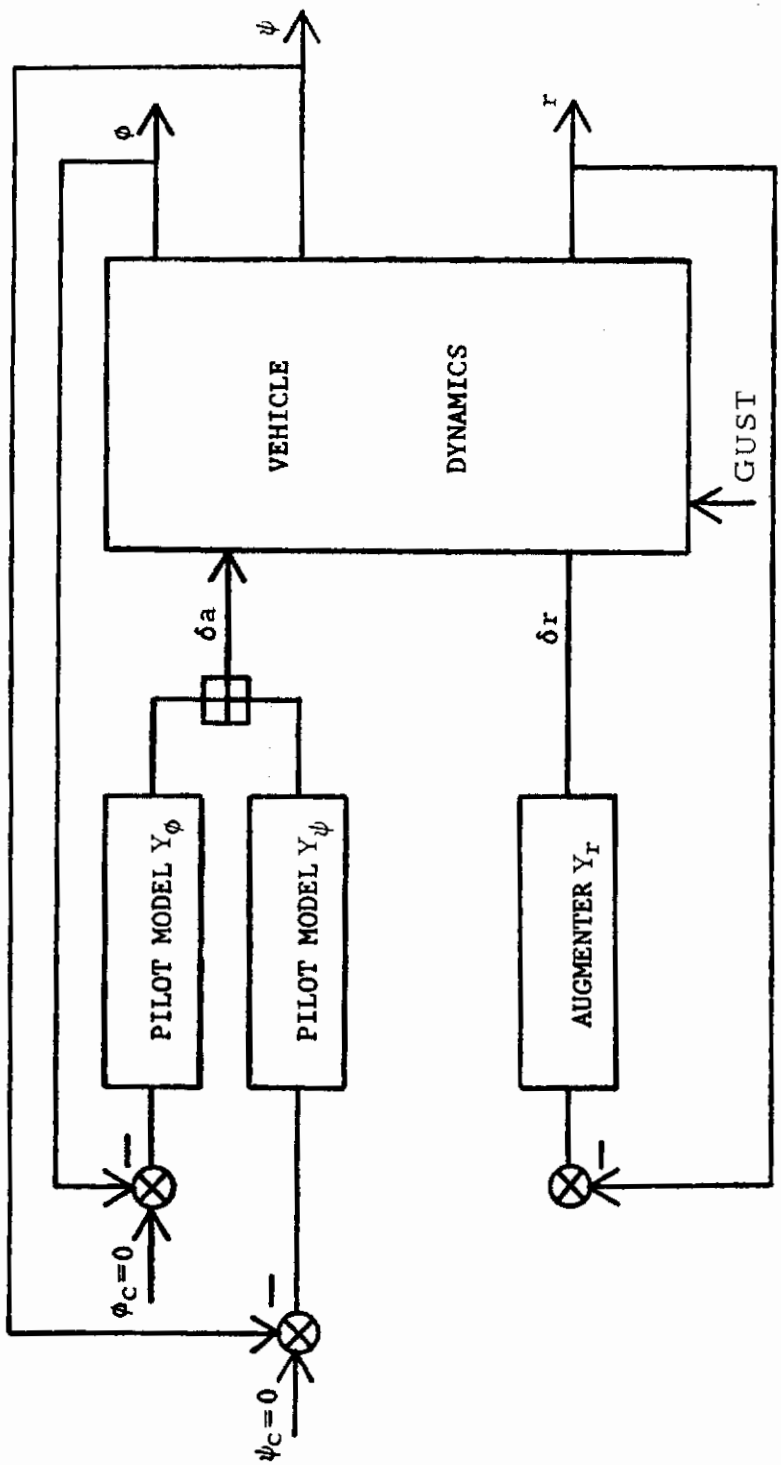

FIGURE 46. LATERAL BLOCK DIAGRAM

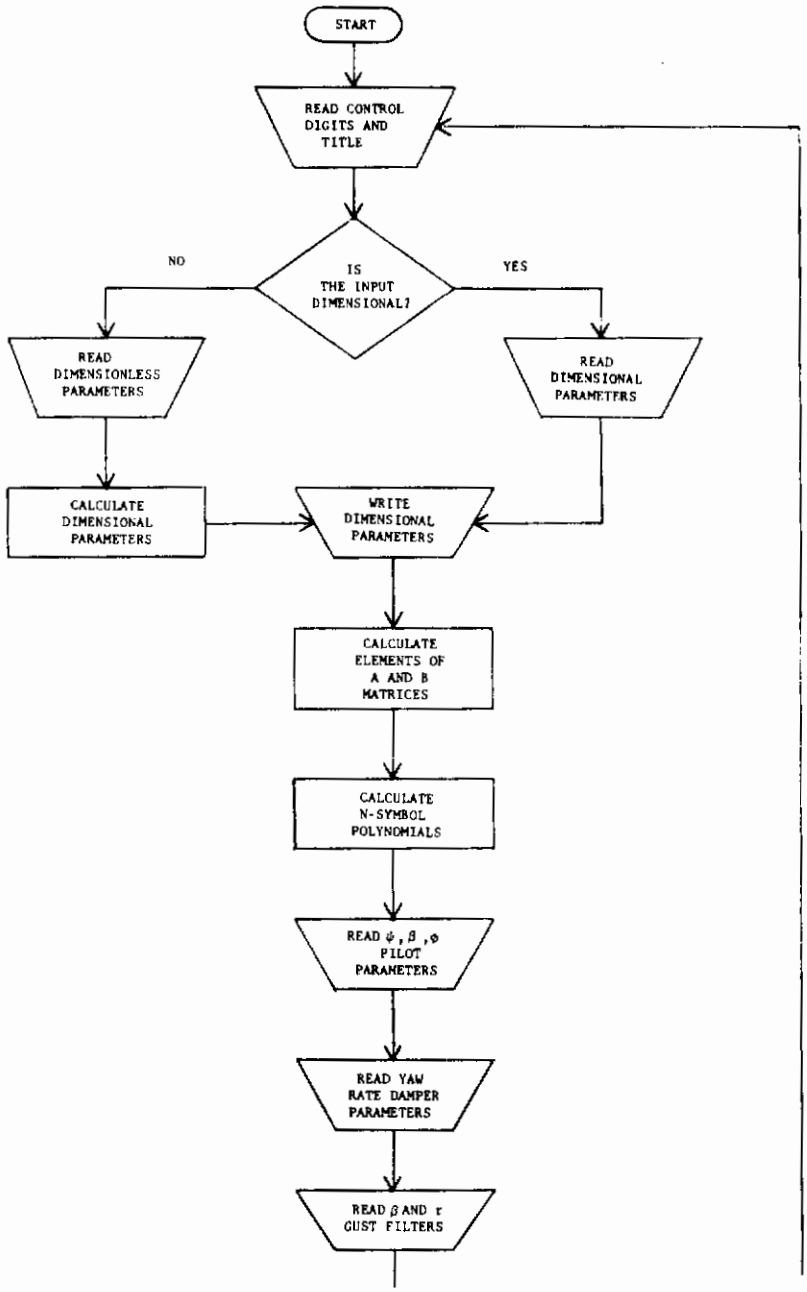

FIGURE 47. LATERAL GUST FLOW CHART

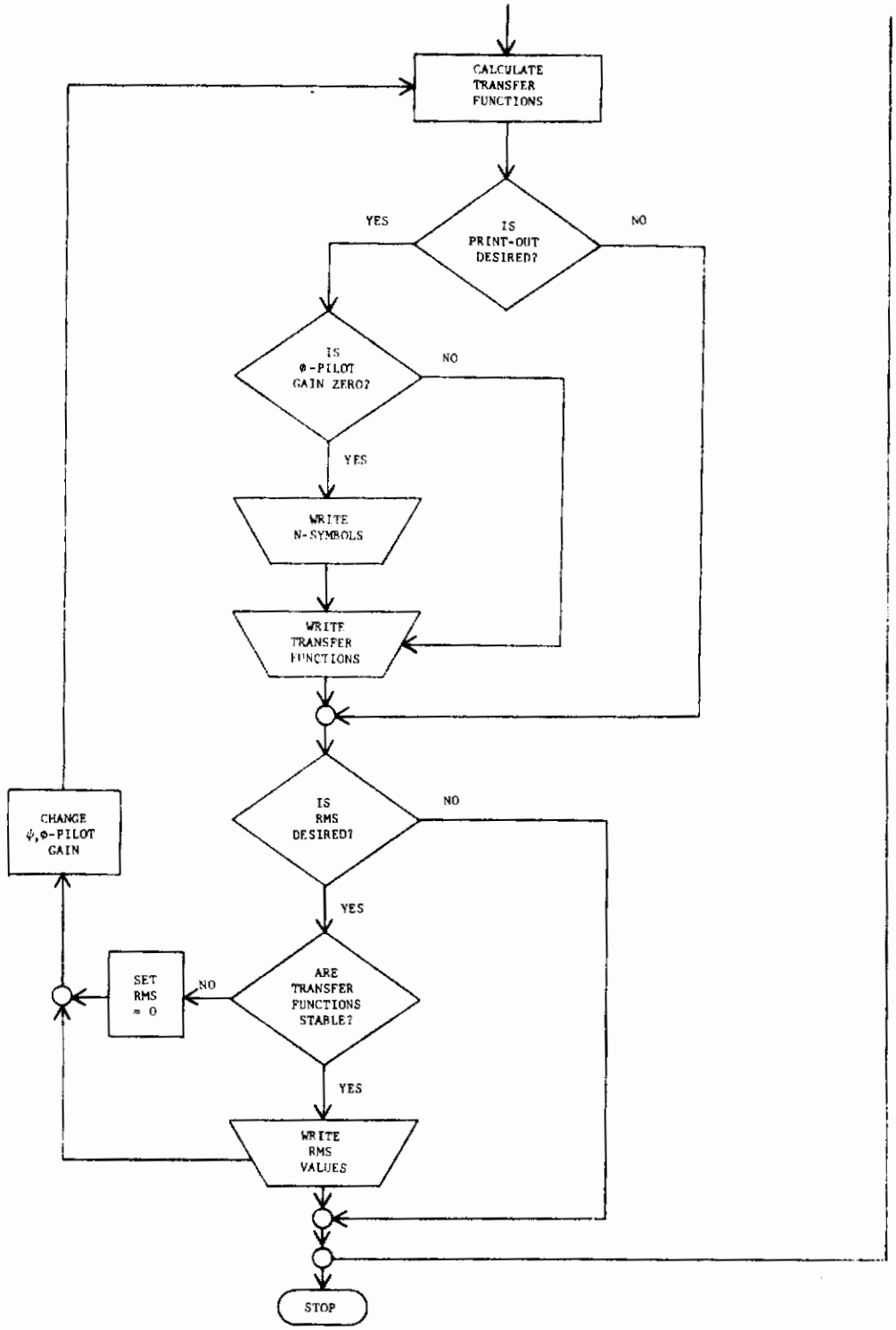

FIGURE 47. (Concluded)

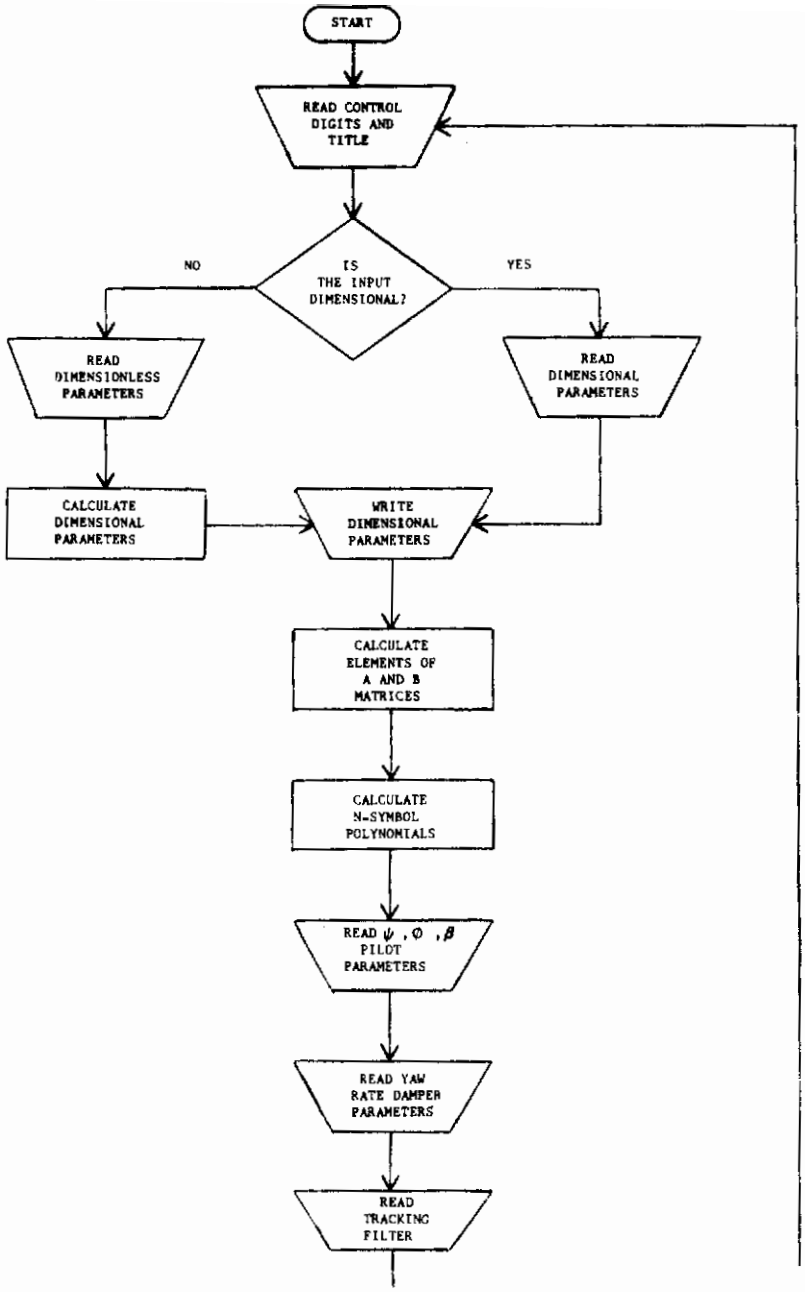

FIGURE 48. LATERAL TRACKING FLOW CHART

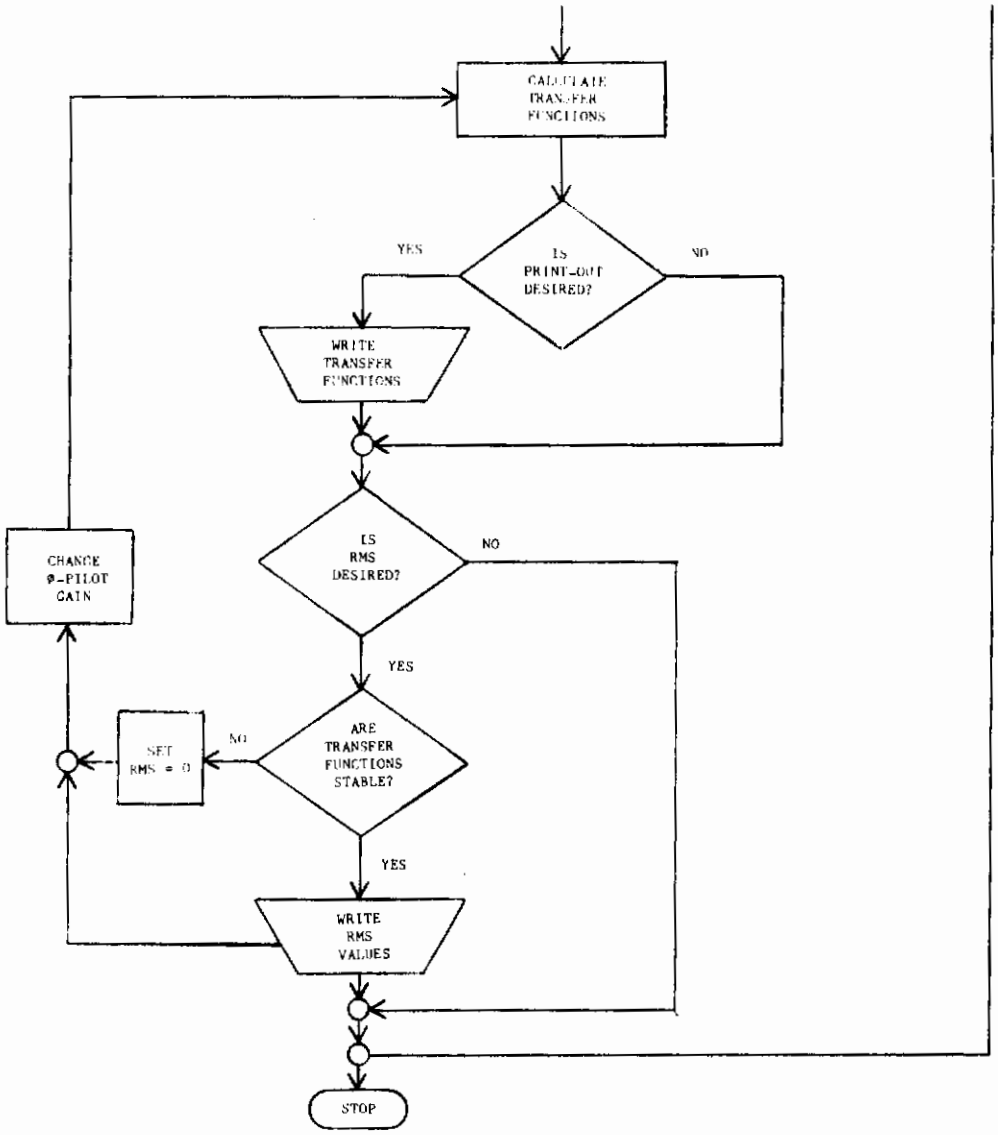

FIGURE 48. (Concluded)

KEY PUNCH FORM - GENERAL PURPOSE

Form 20-706 (R.1-69)

JOB TITLE					ENGINEER	PAGE
DPWA SERIAL NO.	PRE	NDP JOB NO	DASh	FOR ORGN. NO.	ANALYST	DATE

INPUT FOR LATERAL MULTILOOP GUST ANALYSIS PROGRAM

The necessary input format for this program is described below, along with required explanations. Note that the symbol * before a line indicates a data card as apposed to explanations.

NNN A title of up to 64 characters (including blanks) may be entered here

+1 indicates dimensional input; -1 indicates dimensionless input

+1 by-pass rms calculations; -1 gives rms

+1 by-pass N-symbol and transfer function print-outs; -1 gives these print-outs

Dimensional input (prime axis system):

A

Y_V	$Y^*_{\delta_r}$	$Y^*_{\delta_a}$	N'_β	N'_p	N'_r
N'_{δ_r}	N'_{δ_a}	L'_β	L_p	L_r	L_{δ_a}
L_{δ_r}	V_o	θ_o (Deg)	g	$K_{r_{aug}}$	K_{ARI}
α_o(Deg)					

Dimensionless input (body axis system):

B

C_{Y_β}	$C_{Y_{\delta_r}}$	$C_{Y_{\delta_a}}$	C_{n_β}	C_{n_p}	C_{h_r}
$C_{n_{\delta_r}}$	$C_{n_{\delta_a}}$	C_{ℓ_β}	C_{ℓ_p}	C_{ℓ_r}	$C_{\ell_{\beta a}}$
$C_{\ell_{\delta_r}}$	ρ	S	V_o	b	Mass
I_{xx}	I_{zz}	I_{xz}	θ_o (Deg)	g	$K_{r_{aug}}$
K_{ARI}	α_o (Deg)				

N.B. Either A or B must be included in each data set

AA Integer indicating the number of columns in the A matrix

Integer indicating the number of rows in the A matrix

BB Integer indicating the number of columns in the B matrix

Integer indicating the number of rows in the B matrix

FIGURE 49. LATERAL GUST INPUT FORMAT

KEY PUNCH FORM - GENERAL PURPOSE

FORM 20-708 (R-1-69)

JOB TITLE					ENGINEER	PAGE OF
DPWA SERIAL NO.	PRE.	NDP JOB NO.	DASH	FOR ORGN NO.	ANALYST	DATE

M M M M

The ψ - pilot model is entered here in the same manner as the ϕ - pilot model below except that there are no mechanical control polynomials.

L L L L L L

Integer indicating the number of coefficients in mechanical control denominator

Integer indicating the number of coefficients in mechanical control numerator

Integer indicating the number of coefficients in Pade denominator

Integer indicating the number of coefficients in Pade numerator

Integer indicating the number of coefficients in ϕ - pilot compensation denominator

Integer indicating the number of coefficients in ϕ -pilot compensation numerator

ϕ_n	ϕ_{n-1}	ϕ_{n-2}	ϕ_{n-3}	ϕ_{n-4}	

The above card enters the coefficients of the ϕ - pilot compensation numerator in decreasing powers of s. Up to 5 coefficients may be entered.

Coefficients of the ϕ - pilot compensation denominator are entered here in the same manner as above.

Coefficients of Pade numerator are entered in the same manner as above.

Coefficients of Pade denominator are entered in the same manner as above.

Coefficients of mechanical control numerator are entered in the same manner as above.

Coefficients of mechanical control denominator are entered in the same manner as above.

The β - pilot model is entered here in the same manner as the ψ - pilot model above.

FIGURE 49. (Continued)

KEY PUNCH FORM - GENERAL PURPOSE

FORM 20-708 (R.1-69)

JOB TITLE | ENGINEER | PAGE ___ OF ___

OPWA SERIAL NO. | PRE. | NOP JOB NO. | DASH | FOR ORGN. NO. | ANALYST | DATE

K K — Integer indicating the number of coefficients in the yaw rate damper denominator

Integer indicating the number of coefficients in the yaw rate damper numerator

Y_n | Y_{n-1} | Y_{n-2} | Y_{n-3} | Y_{n-4}

The above card enters the coefficients of the yaw rate damper numerator in decreasing powers of s. Up to 5 coefficients may be entered.

Coefficients of the yaw rate damper denominator are entered in the same manner as above.

B B — Integer indicating the number of coefficients in the β - gust filter denominator

Integer indicating the number of coefficients in the β - gust filter numerator

B_n | B_{n-1} | B_{n-2} | B_{n-3} | B_{n-4}

The above card enters the coefficients of the β - gust filter numerator in decreasing powers of s. Up to 5 coefficients may be entered.

Coefficients of the β - gust filter denominator are entered in the same manner as above.

The r-gust filter is entered in the same manner as the β - gust filter above.

F | G | H

H — Incremental change in ψ - pilot gain each computing cycle

G — Incremental change in ϕ - pilot gain each computing cycle

F — Integer indicating the number of computing cycles desired

As many complete data sets may be "stacked" as desired.

FIGURE 49. (Concluded)

KEY PUNCH FORM - GENERAL PURPOSE

FORM 20-708 (R.1 69)

JOB TITLE					ENGINEER	PAGE
DPWA SERIAL NO.	PRE.	NOP JOB NO	DASH	FOR ORGN. NO.	ANALYST	DATE

INPUT FOR LATERAL MULTILOOP COMMAND TRACKING ANALYSIS PROGRAM

The input format for this program is identical to the format for the lateral gust analysis program except that (1) in place of the six cards on which the gust data is entered, the following three cards are substituted:

T	T

Integer indicating the number of coefficients in the tracking filter denominator

Integer indicating the number of coefficients in the tracking filter numerator

T_n	T_{n-1}	T_{n-2}	T_{n-3}	T_{n-4}

The above card enters the coefficients of the command tracking filter numerator, up to 5 coefficients may be entered

Coefficients of the command tracking filter denominator are entered in the same manner as above

and (2) there is no provision for "looping" ψ-pilot gain. Hence the last data card should not include a value for an incremental change in ψ-pilot gain.

FIGURE 50. LATERAL TRACKING INPUT FORMAT

AIRFRAME AND CONTROL SYSTEM EQUATIONS

$$-\left(\alpha_o s + \frac{g \cos \theta_o}{V_o}\right)\phi + \left(1 - \frac{g \sin \theta_o}{V_o s}\right) r + \left(s - Y_v\right)\beta \quad = \quad Y_{\delta_a}{}^{*}\delta_a + Y_{\delta_r}{}^{*}\delta_r + Y_v \beta_g$$

$$s(s - L_p')\phi \qquad - L_r' r \qquad - L_\beta' \beta \quad = \quad L_{\delta_a}' \delta_a + L_{\delta_r}' \delta_r + L_\beta' \beta_g + L_r' r_g$$

$$- s N_p' \phi \qquad + s - N_r' \; r \qquad - N_\beta' \beta \quad = \quad N_{\delta_a}' \delta_a + N_{\delta_r}' \delta_r + N_\beta' \beta_g + N_r' r_g$$

AUXILIARY EQUATIONS

$$\frac{r}{s} = \psi \cos \theta_o$$

$$\frac{p}{s} = \phi$$

$$\delta_a = \delta_{a_{comm}} - K_{r_{aug}} s\phi$$

$$\delta_r = \delta_{r_{comm}} + K_{ARI} \delta_a$$

TRANSFER FUNCTIONS

$$\Delta'' = \Delta + Y_\phi N_{\phi_{\delta_a}} + Y_\psi N_{\psi_{\delta_a}} + Y_\beta N_{\beta_{\delta_r}} + Y_r N_{r_{\delta_r}}$$

$$+ Y_\phi Y_r N^{\phi\ r}_{\delta_a\ \delta_r} + Y_\phi Y_\beta N^{\phi\ \beta}_{\delta_a\ \delta_r} + Y_\psi Y_\beta N^{\psi\ \beta}_{\delta_a\ \delta_r}$$

Gust:

$$\frac{\beta}{\delta_{g_\beta}} = \frac{N_{\beta_{\delta_{g_\beta}}} + Y_\phi N^{\beta\ \phi}_{\delta_{g_\beta}\ \delta_a} + Y_\psi N^{\beta\ \psi}_{\delta_{g_\beta}\ \delta_a} + Y_r N^{\beta\ r}_{\delta_{g_\beta}\ \delta_r}}{\Delta''}$$

$$\frac{\phi}{\delta_{g_\beta}} = \frac{N_{\phi_{\delta_{g_\beta}}} + Y_\psi N^{\phi\ \psi}_{\delta_{g_\beta}\ \delta_a} + Y_\beta N^{\phi\ \beta}_{\delta_{g_\beta}\ \delta_r} + Y_r N^{\phi\ r}_{\delta_{g_\beta}\ \delta_r}}{\Delta''}$$

$$\frac{\psi}{\delta_{g_\beta}} = \frac{N_{\psi_{\delta_{g_\beta}}} + Y_\phi N^{\psi\ \phi}_{\delta_{g_\beta}\ \delta_a} + Y_\beta N^{\psi\ \beta}_{\delta_{g_\beta}\ \delta_r}}{\Delta''}$$

$$\frac{\beta}{\delta_{g_r}} = \frac{N_{\beta_{\delta_{g_r}}} + Y_\phi N^{\beta\ \phi}_{\delta_{g_r}\ \delta_a} + Y_\psi N^{\beta\ \psi}_{\delta_{g_r}\ \delta_a} + Y_r N^{\beta\ r}_{\delta_{g_r}\ \delta_r}}{\Delta''}$$

$$\frac{\phi}{\delta_{g_r}} = \frac{N_{\phi_{\delta_{g_r}}} + Y_\psi N^{\phi\ \psi}_{\delta_{g_r}\ \delta_a} + Y_\beta N^{\phi\ \beta}_{\delta_{g_r}\ \delta_r} + Y_r N^{\phi\ r}_{\delta_{g_r}\ \delta_r}}{\Delta''}$$

$$\frac{\psi}{\delta_{g_r}} = \frac{N_{\psi_{\delta_{g_r}}} + Y_\phi N^{\psi\ \phi}_{\delta_{g_r}\ \delta_a} + Y_\beta N^{\psi\ \beta}_{\delta_{g_r}\ \delta_r}}{\Delta''}$$

The gust component r_g is correlated with β_g. β, ϕ, and ψ for the combination of these two gust components are:

$$\beta = \beta_g \left[\left(\frac{\beta}{\delta g_\beta} \right) + r_g \left(\frac{\beta}{\delta g_r} \right) \right]$$

$$\phi = \beta_g \left[\left(\frac{\phi}{\delta g_\beta} \right) + r_g \left(\frac{\phi}{\delta g_r} \right) \right]$$

$$\psi = \beta_g \left[\left(\frac{\psi}{\delta g_\beta} \right) + r_g \left(\frac{\psi}{\delta g_r} \right) \right]$$

Command Tracking:

$$\frac{\phi}{\phi_c} = \frac{\Delta + Y_\psi N_{\psi_{\delta_a}} + Y_\beta N_{\beta_{\delta_r}} + Y_r N_{r_{\delta_r}} + Y_\psi Y_\beta N^{\psi\ \beta}_{\delta_a\ \delta_r}}{\Delta''}$$

EXAMPLE OUTPUTS

Example cases showing the outputs of the lateral programs are given in Figures 51 and 52. Yaw rate damping is included in these cases but not roll rate feedback or aileron-to-rudder interconnect. Because the yaw rate feedback is provided for by a separate loop, its effect is not reflected in the N-symbols. Roll rate feedback and the interconnect are incorporated into the equations of motion so that their effects would be included in the N-symbols had they been used. In the ϕ-pilot model, a Pade' approximation is used for the gust example case, a first order for the command tracking case. First order leads are used in each case in the ϕ-pilot model. No mechanical control system is included.

In the gust program printout, the errors due to "BETA-GUST" are in degrees rms for a 10-fps rms v-gust. Those due to "BETA-GUST PLUS R-GUST" are for the 10-fps v-gust plus correlated r-gust.

In the command tracking program printout, the errors are in degrees rms due to a 10-degree rms phi command.

The example printouts illustrate "looping" the ϕ-pilot gain. The ψ-pilot gain may be "looped" in the same manner (for turbulence tracking).

```
CHECK CASE FOR BANK-ANGLE CLOSURE, GUST TRACKING

                    DIMENSIONAL DERIVATIVES...PRIME AXIS SYSTEM

YV= -0.61835152E 00   YDR= 0.91010928E-01   YDA=-0.17723188E-01   NB=  0.38409393E 02   NP=  0.15420353E 00
NR= -0.86833566E 00   NDR=-0.12069139E 02   NDA= 0.21127386E 01   LB= -0.74412857E 02   LP= -0.33302040E 01
LR=  0.76676259E 00   LDA= 0.28570419E 02   LDR= 0.13847437E 02

   S**2 DELTA
        -0.10000000E 01     -0.48168898E 01     -0.45077789E 02     -0.12143564E 03     -0.11998739E 01
         0.0                 0.0
   S**2 N/PHI/DA
        -0.28570419E 02     -0.45414047E 02     -0.12715522E 04      0.79306722E 00      0.0
   S**2 N/SI/DA
        -0.21130581E 01     -0.12069016E 02     -0.26911957E 02     -0.45441666E 02      0.0
   S**2 N/B/DR
        -0.91010928E-01     -0.12692935E 02     -0.38851944E 02     -0.76260149E-01      0.0
         0.0
   S**2 N/R/DR
         0.12069139E 02      0.42024643E 02      0.19327698E 02      0.13262909E 02      0.0
         0.0
   S**2 N/PHI/DA/B/DR
        -0.28456402E 01     -0.37653027E 03      0.23644635E 00      0.0
   S**2 N/SI/DA/B/DR
         0.21624625E-01     -0.68967104E 01     -0.13549208E 02      0.0
   S**2 N/R/DR/PHI/DA
         0.37407617E 03      0.12362022E 03      0.0                 0.0
   S**2 N/B/DGB
        -0.61835152E 00     -0.42304291E 02     -0.12143564E 03     -0.11998739E 01      0.0
         0.0
   S**2 N/B/DGB/PHI/DA
        -0.10985382E 02     -0.12715522E 04      0.79306722E 00      0.0
   S**2 N/B/DGB/SI/DA
        -0.62577200E 00     -0.26911957E 02     -0.45441666E 02      0.0
   S**2 N/B/DGB/R/DR
         0.35672956E 01      0.19327698E 02      0.13262909E 02      0.0                 0.0
   S**2 N/PHI/DGB
        -0.74412857E 02     -0.35164444E 02      0.15258789E-03      0.0                 0.0
   S**2 N/PHI/DGB/B/DR
         0.17902002E 01     -0.36771484E 03      0.23150486E 00      0.0
   S**2 N/PHI/DGB/SI/DA
        -0.12547771E 04     -0.24414063E-03      0.0
   S**2 N/PHI/DGB/R/DR
         0.36622754E 03      0.0                 0.0                 0.0
   S**2 N/SI/DGB
         0.38415207E 02      0.11645403E 03     -0.76293945E-05      0.0                 0.0
   S**2 N/SI/DGB/PHI/DA
         0.12547771E 04     -0.45776367E-04      0.0
   S**2 N/SI/DGB/B/DR
        -0.39678974E 01     -0.19330612E 02     -0.13264923E 02      0.0
```

FIGURE 51. LATERAL GUST OUTPUT EXAMPLE

```
   S**2 N/B/DGR
         0.8E1718I6E 00       0.28007154E C1      -0.17532213E-02       0.0                   0.0
   S**2 N/B/DGR/PHI/DA
         0.135E9479E-C1       0.26428665E 02      -0.16706455E-01       0.0
   S**2 N/B/DGR/SI/EA
        -0.15392005E-01       0.41217434E C0       0.45725799E 00       0.0
   S**2 N/B/DGR/R/DR
         0.790280I0E-01       0.30076510E C0       0.10031754E 00       0.0                   0.0
   S**2 N/PHI/DGR
         0.766762S5E CC       0.47412825E 0C      -0.35164429E 02       0.22228640E-01        0.0
   S**2 N/PHI/DGR/B/DR
         0.69783747E-C1      -0.2770C577E C1       0.17510466E-02       0.0
   S**2 N/PHI/DGR/SI/CA
         0.26432663E 02       0.16967587E C2       0.0
   S**2 N/PHI/DGR/R/DR
         0.27700586E 01      -0.14874783E C1       0.0                   0.0
   S**2 N/SI/DGR
        -0.86846733E 00      -0.33109341E 01      -0.23290815E 01      -0.12736721E 01        0.0
   S**2 N/SI/DGR/PHI/CA
        -0.26432663E 02      -0.169680C2E C2       0.0
   S**2 N/SI/DGR/B/DR
        -0.79039991E-01      -0.30081064E 00      -0.10033274E 00       0.0

PHI GAIN =   0.0            LEAD =   0.500          PSI GAIN =   0.0
                THE N/B/DGB NUMERATOR IS BELOW
       -0.30917573E 00      -0.35367371E C2      -0.12351550E 04      -0.211951I3E 05      -0.179944I3E 06
       -0.56865044E 06      -0.56144775E 06      -0.53327148E 04       0.0                   0.0
        0.0
                THE N/PHI/DGB NUMERATOR IS BELOW
       -0.37206421E 02      -0.16937025E 04      -0.33061699E 05      -0.303790S6E 06      -0.93688163E 06
       -0.15628431E 06       0.67816138E 00       0.0                  0.0                   0.0
                THE N/SI/DGB NUMERATOR IS BELOW
        0.19207596E C2       0.86494604E 03       0.16787840E 05       0.15445569E 06       0.90715631E 06
        0.51756800E 06      -0.33980069E-01       0.0                  0.0                   0.0
                THE N/B/DGR NUMERATOR IS BELOW
        0.41636038E 0C       0.18843216E 02       0.36790918E 03       0.34205173E 04       0.115739I4E 05
        0.12304211E 05      -0.77920132E 01       0.0                  0.0                   0.0
                THE N/PHI/DGR NUMERATOR IS BELOW
        0.38338125E 0C       0.15480349E 02       0.24475719E 03       0.109961I3E 04      -0.118597I5E 05
       -0.97421430E 05      -0.15622044E C6       0.98792923E 02       0.0                   0.0
                THE N/SI/DGR NUMERATOR IS BELOW
       -0.43423367E 0C      -0.19893265E 02      -0.39493579E 03      -0.379459S6E 04      -0.14321070E C5
       -0.21919113E 05      -0.1403C871E C5      -0.56607031E 04       0.0                   0.0
                THE OPEN LOOP DENOMINATOR FOR THE GUSTS IS BELOW
       -0.50000000E 00      -0.27149857E 02      -0.65972803E 03      -0.871613I8E 04      -0.632981I1E 05
       -0.25905544E C6      -0.580977C0E 06      -0.56144775E 06      -0.533271I8E 04       0.0
        0.0                  0.0
   THE POLES OF THE CLOSED-LOOP TRANSFER FUNCTIONS ARE BELOW IN REAL-IMAGINARY PAIRS
          0.0                  0.0                  0.0                  0.0                  0.0                   0.0
         -0.95930E-02          0.0                 -0.31623E 01          0.0                 -0.545S2E 01          0.0
         -0.28350E 01         -0.25410E 01         -0.28350E 01          0.25410E 01         -0.15477E 02          0.0
         -0.12261E 02         -0.11697E 02         -0.12261E 02          0.11697E 02
```

FIGURE 51. (Continued)

```
PHI GAIN =  -0.200          LEAD =   0.500          PSI GAIN =   0.0
                THE N/B/DGB NUMERATOR IS BELOW
      -0.30917573E 00     -0.34418091E 02     -0.12057510E 04      -0.22999152E 05     -0.14931794E 06
      -0.70620275E 06     -0.15389540E 07     -0.11349890E 07       0.70494116E 03      0.0
       0.0
                THE N/PHI/DGB NUMERATOR IS BELOW
      -0.37206421E 02     -0.16937825E 04     -0.33061699E 05      -0.30379056E 06     -0.93688163E 06
      -0.15628431E 06      0.67816138E 00      0.0                  0.0                 0.0
                THE N/SI/DGB NUMERATOR IS BELOW
       0.19207596E 02      0.80220703E 03      0.19046438E 05       0.12241494E 06      0.62871900E 06
       0.14656010E 07      0.11153450E 07     -0.40689677E-01       0.0                 0.0
                THE N/B/DGR NUMERATOR IS BELOW
       0.41568089E 00      0.17546234E 02      0.41513452E 03       0.27469482E 04      0.14145012E 05
       0.32282559E 05      0.23471480E 05     -0.14850026E 02       0.0                 0.0
                THE N/PHI/DGR NUMERATOR IS BELOW
       0.38338125E 00      0.15480349E 02      0.24475719E 03       0.10996113E 04     -0.11859715E 05
      -0.97421438E 05     -0.15622044E 06      0.98792923E 02       0.0                 0.0
                THE N/SI/DGR NUMERATOR IS BELOW
      -0.43423367E 00     -0.18571625E 02     -0.44166602E 03      -0.31501833E 04     -0.16448586E 05
      -0.43533887E 05     -0.50346305E 05     -0.20743211E 05       0.0                 0.0
                THE OPEN LOOP DENOMINATOR FOR THE GUSTS IS BELOW
      -0.50000000E 00     -0.25721329E 02     -0.69728760E 03      -0.84415820E 04     -0.60537230E 05
      -0.28639856E 06     -0.87889256E 06     -0.15965090E 07      -0.11349890E 07      0.70494116E 03
       0.0                 0.0
  THE POLES OF THE CLOSED-LOOP TRANSFER FUNCTIONS ARE BELOW IN REAL-IMAGINARY PAIRS
         0.0                 0.0                 0.0                  0.0                 0.62056E-03         0.0
        -0.15058E 01         0.0                -0.54868E 01          0.0                -0.33443E 01        -0.26760E 01
        -0.33443E 01         0.26760E 01        -0.16009E 01         -0.44448E 01        -0.16009E 01         0.44448E 01
        -0.17280E 02        -0.19314E 02        -0.17280E 02          0.19314E 02


                        RMS ERROR CALCULATIONS DUE TO BETA-GUST
          PHI GAIN              LEAD                DELAY             BETA ERROR          PHI ERROR           SI ERROR
          0.0                 0.5000E 00          0.3000E 00          0.7018E 00          0.1148E 01          0.64C7E 00
         -0.2000E 00          0.5000E 00          0.3000E 00          0.0                 0.0                 0.0


                        RMS ERROR CALCULATIONS DUE TO BETA-GUST PLUS R-GUST
          PHI GAIN          BETA ERROR          PHI ERROR           SI ERROR
          0.0               0.6982E 00          0.1228E 01          0.6290E 00
         -0.2000E 00        0.0                 0.0                 0.0
```

FIGURE 51. (Concluded)

```
                CHECK CASE FOR BANK-ANGLE CLOSURE, COMMAND TRACKING


                        DIMENSIONAL DERIVATIVES...PRIME AXIS SYSTEM

YV= -0.61835152E 00   YDR= 0.91010928E-01   YDA=-0.17723188E-01   NB=  0.38409393E 02   NP=  0.15420353E 00

NR= -0.86833566E 00   NDR=-0.12069139E 02   NDA= 0.21127386E 01   LB= -0.74412857E 02   LP= -0.33302040E 01

LR=  0.76676255E 00   LDA= 0.28570419E 02   LDR= 0.13847437E 02


PHI GAIN =   0.0

                    THE SI PER SI ERROR TRANSFER FUNCTION IS BELOW
   NUMERATOR
        -0.10565290E 01      -0.12842779E 02      -0.61732758E 02      -0.16306581E 03      -0.26600952E 03
        -0.20194272E 03       0.0
   DENOMINATOR
        -0.50000000E 00      -0.93718758E 01      -0.72157440E 02      -0.29125098E 03      -0.62292871E 03
        -0.56179712E 03      -0.53322382E 01       0.0                  0.0
                    THE PHI PER PHI ERROR TRANSFER FUNCTION IS BELOW
   NUMERATOR
        -0.71426048E 01      -0.66164017E 02      -0.91904358E 02       0.98688354E 03       0.47512500E 04
         0.56480391E 04      -0.35243893E 01       0.0
   DENOMINATOR
        -0.50000000E 00      -0.93718758E 01      -0.72157440E 02      -0.29125098E 03      -0.62292871E 03
        -0.56179712E 03      -0.53322382E 01       0.0                  0.0
                    THE B PER A ERROR TRANSFER FUNCTION IS BELOW
   NUMERATOR
        -0.45505464E-01      -0.66397038E 01      -0.60727036E 02      -0.18162642E 03      -0.17290370E 03
        -0.33890003E 00       0.0                  0.0
   DENOMINATOR
        -0.50000000E 00      -0.93718758E 01      -0.72157440E 02      -0.29125098E 03      -0.62292871E 03
        -0.56179712E 03      -0.53322382E 01       0.0                  0.0
   THE CLOSED-LOOP POLES OF THE PHI/PHI-COMMAND TRANSFER FUNCTION ARE BELOW IN REAL-IMAGINARY PAIRS
             0.0                  0.0                  0.0                  0.0                 -0.95930F-02          0.0
            -0.31625E 01          0.0                 -0.44436E 01          0.0                 -0.54580E 01          0.0
            -0.28350F 01         -0.25410E 01         -0.28350F 01          0.2541OF 01
```

FIGURE 52. LATERAL COMMAND TRACKING OUTPUT EXAMPLE

```
PHI GAIN =  -0.2C0

                THE SI PER SI ERROR TRANSFER FUNCTION IS BELOW
  NUMERATOR
      -0.10565290E 01     -0.12842779E 02     -0.61732758E 02     -0.16306581E 03     -0.26600952E 03
      -0.20194272E 03      0.0
  DENOMINATOR
      -0.50000000E 00     -0.79433556E 01     -0.58924637E 02     -0.27287012E 03     -0.82030518E 03
      -0.15120474E 04     -0.11349397E 04      0.70487779E 00      0.0
                THE PHI PER PHI ERROR TRANSFER FUNCTION IS BELOW
  NUMERATOR
      -0.7142604AE 01     -0.66164017E 02     -0.91904358E 02      0.98688354E 03      0.47512500E 04
       0.56480391E 04     -0.35243893E 01      0.0
  DENOMINATOR
      -0.50000000E 00     -0.93718758E 01     -0.72157440E 02     -0.2912509AE 03     -0.62292871E 03
      -0.56179712E 03     -0.53223882E 01      0.0                 0.0
                THE B PER B ERROR TRANSFER FUNCTION IS BELOW
  NUMERATOR
      -0.45505464E-01     -0.64974213E 01     -0.41963699E 02     -0.19195721E 03     -0.43478125E 03
      -0.33483594E 03      0.21017110E 00      0.0
  DENOMINATOR
      -0.50000000E 00     -0.79433556E 01     -0.58924637E 02     -0.27287012E 03     -0.82030518E 03
      -0.15120474E 04     -0.11349397E 04      0.70487779E 00      0.0
  THE CLOSED-LOOP POLES OF THE PHI/PHI-COMMAND TRANSFER FUNCTION ARE BELOW IN REAL-IMAGINARY PAIRS
        0.0                 0.0                 0.62056E-03         0.0                 -0.16402E 01        0.0
       -0.54763E 01         0.0                 -0.32669E 01        -0.24500E 01        -0.32669E 01        0.24500E 01
       -0.11186E 01         -0.37305E 01        -0.11186E 01        0.37305E 01


                THE RMS ERROR CALCULATIONS ARE BELOW
        PHI GAIN            LEAD                DELAY               PHI ERROR
       0.0                 0.5000E 00          0.4500E 00          0.1000E 02
      -0.2000E 00          0.5000E 00          0.4500E 00          0.0
```

FIGURE 52. (Concluded)

APPENDIX II

SIMULATOR DATA

LIST OF SYMBOLS FOR APPENDIX II

A_{y_p} - Side acceleration at the pilot's station, ft/sec^2

A_{z_p} - Normal acceleration at the pilot's station, ft/sec^2

$A_{gust}, B_{gust}, C_{gust}, D_{gust}, E_{gust}, F_{gust}, X_{gust}, Y_{gust}, Z_{gust}$ - Gust filter constants, $1/sec$ or $1/sec^2$

A_{tc} - Tracking filter time constant, $1/sec$

b - Airplane wing span, ft

$C_D = D/\frac{1}{2}\rho V_o^2 S$, Airplane drag coefficient

C_{D_o} - Drag coefficient at trim angle of attack

$C_{D_\alpha} = \partial C_D/\partial\alpha$, Nondimensional drag coefficient derivative with respect to angle of attack, $1/rad$

$C_L = L/\frac{1}{2}\rho_o V_o^2 S$, Airplane lift coefficient

C_{L_o} - Lift coefficient at trim angle of attack

$C_{L_\alpha} = \partial C_L/\partial\alpha$, Nondimensional lift coefficient derivative with respect to angle of attack, $1/rad$

$C_{L_{\delta_e}} = \partial C_L/\partial\delta_e$, Nondimensional lift coefficient derivative with respect to elevator control, $1/rad$

D - Airplane drag, lb

g - Acceleration due to gravity, ft/sec^2

h - Altitude, ft

I_x - Moment of inertia about x-axis, ft-lb-sec^2

I_{xz} - Product of inertia in xz-plane, ft-lb-sec^2

I_y - Moment of inertia about y-axis, ft-lb-sec^2

I_z - Moment of inertia about z-axis, ft-lb-sec^2

K = $\left[1 - (I_{xz}^2/I_x I_z)\right]^{-1}$

K_{ari} - Aileron-rudder interconnect gain

K_{a_z} - Fuselage bending constant, rad/g

$K_{a_{z_{aug}}}$ - Pitch augmenter gain, rad/ft/sec

K_{gust} - Gust filter gain for α and β gust filters, rad/volt

$K_{p_{aug}}$ - Roll augmenter gain, rad-sec

K_{p_θ} - Simulator-beam vertical drive signal compensation gain term, rad/volt

K_{p_ψ} - Simulator-beam lateral drive signal compensation gain term, rad/volt

$K_{q_{aug}}$ - Pitch augmenter gain, rad-sec

$K_{\dot{q}_{aug}}$ - Pitch augmenter gain, rad-sec^2

$K_{r_{aug}}$ - Yaw augmenter gain, rad-sec^2

K_{tc} - Tracking filter gain, rad/volt-sec^2

K_θ - Simulator-cockpit pitch drive signal gain

$K_{\ddot{\theta}}$ - Simulator-beam vertical drive signal washout gain

K_{θ_M} - Simulator-cockpit pitch drive signal compensation gain term, rad/volt

K_{ϕ} - Simulator-cockpit roll drive signal washout gain

K_{ϕ_M} - Simulator-cockpit roll drive signal compensation gain term, rad/volt

K_{ψ} - Simulator-cockpit yaw drive signal washout gain

$K_{\ddot{\psi}}$ - Simulator-beam lateral drive signal washout gain

K_{ψ_M} - Simulator-cockpit yaw drive signal compensation gain term, rad/volt

ℓ_B - Distance between simulator cockpit gimbal center and simulator beam gimbal center, ft

ℓ_x - Distance from airplane center of gravity to the pilot's station along the x-axis, ft

L - Rolling moment, ft-lb; Lift, lb

$L'_i = K\left[L_i + (I_{xz}/I_x)\, N_i\right]$; $i = \beta, p, r, \delta_a, \delta_r$

$L_p = (1/I_x)\,(\partial L/\partial p)$, 1/sec

$L_r = (1/I_x)\,(\partial L/\partial r)$, 1/sec

$L_\beta = (1/I_x)\,(\partial L/\partial \beta)$, $1/sec^2$

$L_{\delta_a} = (1/I_x)\,(\partial L/\partial \delta_a)$, $1/sec^2$-rad

$L_{\delta_r} = (1/I_x)\,(\partial L/\partial \delta_r)$, $1/sec^2$-rad

m - W/g, lb-sec^2/ft

M - Pitching moment, ft-lb

$M_q = (1/I_z)\,(\partial M/\partial q)$, 1/sec

$M_\alpha = (1/I_z)\,(\partial M/\partial \alpha)$, $1/sec^2$

$M_{\dot{\alpha}} = (1/I_z)\,(\partial M/\partial \dot{\alpha})$, 1/sec

$M_{\delta_e} = (1/I_z)\,(\partial M/\partial \delta_e)$, $1/sec^2$

N - Yawing moment, ft-lb

N'_i = $K\left[N_i + (I_{xz}/I_x)\, L_i\right]$; $i = \beta, p, r, \delta_a, \delta_r$

N_g - Noise generator signal, Gaussian, 50 Hz bandwidth, infinite random sequence length

N_p = $(1/I_z)\,(\partial N/\partial p)$, 1/sec

N_r = $(1/I_z)\,(\partial N/\partial r)$, 1/sec

$N_{y_{cg}}$ - Side acceleration at airplane center of gravity, g units

$N_{z_{cg}}$ - Normal acceleration at airplane center of gravity, g units

N_β = $(1/I_z)\,(\partial N/\partial \beta)$, $1/sec^2$

N_{δ_a} = $(1/I_z)\,(\partial N/\partial \delta_a)$, $1/sec^2$-rad

N_{δ_r} = $(1/I_z)\,(\partial N/\partial \delta_r)$, $1/sec^2$-rad

p - Roll rate, rad/sec

q - Pitch rate, rad/sec

q_o - $(1/2)\rho\, V_o^2$, dynamic pressure, lbs/ft^2

r - Yaw rate, rad/sec

s - Laplace operator, 1/sec

S - Wing area, ft^2

T_x - Thrust, lb

T_{θ_1} - Simulator-beam vertical drive signal rate washout constant, sec

T_{θ_2} - Simulator-beam vertical drive signal position washout constant, sec^2

T_{ψ_1} - Simulator-beam lateral drive signal rate washout constant, sec

T_{ψ_2} - Simulator-beam lateral drive signal position washout constant, sec^2

V - True airspeed, ft/sec

V_o	- Initial true airspeed, ft/sec
ΔV	- Perturbation true airspeed, ft/sec
W	- Airplane weight, lb
x,y,z	- Stability axes (i.e., a right hand orthogonal body-axis system with origin at the center of gravity, the z-axis in the plane of symmetry, and the x-axis aligned with the relative wind of zero sideslip trimmed flight)
X	- Force in x-direction, lb
Y	- Force in y-direction, lb
Y_v	= $(1/m V_o)(\partial Y/\partial \beta)$, 1/sec
$Y^*_{\delta_r}$	= $(1/m V_o)(\partial Y/\partial \delta_r)$, 1/sec-rad
Z	- Force in z-direction, lb
α	- Angle of attack perturbation from trim, rad
β	- Angle of sideslip, rad
δ_a	- Aileron deflection, rad. Positive right aileron up
$\delta_{a_{comm}}$	- Commanded aileron deflection, inches of control deflection at stick grip, positive to right
δ_e	- Elevator deflection, rad. Positive trailing edge up
$\delta_{e_{comm}}$	- Commanded elevator deflection, inches of control deflection at stick grip, positive forward
δ_r	- Rudder deflection, rad. Positive trailing edge left
$\delta_{r_{comm}}$	- Commanded rudder deflection, inches of pedal travel, positive left pedal forward
$\Delta\delta_{a_{aug}}$	- Increment in aileron deflection due to roll augmenter, rad
$\Delta\delta_{e_{aug}}$	- Increment in elevator deflection due to pitch augmenter, rad
$\Delta\delta_{e_{bend}}$	- Increment in elevator deflection due to fuselage bending, rad

$\Delta\delta_{r_{aug}}$ - Increment in rudder deflection due to yaw augmenter, rad

$\Delta\delta_{r_i}$ - Increment in rudder deflection due to aileron-rudder interconnect, rad

θ - Pitch angle, rad

θ_{BD} - Washed-out simulator-beam vertical drive signal with compensation

θ_{BW} - Washed-out simulator-beam vertical drive signal without compensation

θ_C - Simulator-cockpit pitch drive signal with compensation

θ_M - Simulator-cockpit pitch drive signal without compensation

ρ - Atmospheric density, lbs-sec^2/ft^4

$\tau_{q_{aug}}$ - Pitch augmenter time constant, sec

$\tau_{r_{aug}}$ - Yaw augmenter time constant, sec

τ_1, τ_2 - Simulator-beam lateral drive signal compensation time constants, sec

τ_3, τ_4 - Simulator-beam vertical drive signal compensation time constants, sec

τ_{θ_M} - Simulator-cockpit pitch drive signal compensation time constant, sec

τ_{ϕ_M} - Simulator-cockpit roll drive signal compensation time constant, sec

τ_{ϕ_W} - Simulator-cockpit roll drive signal washout time constant, sec

τ_{ψ_M} - Simulator-cockpit yaw drive signal compensation time constant, sec

τ_{ψ_W} - Simulator-cockpit yaw drive signal washout time constant, sec

ϕ - Roll angle, rad

ϕ_C	- Washed-out simulator-cockpit roll drive signal with compensation
ϕ_M	- Washed-out simulator-cockpit roll drive signal without compensation
ψ	- Yaw angle, rad
ψ_{BD}	- Washed-out simulator-beam lateral drive signal with compensation
ψ_{BW}	- Washed-out simulator-beam lateral drive signal without compensation
ψ_C	- Washed-out simulator-cockpit yaw drive signal with compensation
ψ_M	- Washed-out simulator-cockpit yaw drive signal without compensation

APPENDIX II. SIMULATOR DATA

INTRODUCTION

The following discussion presents the experiments performed on the Northrop Large Amplitude Flight Simulator. The simulator dynamics and the tasks were carefully controlled to provide the best possible data. Descriptions of the simulator and equations programmed follow.

SIMULATION

An external view of the Northrop 3-Axis Large Amplitude Flight Simulator is shown in Figure 82 of Reference 1. The motion system of the moving base simulator employs a gimbaled cockpit suspended at the end of a beam as shown. The three rotational degrees of freedom are obtained through the gimbals. The beam is pivoted on a clevis and driven by front and rear hydraulic actuators to provide vertical translation. Lateral translation is derived through a pivoting mechanism between the clevis and the post, driven by hydraulic actuators.

A satisfactory level of fidelity in the output characteristics of the simulator response must be achieved within the limitations imposed by the following constraints:

1. Available hydraulic power imposes magnitude limits on acceleration and velocity motion response.
2. Total travel of the simulators sets limits on displacement.
3. The motion control servo sets upper and lower limits on the dynamic response of the simulator.
4. Coulomb and breakaway friction exist in the output of the servodrive. The motion performance capability of the simulator is summarized in Figure 53. Figure 54 shows a typical response of the simulator translation motion system to sinusoidal inputs, and indicates how velocity saturation sets amplitude limits on motion response over midrange frequencies. Acceleration saturation determines amplitude limits at high frequencies, and position saturation sets displacement limits at low frequency.

				TWO-PLACE COCKPIT –		ONE-PLACE COCKPIT –	
				BEAM STATIONARY	BEAM MAX ACCEL	BEAM STATIONARY	BEAM MAX ACCEL
		DISPLACE-MENT	VELOCITY	ACCEL-ERATION	ACCEL-ERATION	ACCEL-ERATION	ACCEL-ERATION
BEAM	VERTICAL	±10 FEET	±16.2 FT/SEC	–	±4.8 g	–	±5.8 g
	LATERAL	±4 FEET	±21.6 FT/SEC	–	±1.8 g	–	±2.2 g
COCKPIT	PITCH	±30°	±1.1 RAD/SEC	±24.4 RAD/SEC^2	±14.4 RAD/SEC^2	SAME AS TWO--PLACE COCKPIT	
	YAW	±30°	±1.5 RAD/SEC	±20.3 RAD/SEC^2	±15.0 RAD/SEC^2		
	ROLL	±45°	±2.7 RAD/SEC	±35.3 RAD/SEC^2	±29.1 RAD/SEC^2		

FIGURE 53. PERFORMANCE SUMMARY, LARGE AMPLITUDE 3-AXIS FLIGHT SIMULATOR

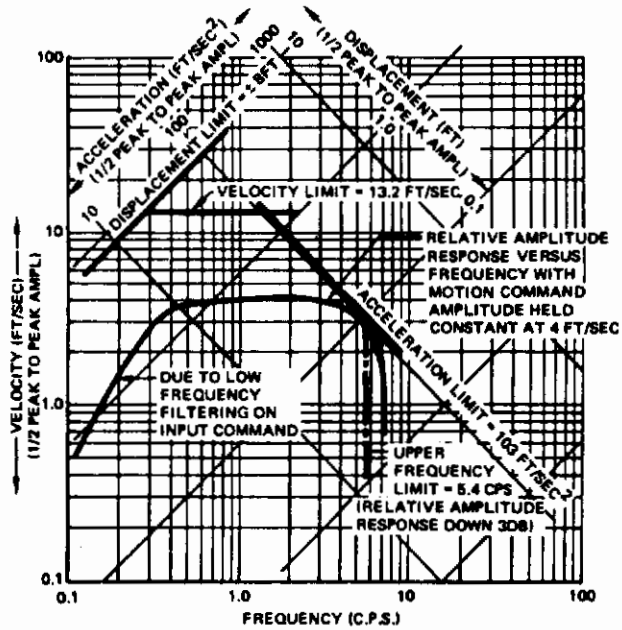

FIGURE 54. RESPONSE OF VERTICAL TRANSLATED MOTION SYSTEM AT PILOT'S STATION TO STEADY SINUSOIDAL MOTION

An external visual display is also available for use with the simulator. However, all experiments were performed under instrument flight rules and no external visual display was used.

A pictorial description of the drive philosophy is given in Figure 55 . Note that the essential requirements are that beam movements provide linear acceleration cues and that cab movements provide rotational and attitude cues. In practice, the drive system filters must be "tuned" to provide the maximum possible fidelity within the limits of the equipment. Since the tasks involved in this simulation required no large amplitude maneuvers, very good motion cues could be obtained without fear of reaching simulator limits. The frequency response obtained by "tuning" the simulation is given in Figure 56. Details of the drive equation and vehicle dynamics are given in Tables II through XIV of Reference 1. Note that the full five degrees of freedom of the simulator were used in conjunction with the six-degree-of-freedom representation of the vehicle on the analog computers.

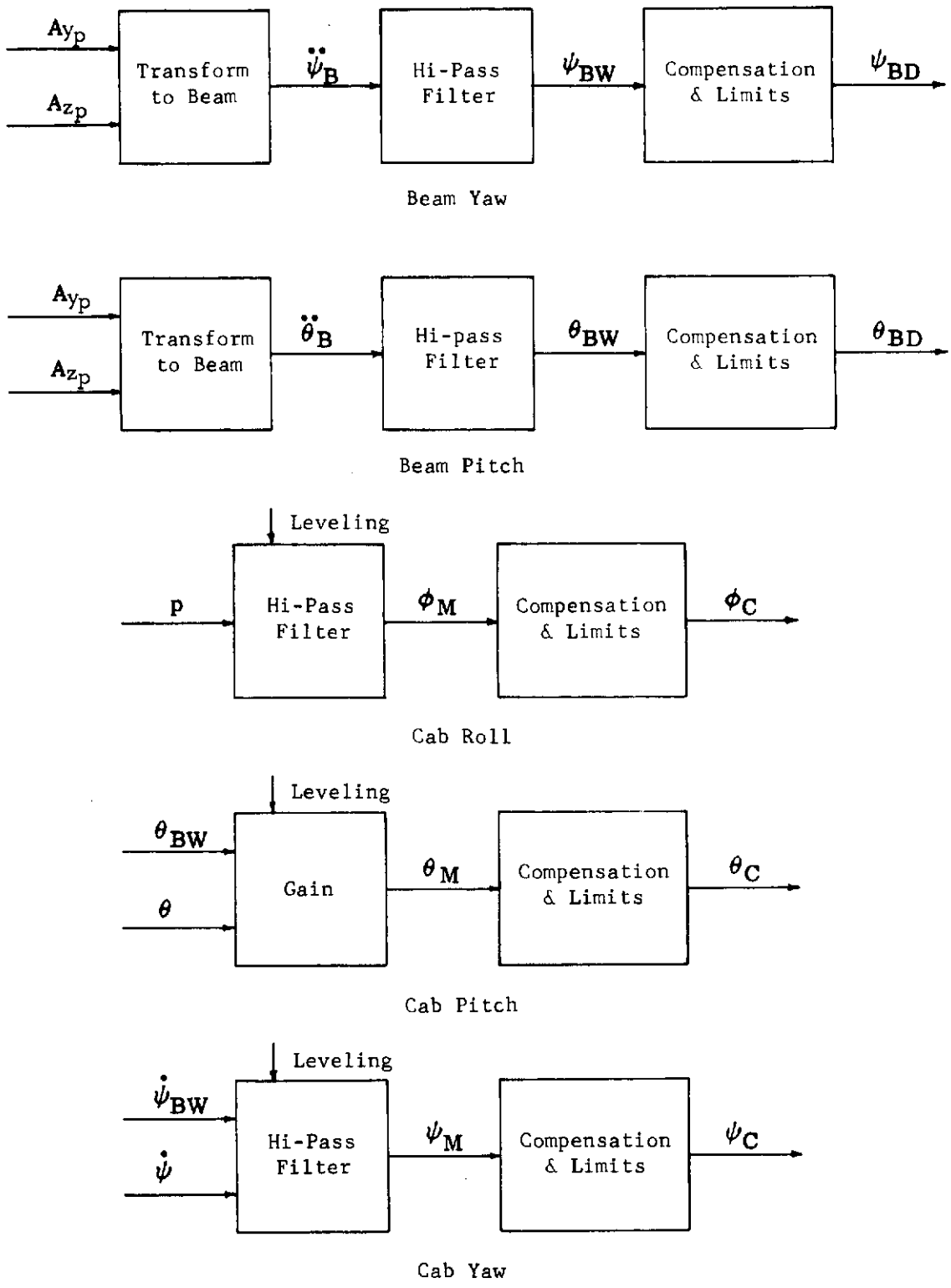

FIGURE 55. SIMULATOR DRIVE PHILOSOPHY

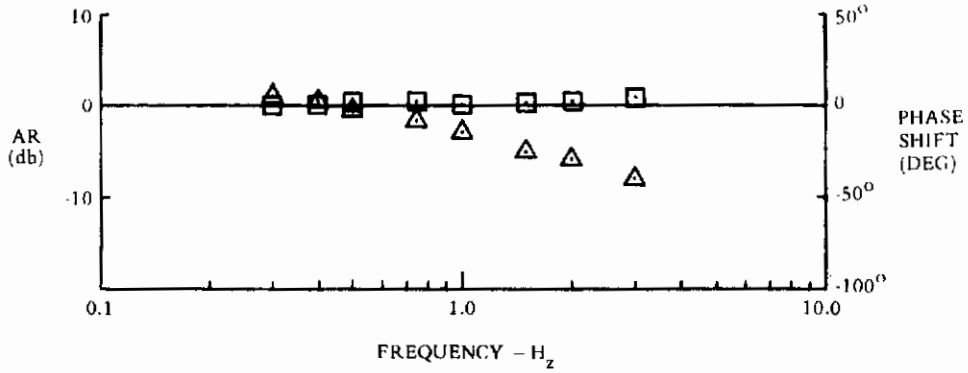

CAB PITCH

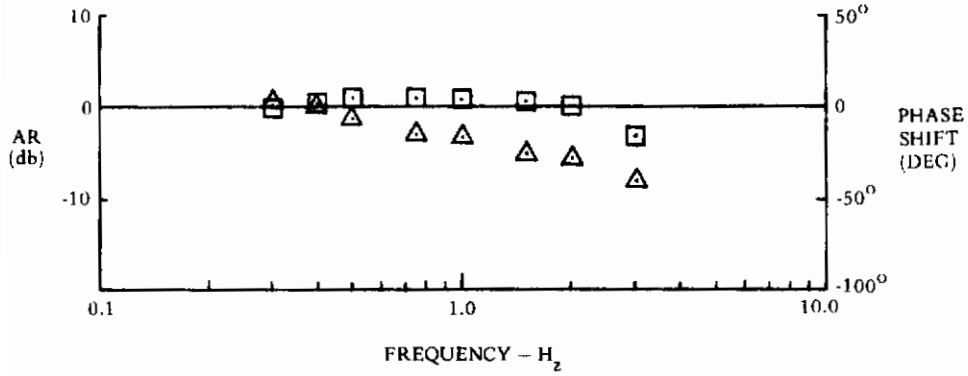

CAB YAW

△ PHASE

⊡ AMPLITUDE

FIGURE 56. SIMULATOR FREQUENCY RESPONSE

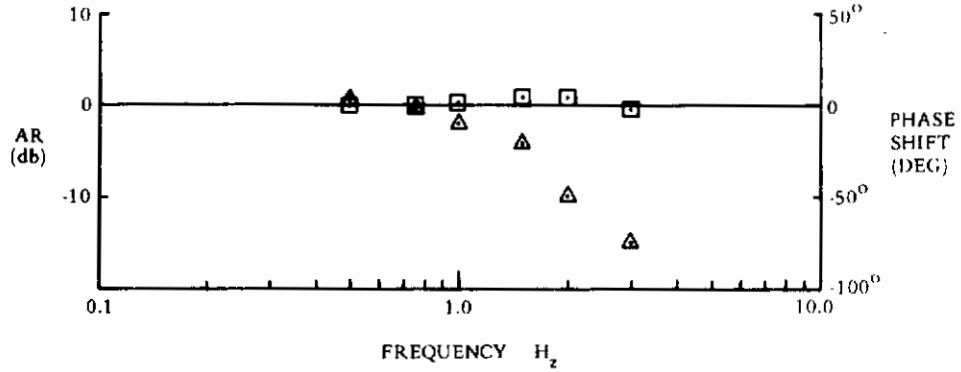

BEAM YAW

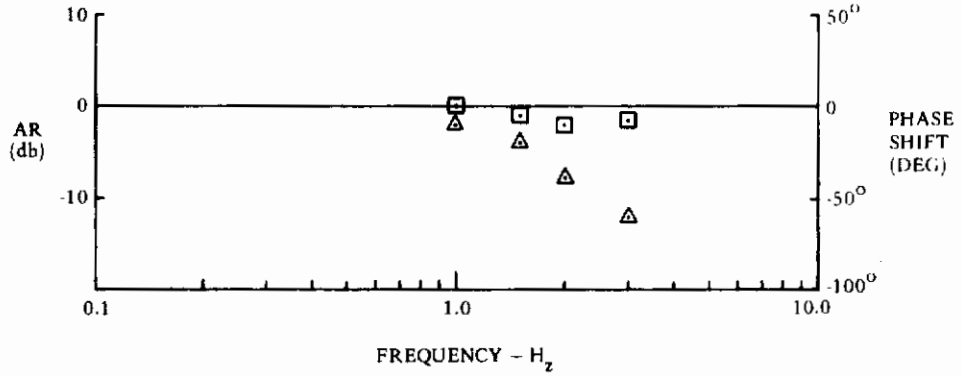

BEAM PITCH

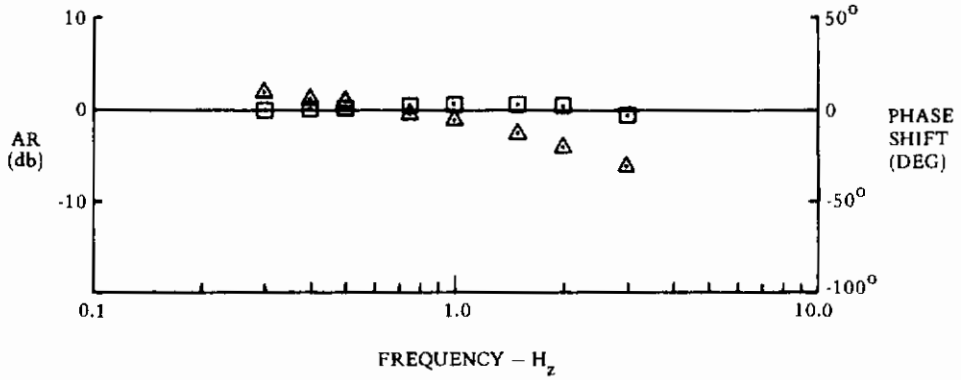

CAB ROLL

FIGURE 56 SIMULATOR FREQUENCY RESPONSE (Concluded)

$$\dot{\beta} = \frac{Y}{mV_o} + \frac{g \sin \phi}{V_o} + \alpha_{iner}\, p_{iner} - r_{iner}$$

$$\beta_{iner} = \int \dot{\beta}\, dt$$

$$\beta_{aero} = \beta_{iner} + \beta_{gust}$$

$$\frac{Y}{mV_o} = Y_v \beta_{aero} + Y^*_{\delta_r} \delta_r$$

$$\dot{p} = L'_\beta \beta_{aero} + L'_p p_{aero} + L'_r r_{aero} + L'_{\delta_a} \delta_a + L'_{\delta_r} \delta_r$$

$$p_{iner} = \int \dot{p}\, dt$$

$$p_{aero} = p_{iner} + p_{gust}$$

$$\dot{r} = N'_\beta \beta_{aero} + N'_p p_{aero} + N'_r r_{aero} + N'_{\delta_a} \delta_a + N'_{\delta_r} \delta_r$$

$$r_{iner} = \int \dot{r}\, dt$$

$$r_{aero} = r_{iner} + r_{gust}$$

$$a_{y_p} = \dot{V}\beta_{aero} + \ell_x \dot{r} - g \sin \phi + V_o (\dot{\beta} + r_{iner})$$

$$N_{y_{cg}} = \frac{a_{y_p}}{g} - \frac{\ell_x \dot{r}}{g}$$

$$\frac{\Delta\delta_{r_{aug}}}{r_{iner}} = \frac{K_{r_{aug}}\, s}{\tau_{r_{aug}}\, s + 1}$$

$$\frac{\Delta\delta_{a_{aug}}}{p_{iner}} = K_{p_{aug}}$$

$$\Delta\delta_{r_i} = K_{ari}\,\delta_a$$

$$\delta_a = \left(K_{a_1} + \frac{K_{a_2}}{s+3}\right)\delta_{a_{comm}} + \Delta\delta_{a_{aug}}$$

$$\delta_r = K_r\,\delta_{r_{comm}} + \Delta\delta_{r_{aug}} + \Delta\delta_{r_i}$$

LONGITUDINAL AIRFRAME EQUATIONS

$$\dot{V} = \frac{X}{m} + \frac{T_x}{m} - g\theta + g\alpha_{iner}\cos\phi$$

$$\Delta V_{iner} = \int \dot{V}\, dt$$

$$\Delta V_{aero} = \Delta V_{iner} + V_{gust}$$

$$V = V_o + \Delta V_{aero}$$

$$X = -q_o S\,(C_{D_o} + C_{d_\alpha}\alpha) - \frac{2q_o S \Delta V_{aero}}{V_o}\,(C_{D_o} + C_{d_\alpha}\alpha)$$

$$\frac{T_x}{m} = \text{constant}$$

$$\dot{\alpha} = \frac{Z}{V_o m} + \frac{g\cos\phi}{V_o} + q_{iner}$$

$$\alpha_{iner} = \int \dot{\alpha}\, dt$$

$$\alpha_{aero} = \alpha_{iner} + \alpha_{gust}$$

$$Z = -q_o S\,(C_{L_o} + C_{L_\alpha}\alpha_{aero} + C_{L_{\delta_e}}\delta_e) - \frac{2q_o S \Delta V_{aero}}{V_o}\,(C_{L_o} + C_{L_\alpha}\alpha_{aero})$$

$$\dot{q} = M_\alpha \alpha_{aero} + M_{\delta_e}\delta_e + M_{\dot{\alpha}}\dot{\alpha} + M_q q_{aero}$$

$$q_{iner} = \int \dot{q}\, dt$$

$$q_{aero} = q_{iner} + q_{gust}$$

$$a_{z_p} = \dot{V}\alpha_{iner} - \ell_x \dot{q} - g\cos\phi - V_o(q_{iner} - \dot{\alpha})$$

$$N_{z_{cg}} = -\frac{a_{z_p}}{g} - \frac{\ell_x \dot{q}}{g}$$

$$\Delta\delta_{e_{aug}} = \left(\frac{K_{q_{aug}}\, s}{\tau_{q_{aug}}\, s + 1} + K_{q_{aug}}\right) q_{iner} + K_{a_{z_{aug}}} \Delta a_{z_p}$$

$$\Delta\delta_{e_{bend}} = K_{a_z}(N_{z_{cg}} - 1.0)$$

$$\dot{h} = V\theta - \alpha_{iner}\cos\phi - \beta_{iner}\sin\phi$$

$$\delta_e = \left(K_{e_1} + \frac{K_{e_2}}{s + 2}\right)\delta_{e_{comm}} + \Delta\delta_{e_{aug}} + \Delta\delta_{e_{bend}}$$

SIMULATOR COCKPIT EQUATIONS

$$\phi_M = \frac{K_\phi (p - \dot{\theta} \tan \psi) + \dot{\psi}_{BW} \sin (\theta_M + \theta_{BW})}{s + \frac{1}{\tau_{\phi_W}}}$$

$$\phi_C = \frac{(\tau_{\phi_M} s + 1) \phi_M}{K_{\phi_M}}$$

$$\dot{\theta}_M + \dot{\theta}_{BW} = \frac{K_\theta \dot{\theta}}{\cos \psi} - \psi_{BW} \sin (\theta_M + \theta_{BW}) \sin \psi_M$$

$$\theta_C = \frac{(\tau_{\theta_M} s + 1) \theta_M}{K_{\theta_M}}$$

$$\psi_M = \frac{K_\psi \dot{\psi} - \dot{\psi}_{BW} \cos (\theta_M + \theta_{BW}) \cos \psi_M}{s + \frac{1}{\tau_{\psi_W}}}$$

$$\psi_C = \frac{(\tau_{\psi_M} s + 1) \psi_M}{K_{\psi_M}}$$

SIMULATOR DATA

ℓ_B	=	23.34 ft
$\tau_1 \tau_2$	=	0.762 sec^2
$\tau_1+\tau_2$	=	1.310 sec
$1/K_{p_\psi}$	=	261 volts/rad
T_{ψ_1}	=	0.500 sec
T_{ψ_2}	=	0.200 sec
$K_{\dot{\psi}}$	=	0.200 (bank angle task)
	=	0.080 (heading and pitch angle tasks)
$\tau_3 \tau_4$	=	0.080 sec^2
$\tau_3+\tau_4$	=	1.234 sec
$1/K_{p_\theta}$	=	121.7
T_{θ_1}	=	0.100 sec
T_{θ_2}	=	0.03185 sec^2
$K_{\dot{\theta}}$	=	0.100 (bank angle and heading tasks)
	=	0.500 (pitch angle task)
K_ϕ	=	0.400
τ_{ϕ_W}	=	1.00 sec
τ_{ϕ_M}	=	0.473 sec
$1/K_{\phi_M}$	=	60.4 volts/rad
K_θ	=	0.400
τ_{θ_M}	=	1.220 sec
$1/K_{\theta_M}$	=	115.5 volts/rad
K_ψ	=	0.400
τ_{ψ_W}	=	2.000 sec
τ_{ψ_M}	=	0.355 sec
$1/K_{\psi_M}$	=	123.0 volts/rad

GUST SIMULATION

$$\alpha_{gust} = \beta_{gust} = (N_g)(K_{gust}) \frac{A_{gust}\, s + 1}{B_{gust}\, s^2 + C_{gust}\, s + 1}$$

$$r_{gust} = \frac{s}{D_{gust}\, s + 1} \beta_{gust}$$

$$p_{gust} = (N_g) \frac{E_{gust}}{F_{gust}\, s + 1}$$

$$V_{gust} = (N_g) \frac{X_{gust}}{Y_{gust}\, s + 1}$$

$$q_{gust} = \frac{s}{Z_{gust}\, s + 1} \alpha_{gust}$$

TRACKING SIGNAL

$$\theta_{tc}, \phi_{tc}, \text{ or } \psi_{tc} = (N_g) \frac{K_{tc}}{(s + A_{tc})^2}$$

ROOT MEAN SQUARE COMPUTATIONS

$$x_{ms} = \frac{1}{100} \int_0^{100} \left[x(t)\right]^2 dt \qquad \text{(Analog Computer)}$$

$$x_{rms} = (x_{ms})^{1/2} \qquad \text{(Digital Calculation)}$$

Lateral task, x(t): $V_o \beta_{gust}, r_{gust}, \beta_{iner}, r_{iner}, \phi, \phi_\epsilon, \psi, \psi_\epsilon, \phi_{tc}$

Longitudinal task, x(t): $V_o \alpha_{gust}, q_{gust}, V_{gust}, \alpha_{iner}, q_{iner}, \theta_\epsilon, \theta_{tc}$

SIMULATOR COCKPIT INSTRUMENTS

Attitude Director Indicator (ADI)

Pitch Indicator:	θ
Roll Indicator:	ϕ
Steering Bar:	
(Tracking Command Display)	$\phi_\epsilon = \phi - \phi_{tc}$
or	$\psi_\epsilon = \psi - \psi_{tc}$
or	$\theta_\epsilon = \theta - \theta_{tc}$
Horizontal Situation Indicator (HSI):	ψ
Airspeed Indicator:	$V_o + \Delta V$
Altimeter:	$\int \dot{h}\, dt + h_o$
Vertical Velocity Indicator:	$\dot{h}$
G-meter	$N_{z_{cg}}$

APPENDIX III

PILOT RESUMÉS

AERODYNAMIC AND CONTROL DATA FOR THE F-5 AND THE A-7 SIMULATION

APPENDIX III

PILOT RESUMÉS

AERODYNAMIC AND CONTROL DATA FOR
THE F-5 AND THE A-7 SIMULATION

J. B. JORDAN (J. B. J.)

Mr. Jordan, who recently joined Northrop Corporation, has had over 18 years and 6000 hours of pilot experience with the United States Air Force. Ten years of this has been in the field of Engineering Flight Test. He is a graduate of USAF Aerospace Research Pilots School and the USAF Fighter Weapons School, and has been involved with many flight test programs, including the F-105 and F-111A airplanes.

W. W. KOEPCKE (W. W. K.)

Mr. Koepcke is currently employed in the Northrop Aircraft Division Research and Development department. At Northrop he has participated as an engineer-pilot in several conventional aircraft and VTOL simulation studies, including an auto-rotation and stability augmentation failure study of the CH-46 helicopter, and A-X dive bombing evaluations. He has flown the Northrop T-38A and F-5B, and the experimental S-1. Prior to joining Northrop, he served in the U. S. Navy as an operational pilot with the fleet and as a test pilot at the Naval Air Test Center, Patuxent River, Maryland. He is a graduate of the U. S. Naval Test Pilot School. He holds conventional airplane and helicopter commercial flying licenses, and has approximately 4000 hours of flying time.

J. T. THOMAS (J. T. T.)

Mr. Thomas has 23 years of experience in military aviation with the U. S. Air Force, and is presently Manager of Tactical Requirements in Tactical Operations Analysis at Northrop. His flying experience includes 5300 hours in numerous fighters and trainers, including the F-86, F-84 and F-100 airplanes.

SIMULATION MECHANIZATION

The following Figures, 57 through 62, include all relevant details of the simulation.

	F-5				A-7			
	CASE 1	CASE 2	CASE 3	CASE 4	CASE 1	CASE 2	CASE 3	CASE 4
Altitude, ft.	5,135	4,950	5,000	32,150	15,000	15,000	35,000	35,000
Mach No.	0.81	0.40	0.90	0.80	0.6	0.9	0.6	0.9
V_o, ft/sec	889	439	988	789	635	952	584	876
q_o, lbs/ft^2	804.4	197.5	998.2	255.1	301	677	126	283
m, slugs	354	346	343	372	680	680	680	680
S, ft^2	170	170	170	170	375	375	375	375
l_x, ft	12	12	12	12	16	16	16	16
c, ft	7.73				10.8			
b, ft	25.25				38.7			
I_x, slug-ft^2	4,200				13,635			
I_y, slug-ft^2	32,000				58,966			
I_z, slug-ft^2	33,000				67,560			
I_{xz}, slug-ft^2	-200				2,933			

FIGURE 57. F-5 AND A-7 FLIGHT CONDITIONS

	F-5				A-7			
	CASE 1	CASE 2	CASE 3	CASE 4	CASE 1	CASE 2	CASE 3	CASE 4
L'_β, $1/sec^2$	-74.8	-22.4	-102.1	-27.6	-29.2	-66.0	-14.90	-30.6
L'_p, $1/sec$	-3.28	-1.746	-3.57	-.1360	-2.73	-6.19	-1.400	-3.00
L'_r, $1/sec$	0.801	0.395	1.028	0.231	0.868	0.843	0.599	0.563
$L'_{\delta a}$, $1/sec^2$	28.0	8.43	26.5	12.01	17.60	24.1	7.96	14.20
$L'_{\delta r}$, $1/sec^2$	13.80	4.23	12.28	5.16	7.27	11.20	3.09	6.55
N'_β, $1/sec$	39.6	7.43	56.3	11.54	3.12	10.20	1.380	4.72
N'_p, $1/sec$	0.1539	0.0623	0.1878	0.0508	-0.1160	-0.207	-0.0799	-0.1120
N'_r, $1/sec$	-0.839	-0.365	-1.020	-0.283	-0.541	-0.975	-0.247	-0.455
$N'_{\delta a}$, $1/sec^2$	2.04	0.1931	2.80	0.619	1.370	1.640	0.652	1.010
$N'_{\delta r_r}$, $1/sec^2$	-12.15	-3.74	-12.34	-4.75	-5.54	-8.80	-2.54	-5.11
Y_v, $1/sec$	-0.584	-0.288	-0.787	-0.1924	-0.1870	-0.310	-0.0847	-0.1450
$Y^*_{\delta r}$, $1/sec$	0.0949	0.0608	0.0862	0.0407	0.0537	0.0550	0.0267	0.0347

FIGURE 58. F-5 AND A-7 LATERAL DATA

	F-5				A-7			
	CASE 1	CASE 2	CASE 3	CASE 4	CASE 1	CASE 2	CASE 3	CASE 4
C_{L_o}	0.0835	0.332	0.0651	0.276	0.194	0.0862	0.463	0.206
C_{L_α}, 1/rad	3.95	4.18	3.98	4.61	4.40	5.40	4.50	5.60
$C_{L_{\delta e}}$, 1/rad	0.859	0.745	0.917	0.888	0.600	0.550	0.630	0.650
C_{D_o}	0.020	0.0207	0.0217	0.020	0.020	0.020	0.040	0.022
C_{D_α}, 1/rad	-0.088	0.450	-0.1043	0.265	0.300	0.240	0.950	0.400
M_α, $1/sec^2$	-10.30	-3.59	-11.40	-4.11	-9.08	-27.8	-4.15	-13.14
$M_{\dot{\alpha}}$, 1/sec	-0.0646	-0.00357	-0.1523	-0.0282	-0.133	-0.267	-0.0648	-0.143
M_q, 1/sec	-1.350	-0.478	-2.04	-0.493	-0.696	-1.070	-0.330	-0.539
$M_{\delta e}$, $1/sec^2$	-47.2	-10.50	-64.4	-15.48	-18.90	-41.7	-8.19	-20.2

FIGURE 59. F-5 AND A-7 LONGITUDINAL DATA

	CONFIGURATION							
	F-5				A-7			
	CASE 1	CASE 2	CASE 3	CASE 4	CASE 1	CASE 2	CASE 3	CASE 4
$K_{q_{aug}}$, sec	0.055	0.123	0.055	0.090	0.25	0.25	0.25	0.25
$K_{\dot{q}_{aug}}$, sec^2	0.0080	-0.0312	0.0080	-0.0312	0	0	0	0
$\tau_{q_{aug}}$, sec	0.08	0.08	0.08	0.08	0	0	0	0
$K_{a_{z_{aug}}}$, rad/ft/sec	0	0 0	0	0	-0.000542	-0.000542	-0.000542	-0.000542
K_{a_z}, rad/g	0.00522	0.00522	0.00522	0.00522	0	0	0	0
K_{e_1}, rad/in	0.015	0.015	0.015	0.015	0.0635	0.0635	0.0635	0.0635
K_{e_2}, rad-sec/in	0	0	0	0	0.0912	0.0912	0.0912	0.0912
$K_{r_{aug}}$, sec^2	0.31	0.62	0.27	0.52	0.25	0.25	0.25	0.25
$\tau_{r_{aug}}$, sec	0.5	0.5	0.5	0.5	0.1	0.1	0.1	0.1
$K_{p_{aug}}$, sec	0	0	0	0	-0.1	-0.1	-0.1	-0.1
K_{a_1}, rad/in	.065	.065	.065	.065	0.230	0.230	0.230	0.230
K_a, rad-sec/in	0	0	0	0	0.345	0.345	0.345	0.345
K_r, rad/in	.14	.14	.14	.14	0.05	0.05	0.05	0.05
K_{ari}	0	0	0	0	0.1467	0.1533	0.200	0.200

FIGURE 60. F-5 AND A-7 CONTROL DATA

Longitudinal

$$\Delta\delta e_{aug} = \left(\frac{K_{\dot{q}_{aug}} \; s}{\tau_{q_{aug}} \; s + 1} + K_{q_{aug}} \right) q + K_{a_{z_{aug}}} \; \Delta a_{z_p}$$

$$\Delta\delta e_{bend} = K_{a_z} \left(N_{z_{cg}} - 1.0 \right)$$

$$\delta e = \left(K_{e_1} + \frac{K_{e_2}}{s + 2} \right) \delta e_{comm} + \Delta\delta e_{aug} + \Delta\delta e_{bend}$$

$$N_{z_{cg}} = - \frac{a_{z_p}}{g} - \frac{\ell_x \dot{q}}{g}$$

Lateral — Directional

$$\Delta\delta r_{aug} = \left(\frac{K_{r_{aug}} \; s}{\tau_{r_{aug}} \; s + 1} \right) r$$

$$\Delta\delta a_{aug} = K_{b_{aug}} \; p$$

$$\Delta\delta r_{interconnect} = K_{ari} \; \delta a$$

$$\delta a = \left(K_{a_1} + \frac{K_{a_2}}{s + 3} \right) \delta a_{comm} + \Delta\delta a_{aug}$$

$$\delta r = K_r \; \delta r_{comm} + \Delta\delta r_{aug} + \Delta\delta r_{interconnect}$$

FIGURE 61. CONTROL SYSTEMS

LATERAL FAILURE MODES

F-5 Control System as shown except for

$$K_{r_{aug}} = 0$$

A-7 Control System as shown except for

w/o AUG $K_{r_{aug}} = 0$

$K_{P_{aug}} = 0$

Failure with AUG $K_{a_2} = 0$

Failure w/o AUG $K_{a_2} = 0$

$K_{r_{aug}} = 0$

$K_{P_{aug}} = 0$

LONGITUDINAL FAILURE MODES

F-5 Control System as shown except for

$$K_{q_{aug}} = 0$$

$$K_{\dot{q}_{aug}} = 0$$

A-7 Control System as shown except for

$$K_{q_{aug}} = 0$$

$$K_{a_{z_{aug}}} = 0$$

FIGURE 62. FAILURE MODES

APPENDIX IV

SIMULATOR FLIGHT DATA AND PREDICTION GRAPHS

APPENDIX IV

SIMULATOR FLIGHT DATA AND PREDICTION GRAPHS

The data collected in Appendix IV consists of two groupings. The first contains the numerical simulation results arranged in the categories of bank angle, heading angle, and pitch angle. All flights recorded during the simulation are reported and no data have been excluded from the analysis for any reason. Pilot ratings are according to the scale and instructions described in Section III, and rms tracking errors and gust levels are reported for each flight.

The second set of data is graphical in nature and is also arranged in the order bank angle, heading angle, and pitch angle. For each configuration, the tracking error is graphed versus the gust level. The pilot is identified by symbol and the attached numbers are pilot ratings. Since the pilot model is linear, the predicted tracking error at 10 ft/sec rms turbulence defines a prediction line through the origin and the computed error. The lines have been drawn on these simulation data graphs which are preceded by the pilot model gain and lead variation graphs described in Section III* Root locus diagrams of the bank angle and pitch angle configurations have been included. They were made during the course of a preliminary analysis when it was useful to have information about the stability of the short period eigenvalues. Low frequency roots are not shown and the pilot models incorporate only first order Padè delays. Control and augmentation dynamics have also contributed loci to these diagrams.

---

* These plots of pilot parameters were all generated for the turbulence tracking task.

F-5 CASE 1 WITH AUGMENTER

Flight	rms v_g	rms ϕ_c	rms ϕ_e	PR	Pilot
1	5.06		1.01		JTT
2	5.86		.81	3	
3	9.55		1.30		
4	9.94		1.33	6	
5	11.26		1.56		
6	13.22		1.64		
7	13.26		1.52	7.5	
8	8.57		1.28		
9	5.97		.87		
10		6.31	2.48		
11		6.12	2.38		
12	5.66		.99		WWK
13	6.02		.83	3.5	
14	8.68		1.57		
15	9.37		1.43		
16	9.46		1.53	4.5	
17	11.17		1.87		
18	11.97		1.91	5.5	
19		4.18	2.52		
20		4.50	2.40		
21	5.24		.26		JBJ
22	4.98		.94	3.5	
23	9.88		1.59		
24	10.09		1.46		
25	9.76		1.61	5	
26	12.40		1.88		
27	11.49		2.07	6	
28		7.80	2.77		
29		5.38	3.20		

F-5 CASE 1 WITHOUT AUGMENTER

Flight	rms v_g	rms ϕ_c	rms ϕ_e	PR	Pilot
30	5.09		.91		JTT
31	5.31		1.08	5	
32	9.48		1.76		
33	8.90		1.59		
34	10.25		1.75	7	
35	11.38		1.95		
36	11.71		2.17		
37	11.90		2.04	8	
38		7.88	2.85		
39		6.38	2.82		
40	5.25		.79		WWK
41	5.35		.96	4	
42	9.59		1.78		
43	8.91		1.56		
44	9.34		1.70	5.5	
45	13.61		2.35		
46	11.19		2.02	7	
47		4.73	2.46		
48		4.50	2.22		
49	6.09		.91		JBJ
50	8.08		1.06	4	
51	10.42		1.76		
52	8.43		1.54		
53	9.02		1.58	6.5	
54	12.48		2.47		
55	11.27		2.60	8	
56		5.58	3.50		
57		4.78	2.82		

F-5 CASE 2 WITH AUGMENTER

Flight	rms v_g	rms ϕ_c	rms ϕ_e	PR	Pilot
58	4.39		1.51		JTT
59	4.32		1.29	4	
60	9.22		2.71		
61	10.87		2.55	5	
62	8.90		2.28		
63	12.61		3.37		
64	13.54		3.41	6	
65		8.81	3.92		
66		6.14	2.28		
67	4.46		1.16		WWK
68	4.90		1.0	4	
69	9.13		2.01		
70	9.34		1.88	6	
71	12.98		2.55		
72	14.28		2.67	7.5	
73		5.19	2.56		
74		5.67	2.86		
75	4.41		1.19		JBJ
76	4.55		1.21	2	
77	8.16		2.97	4	
78	9.13		2.27		
79	7.90		2.35	5	
80	13.22		3.56		
81	13.80		3.73	7	
82		6.56	2.59		
83		4.78	2.01		

F-5 CASE 2 WITHOUT AUGMENTER

Flight	rms v_g	rms ϕ_c	rms ϕ_e	PR	Pilot
84	4.57		1.53		JTT
85	4.44		1.54	4	
86	9.96		2.81		
87	9.44		2.93	6	
88	12.83		2.96		
89	14.69		3.49	8	
90		5.06	2.02		
91		6.62	2.74		
92	4.48		1.30		WWK
93	4.34		1.43	5	
94	10.52		2.50		
95	8.55		2.01	7	
96	14.25		3.14		
97	17.34		4.18	9.5	
98		5.63	2.91		
99		5.78	2.98		
100	4.05		1.40		JBJ
101	4.55		1.32	2	
102	8.81		3.17	6	
103	8.96		2.99		
104	8.87		2.74	4	
105	14.86		5.70		
106	13.82		6.37	10	
107		4.21	1.30		
108		5.80	2.44		

F-5 CASE 3 WITH AUGMENTER

Flight	rms v_g	rms ϕ_c	rms ϕ_e	PR	Pilot
109	8.02		1.30		JBJ
110	5.55		.93	3	
111	11.88		1.93		
112	12.91		1.76	4	
113	14.72		2.37		
114	13.83		2.40	8	
115		6.09	2.42		
116		4.14	2.14		
117	5.83		.95		JTT
118	5.97		.95	3	
119	12.86		1.64	6	
120	11.84		1.70	6.5	
121	13.21		1.62	6.5	
122	15.20		2.18		
123	14.36		1.82	7	
124		5.20	2.04		
125		5.38	2.30		
126	8.41		1.00		WWK
127	8.36		.95	2.5	
128	11.89		1.70		
129	12.03		1.62	4	
130	15.53		2.24		
131	14.98		2.29	7.5	
132		4.47	2.75		
133		6.25	3.29		

F-5 CASE 3 WITHOUT AUGMENTER

Flight	rms v_g	rms ϕ_c	rms ϕ_e	PR	Pilot
134	5.72		.95		JBJ
135	5.55		.96	3.5	
136	11.64		2.04		
137	11.46		1.79	6.5	
138	15.87		2.96		
139	14.25		3.08	9	
140		5.53	2.42		
141		5.73	2.43		
142	5.54		.84		JTT
143	5.11		.94	4	
144	12.10		2.04		
145	11.13		1.78	7	
146	13.65		2.36	8.5	
147	15.71		2.79		
148	14.98		2.46	8	
149		5.48	2.16		
150		5.25	2.62		
151	5.66		.88		WWK
152	6.01		1.10	3.5	
153	12.11		1.80		
154	11.06		1.58	7	
155	15.50		2.98		
156	14.64		3.49	9.5	
157		6.91	2.89		
158		5.05	2.40		

F-5 CASE 4 WITH AUGMENTER

Flight	rms v_g	rms ϕ_c	rms ϕ_e	PR	Pilot
159	5.93		1.36		WWK
160	6.95		1.61	2	
161	11.99		2.96		
162	12.20		2.86	7	
163	17.80		3.72		
164	17.51		3.66	9	
165		5.67	3.07		
166	6.79		1.73		JBJ
167	6.63		1.36	3	
168	10.64		1.92		
169	9.83		2.15	5	
170	11.68		3.05		
171	12.88		2.95	6	
172		5.95	2.78		
173		5.52	2.80		
174	5.52		1.10		JTT
175	6.68		1.38	3	
176	7.96		1.59		
177	10.26		1.95	4	
178	10.40		2.29		
179	11.52		1.91	5	
180		6.39	2.55		
181		6.30	2.93		

F-5 CASE 4 WITHOUT AUGMENTER

Flight	rms v_g	rms ϕ_c	rms ϕ_e	PR	Pilot
182	6.07		2.39		WWK
183	7.06		2.75	5	
184	15.07		4.86	10	
185		5.67	3.07		
186	6.36		2.05		JBJ
187	6.83		2.11	6	
188	8.95		4.05		
189	9.14		3.79	7.5	
190	11.86		4.37		
191	12.28		5.45	8	
192		5.95	2.78		
193		5.52	2.80		
194	6.83		2.96		JTT
195	6.18		2.33	5	
196	9.17		2.68		
197	9.01		2.43	5.5	
198	11.16		5.70		
199	12.10		4.20	8	
200		6.39	2.55		
201		6.30	2.93		

A-7 CASE 1 WITH AUGMENTER

Flight	rms v_g	rms ϕ_c	rms ϕ_e	PR	Pilot
202	4.82		.94		WWK
203	5.11		1.25	4.5	
204	6.72		1.30		
205	7.40		1.40	5	
206	10.65		1.87		
207	8.72		1.63	7	
208		5.69	2.98		
209		7.98	3.31		
210	4.34		.78		JBJ
211	5.48		.93	4	
212	7.64		1.24		
213	7.84		1.33	5	
214	7.47		1.95		
215	10.13		1.70	7	
216		6.57	5.29		
217		4.65	4.61		
218	4.82		.88		JTT
219	4.96		.82	5	
220	8.08		1.09		
221	6.42		1.06	5	
222	12.17		1.37		
223	9.83		1.10	7.5	
224		5.29	2.03		
225		6.75	2.16		

A-7 CASE 1 WITHOUT AUGMENTOR

Flight	rms v_g	rms ϕ_c	rms ϕ_e	PR	Pilot
226	4.89		1.62		WWK
227	4.94		1.53	5	
228	7.04		1.92		
229	6.94		1.55	6.5	
230	9.62		2.13		
231	8.95		2.09	7.5	
232		6.36	2.83		
233		4.85	2.67		
234	4.98		1.40		JBJ
235	5.97		1.41	5.5	
236	6.47		1.57		
237	7.47		1.95	6.5	
238	10.68		2.46		
239	9.94		2.85	8	
240		5.45	4.71		
241		5.89	4.10		
242	4.43		.88		JTT
243	4.93		.97	6	
244	7.68		1.45		
245	6.85		1.29	7.5	
246	9.22		1.67		
247	9.10		1.57	8.5	
248		7.15	2.19		
249		6.31	1.76		

A-7 CASE 1 FAILURE WITH AUGMENTER

Flight	rms v_g	rms ϕ_c	rms ϕ_e	PR	Pilot
250	5.47		1.40		WWK
251	6.43		1.51	4.5	
252	14.35		3.16		
253	14.26		3.33	9	
254	3.86		1.01		
255	3.49		1.10	3.5	
256	1.62		.77	4	
257		5.27	3.42		
258		5.79	3.93		
259	3.63		.88		JBJ
260	3.71		.91	3	
261	5.94		1.34		
262	6.14		1.21	5.5	
263	11.15		2.69		
264	9.65		2.01	7.5	
265		5.23	2.22		
266		5.09	2.00		
267	4.00		.71		JTT
268	3.79		.79	2	
269	7.22		1.41		
270	6.67		1.03	4.5	
271	10.22		1.37		
272	10.50		1.32	7	
273	9.25		1.48		
274	9.67		1.78	8	
275		6.23	2.30		
276		3.69	1.93		

A-7 CASE 1 FAILURE WITHOUT AUGMENTER

Flight	rms v_g	rms ϕ_c	rms ϕ_e	PR	Pilot
277	6.88		2.42		WWK
278	5.73		2.34	5.5	
279	10.62		3.77		
280	12.79		4.38	8.5	
281	3.47		1.75		
282	3.57		1.72	5	
283	1.89		.88	4.5	
284		5.51	3.48		
285		6.80	4.01		
286	3.89		1.29		JBJ
287	3.90		1.36		
288	3.65		1.09	4.5	
289	6.07		2.10		
290	5.88		1.73	6.5	
291	9.22		2.42		
292	9.61		2.78	8.5	
293		5.37	2.13		
294		5.15	1.96		
295	3.67		.87		JTT
296	3.19		.84	3	
297	6.11		1.30		
298	5.74		1.23	5.5	
299	10.85		1.95		
300	9.13		1.69	7.5	
301	10.65		2.19		
302	10.66		2.09	8	
303		4.70	1.77		
304		5.45	2.03		

A-7 CASE 2 WITH AUGMENTER

Flight	rms v_g	rms ϕ_c	rms ϕ_e	PR	Pilot
305	6.38		.67		JTT
306	6.22		.57	4	
307	7.33		.73		
308	10.29		.81	7	
309	11.84		.94		
310	11.71		.97	8.5	
311		5.90	2.65		
312		5.12	1.65		
313	6.04		.77		WWK
314	6.74		.89	4	
315	9.52		1.11		
316	8.74		1.14	5.5	
317	11.37		1.55		
318	12.48		1.58	5.5	
319		6.64	2.89		
320		5.83	2.68		
321	6.02		.73		JBJ
322	5.93		.69	3	
323	9.10		.91		
324	9.40		.91	4.5	
325	11.97		1.49		
326	12.88		1.41	7	
327		4.65	1.96		
328		5.91	1.84		

A-7 CASE 2 WITHOUT AUGMENTER

Flight	rms v_g	rms ϕ_c	rms ϕ_e	PR	Pilot
329	6.84		.82		JTT
330	7.33		.73	5.5	
331	9.48		1.06		
332	8.90		.94	8	
333	12.25		1.38		
334	11.47		1.19	9	
335		5.59	1.68		
336		4.99	1.79		
337	5.75		1.40		WWK
338	6.25		1.20	5.5	
339	9.85		1.76		
340	10.47		1.73	6	
341	11.61		2.17		
342	12.65		2.33	7	
343		5.61	2.73		
344		5.11	2.67		
345	6.83		1.13		JBJ
346	6.33		.98	4	
347	10.36		1.63		
348	10.30		1.36	6.5	
349	12.69		1.79		
350	14.04		1.97	8	
351		6.12	2.06		
352		5.65	2.19		

A-7 CASE 2 FAILURE WITH AUGMENTER

Flight	rms v_g	rms ϕ_c	rms ϕ_e	PR	Pilot
353	6.71		1.18		JBJ
354	7.13		1.07	3	
355	9.85		1.58		
356	9.27		1.49	6.5	
357	9.89		1.70		
358	11.38		2.07		
359	12.11		2.16	7	
360	3.78		.82		
361	4.00		.71	2.5	
362		6.13	2.61		
363		5.37	2.77		
364	5.95		.99		JTT
365	4.94		.77	3	
366	9.95		1.23		
367	8.49		1.04		
368	9.23		1.08	5.5	
369	12.07		1.40		
370	11.59		1.43	6.5	
371		7.60	2.47		
372		5.18	2.08		
373	5.03		.84		WWK
374	5.61		.92	4	
375	8.62		1.24		
376	9.28		1.41		
377	8.15		1.39	5	
378	11.62		1.84		
379	13.38		2.27	6.5	
380		6.58	2.74		
381		8.04	2.67		

A-7 CASE 2 FAILURE WITHOUT AUGMENTER

Flight	rms v_g	rms ϕ_c	rms ϕ_e	PR	Pilot
382	6.80		1.44		JBJ
383	6.52		1.55	5	
384	9.51		2.01		
385	11.19		2.43	8	
386	12.98		3.00		
387	10.86		2.84	8.5	
388	3.95		1.10		
389	4.15		1.09	3.5	
390		5.61	2.46		
391		5.34	2.83		
392	5.40		.99		JTT
393	6.03		1.01	4	
394	11.04		1.58		
395	10.06		1.40		
396	9.18		1.39	6	
397	13.04		2.00		
398	10.65		1.75	7	
399		3.90	1.89		
400		4.71	2.15		
401	5.12		1.15		WWK
402	5.60		1.09	4.5	
403	7.97		1.78		
404	8.51		1.73		
405	8.33		1.62	6	
406	12.29		2.50		
407	12.10		2.50	6	
408		5.54	3.06		
409		4.12	2.66		

A-7 CASE 3 WITH AUGMENTER

Flight	rms v_g	rms ϕ_c	rms ϕ_e	PR	Pilot
410	4.51		.92		JBJ
411	4.40		.82	3	
412	7.56		1.42		
413	6.65		1.29	5.5	
414	9.05		1.56		
415	8.36		1.35	6.5	
416		5.41	2.30		
417		5.13	2.27		
418	5.09		1.24		JTT
419	4.74		.88	3	
420	6.72		1.03		
421	5.61		.96	5	
422	9.20		1.31		
423	9.65		1.51	6	
424		5.77	2.08		
425		5.52	2.06		
426	4.87		1.13		WWK
427	5.07		1.13	4.5	
428	6.81		1.40		
429	6.46		1.41	4.5	
430	9.69		1.87		
431	8.21		1.25	5	
432		4.85	3.52		
433		5.68	3.32		

A-7 CASE 3 WITHOUT AUGMENTER

Flight	rms v_g	rms ϕ_c	rms ϕ_e	PR	Pilot
434	4.36		1.14		JBJ
435	4.39		1.17	4.5	
436	6.67		1.33		
437	6.85		1.22	5	
438	6.62		1.44		
439	9.50		2.02		
440	8.57		1.87	7	
441		6.27	2.77		
442		5.22	2.44		
443	4.19		.97		
					JTT
444	4.00		1.08	3.5	
445	6.50		1.21		
446	6.84		1.17	5.5	
447	9.07		1.75		
448	8.34		1.44	7.5	
449		5.39	2.09		
450		4.95	2.24		
451	4.94		1.15		WWK
452	4.67		1.41	5	
453	6.85		1.72		
454	7.11		1.93	5.5	
455	9.97		1.82		
456	10.73		2.49	6.5	
457		5.37	3.51		
458		6.76	4.49		

A-7 CASE 3 FAILURE WITH AUGMENTER

Flight	rms v_g	rms ϕ_c	rms ϕ_e	PR	Pilot
459	4.55		1.28		JTT
460	4.60		1.04	4	
461	6.29		1.35		
462	6.41		1.31	5	
463	7.38		1.66		
464	7.60		1.47	6.5	
465	3.04		1.25		
466	2.72		.69	4	
467		6.34	2.71		
468		6.29	2.61		
469	3.85		.93		WWK
470	3.99		.97	4.5	
471	6.63		1.49		
472	7.28		1.45	5.5	
473	8.98		2.05		
474	8.85		2.25	6	
475		5.77	2.94		
476		5.67	2.98		
477	3.64		1.04		JBJ
478	3.98		.89	3	
479	6.27		1.30		
480	7.15		1.72	5.5	
481	7.62		2.11		
482	8.72		2.25	7	
483		5.75	3.31		
484		6.00	2.67		

A-7 CASE 3 FAILURE WITHOUT AUGMENTER

Flight	rms v_g	rms ϕ_c	rms ϕ_e	PR	Pilot
485	4.38		1.24		JTT
486	4.41		1.29	4.5	
487	6.88		1.81		
488	7.42		1.83	6	
489	7.74		1.79		
490	7.30		2.00	7	
491	3.09		.83		
492	2.60		.94	4	
493		4.94	2.13		
494		5.19	2.17		
495	4.30		1.33		WWK
496	3.98		1.17	5	
497	7.47		1.54		
498	7.26		1.77	5	
499	8.36		2.07		
500	8.13		2.14	5.5	
501		7.30	2.76		
502		5.92	3.54		
503	3.92		1.05		JBJ
504	4.17		1.2u	4.5	
505	5.89		1.92		
506	6.38		1.87	6.5	
507	7.34		2.44		
508	7.04		2.43	8	
509		5.51	2.71		
510		5.58	2.71		

A-7 CASE 4 WITH AUGMENTER

Flight	rms v_g	rms ϕ_c	rms ϕ_e	PR	Pilot
511	5.62		1.21		WWK
512	5.98		1.03	4	
513	5.90		1.47		
514	10.48		1.48	5	
515	11.24		1.52		
516	12.36		1.85	6	
517	2.64		.57	3.5	
518	4.72		.79		JBJ
519	4.66		.80	3	
520	8.51		1.21		
521	8.22		1.02	4	
522	11.37		1.75		
523	13.08		1.80	6	
524		6.65	3.54		
525		7.07	2.49		
526	4.49		.85		JTT
527	5.31		.68	3	
528	8.34		1.13		
529	7.83		1.02	4.5	
530	12.49		1.41		
531	11.18		1.14	7	
532		5.59	2.00		
533		6.43	1.89		

A-7 CASE 4 WITHOUT AUGMENTER

Flight	rms v_g	rms ϕ_c	rms ϕ_e	PR	Pilot
534	5.42		1.12		WWK
535	6.38		1.35	4.5	
536	7.34		1.55		
537	9.28		1.75	6	
538	11.04		2.11		
539	12.20		1.73	6.5	
540	4.79		1.14		JBJ
541	4.91		1.05	4	
542	8.03		1.71		
543	8.16		1.68	5	
544	11.22		2.26		
545	12.91		2.02	7	
546		5.87	2.49		
547		5.05	2.16		
548	4.44		.92		JTT
549	4.49		1.02	3.5	
550	7.48		1.14		
551	8.57		1.26	5.5	
552	12.49		1.51		
553	13.27		1.48	7.5	
554		5.68	2.04		
555		6.41	2.14		

A-7 CASE 4 FAILURE WITH AUGMENTER

Flight	rms v_g	rms ϕ_c	rms ϕ_e	PR	Pilot
556	3.50		.96		JBJ
557	3.39		.82	3.5	
558	5.65		1.39		
559	5.66		1.44	5.5	
560	7.52		1.81		
561	7.27		1.76	7	
562		5.70	2.75		
563		6.06	2.51		
564	3.05		.75		JTT
565	3.40		.82	3	
566	5.58		1.44		
567	5.50		.94	5	
568	6.14		1.21		
569	8.06		1.52	7	
570		6.59	2.66		
571		5.22	2.34		
572	3.42		.94		WWK
573	3.50		1.06	4	
574	5.66		1.21		
575	6.36		1.69	5.5	
576	7.42		2.10		
577	6.84		1.82	6	
578		5.89	3.28		
579		5.64	3.15		

A-7 CASE 4 FAILURE WITHOUT AUGMENTER

Flight	rms v_g	rms ϕ_c	rms ϕ_e	PR	Pilot
580	3.29		1.08		JBJ
581	3.38		1.04	4	
582	5.77		1.84		
583	6.13		1.68	6.5	
584	6.89		1.91		
585	7.45		2.31	7.5	
586		5.36	2.30		
587		5.48	2.34		
588	3.56		1.00		JTT
589	3.46		.91	3	
590	5.99		1.54		
591	5.45		1.25	6.5	
592	7.26		1.75		
593	8.37		2.08	7.5	
594		5.30	2.13		
595		4.58	1.91		
596	3.78		1.29		WWK
597	3.46		1.27	4.5	
598	5.78		1.74		
599	5.32		1.56	6.0	
600	6.94		2.39		
601	7.22		2.46	6.5	
602		5.45	2.80		
603		5.4	3.23		

F-5 CASE 1 WITH AUGMENTER

Flight	rms v_g	rms ψ_e	rms β	rms ϕ	rms r	PR	Pilot
604	5.26	.66	.45	4.22	.16		JTT
605	5.34	.48	.46	2.74	.16	2.5	
606	9.52	.80	.79	3.98	.31		
607	9.60	.85	.79	7.38	.31	5	
608	12.40	1.18	1.03	8.38	.40		
609	11.91	1.02	.99	6.30	.38	5	
610	6.28	.68	.56	4.16	.19		WWK
611	5.47	.52	.48	2.44	.15	2.5	
612	8.20	.70	.70	3.72	.27		
613	9.75	.79	.82	4.40	.29	3.5	
614	12.65	1.08	1.05	4.38	.36		
615	12.35	1.10	1.06	3.74	.38	4.0	
616	5.03	.60	.45	2.84	.15		JBJ
617	5.32	.53	.47	2.44	.16	3	
618	9.93	.93	.87	4.08	.31		
619	10.16	.89	.88	3.46	.32	5	
620	14.97	1.03	1.00	5.56	.38		
621	13.73	1.21	1.15	4.76	.38	7	

F-5 CASE 1 WITHOUT AUGMENTER

Flight	rms v_g	rms ψ_e	rms β	rms ϕ	rms r	PR	Pilot
622	7.44	.79	.71	5.43	.41		JTT
623	5.82	.71	.57	6.10	.37	3.5	
624	8.88	1.11	.89	9.83	.65		
625	9.07	.9	.95	8.50	.73	6.5	
626	12.30	1.53	1.24	17.64	.88		
627	11.72	1.42	1.22	14.40	.95	8.0	
628	4.97	.54	.51	3.54	.35		WWK
629	5.17	.57	.53	3.96	.35	3.0	
630	8.94	.93	.88	3.94	.60		
631	8.45	.87	.91	2.46	.66	3.0	
632	11.78	1.14	1.22	4.64	.88		
633	10.62	1.14	1.10	4.30	.79	6.5	
634	5.48	.64	.58	4.16	.41		JBJ
635	5.02	.65	.52	3.10	.34	4.0	
636	9.65	.97	.91	4.16	.56		
637	8.63	.94	.87	4.52	.59	6.0	
638	12.87	1.42	1.26	4.82	.84		
639	13.60	1.40	1.32	6.88	.85	8.0	

F-5 CASE 2 WITH AUGMENTER

Flight	rms v_g	rms ψ_e	rms β	rms ϕ	rms r	PR	Pilot
640	4.57	1.18	.99	8.72	.26	4	JTT
641	5.62	1.00	1.10	8.78	.24		
642	8.81	1.63	1.70	5.84	.37		
643	10.55	2.05	2.08	6.03	.41	6	
644	5.32	.90	1.01	3.53	.18		WWK
645	4.37	.92	.90	3.58	.18	3	
646	11.24	2.18	2.15	5.63	.42		
647	10.38	1.83	1.97	4.97	.43	5.5	
648	4.39	.87	.85	4.40	.18		JBJ
649	5.23	1.01	.98	4.57	.18	2	
650	11.84	2.41	2.33	9.03	.41		
651	11.67	2.25	2.30	8.80	.48	8	
652	8.50	1.76	1.63	7.03	.31		
653	8.15	1.89	1.71	9.45	.35	5	

F-5 CASE 2 WITHOUT AUGMENTER

Flight	rms v_g	rms ψ_e	rms β	rms ϕ	rms r	PR	Pilot
654	4.96	1.09	1.04	5.01	.37		JTT
655	4.69	.98	1.00	3.08	.33	7	
656	9.73	2.11	2.15	4.84	.76		
657	9.02	2.09	2.08	4.93	.76	5.5	
658	4.48	1.04	1.09	2.18	.41		WWK
659	4.54	1.06	1.01	2.20	.36	4.5	
660	12.15	2.97	2.74	8.32	.99	6.5	
661	10.85	2.75	2.72	5.70	1.01	7	
662	3.59	1.02	.92	3.37	.37		JBJ
663	4.53	1.41	1.04	5.55	.38	4	
664	9.69	2.39	2.17	8.15	.80		
665	11.47	3.29	2.89	10.15	1.06	9	
666	7.71	2.23	1.80	10.50	.69		
667	7.92	2.20	1.79	10.52	.65	7.5	

F-5 CASE 3 WITH AUGMENTER

Flight	rms v_g	rms ψ_e	rms β	rms ϕ	rms r	PR	Pilot
668	5.18	.50	.41	2.70	.19		JBJ
669	5.43	.50	.42	3.10	.19	2	
670	12.98	1.14	1.39	6.82	.44		
671	11.25	.94	.98	4.75	.39	5.5	
672	5.88	.57	.46	3.96	.20		JTT
673	5.50	.48	.44	2.78	.20	3	
674	12.99	.76	.74	5.40	.38		
675	11.97	.98	.90	5.50	.43	7	
676	15.92	1.20	1.18	4.68	.53		
677	14.81	1.18	1.07	7.28	.54	7	
678	5.62	.60	.44	3.44	.18		WWK
679	5.20	.46	.41	2.72	.19	3	
680	11.24	.85	.87	5.00	.38		
681	10.77	.82	.82	5.90	.39	5	

F-5 CASE 3 WITHOUT AUGMENTER

Flight	rms v_g	rms ψ_e	rms β	rms ϕ	rms r	PR	Pilot
682	5.12	.57	.48	3.94	.37		JBJ
683	5.68	.64	.52	4.42	.41	3	
684	10.39	.96	.94	5.26	.76		
685	10.66	1.11	.97	6.74	.79	7	
686	5.52	.66	.53	3.94	.40		JTT
687	6.35	.69	.54	5.24	.42	5	
688	11.52	1.06	1.05	4.98	.89		
689	9.74	.88	.92	3.98	.79	6.5	
690	15.49	1.52	1.34	8.74	1.02	8	
691	14.41	1.38	1.29	8.64	1.04		
692	5.87	.58	.53	3.84	.42		WWK
693	5.84	.61	.53	3.96	.42	4	
694	15.34	.98	.96	5.78	.77		
695	12.34	1.07	1.05	6.38	.76	6	

F-5 CASE 4 WITH AUGMENTER

Flight	rms v_g	rms ψ_e	rms β	rms ϕ	rms r	PR	Pilot
696	6.95	.71	.71	2.92	.17		WWK
697	5.92	.64	.65	2.70	.17	3	
698	8.92	1.03	.93	3.44	.23		
699	9.22	1.01	1.04	3.62	.28	4.5	
700	13.06	1.51	1.40	5.84	.36		
701	11.12	1.10	1.17	4.00	.31	4.5	
702	4.44	.64	.47	3.46	.12		JBJ
703	5.12	.64	.57	2.60	.14	3	
704	9.29	1.00	.95	4.34	.23		
705	7.75	.87	.82	2.78	.22	4	
706	6.15	.74	.65	2.64	.16		
707	6.21	.75	.64	3.08	.16	3	
708	6.09	.62	.63	2.64	.15		JTT
709	5.77	.62	.62	3.64	.15	3	
710	8.06	.90	.85	4.58	.22		
711	6.54	.63	.66	6.56	.18	4	
712	11.12	1.15	1.18	11.96	.30		
713	9.34	1.02	.99	7.08	.27	5	

F-5 CASE 4 WITHOUT AUGMENTER

Flight	rms v_g	rms ψ_e	rms β	rms ϕ	rms r	PR	Pilot
714	5.67	1.09	1.05	3.54	.55		WWK
715	6.26	1.19	1.00	3.50	.50	5	
716	9.23	1.26	1.30	3.96	.62		
717	9.36	1.47	1.51	4.92	.75	6	
718	13.11	2.24	2.23	7.02	1.15		
719	14.39	2.04	1.96	6.16	.89	7.5	
720	4.67	.75	.63	4.56	.29		JBJ
721	4.66	.77	.73	3.90	.35	4.5	
722	8.77	1.51	1.46	6.84	.75		
723	9.20	1.48	1.55	6.22	.71	7.5	
724	6.96	1.34	1.08	6.30	.53		
725	6.88	1.00	.94	5.06	.46	5	
726	5.61	1.05	.81	7.50	.41		JTT
727	6.14	.96	.82	7.10	.41	4	
728	7.93	1.33	1.11	8.94	.55		
729	7.80	1.29	1.07	10.44	.52	5	
730	9.68	1.92	1.44	15.62	.76		
731	10.58	1.40	1.33	8.66	.63	6	

A-7 CASE 1 WITH AUGMENTER

Flight	rms v_g	rms ψ_e	rms β	rms ϕ	rms r	PR	Pilot
732	4.66	.70	.60	4.08	.11		WWK
733	4.89	.63	.64	2.88	.12	5	
734	7.14	.80	.87	3.96	.17		
735	6.54	.81	.73	3.16	.16	4.5	
736	9.74	1.13	1.22	4.63	.24		
737	9.48	1.16	1.21	4.95	.22	5	
738	4.94	.59	.64	4.20	.11		JBJ
739	5.03	.57	.66	3.41	.12	3	
740	7.46	.79	.96	9.50	.19		
741	7.26	.79	.97	7.89	.20	5	
742	8.85	.97	1.04	10.99	.25		
743	8.42	1.01	1.06	11.10	.23	6.5	
744	4.14	1.11	.83	18.98	.19		JTT
745	4.48	1.16	1.00	22.32	.22	7.5	
746	7.31	.73	.84	10.73	.16		
747	6.26	.96	.89	14.76	.21	6	
748	9.65	1.55	1.44	19.15	.30		
749	9.21	1.11	1.39	15.08	.23	6.5	

A-7 CASE 1 WITHOUT AUGMENTER

Flight	rms v_g	rms ψ_e	rms β	rms ϕ	rms r	PR	Pilot
750	4.83	.74	.71	4.25	.18		WWK
751	5.18	.87	.79	5.38	.21	5.5	
752	7.26	1.00	1.11	4.51	.30		
753	7.29	1.11	1.35	5.17	.27	5	
754	9.73	1.57	1.46	6.14	.41		
755	10.76	1.56	1.58	7.40	.41	5.5	
756	5.34	.87	.85	6.15	.23		JBJ
757	5.08	.99	.94	8.81	.28	5	
758	8.14	1.20	1.30	7.71	.34		
759	7.84	1.33	1.22	9.01	.34	6	
760	9.51	1.57	1.56	11.13	.46		
761	9.53	1.37	1.47	11.83	.41	7	
762	5.11	1.05	.96	19.51	.27		JTT
763	5.01	.83	.82	11.99	.23	7	
764	7.40	1.17	1.34	14.42	.34		
765	7.72	1.44	1.28	18.35	.37	8.5	
766	10.24	1.49	1.54	18.08	.41		
767	10.94	1.61	1.61	18.73	.42	8	

A-7 CASE 1 FAILURE WITH AUGMENTER

Flight	rms v_g	rms ψ_e	rms β	rms ϕ	rms r	PR	Pilot
768	6.04	.86	.79	3.45	.24		WWK
769	5.47	.82	.71	3.47	.22	3.5	
770	3.58	.57	.56	2.47	.10		JBJ
771	3.57	.57	.52	2.27	.09	2	
772	6.73	1.04	1.19	10.81	.24		
773	5.66	.88	.87	13.22	.20	6	
774	8.32	.97	1.14	10.99	.25		
775	10.23	1.15	1.40	12.68	.28	6.5	
776	4.17	.67	.61	7.19	.12		JTT
777	3.42	.61	.57	6.82	.12	3	
778	6.55	.90	.93	9.88	.20		
779	5.97	.67	.82	5.02	.15	5	
780	9.38	1.15	1.17	8.75	.26		
781	10.05	1.28	1.37	12.28	.29	6.5	

A-7 CASE 1 FAILURE WITHOUT AUGMENTER

Flight	rms v_g	rms ψ_e	rms β	rms ϕ	rms r	PR	Pilot
782	6.90	.83	.88	4.58	.19		WWK
783	7.02	.87	.89	5.80	.20	4	
784	3.14	.49	.57	2.79	.10		JBJ
785	3.43	.65	.80	8.31	.14	3.5	
786	6.06	1.08	1.16	17.06	.25		
787	5.86	.75	.81	9.58	.17	5	
788	8.76	.85	1.41	15.78	.24		
789	7.90	1.02	1.23	17.43	.27	7	
790	3.78	.65	.73	11.29	.13		JTT
791	3.50	.56	.53	8.41	.12	5	
792	6.15	.91	.97	13.47	.17		
793	5.67	.86	.87	13.44	.19	6	
794	9.71	1.32	1.50	17.86	.27		
795	10.11	1.13	1.39	11.47	.28	6.5	

A-7 CASE 2 WITH AUGMENTER

Flight	rms v_g	rms ψ_e	rms β	rms ϕ	rms r	PR	Pilot
796	6.78	.52	.53	3.11	.15		JTT
797	5.91	.50	.46	5.80	.15	3	
798	9.75	.65	.71	5.81	.22		
799	9.05	.66	.68	5.00	.22	5	
800	11.92	.84	.89	4.50	.28		
801	12.89	.80	.89	5.49	.28	6.5	
802	7.16	.67	.61	5.75	.15		WWK
803	6.36	.54	.54	4.56	.15	4.5	
804	10.10	.75	.81	3.52	.22		
805	9.20	.72	.72	3.90	.20	5	
806	13.06	.96	1.03	4.96	.31		
807	13.86	1.02	1.08	5.18	.29	5.5	
808	6.17	.60	.50	2.12	.13		JBJ
809	6.62	.51	.57	2.37	.15	3	
810	8.73	.70	.67	2.36	.19		
811	9.80	.67	.75	2.44	.20	4	
812	13.21	.93	1.00	2.71	.26		
813	13.14	.89	1.01	2.55	.27	6.5	

A-7 CASE 2 WITHOUT AUGMENTER

Flight	rms v_g	rms ψ_e	rms β	rms ϕ	rms r	PR	Pilot
814	6.04	.57	.64	4.45	.27		JTT
815	6.00	.57	.58	3.67	.25	4.5	
816	11.21	1.06	1.12	5.30	.51		
817	10.41	.93	.93	5.34	.39	6	
818	12.11	1.07	1.14	5.27	.56		
819	13.97	1.12	1.22	5.05	.56	6.5	
820	5.88	.61	.57	4.66	.24		WWK
821	5.77	.59	.57	3.77	.24	4	
822	9.71	.90	.93	4.35	.38		
823	9.21	.83	.87	3.63	.36	5.5	
824	12.33	1.08	1.17	3.97	.49		
825	11.68	1.14	1.15	5.02	.50	6.5	
826	6.86	.61	.64	2.13	.24		JBJ
827	6.49	.57	.59	1.72	.22	3.5	
828	10.69	.89	.94	2.32	.35		
829	10.19	.83	.88	2.24	.33	5	
830	12.32	1.10	1.13	2.86	.49		
831	12.60	1.18	1.22	3.38	.51	7.5	

A-7 CASE 2 FAILURE WITH AUGMENTER

Flight	rms v_g	rms ψ_e	rms β	rms ϕ	rms r	PR	Pilot
832	6.60	.67	.58	3.21	.19		JBJ
833	6.45	.65	.58	2.72	.19	3	
834	10.15	.70	.84	2.53	.30		
835	9.57	.82	.82	2.41	.27	5	
836	10.62	.95	.94	4.40	.35		
837	12.49	1.09	1.08	4.90	.36	7.5	
838	5.62	.57	.47	5.41	.19		JTT
839	5.92	.50	.50	2.40	.18	2	
840	9.72	.79	.79	2.93	.27		
841	10.48	.86	.85	4.63	.29	5	
842	10.79	.83	.86	3.68	.32		
843	13.15	1.05	.97	7.46	.32	6	
844	5.72	.57	.50	4.76	.18		WWK
845	5.67	.55	.52	5.24	.19	3	
846	9.26	.87	.78	5.83	.29		
847	8.96	.74	.75	4.82	.26	4.5	
848	13.18	1.13	1.09	7.76	.34		
849	12.21	1.05	1.00	5.30	.34	5	

A-7 CASE 2 FAILURE WITHOUT AUGMENTER

Flight	rms v_g	rms ψ_e	rms β	rms ϕ	rms r	PR	Pilot
850	5.89	.56	.53	2.84	.18		JBJ
851	5.77	.54	.51	2.92	.17	4	
852	10.49	.94	.92	4.90	.30		
853	11.33	.83	.88	4.32	.29	6.5	
854	12.69	1.00	5.62	.36			
855	12.41	.97	1.05	4.03	.34	7	
856	5.60	.45	.48	2.22	.15		JTT
857	5.70	.46	.49	1.93	.17	3.5	
858	10.26	.84	.79	7.36	.26		
859	9.17	.82	.75	6.99	.26	4.5	
860	10.91	.77	.84	7.37	.30		
861	12.09	.85	.89	8.89	.32	6	
862	5.36	.54	.48	4.94	.17	2.5	WWK
863	5.61	.53	.50	4.44	.18		
864	9.68	.77	.81	5.71	.27		
865	8.85	.73	.77	4.32	.25	4	
866	12.52	1.08	1.08	6.04	.35		
867	11.74	.95	.99	5.35	.33	5.5	

A-7 CASE 3 WITH AUGMENTER

Flight	rms v_g	rms ψ_e	rms β	rms ϕ	rms r	PR	Pilot
868	4.29	.97	.85	4.06	.14		JBJ
869	4.25	1.11	.99	5.00	.16	4	
870	6.40	1.06	1.13	7.79	.21		
871	6.64	1.10	1.40	13.96	.25	6.5	
872	11.35	1.49	1.53	14.39	.32		
873	9.71	1.44	1.68	14.03	.31	8	
874	7.89	1.49	1.42	4.69	.22		WWK
875	6.32	1.14	1.13	4.39	.18	4.5	
876	9.51	1.62	1.68	4.08	.25		
877	9.86	1.95	1.86	4.69	.27	5.5	

A-7 CASE 3 WITHOUT AUGMENTER

Flight	rms v_g	rms ψ_e	rms β	rms ϕ	rms r	PR	Pilot
878	4.78	1.01	1.12	4.24	.22		JBJ
879	4.69	1.01	1.10	4.31	.22	5	
880	7.13	1.62	1.70	11.30	.39		
881	6.81	1.66	1.85	10.10	.45	7.5	
882	6.20	1.52	1.43	4.09	.29		WWK
883	7.17	1.79	1.72	4.20	.34	6	
884	8.81	1.83	1.85	3.93	.35		
885	9.32	2.02	2.05	4.35	.41	6	

A-7 CASE 3 FAILURE WITH AUGMENTER

Flight	rms v_g	rms ψ_e	rms β	rms ϕ	rms r	PR	Pilot
886	3.62	.76	.69	9.70	.13		JTT
887	4.25	.74	.81	9.67	.13	5	
888	6.09	.90	1.07	11.48	.17		
889	5.10	.81	.91	9.12	.16	5.5	
890	7.10	.86	1.00	8.66	.18		
891	8.20	.80	1.38	14.02	.18	6	
892	4.28	1.02	1.06	4.28	.17		WWK
893	4.03	1.02	.92	4.04	.15	4.5	
894	6.73	1.25	1.36	3.63	.21		
895	7.14	1.45	1.58	4.45	.26	5.5	
896	7.49	1.57	1.63	5.46	.25		JBJ
897	7.07	1.92	1.72	7.66	.27	5.5	
898	7.54	1.99	1.88	8.84	.33		
899	8.31	2.53	2.10	11.77	.37	6.5	

A-7 CASE 3 FAILURE WITHOUT AUGMENTER

Flight	rms v_g	rms ψ_e	rms β	rms ϕ	rms r	PR	Pilot
900	3.88	.84	1.00	17.39	.16		JTT
901	4.85	.69	1.01	14.64	.15	6	
902	5.45	1.07	1.10	11.70	.17		
903	5.36	1.00	1.10	14.55	.19	7	
904	6.97	1.03	1.37	17.99	.21		
905	6.35	1.28	1.60	18.09	.26	7.5	
906	3.96	.88	.96	4.22	.15		WWK
907	4.17	1.01	1.01	3.54	.16	4	
908	6.33	1.44	1.42	5.40	.23		
909	6.45	1.65	1.52	5.65	.15	5	
910	6.69	2.32	1.99	11.94	.36	6.5	JBJ
911	8.47	1.48	1.94	14.70	.23		
912	8.33	1.03	1.40	13.13	.22	4	

A-7 CASE 4 WITH AUGMENTER

Flight	rms v_g	rms ψ_e	rms β	rms ϕ	rms r	PR	Pilot
913	5.99	.66	.62	2.88	.18		WWK
914	5.97	.63	.61	2.97	.12	4	
915	11.82	1.18	1.12	4.97	.24		
916	10.42	.98	.99	3.61	.23	5	
917	4.33	.62	.57	3.21	.13		JBJ
918	5.12	.61	.56	2.66	.12	3	
919	7.09	.71	.65	2.23	.16		
920	7.76	.72	.75	2.13	.18	4	
921	11.95	4.89	3.61	15.54	.58		
922	10.16	2.13	1.99	8.08	.43	9	

A-7 CASE 4 WITHOUT AUGMENTER

Flight	rms v_g	rms ψ_e	rms β	rms ϕ	rms r	PR	Pilot
923	6.53	1.02	.88	5.12	.27		WWK
924	5.67	.78	.73	2.83	.22	4.5	
925	9.63	1.14	1.15	3.42	.35		
926	12.41	1.40	1.40	3.55	.41	5	
927	4.56	.66	.71	2.95	.23		JBJ
928	4.13	.62	.49	1.70	.15	3.5	
929	7.90	1.13	1.08	3.21	.34		
930	8.26	1.59	1.50	4.29	.39	5.5	
931	12.58	4.04	3.90	17.33	1.07	10.0	

A-7 CASE 4 FAILURE WITH AUGMENTER

Flight	rms v_g	rms ψ_e	rms β	rms ϕ	rms r	PR	Pilot
932	3.26	.60	.54	2.18	.12		JBJ
933	3.66	.60	.57	1.89	.12	3	
934	5.81	.89	.93	2.68	.20		
935	4.89	.98	.87	3.78	.21	4.5	
936	7.08	.92	.97	3.16	.25		
937	7.07	.72	.96	2.96	.25	5.5	
938	3.24	.59	.55	5.58	.14		JTT
939	3.70	.64	.62	4.90	.16	4	
940	6.42	.95	1.03	6.16	.27		
941	5.56	.81	.86	4.73	.24	4.5	
942	7.73	1.10	.94	8.22	.26		
943	6.80	.95	.97	5.22	.27	5	
944	3.29	.73	.58	3.32	.13		WWK
945	3.98	.81	.74	3.42	.17	4	
946	5.18	.93	.85	2.89	.19		
947	6.10	.97	.99	2.77	.21	4	
948	7.12	1.12	1.16	2.88	.26		
949	6.97	1.16	1.15	3.21	.27	4.5	

A-7 CASE 4 FAILURE WITHOUT AUGMENTER

Flight	rms v_g	rms ψ_e	rms β	rms ϕ	rms r	PR	Pilot
950	3.24	.62	.54	2.32	.13		JBJ
951	3.61	.71	.66	2.37	.14	3.5	
952	5.46	.88	.88	6.02	.22		
953	5.03	.75	.78	4.26	.17	5.5	
954	7.61	1.10	1.11	4.57	.26		
955	7.11	1.04	1.04	4.60	.25	6.5	
956	3.67	.71	.66	6.95	.14		JTT
957	3.93	.63	.65	5.33	.16	4.5	
958	5.49	.72	.77	5.51	.22		
959	5.41	.85	.85	6.28	.23	5	
960	7.10	.92	1.10	8.84	.25		
961	7.32	.93	1.10	8.97	.29	6.5	
962	3.09	.66	.57	2.82	.15		WWK
963	3.33	.57	.56	3.01	.13	3	
964	5.55	.88	.92	3.48	.22		
965	5.86	.95	.99	3.30	.22	4.5	
966	6.86	1.14	1.18	3.78	.29		
967	7.82	1.40	1.35	4.09	.31	4.5	

F-5 CASE 1 WITH AUGMENTER

Flight	rms w_g	rms θ_c	rms θ_e	PR	Pilot
968	6.25		.49		JTT
969	5.91		.36	4	
970	10.66		.73		
971	10.58		.74	7	
972	3.54		.24		WWK
973	3.58		.25	3.5	
974	6.67		.48		
975	8.33		.61	5.5	
976		1.74	.50		
977		1.85	.42		
978	4.09		.29		JBJ
979	3.78		.29	4	
980	6.30		.44		
981	7.29		.50	7.5	
982	1.84		.16		
983	1.82		.19	4	
984		1.37	.41		
985		1.44	.48		

F-5 CASE 1 WITHOUT AUGMENTER

Flight	rms w_g	rms θ_c	rms θ_e	PR	Pilot
986	5.13		.50		JTT
987	5.54		.47	5	
988	3.36		.37		WWK
989	4.02		.47	4	
990	7.09		.66		
991	6.84		.66	7	
992		2.24	.46		
993		1.50	.52		
994	3.72		.38		JBJ
995	3.81		.37	6	
996	5.69		.57	8	
997	1.93		.19	4.5	
998	1.81		.24		
999		1.58	.46		
1000		1.37	.39		

F-5 CASE 2 WITH AUGMENTER

Flight	rms w_g	rms θ_c	rms θ_e	PR	Pilot
1001	3.14		.35		WWK
1002	2.99		.29	4	
1003	4.41		.45		
1004	5.28		.60	4.5	
1005	9.55		.92		
1006	9.33		.88	5.5	
1007		1.62	.54		
1008		1.54	.50		
1009	1.57		.18		JBJ
1010	1.67		.19	4.5	
1011	2.58		.28		
1012	2.52		.26	5.5	
1013	4.37		.41		
1014	3.48		.37	7	
1015		1.10	.42		
1016		1.59	.52		
1017	3.47		.34		JTT
1018	2.97		.30	3	
1019	5.16		.49		
1020	5.02		.47	4.5	
1021	7.38		.71	7	
1022	7.39		.68		
1023		1.33	.55		
1024		1.33	.45		

F-5 CASE 2 WITHOUT AUGMENTER

Flight	rms w_g	rms θ_c	rms θ_e	PR	Pilot
1025	3.32		.51		WWK
1026	3.33		.51	5	
1027	5.20		.78		
1028	4.66		.77	5.5	
1029	9.19		1.25		
1030	8.47		1.17	6.5	
1031		1.95	.68		
1032		1.56	.53		
1033	1.60		.23		JBJ
1034	1.54		.23	5	
1035	2.57		.37		
1036	2.50		.34	6	
1037	3.97		.63		
1038	4.40		.57	7.5	
1039		1.22	.51		
1040		1.70	.59		
1041	2.85		.38		JTT
1042	2.78		.33	5.5	
1043	4.92		.59		
1044	5.64		.63	6.5	
1045	7.17		.86		
1046	7.49		.96	7.5	
1047		1.42	.45		
1048		1.40	.62		

F-5 CASE 3 WITH AUGMENTER

Flight	rms w_g	rms θ_c	rms θ_e	PR	Pilot
1049	5.47		.28		JBJ
1050	5.94		.32	2.5	
1051	9.02		.52		
1052	8.74		.50	3.5	
1053	14.09		.79		
1054	13.02		.71	6	
1055		1.31	.47		
1056		1.45	.50		
1057	5.79		.37		JTT
1058	5.37		.38	4.5	
1059	9.02		.57		
1060	10.55		.63	8	
1061	2.48		.28		
1062	2.34		.18	2	
1063		1.60	.42		
1064		1.48	.44		
1065	2.32		..18		WWK
1066	2.24		.14	2.5	
1067	6.13		.38		
1068	5.82		.36	5	
1069	8.95		.63		
1070	8.60		.55	7.5	
1071		1.15	.50		
1072		1.96	.47		

F-5 CASE 3 WITHOUT AUGMENTER

Flight	rms w_g	rms θ_c	rms θ_e	PR	Pilot
1073	6.62		.44		JBJ
1074	6.15		.46	3	
1075	8.83		.69		
1076	8.47		.67	5	
1077	15.02		1.04		
1078	12.87		1.06		
1079		1.08	.40		
1080		1.11	.40		
1081	5.43		.52		JTT
1082	5.40		.45	6	
1083	8.94		.84	9	
1084	2.60		.26		
1085	2.23		.25	3.5	
1086		1.36	.44		
1087		1.48	.52		
1088	2.65		.24		WWK
1089	2.34		.19	4	
1090	5.65		.45		
1091	5.34		.46	6.5	
1092	7.71		.62		
1093	7.03		.60	8	
1094		1.27	.48		
1095		1.22	.47		

F-5 CASE 4 WITH AUGMENTER

Flight	rms w_g	rms θ_c	rms θ_e	PR	Pilot
1096	7.17		.43		JBJ
1097	6.90		.40	3	
1098	12.70		.73		
1099	11.70		.73	5	
1100	17.70		.96		
1101	17.28		1.00	6.5	
1102		1.57	.52		
1103		1.26	.44		
1104	7.05		.48		JTT
1105	6.68		.49	3	
1106	12.38		.90		
1107	11.75		.84	5.5	
1108	17.05		1.07		
1109	17.66		1.18	7	
1110		1.62	.66		
1111		1.46	.52		
1112	7.65		.55		WWK
1113	6.86		.49	4.5	
1114	12.73		.96		
1115	12.48		.89	6	
1116	3.87		.27		
1117	4.39		.31	4	
1118		1.58	.60		
1119		1.51	.59		

F-5 CASE 4 WITHOUT AUGMENTER

Flight	rms w_g	rms θ_c	rms θ_e	PR	Pilot
1120	6.62		.54		JBJ
1121	7.37		.54	4	
1122	10.88		.97		
1123	12.32		.94	6.5	
1124	15.07		1.12		
1125	17.83		1.16	7.5	
1126		1.56	.71		
1127		1.41	.55		
1128	7.44		.67		JTT
1129	7.35		.74	4	
1130	12.97		1.10		
1131	11.79		1.00	6.5	
1132	16.52		1.26		
1133	17.15		1.31	8	
1134		1.49	.56		
1135		1.30	.62		
1136	6.58		.73		WWK
1137	7.05		.71	5.5	
1138	11.10		1.16		
1139	10.58		1.20	7	
1140	4.34		.46		
1141	4.11		.45	4.5	
1142		1.09	.60		
1143		1.31	.66		

A-7 CASE 1 WITH AUGMENTER

Flight	rms w_g	rms θ_c	rms θ_e	PR	Pilot
1144	5.81		.54		JTT
1145	6.01		.52	3.5	
1146	9.74		.71		
1147	11.27		.74	6	
1148	12.18		.81		
1149	11.69		.80	7.5	
1150		1.73	.65		
1151		1.44	.51		
1152	6.00		.44		WWK
1153	6.34		.42	4.5	
1154	11.14		.78		
1155	11.11		.78	5.5	
1156	14.67		1.03		
1157	13.75		.86	6	
1158		1.45	.42		
1159		1.28	.35		
1160	4.68		.32	4	
1161	4.66		.39		JBJ
1162	4.87		.35	3	
1163	8.33		.53		
1164	8.23		.56	5.5	
1165	11.86		.81		
1166	11.40		.84	7	
1167		1.26	.44		
1168		1.42	.42		

A-7 CASE 1 WITHOUT AUGMENTER

Flight	rms w_g	rms θ_c	rms θ_e	PR	Pilot
1169	5.57		.66		JTT
1170	5.95		.66	5	
1171	12.19		1.06		
1172	10.87		.95	7.5	
1173	13.11		1.26		
1174	12.29		1.02	8.5	
1175		1.12	.49		
1176		1.37	.51		
1177	6.21		.88		WWK
1178	5.97		.73	6	
1179	10.14		1.31		
1180	11.40		1.39	7.5	
1181		1.13	.46		
1182		1.27	.44		
1183	3.84		.54		JBJ
1184	4.18		.53	4.5	
1185	10.08		.98		
1186	8.76		.82	6.5	
1187	12.60		1.30	8	
1188		1.60	.39		
1189		1.06	.39		

A-7 CASE 2 WITH AUGMENTER

Flight	rms w_g	rms θ_c	rms θ_e	PR	Pilot
1190	6.41		.45		JTT
1191	6.71		.45	5	
1192	7.59		.45		
1193	8.24		.47	7	
1194	3.05		.25		
1195	3.20		.25	3	
1196		1.48	.42		
1197		1.42	.46		
1198	2.91		.18		WWK
1199	3.22		.20	3	
1200	6.21		.36		
1201	5.73		.31	4	
1202	9.11		.51		
1203	8.45		.52	6.5	
1204		1.71	.45		
1205		1.76	.35		
1206	3.20		.30		JBJ
1207	3.09		.30	2.5	
1208	6.21		.39		
1209	5.63		.32	4	
1210	9.23		.57		
1211	9.57		.59	6.5	
1212		1.21	.39		
1213		1.30	.36		

A-7 CASE 2 WITHOUT AUGMENTER

Flight	rms w_g	rms θ_c	rms θ_e	PR	Pilot
1214	3.07		.33		JTT
1215	2.69		.28	5	
1216		1.78	.58		
1217		1.58	.57		
1218	3.40		.30		WWK
1219	2.82		.31	4	
1220	6.42		.63		
1221	7.20		.59	6	
1222	8.81		.77	9.5	
1223		2.21	.42		
1224		1.70	.41		
1225	3.29		.39		JBJ
1226	3.39		.42	4	
1227	7.43		.71		
1228	7.04		.64	7	
1229	8.44		1.02	9	
1230		1.37	.42		
1231		1.60	.45		

A-7 CASE 3 WITH AUGMENTER

Flight	rms w_g	rms θ_c	rms θ_e	PR	Pilot
1232	5.95		.29		JBJ
1233	6.34		.26	2.5	
1234	10.76		.43		
1235	11.55		.43	5	
1236	16.77		.97		
1237	18.65		1.11	7	
1238		1.50	.38		
1239		1.94	.38		
1240	6.24		.39		JTT
1241	6.03		.37	4	
1242	11.86		.68		
1243	11.30		.58	6.5	
1444	16.56		.84		
1245	17.08		.87	8	
1246		1.84	.41		
1247		1.36	.39		
1248	5.46		.41		WWK
1249	6.02		.52	4.5	
1250	12.70		1.00		
1251	11.44		.83	6	
1252	16.29		1.23	7.5	
1253	19.40		1.30	7.5	
1254		1.29	.72		
1255		1.53	.50		

A-7 CASE 3 WITHOUT AUGMENTER

Flight	rms w_g	rms θ_c	rms θ_e	PR	Pilot
1256	5.73		.35		JBJ
1257	5.81		.33	3.5	
1258	11.70		.87		
1259	11.86		.85	6	
1260	17.61		1.24		
1261	16.68		1.15	8.5	
1262		1.61	.48		
1263		2.20	.49		
1264	5.77		.44		JTT
1265	5.38		.40	5	
1266	12.96		.82		
1267	10.65		.82	7.5	
1268	17.66		1.05		
1269	17.81		1.17	8.5	
1270		1.58	.41		
1271		1.49	.43		
1272	5.79		.81		WWK
1273	7.06		.85	6	
1274	11.61		1.30		
1275	11.53		1.20	7	
1276	15.24		1.70	8.5	
1277		1.30	.65		
1278		1.69	.76		

A-7 CASE 4 WITH AUGMENTER

Flight	rms w_g	rms θ_c	rms θ_e	PR	Pilot
1279	3.15		.19		JBJ
1280	2.72		.21	2	
1281	6.75		.42		
1282	5.97		.31	3	
1283	8.46		.50		
1284	8.97		.51	4.5	
1285		1.58	.47		
1286		1.48	.40		
1287	2.78		.16		JTT
1288	3.58		.19	1.5	
1289	6.37		.33		
1290	6.47		.32	4	
1291	8.54		.45		
1292	9.32		.47	6.5	
1293		1.59	.48		
1294		1.24	.34		
1295	3.22		.23		WWK
1296	3.27		.23	3.5	
1297	5.96		.36		
1298	7.00		.46	4.5	
1299	9.06		.53		
1300	8.65		.51	5.5	
1301		1.64	.66		
1302		1.47	.49		

A-7 CASE 4 WITHOUT AUGMENTER

Flight	rms w_g	rms θ_c	rms θ_e	PR	Pilot
1303	2.86		.29		JBJ
1304	3.02		.30	3	
1305	6.01		.52		
1306	5.74		.54	4	
1307	9.39		.87		
1308	9.84		.80	6	
1309		1.93	.48		
1310		1.47	.44		
1311	3.45		.29		JTT
1312	3.56		.28	2.5	
1313	6.09		.51		
1314	5.63		.46	6	
1315	9.43		.73		
1316	10.73		.85	8	
1317		1.12	.37		
1318		1.29	.41		
1319	3.05		.33		WWK
1320	2.70		.33	4.5	
1321	5.68		.58		
1322	6.34		.65	5.5	
1323	8.77		.93		
1324	9.31		.92	6	
1325		1.56	.63		
1326		2.21	.62		

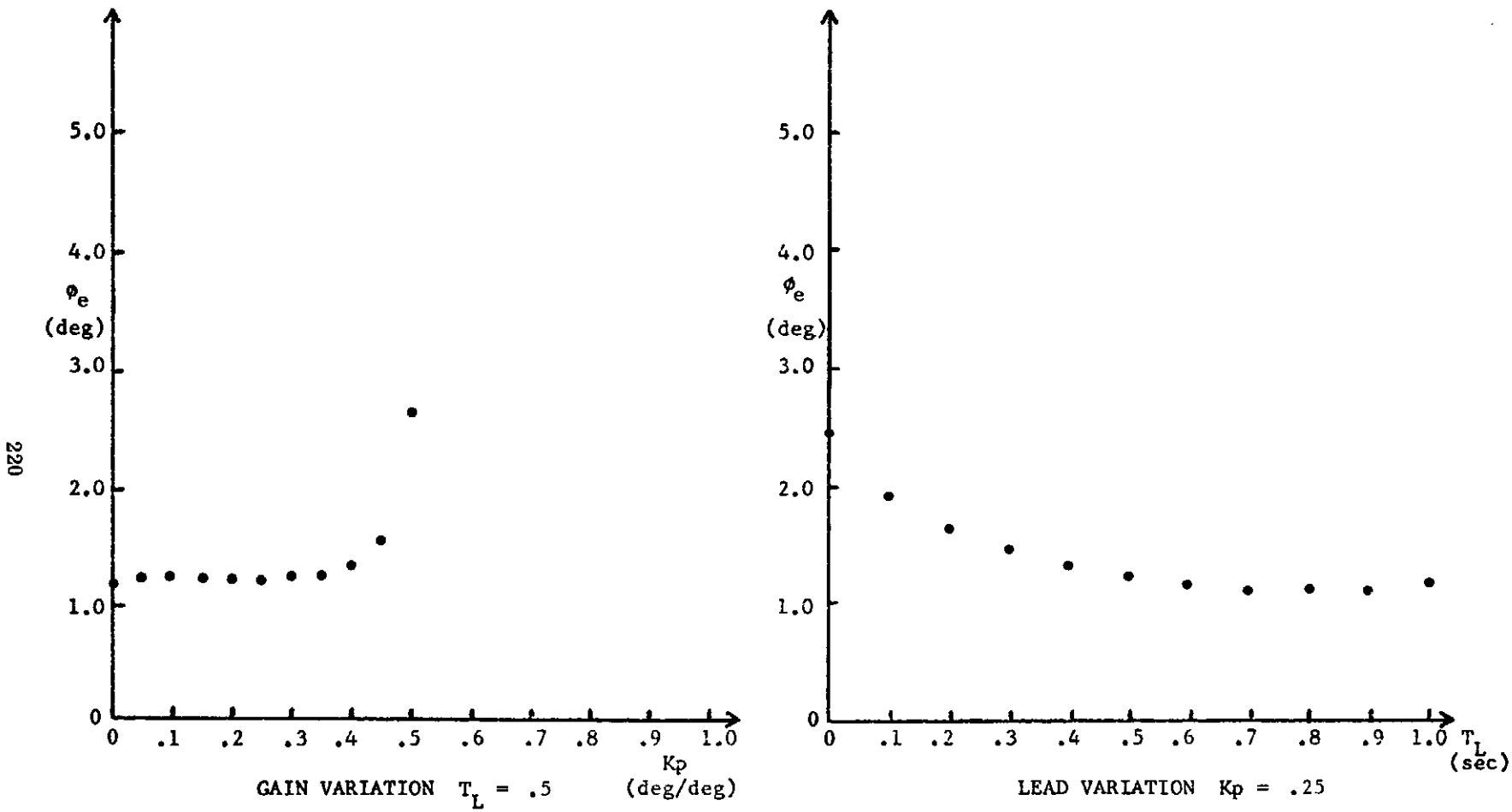

FIGURE 63. PILOT LEAD AND GAIN VARIATIONS
F-5 FLIGHT CONDITION 1
WITH AUGMENTER

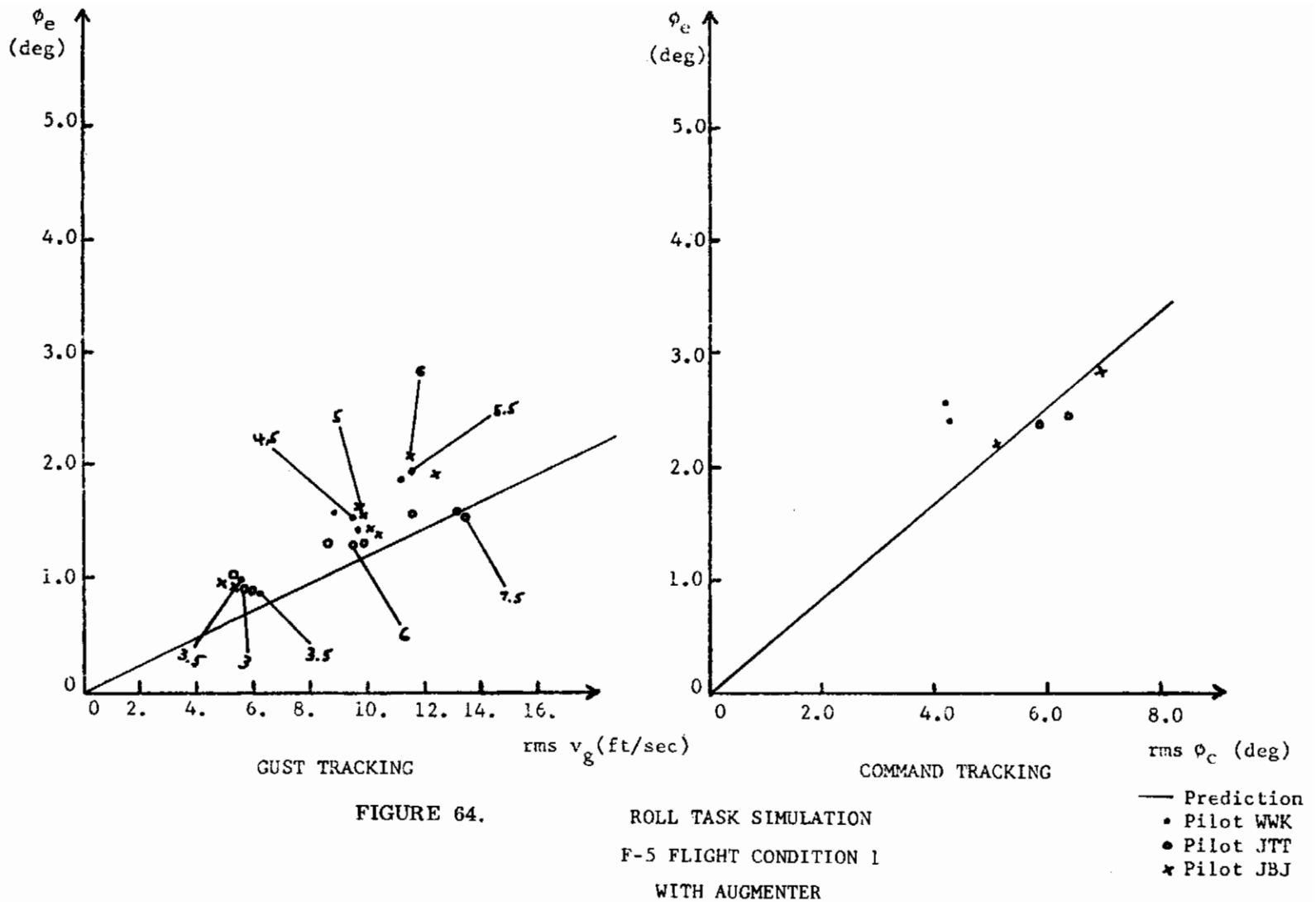

FIGURE 64. ROLL TASK SIMULATION
F-5 FLIGHT CONDITION 1
WITH AUGMENTER

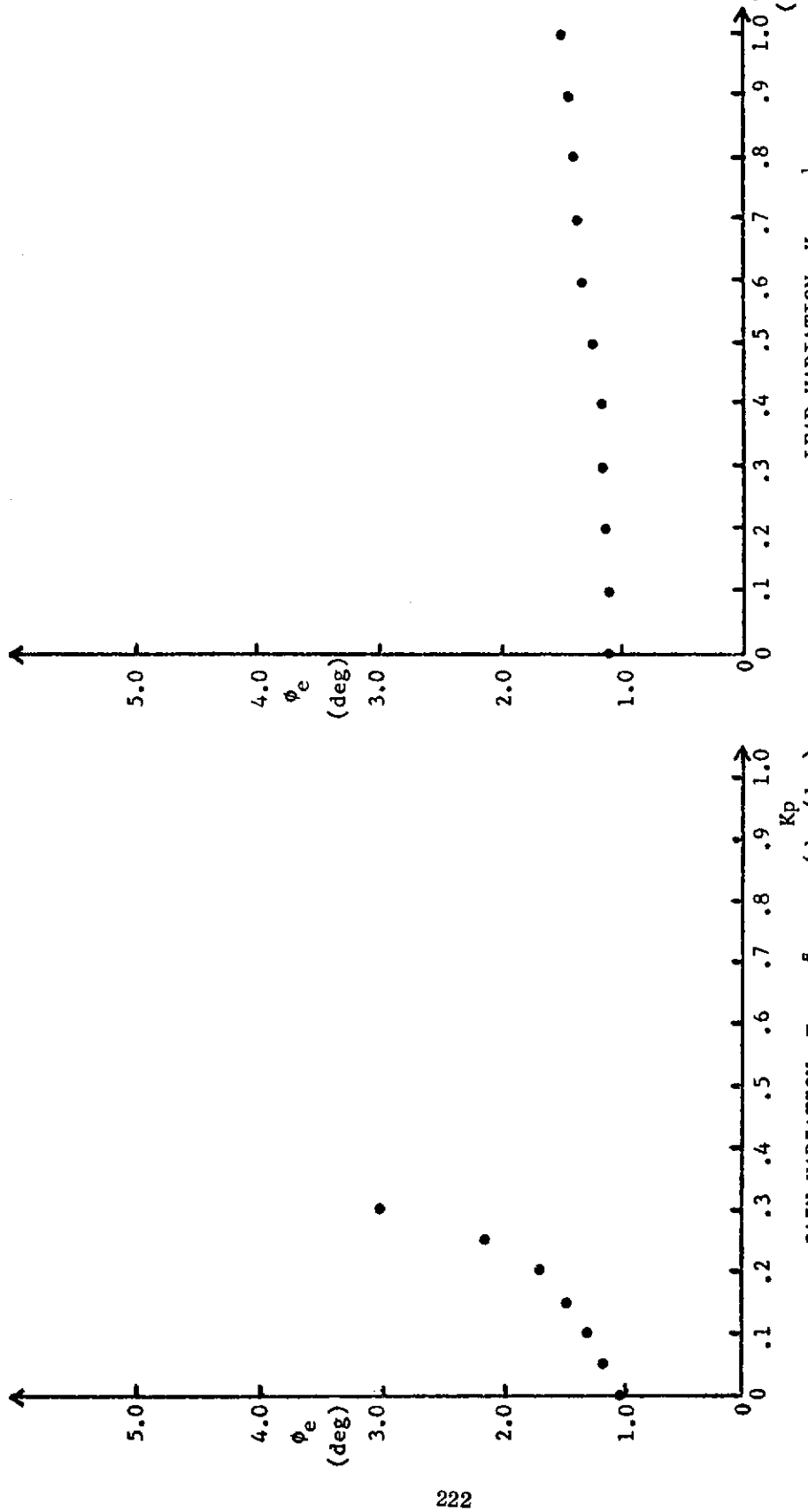

FIGURE 65. PILOT LEAD AND GAIN VARIATIONS
F-5 FLIGHT CONDITION 1
WITHOUT AUGMENTER

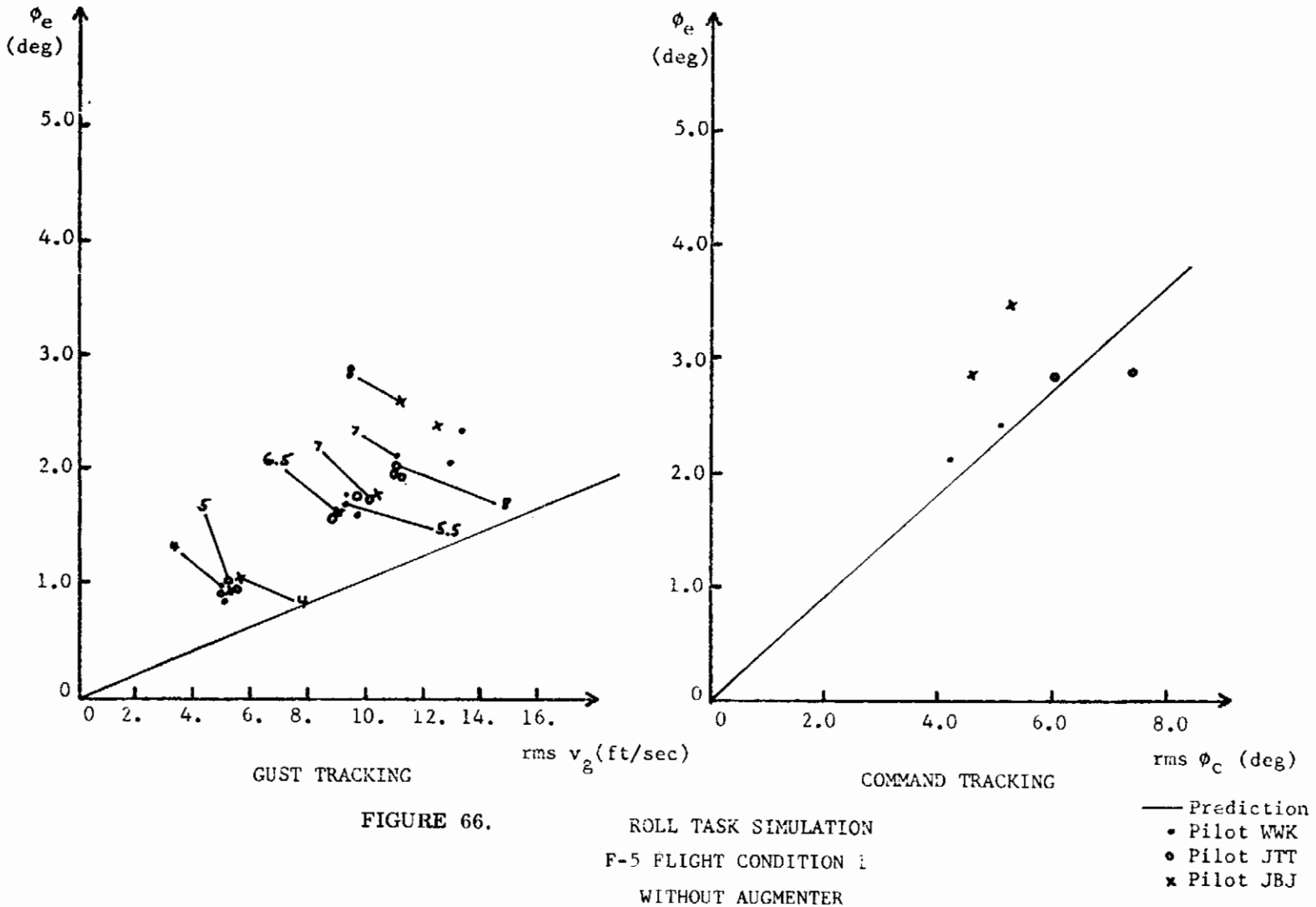

FIGURE 66. ROLL TASK SIMULATION
F-5 FLIGHT CONDITION 1
WITHOUT AUGMENTER

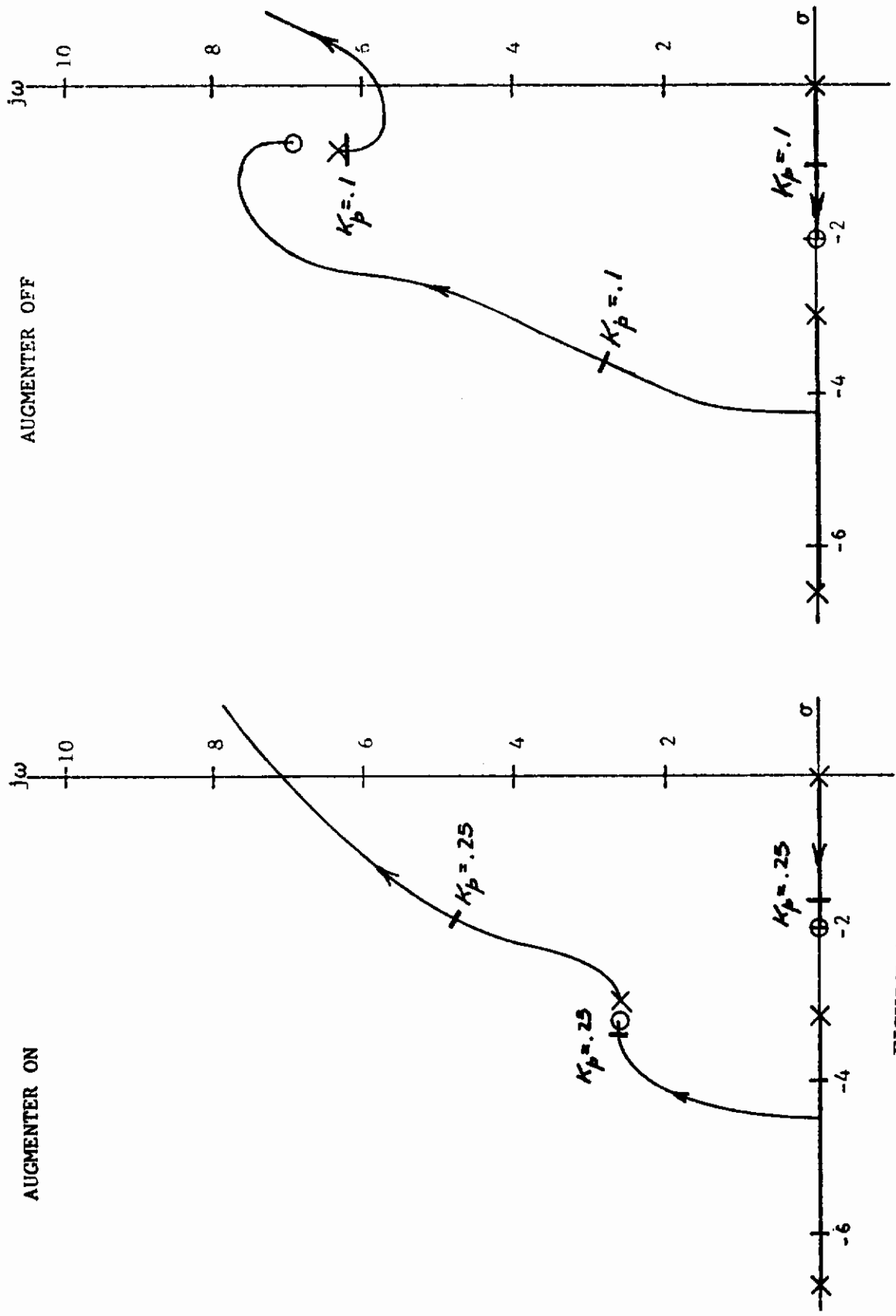

FIGURE 67. ROOT LOCUS FOR BANK ANGLE TRACKING
F-5 FLIGHT CONDITION 1
T_L = 0.5 SEC

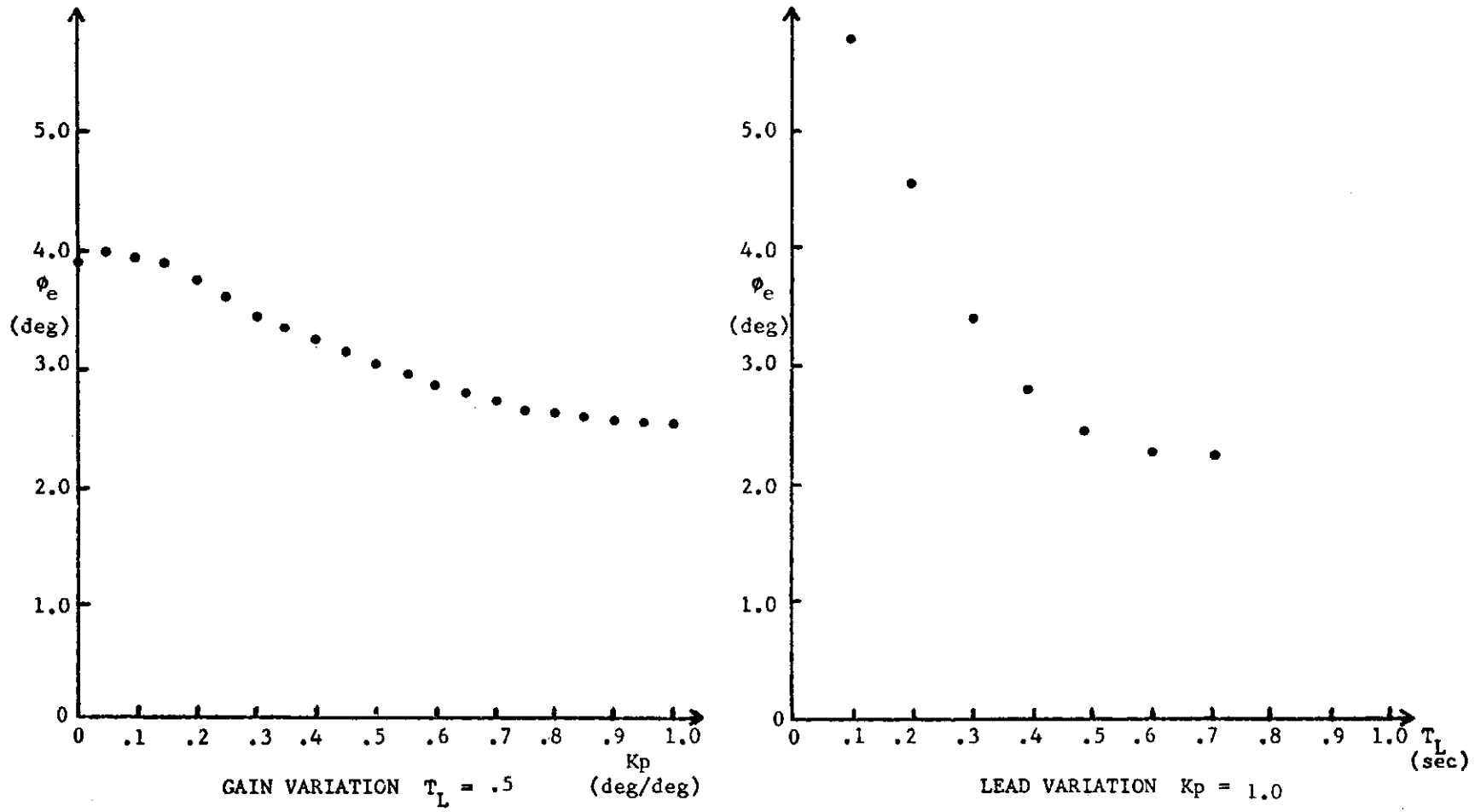

FIGURE 68. PILOT LEAD AND GAIN VARIATIONS
F-5 FLIGHT CONDITION 2
WITH AUGMENTER

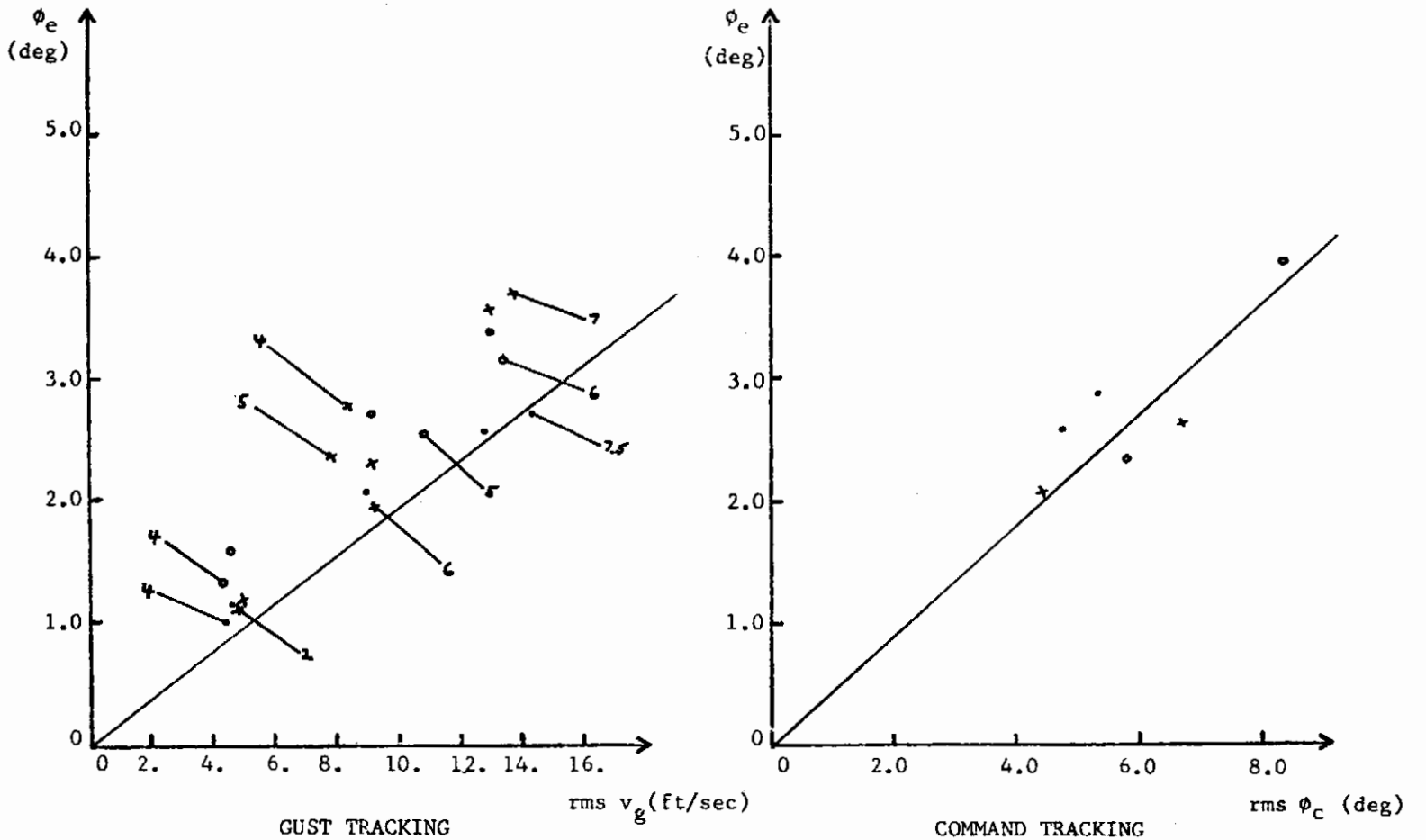

FIGURE 69. ROLL TASK SIMULATION
F-5 FLIGHT CONDITION 7
WITH AUGMENTER

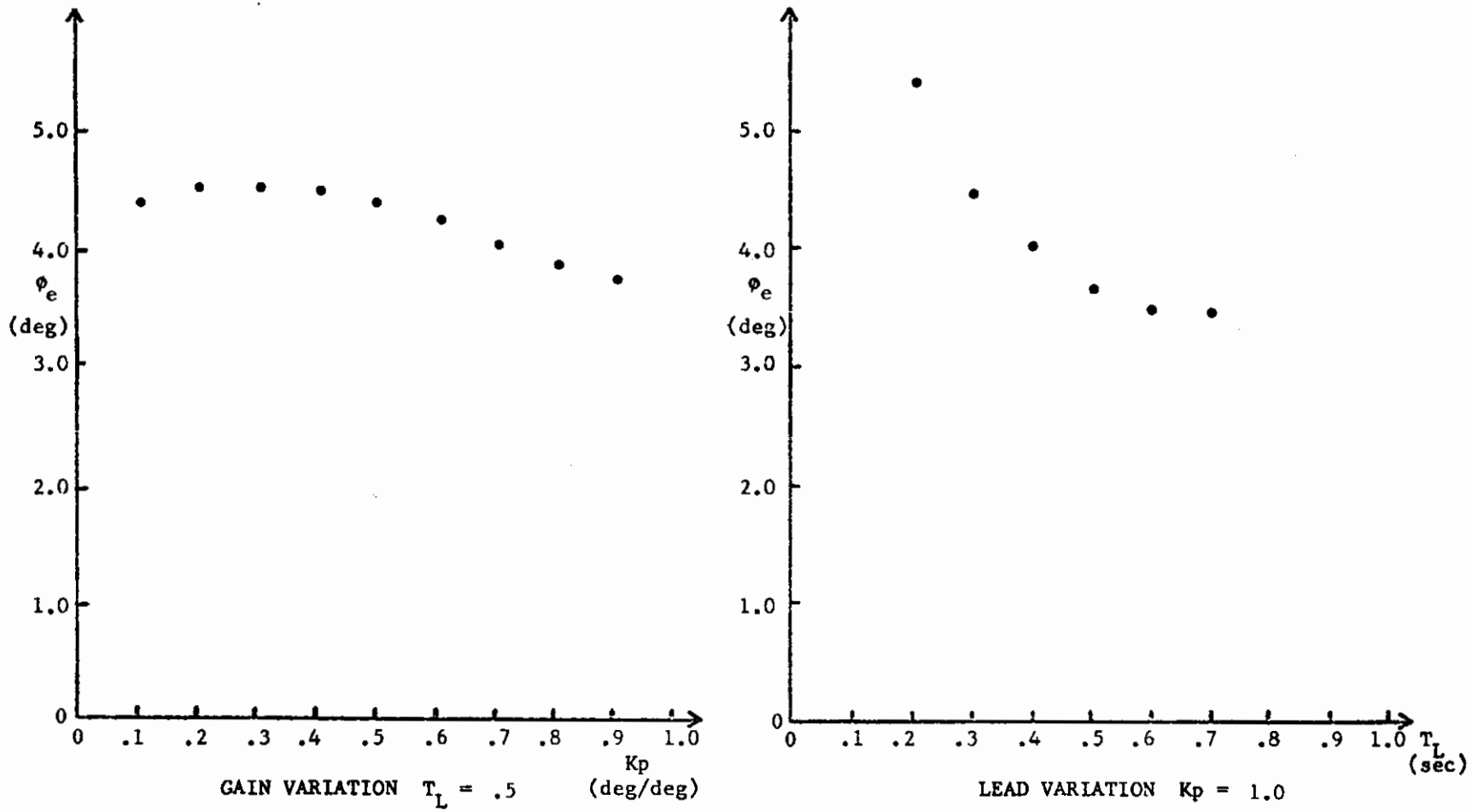

FIGURE 70. PILOT LEAD AND GAIN VARIATIONS
F-5 FLIGHT CONDITION 2
WITHOUT AUGMENTER

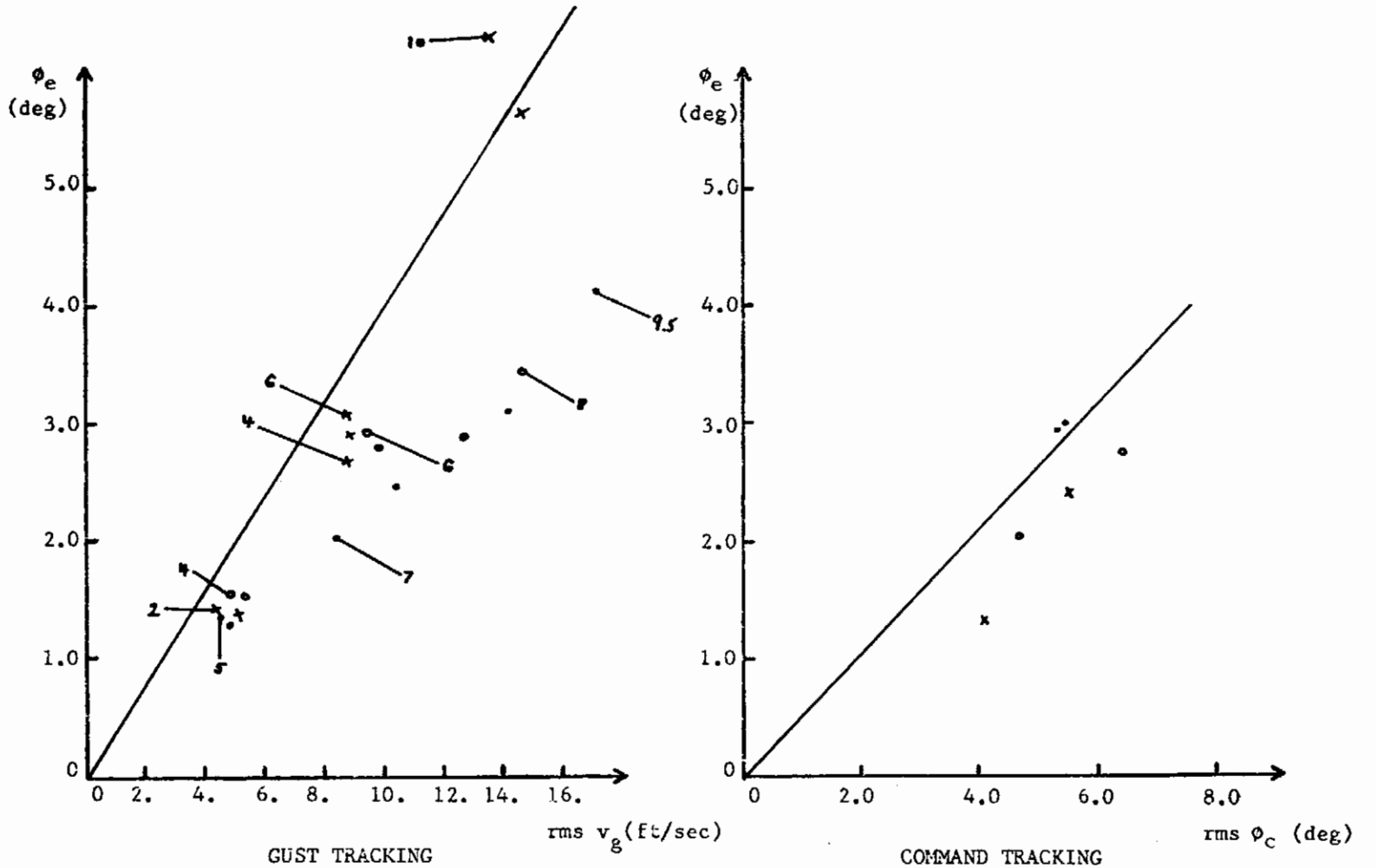

FIGURE 71. ROLL TASK SIMULATION
F-5 FLIGHT CONDITION 2
WITHOUT AUGMENTER

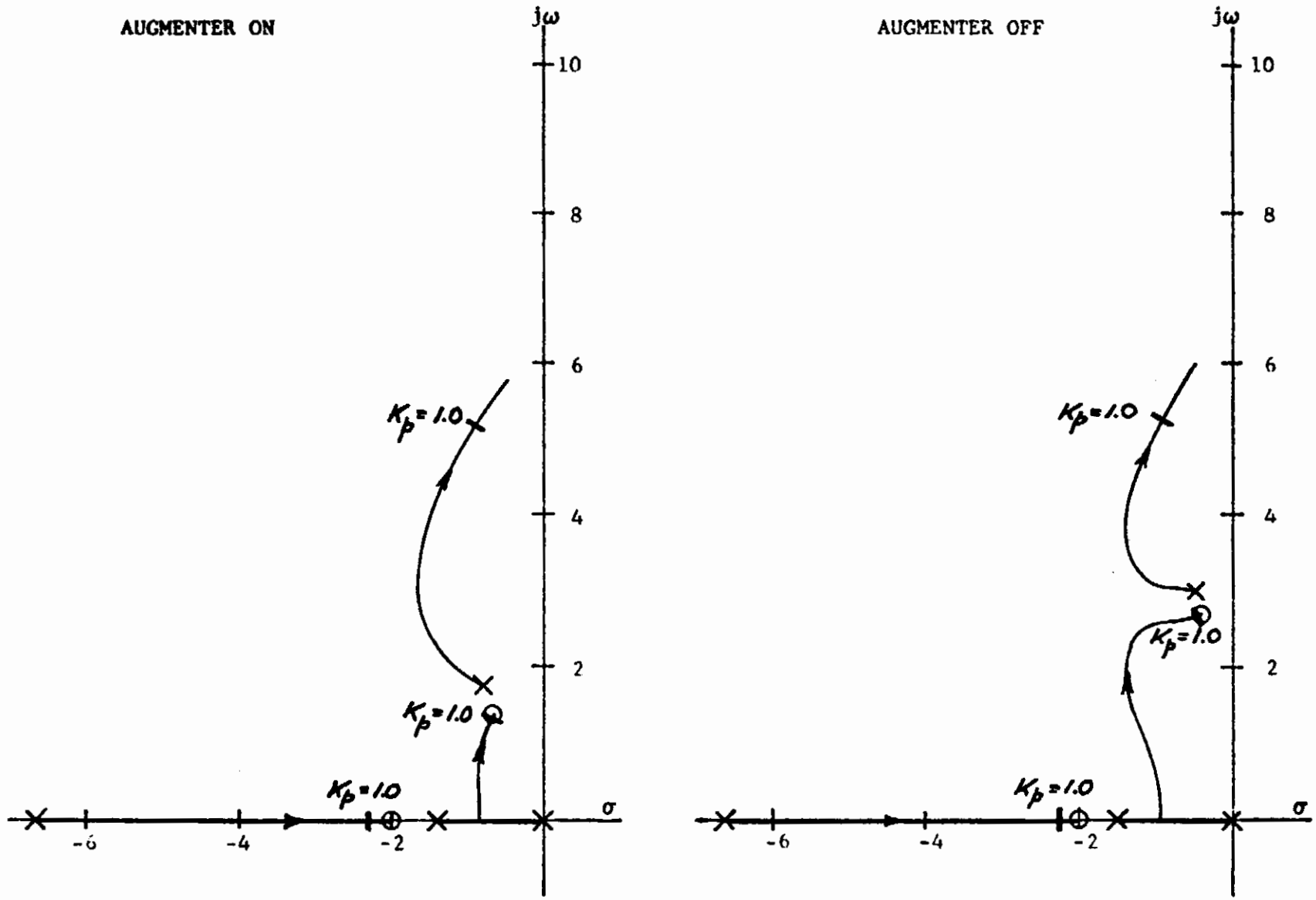

FIGURE 72. ROOT LOCUS FOR BANK ANGLE TRACKING
F-5 FLIGHT CONDITION 2
T_L = 0.5 SEC

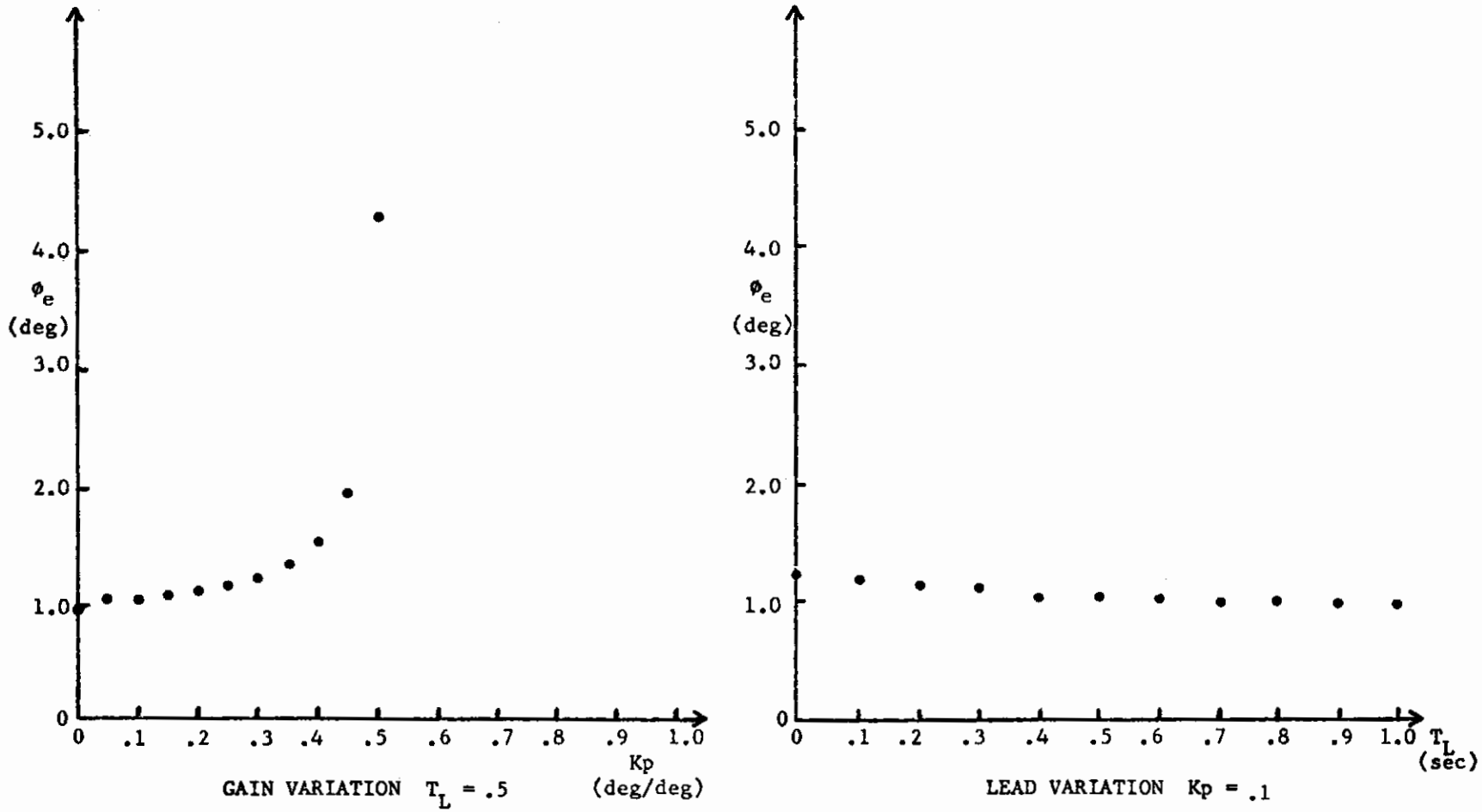

FIGURE 73. PILOT LEAD AND GAIN VARIATIONS
F-5 FLIGHT CONDITION 3
WITH AUGMENTER

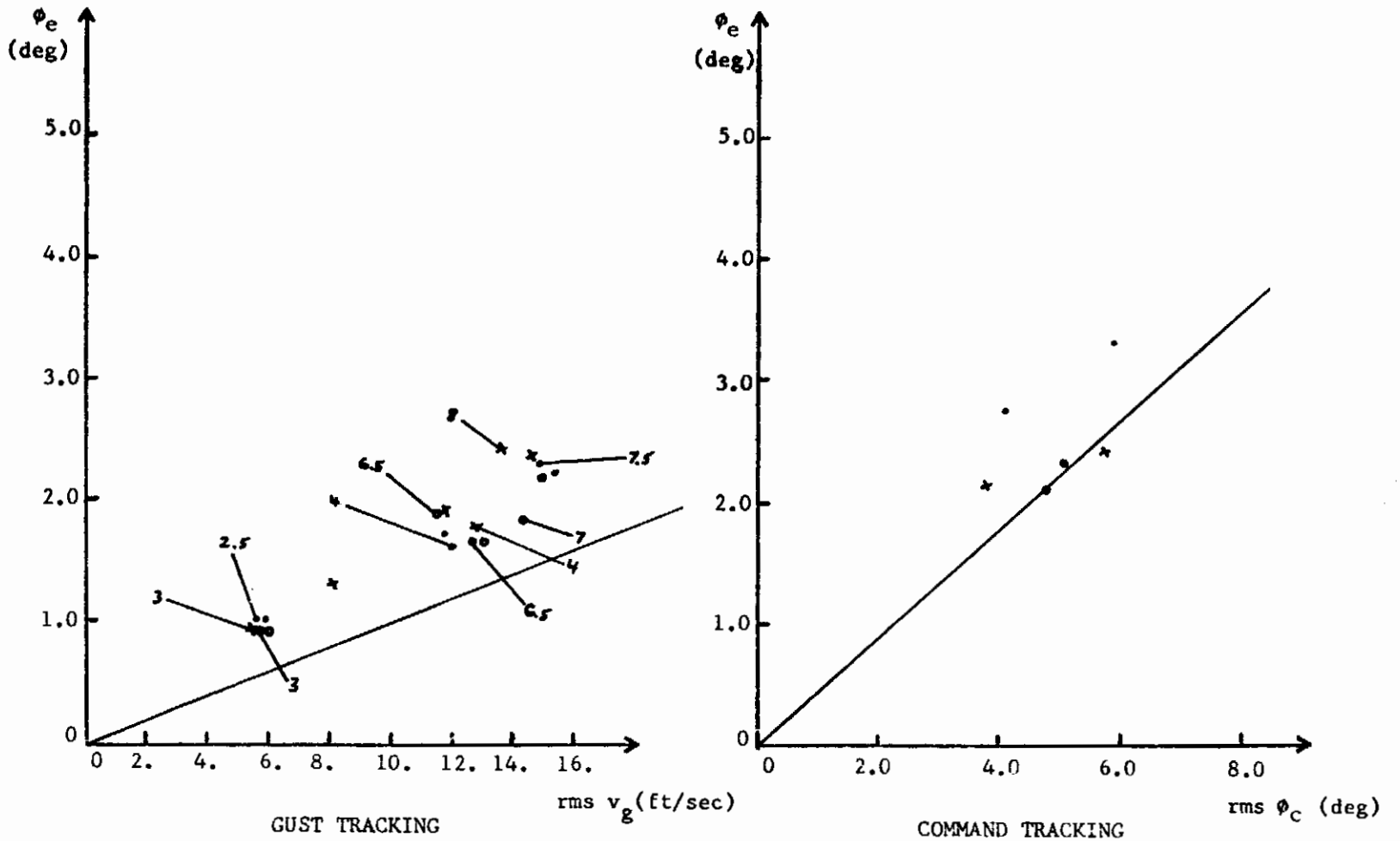

FIGURE 74.

ROLL TASK SIMULATION
F-5 FLIGHT CONDITION 3
WITH AUGMENTER

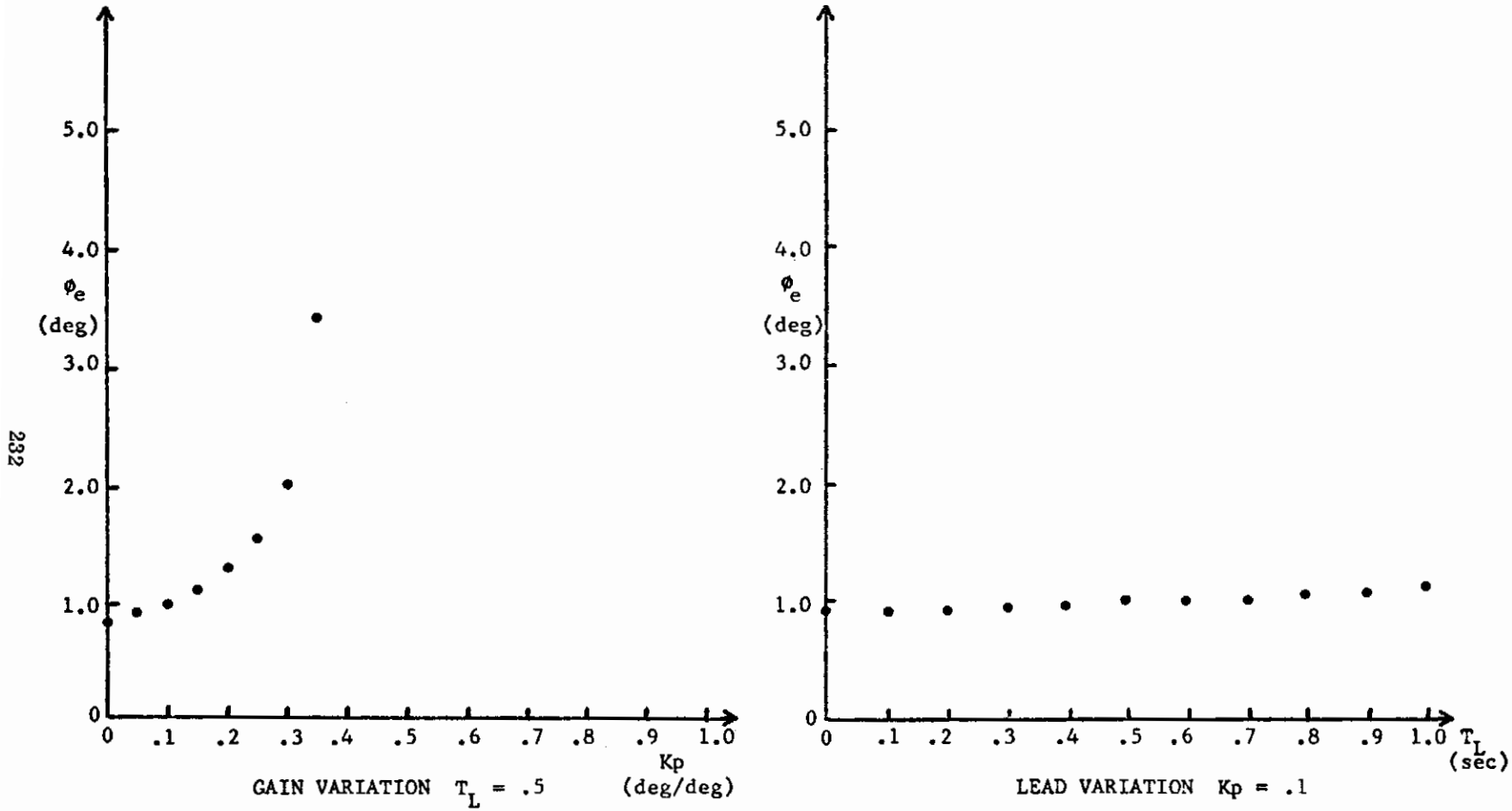

FIGURE 75. PILOT LEAD AND GAIN VARIATIONS
F-5 FLIGHT CONDITION 3
WITHOUT AUGMENTER

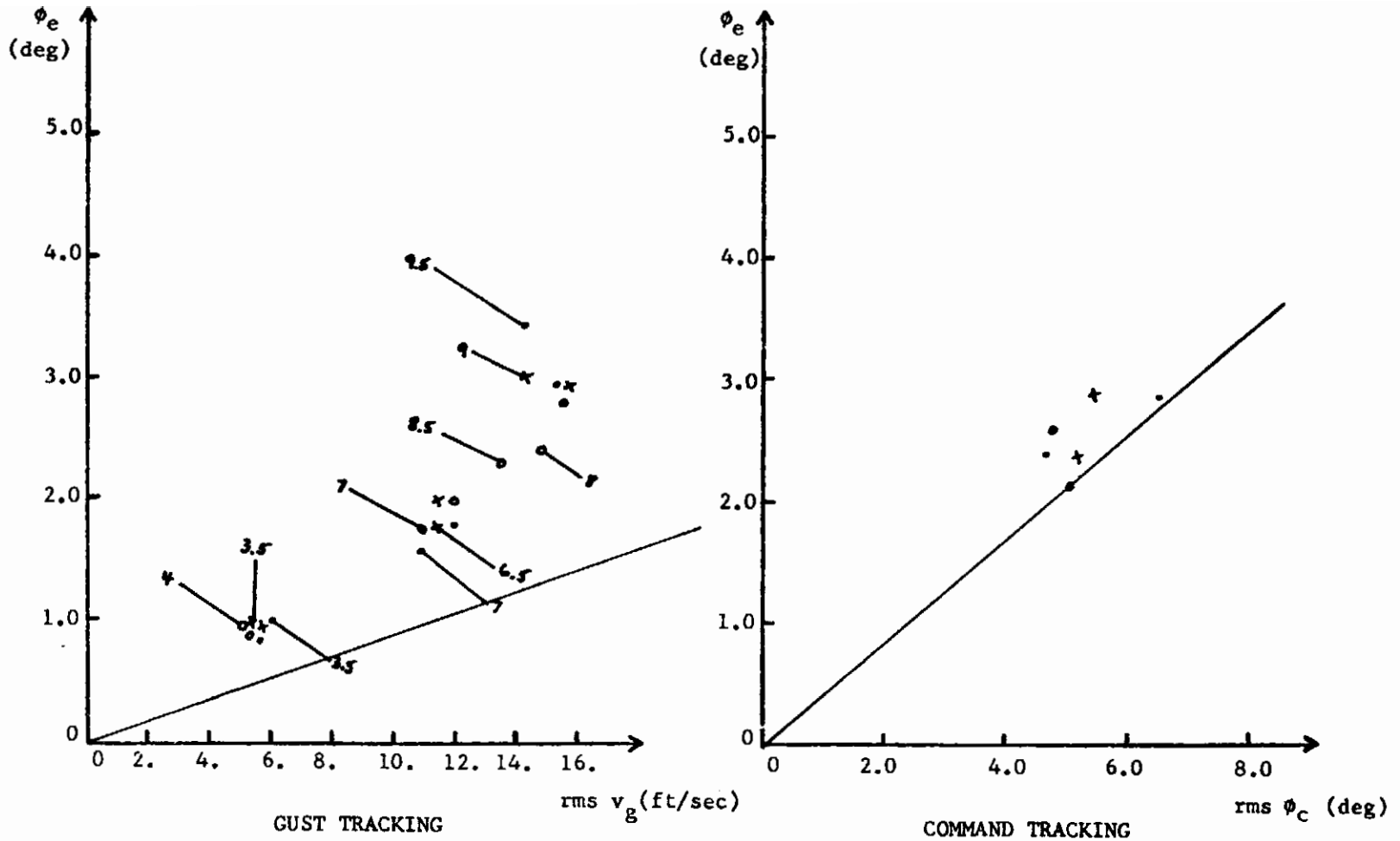

FIGURE 76. ROLL TASK SIMULATION
F-5 FLIGHT CONDITION 3
WITHOUT AUGMENTER

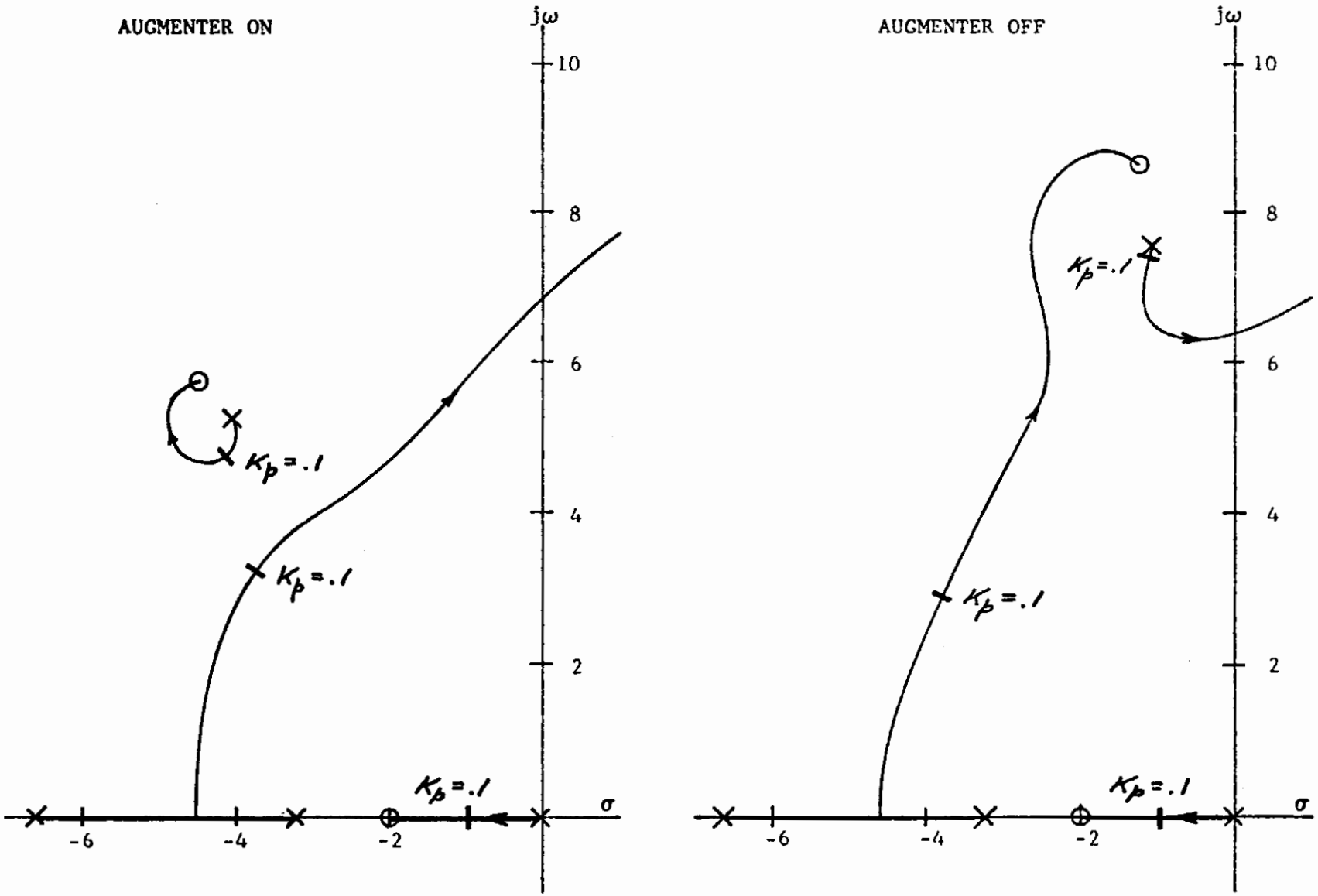

FIGURE 77. ROOT LOCUS FOR BANK ANGLE TRACKING
F-5 FLIGHT CONDITION 3
T_L = 0.5 SEC

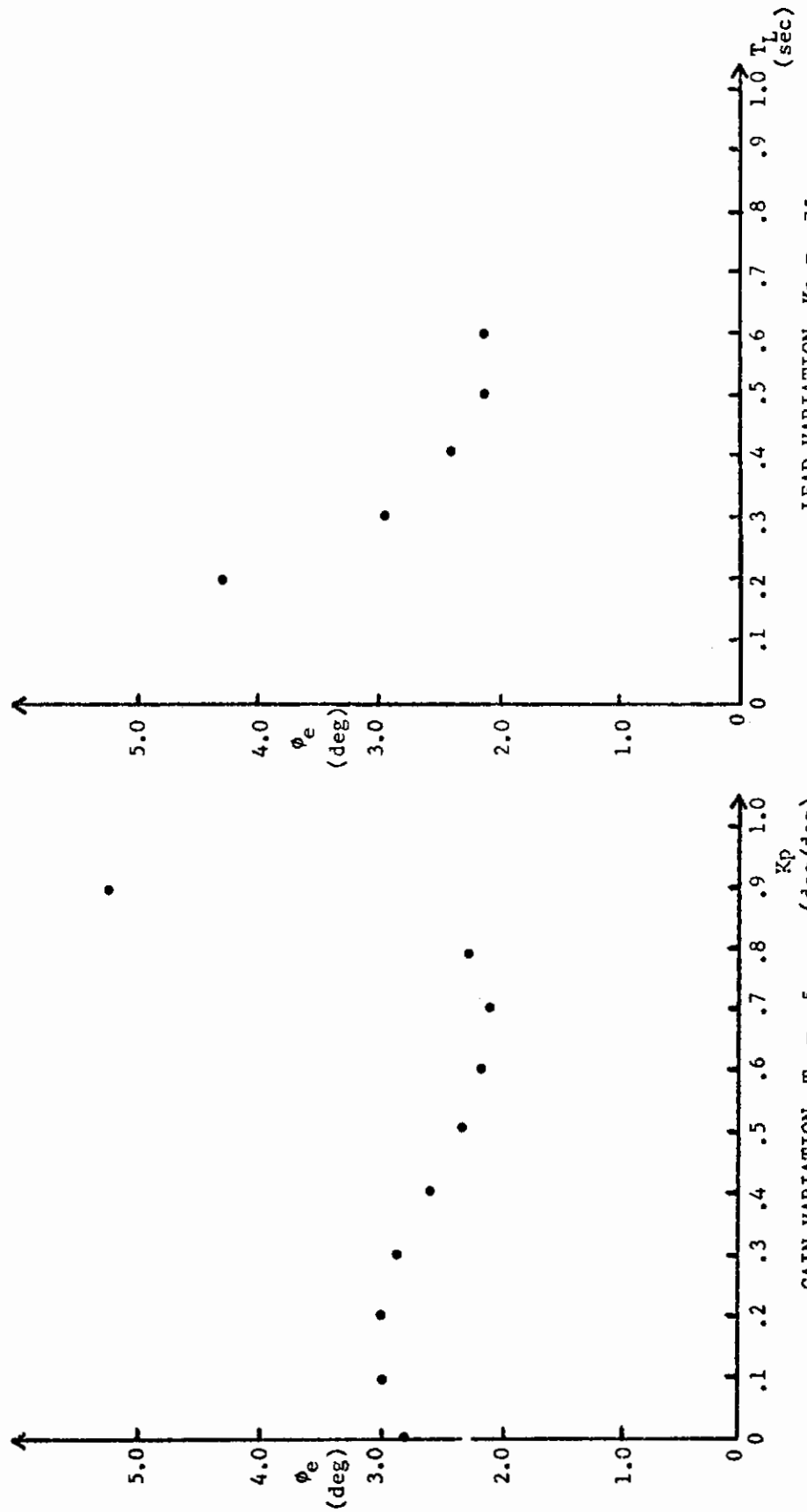

FIGURE 78. PILOT LEAD AND GAIN VARIATIONS
F-5 FLIGHT CONDITION 4
WITH AUGMENTER

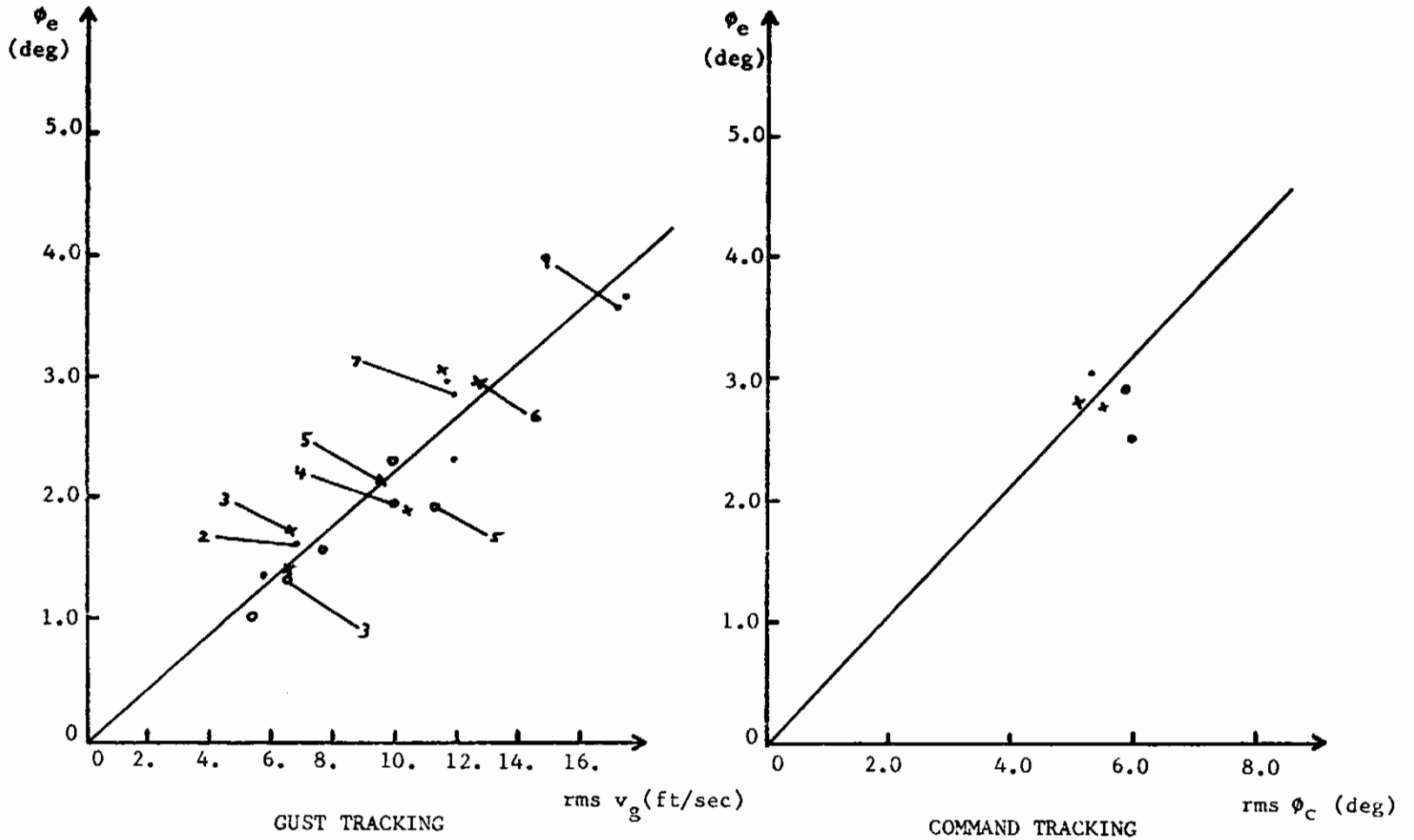

FIGURE 79. ROLL TASK SIMULATION
F-5 FLIGHT CONDITION 4
WITH AUGMENTER

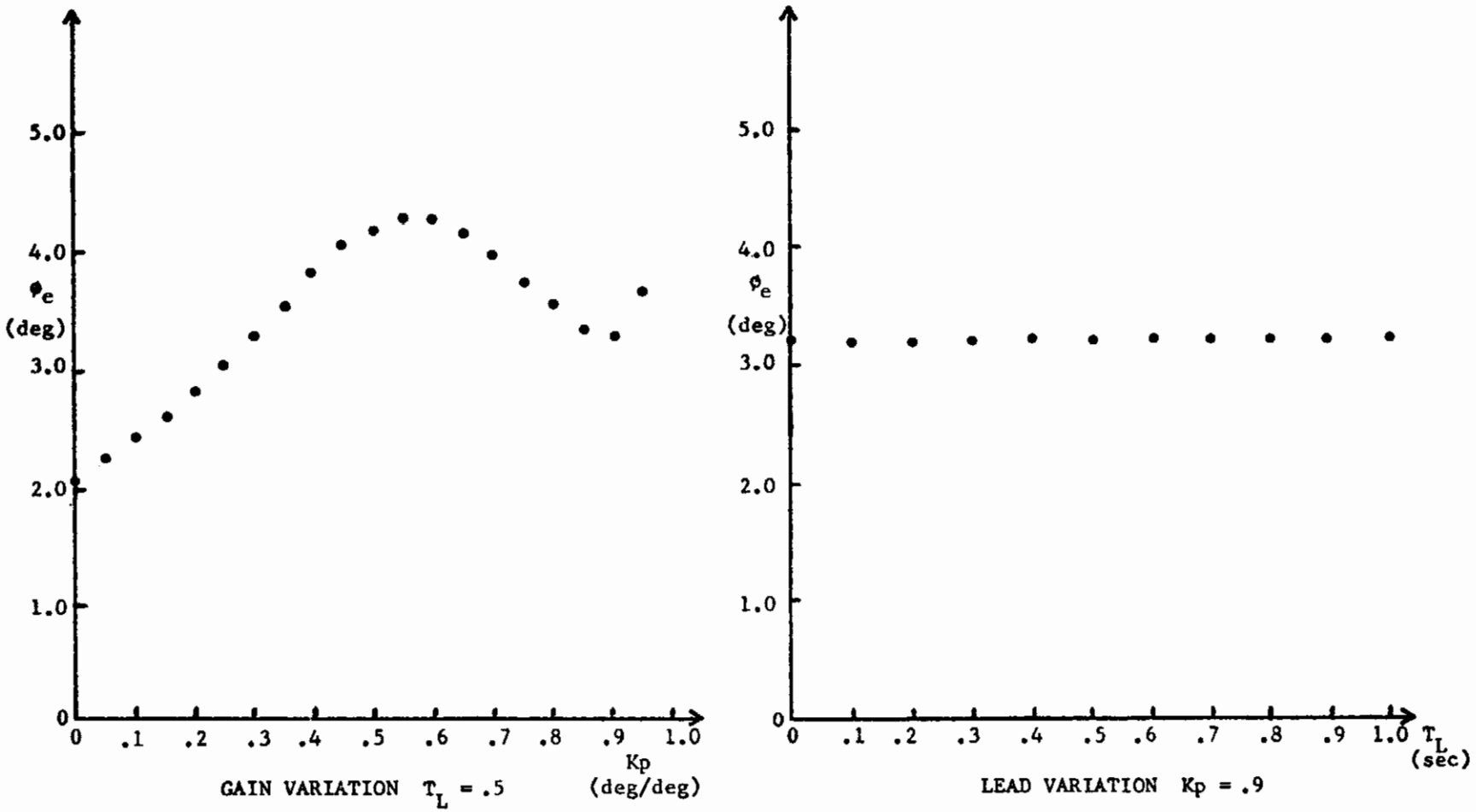

FIGURE 80. PILOT LEAD AND GAIN VARIATIONS
F-5 FLIGHT CONDITION 4
WITHOUT AUGMENTER

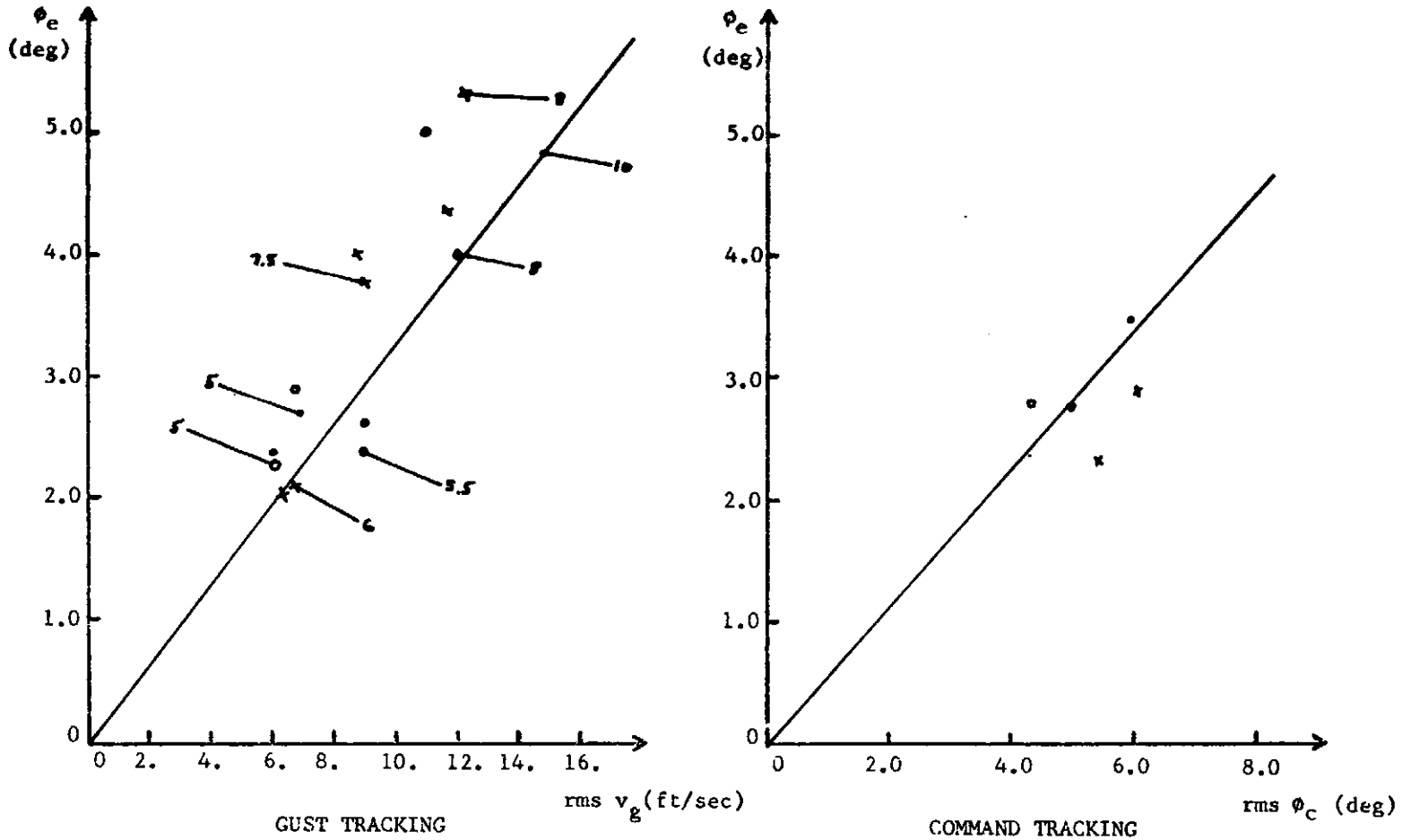

FIGURE 81. ROLL TASK SIMULATION
F-5 FLIGHT CONDITION 4
WITHOUT AUGMENTER

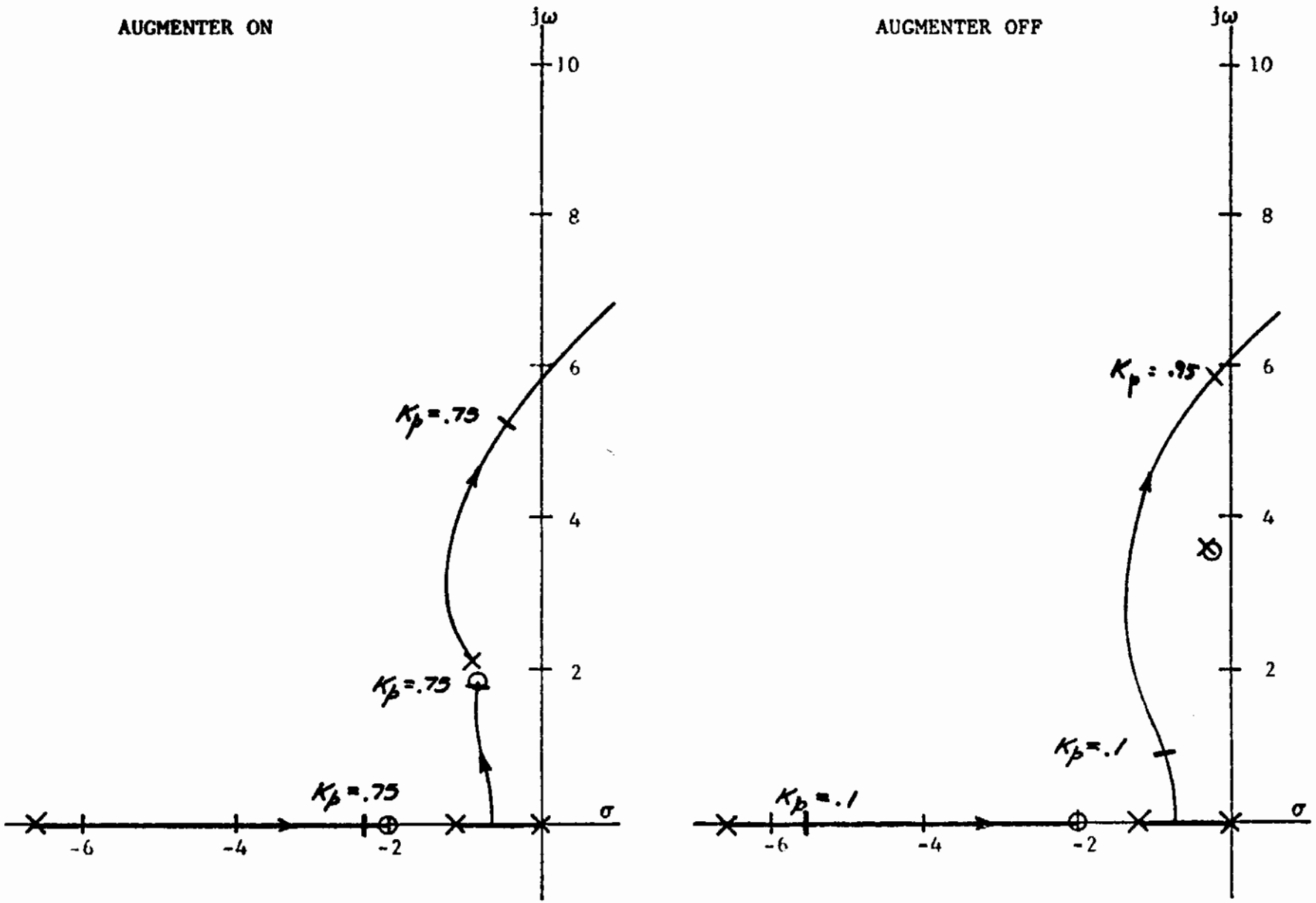

FIGURE 82. ROOT LOCUS FOR BANK ANGLE TRACKING
F-5 FLIGHT CONDITION 4
T_L = 0.5 SEC

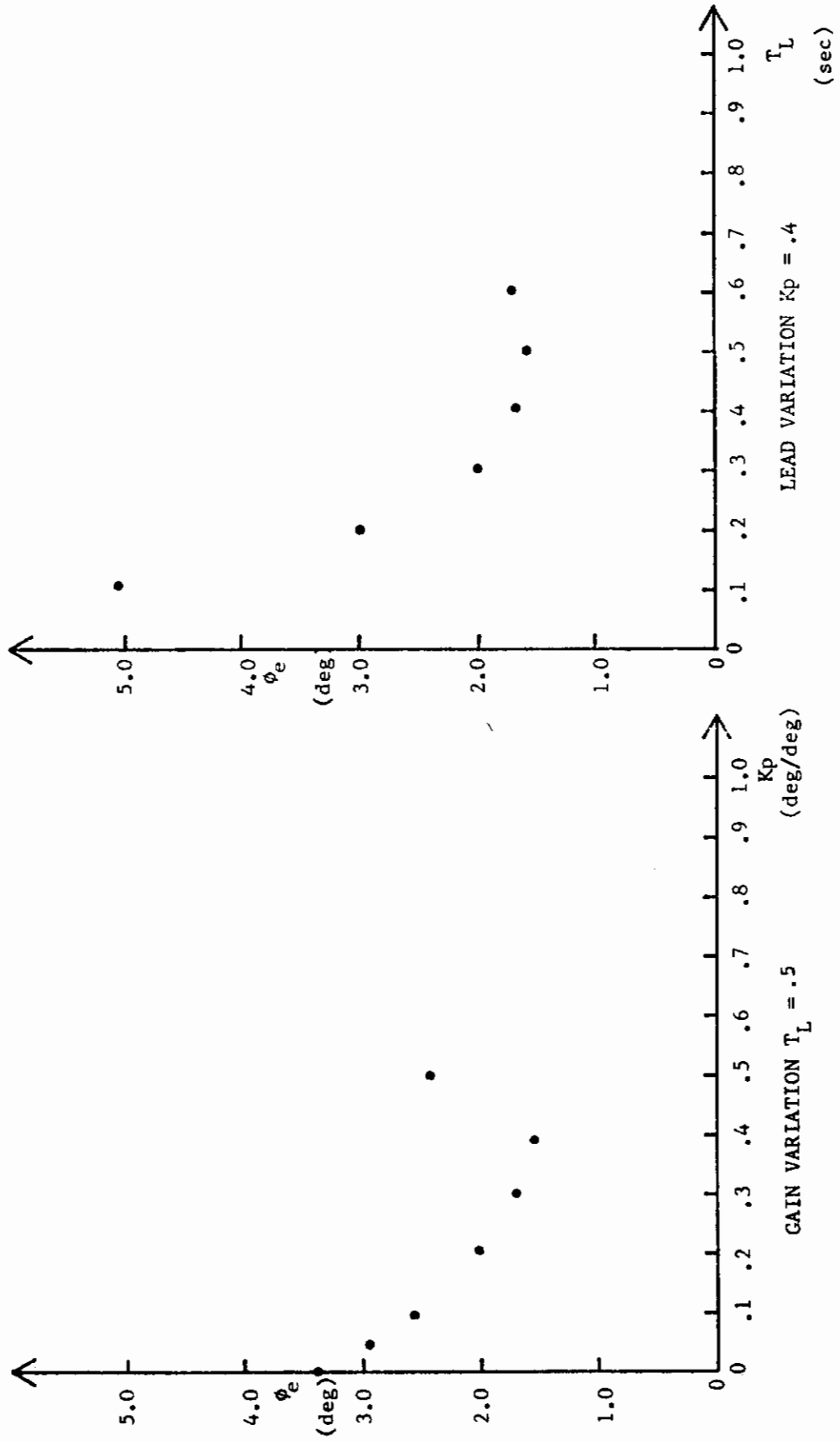

FIGURE 83. PILOT LEAD AND GAIN VARIATIONS
A-7 FLIGHT CONDITION 1
WITH AUGMENTER

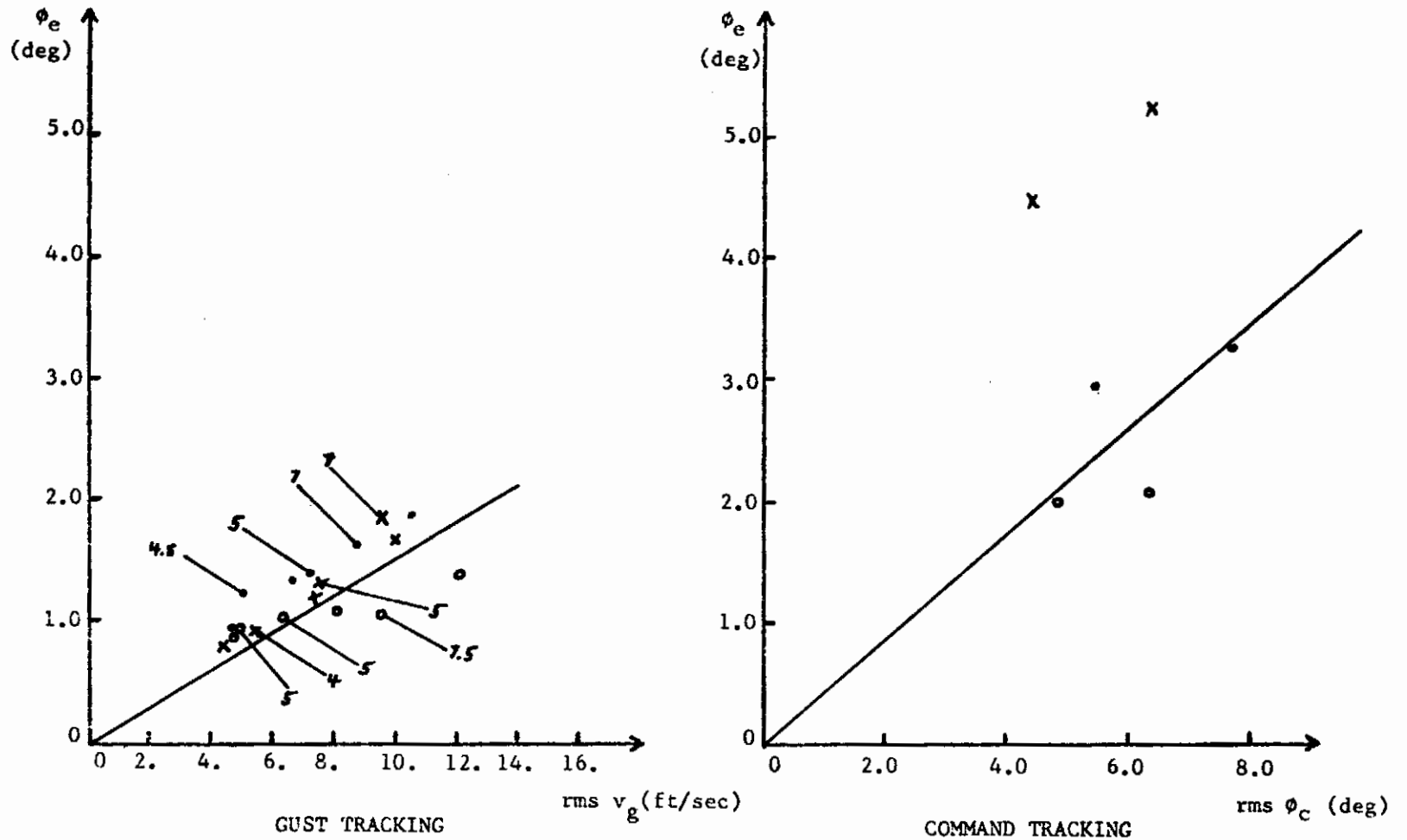

FIGURE 84. ROLL TASK SIMULATION
A-7 FLIGHT CONDITION 1
WITH AUGMENTER

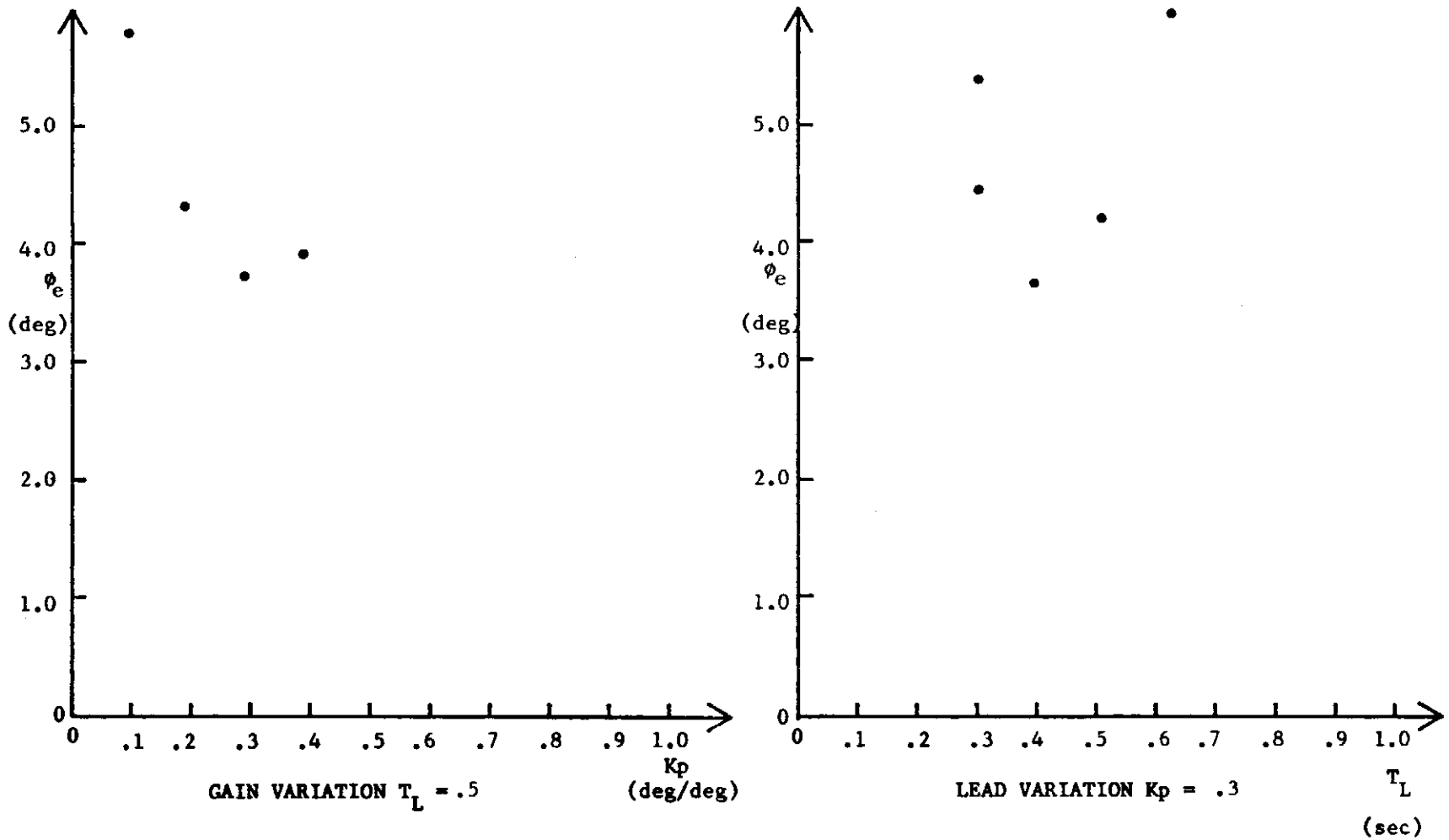

FIGURE 85. PILOT LEAD AND GAIN VARIATIONS
A-7 FLIGHT CONDITION 1
WITHOUT AUGMENTER

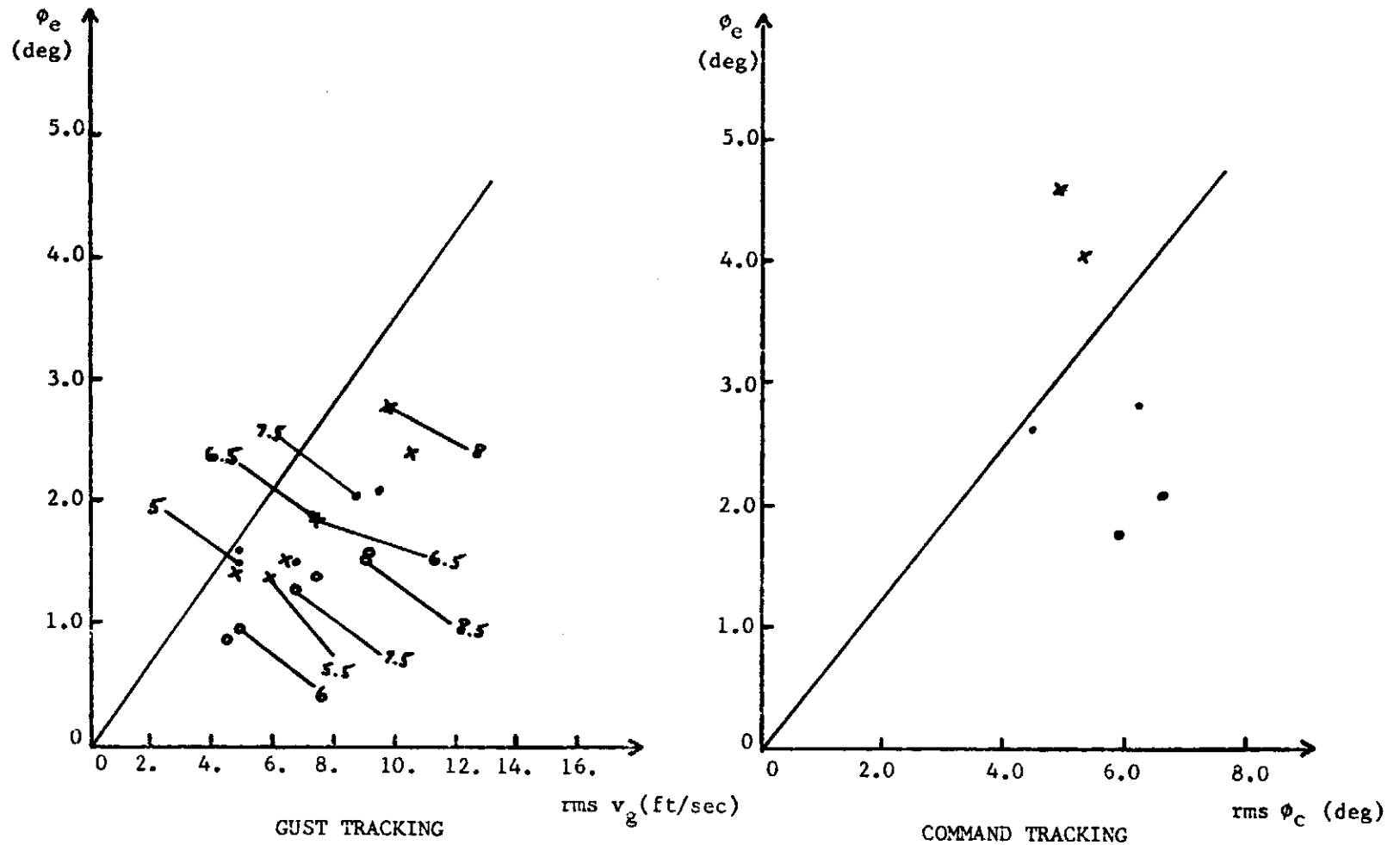

GUST TRACKING

COMMAND TRACKING

FIGURE 86. ROLL TASK SIMULATION
A-7 FLIGHT CONDITION 1
WITHOUT AUGMENTER

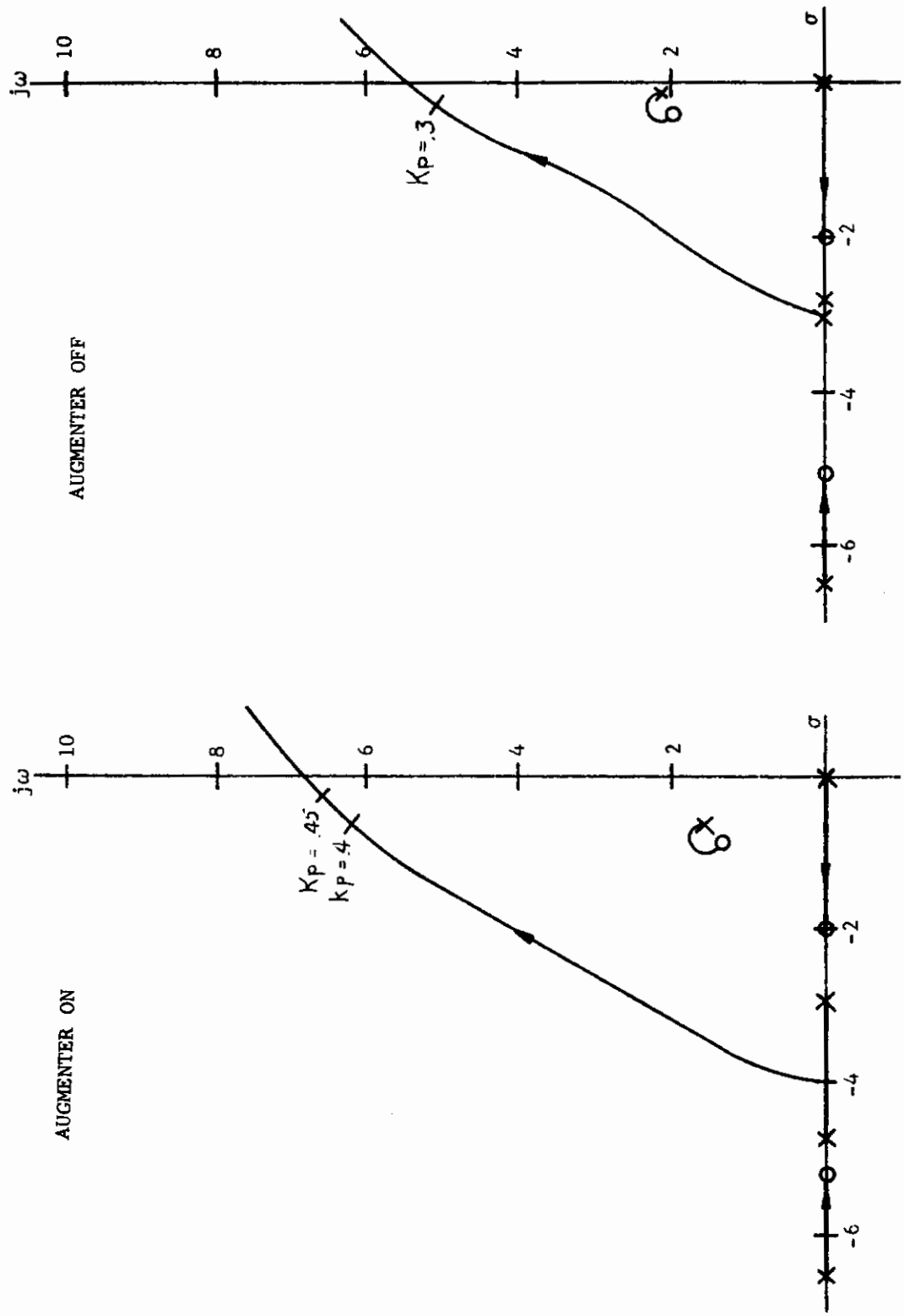

FIGURE 87. ROOT LOCUS FOR BANK ANGLE TRACKING
A-7 FLIGHT CONDITION 1
$T_L = 0.5$ SEC

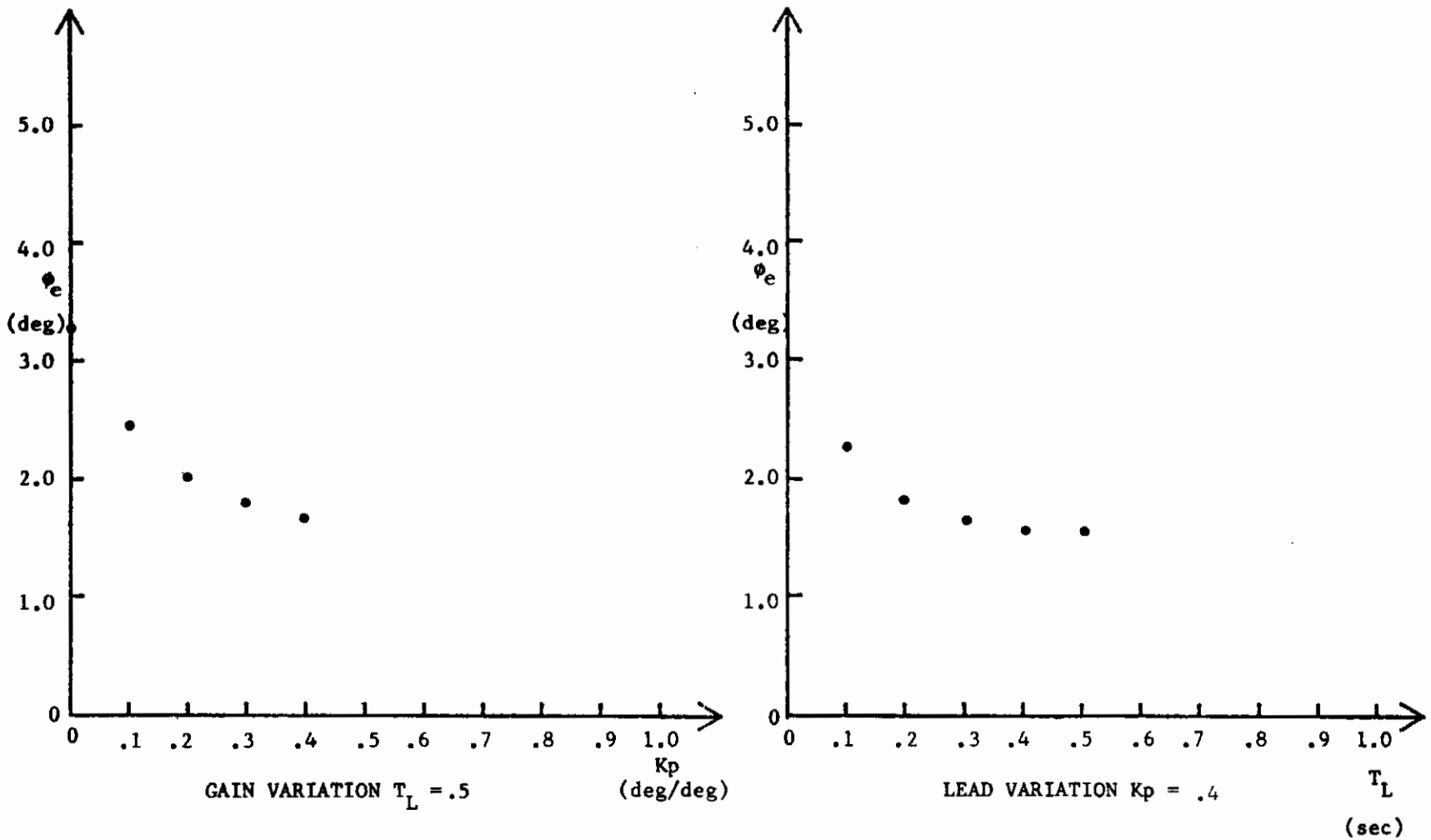

FIGURE 88. PILOT LEAD AND GAIN VARIATIONS
A-7 FLIGHT CONDITION 1
FAILURE WITH AUGMENTER

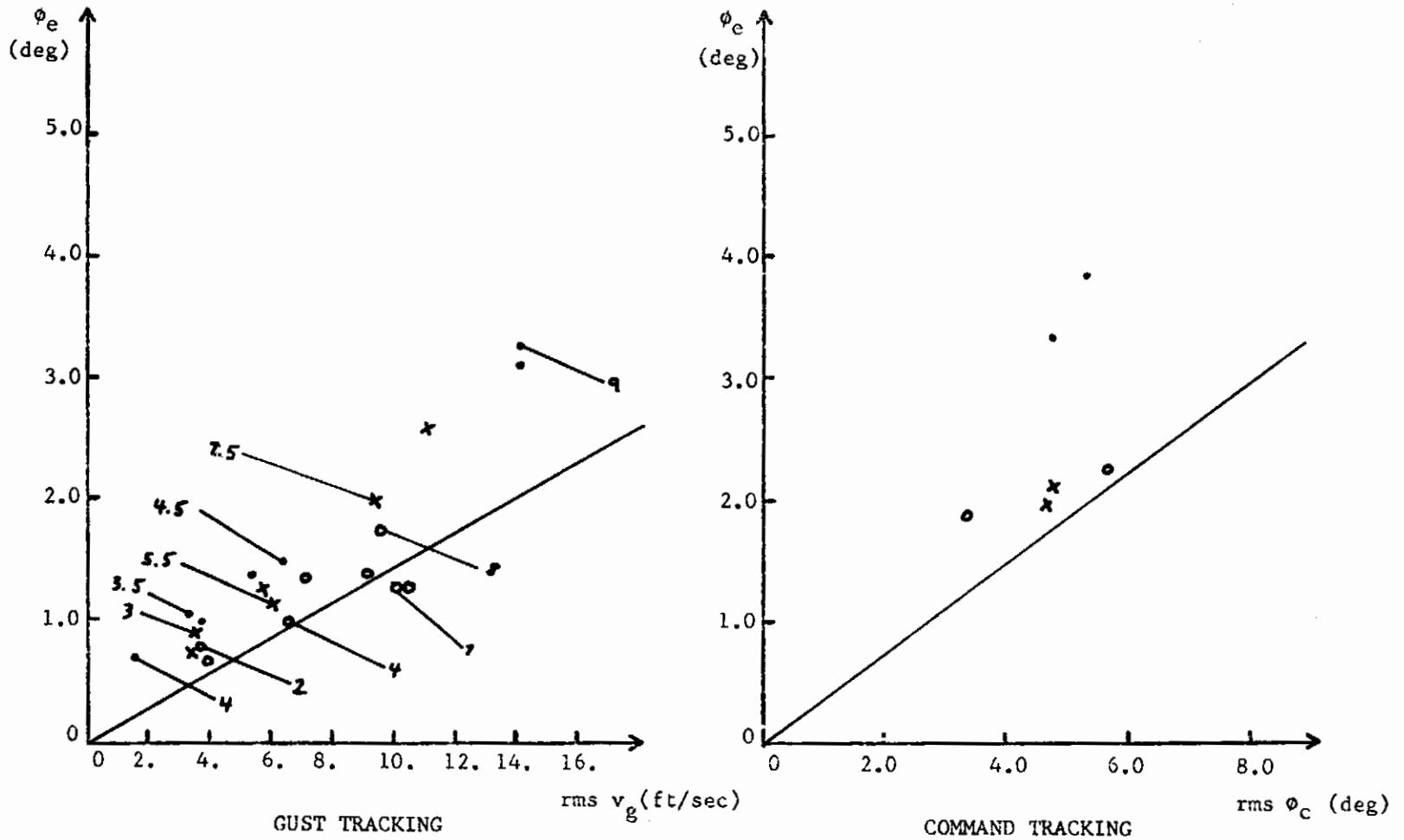

FIGURE 89. ROLL TASK SIMULATION
A-7 FLIGHT CONDITION 1
FAILURE WITH AUGMENTER

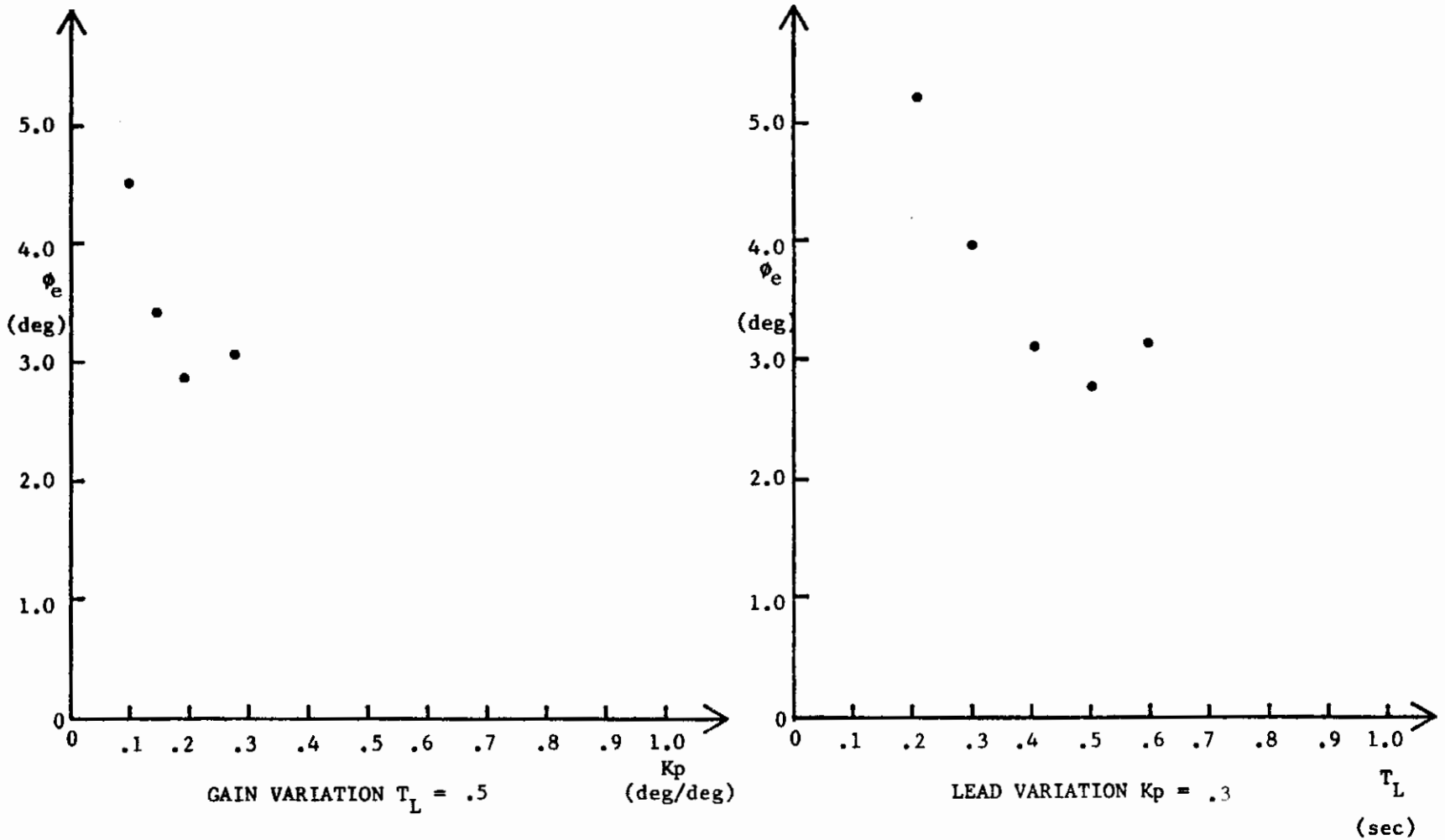

FIGURE 90. PILOT LEAD AND GAIN VARIATIONS
A-7 FLIGHT CONDITION 1
FAILURE WITHOUT AUGMENTER

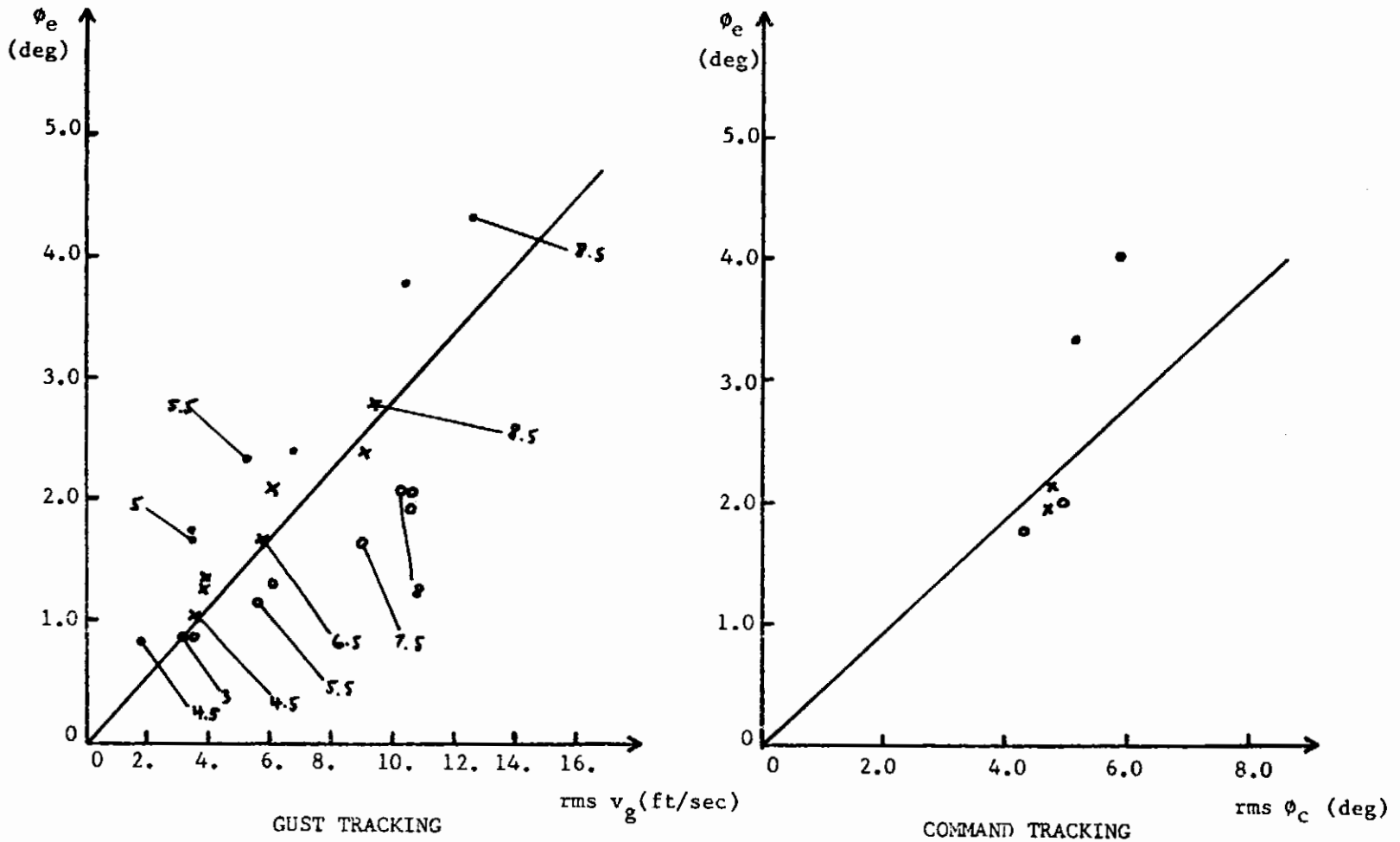

FIGURE 91. ROLL TASK SIMULATION
A-7 FLIGHT CONDITION 1
FAILURE WITHOUT AUGMENTER

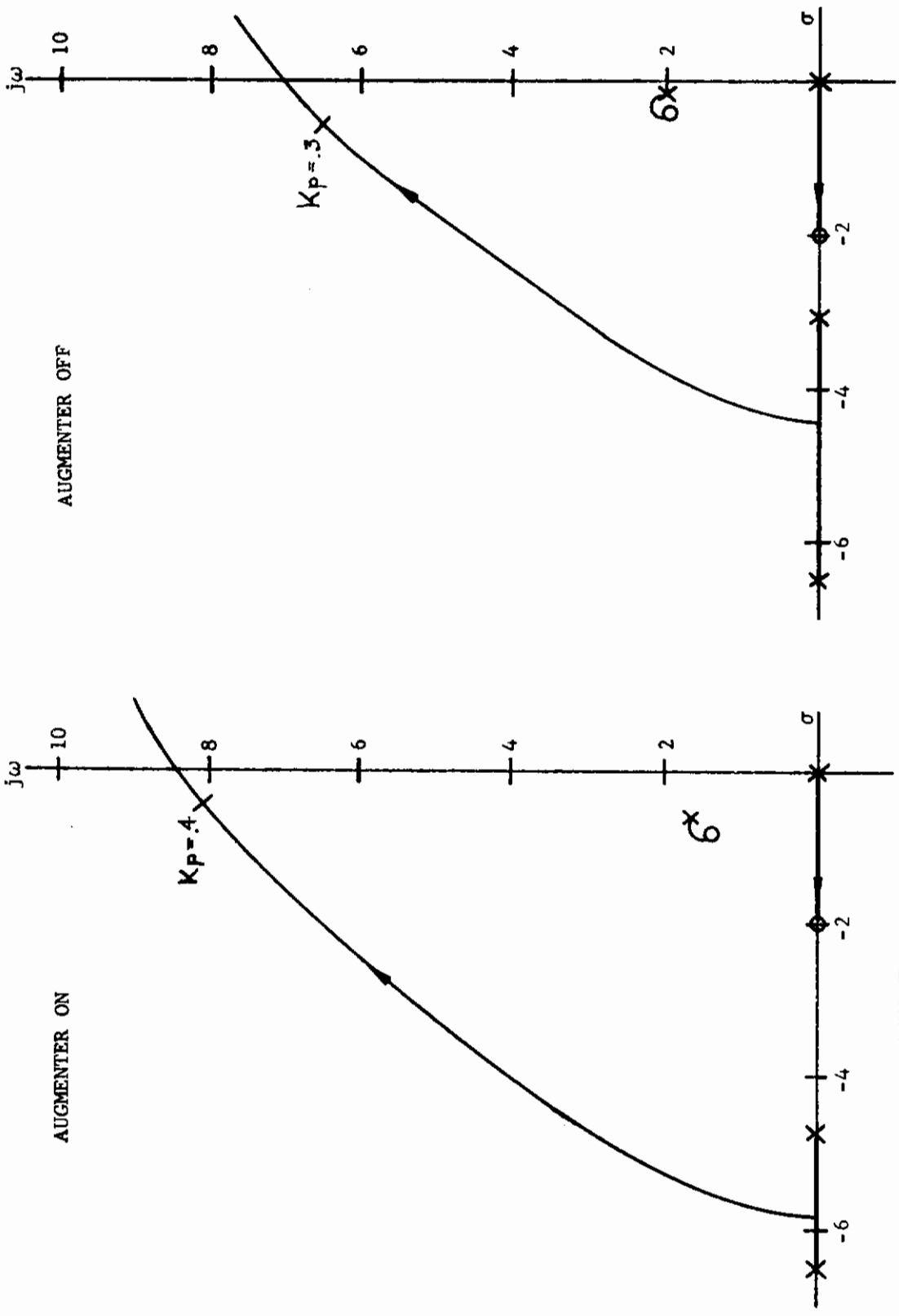

FIGURE 92 ROOT LOCUS FOR BANK ANGLE TRACKING
A-7 FLIGHT CONDITION 1
T_L = 0.5 SEC
FAILURE

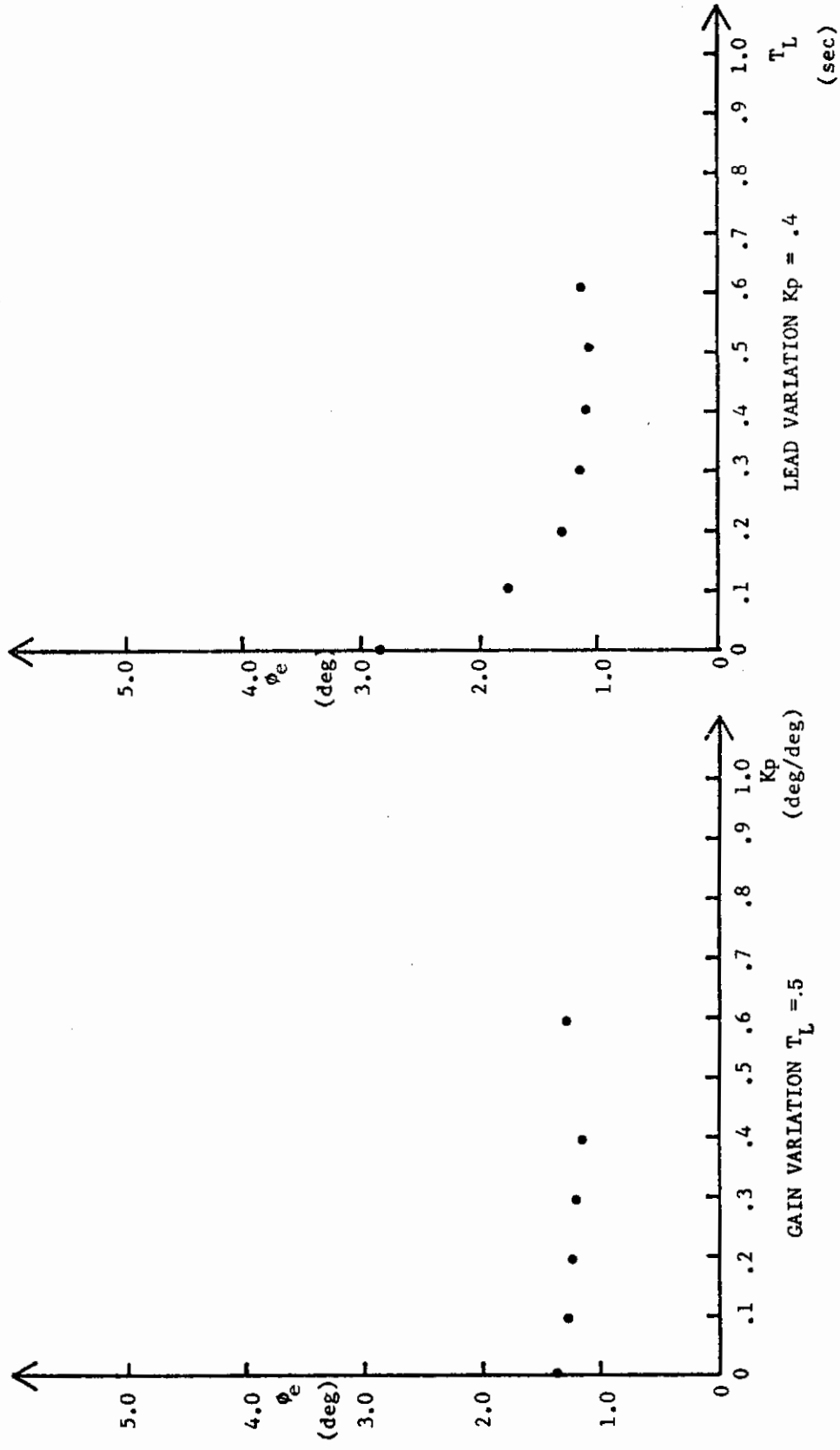

FIGURE 93. PILOT LEAD AND GAIN VARIATIONS
A-7 FLIGHT CONDITION 2
WITH AUGMENTER

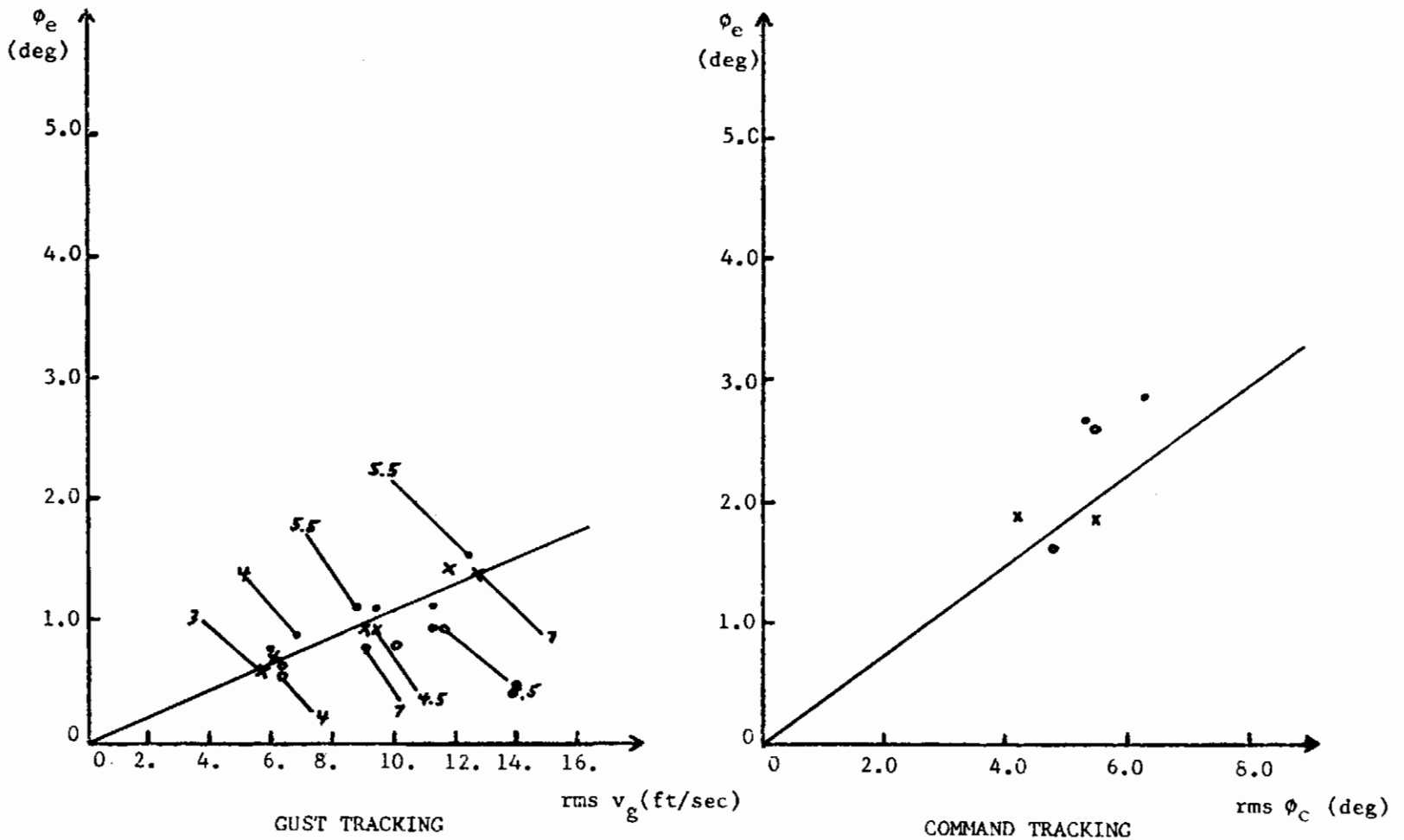

GUST TRACKING

COMMAND TRACKING

FIGURE 94. ROLL TASK SIMULATION
A-7 FLIGHT CONDITION 2
WITH AUGMENTER

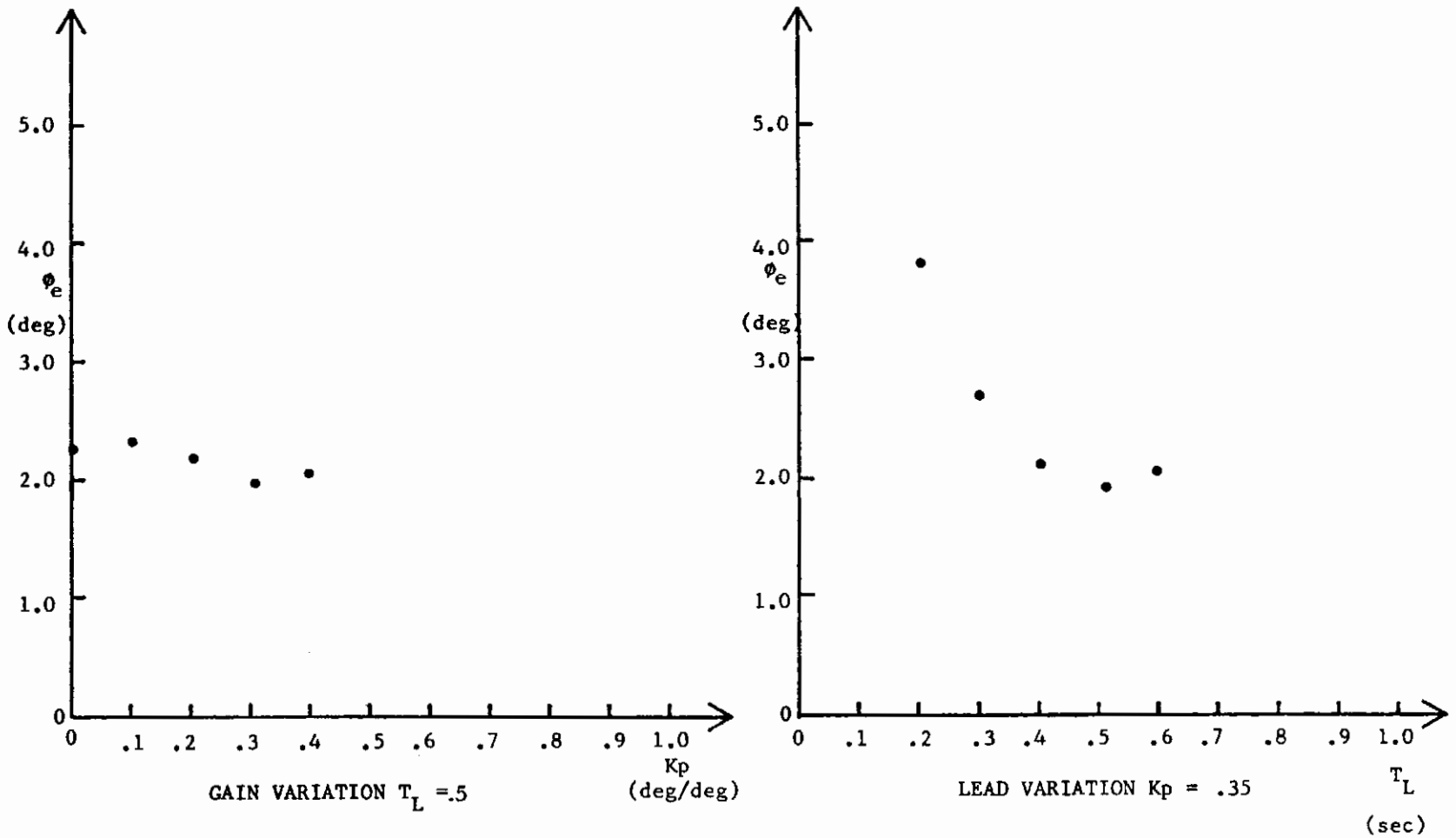

FIGURE 95. PILOT LEAD AND GAIN VARIATIONS
A-7 FLIGHT CONDITION 2
WITHOUT AUGMENTER

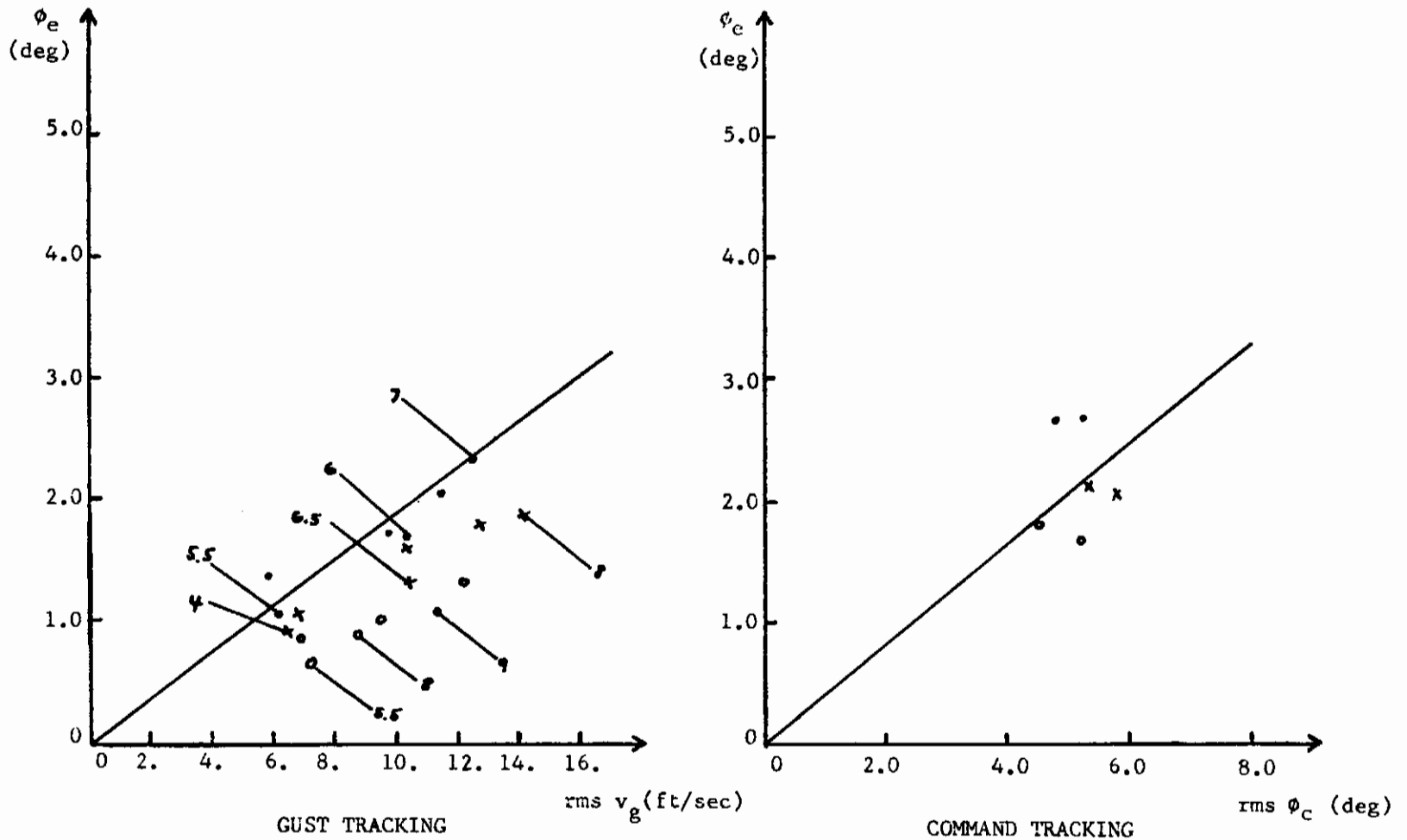

FIGURE 96. ROLL TASK SIMULATION
A-7 FLIGHT CONDITION 2
WITHOUT AUGMENTER

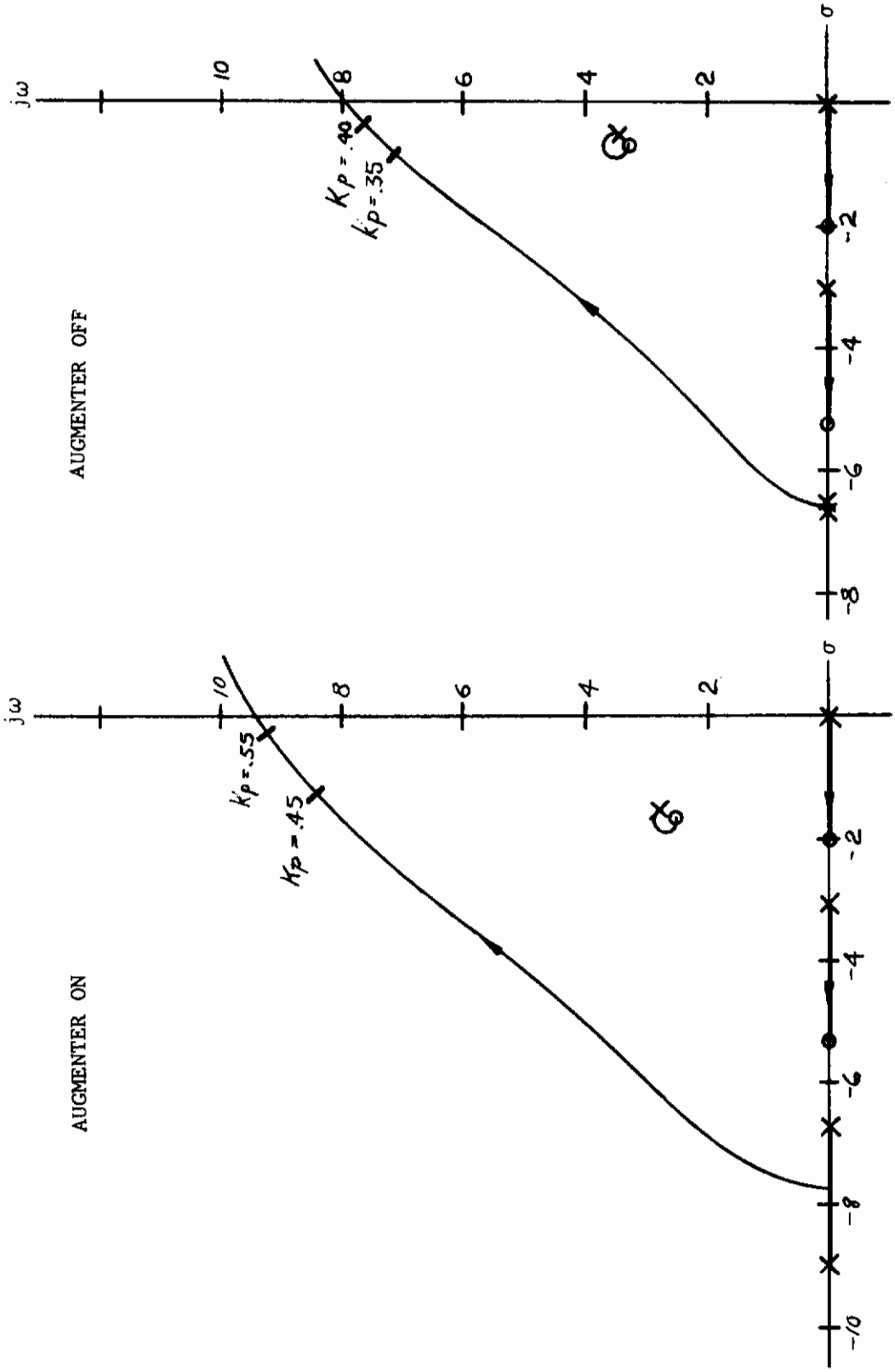

FIGURE 97. A-7 FLIGHT CONDITION 2

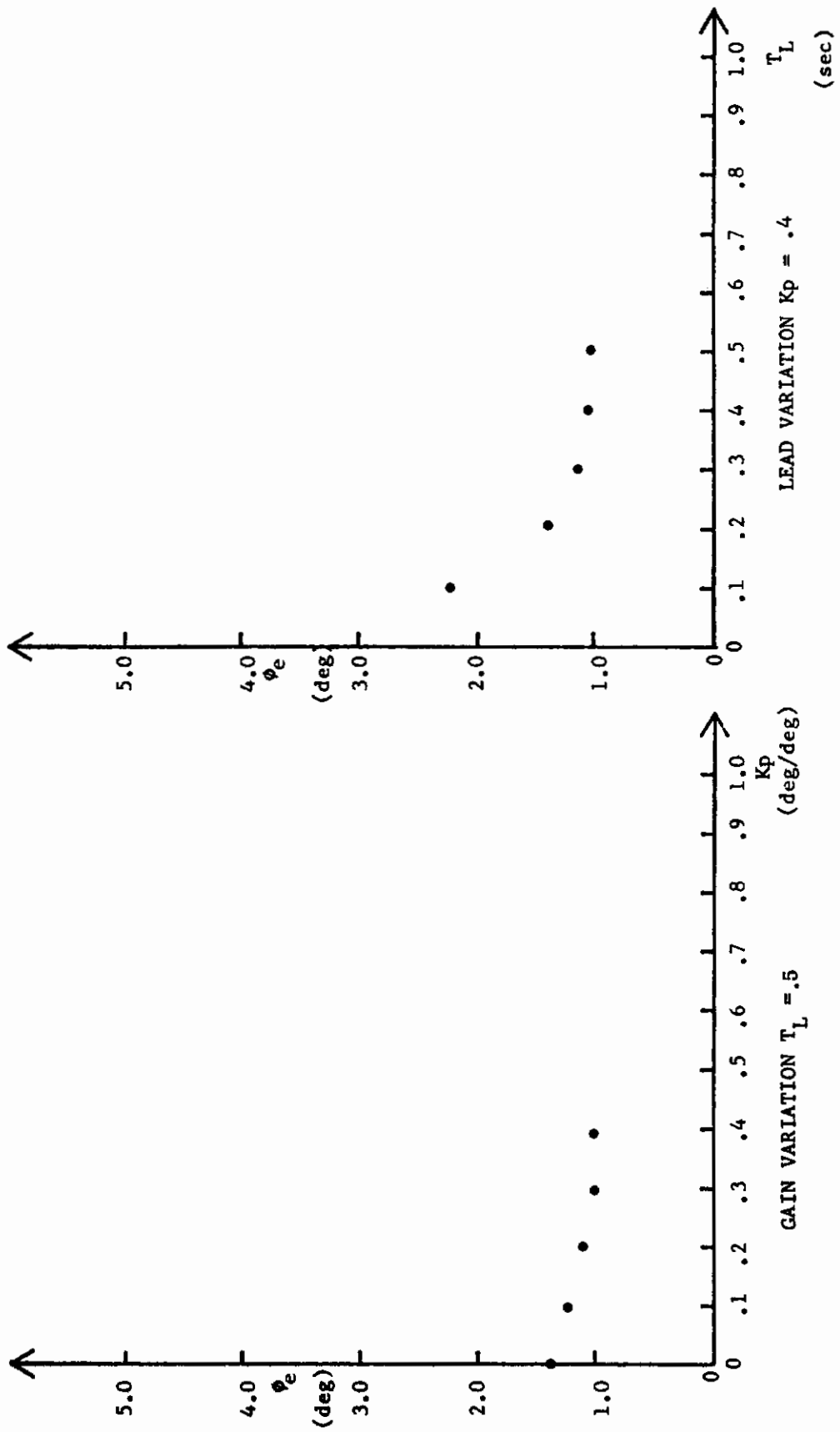

FIGURE 98. PILOT LEAD AND GAIN VARIATIONS
A-7 FLIGHT CONDITION 2 FAILURE
WITH AUGMENTER

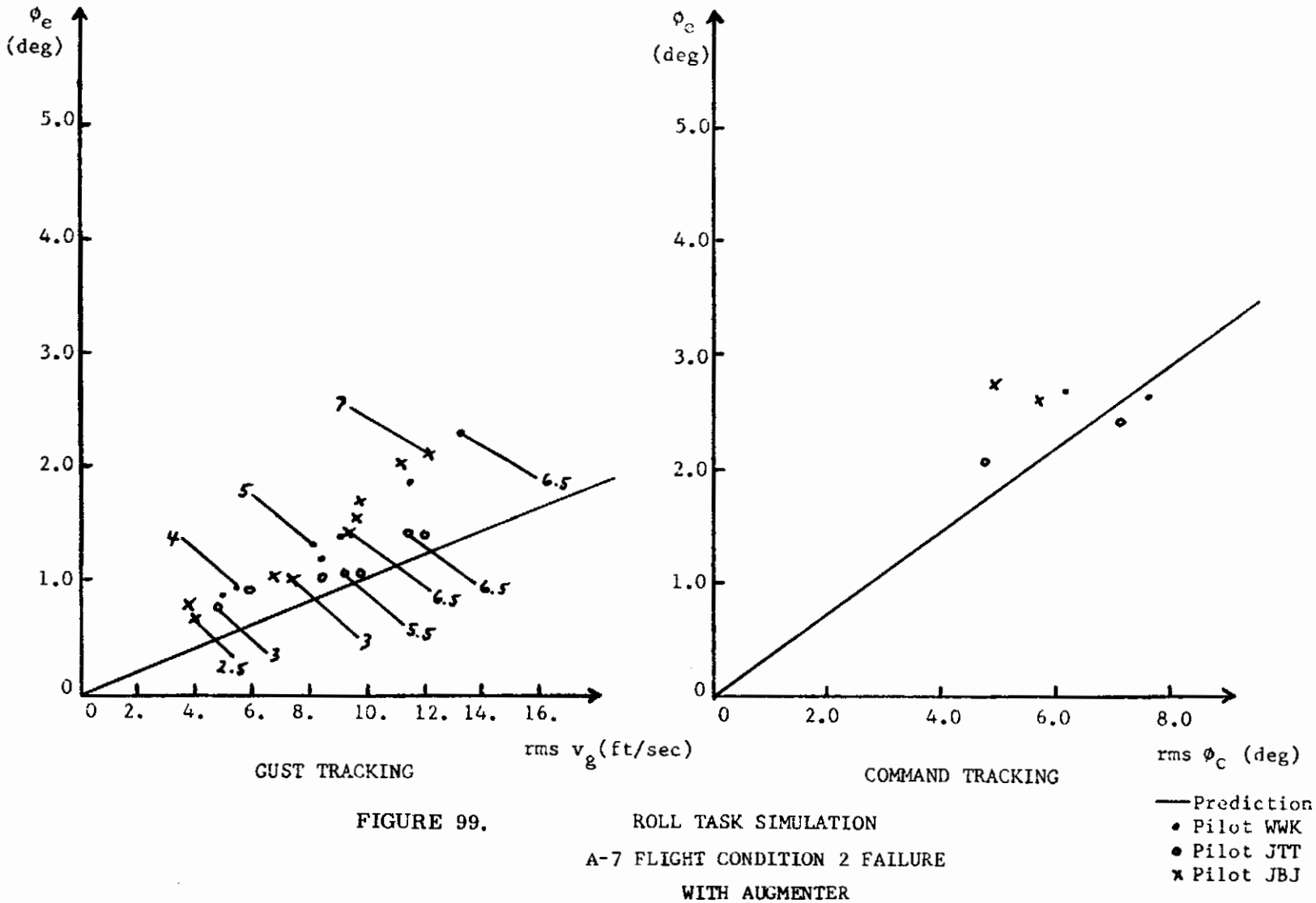

FIGURE 99. ROLL TASK SIMULATION
A-7 FLIGHT CONDITION 2 FAILURE
WITH AUGMENTER

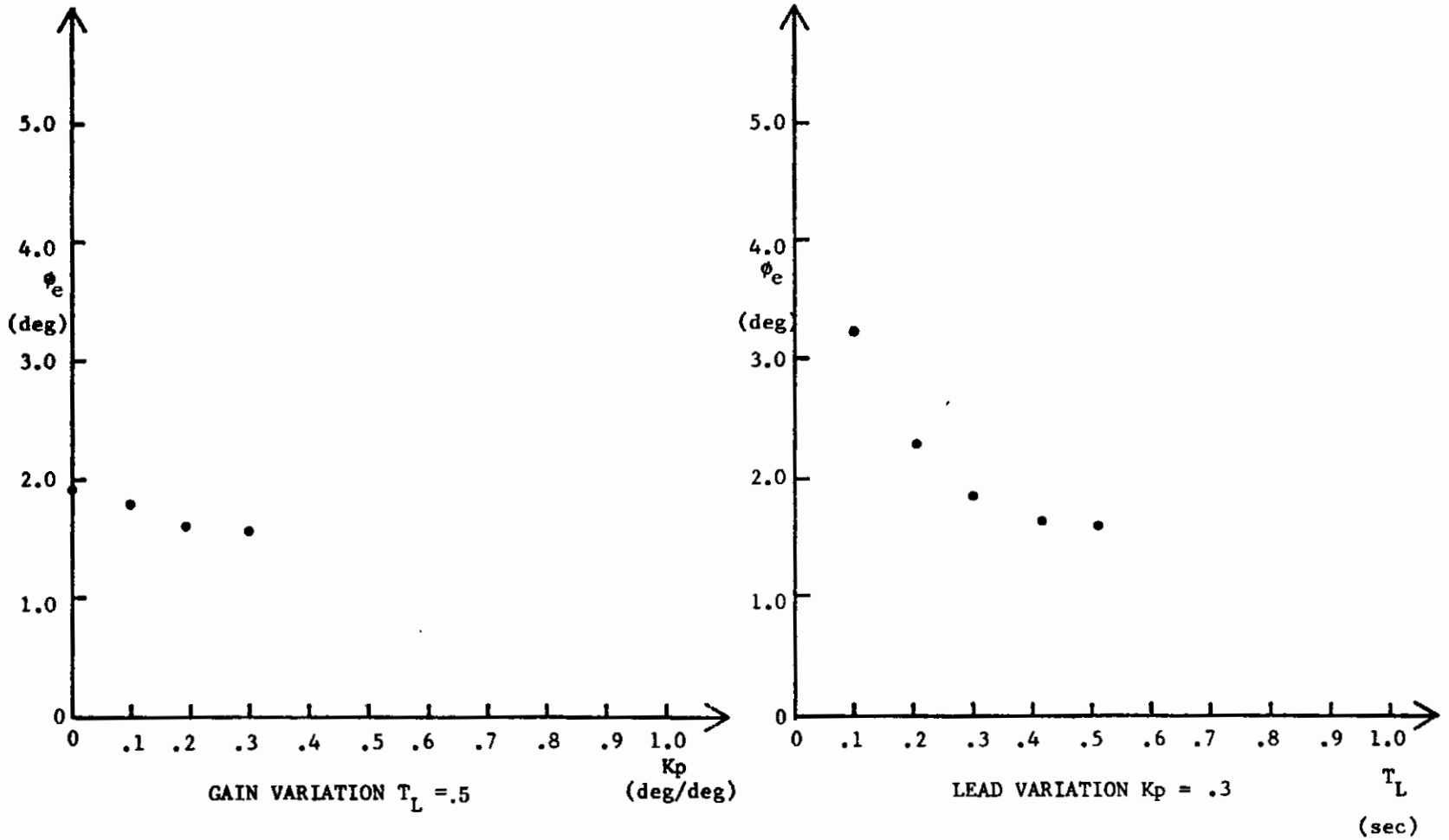

FIGURE 100. PILOT LEAD AND GAIN VARIATIONS
A-7 FLIGHT CONDITION 2 FAILURE
WITHOUT AUGMENTER

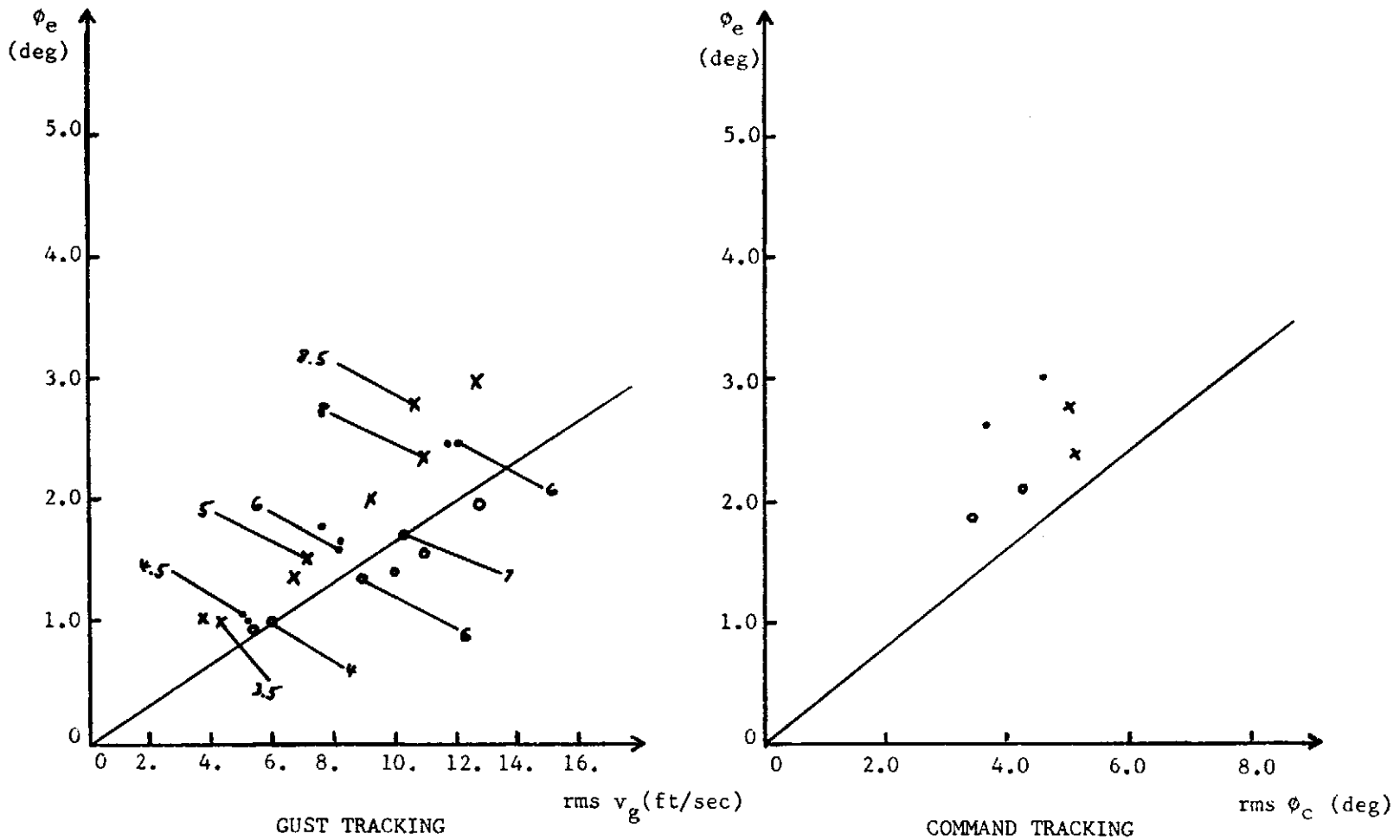

FIGURE 101. ROLL TASK SIMULATION
A-7 FLIGHT CONDITION 2 FAILURE
WITHOUT AUGMENTER

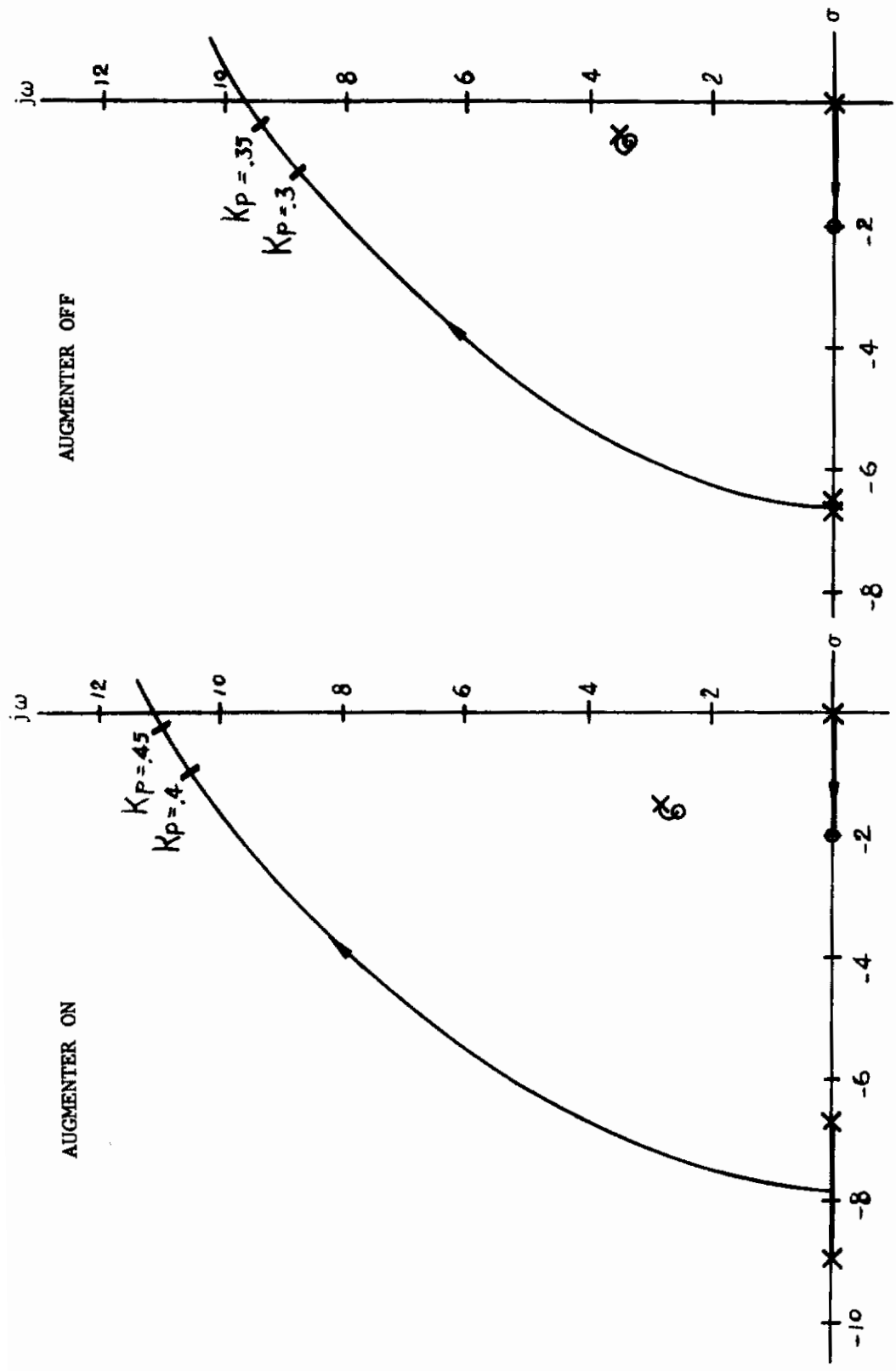

FIGURE 102. A-7 FLIGHT CONDITION 2 FAILURE

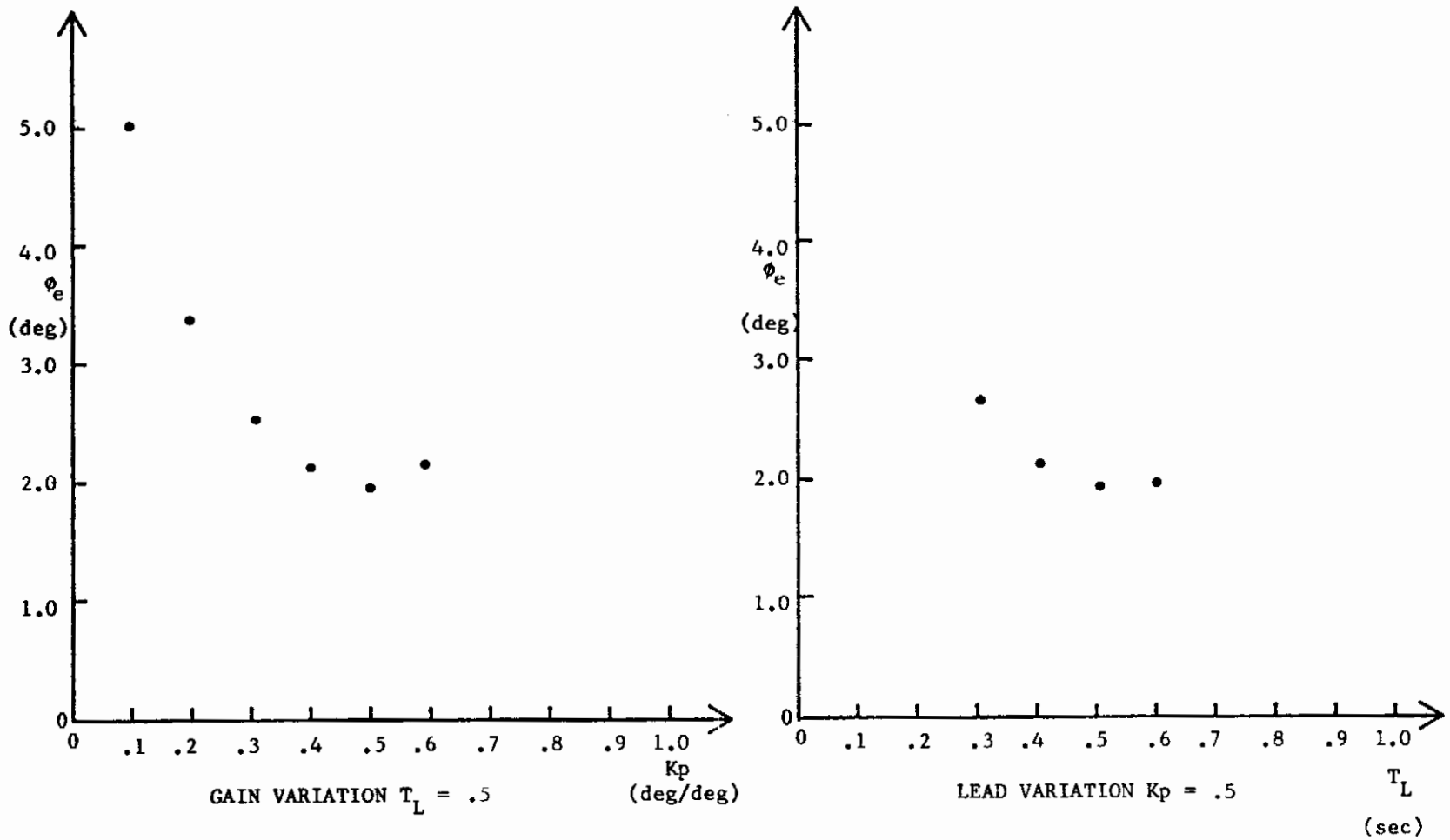

FIGURE 103. PILOT LEAD AND GAIN VARIATIONS
A-7 FLIGHT CONDITION 3
WITH AUGMENTER

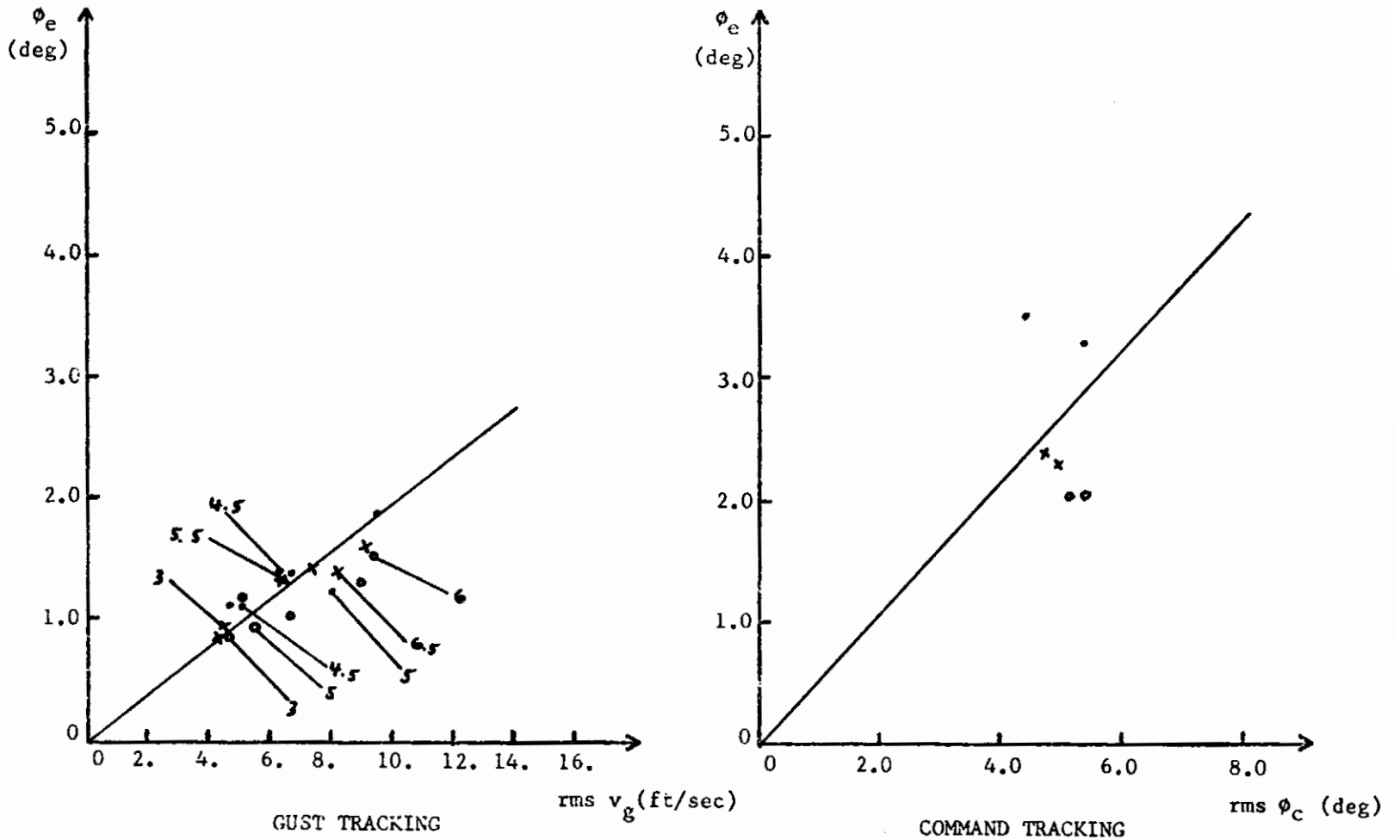

FIGURE 104. ROLL TASK SIMULATION
A-7 FLIGHT CONDITION 3
WITH AUGMENTER

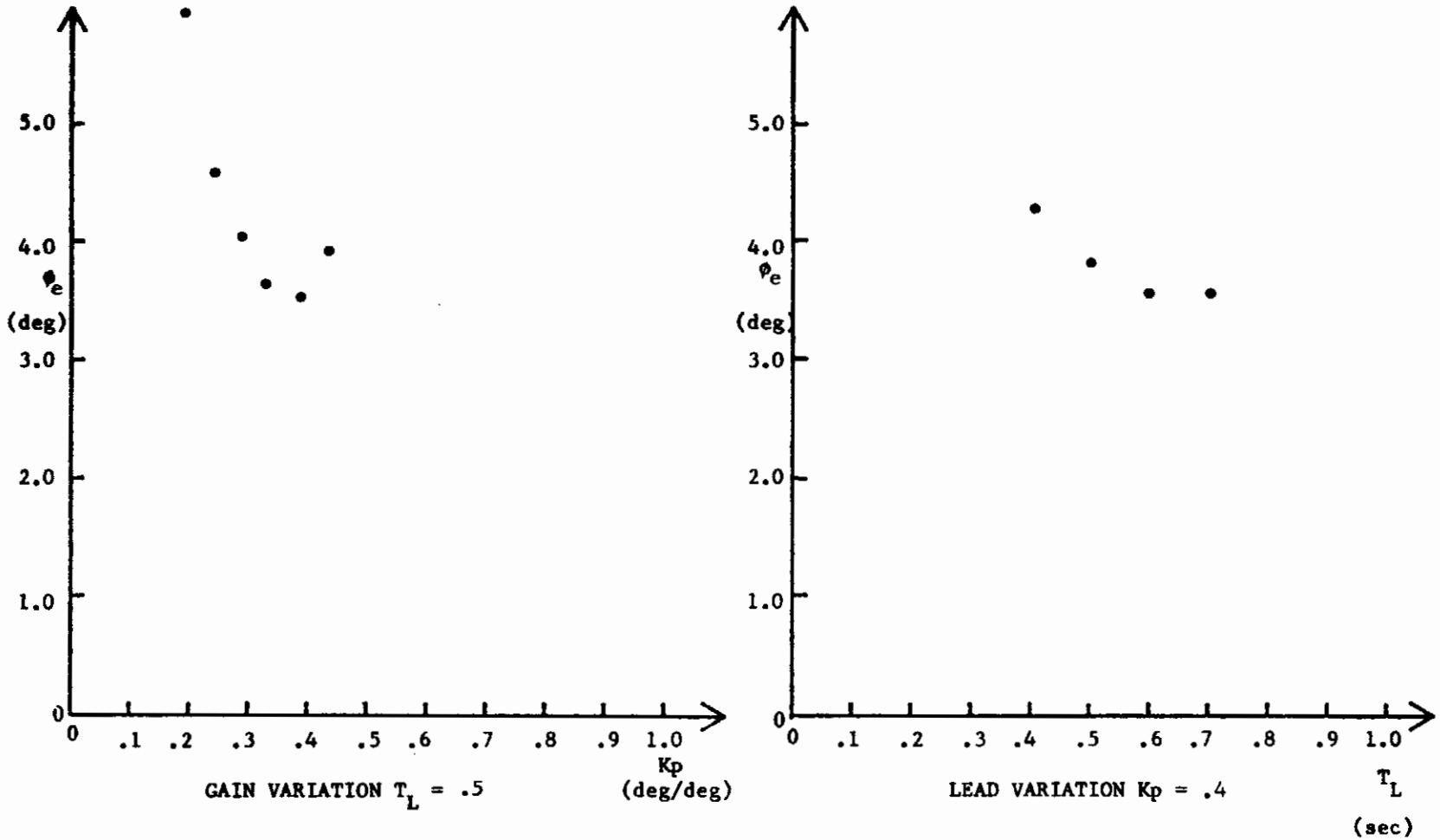

FIGURE 105. PILOT LEAD AND GAIN VARIATIONS

A-7 FLIGHT CONDITION 3

WITHOUT AUGMENTER

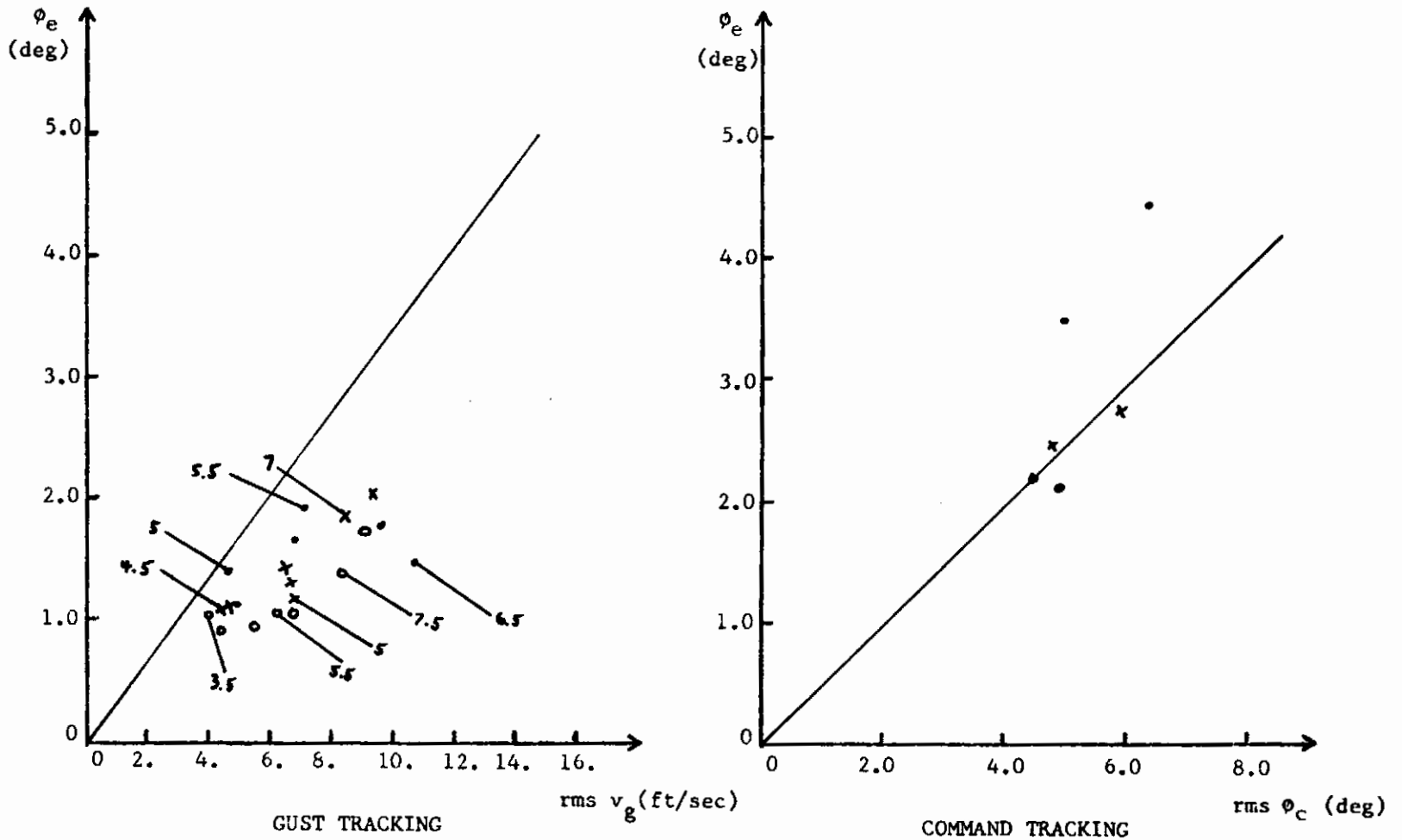

FIGURE 106. ROLL TASK SIMULATION
A-7 FLIGHT CONDITION 3
WITHOUT AUGMENTER

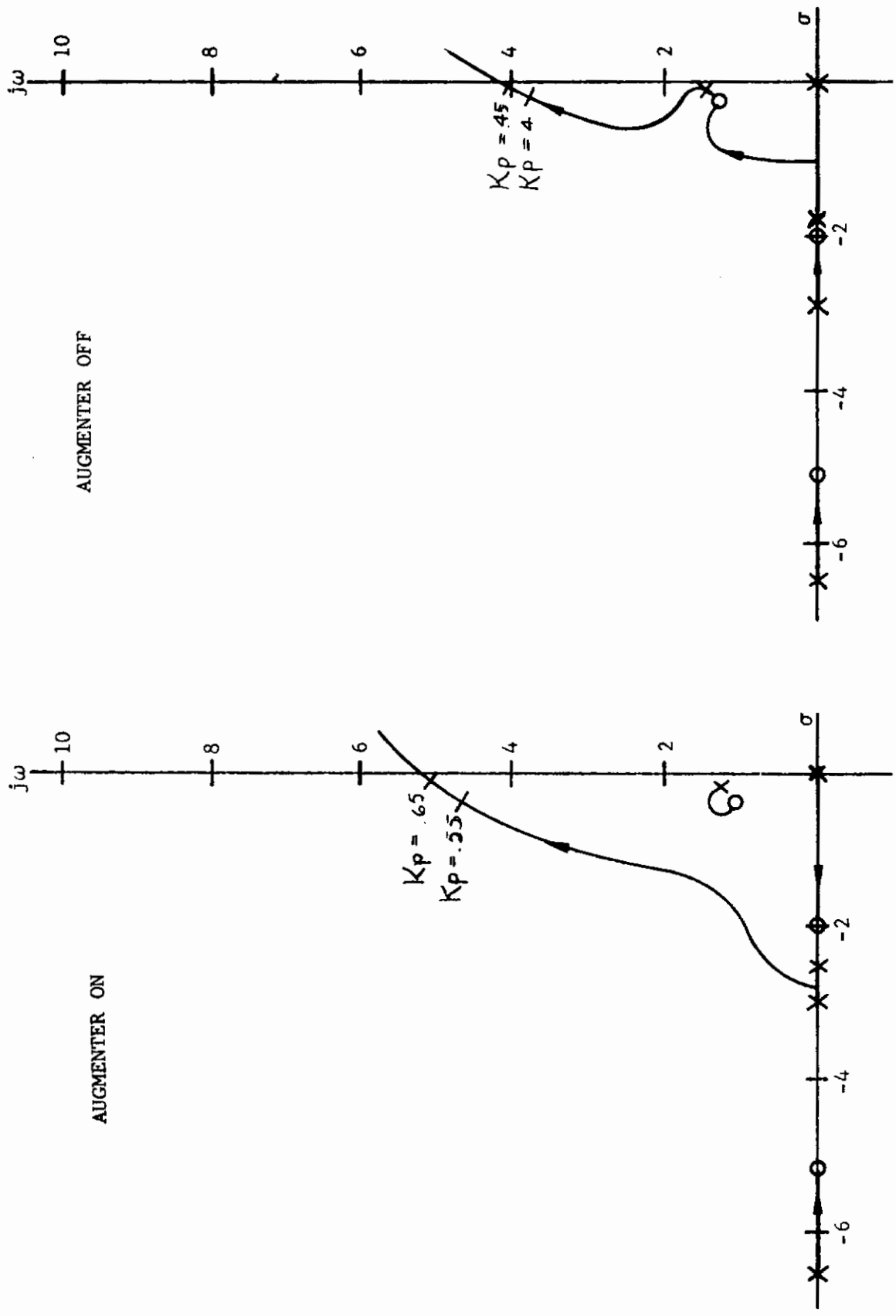

FIGURE 107. ROOT LOCUS FOR BANK ANGLE TRACKING
A-7 FLIGHT CONDITION 3
T_L = 0.5 SEC

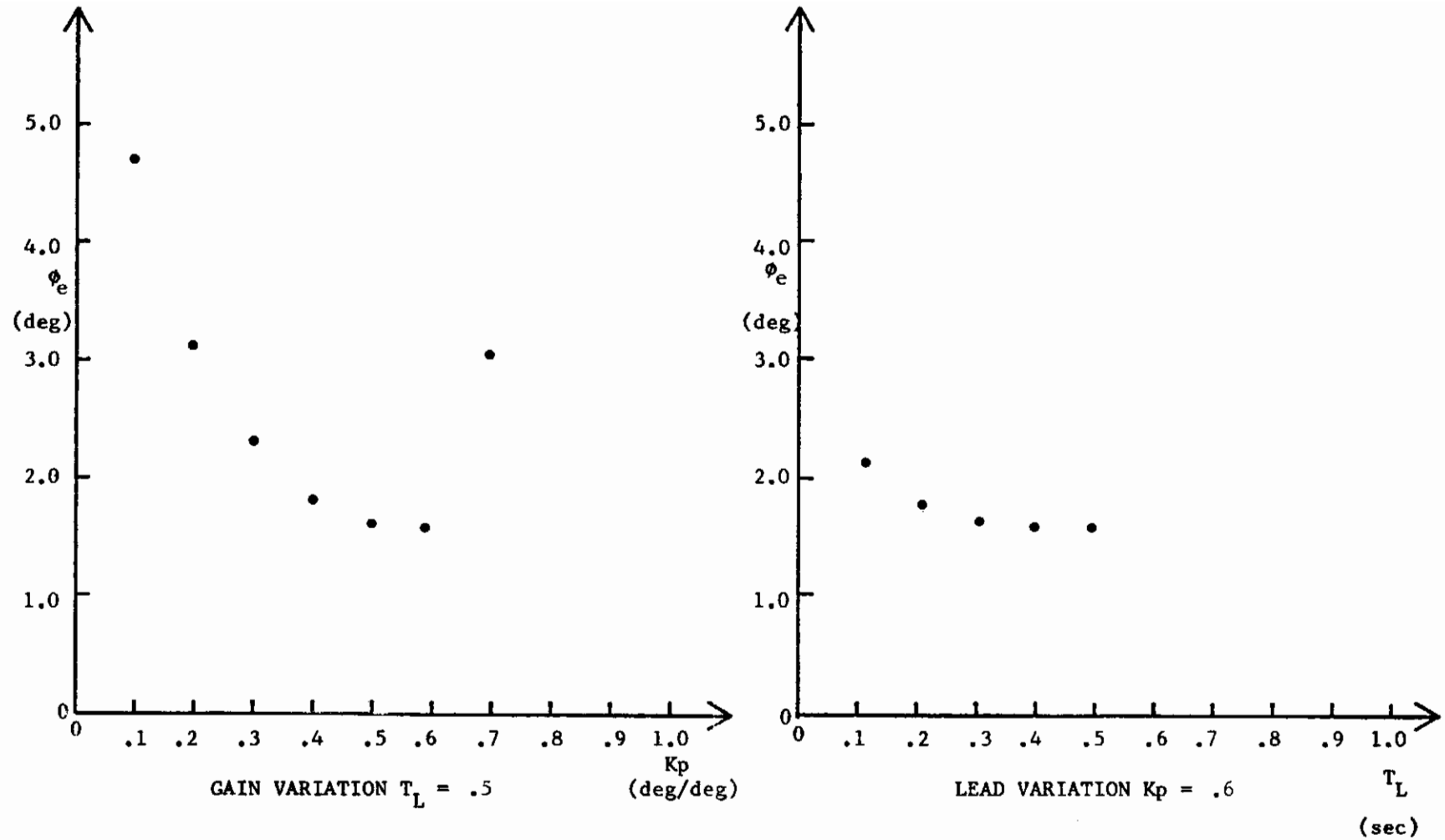

FIGURE 108. PILOT LEAD AND GAIN VARIATIONS
A-7 FLIGHT CONDITION 3 FAILURE
WITH AUGMENTER

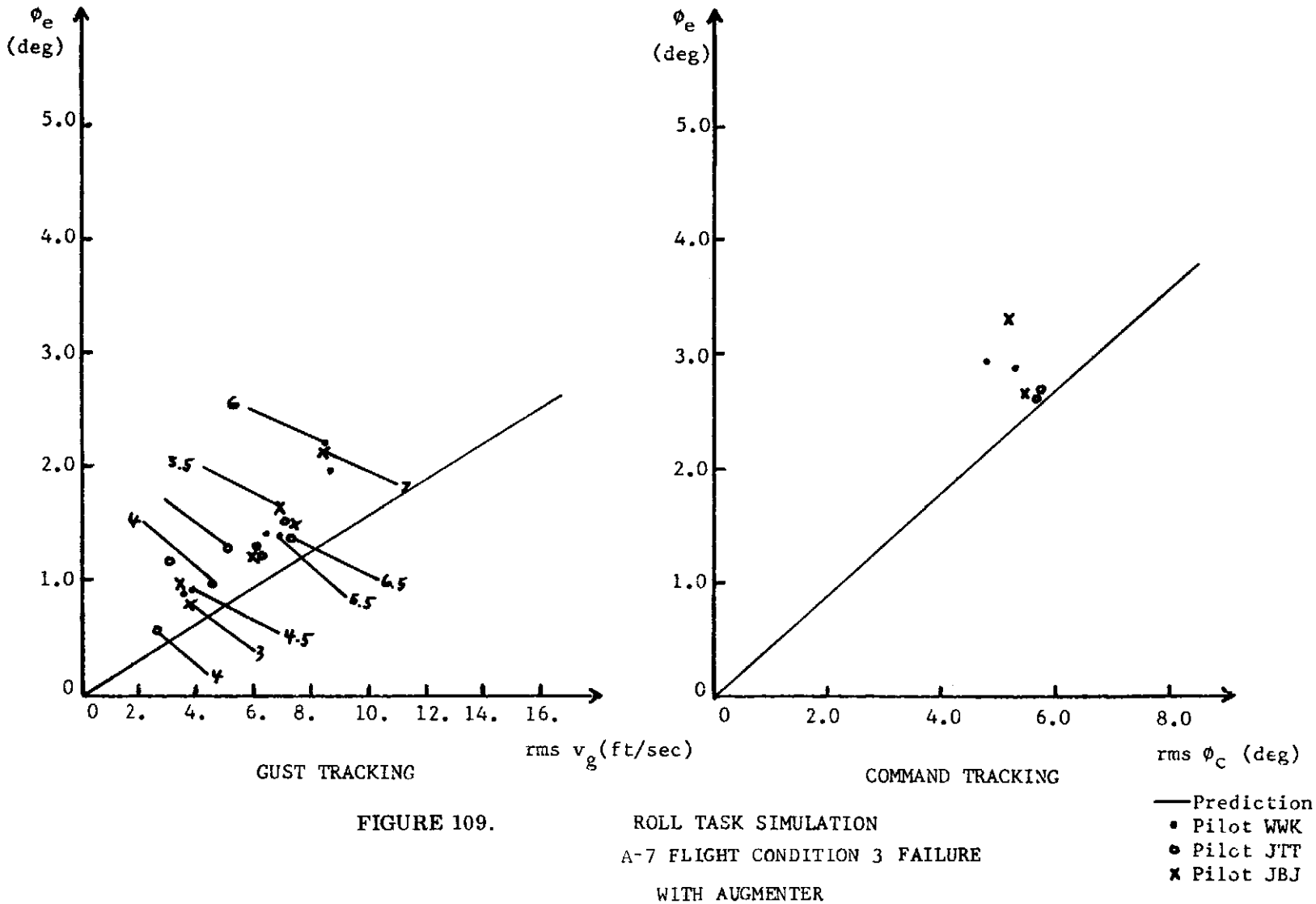

FIGURE 109. ROLL TASK SIMULATION
A-7 FLIGHT CONDITION 3 FAILURE
WITH AUGMENTER

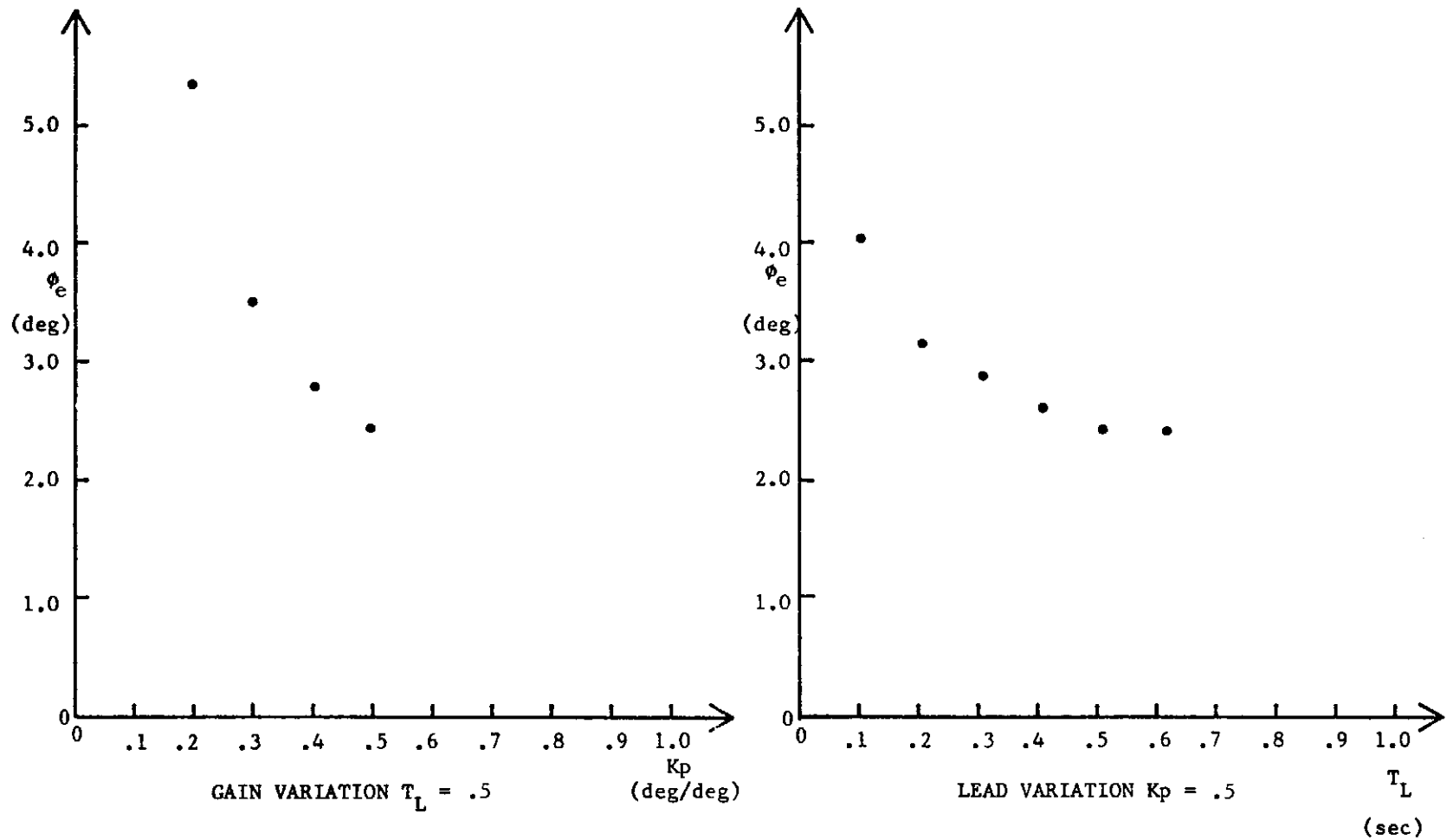

FIGURE 110. PILOT LEAD AND GAIN VARIATIONS
A-7 FLIGHT CONDITION 3 FAILURE
WITHOUT AUGMENTER

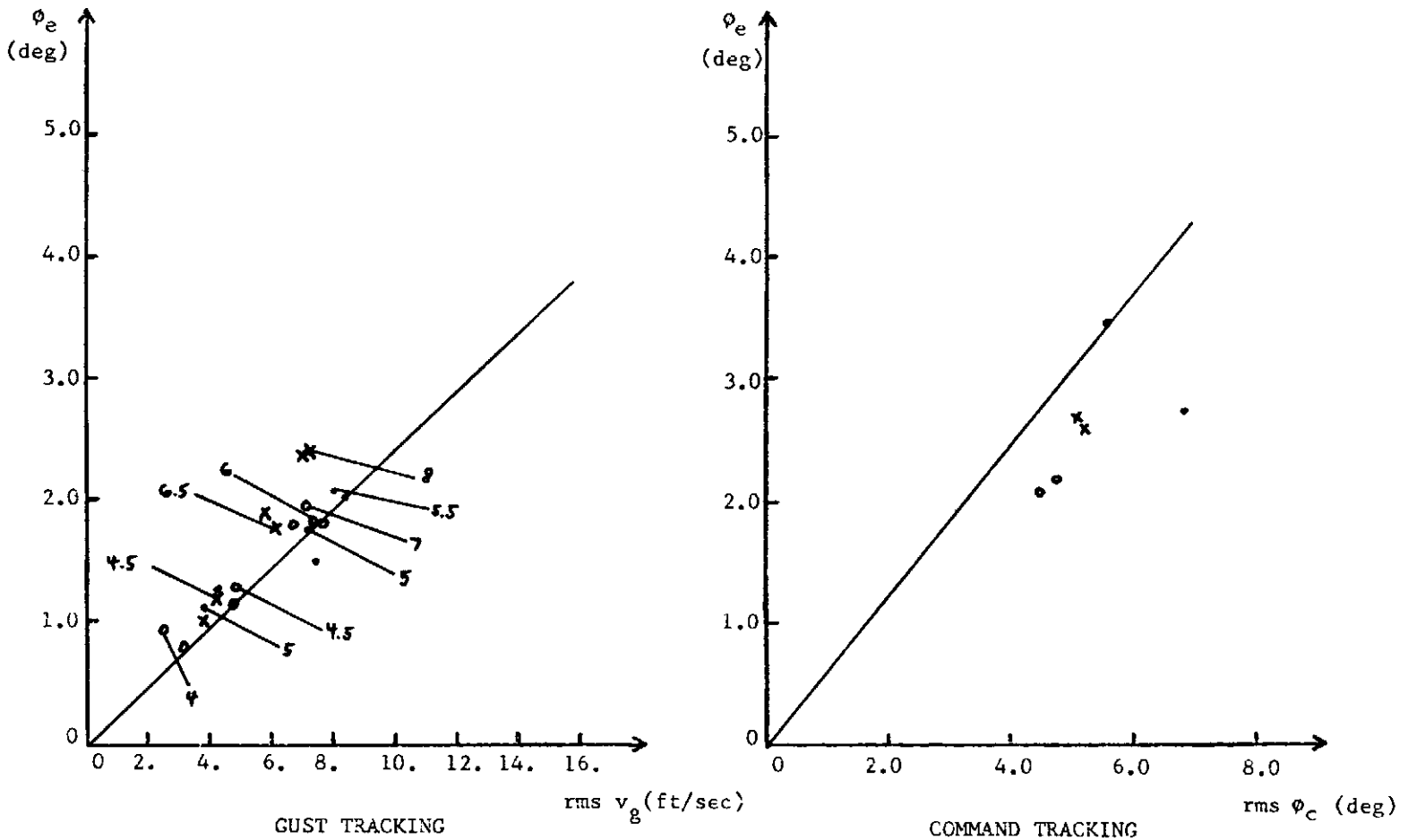

FIGURE 111. ROLL TASK SIMULATION
A-7 FLIGHT CONDITION 3 FAILURE
WITHOUT AUGMENTER

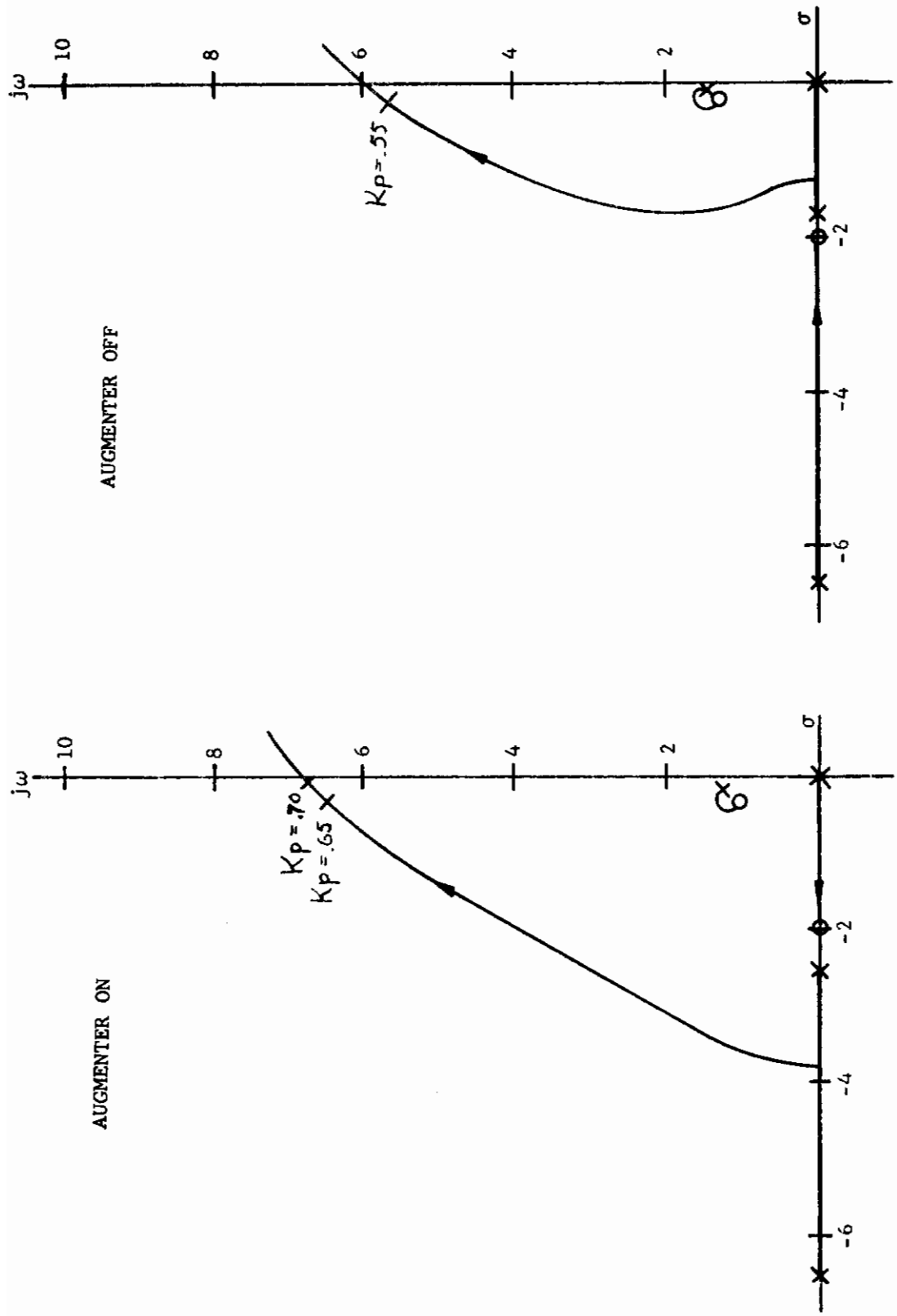

FIGURE 112. ROOT LOCUS FOR BANK ANGLE TRACKING
A-7 FLIGHT CONDITION 3 FAILURE
T_L = 0.5 SEC

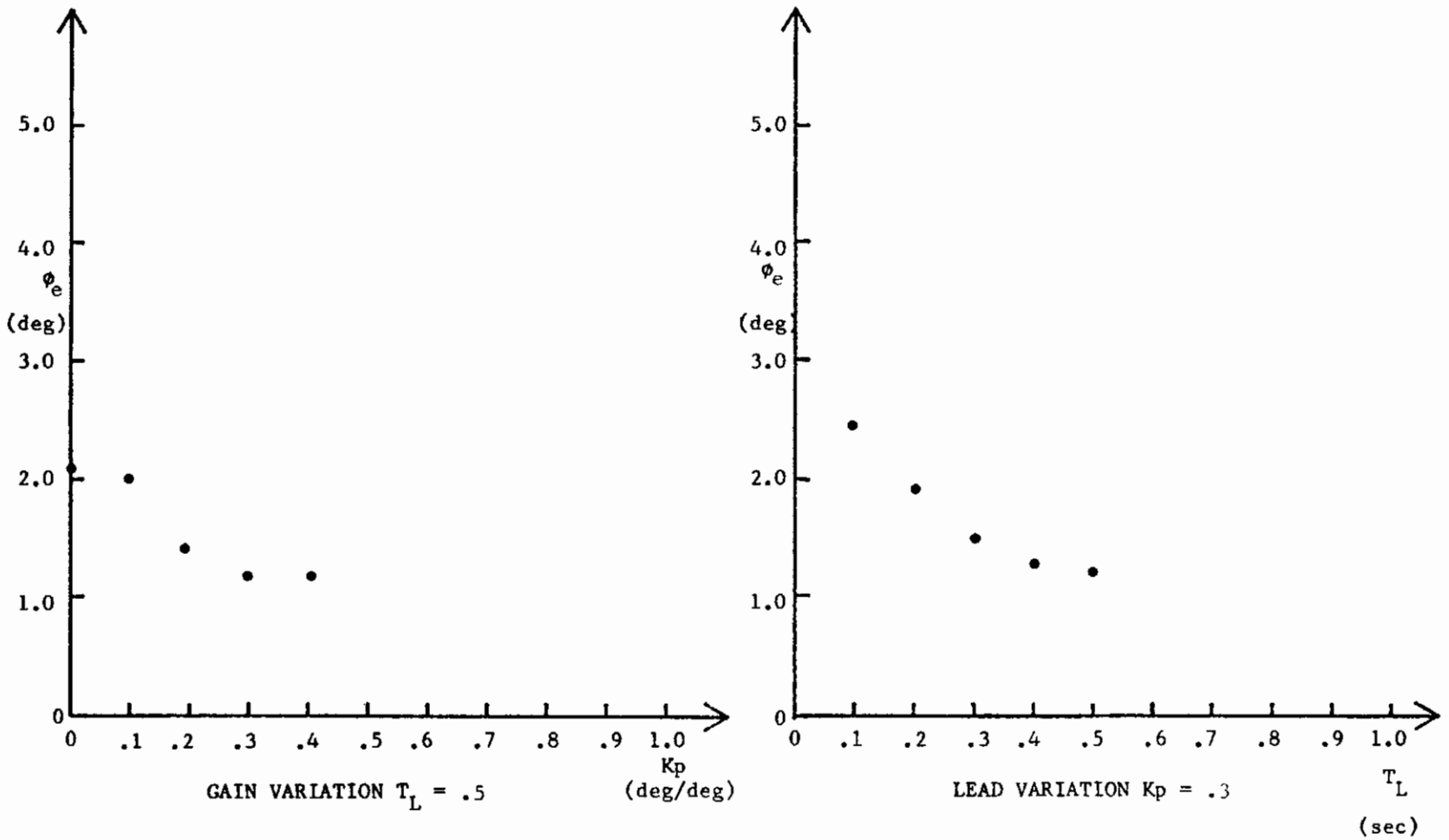

FIGURE 113. PILOT LEAD AND GAIN VARIATIONS
A-7 FLIGHT CONDITION 4
WITH AUGMENTER

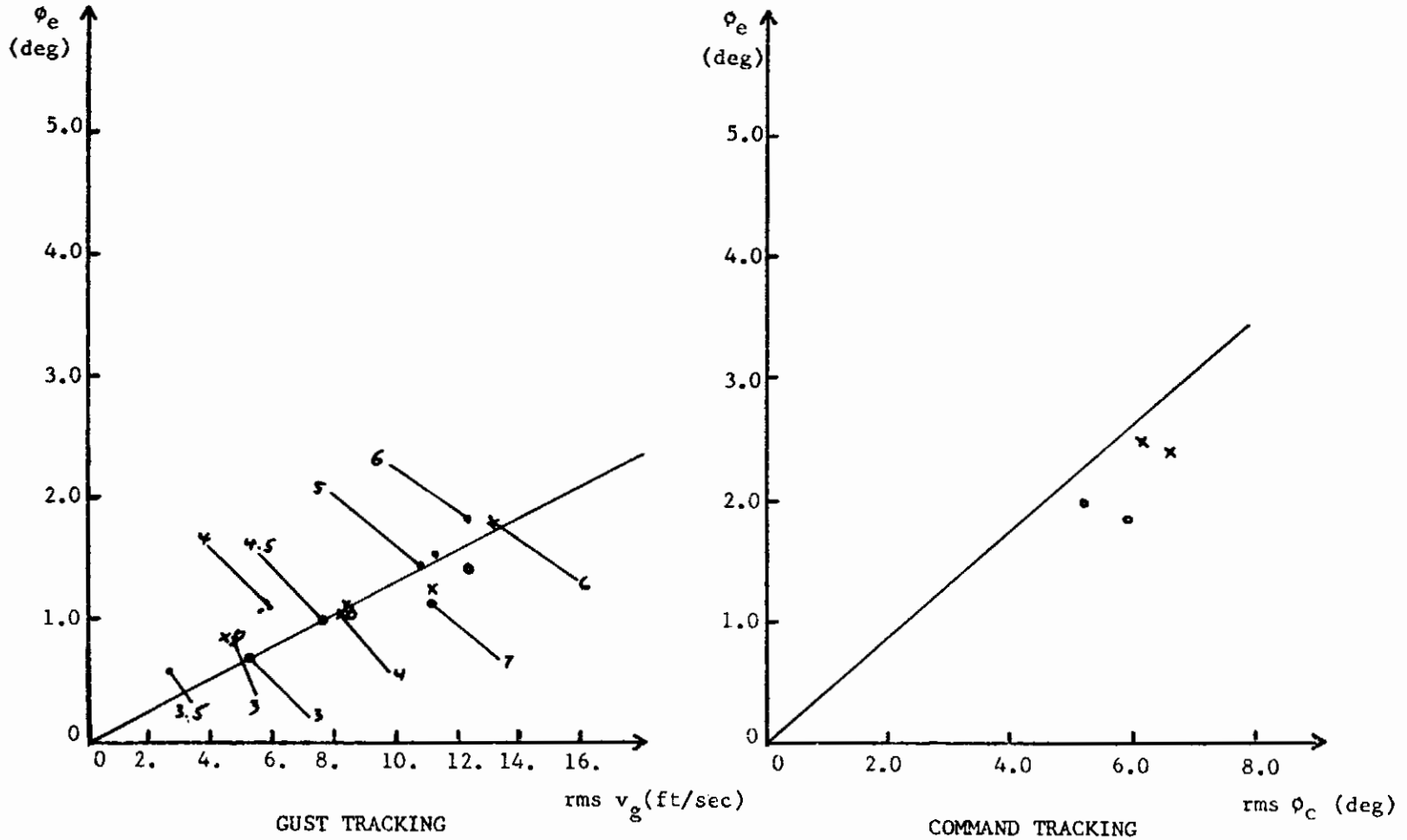

FIGURE 114. ROLL TASK SIMULATION
A-7 FLIGHT CONDITION 4
WITH AUGMENTER

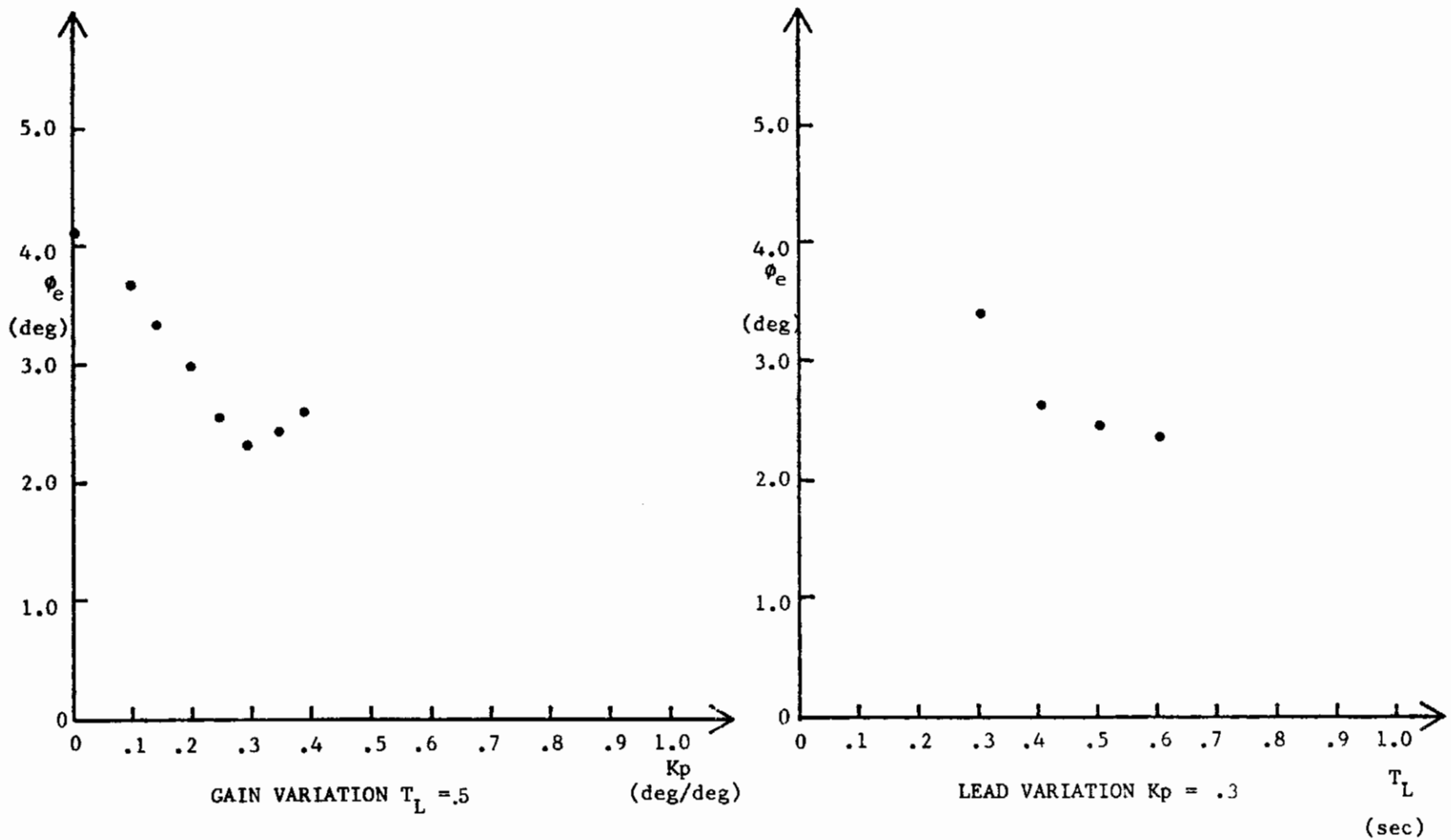

FIGURE 115. PILOT LEAD AND GAIN VARIATIONS

A-7 FLIGHT CONDITION 4

WITHOUT AUGMENTER

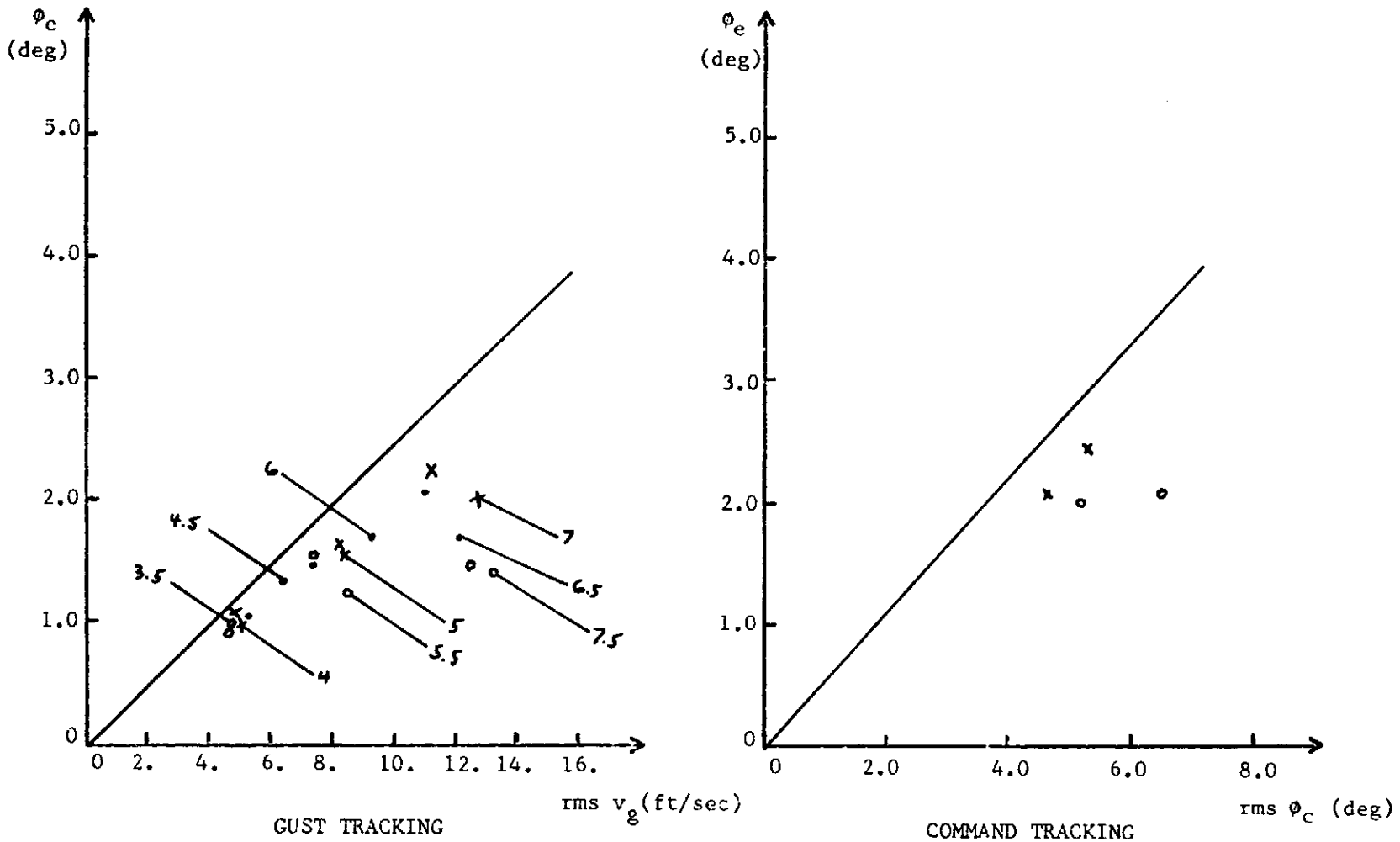

GUST TRACKING

COMMAND TRACKING

FIGURE 116. ROLL TASK SIMULATION
A-7 FLIGHT CONDITION 4
WITHOUT AUGMENTER

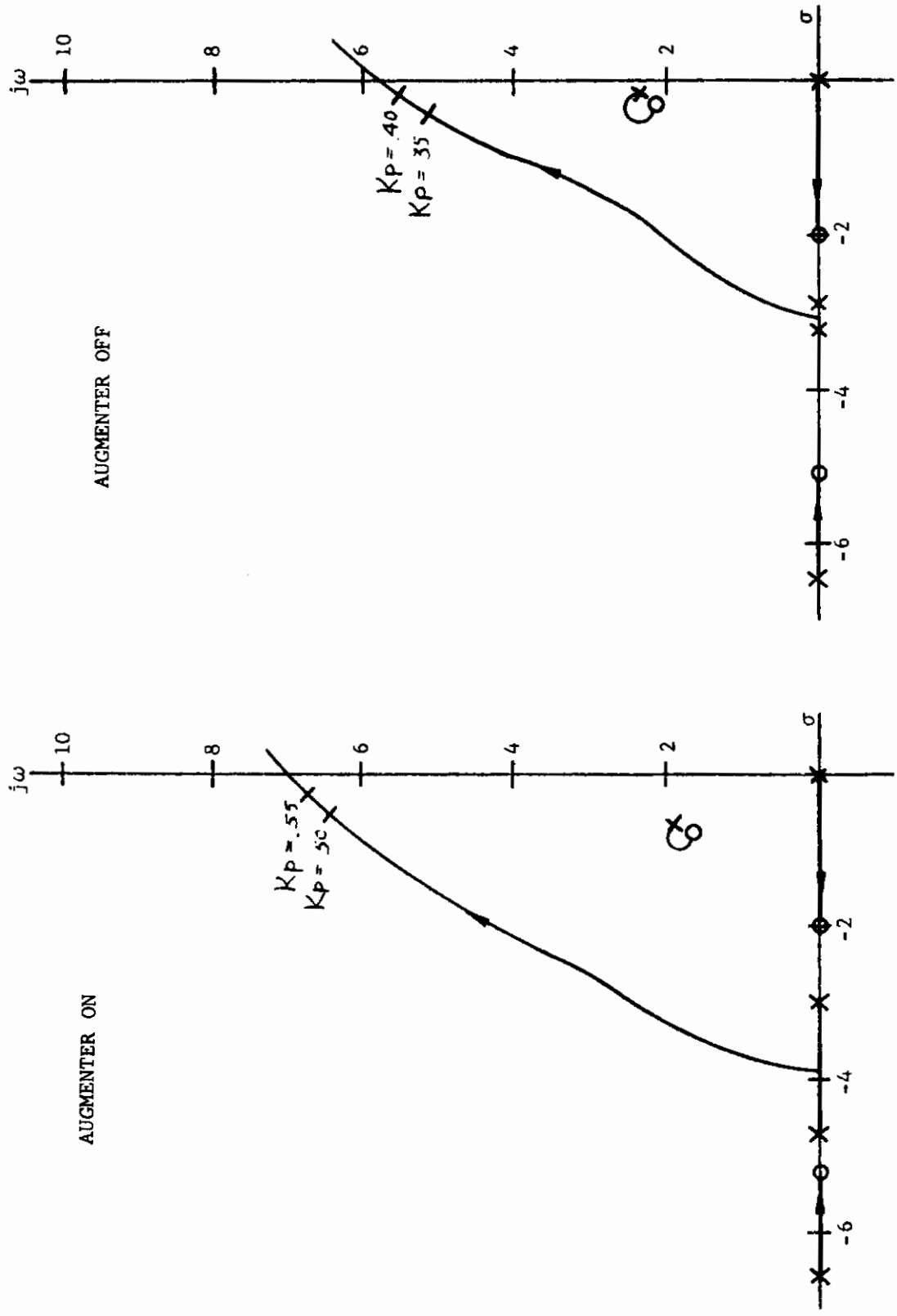

FIGURE 117. ROOT LOCUS FOR BANK ANGLE TRACKING
A-7 FLIGHT CONDITION 4
T_L = 0.5 SEC

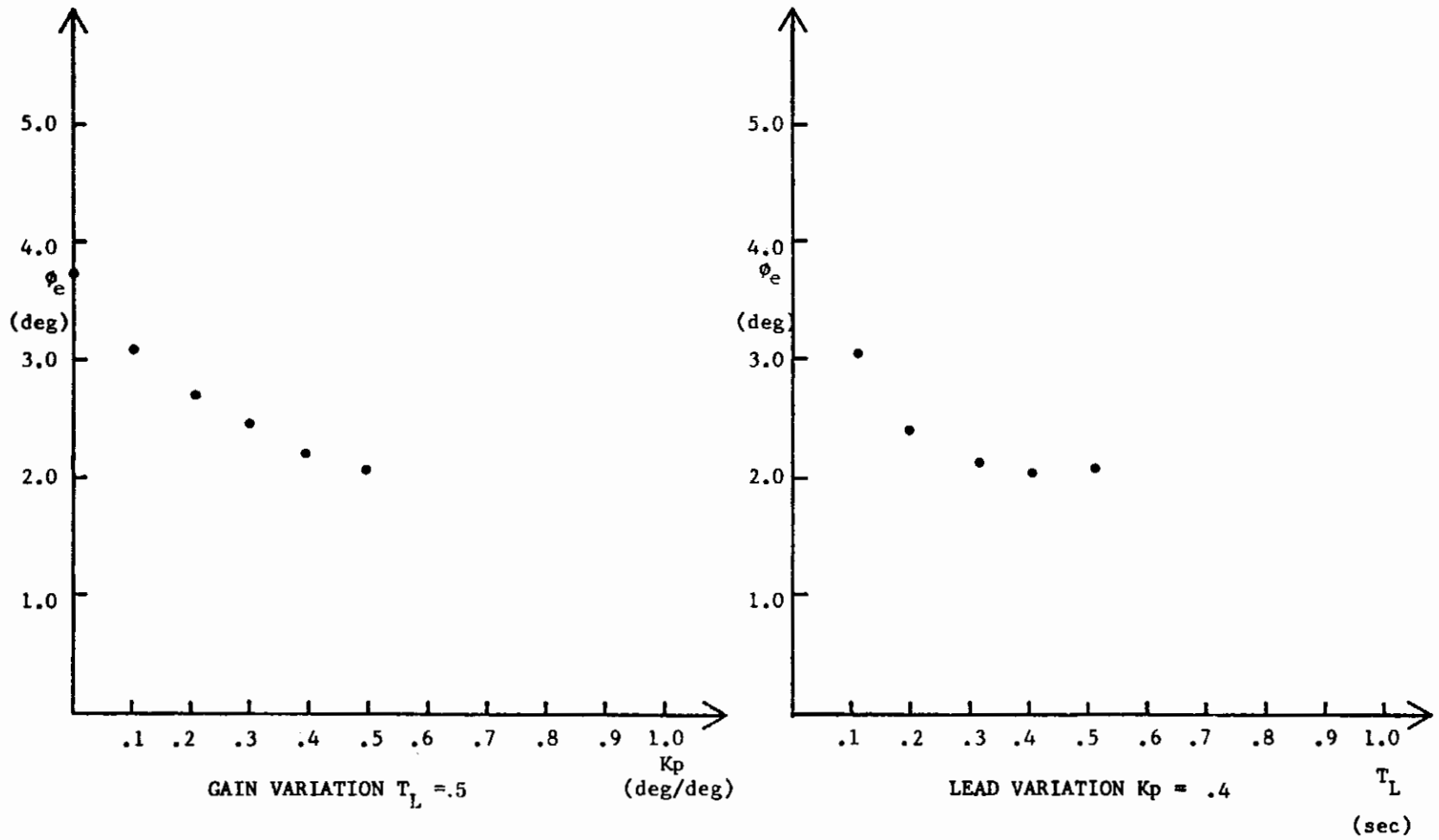

FIGURE 118. PILOT LEAD AND GAIN VARIATIONS

A-7 FLIGHT CONDITION 4

FAILURE

WITH AUGMENTER

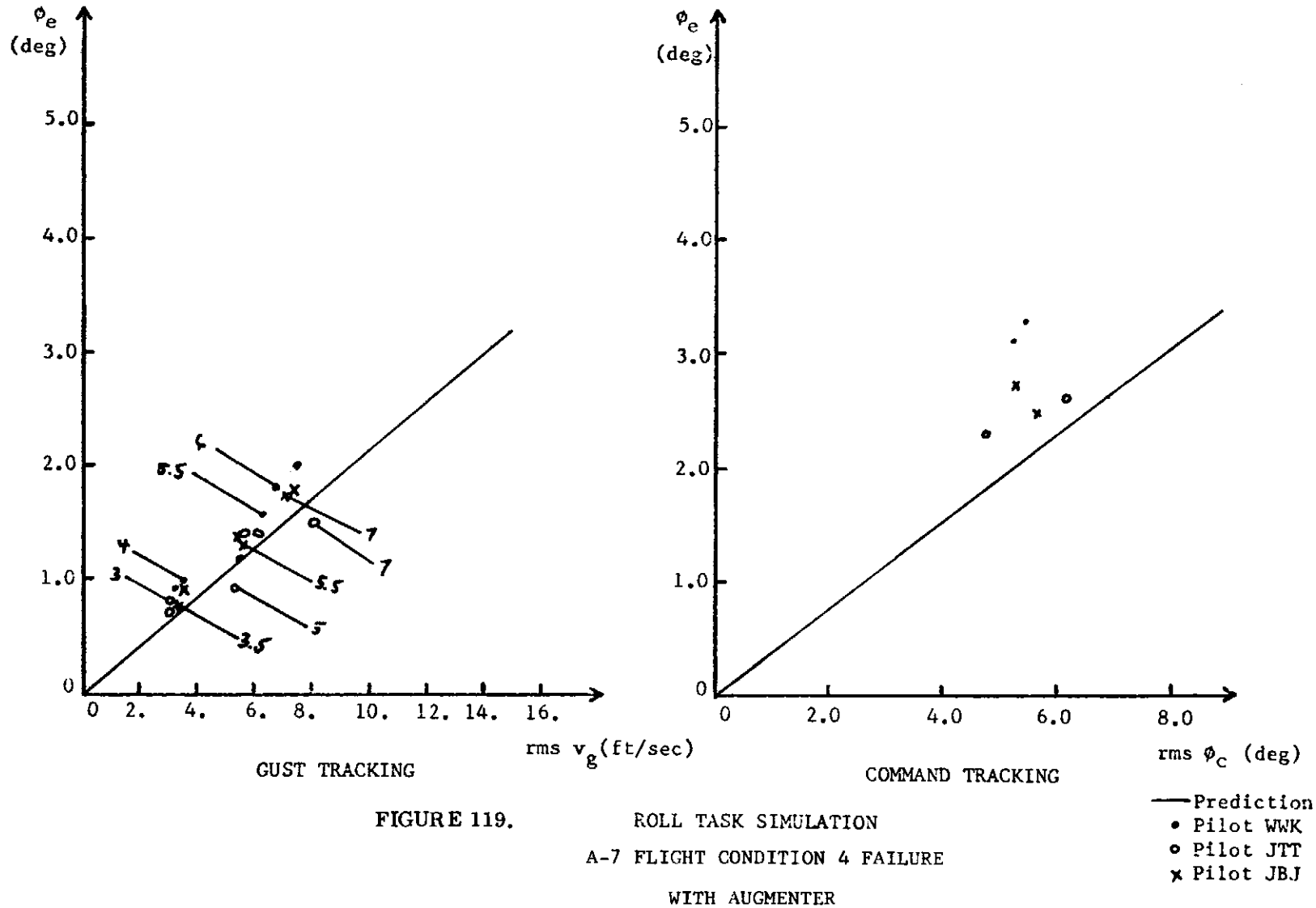

FIGURE 119. ROLL TASK SIMULATION
A-7 FLIGHT CONDITION 4 FAILURE
WITH AUGMENTER

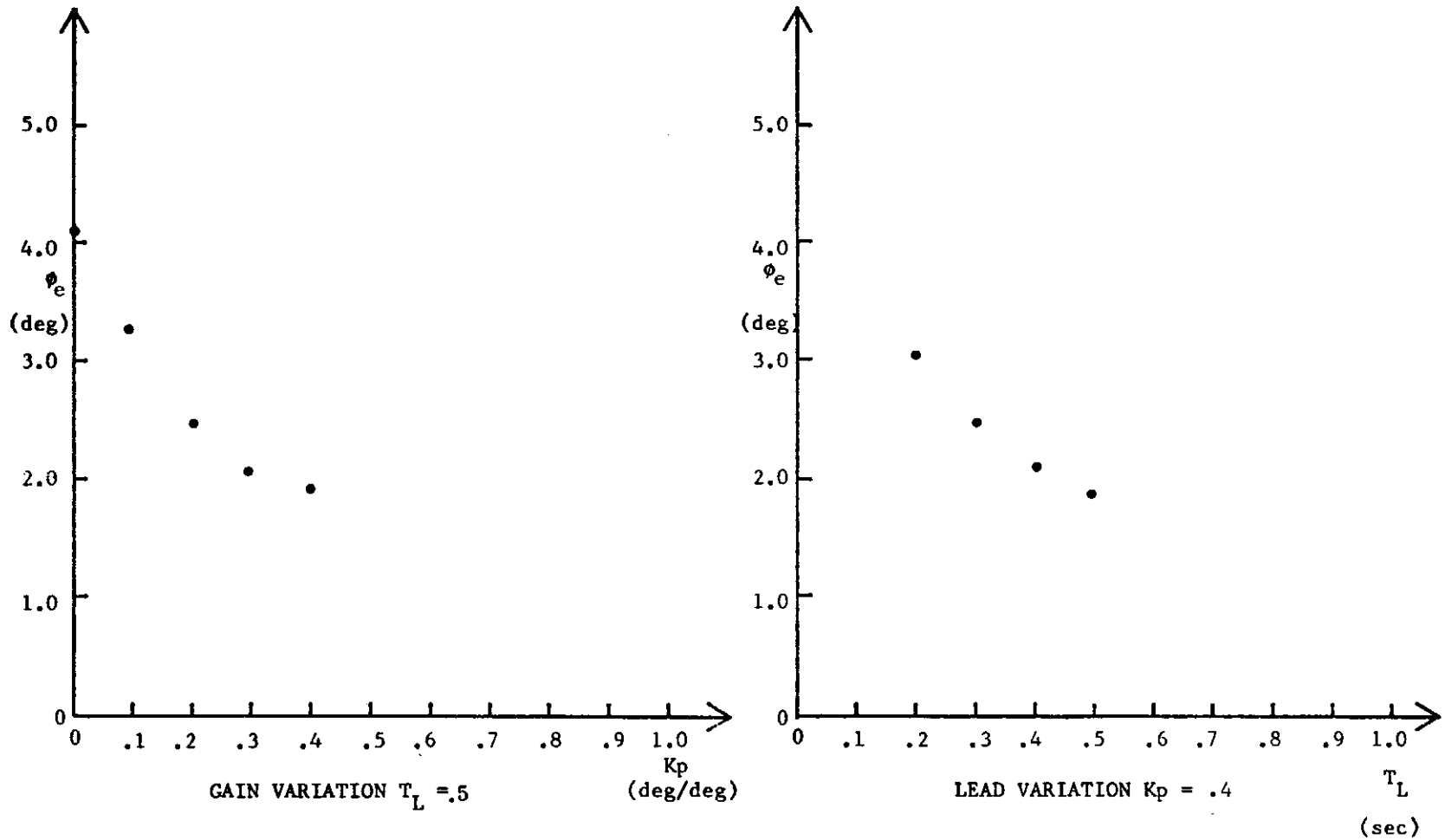

FIGURE 120. PILOT LEAD AND GAIN VARIATIONS
A-7 FLIGHT CONDITION 4 FAILURE
WITHOUT AUGMENTER

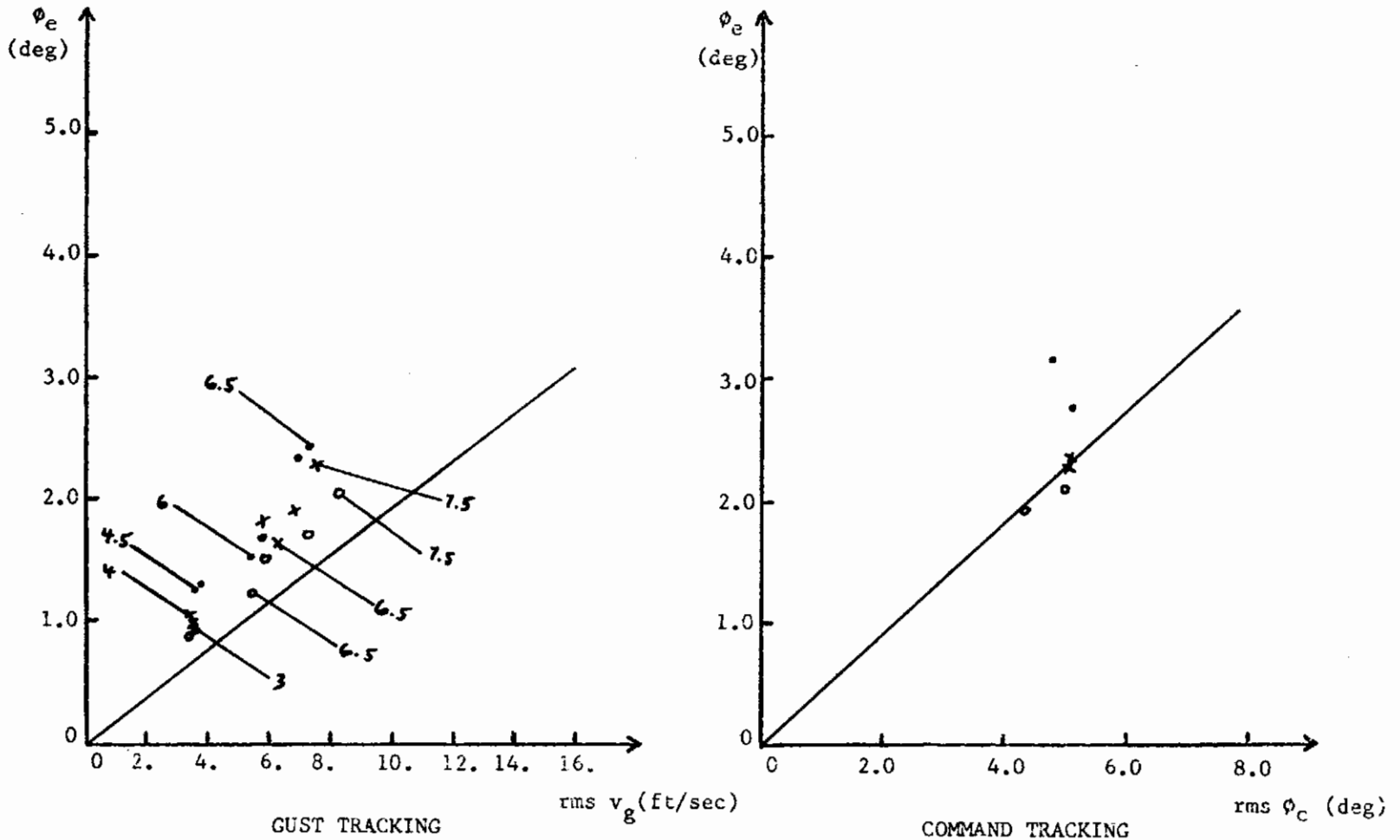

FIGURE 121. ROLL TASK SIMULATION
A-7 FLIGHT CONDITION 4 FAILURE
WITHOUT AUGMENTER

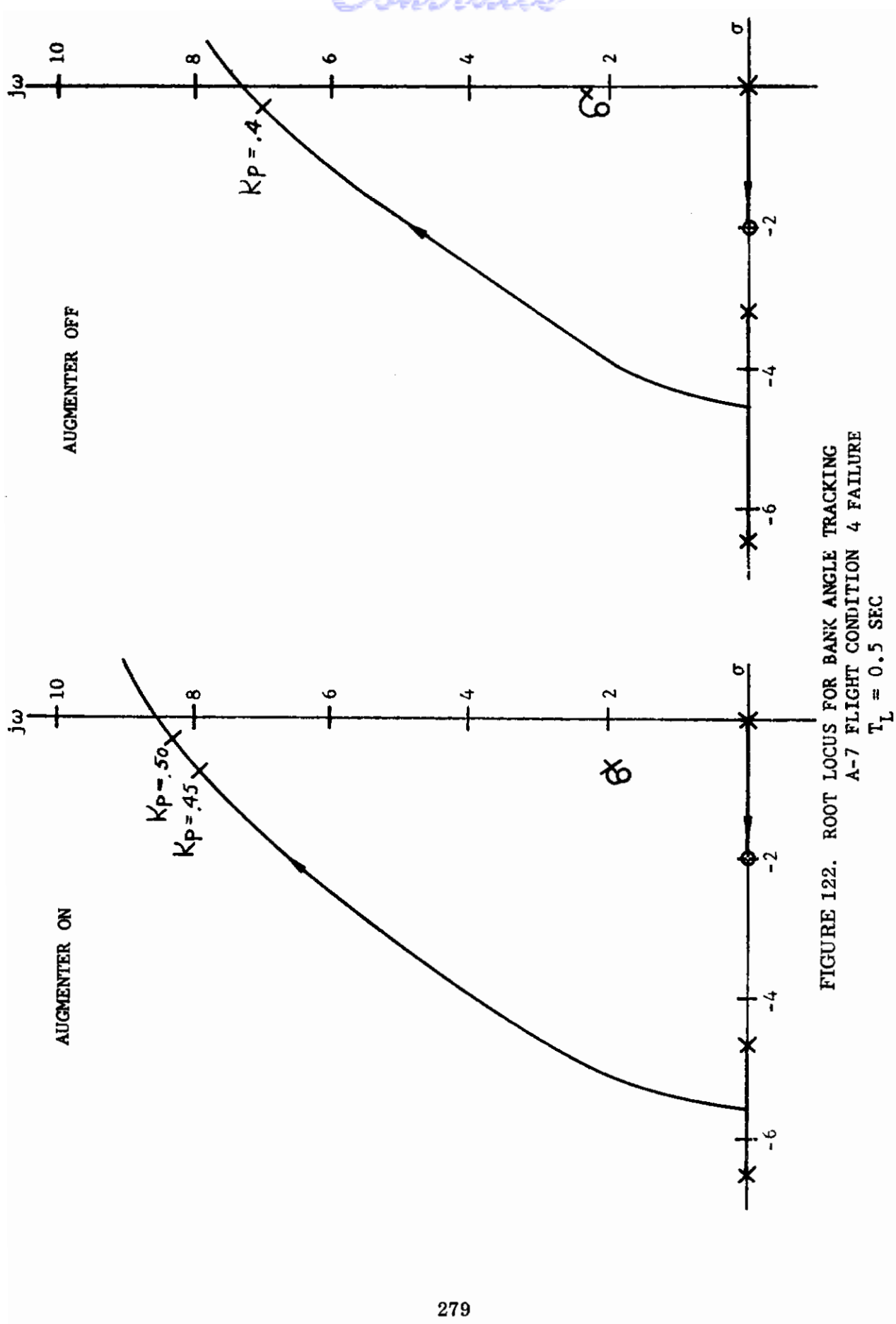

FIGURE 122. ROOT LOCUS FOR BANK ANGLE TRACKING
A-7 FLIGHT CONDITION 4 FAILURE
T_L = 0.5 SEC

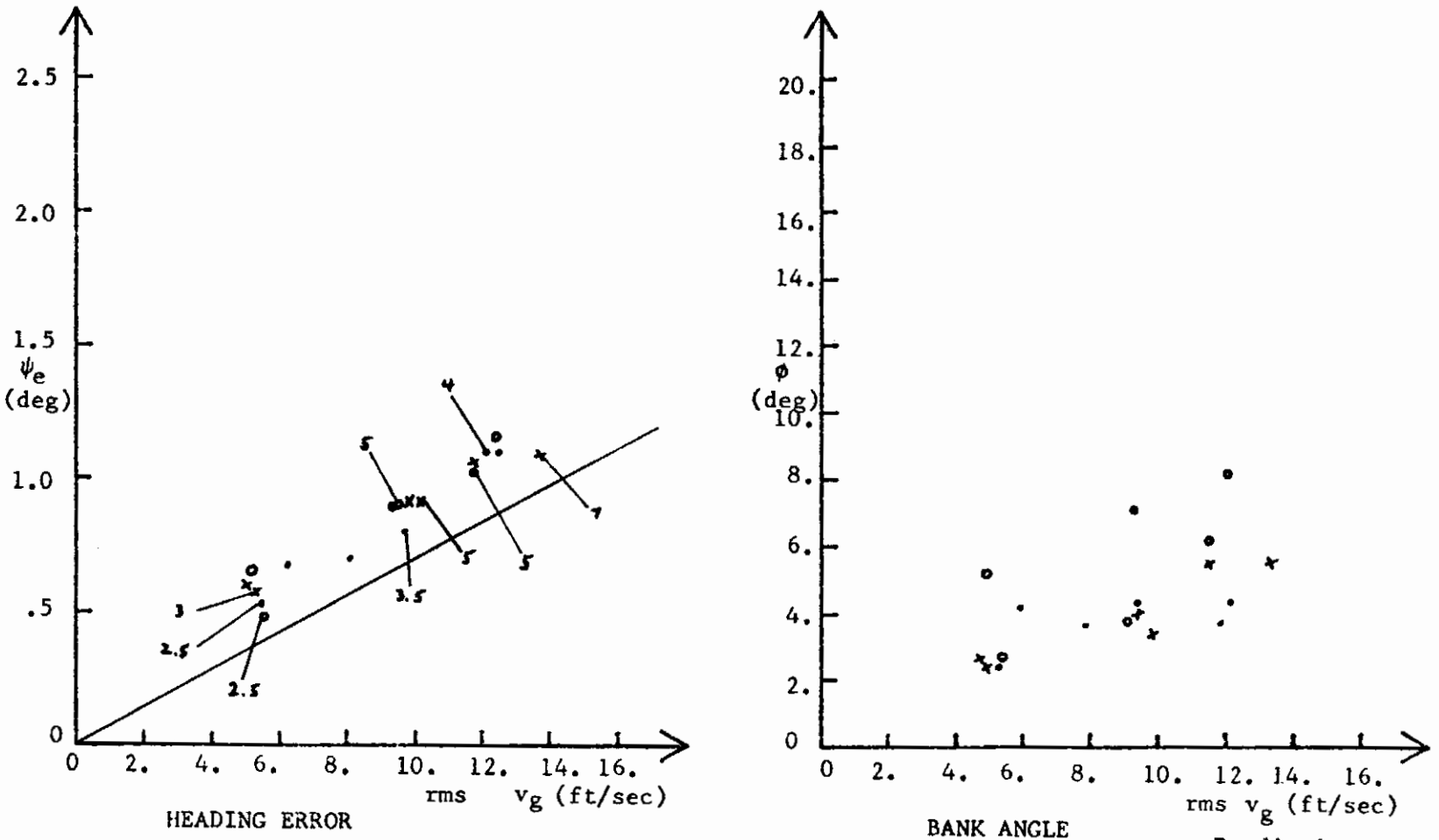

FIGURE 123. HEADING TASK SIMULATION
F-5 FLIGHT CONDITION 1
WITH AUGMENTER

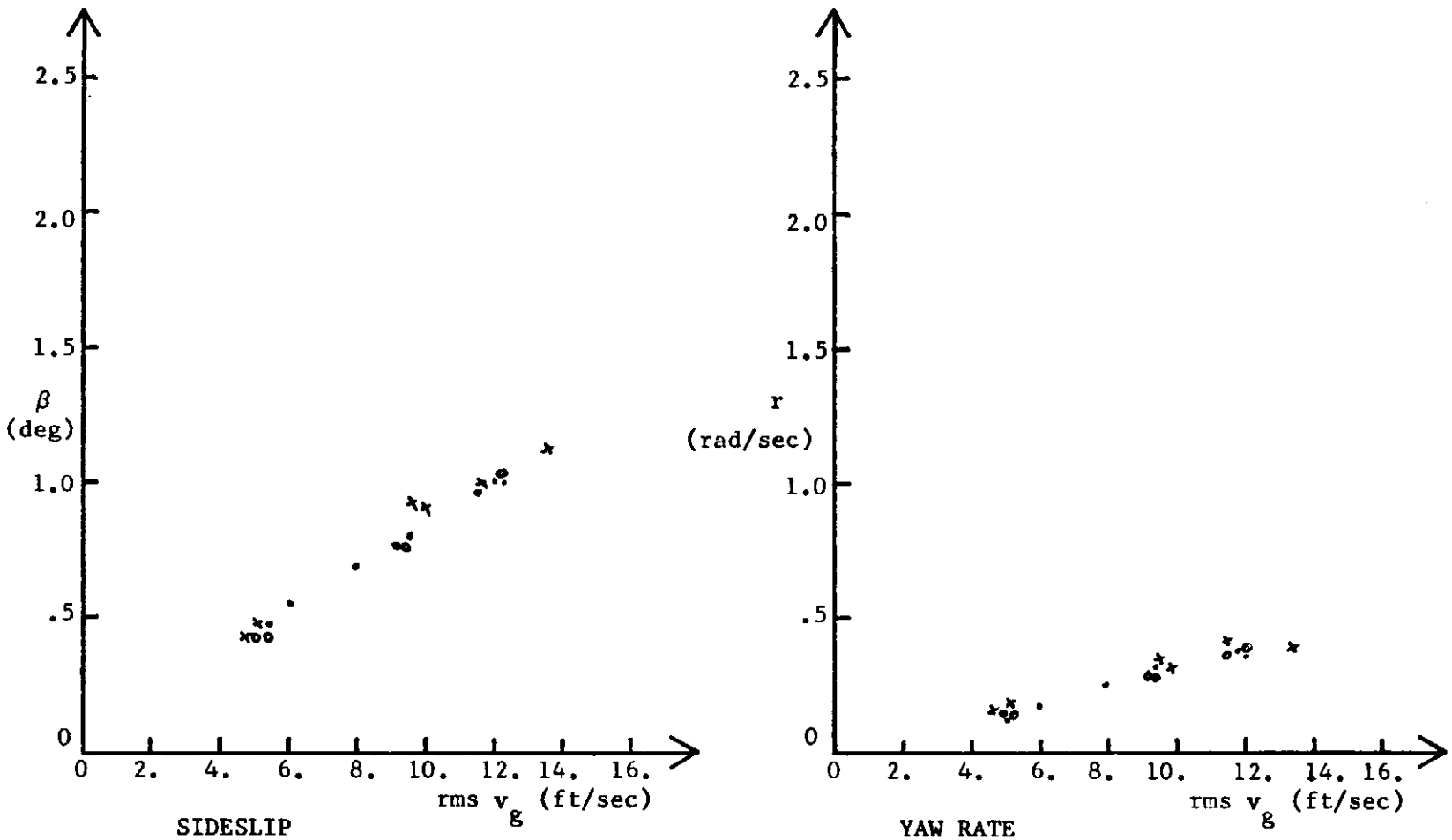

FIGURE 124. HEADING TASK SIMULATION
F-5 FLIGHT CONDITION 1
WITH AUGMENTER

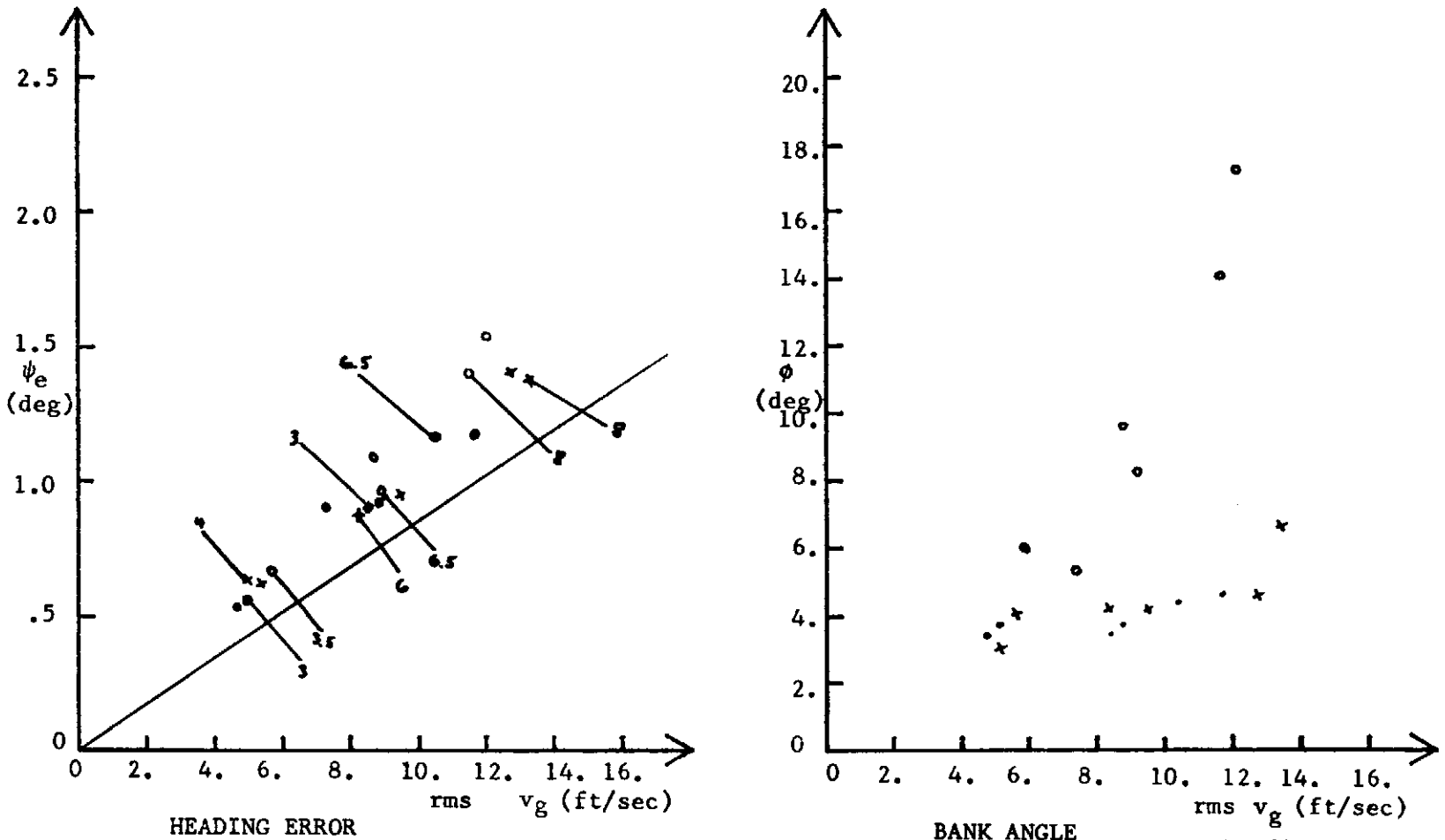

FIGURE 125. HEADING TASK SIMULATION

F-5 FLIGHT CONDITION 1

WITHOUT AUGMENTER

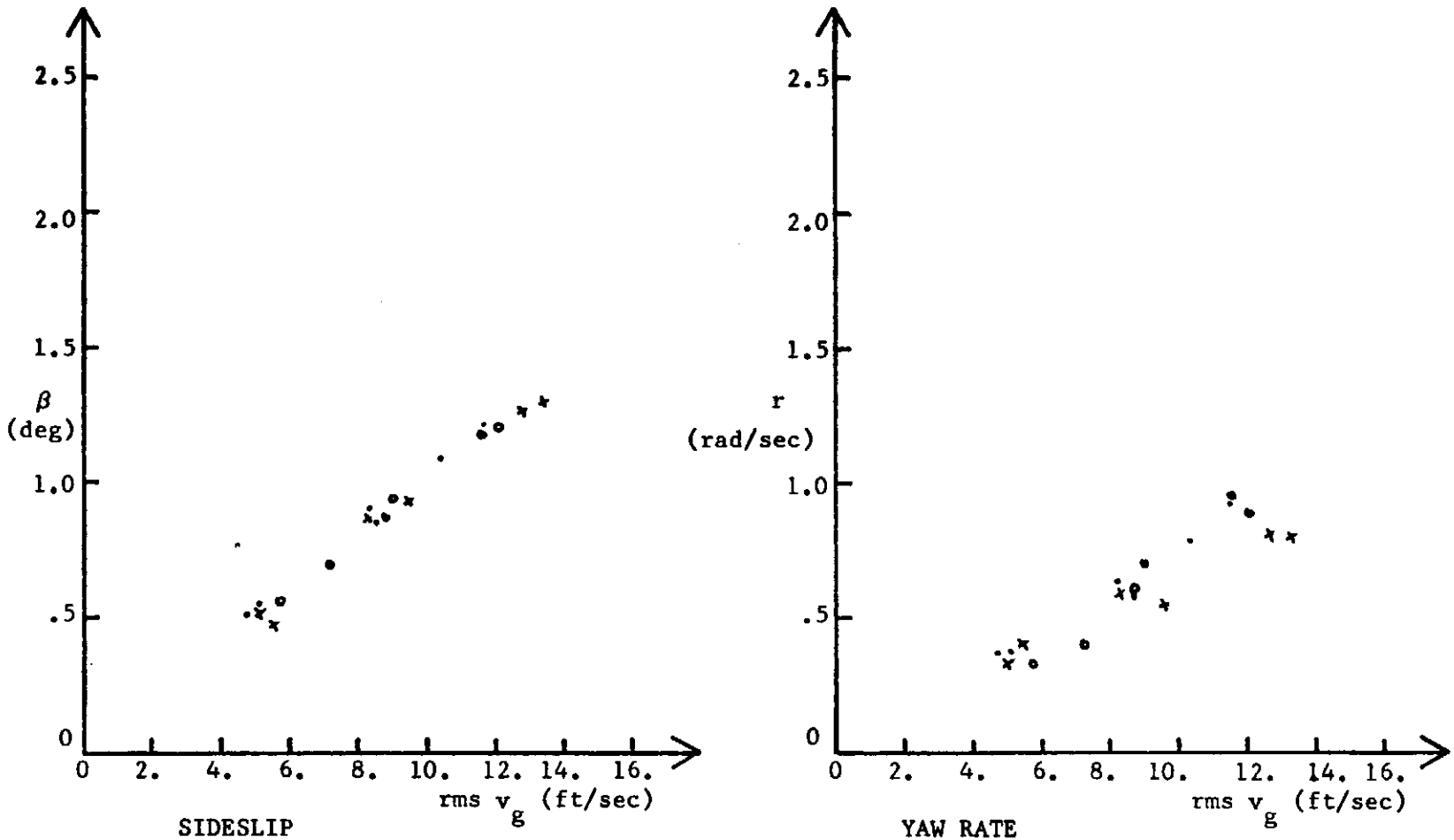

FIGURE 126. HEADING TASK SIMULATION

F-5 FLIGHT CONDITION 1

WITHOUT AUGMENTER

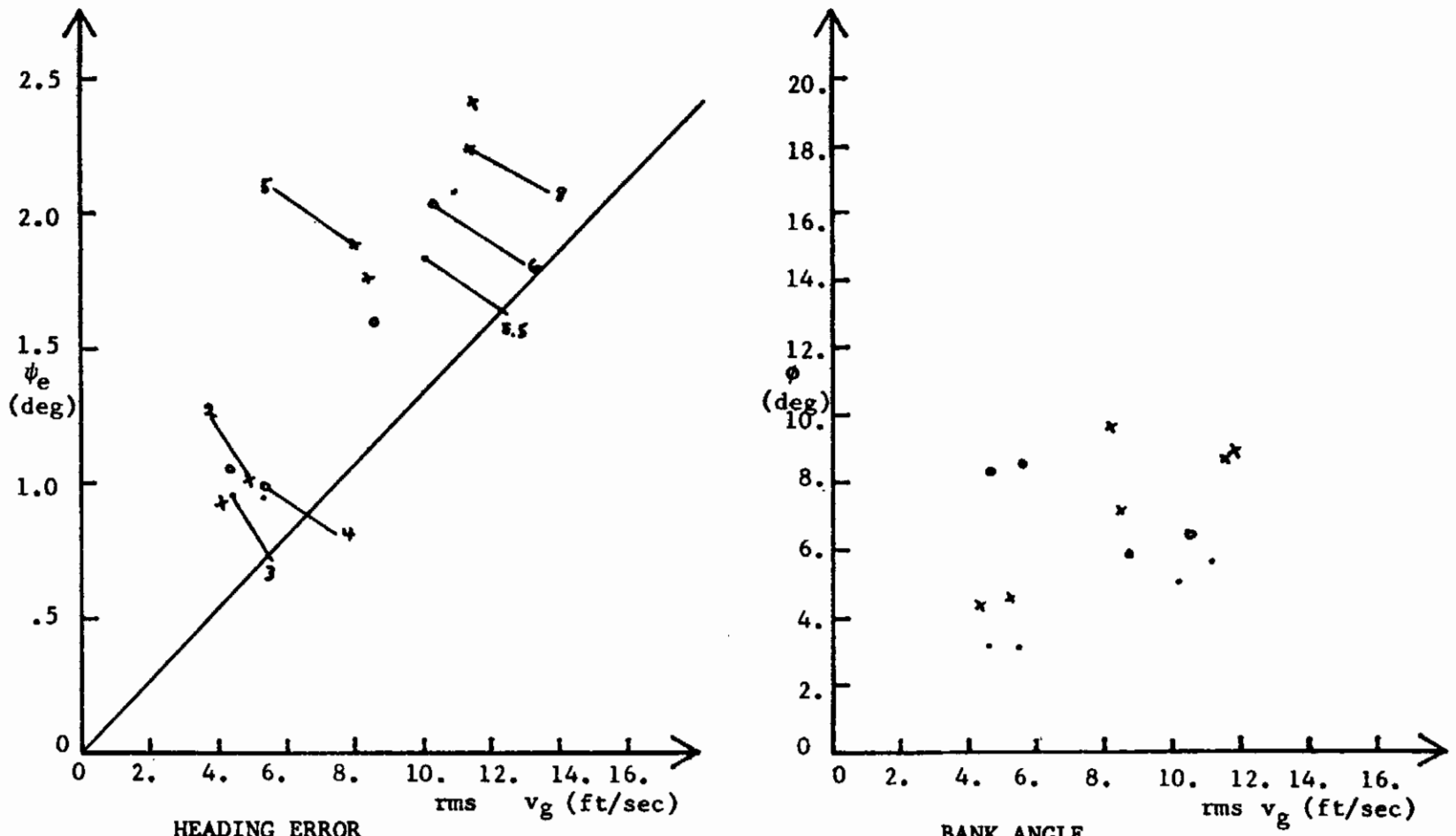

FIGURE 127. HEADING TASK SIMULATION
F-5 FLIGHT CONDITION 2
WITH AUGMENTER

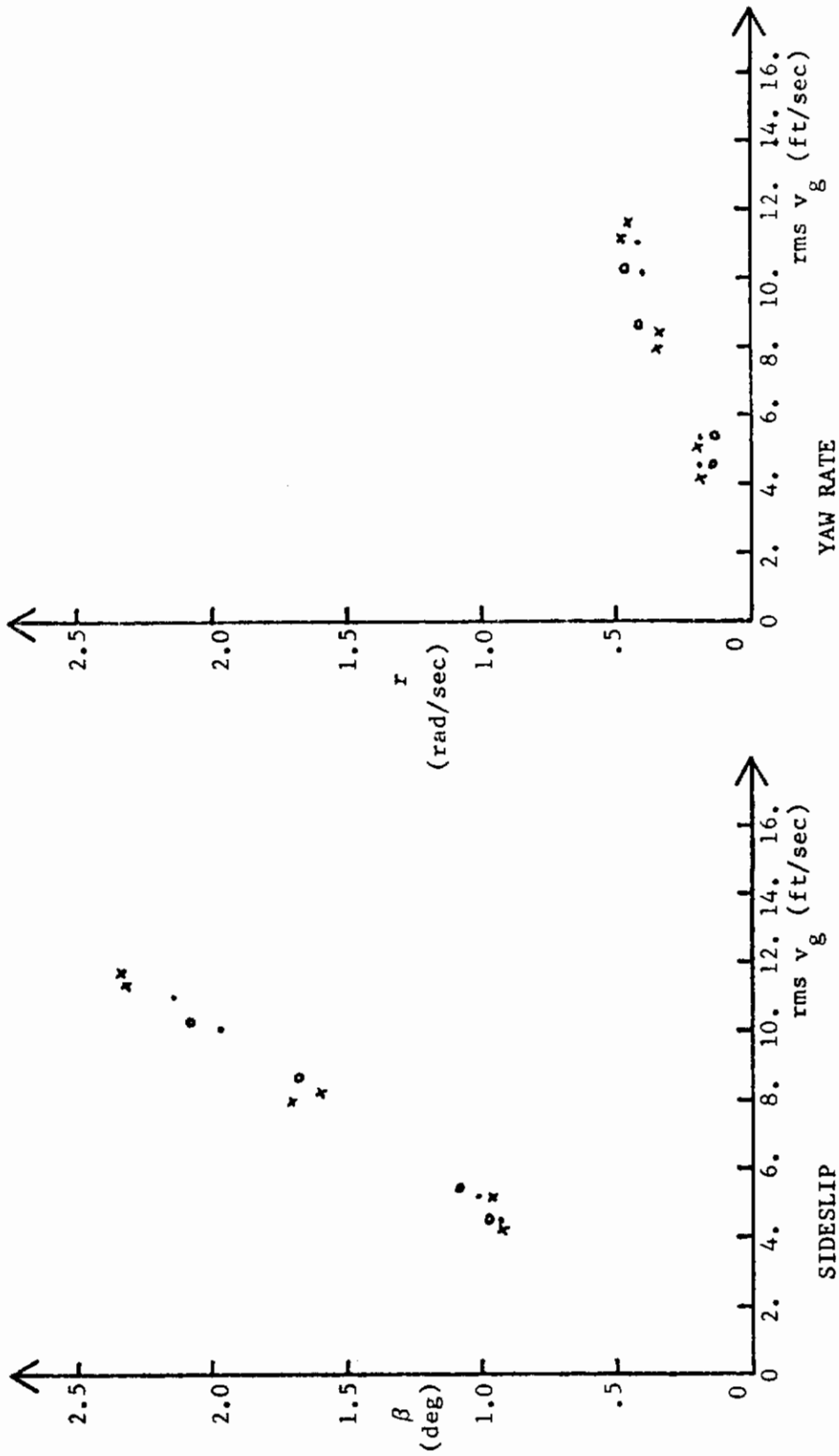

FIGURE 128. HEADING TASK SIMULATION
F-5 FLIGHT CONDITION 2
WITH AUGMENTER

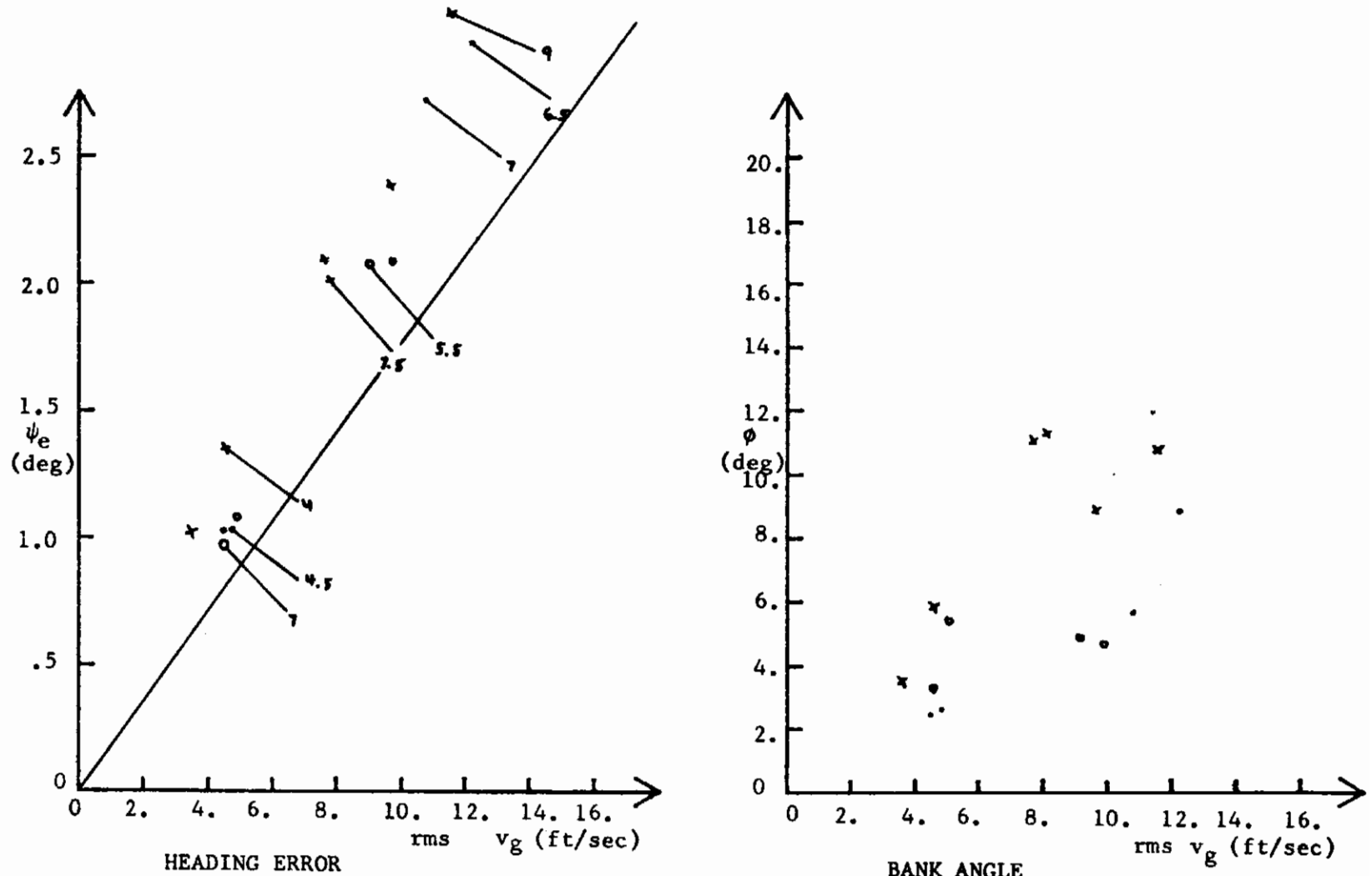

FIGURE 129. HEADING TASK SIMULATION
F-5 FLIGHT CONDITION 2
WITHOUT AUGMENTER

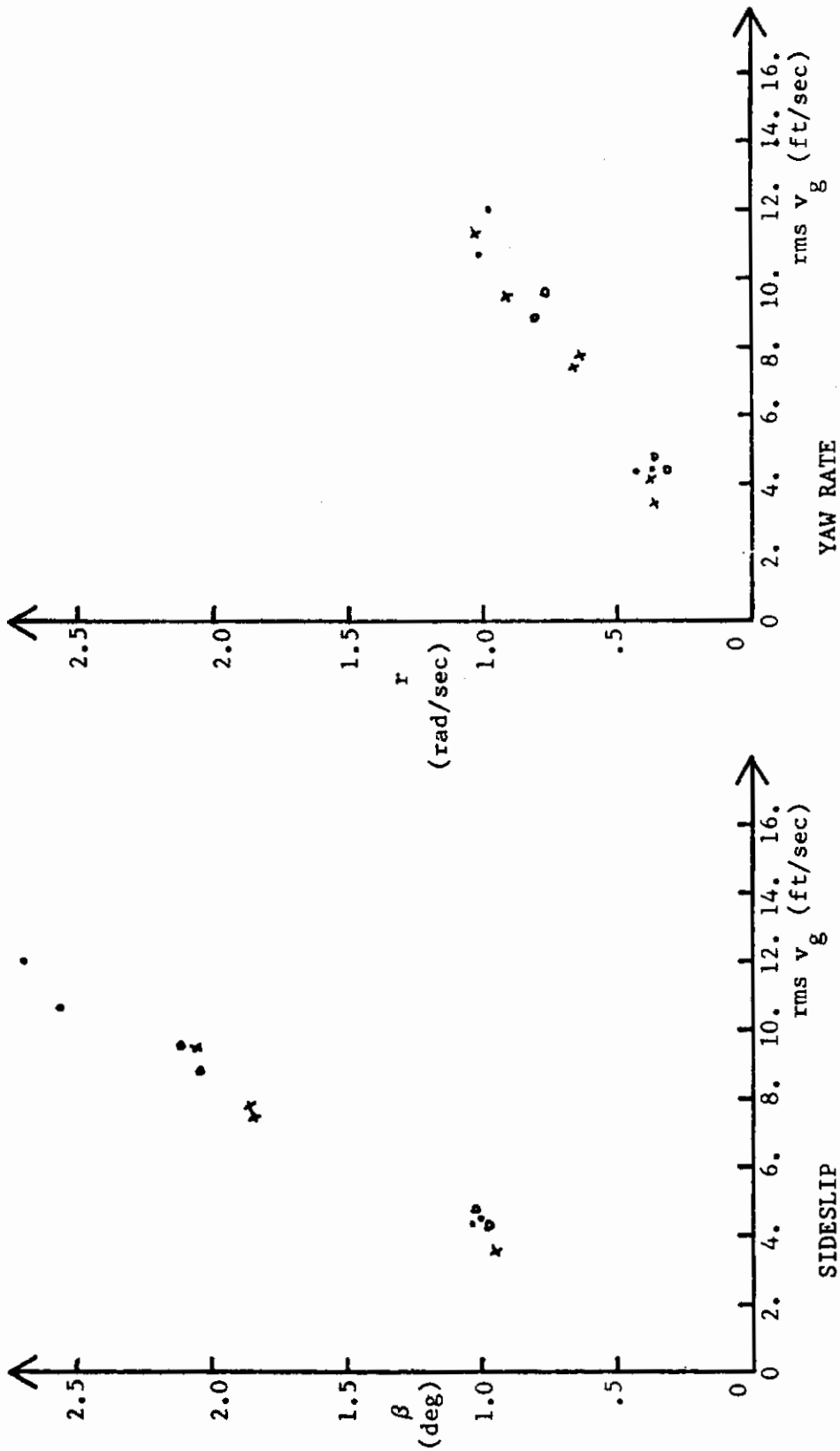

FIGURE 130. HEADING TASK SIMULATION
F-5 FLIGHT CONDITION 2
WITHOUT AUGMENTER

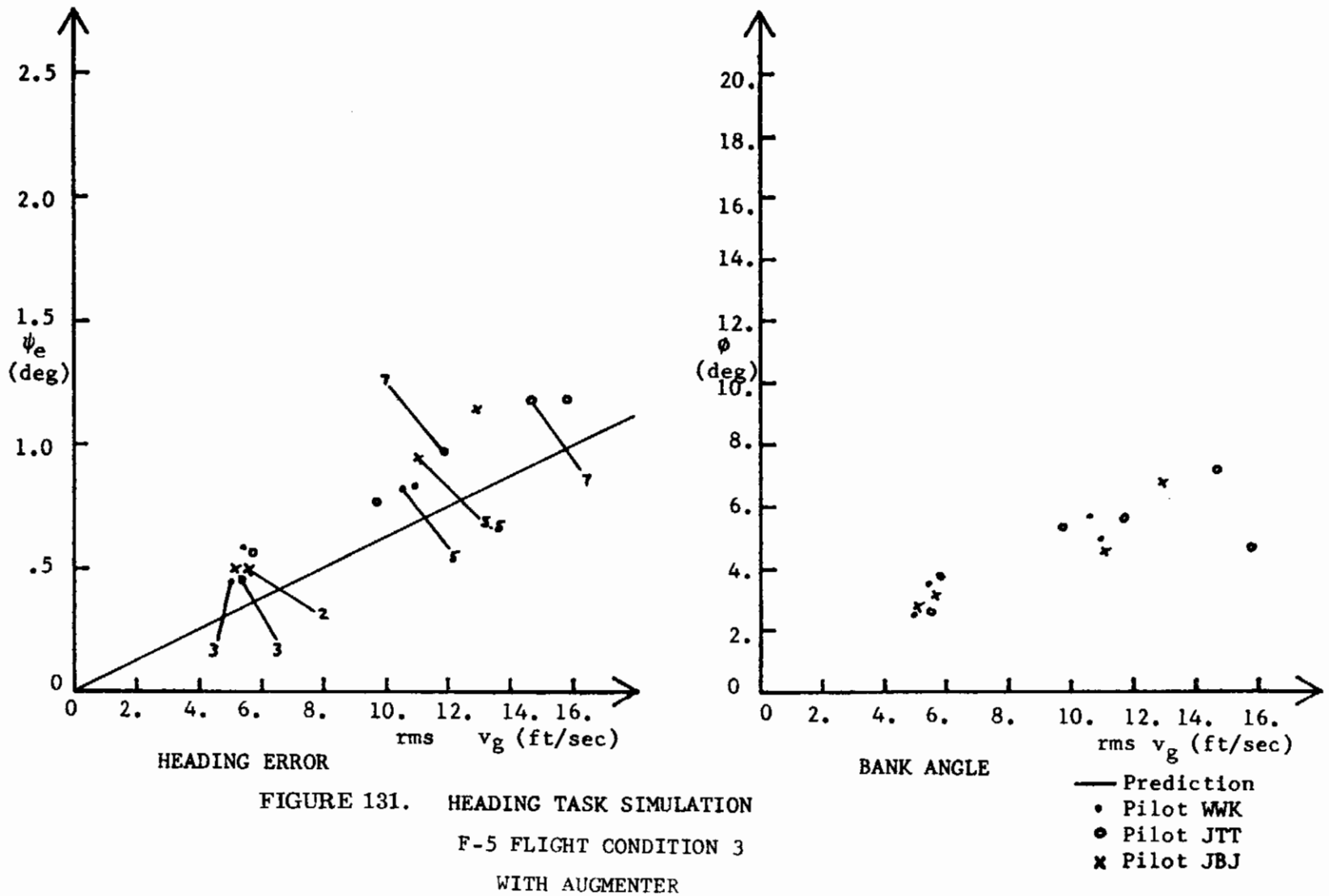

FIGURE 131. HEADING TASK SIMULATION

F-5 FLIGHT CONDITION 3

WITH AUGMENTER

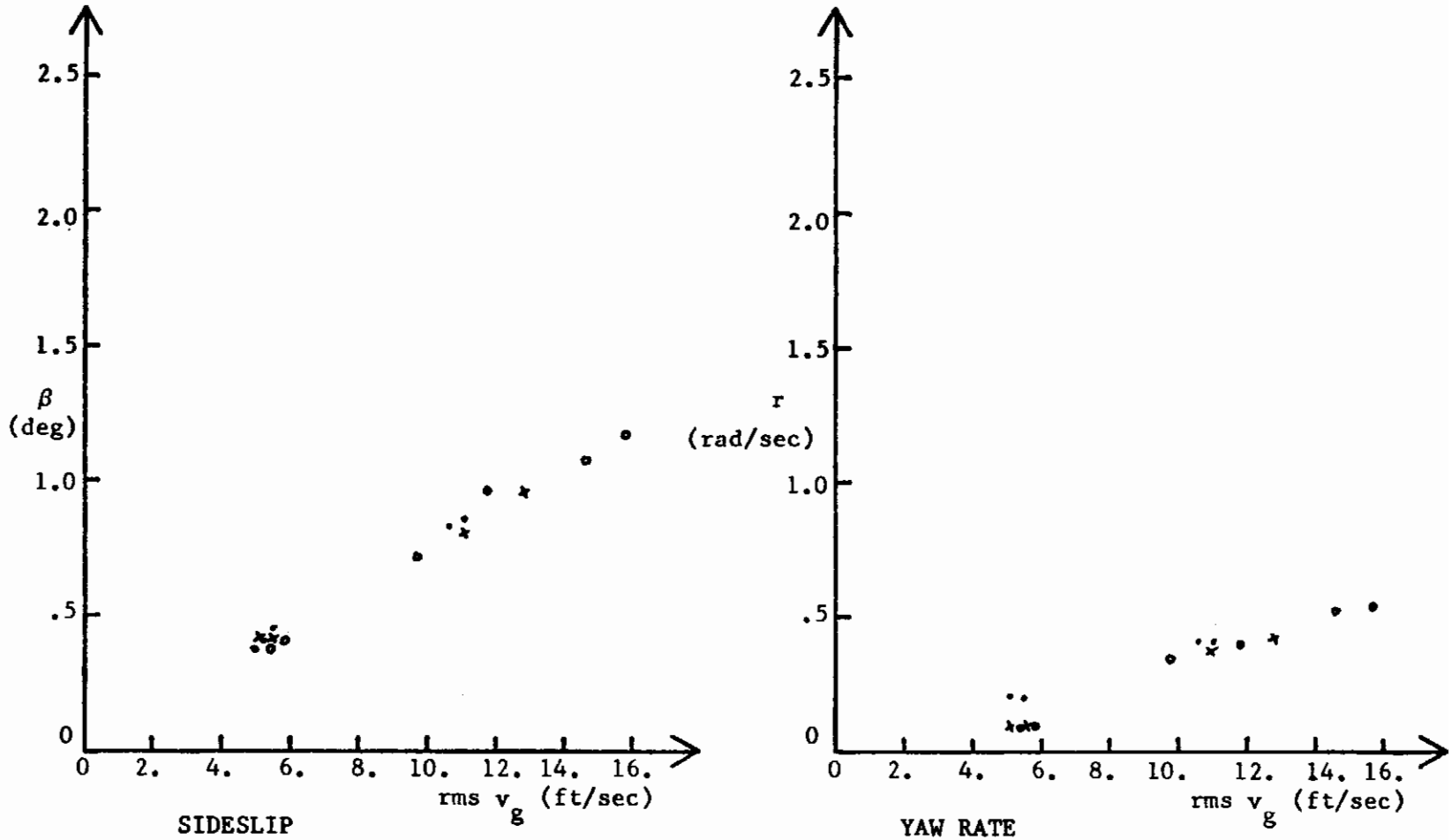

FIGURE 132. HEADING TASK SIMULATION
F-5 FLIGHT CONDITION 3
WITH AUGMENTER

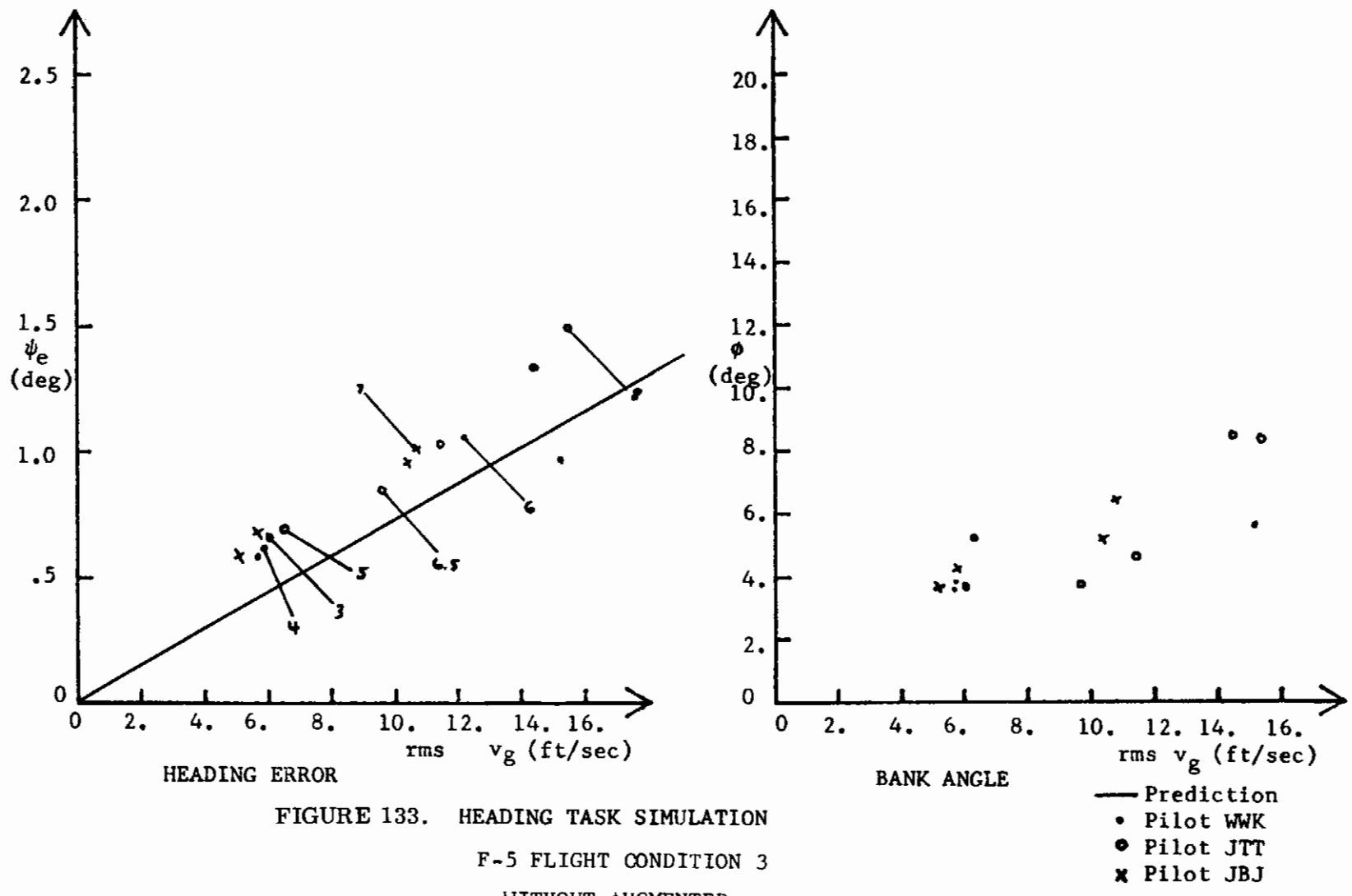

FIGURE 133. HEADING TASK SIMULATION

F-5 FLIGHT CONDITION 3

WITHOUT AUGMENTER

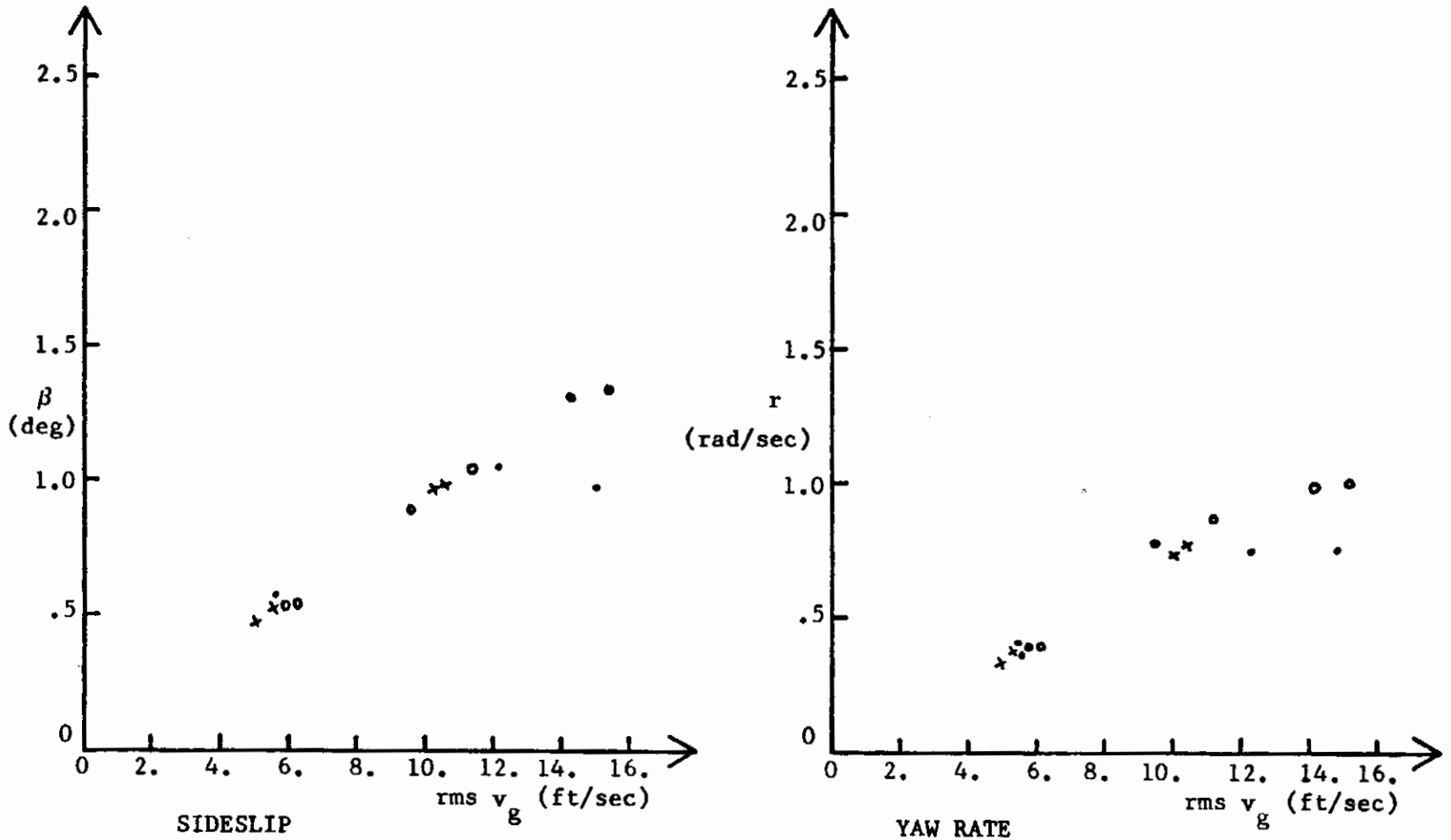

FIGURE 134. HEADING TASK SIMULATION
F-5 FLIGHT CONDITION 3
WITHOUT AUGMENTER

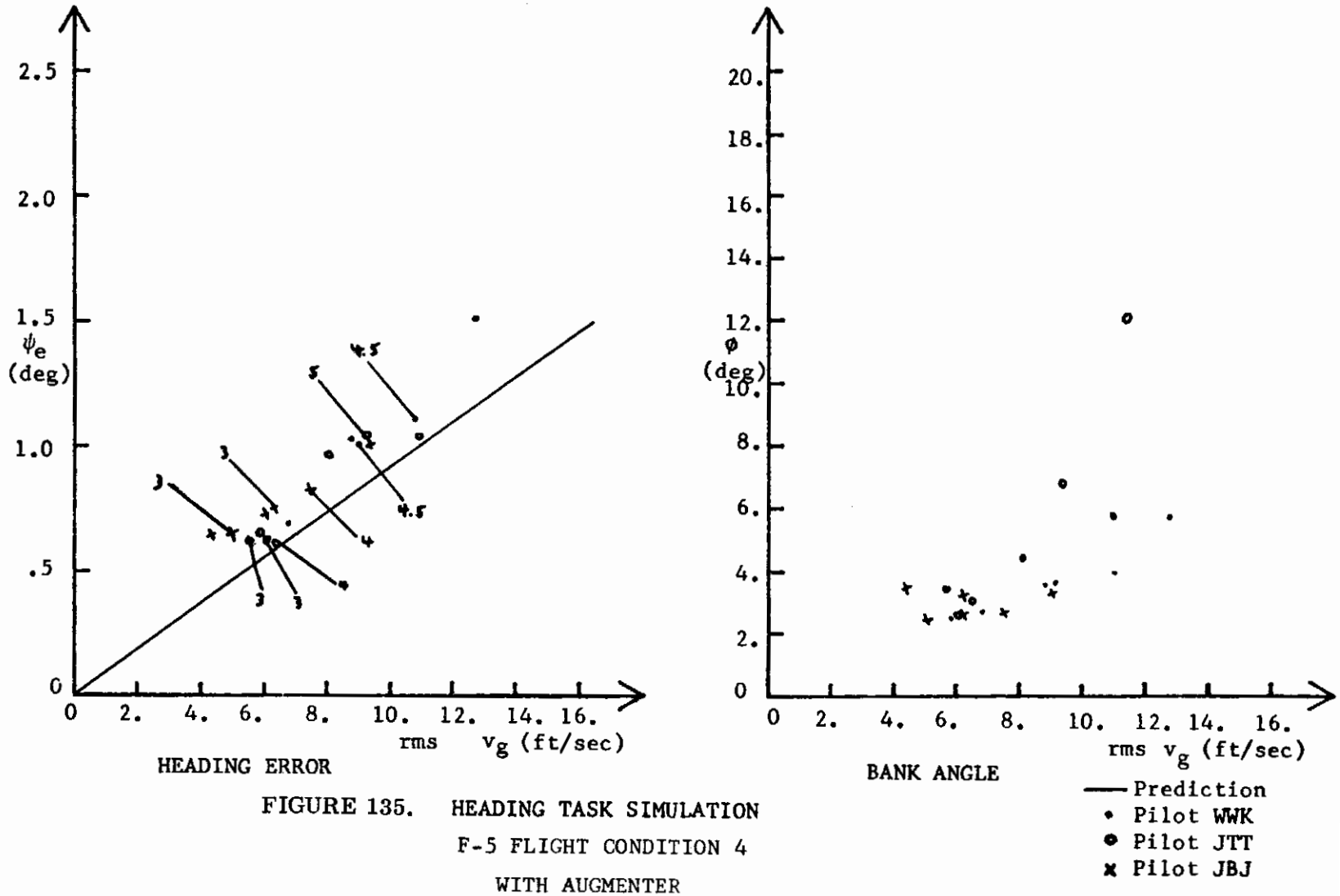

FIGURE 135. HEADING TASK SIMULATION
F-5 FLIGHT CONDITION 4
WITH AUGMENTER

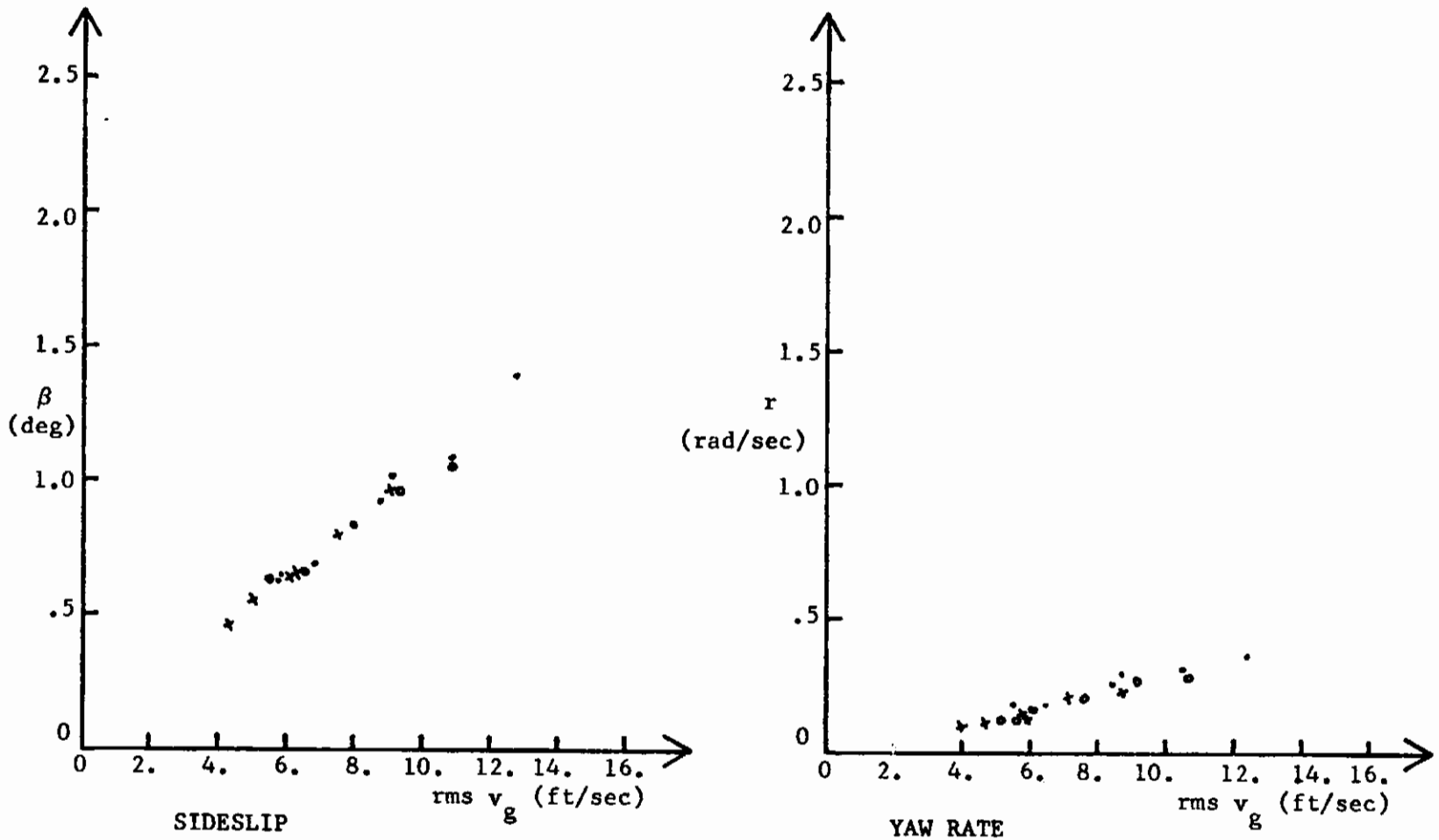

FIGURE 136. HEADING TASK SIMULATION

F-5 FLIGHT CONDITION 4

WITH AUGMENTER

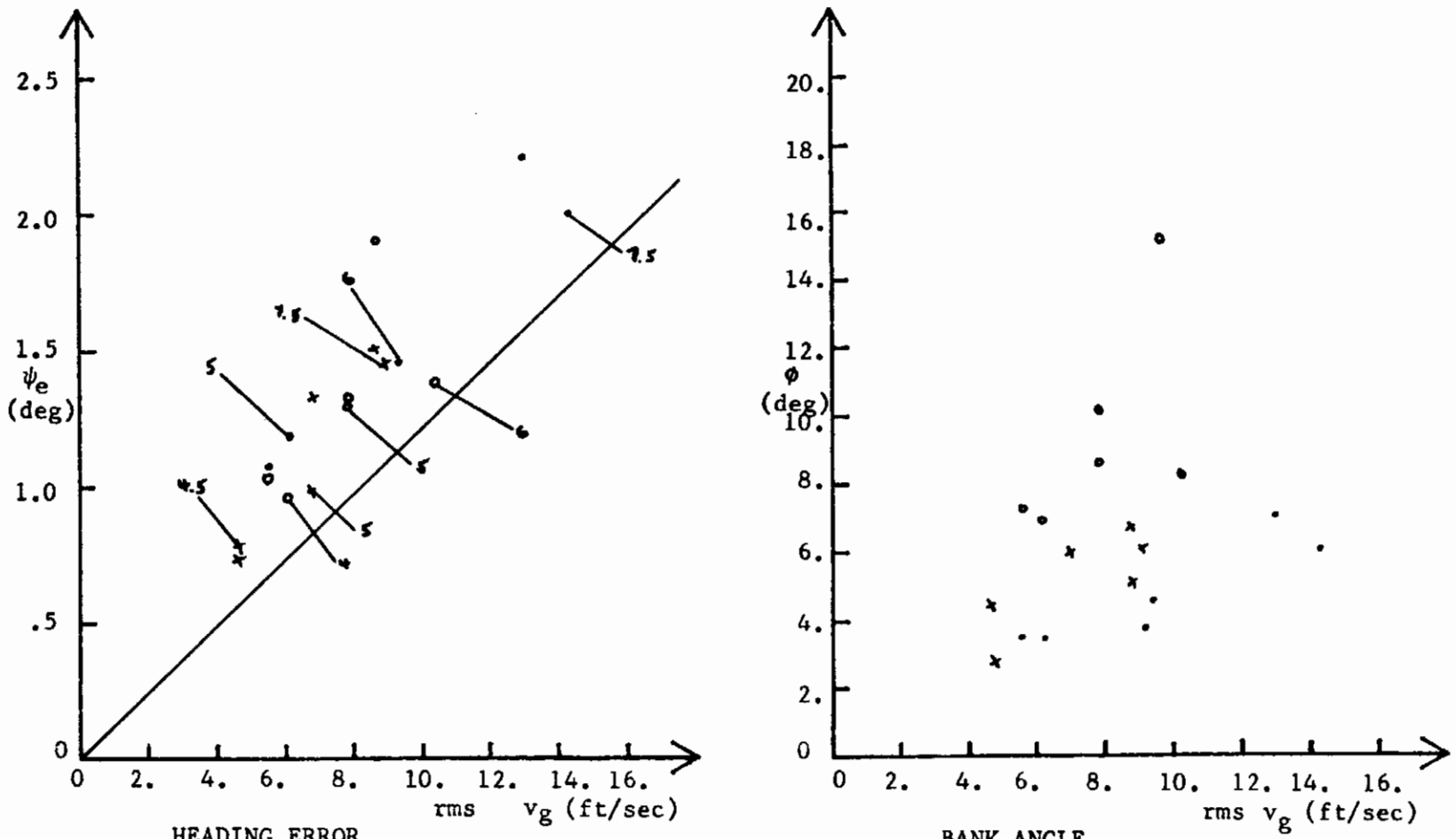

FIGURE 137. HEADING TASK SIMULATION

F-5 FLIGHT CONDITION 4

WITHOUT AUGMENTER

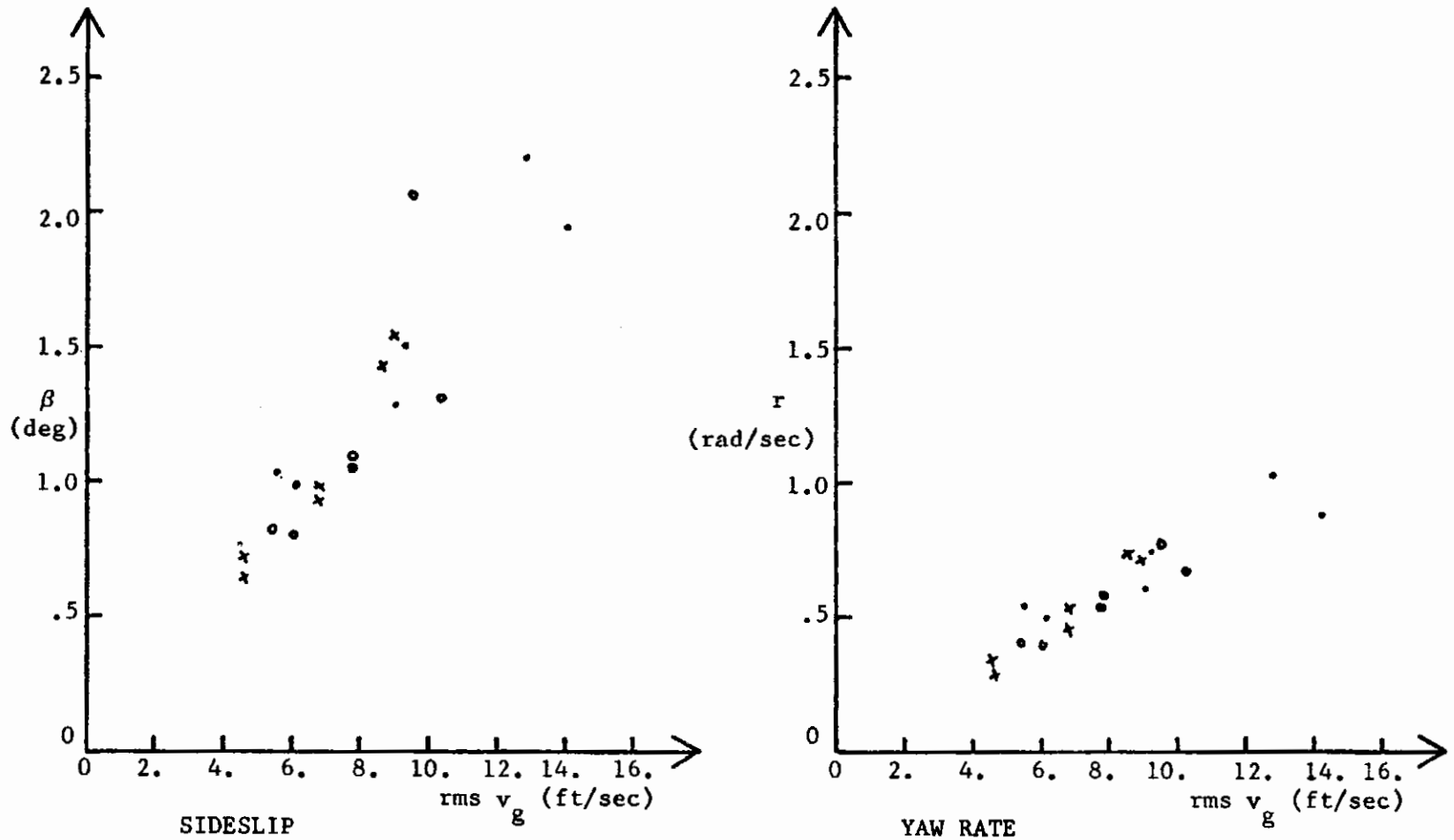

FIGURE 138. HEADING TASK SIMULATION

F-5 FLIGHT CONDITION 4

WITHOUT AUGMENTER

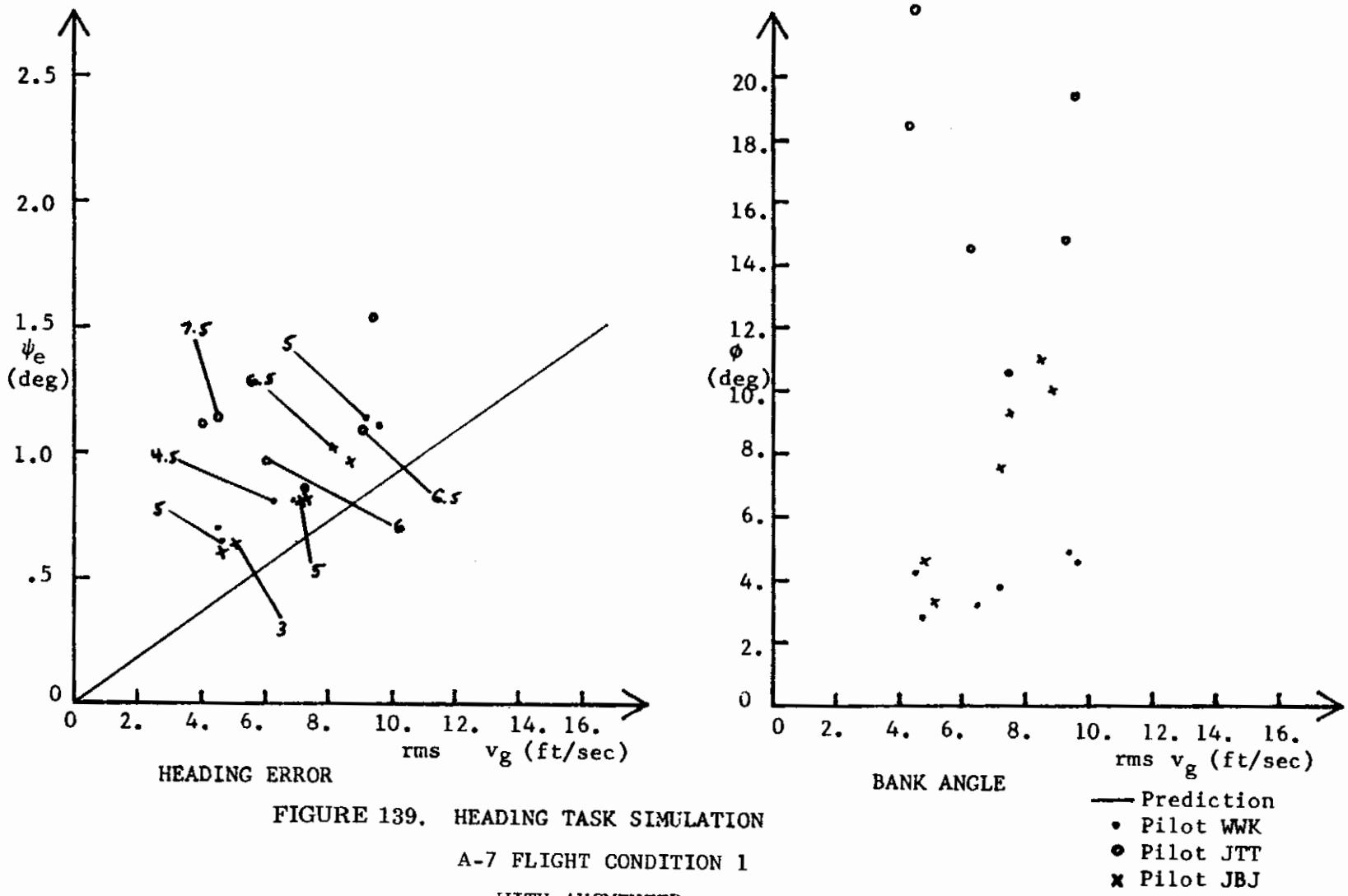

FIGURE 139. HEADING TASK SIMULATION

A-7 FLIGHT CONDITION 1

WITH AUGMENTER

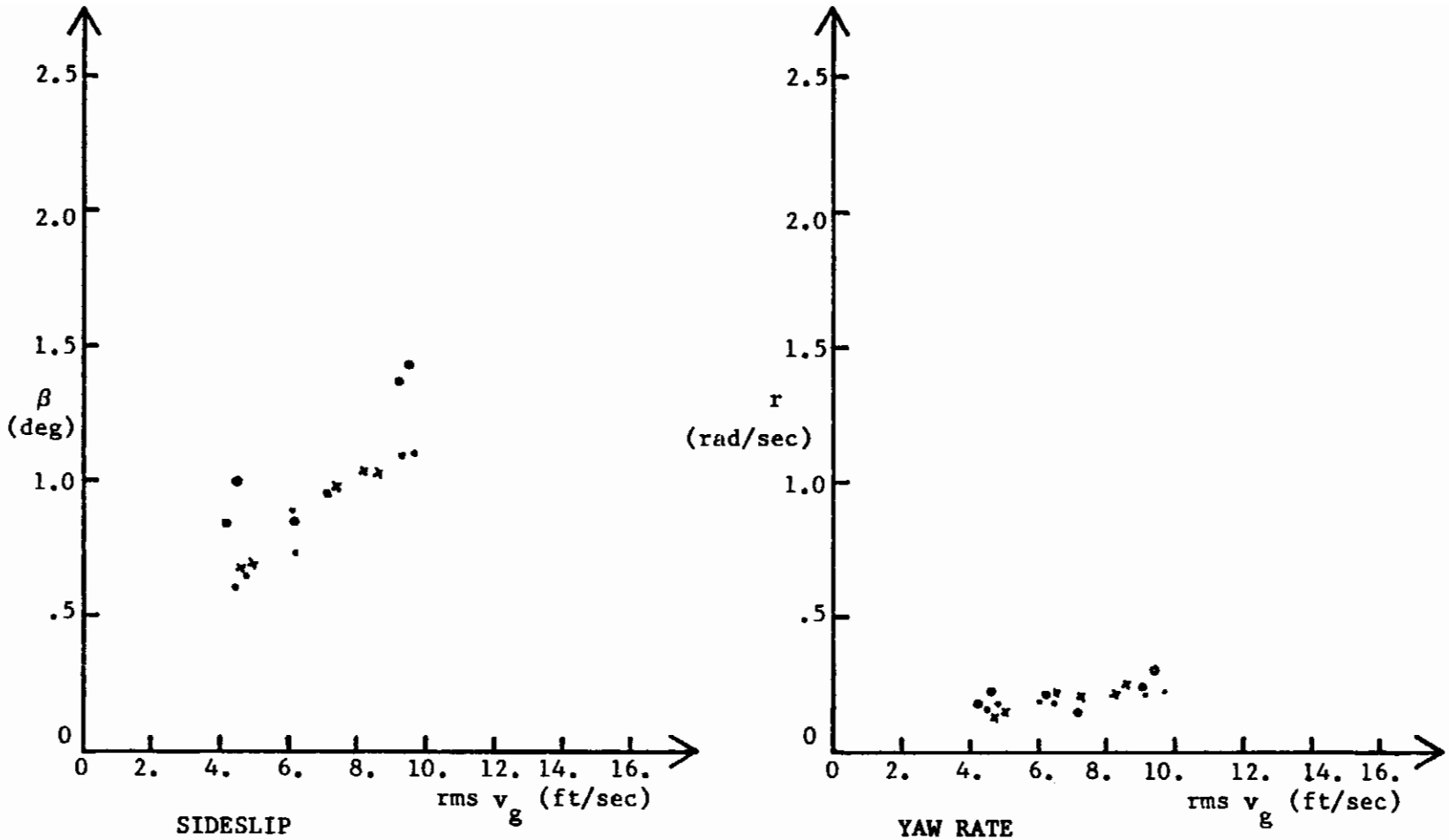

FIGURE 140. HEADING TASK SIMULATION
A-7 FLIGHT CONDITION 1
WITH AUGMENTER

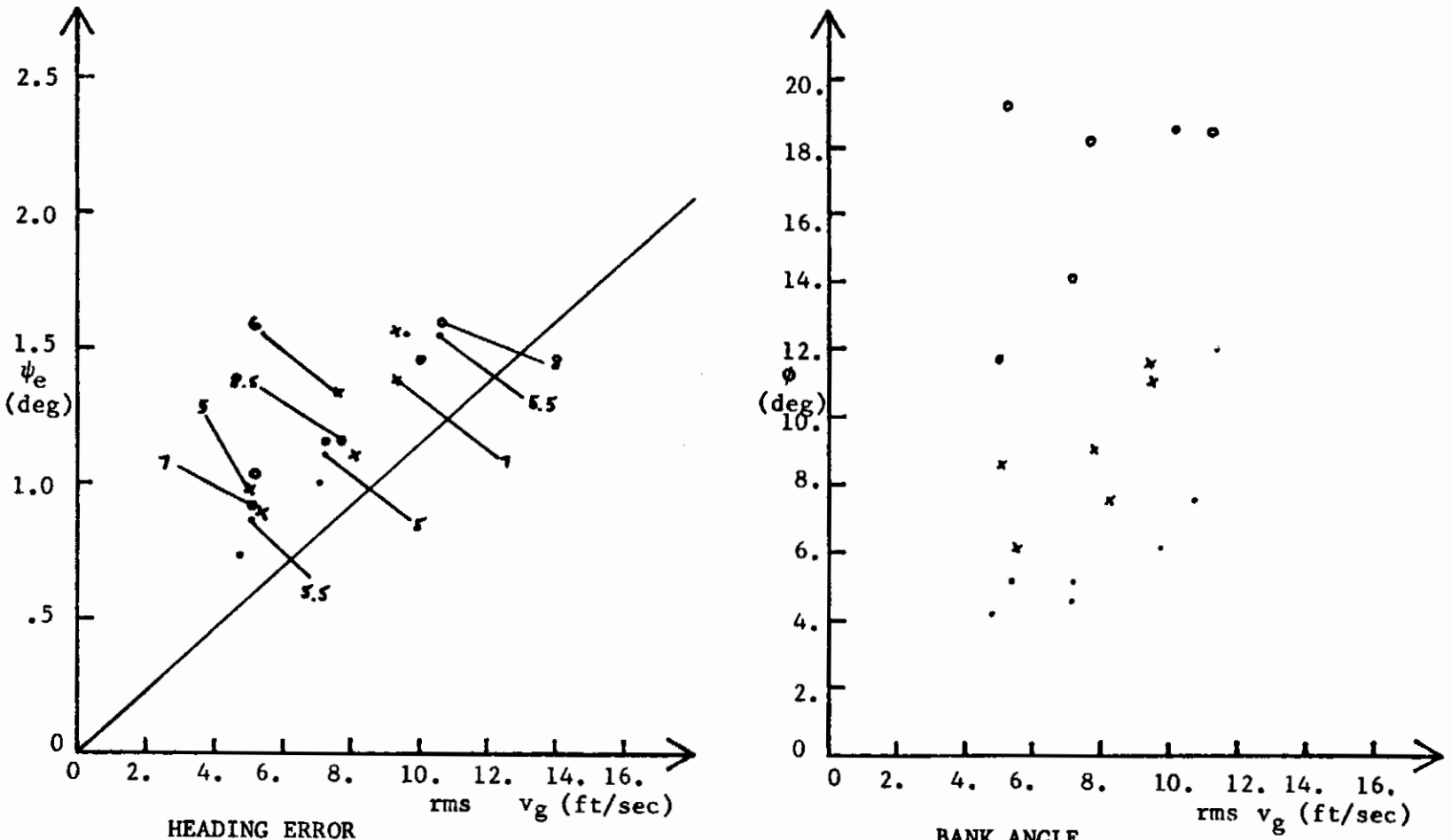

FIGURE 141. HEADING TASK SIMULATION
A-7 FLIGHT CONDITION 1
WITHOUT AUGMENTER

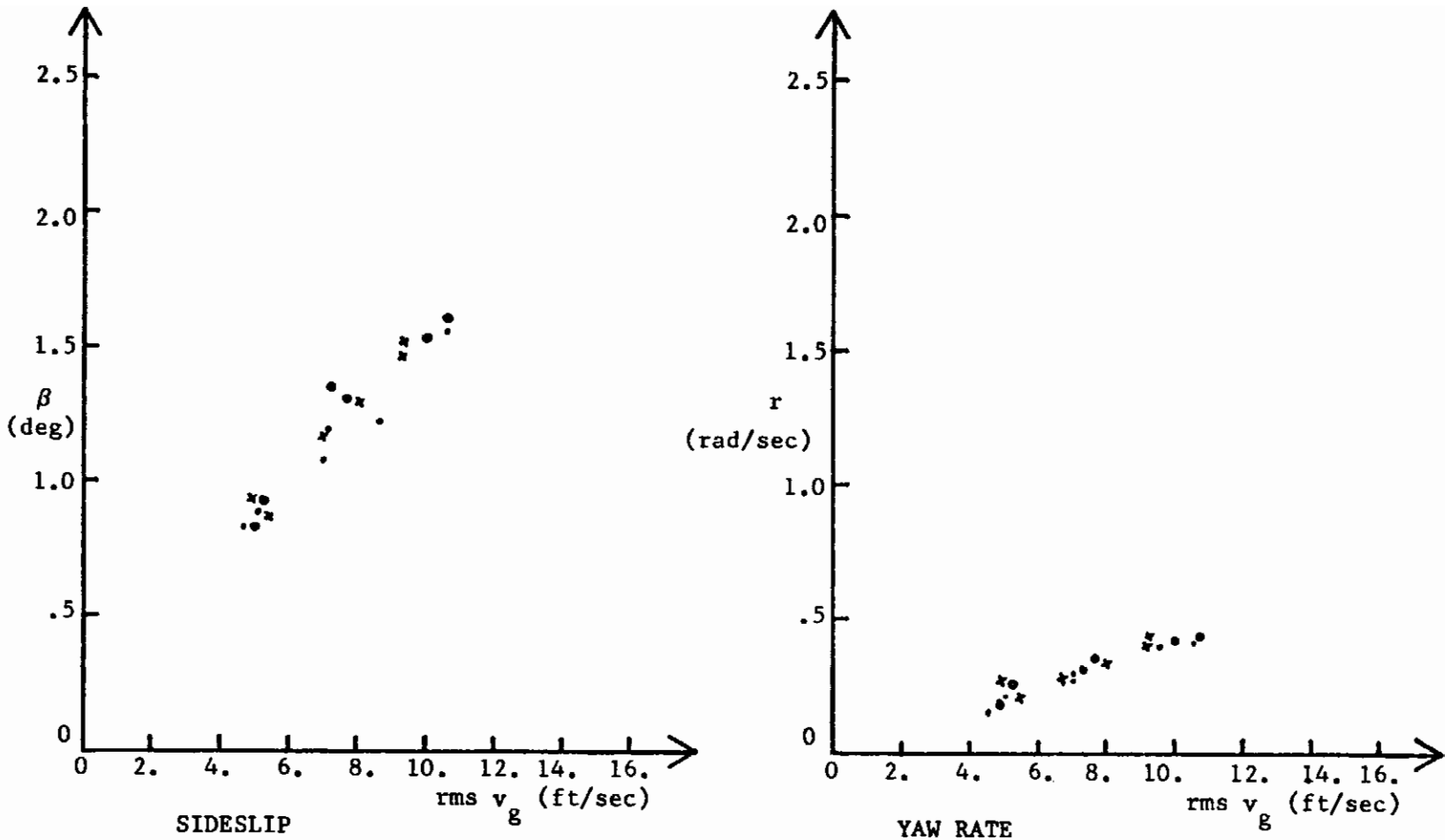

FIGURE 142. HEADING TASK SIMULATION

A-7 FLIGHT CONDITION 1

WITHOUT AUGMENTER

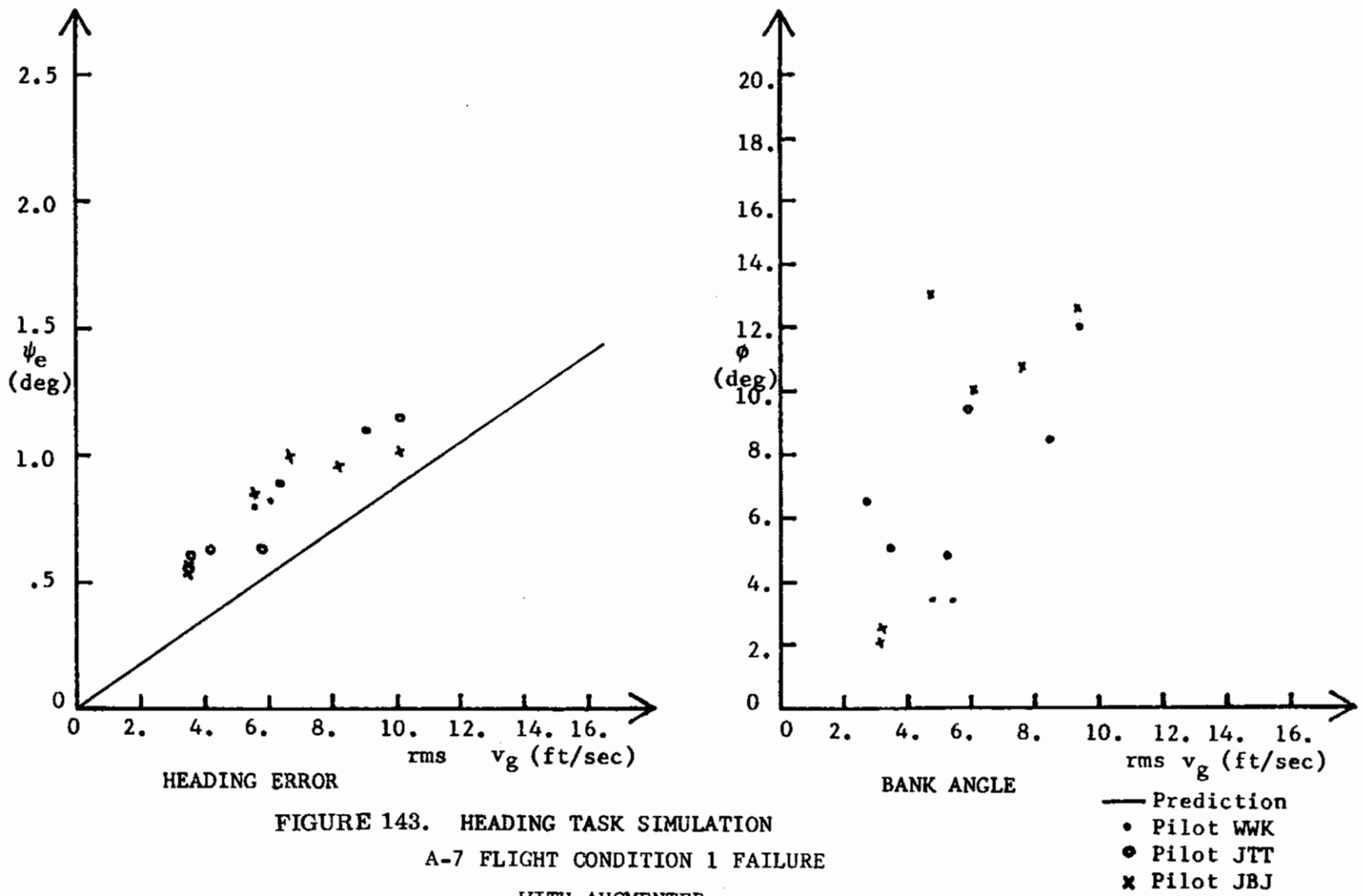

FIGURE 143. HEADING TASK SIMULATION
A-7 FLIGHT CONDITION 1 FAILURE
WITH AUGMENTER

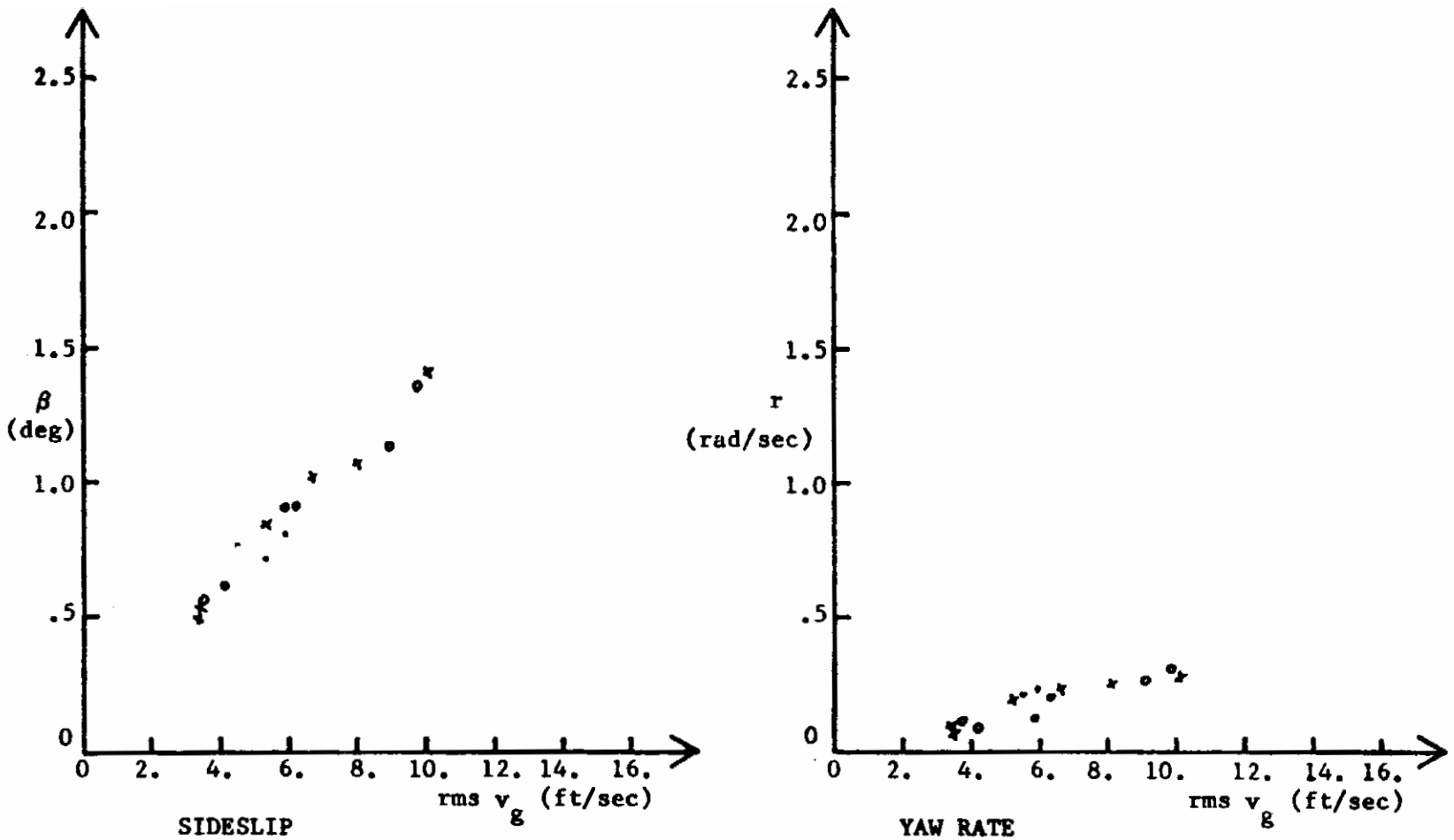

FIGURE 144. HEADING TASK SIMULATION

A-7 FLIGHT CONDITION 1 FAILURE

WITH AUGMENTER

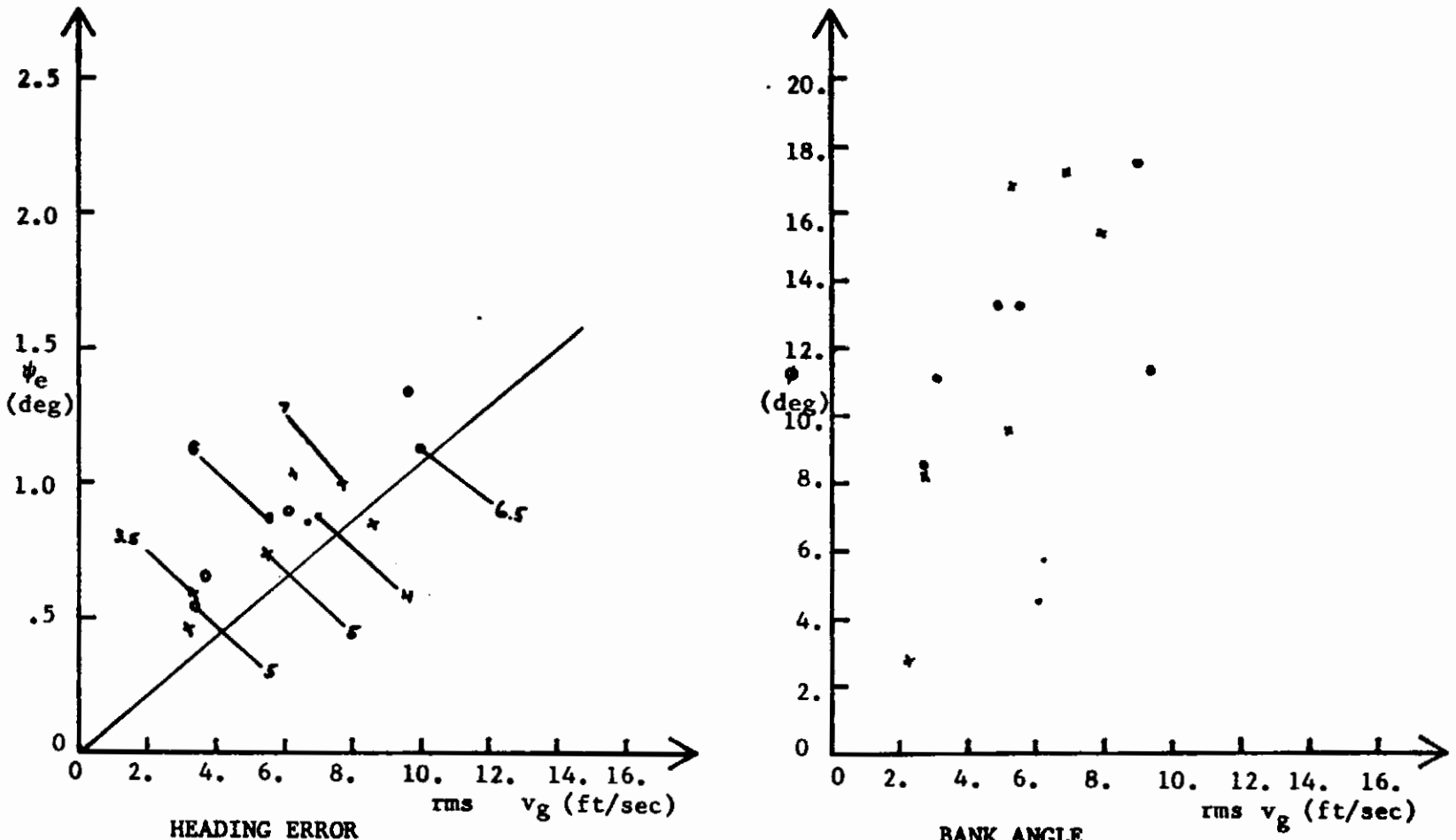

FIGURE 145. HEADING TASK SIMULATION

A-7 FLIGHT CONDITION 1 FAILURE

WITHOUT AUGMENTER

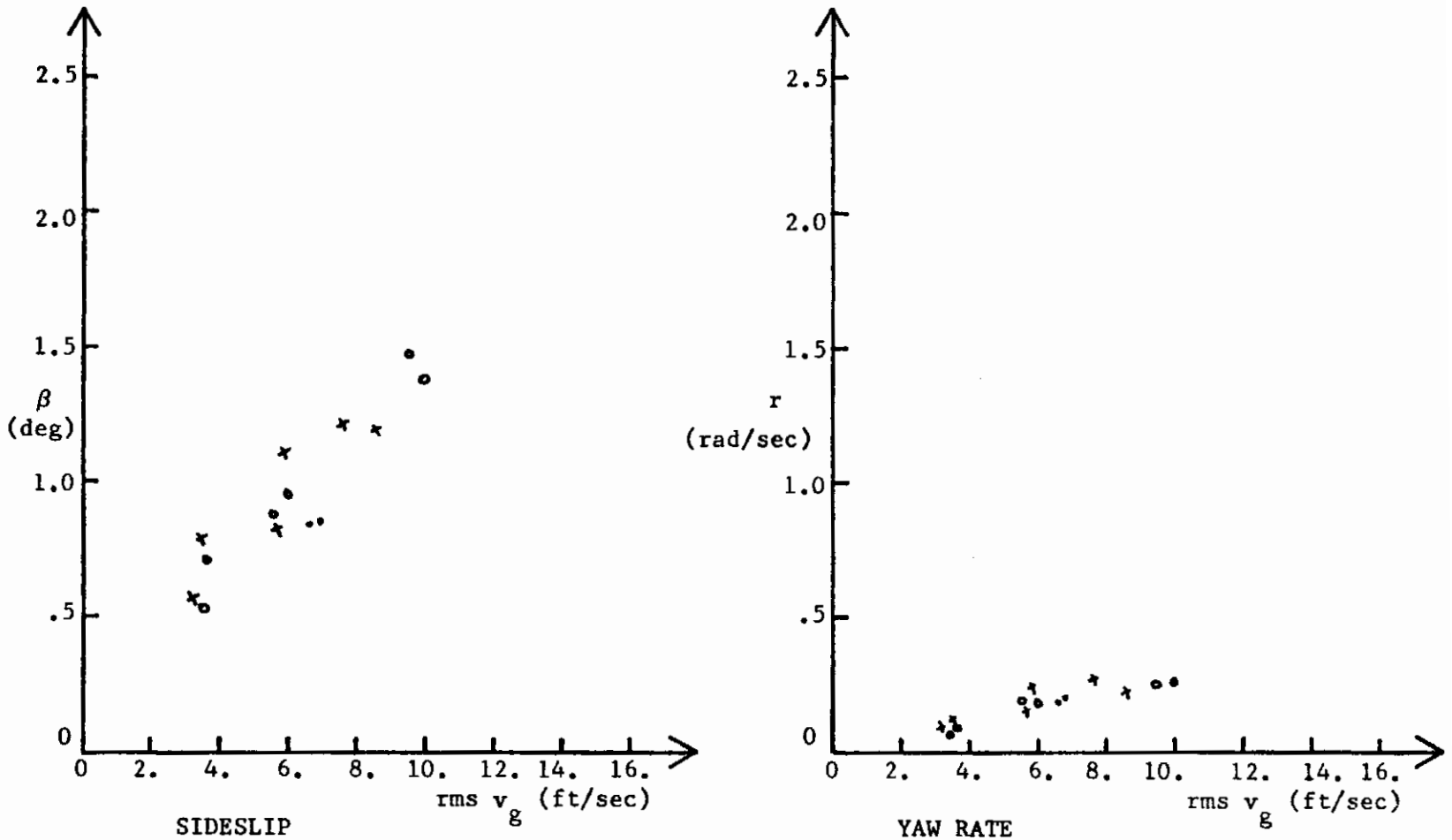

FIGURE 146. HEADING TASK SIMULATION

A-7 FLIGHT CONDITION 1 FAILURE

WITHOUT AUGMENTER

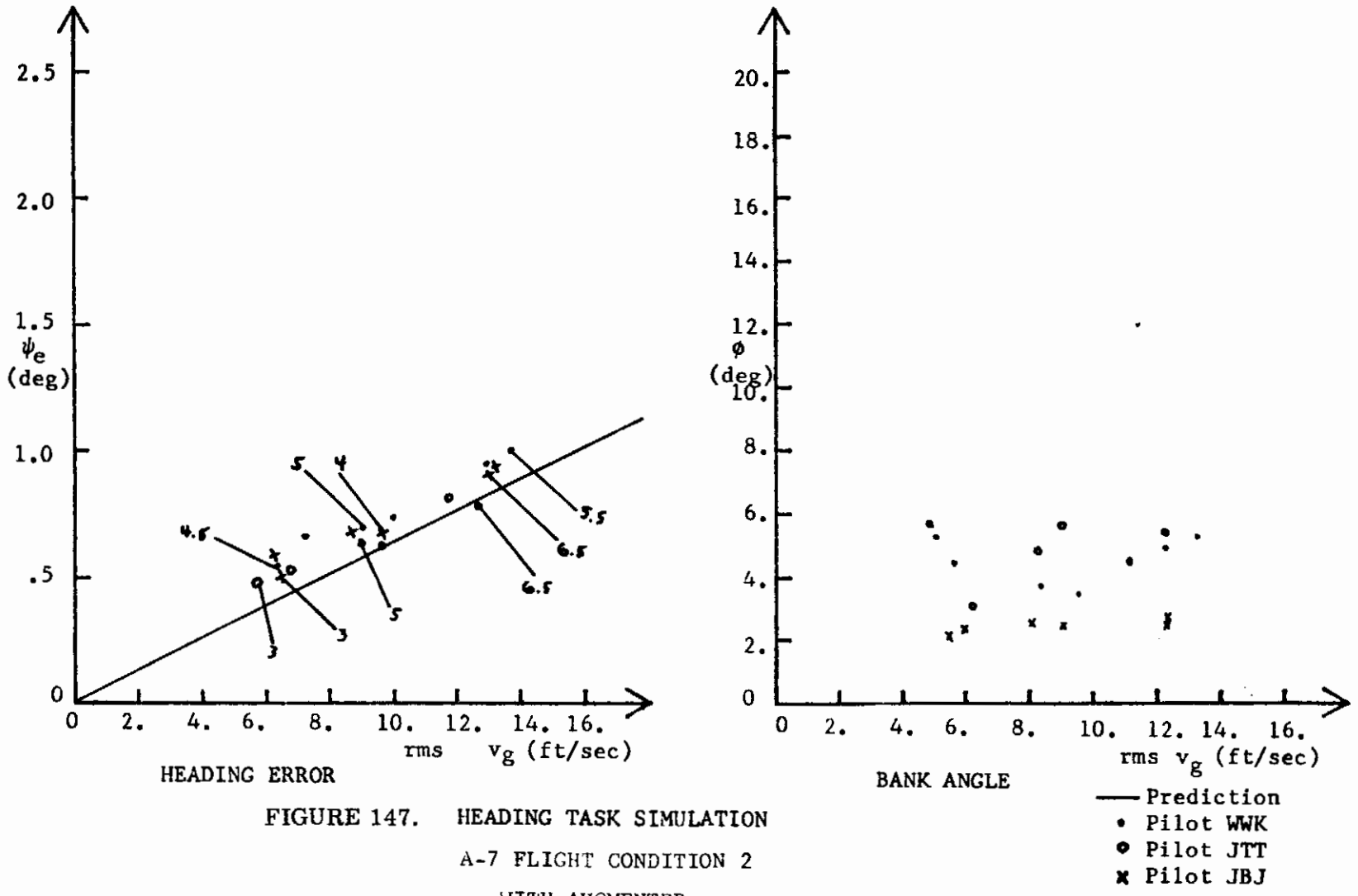

FIGURE 147. HEADING TASK SIMULATION

A-7 FLIGHT CONDITION 2

WITH AUGMENTER

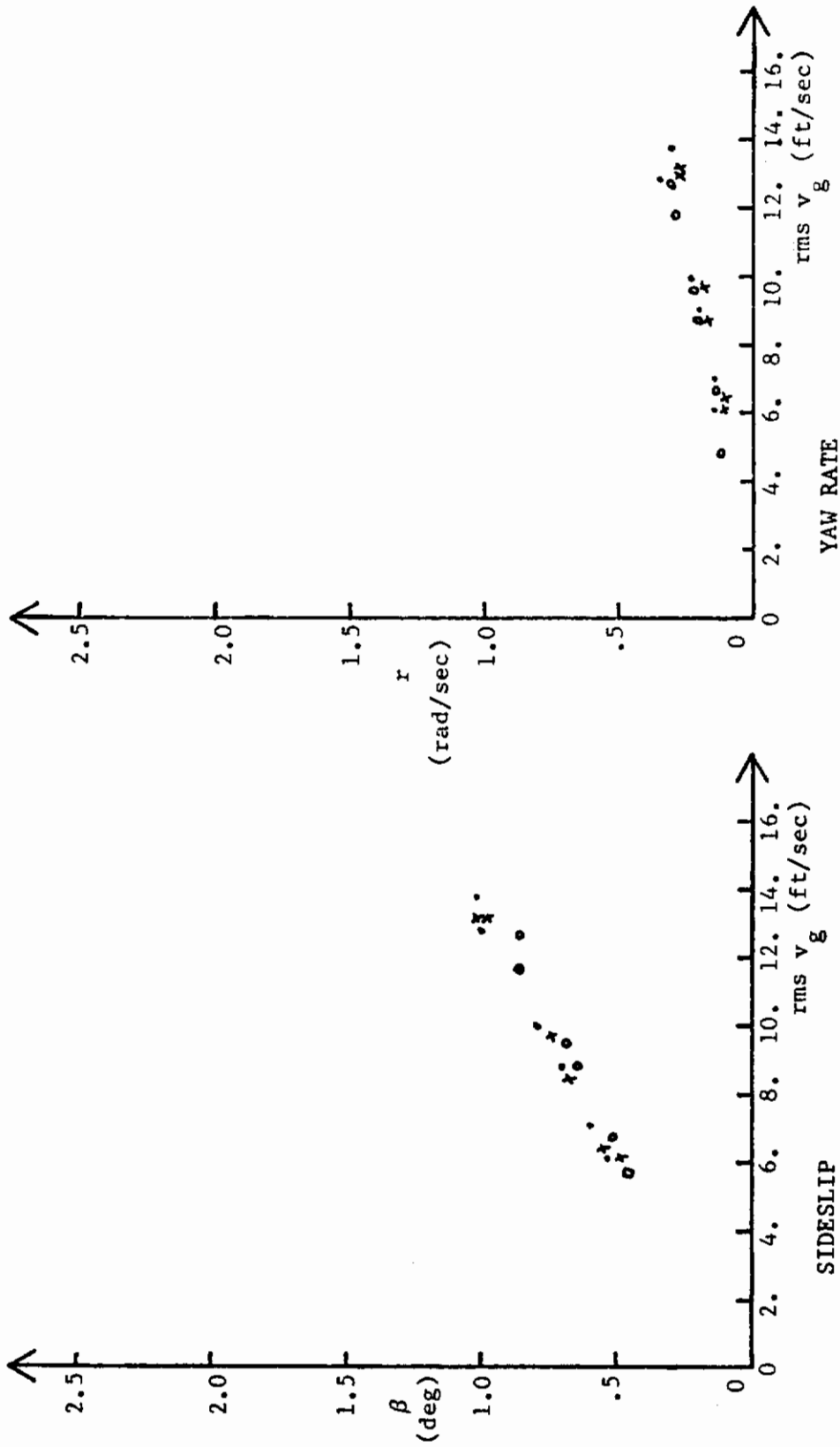

FIGURE 148. HEADING TASK SIMULATION

A-7 FLIGHT CONDITION 2

WITH AUGMENTER

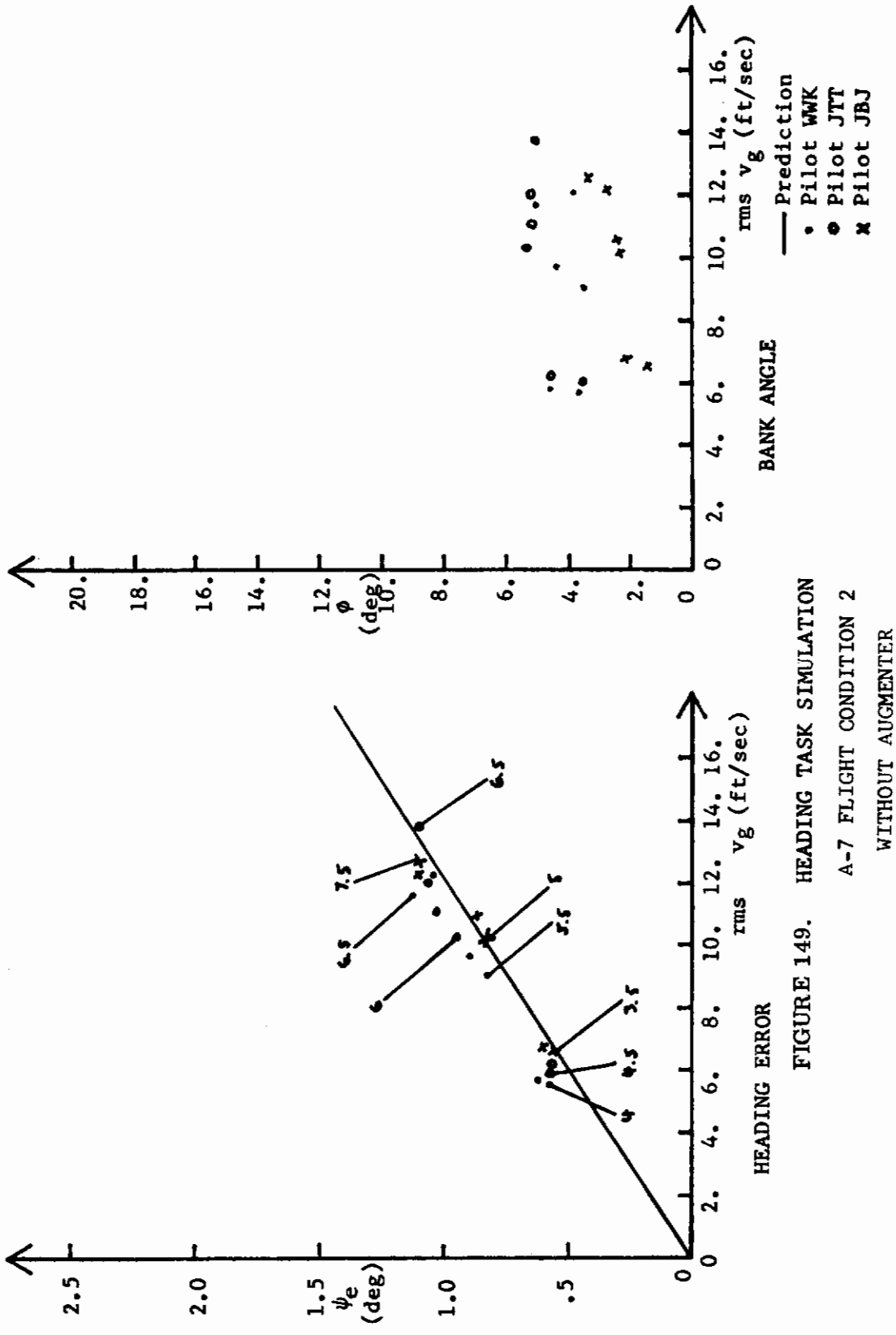

FIGURE 149. HEADING TASK SIMULATION
A-7 FLIGHT CONDITION 2
WITHOUT AUGMENTER

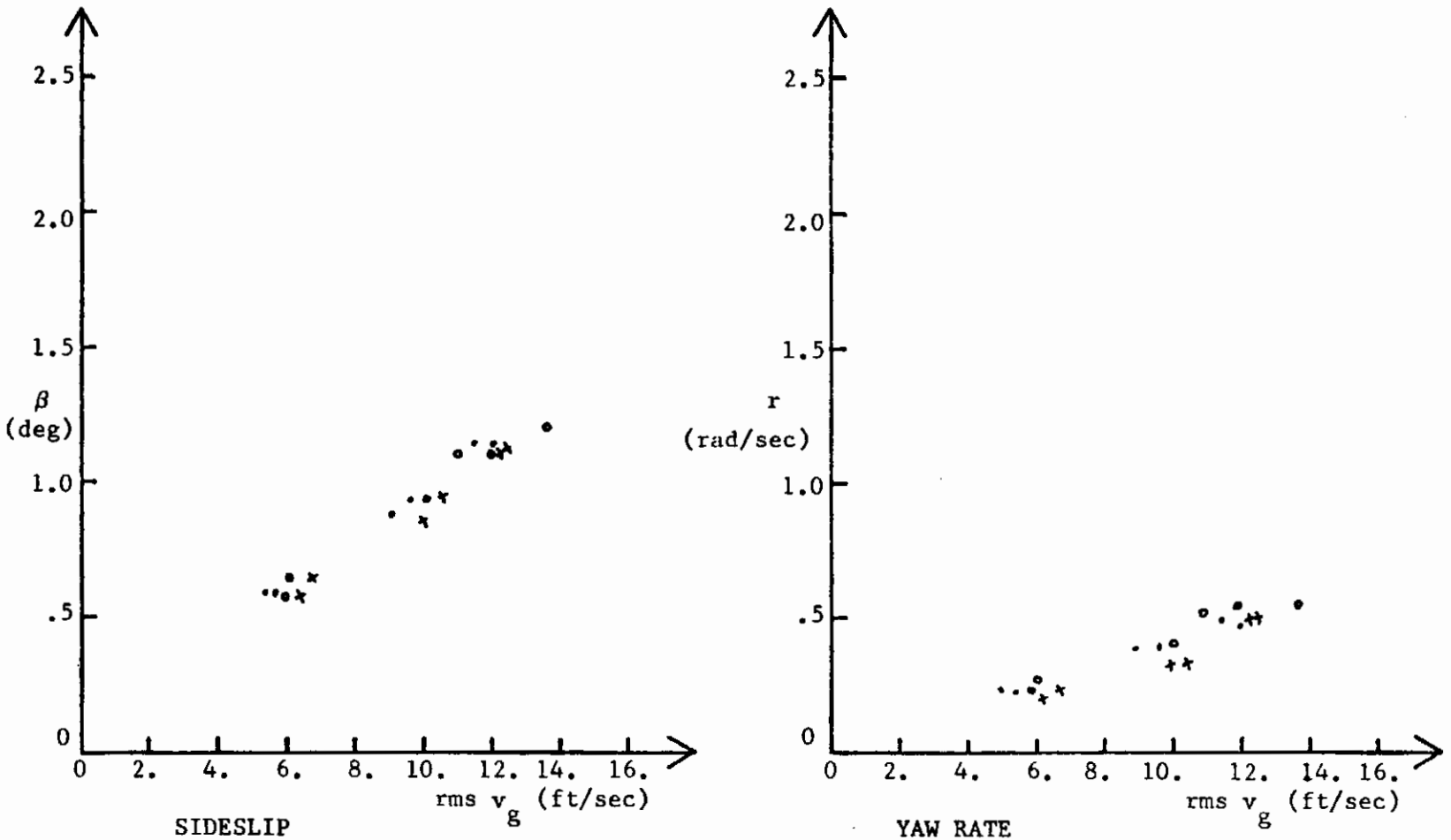

FIGURE 150. HEADING TASK SIMULATION

A-7 FLIGHT CONDITION 2

WITHOUT AUGMENTER

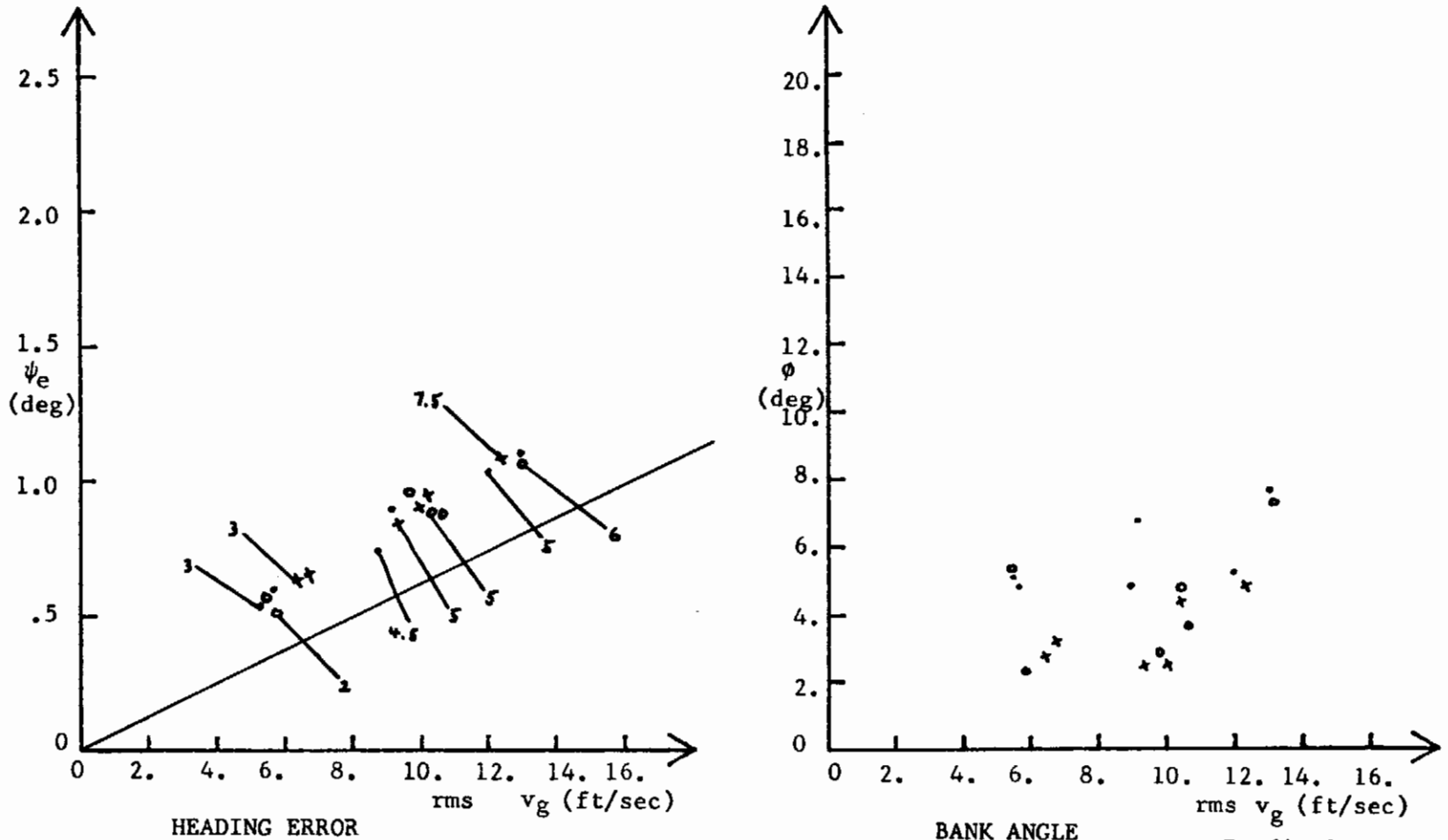

FIGURE 151. HEADING TASK SIMULATION

A-7 FLIGHT CONDITION 2 FAILURE

WITH AUGMENTER

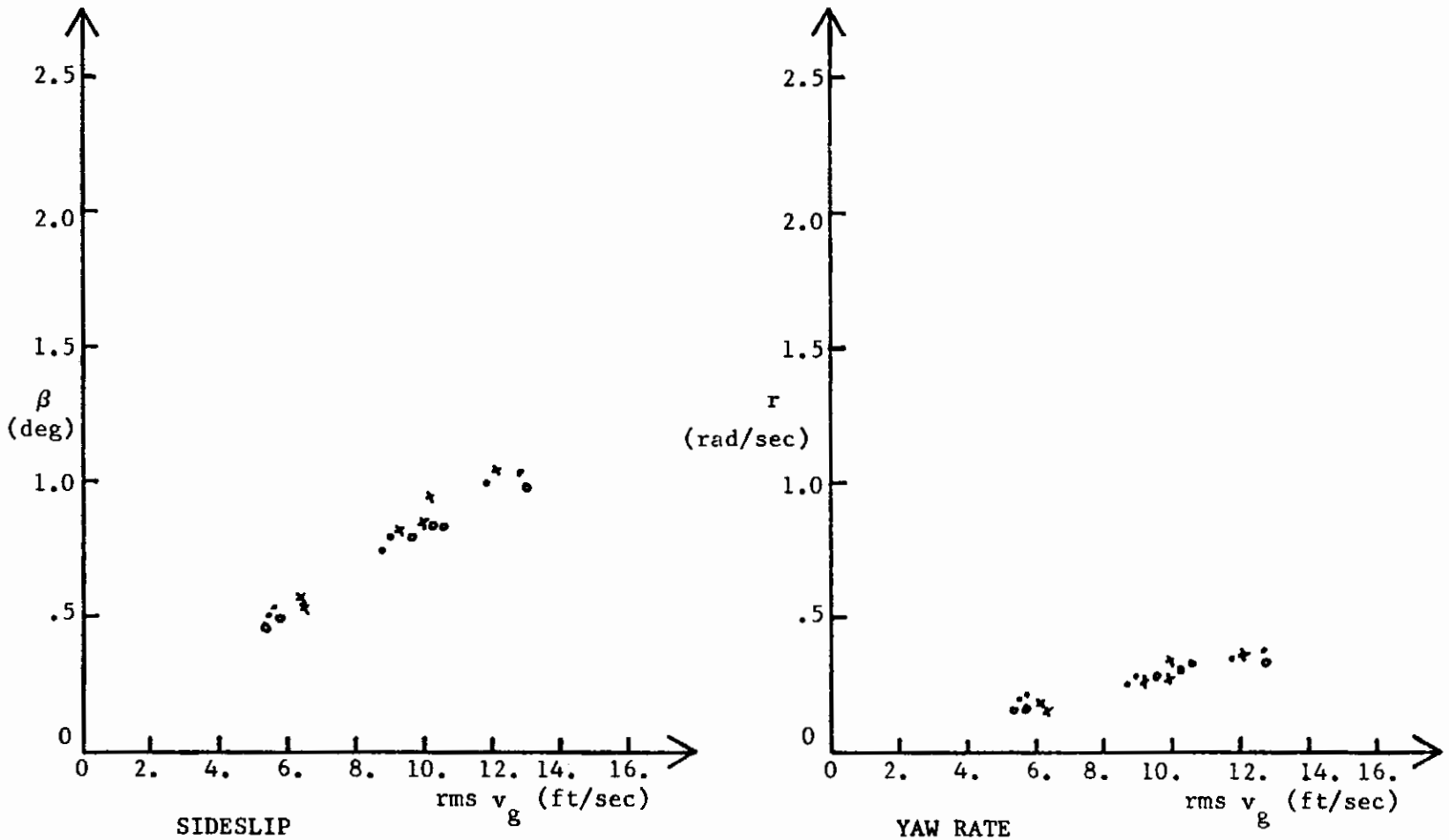

FIGURE 152. HEADING TASK SIMULATION
A-7 FLIGHT CONDITION 2 FAILURE
WITH AUGMENTER

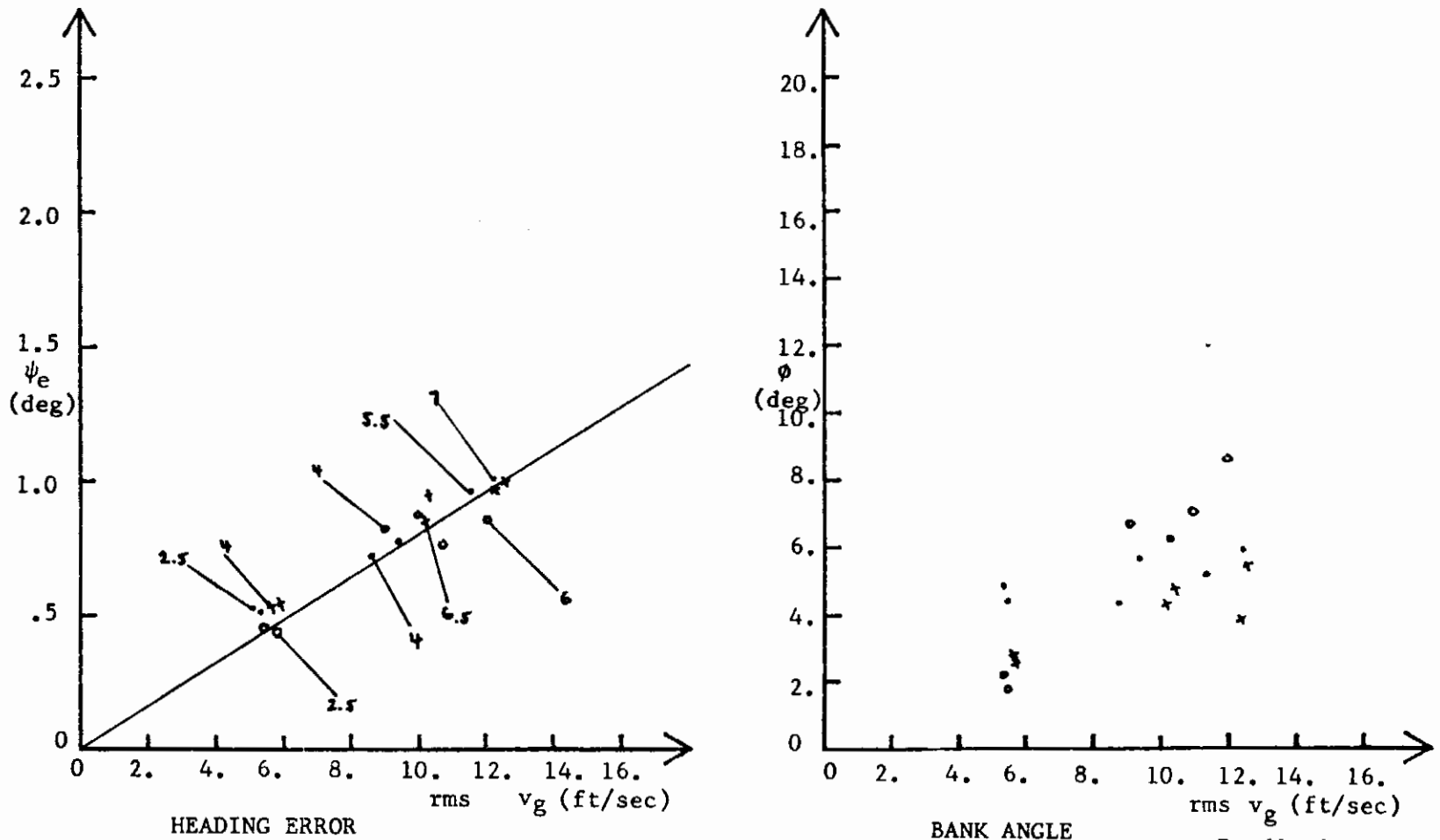

FIGURE 153. HEADING TASK SIMULATION

A-7 FLIGHT CONDITION 2 FAILURE

WITHOUT AUGMENTER

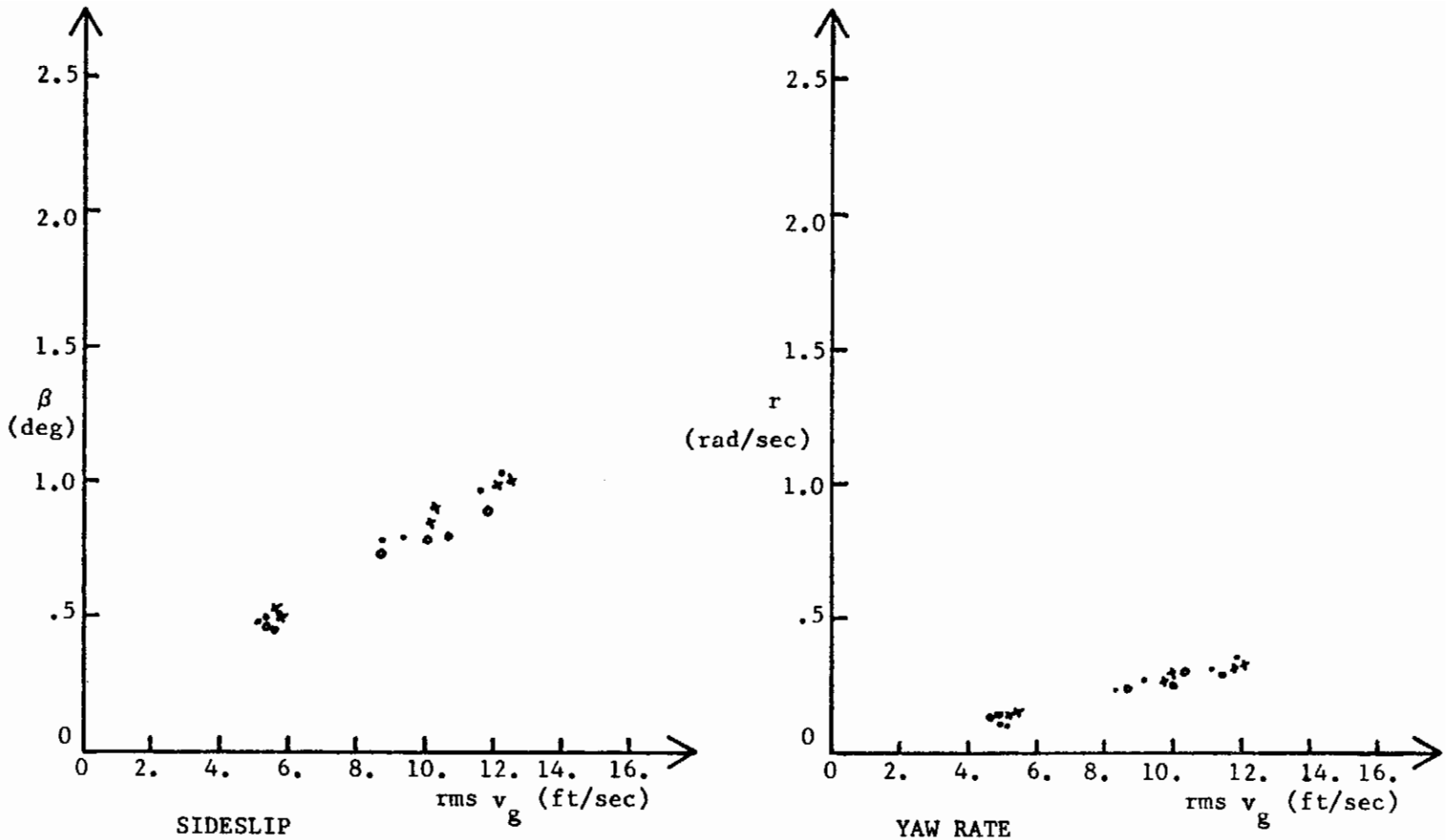

FIGURE 154. HEADING TASK SIMULATION

A-7 FLIGHT CONDITION 2 FAILURE

WITHOUT AUGMENTER

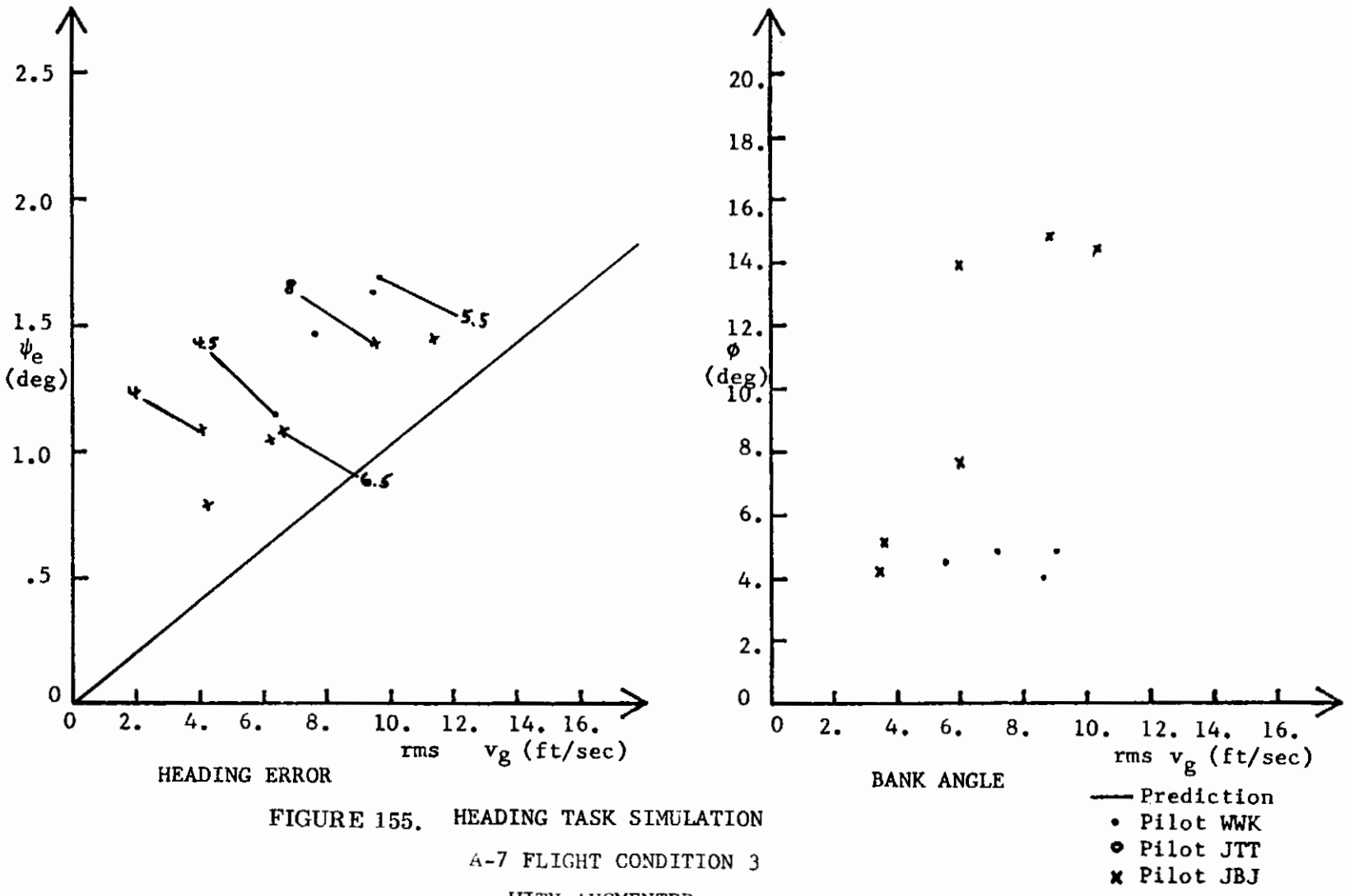

FIGURE 155. HEADING TASK SIMULATION

A-7 FLIGHT CONDITION 3

WITH AUGMENTER

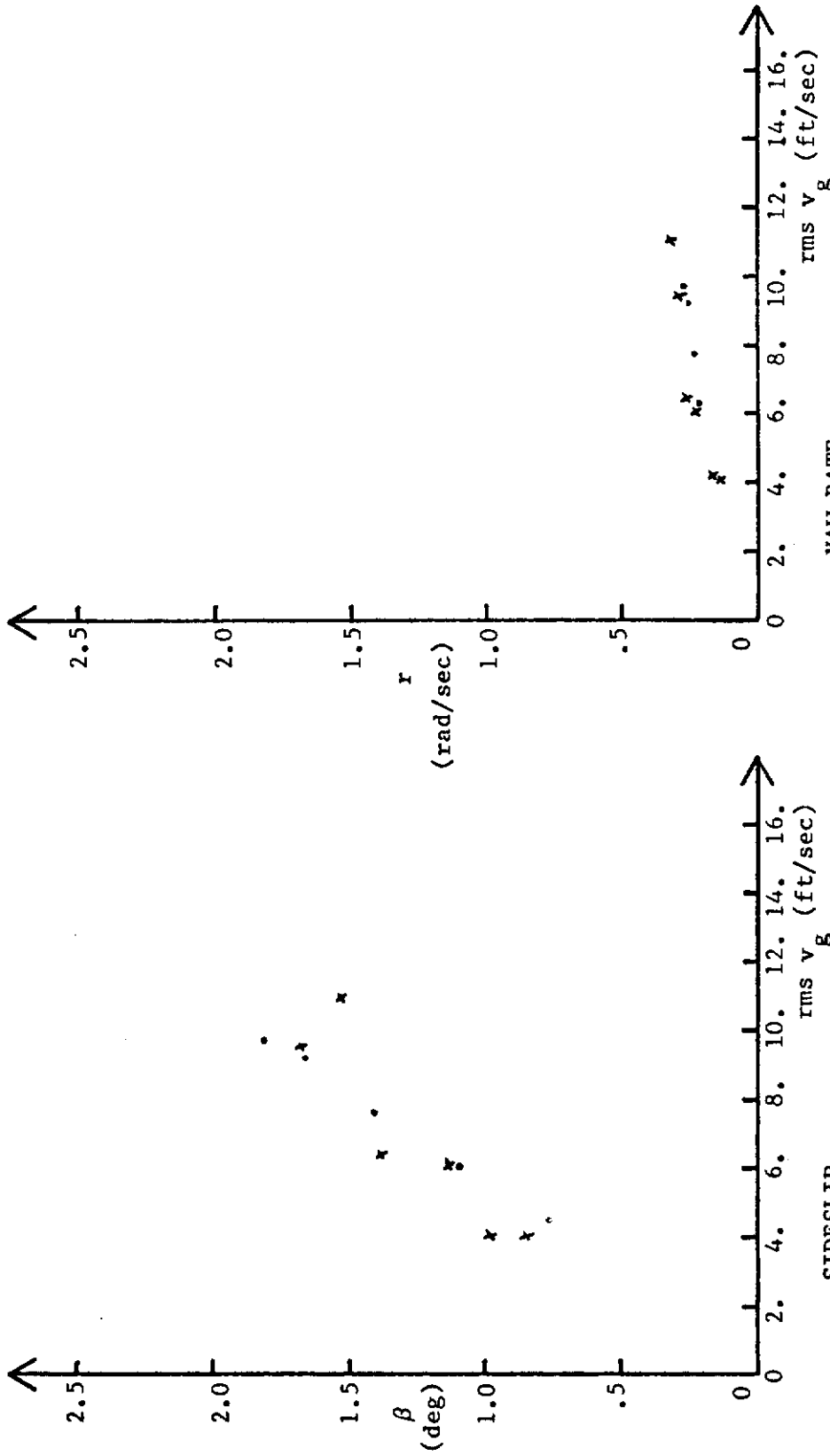

FIGURE 156. HEADING TASK SIMULATION
A-7 FLIGHT CONDITION 3
WITH AUGMENTER

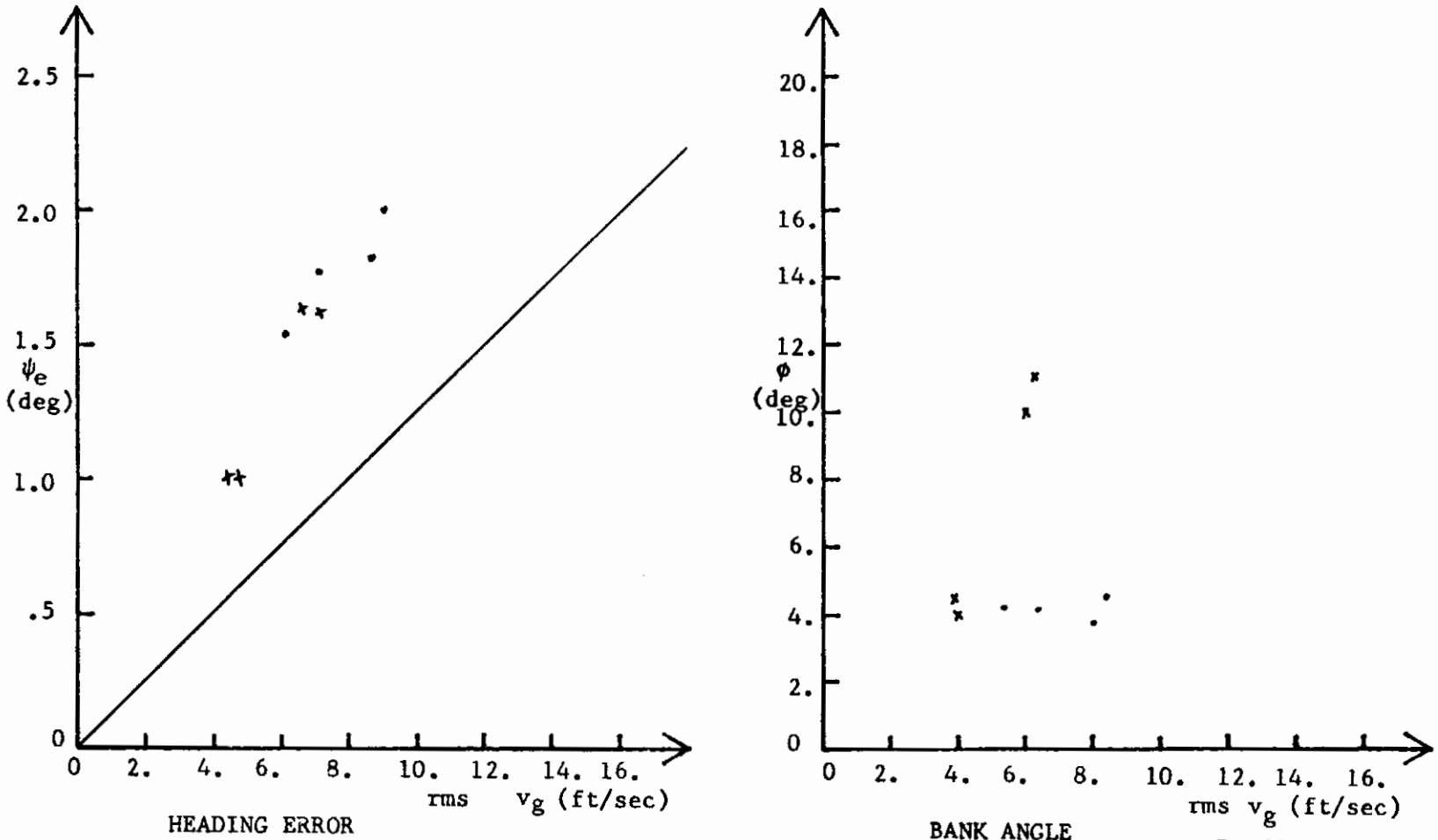

FIGURE 157. HEADING TASK SIMULATION

A-7 FLIGHT CONDITION 3

WITHOUT AUGMENTER

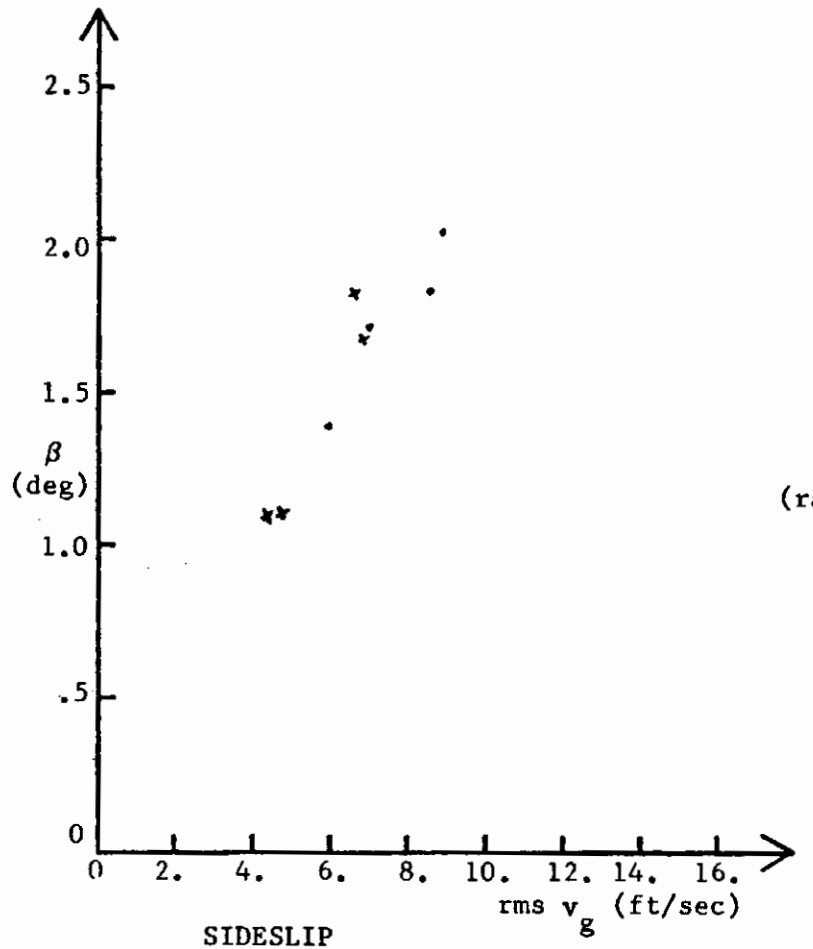

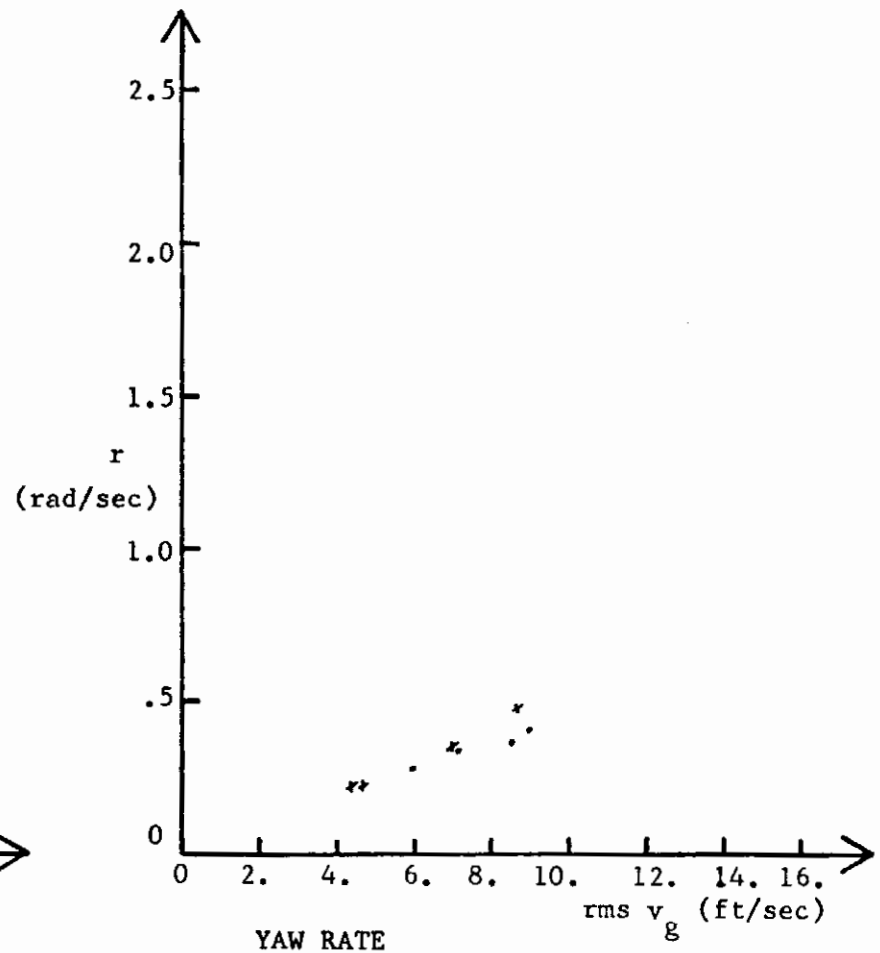

FIGURE 158. HEADING TASK SIMULATION

A-7 FLIGHT CONDITION 3

WITHOUT AUGMENTER

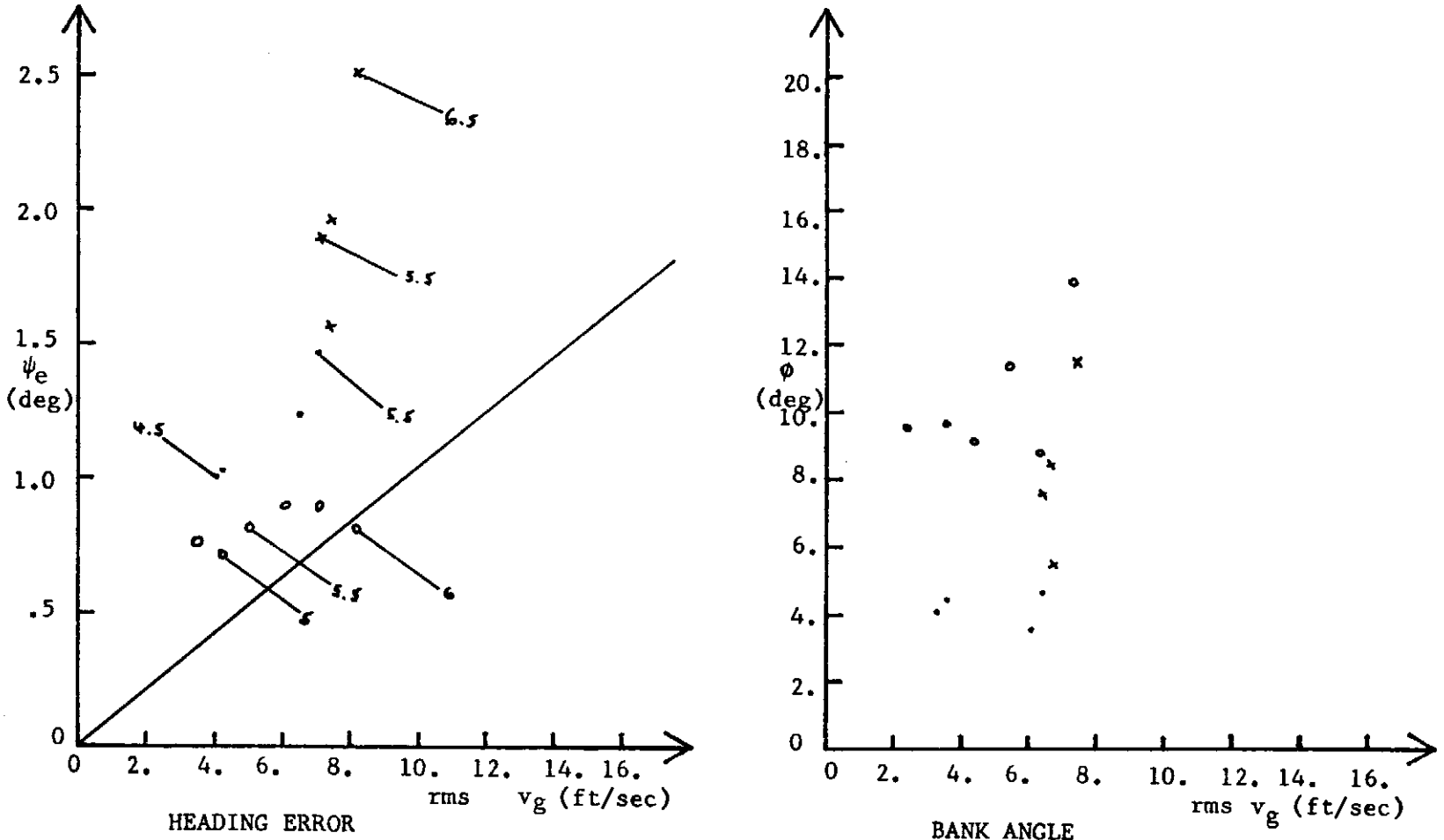

FIGURE 159. HEADING TASK SIMULATION

A-7 FLIGHT CONDITION 3 FAILURE

WITH AUGMENTER

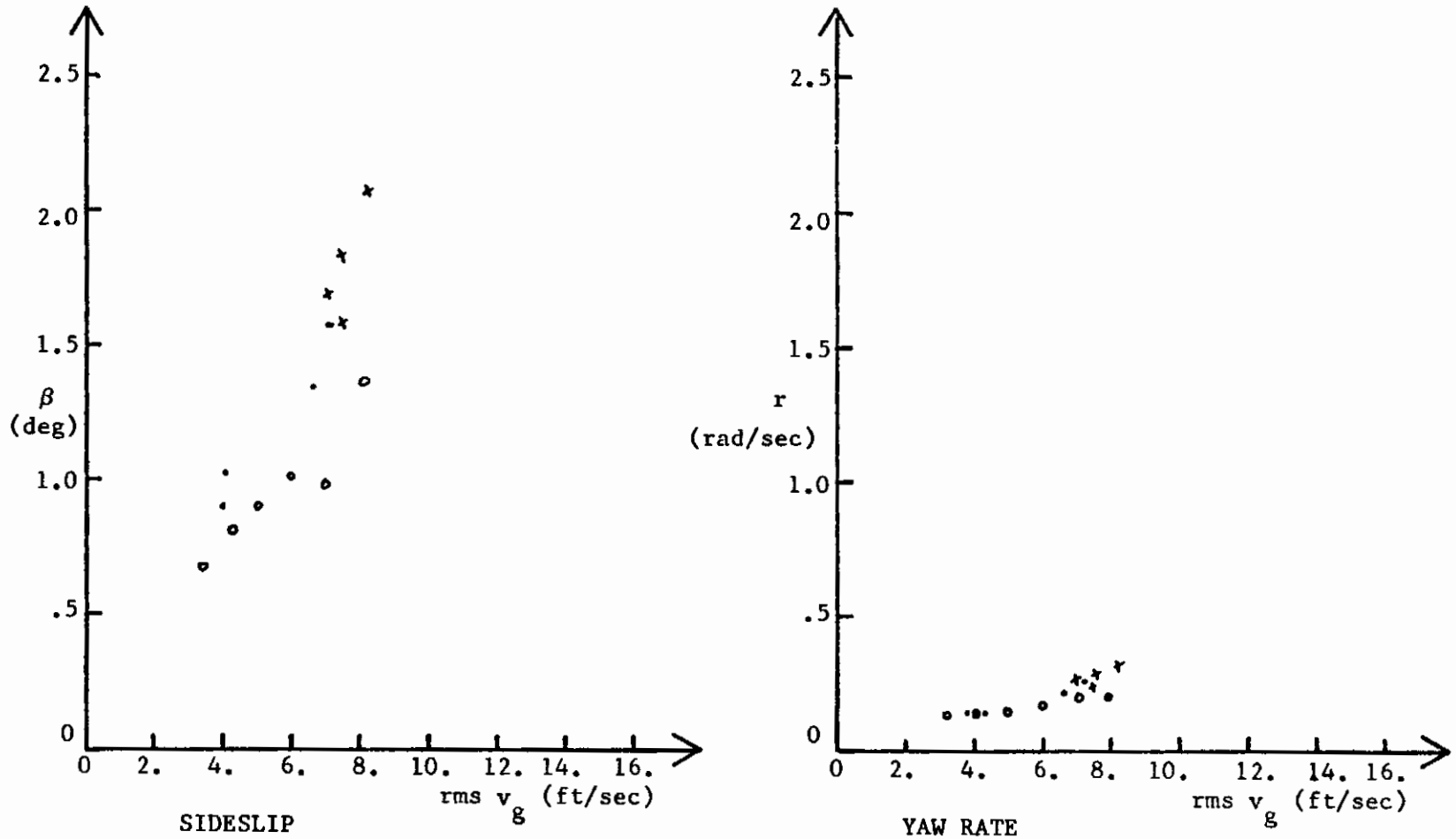

FIGURE 160. HEADING TASK SIMULATION

A-7 FLIGHT CONDITION 3 FAILURE

WITH AUGMENTER

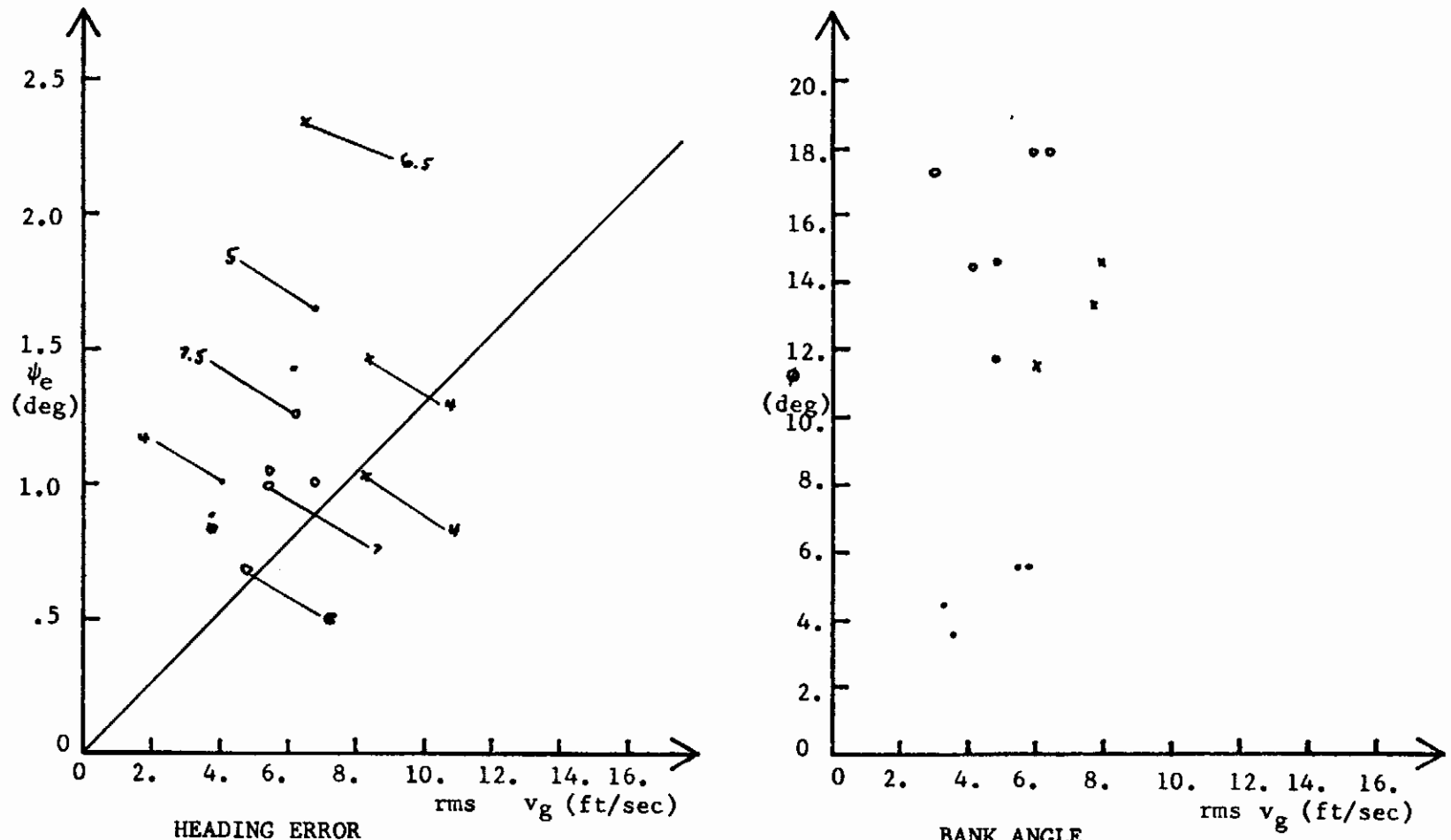

FIGURE 161. HEADING TASK SIMULATION

A-7 FLIGHT CONDITION 3 FAILURE

WITHOUT AUGMENTER

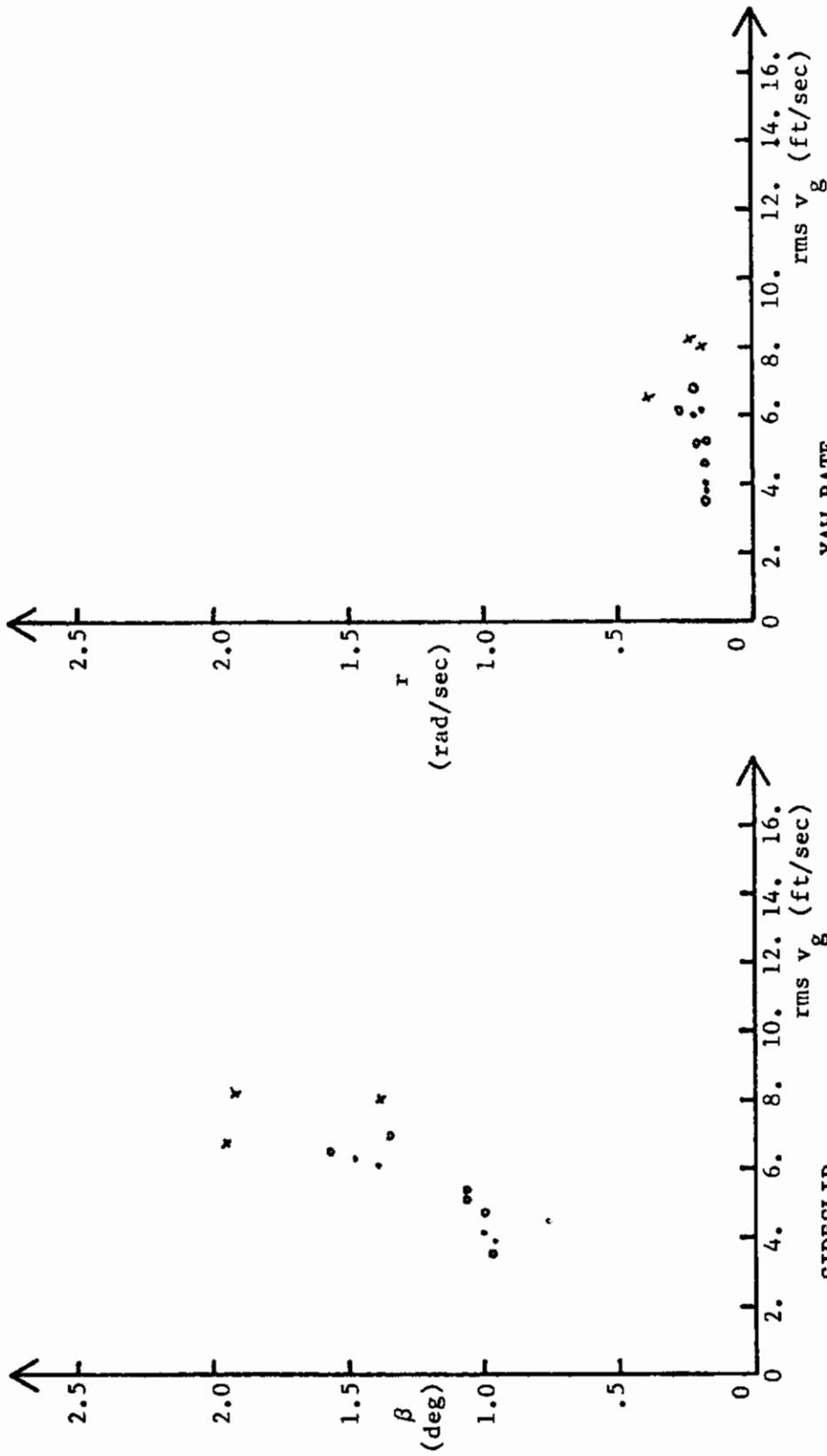

FIGURE 162. HEADING TASK SIMULATION
A-7 FLIGHT CONDITION 3 FAILURE
WITHOUT AUGMENTER

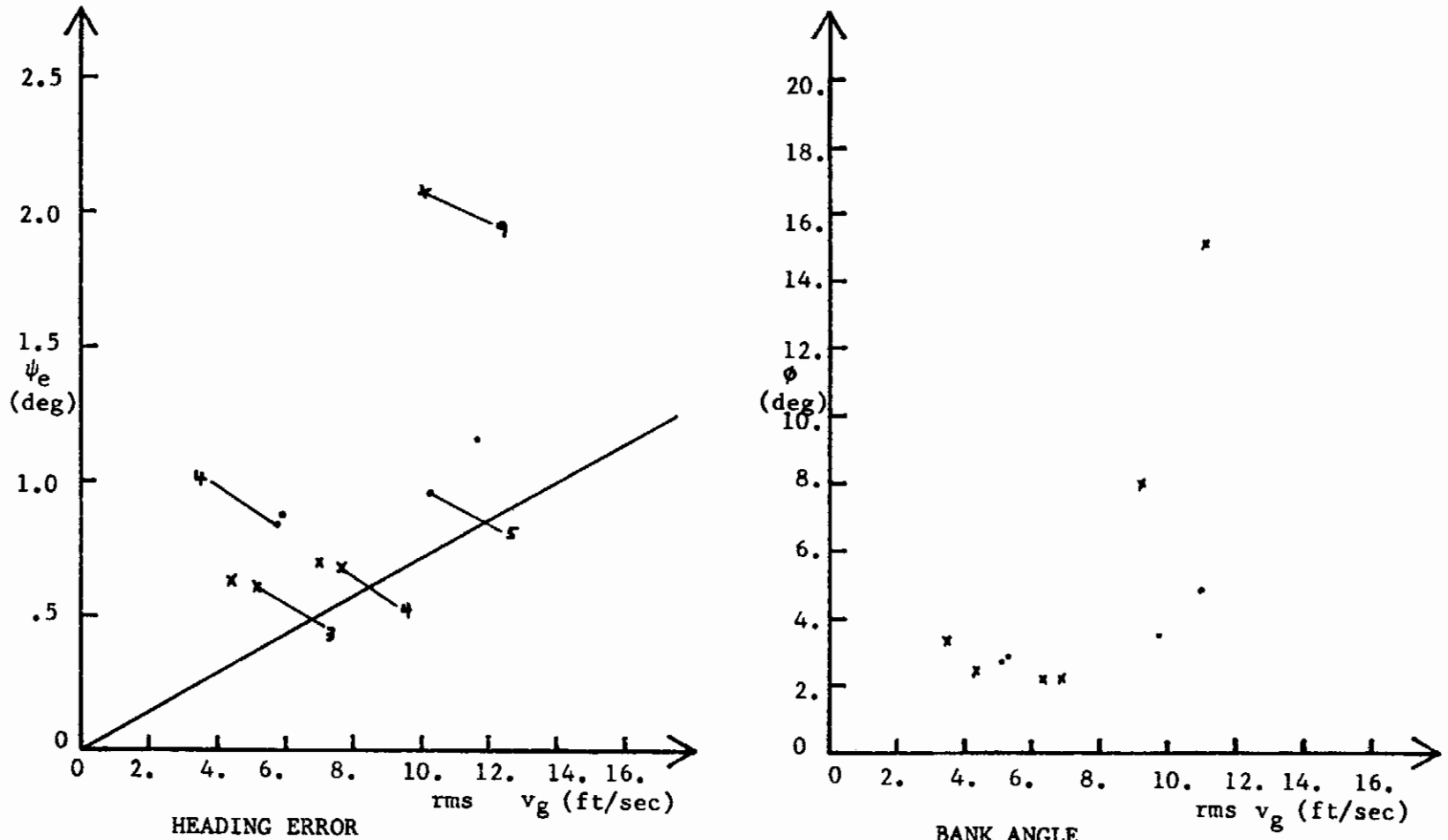

FIGURE 163. HEADING TASK SIMULATION

A-7 FLIGHT CONDITION 4

WITH AUGMENTER

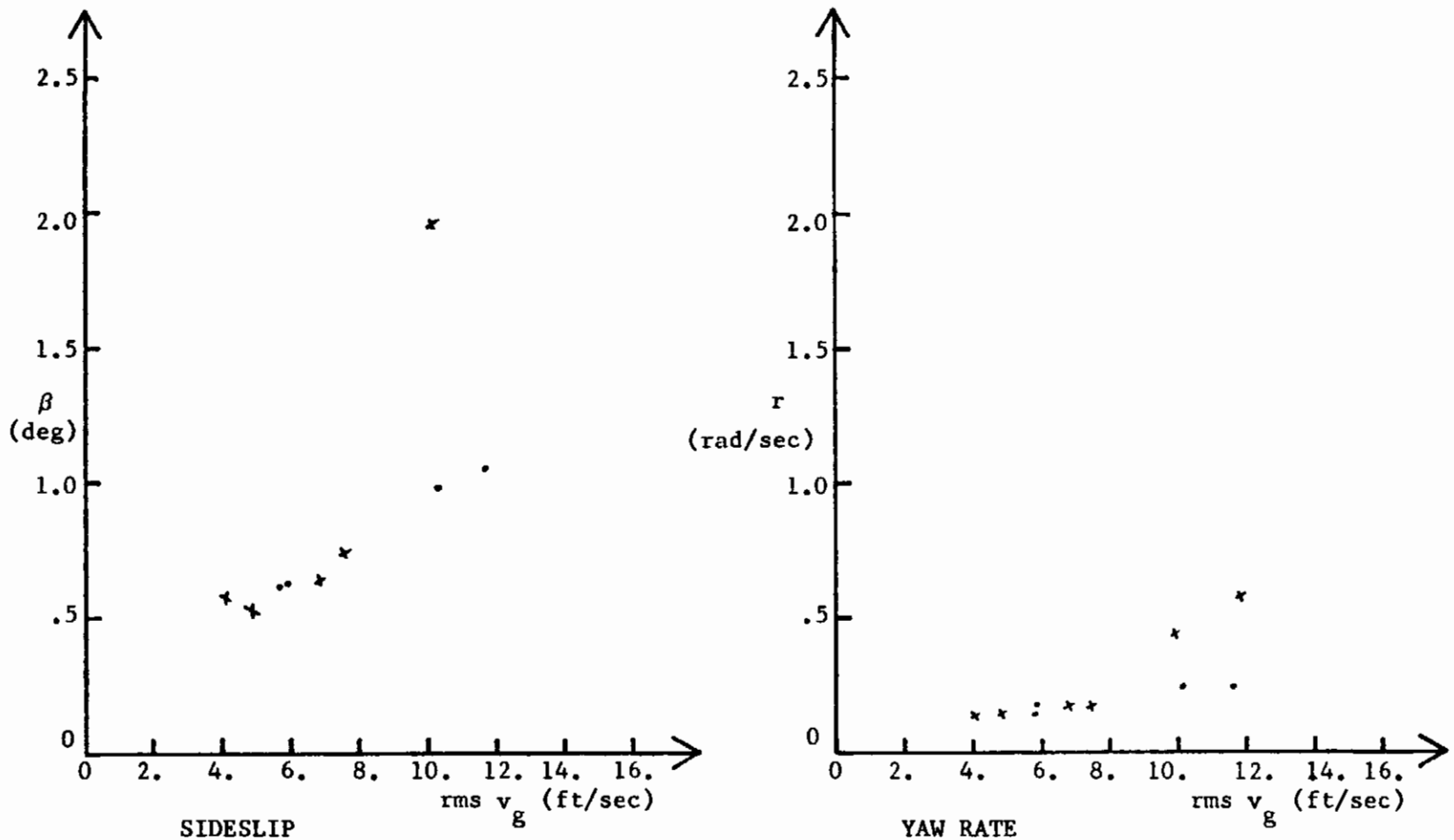

FIGURE 164. HEADING TASK SIMULATION

A-7 FLIGHT CONDITION 4

WITH AUGMENTER

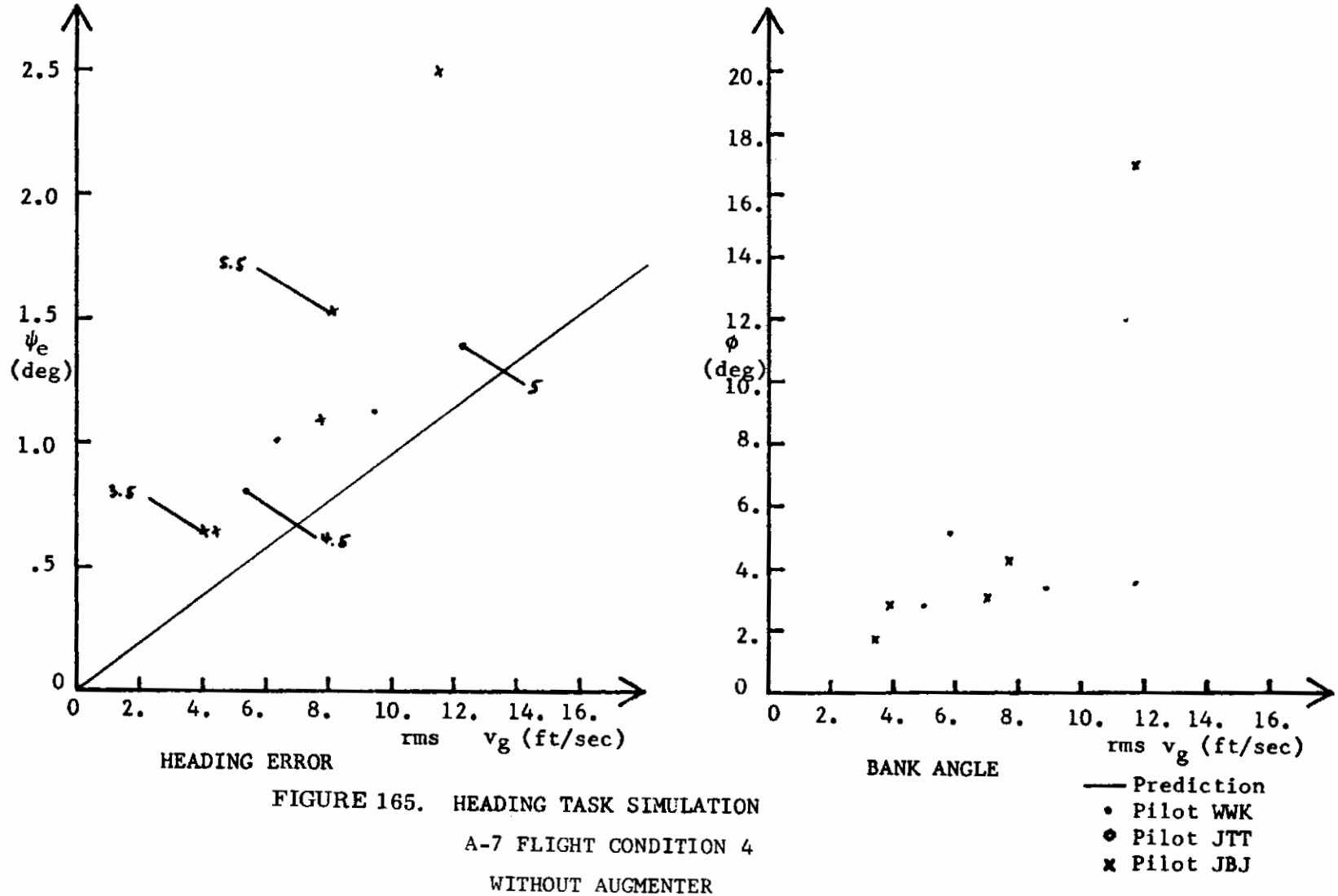

FIGURE 165. HEADING TASK SIMULATION

A-7 FLIGHT CONDITION 4

WITHOUT AUGMENTER

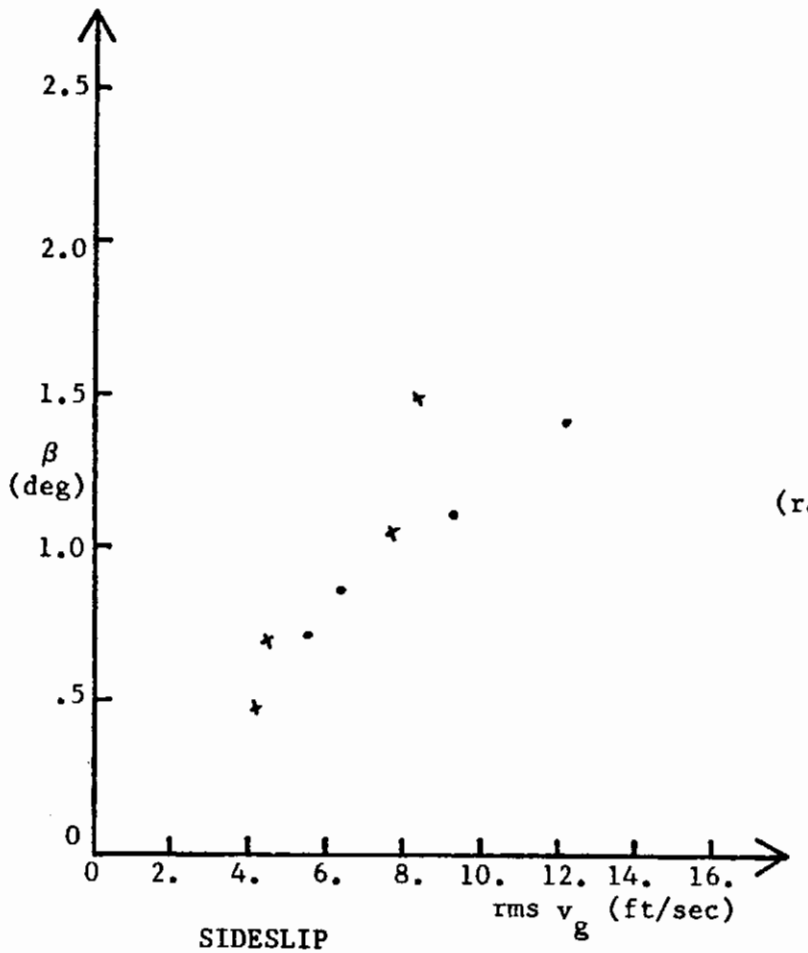

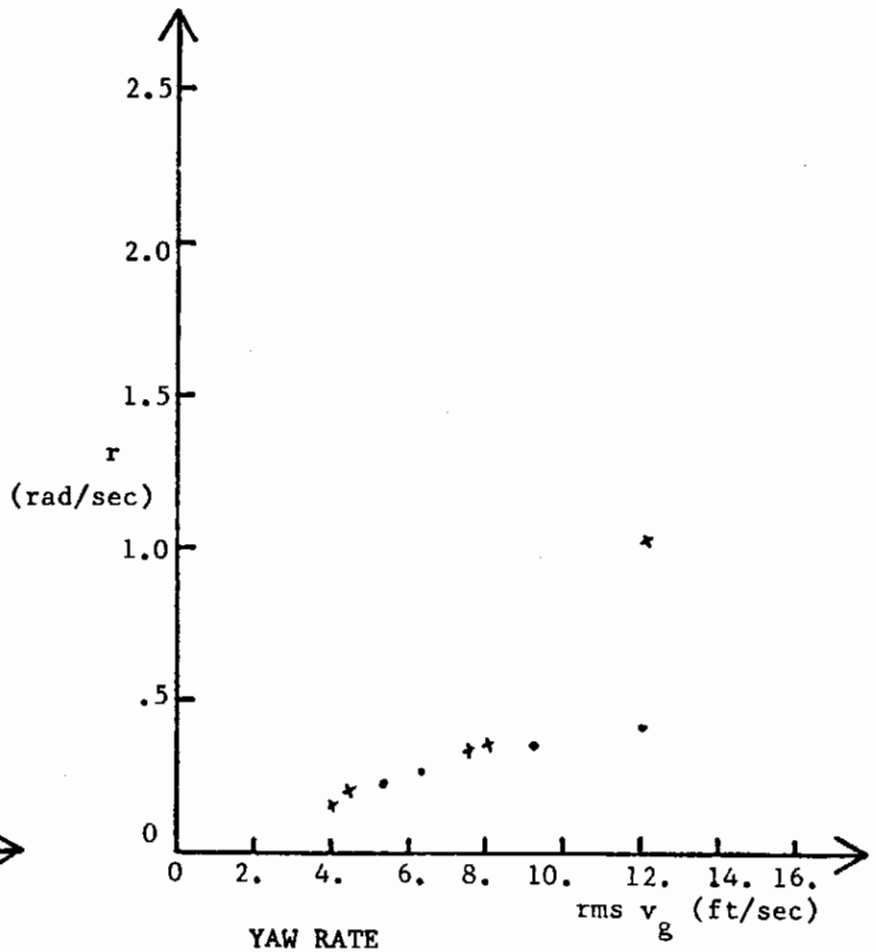

FIGURE 166. HEADING TASK SIMULATION
A-7 FLIGHT CONDITION 4
WITHOUT AUGMENTER

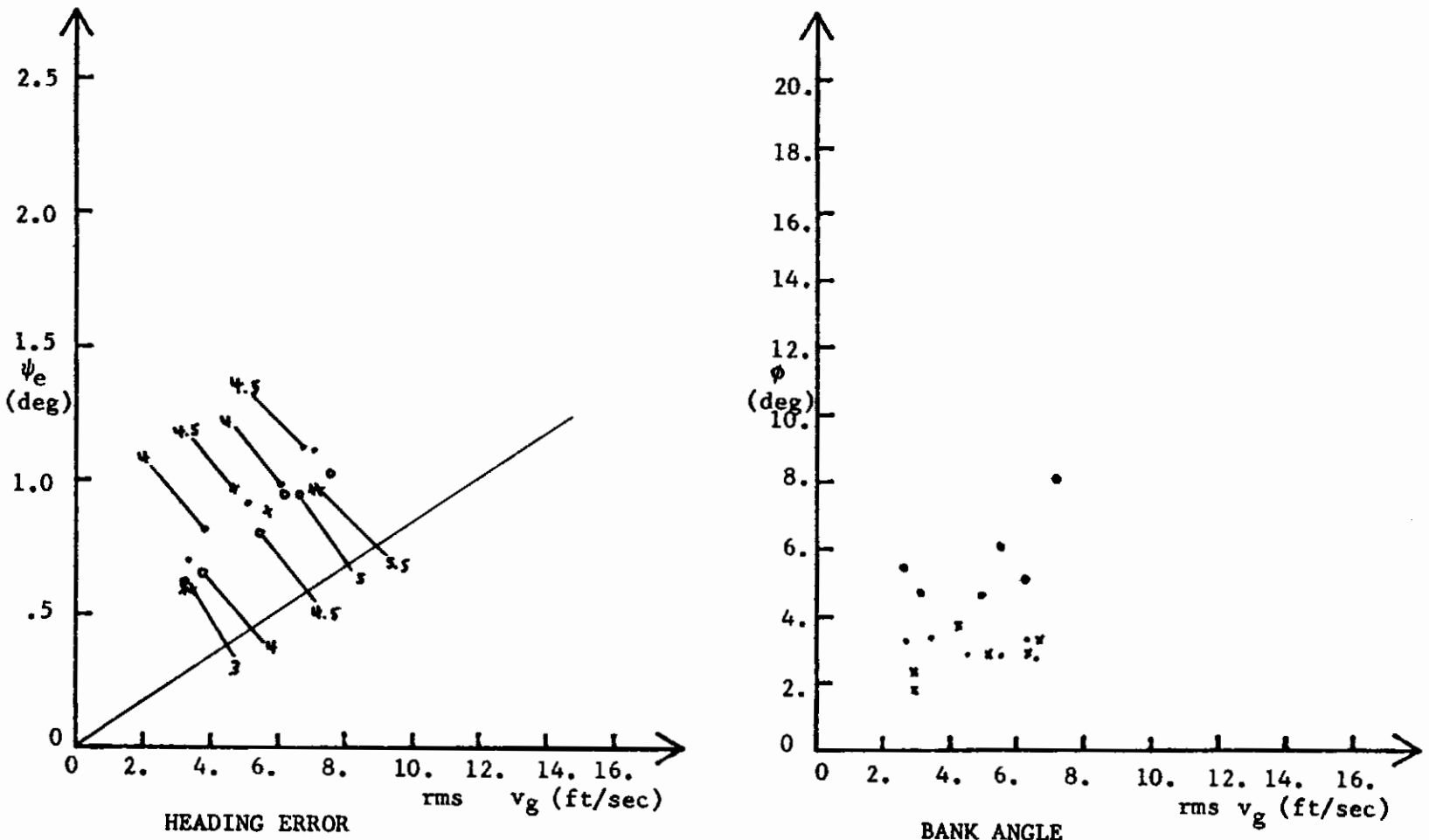

FIGURE 167. HEADING TASK SIMULATION

A-7 FLIGHT CONDITION 4 FAILURE

WITH AUGMENTER

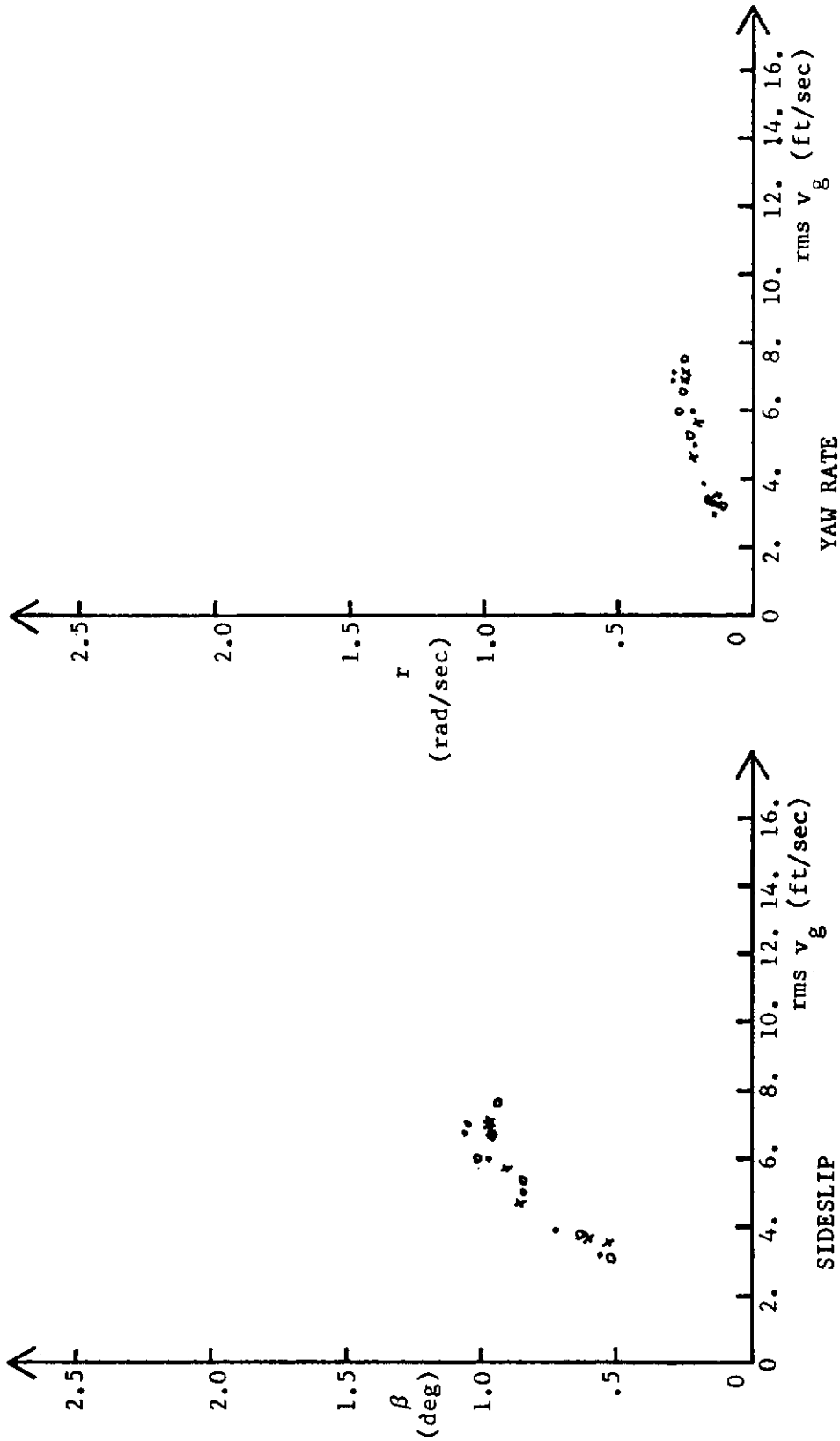

FIGURE 168. HEADING TASK SIMULATION
A-7 FLIGHT CONDITION 4 FAILURE
WITH AUGMENTER

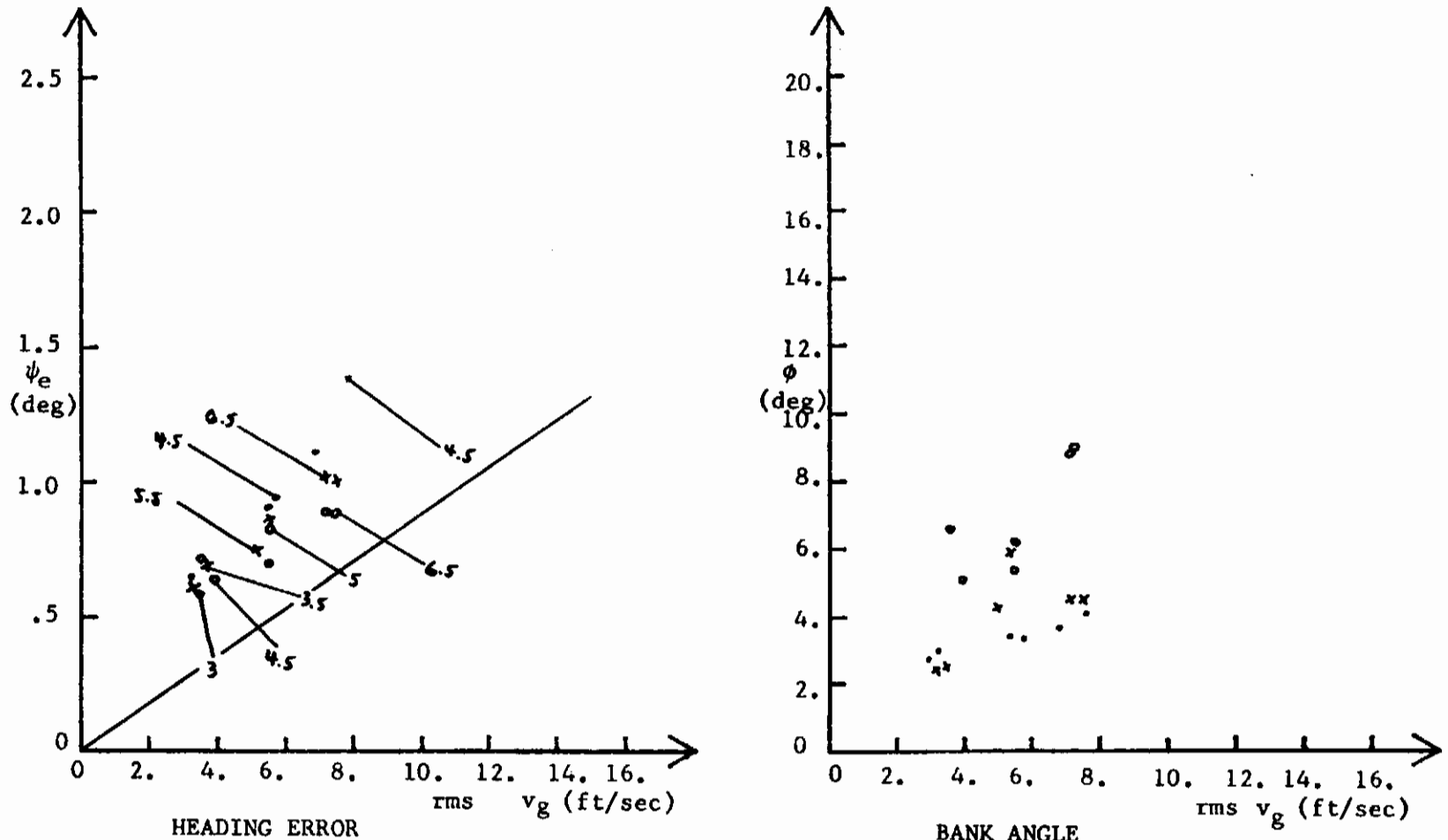

FIGURE 169. HEADING TASK SIMULATION

A-7 FLIGHT CONDITION 4 FAILURE

WITHOUT AUGMENTER

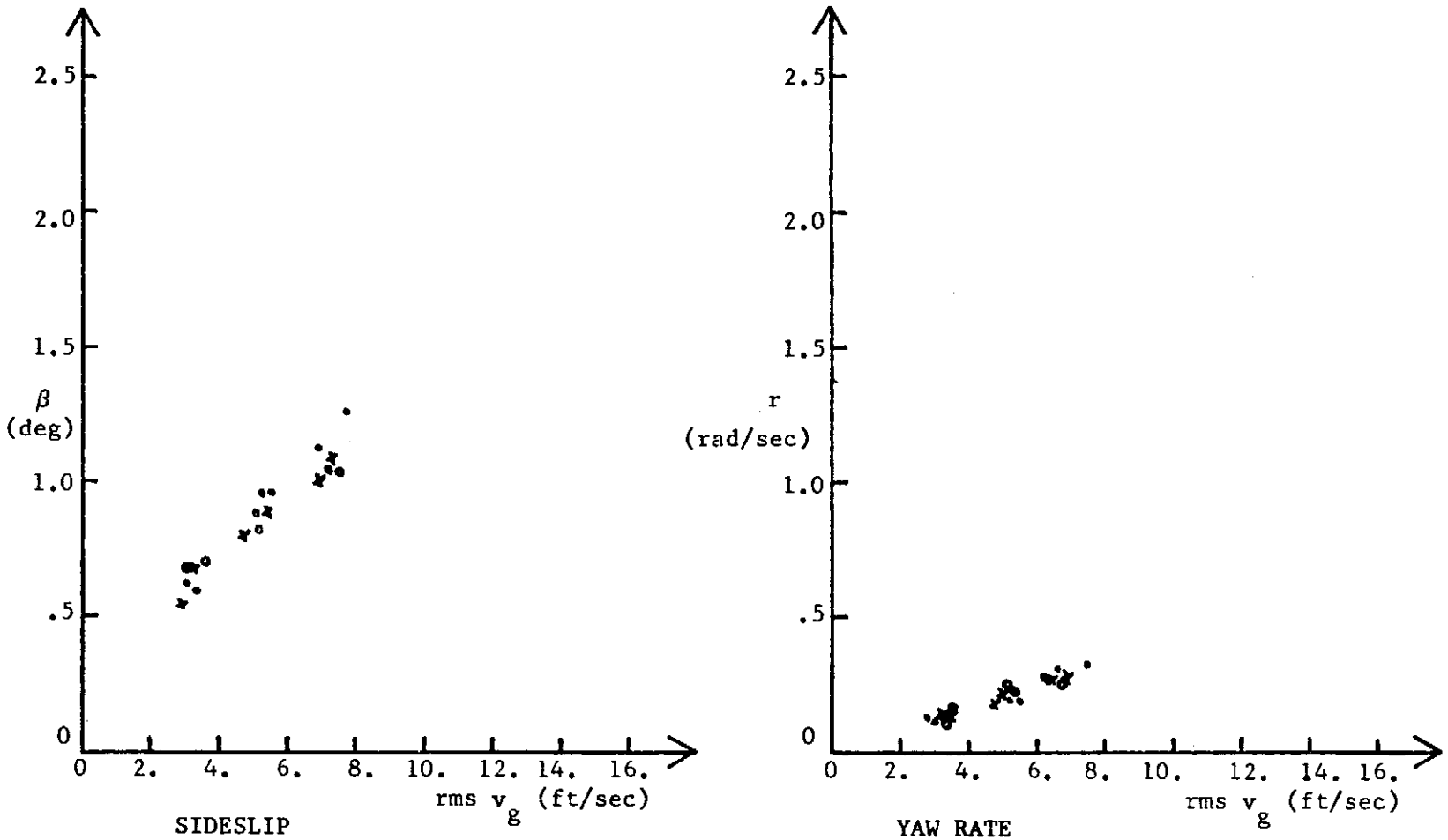

FIGURE 170. HEADING TASK SIMULATION
A-7 FLIGHT CONDITION 4 FAILURE
WITHOUT AUGMENTER

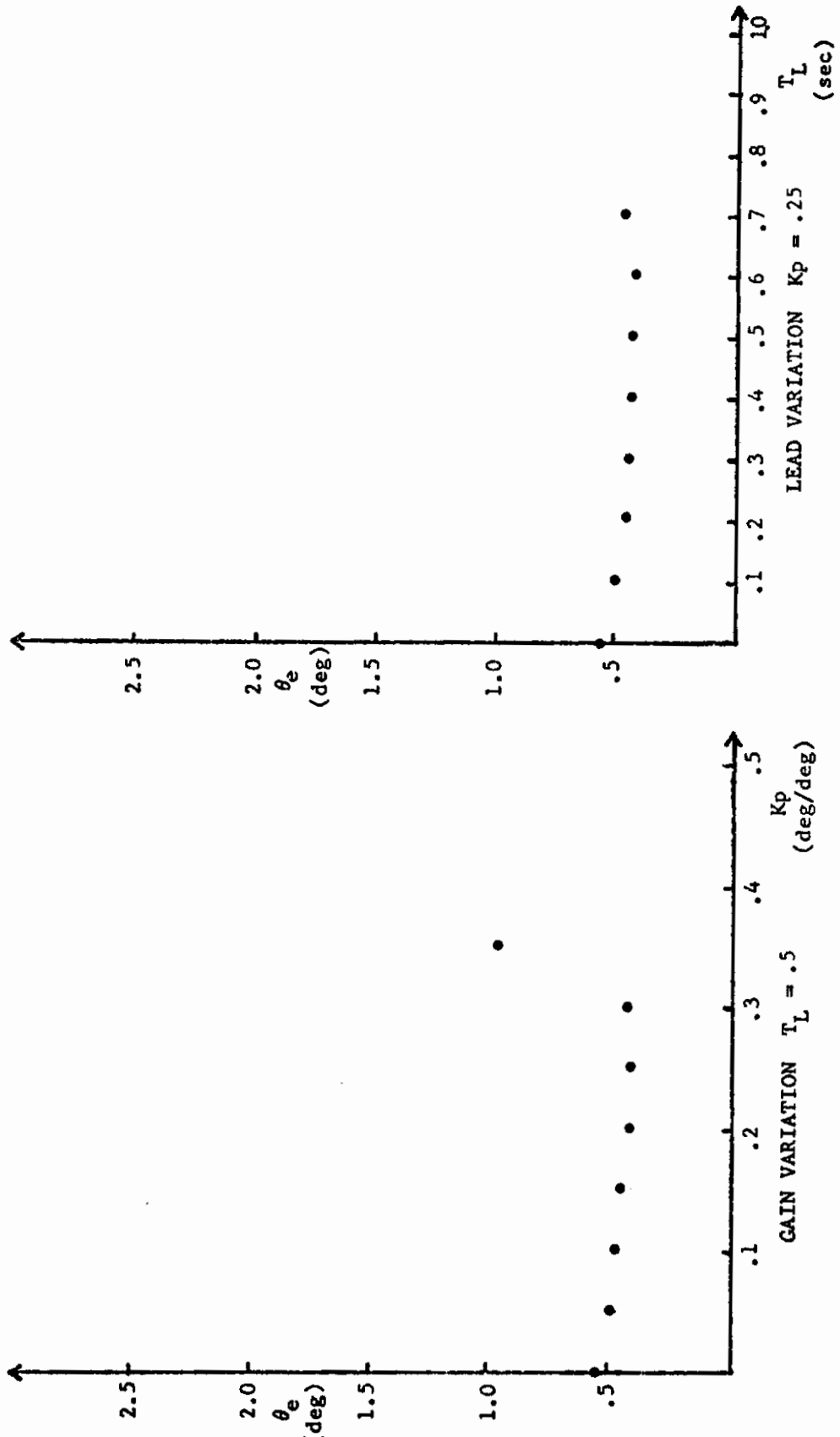

FIGURE 171. PILOT LEAD AND GAIN VARIATION
F-5 FLIGHT CONDITION 1
WITH AUGMENTER

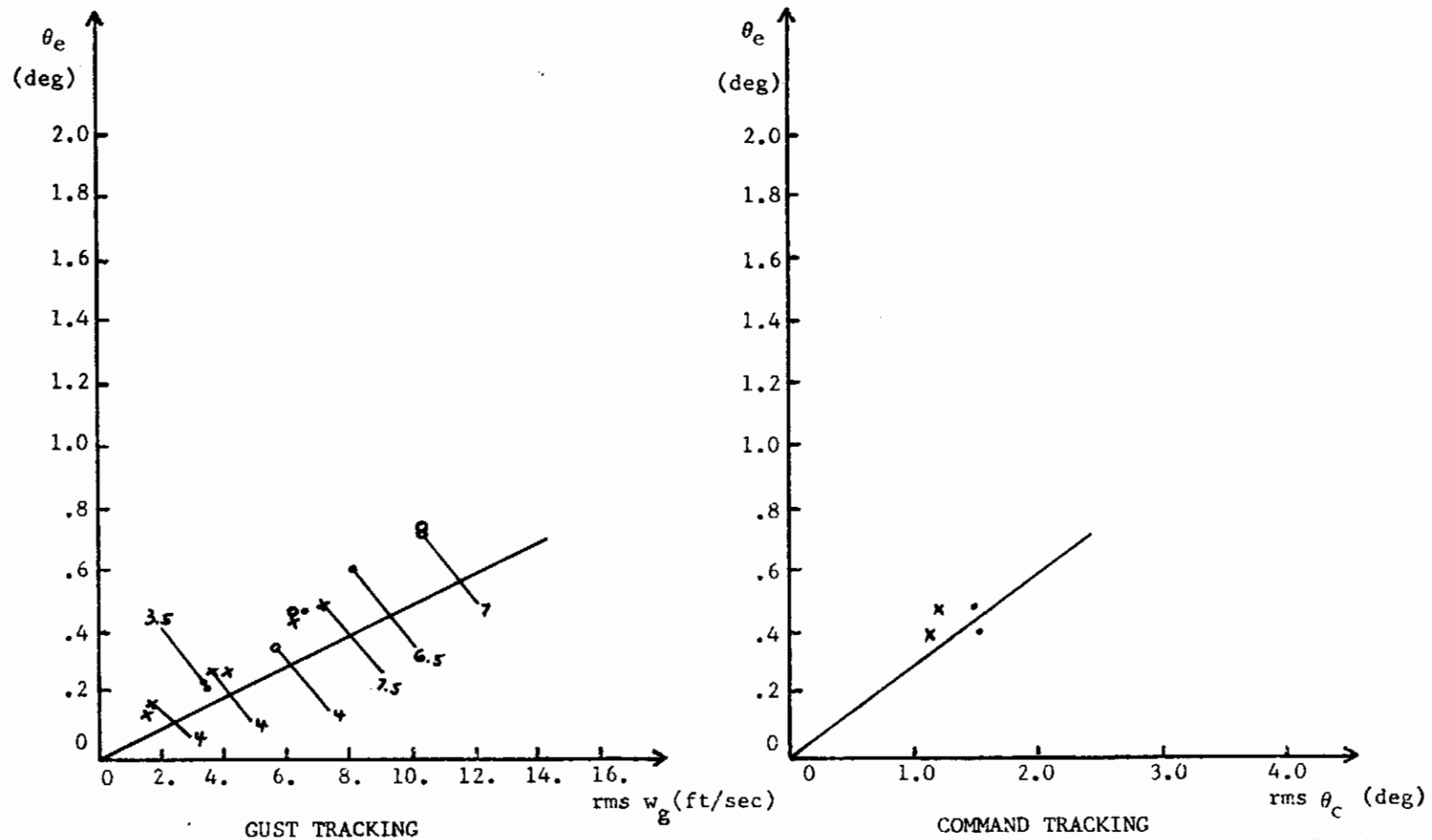

FIGURE 172. PITCH TASK SIMULATION
F-5 FLIGHT CONDITION 1
WITH AUGMENTER

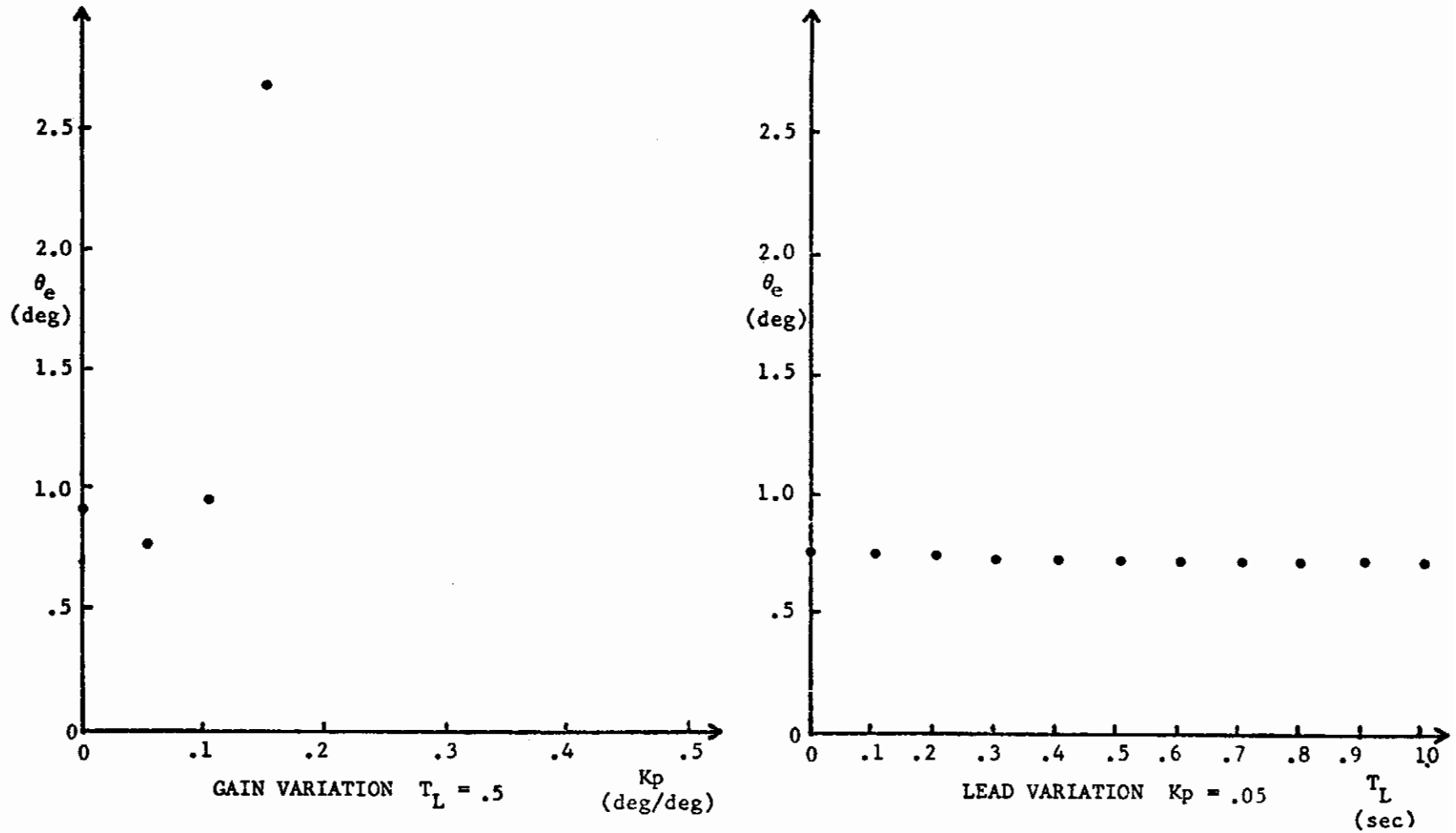

FIGURE 173. PILOT LEAD AND GAIN VARIATION
F-5 FLIGHT CONDITION 1
WITHOUT AUGMENTER

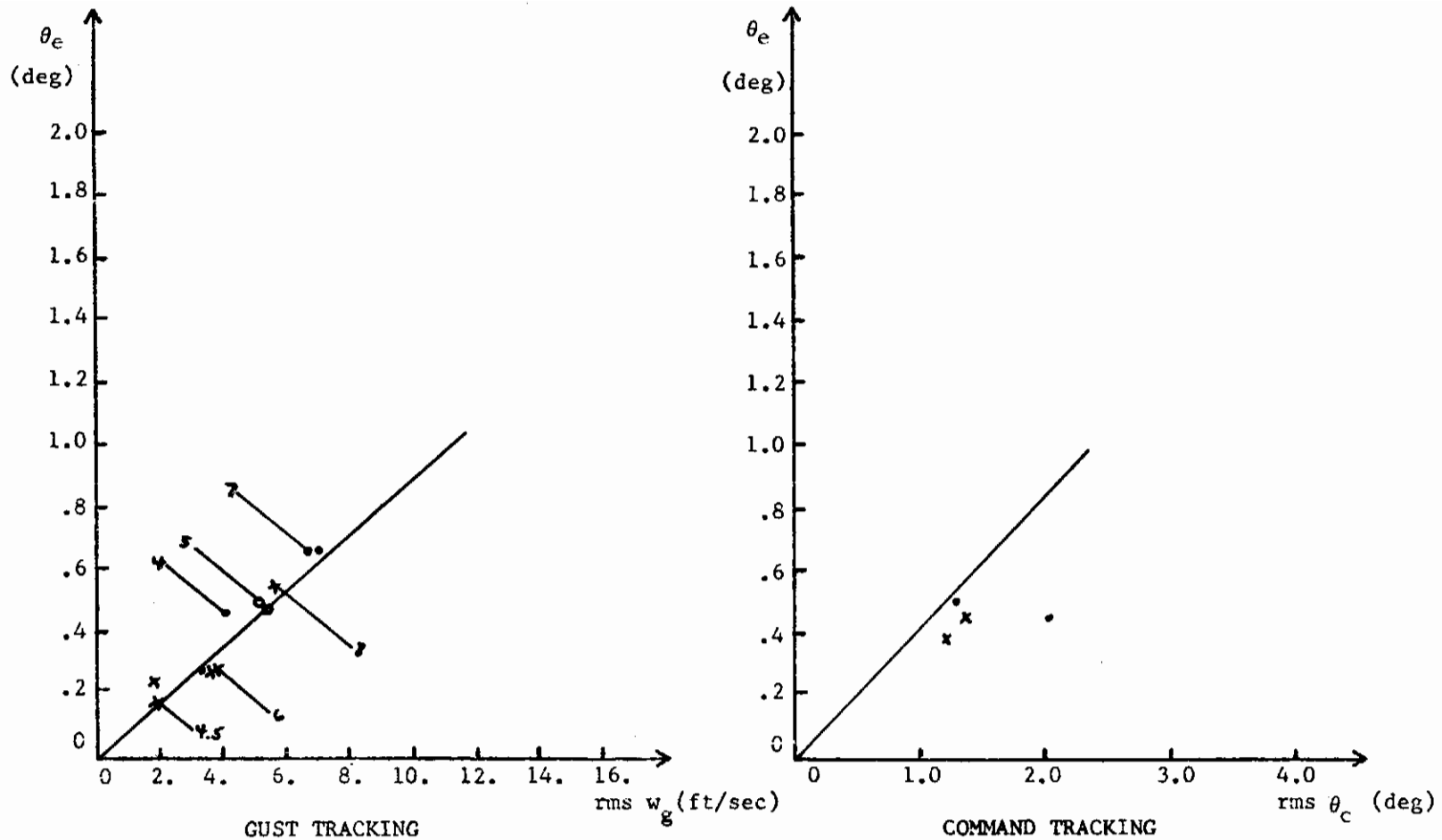

FIGURE 174. PITCH TASK SIMULATION
F-5 FLIGHT CONDITION 1
WITHOUT AUGMENTER

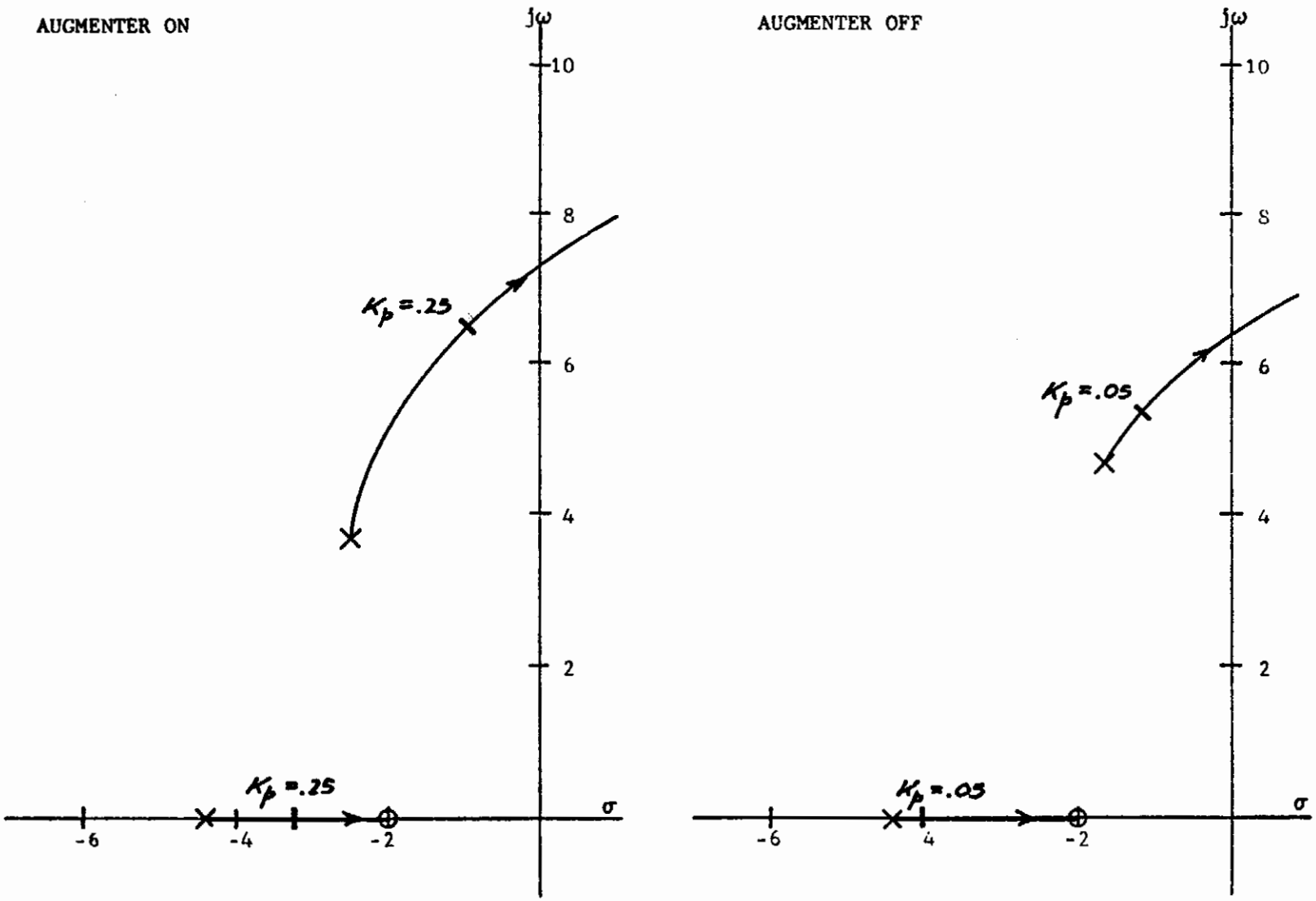

FIGURE 175. ROOT LOCUS FOR PITCH ANGLE TRACKING
F-5 FLIGHT CONDITION 1
T_L = 0.5 SEC

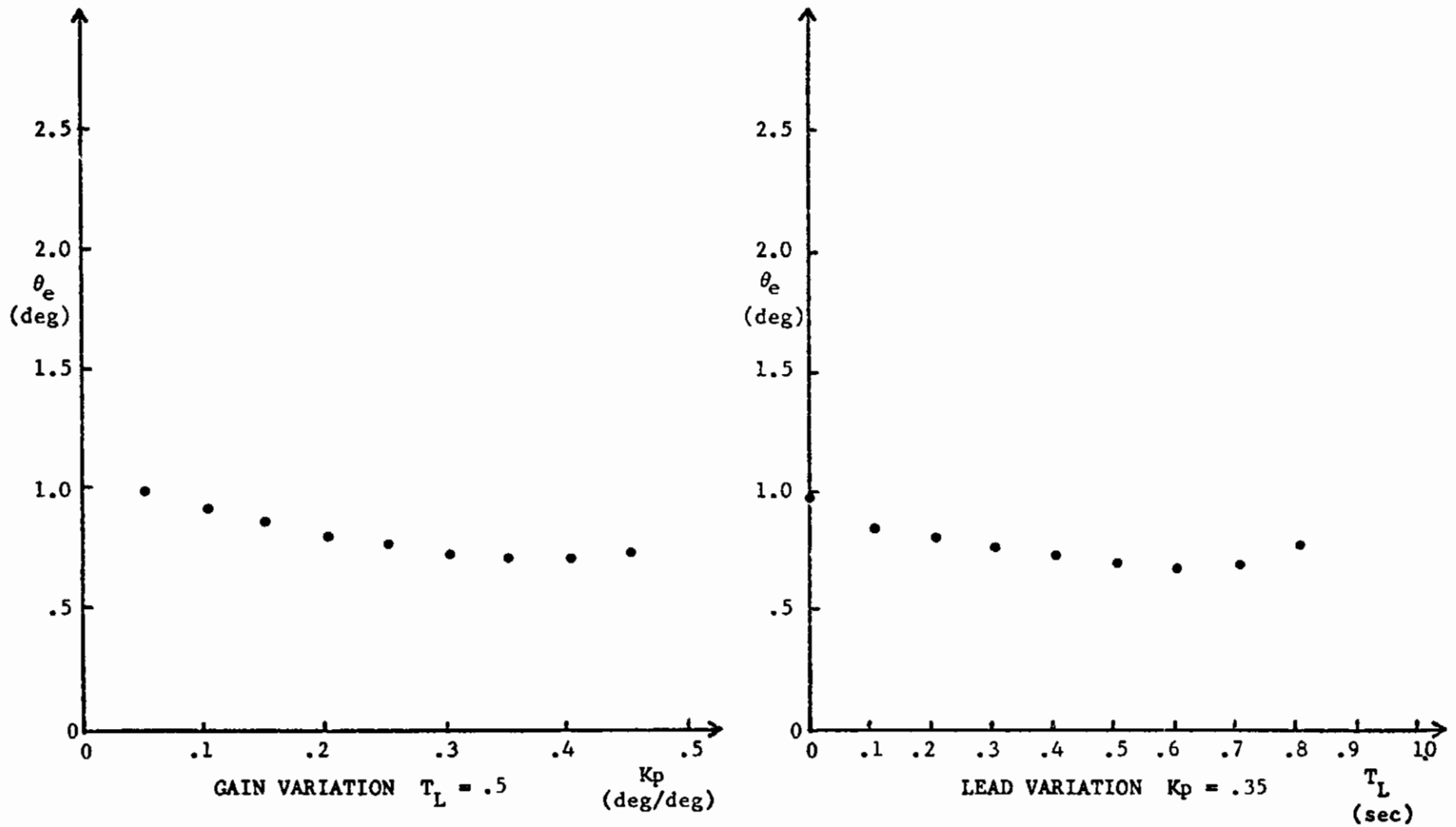

FIGURE 176. PILOT LEAD AND GAIN VARIATION
F-5 FLIGHT CONDITION 2
WITH AUGMENTER

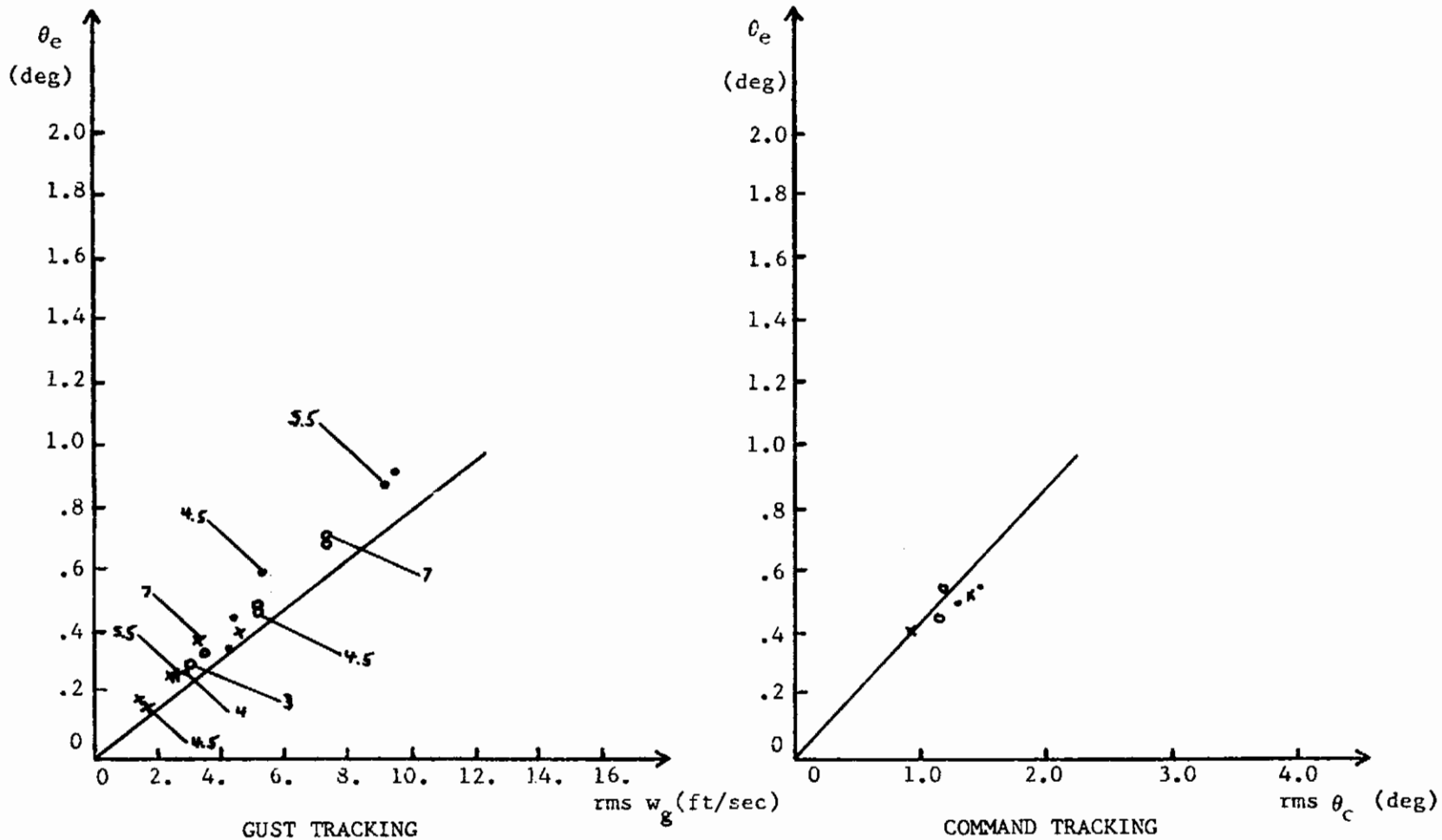

FIGURE 177. PITCH TASK SIMULATION
F-5 FLIGHT CONDITION 2
WITH AUGMENTER

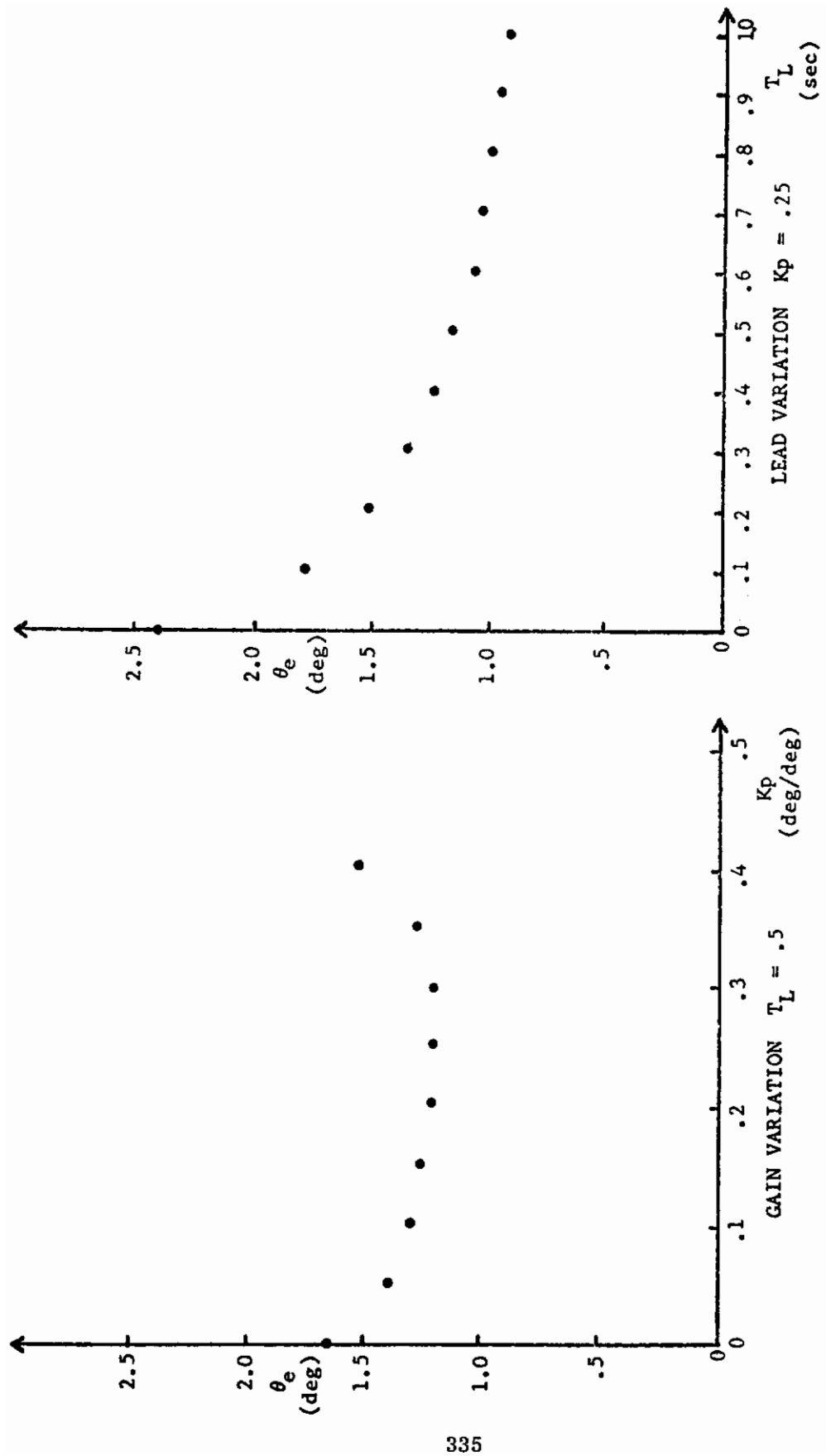

FIGURE 178. PILOT LEAD AND GAIN VARIATION
F-5 FLIGHT CONDITION 2
WITHOUT AUGMENTER

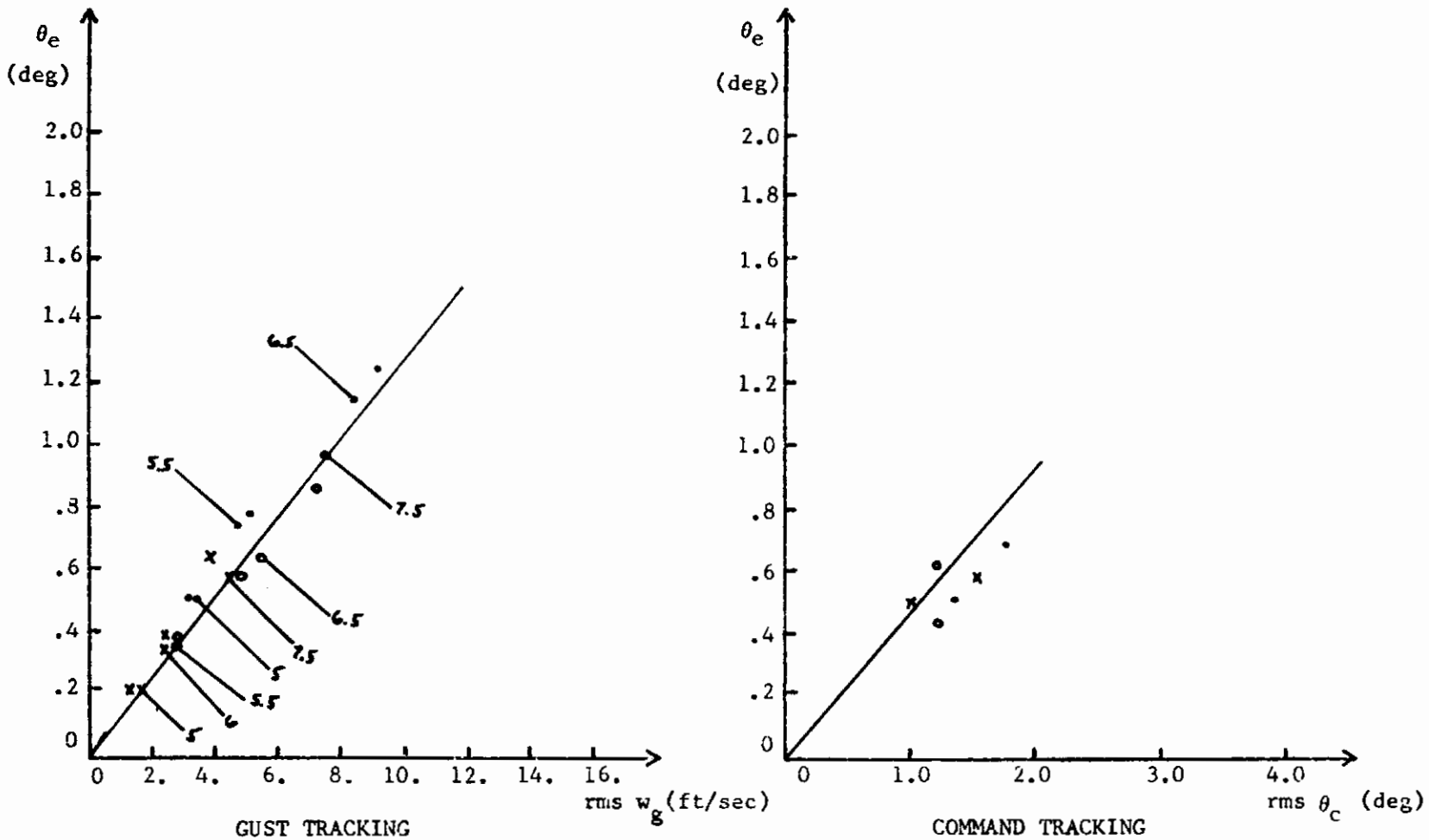

FIGURE 179. PITCH TASK SIMULATION

F-5 FLIGHT CONDITION 2

WITHOUT AUGMENTER

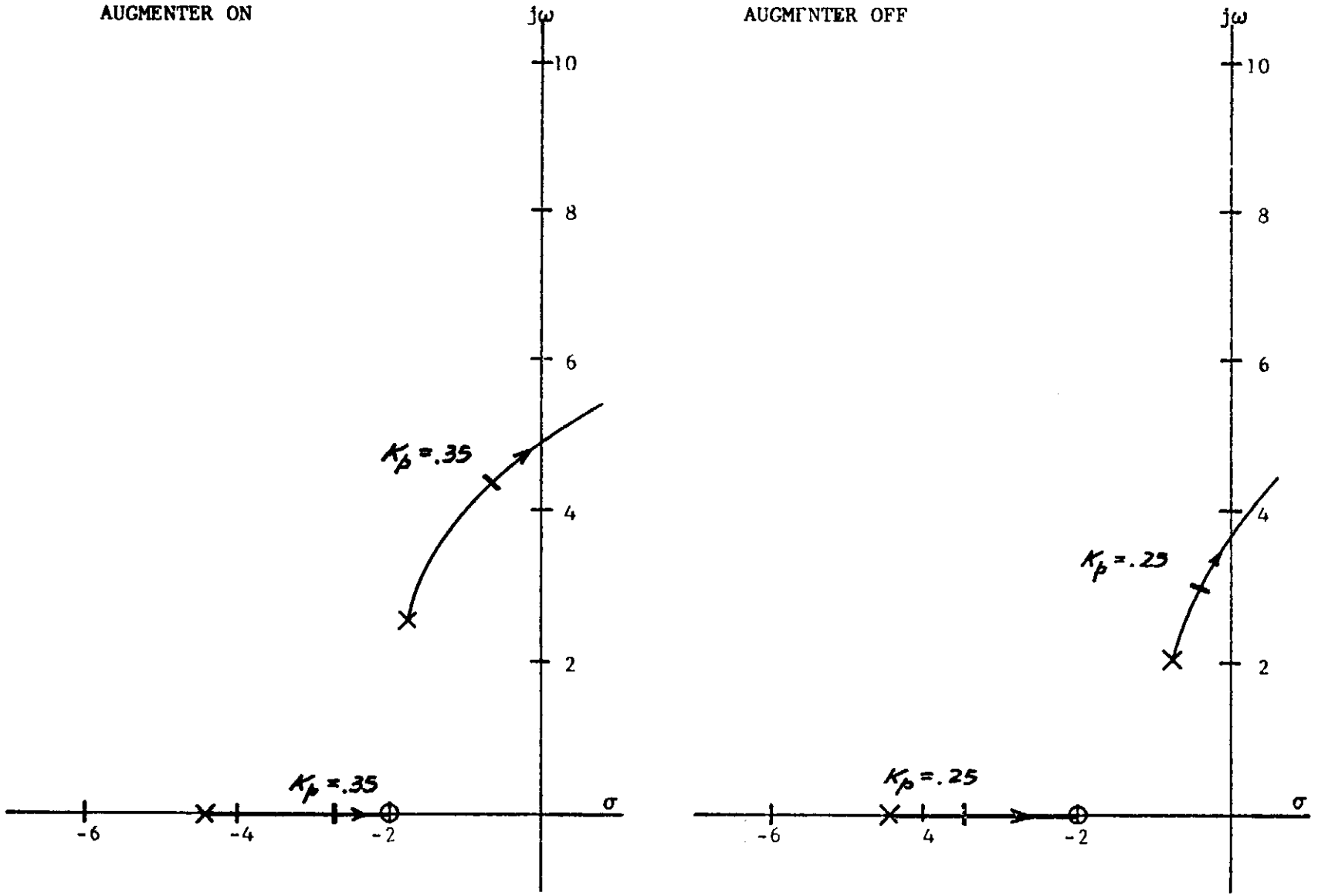

FIGURE 180. ROOT LOCUS FOR PITCH ANGLE TRACKING
F-5 FLIGHT CONDITION 2
T_L = 0.5 SEC

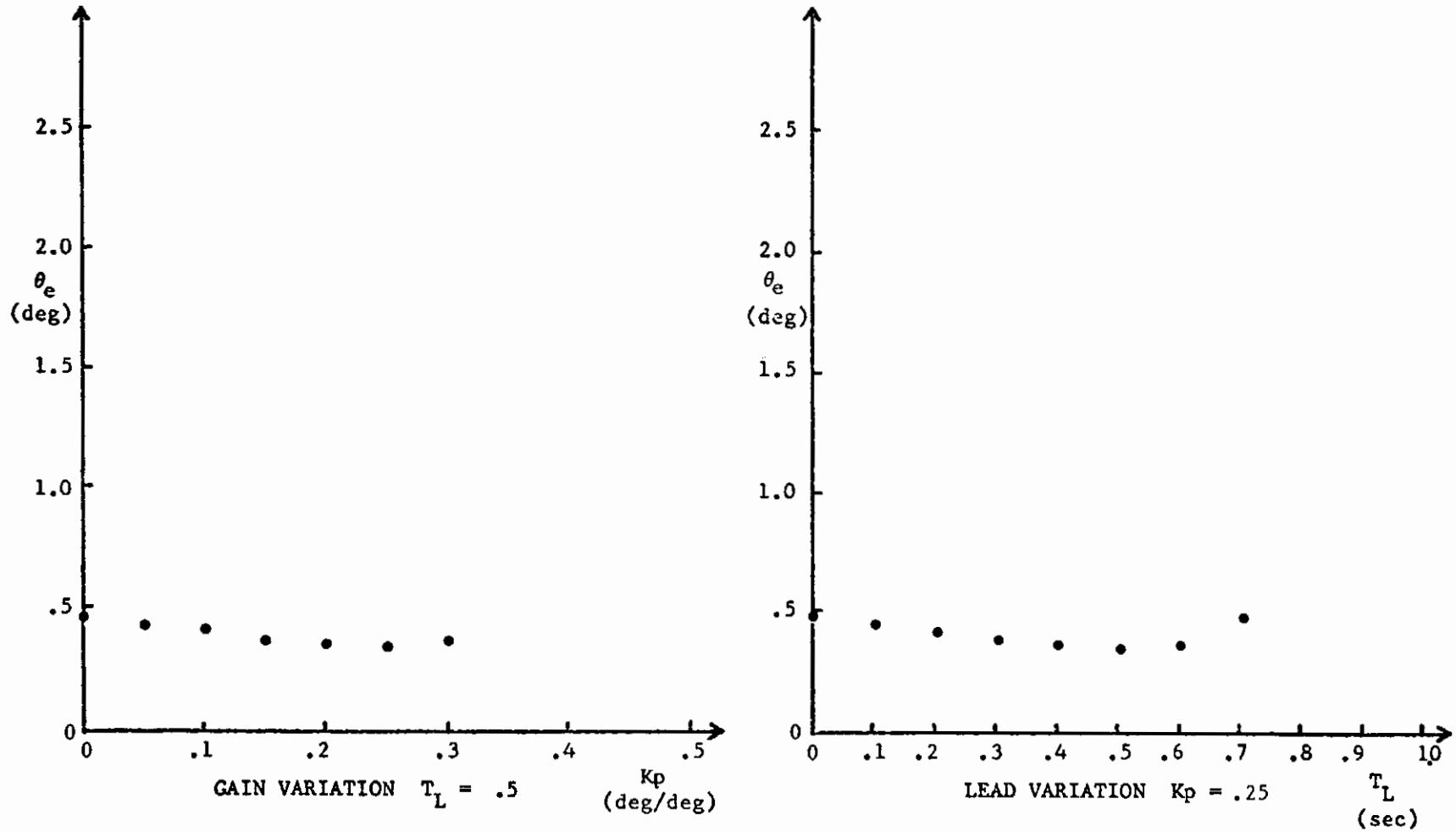

FIGURE 181. PILOT LEAD AND GAIN VARIATION
F-5 FLIGHT CONDITION 3
WITH AUGMENTER

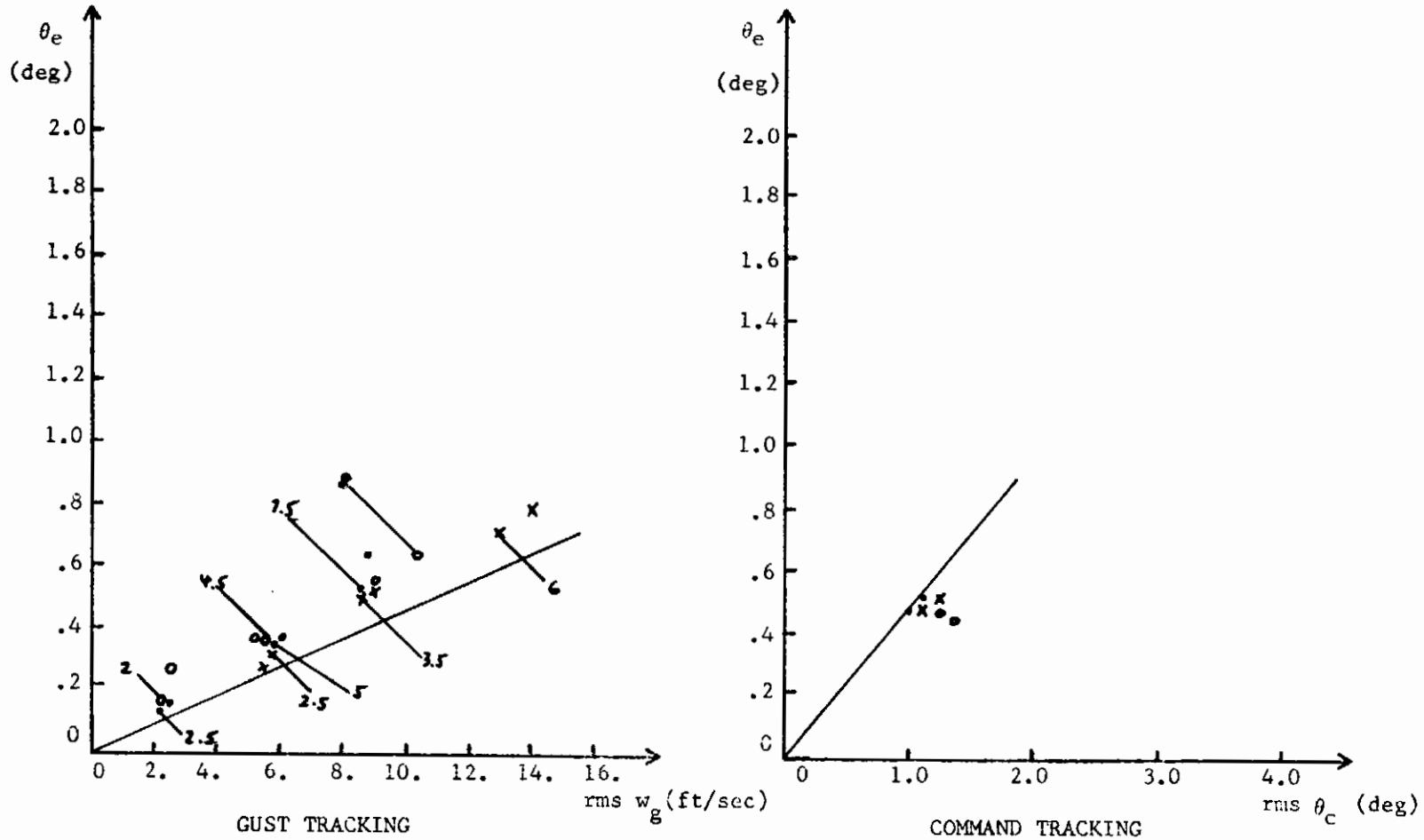

FIGURE 182. PITCH TASK SIMULATION
F-5 FLIGHT CONDITION 3
WITH AUGMENTER

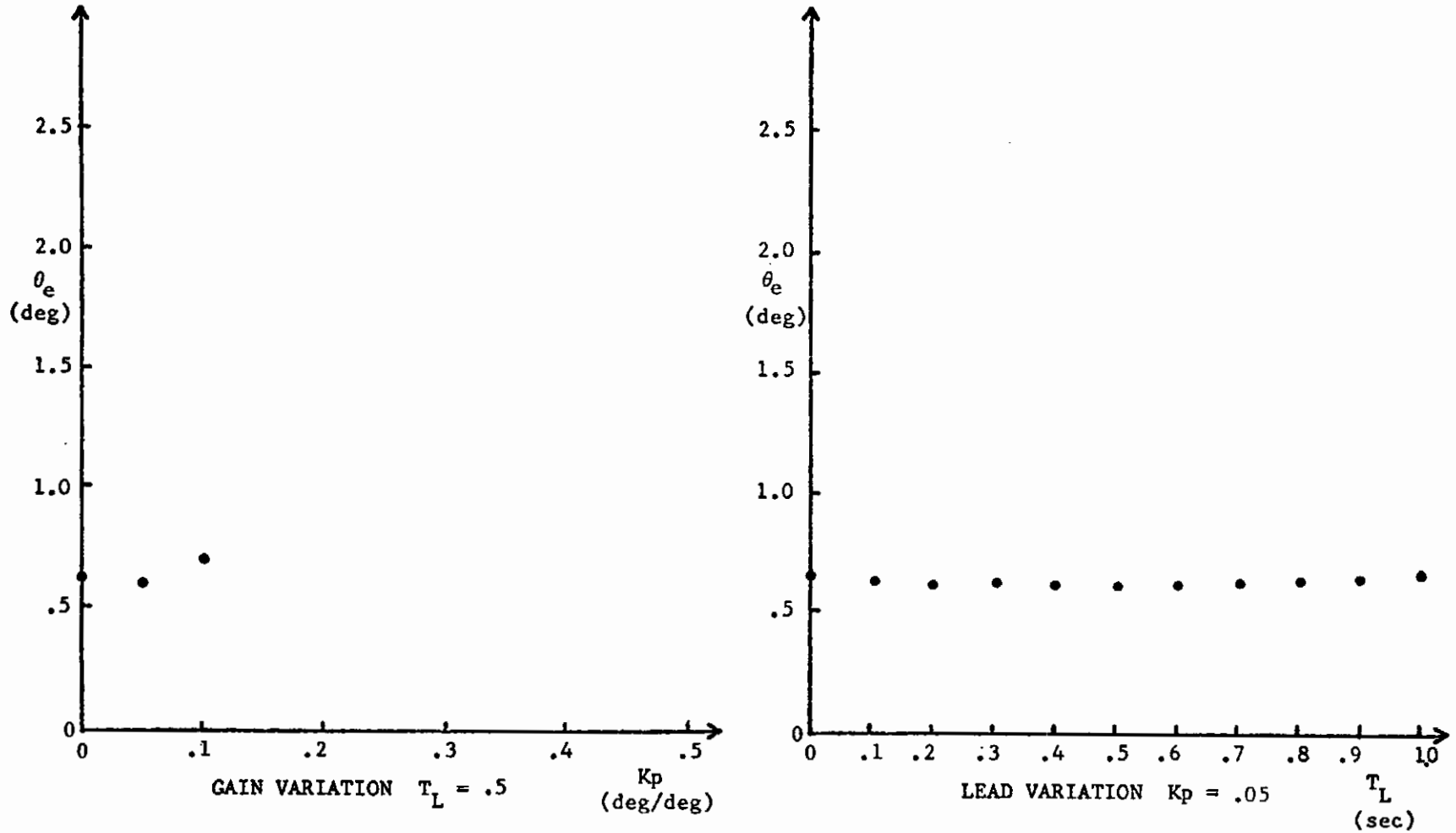

FIGURE 183. PILOT LEAD AND GAIN VARIATION
F-5 FLIGHT CONDITION 3
WITHOUT AUGMENTER

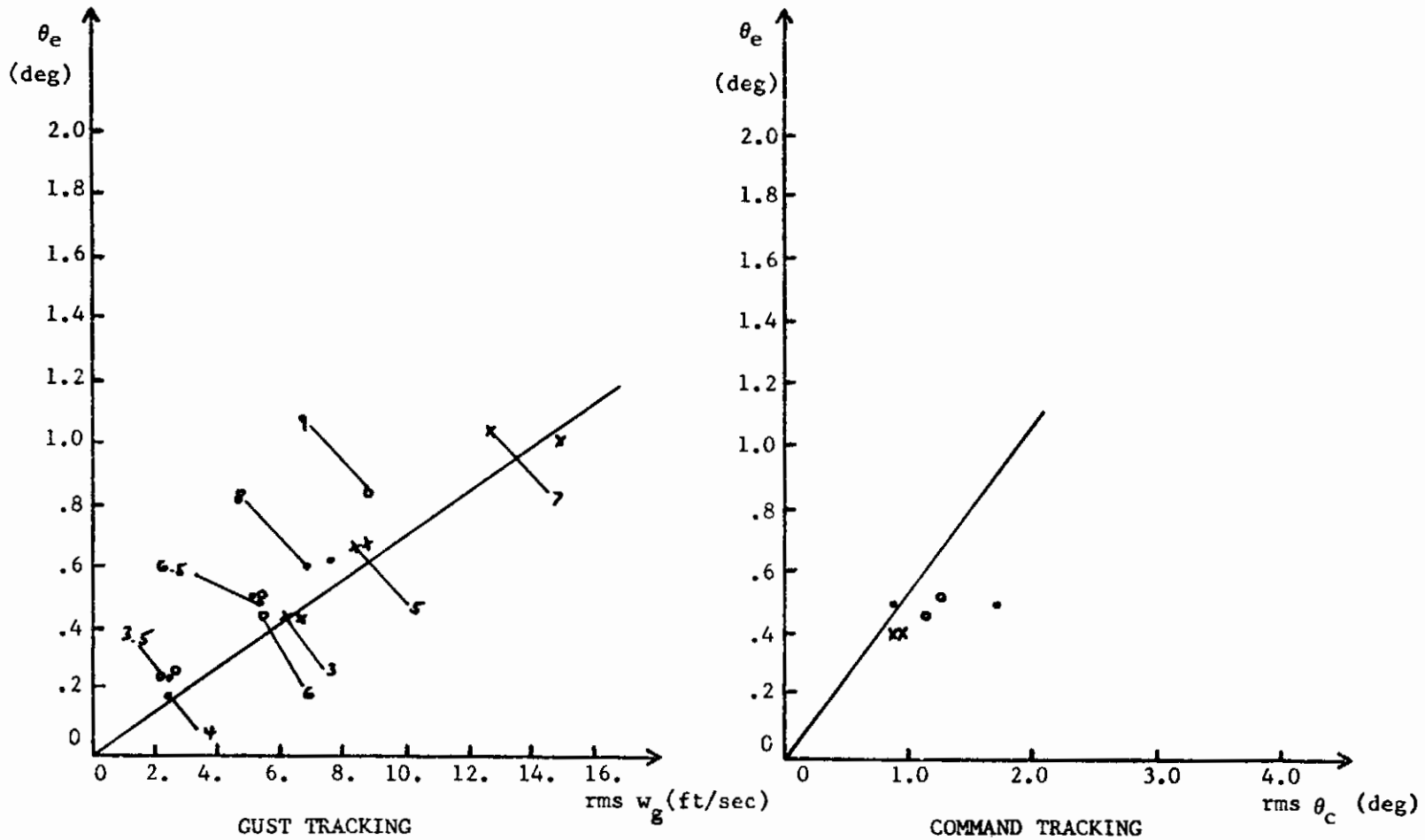

FIGURE 184. PITCH TASK SIMULATION
F-5 FLIGHT CONDITION 3
WITHOUT AUGMENTER

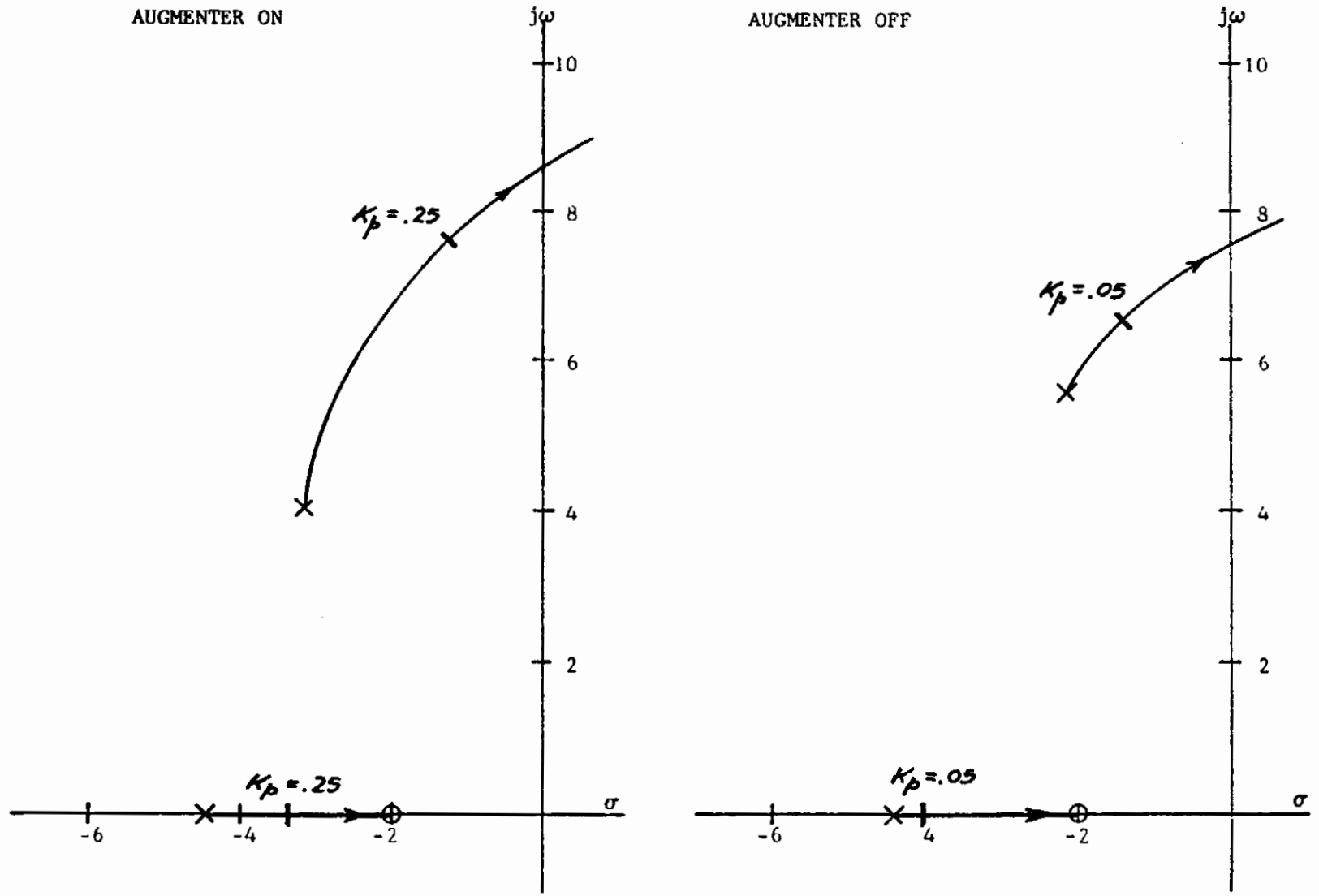

FIGURE 185. ROOT LOCUS FOR PITCH ANGLE TRACKING
F-5 FLIGHT CONDITION 3
T_L = 0.5 SEC

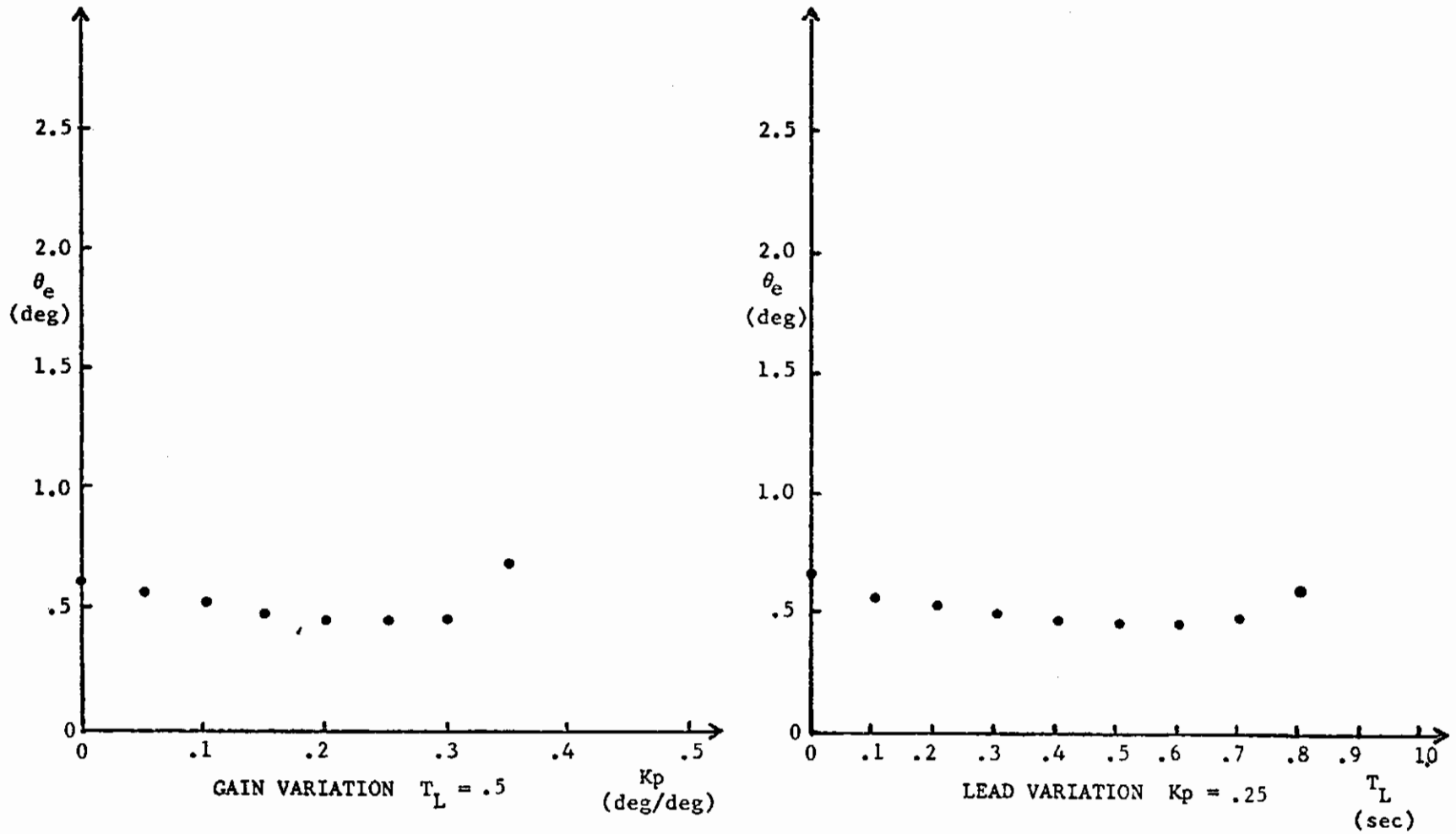

FIGURE 186. PILOT LEAD AND GAIN VARIATION
F-5 FLIGHT CONDITION 4
WITH AUGMENTER

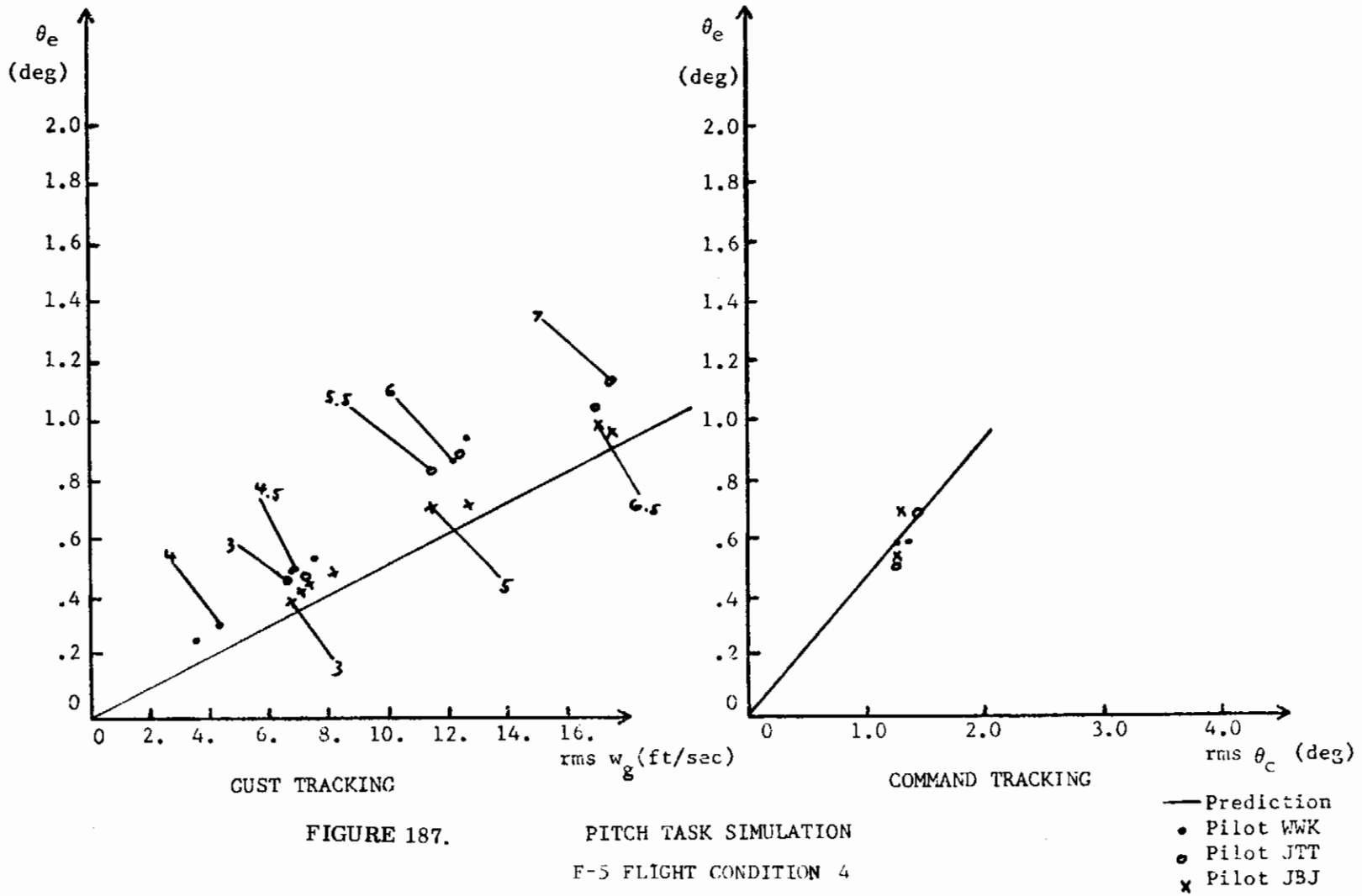

FIGURE 187. PITCH TASK SIMULATION
F-5 FLIGHT CONDITION 4
WITH AUGMENTER

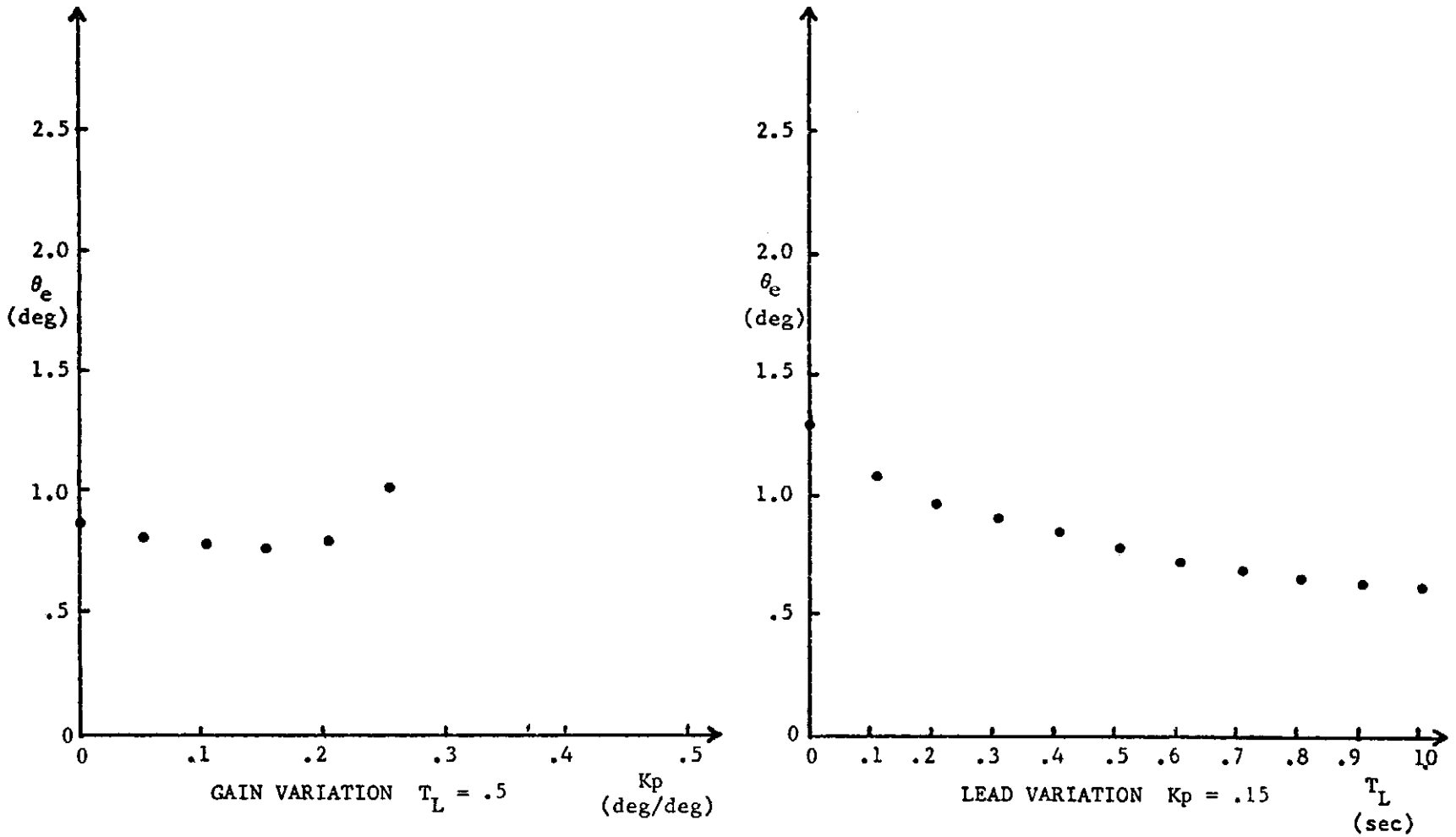

FIGURE 188. PILOT LEAD AND GAIN VARIATION
F-5 FLIGHT CONDITION 4
WITHOUT AUGMENTER

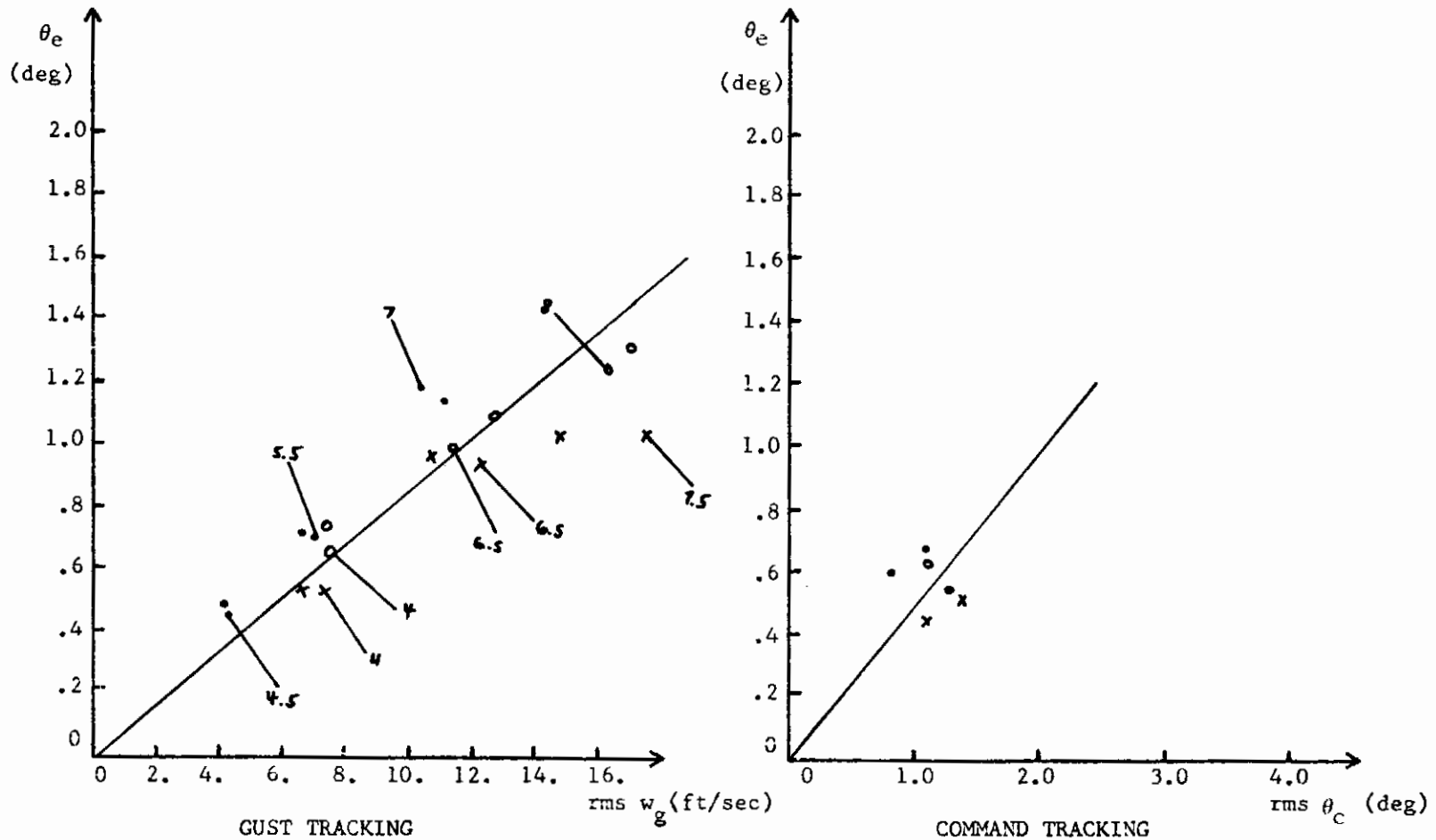

FIGURE 189. PITCH TASK SIMULATION

F-5 FLIGHT CONDITION 4

WITHOUT AUGMENTER

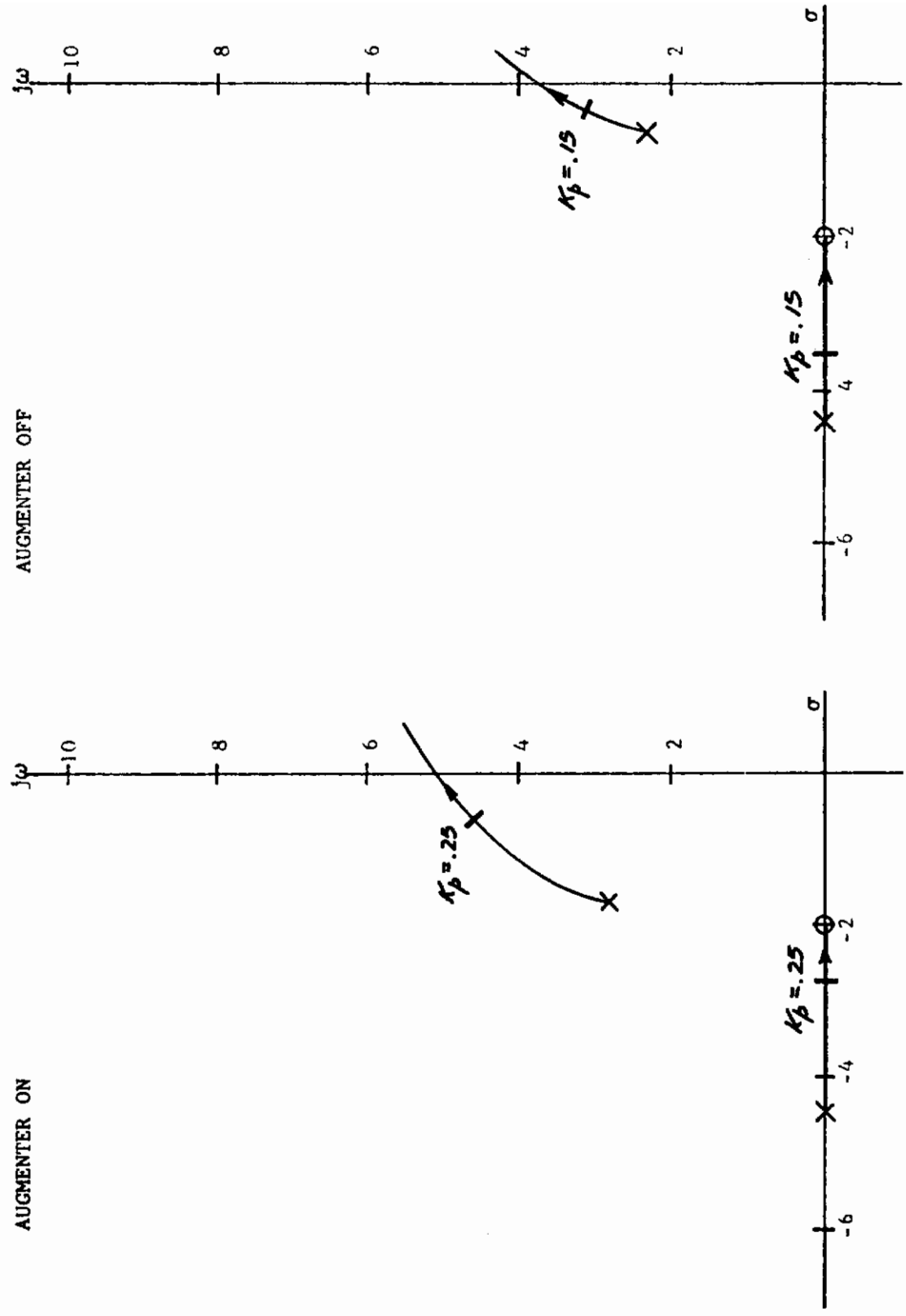

FIGURE 190. ROOT LOCUS FOR PITCH ANGLE TRACKING
F-5 FLIGHT CONDITION 4
T_L = 0.5 SEC

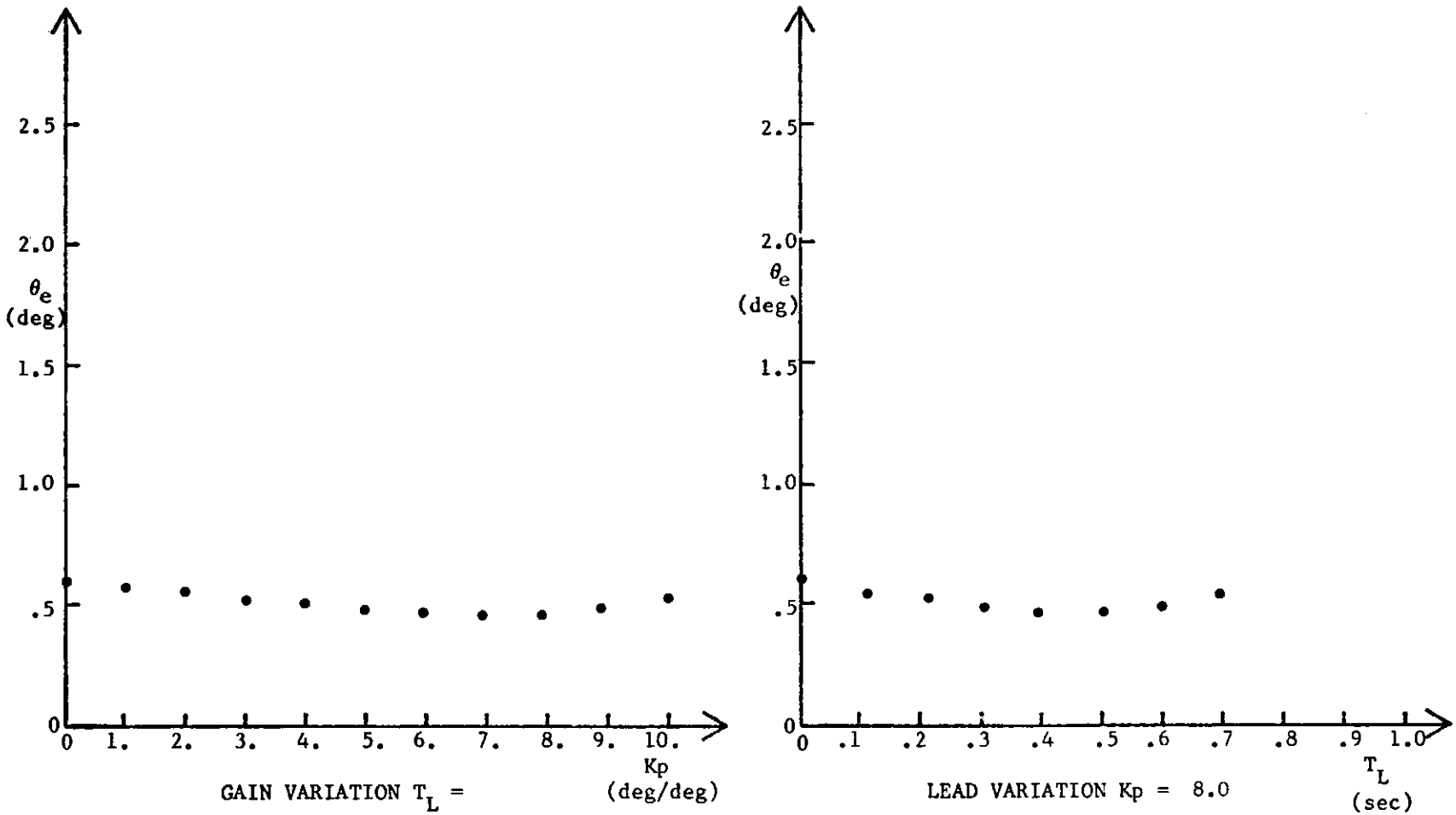

FIGURE 191. PILOT LEAD AND GAIN VARIATION
A-7 FLIGHT CONDITION 1
WITH AUGMENTER

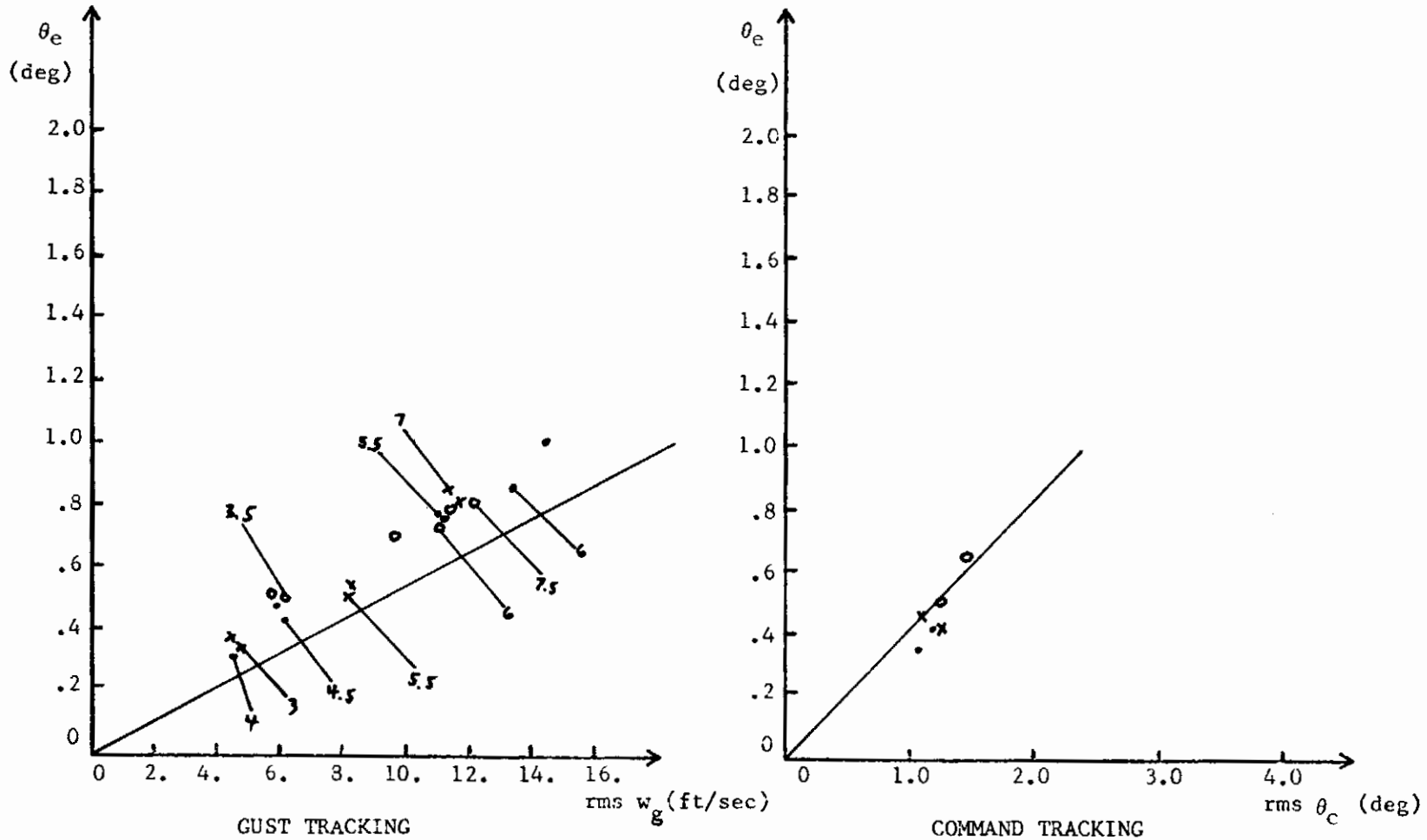

FIGURE 192. PITCH TASK SIMULATION

A-7 FLIGHT CONDITION 1

WITH AUGMENTER

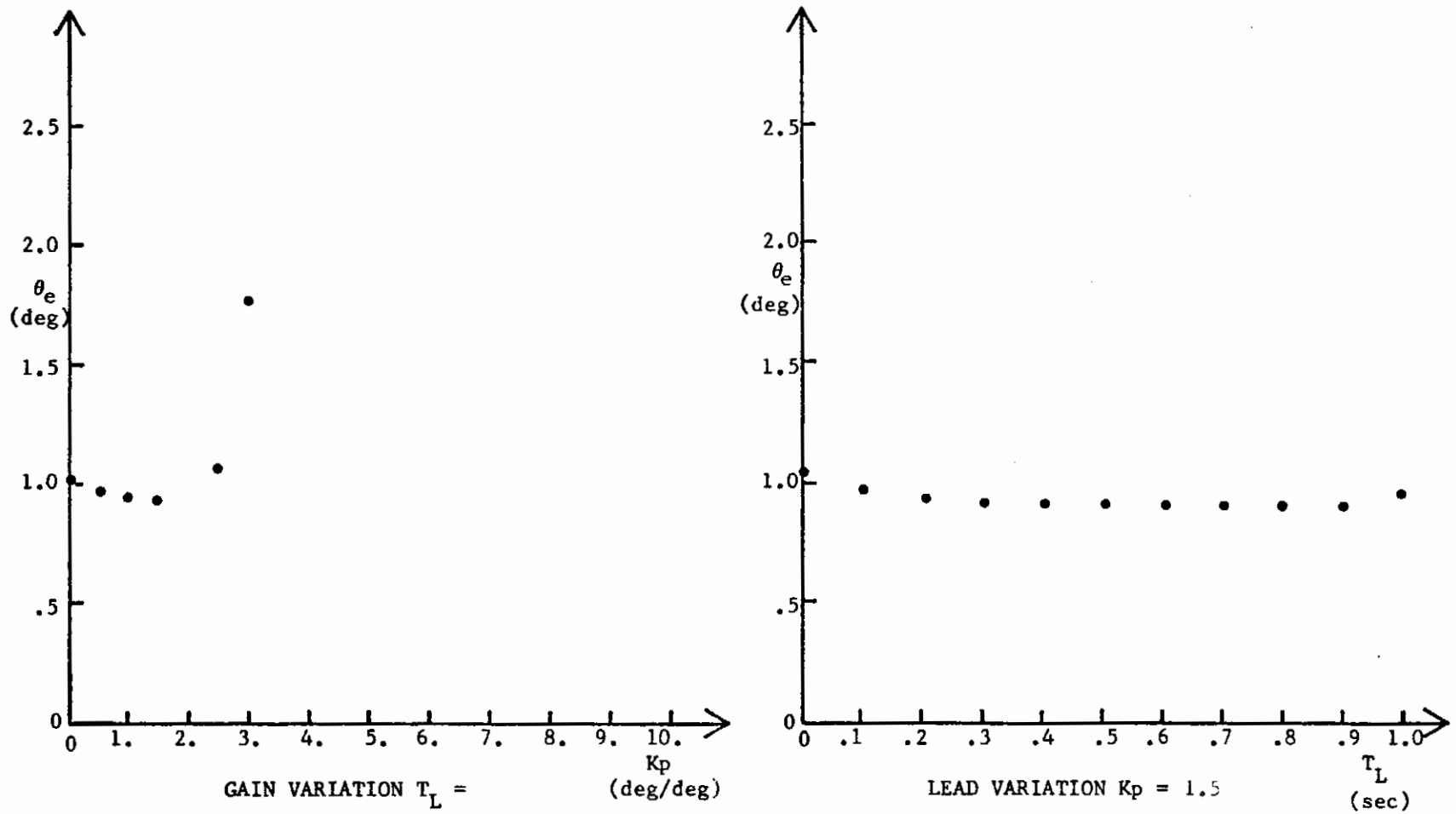

FIGURE 193. PILOT LEAD AND GAIN VARIATION

A-7 FLIGHT CONDITION 1

WITHOUT AUGMENTER

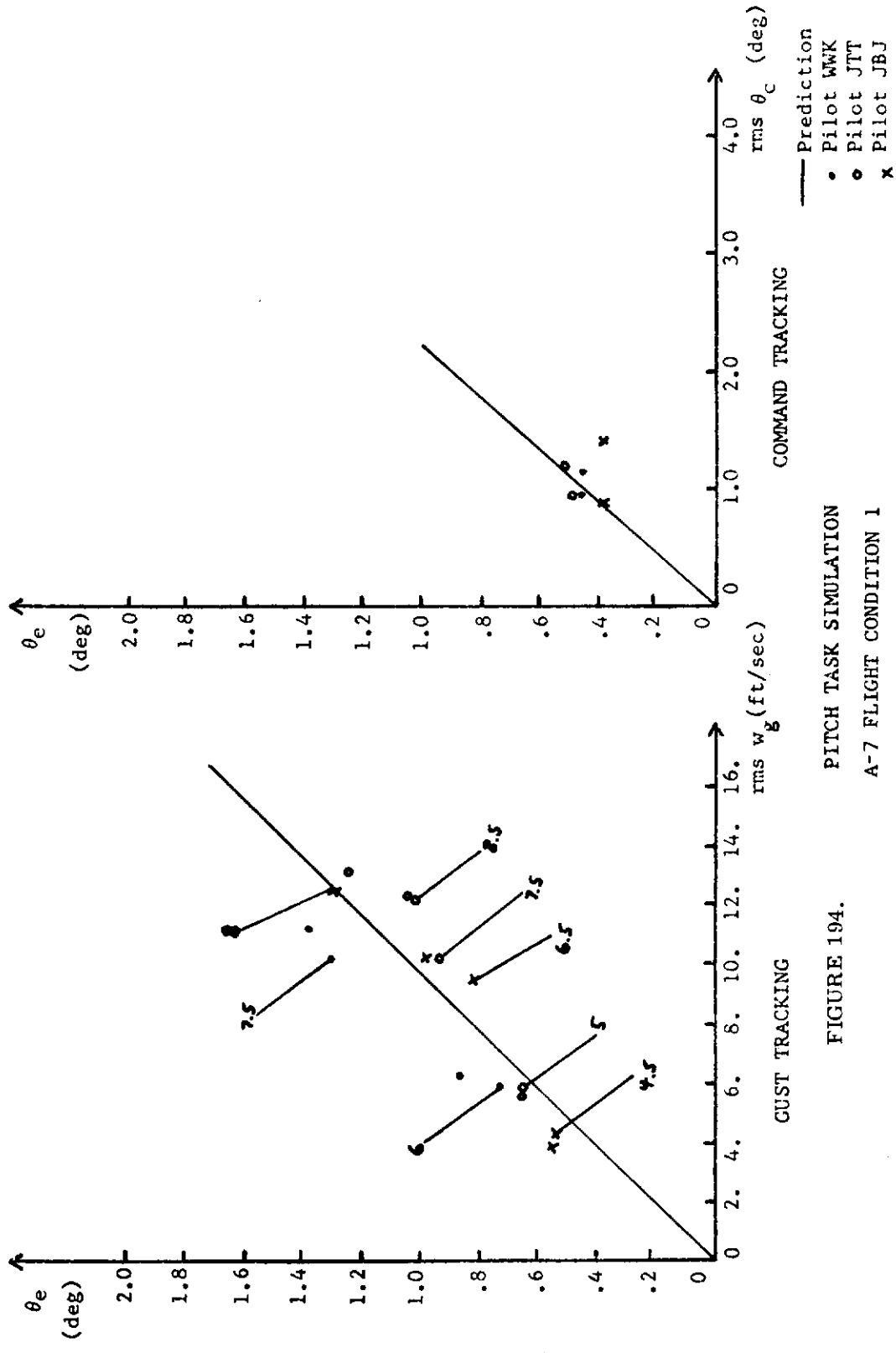

FIGURE 194. PITCH TASK SIMULATION
A-7 FLIGHT CONDITION 1
WITHOUT AUGMENTER

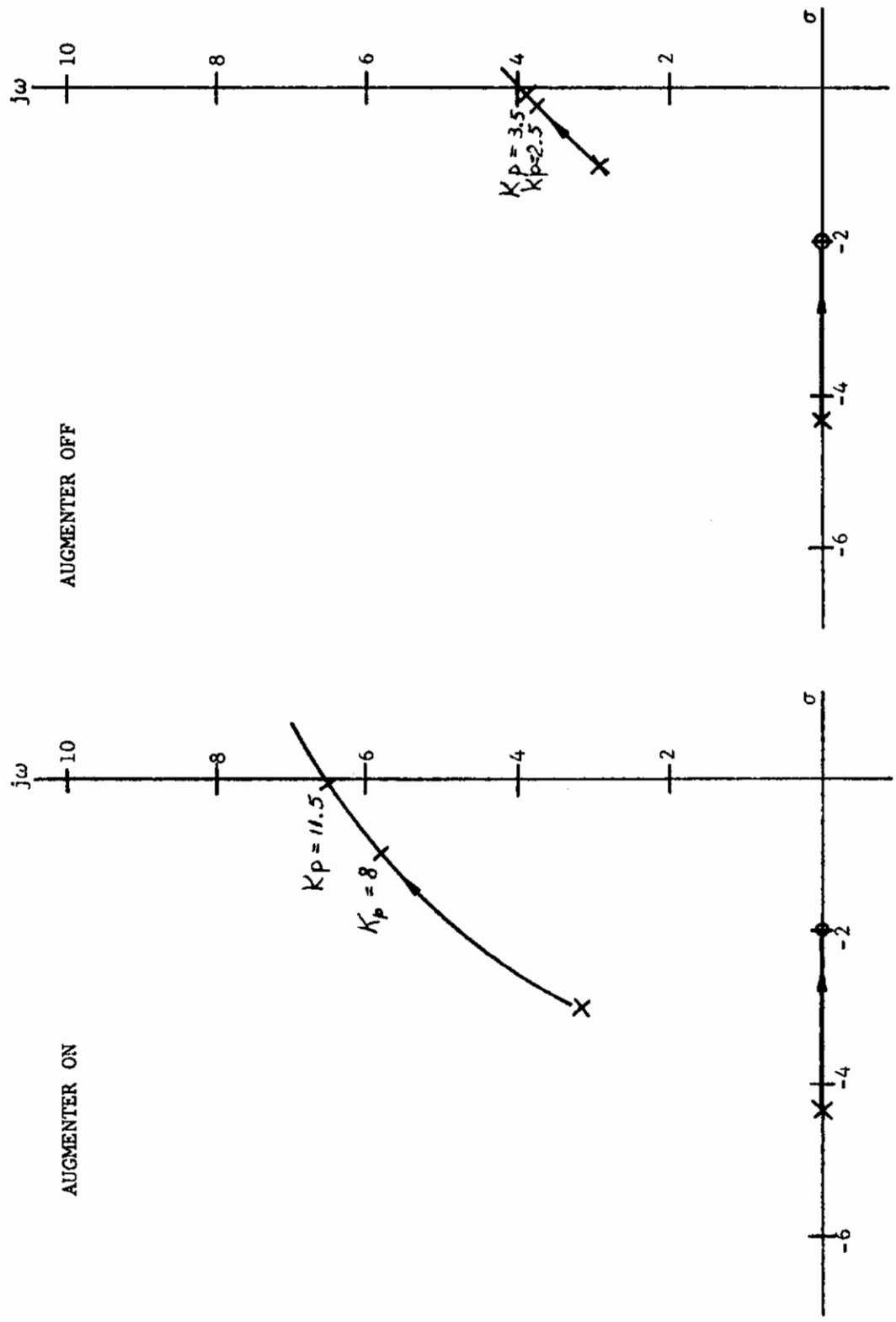

FIGURE 195. ROOT LOCUS FOR PITCH ANGLE TRACKING
A-7 FLIGHT CONDITION 1
$T_L = 0.5$ SEC

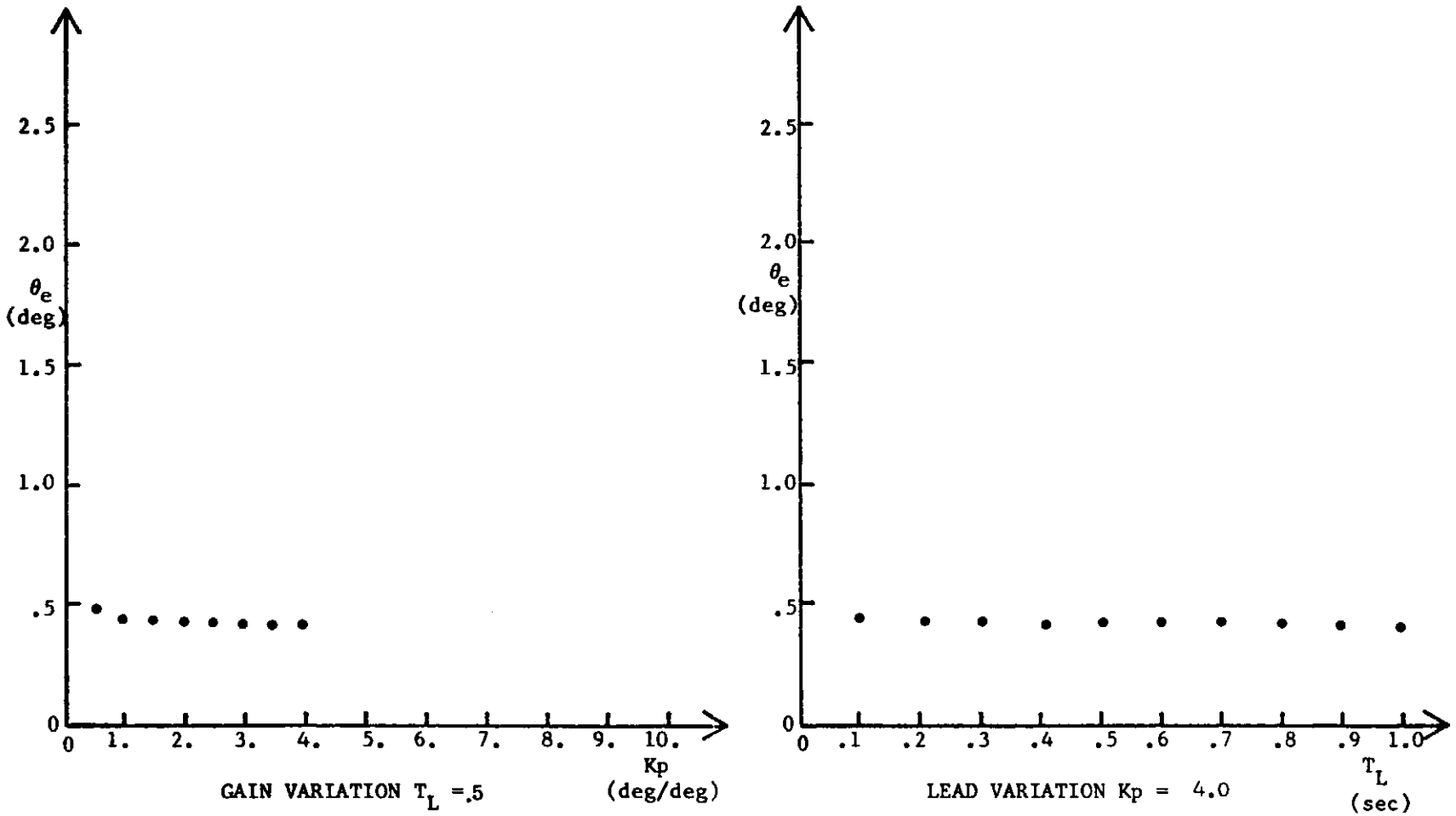

FIGURE 196. PILOT LEAD AND GAIN VARIATION
A-7 FLIGHT CONDITION 2
WITH AUGMENTER

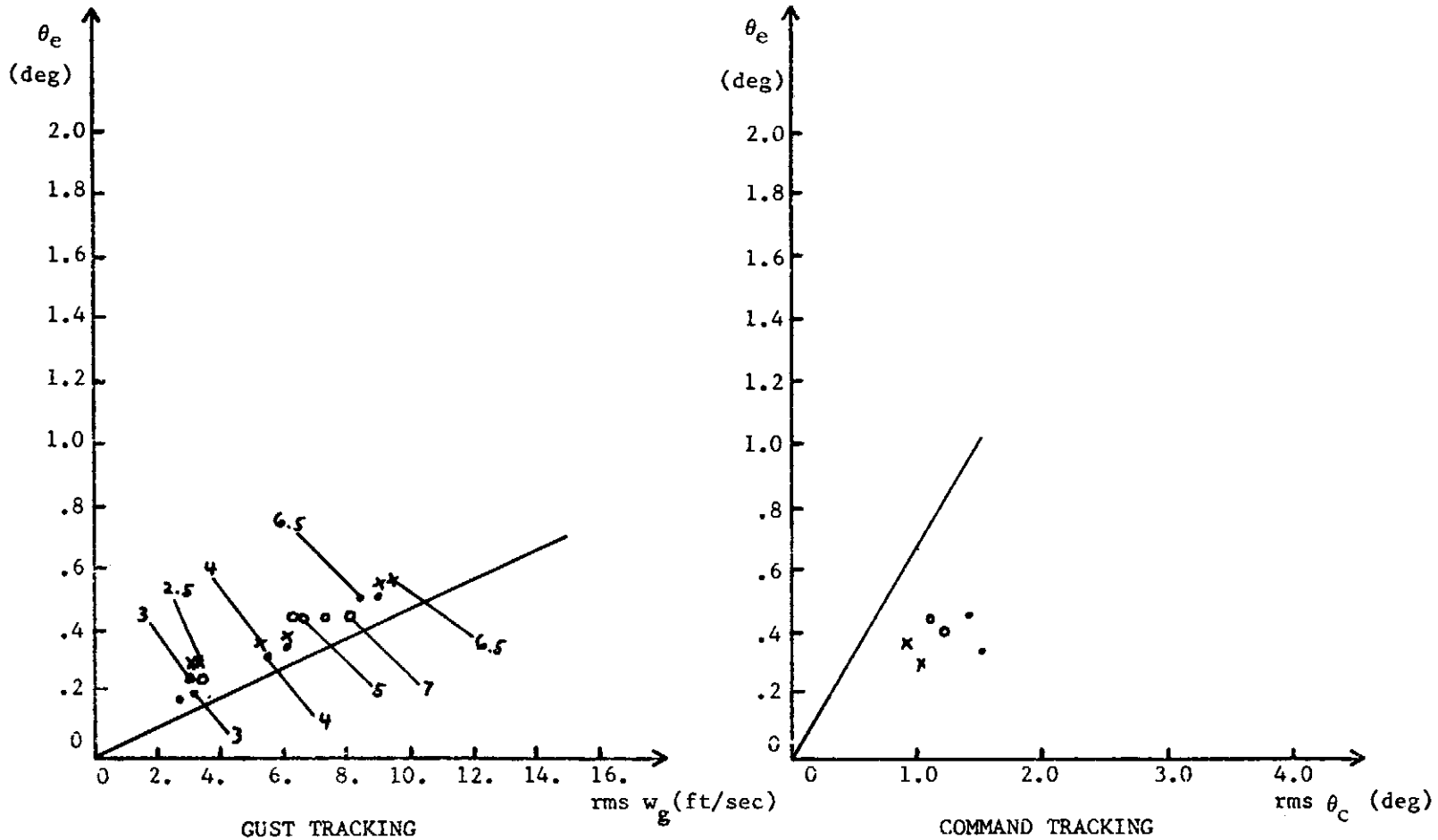

FIGURE 197. PITCH TASK SIMULATION
A-7 FLIGHT CONDITION 2
WITH AUGMENTER

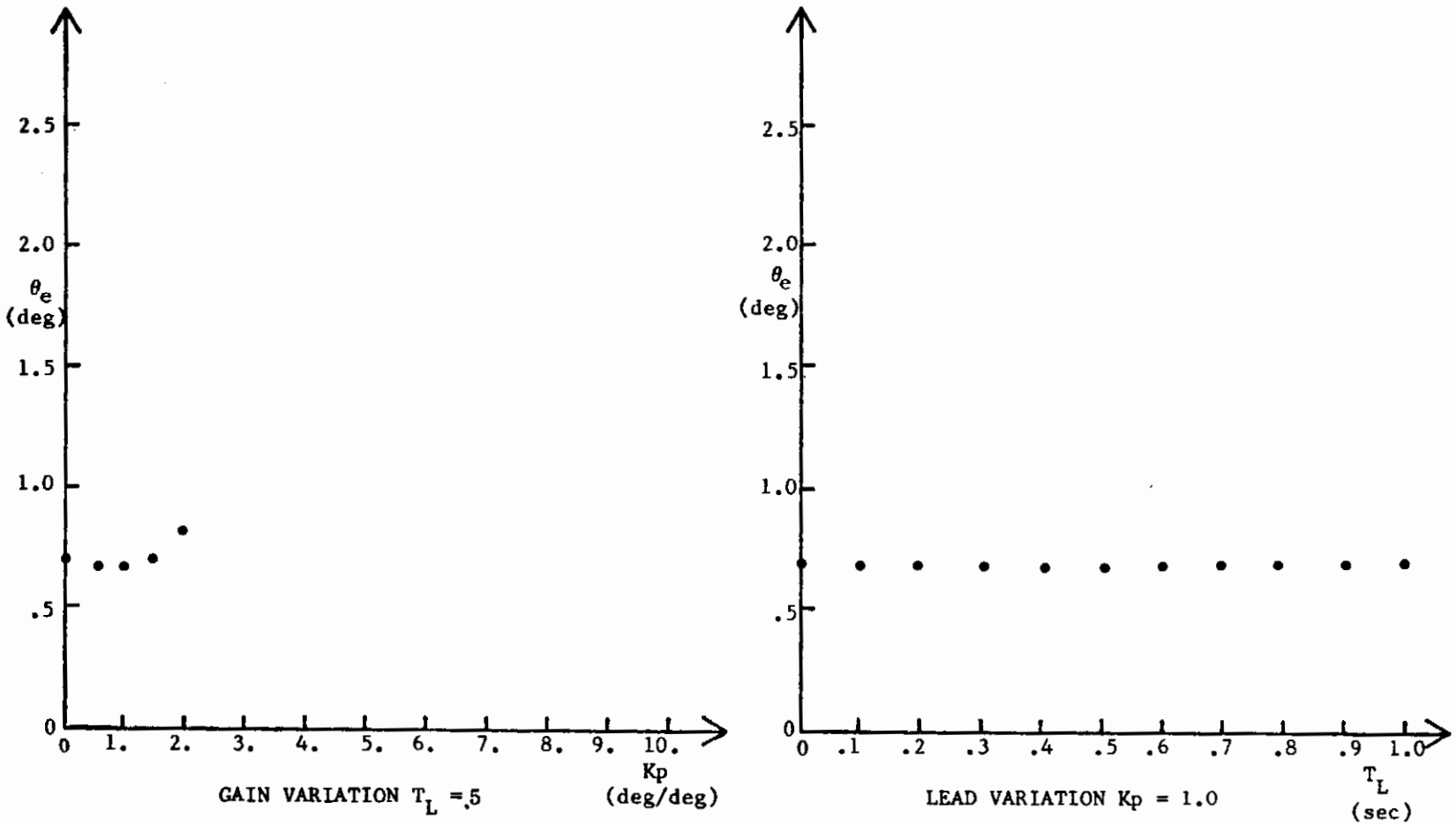

FIGURE 198. PILOT LEAD AND GAIN VARIATION

A-7 FLIGHT CONDITION 2

WITHOUT AUGMENTER

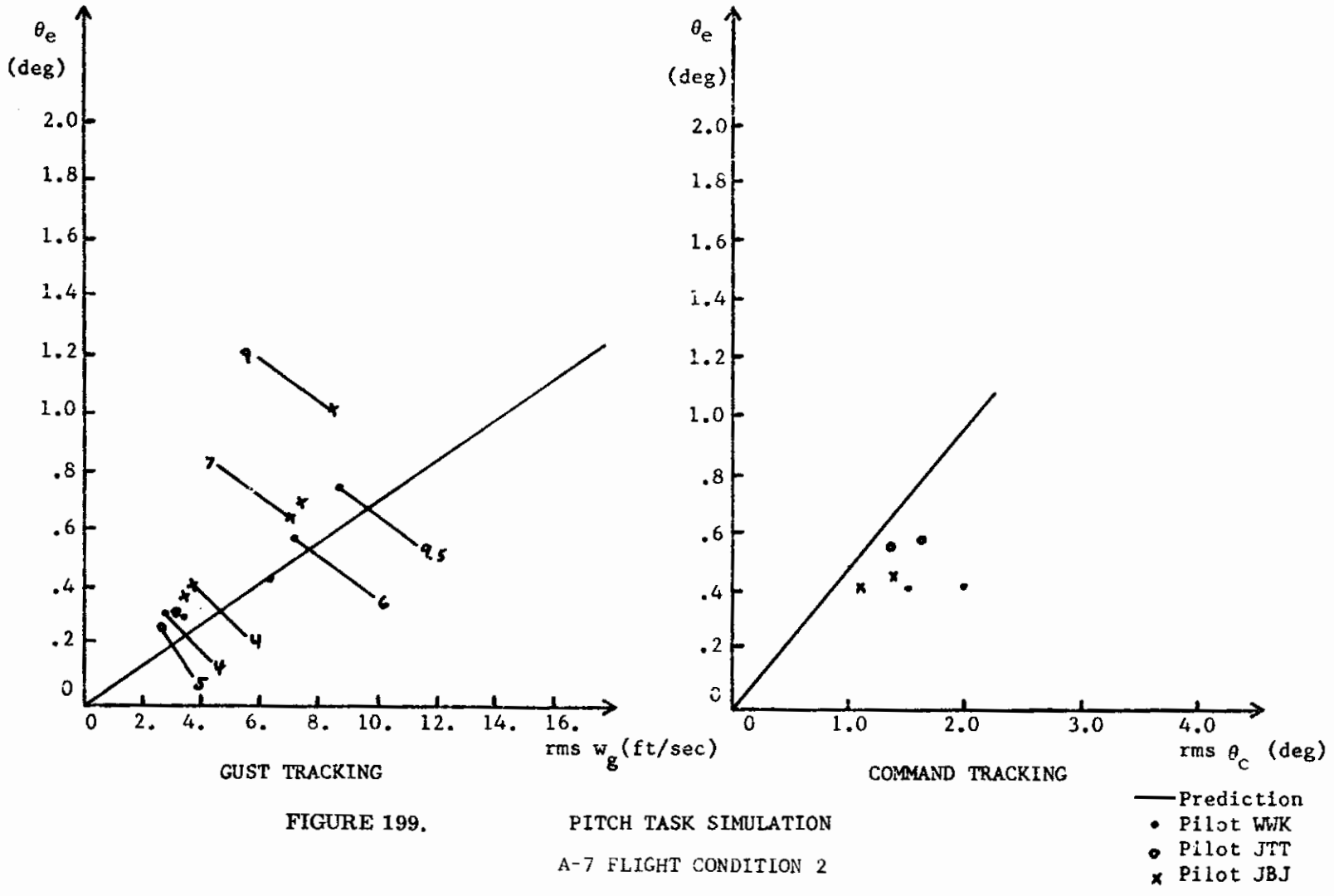

FIGURE 199. PITCH TASK SIMULATION

A-7 FLIGHT CONDITION 2

WITHOUT AUGMENTER

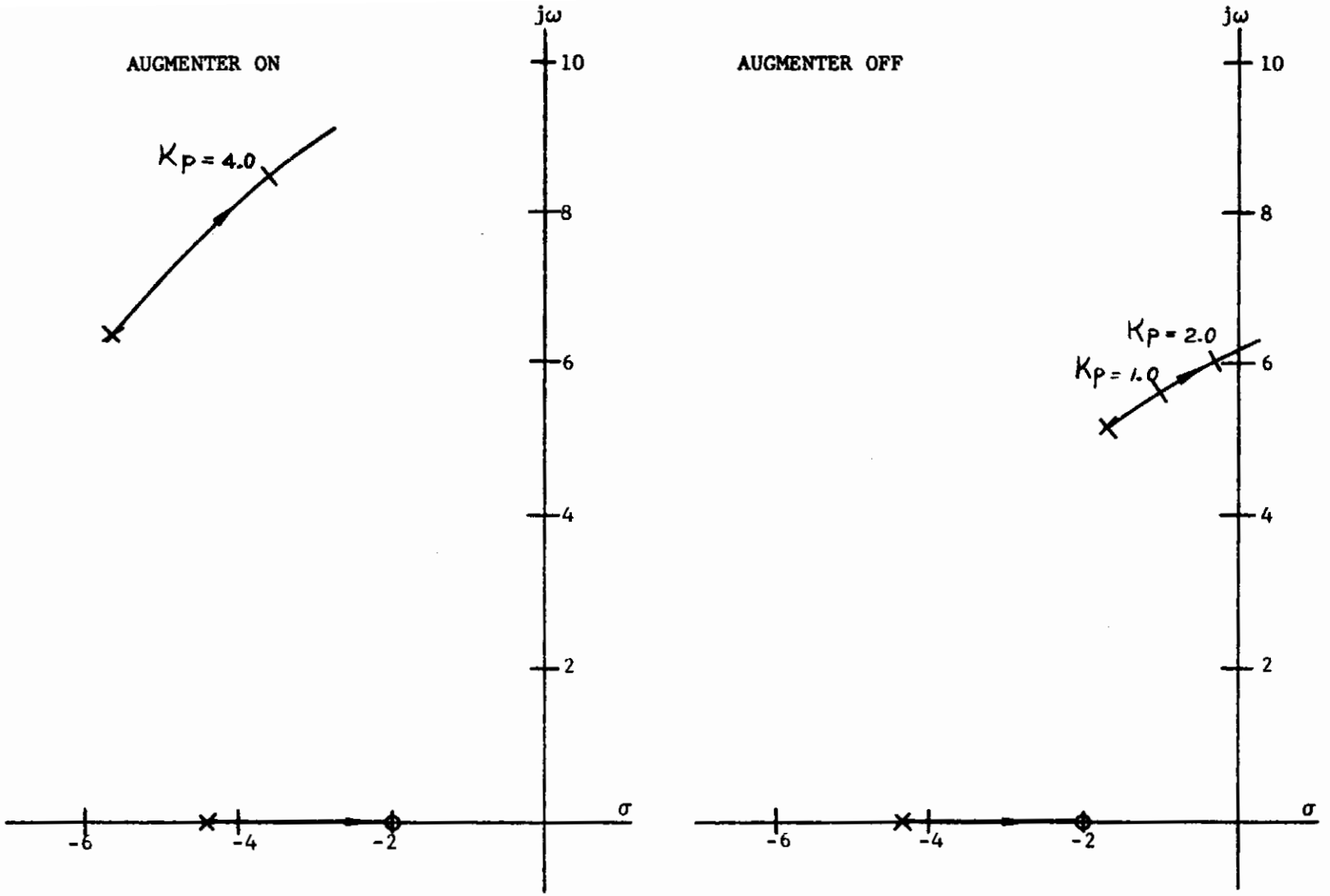

FIGURE 200. ROOT LOCUS FOR PITCH ANGLE TRACKING
A-7 FLIGHT CONDITION 2
T_L = 0.5 SEC

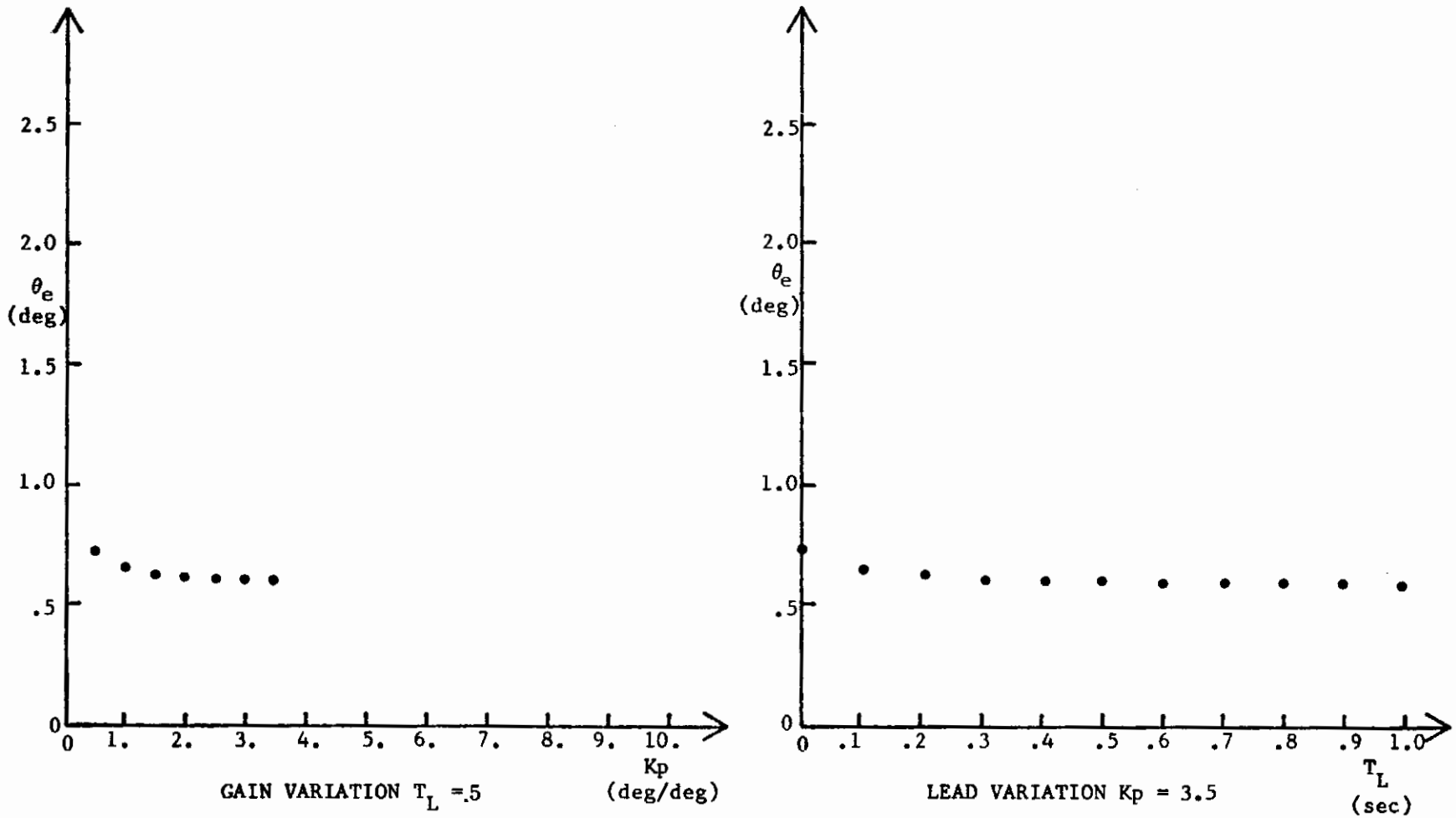

FIGURE 201. PILOT LEAD AND GAIN VARIATION

A-7 FLIGHT CONDITION 3

WITH AUGMENTER

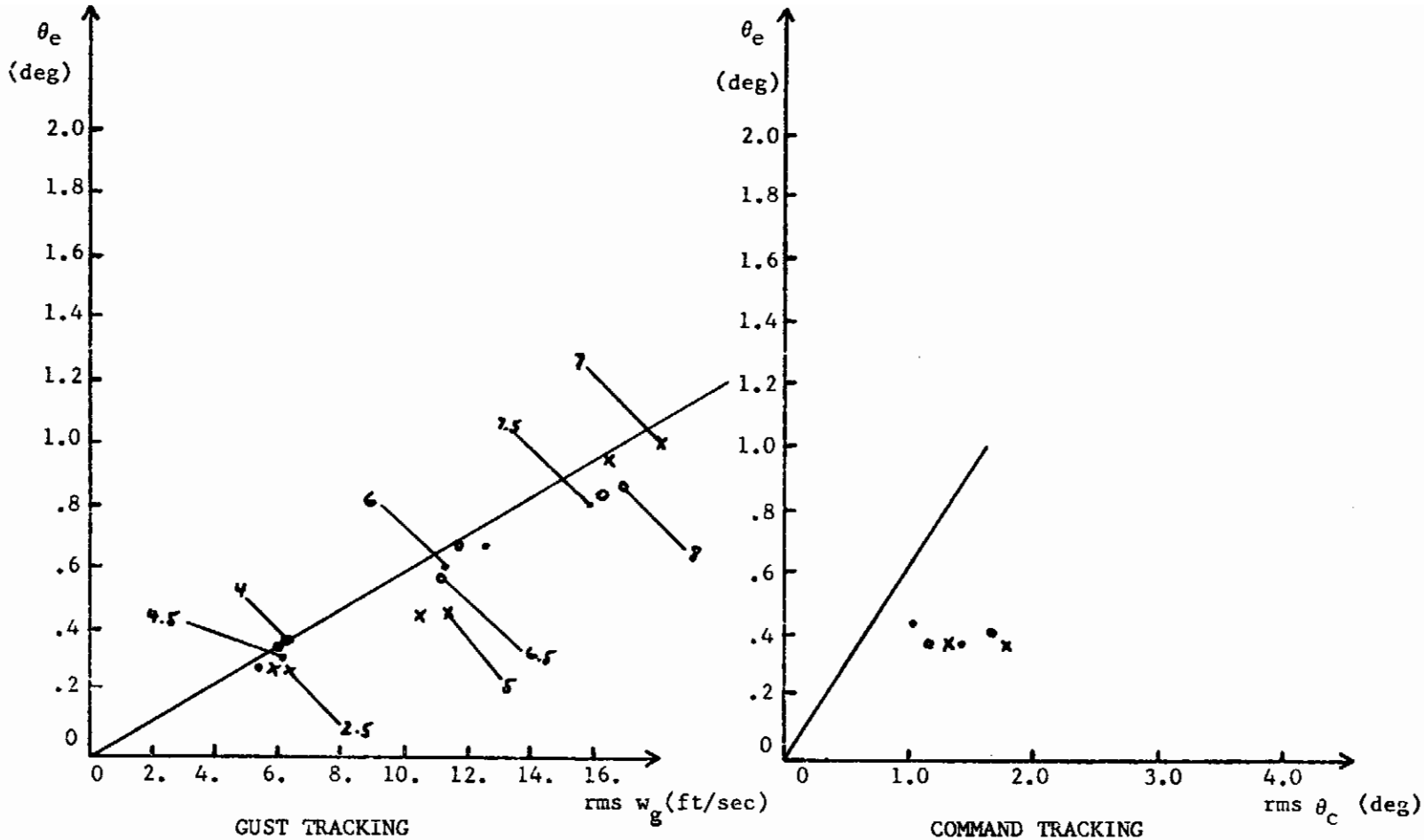

FIGURE 202. PITCH TASK SIMULATION
A-7 FLIGHT CONDITION 3
WITH AUGMENTER

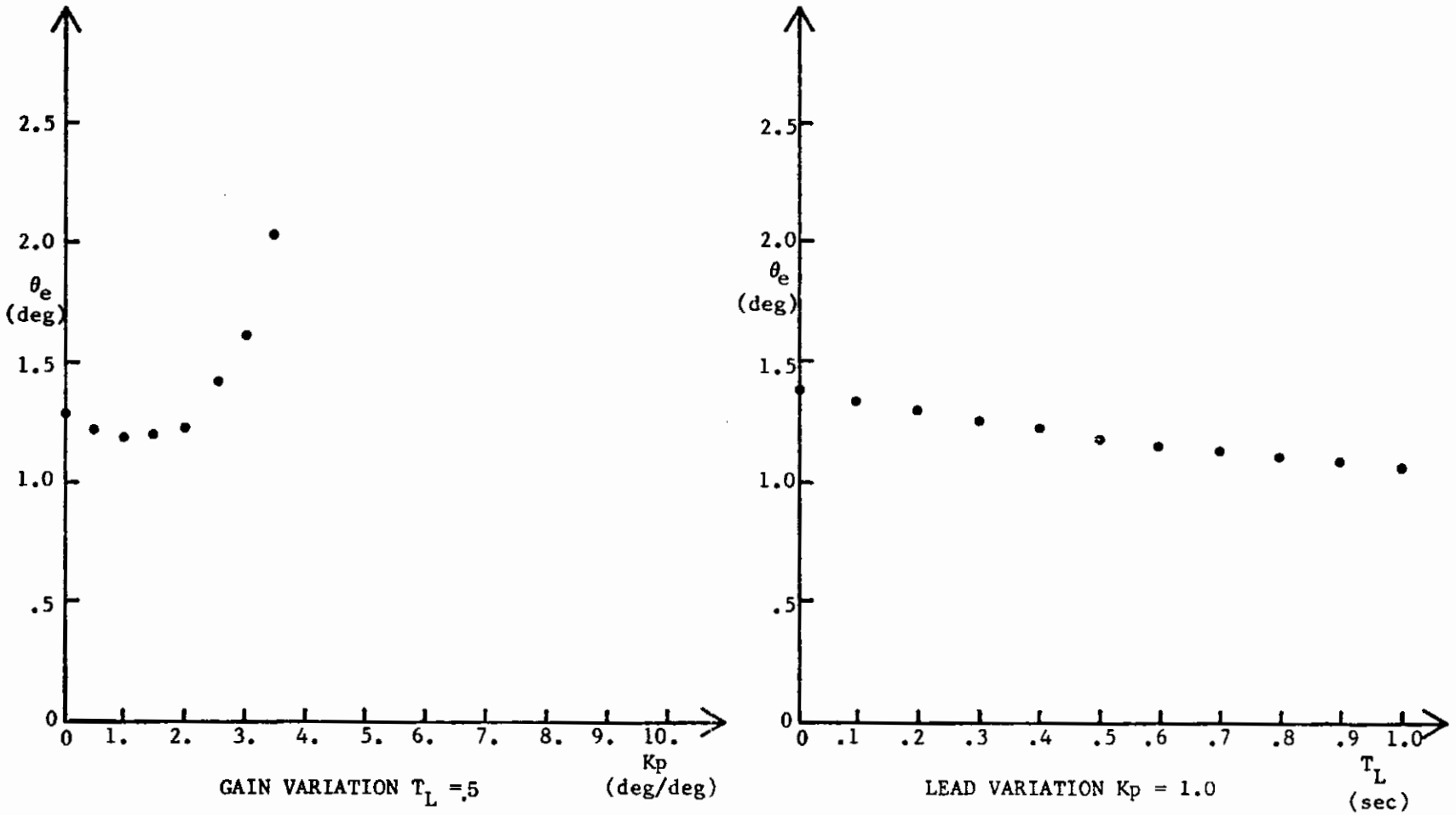

FIGURE 203. PILOT LEAD AND GAIN VARIATION

A-7 FLIGHT CONDITION 3

WITHOUT AUGMENTER

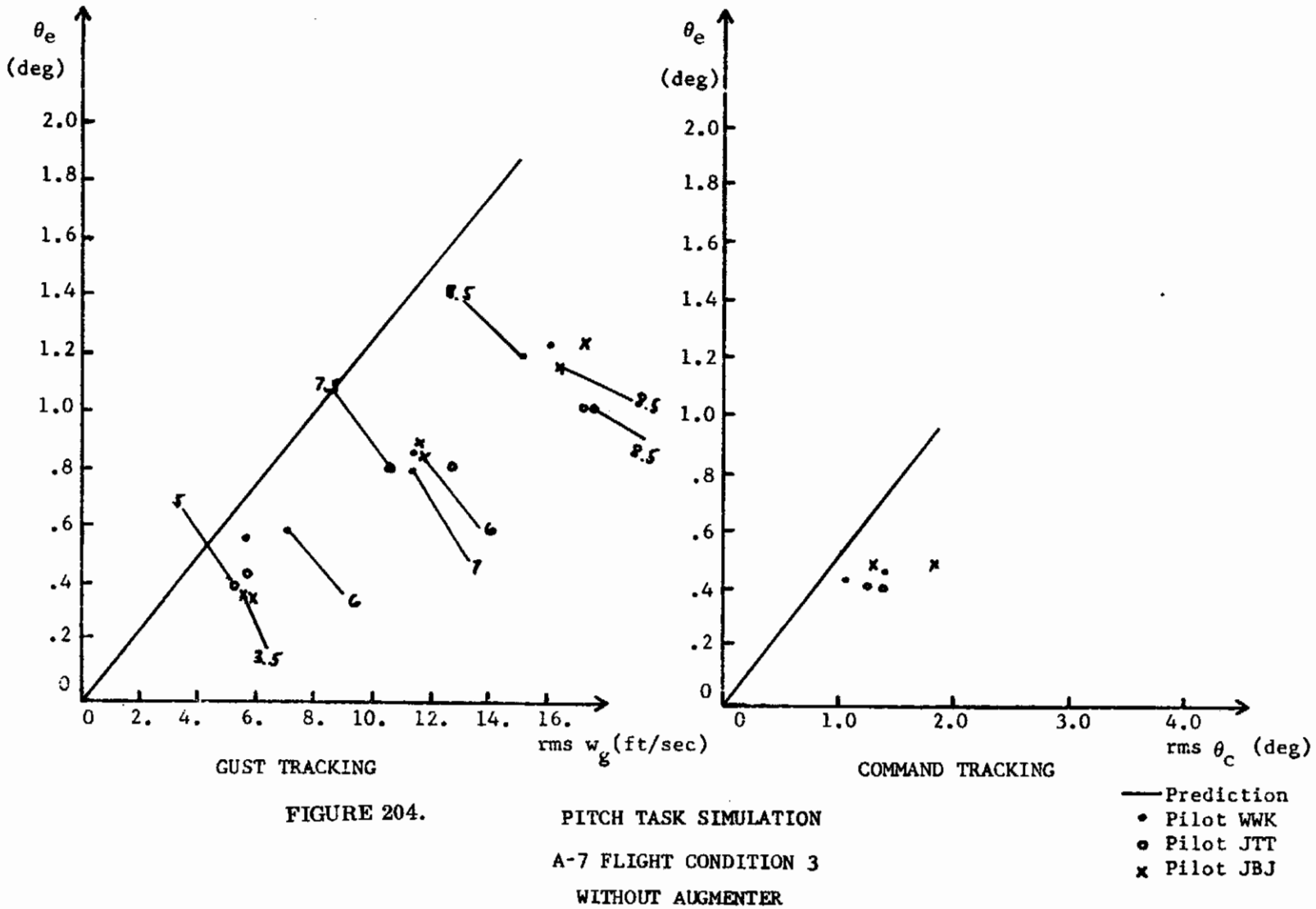

FIGURE 204. PITCH TASK SIMULATION
A-7 FLIGHT CONDITION 3
WITHOUT AUGMENTER

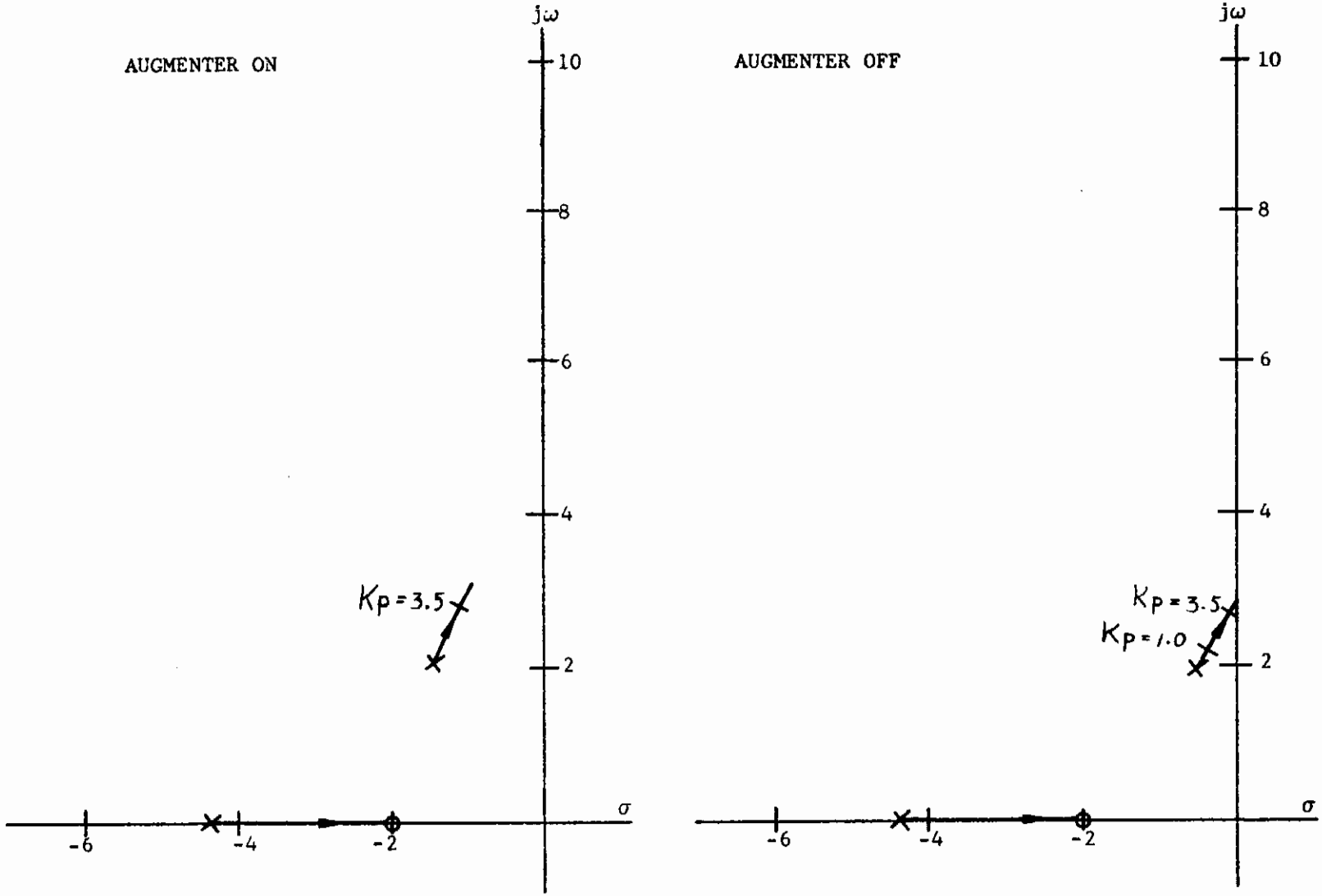

FIGURE 205. ROOT LOCUS FOR PITCH ANGLE TRACKING
A-7 FLIGHT CONDITION 3
T_L = 0.5 SEC

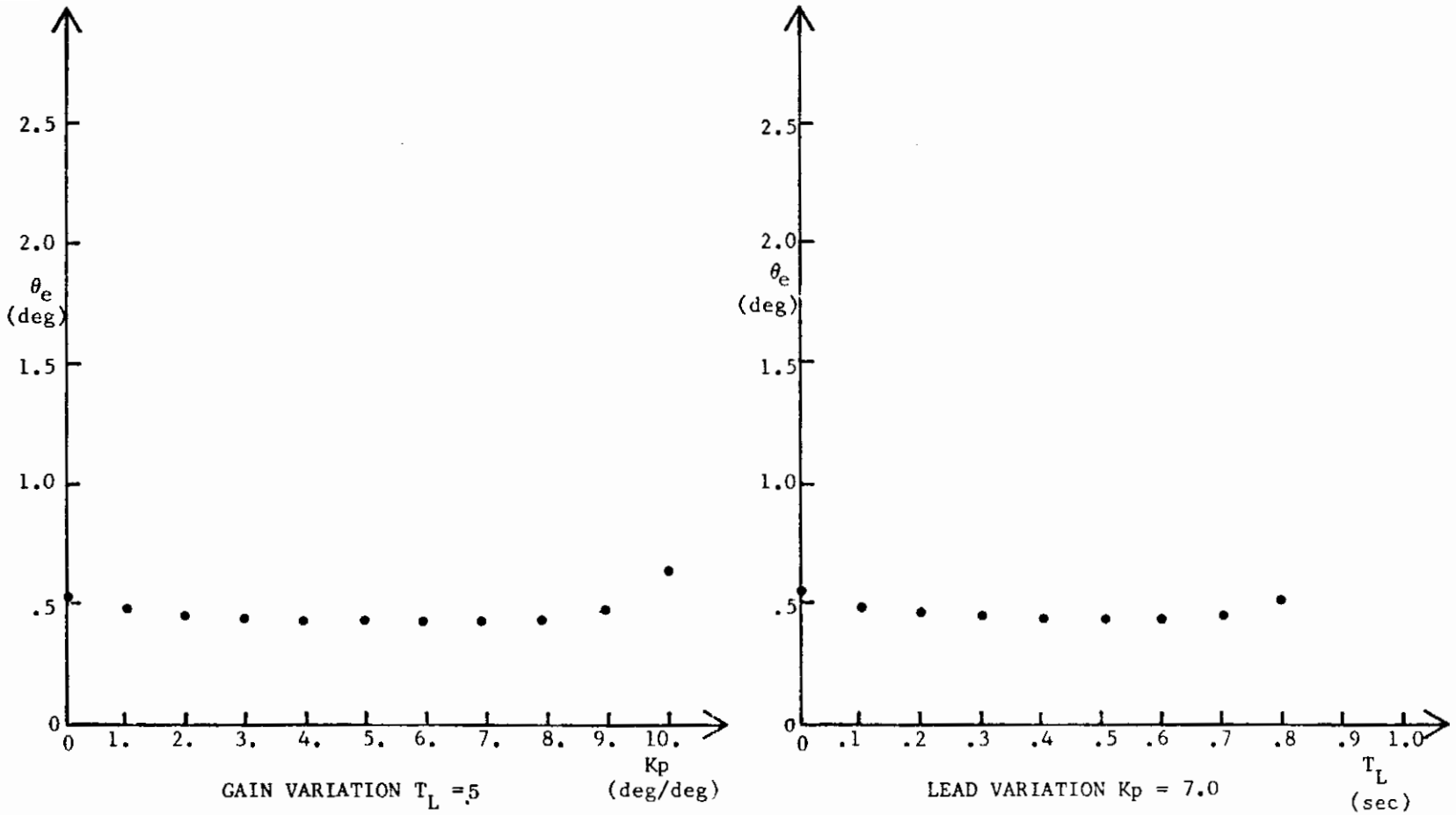

FIGURE 206. PILOT LEAD AND GAIN VARIATION
A-7 FLIGHT CONDITION 4
WITH AUGMENTER

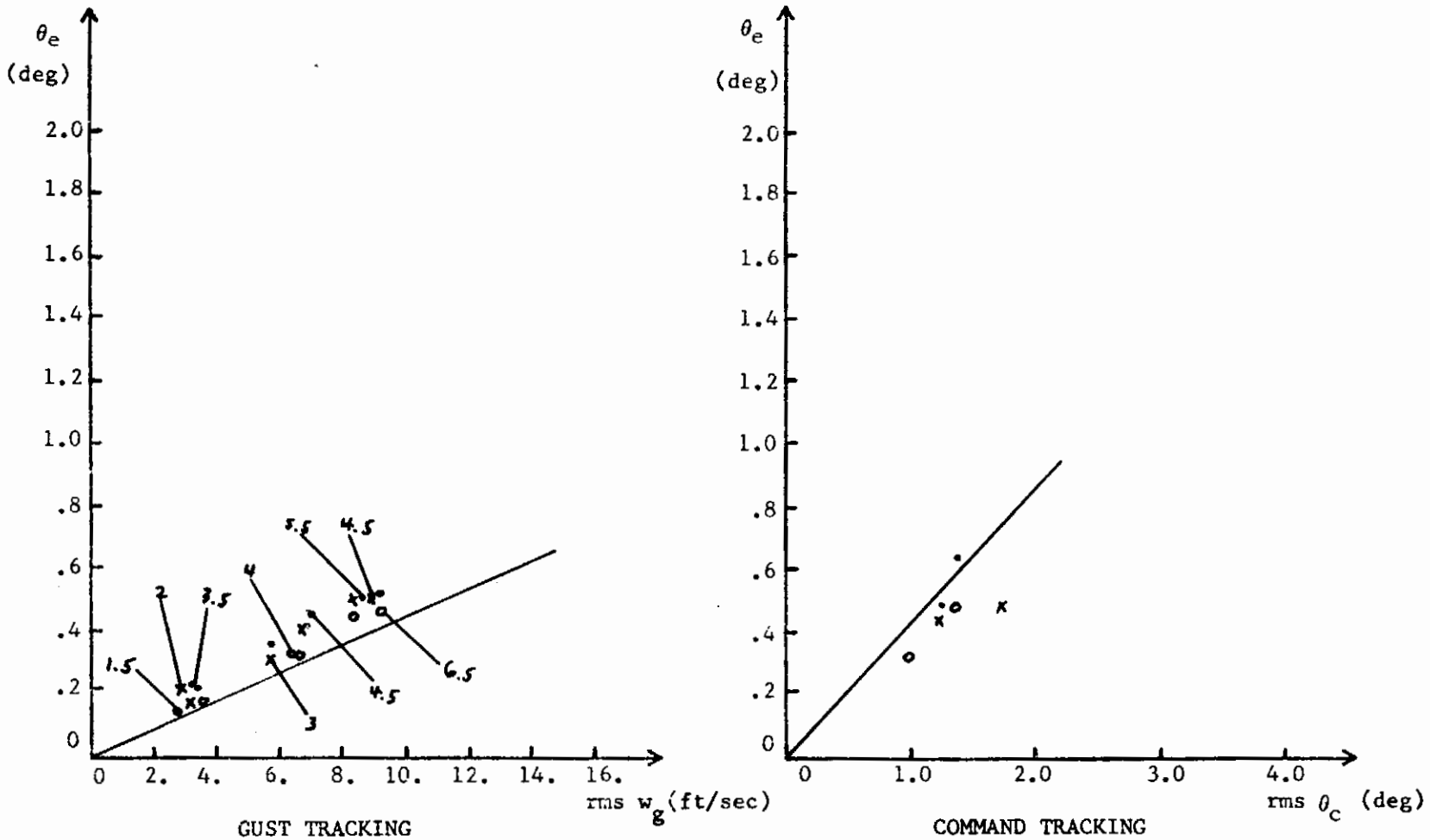

FIGURE 207. PITCH TASK SIMULATION
A-7 FLIGHT CONDITION 4
WITH AUGMENTER

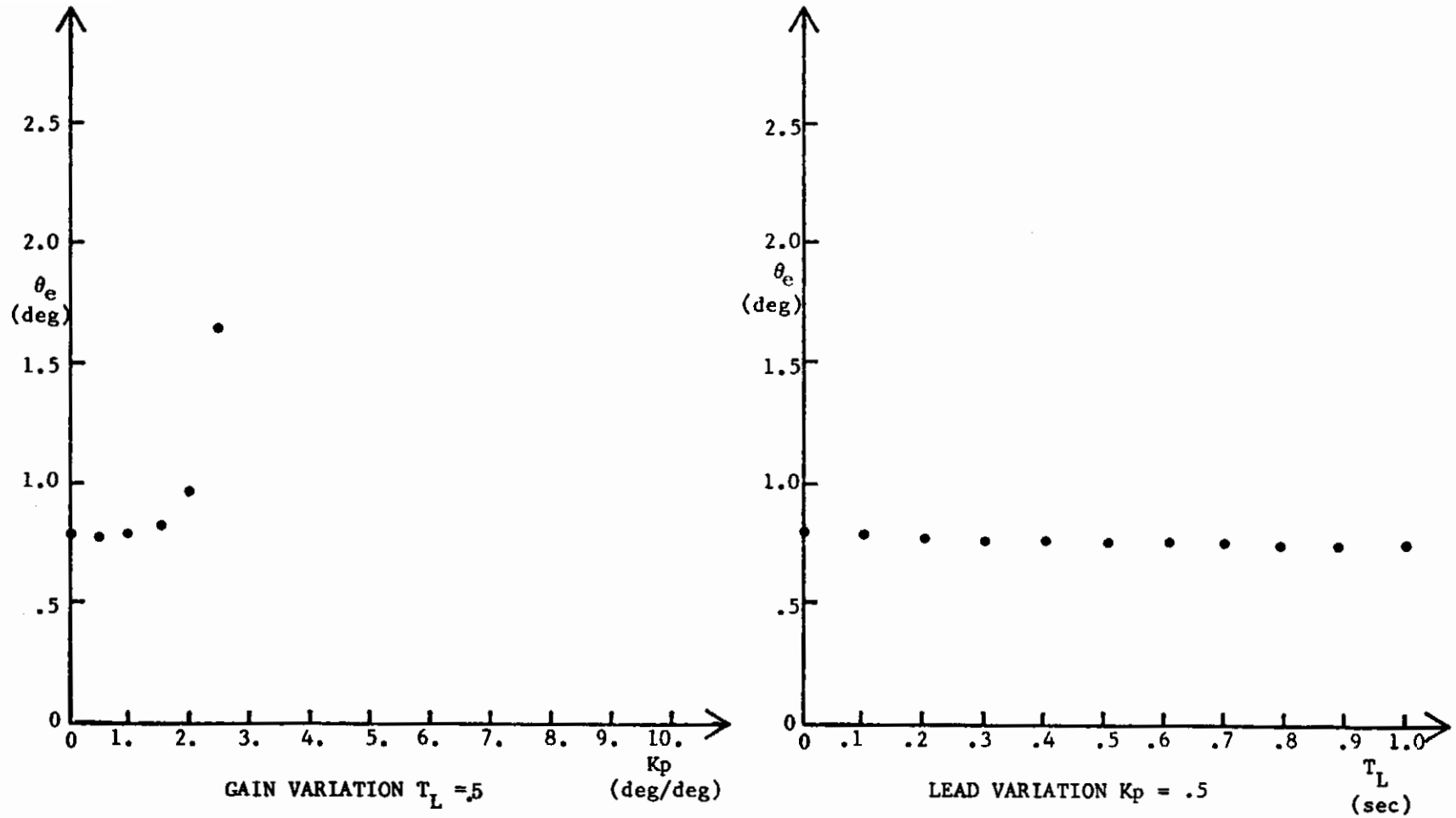

FIGURE 208. PILOT LEAD AND GAIN VARIATION

A-7 FLIGHT CONDITION 4

WITHOUT AUGMENTER

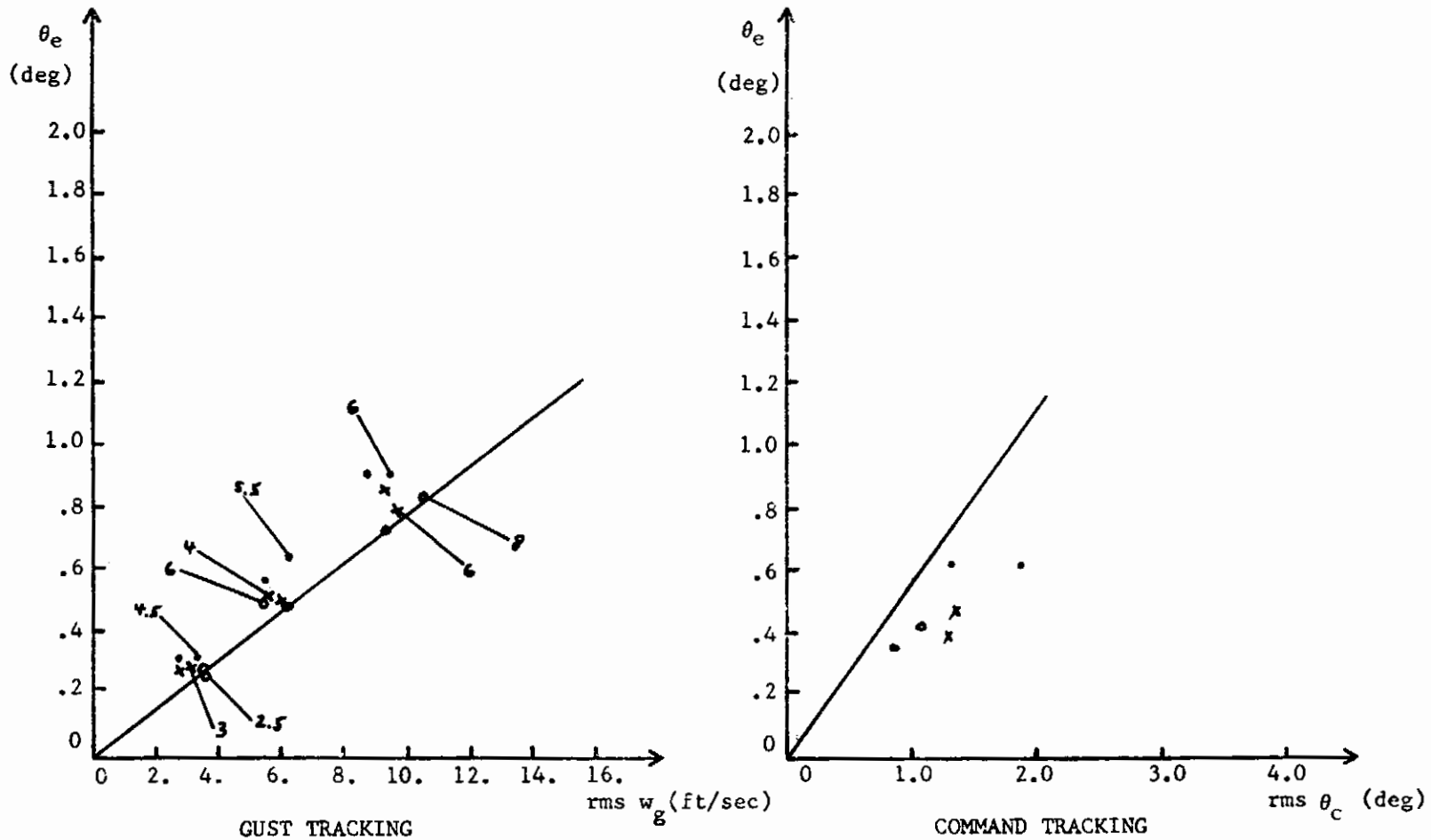

FIGURE 209. PITCH TASK SIMULATION
A-7 FLIGHT CONDITION 4
WITHOUT AUGMENTER

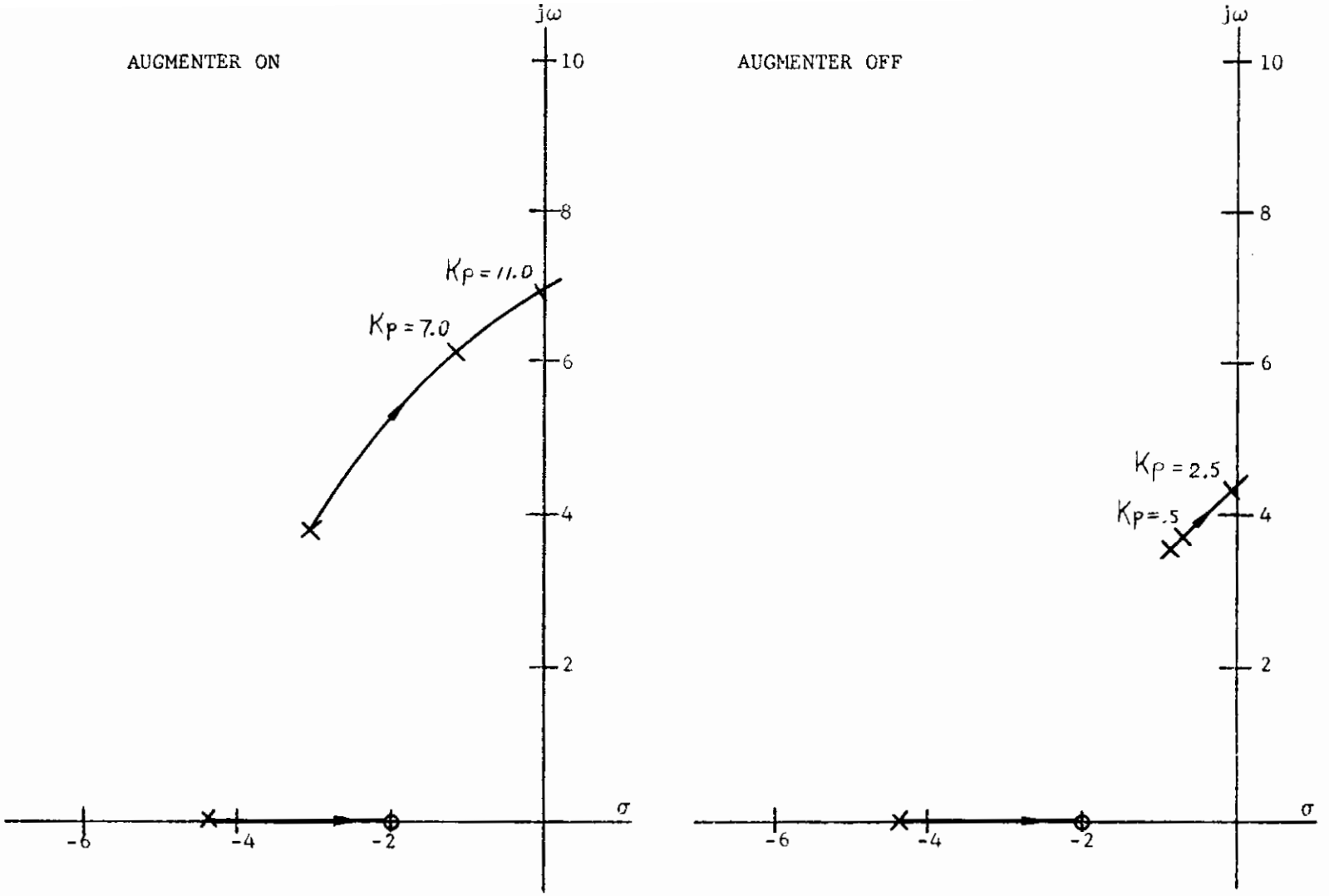

FIGURE 210. ROOT LOCUS FOR PITCH ANGLE TRACKING
A-7 FLIGHT CONDITION 4
T_L = 0.5 SEC

Unclassified
Security Classification

DOCUMENT CONTROL DATA - R & D

(Security classification of title, body of abstract and indexing annotation must be entered when the overall report is classified)

1. ORIGINATING ACTIVITY (Corporate author)	2a. REPORT SECURITY CLASSIFICATION
Northrop Corporation, Aircraft Division 3901 West Broadway Hawthorne, California 90250	Unclassified 2b. GROUP

3. REPORT TITLE

Prediction and Evaluation of Flying Qualities in Turbulence

4. DESCRIPTIVE NOTES (Type of report and inclusive dates)

Final Report — 4 December 1970 to 4 October 1971

5. AUTHOR(S) (First name, middle initial, last name)

Edward D. Onstott
Ernest P. Salmon
Ralph L. McCormick

6. REPORT DATE	7a. TOTAL NO. OF PAGES	7b. NO. OF REFS
February 1972	388	4

8a. CONTRACT OR GRANT NO.	9a. ORIGINATOR'S REPORT NUMBER(S)
F33615-71-C-1076	NOR-71-139
b. PROJECT NO. 8219 c. Task No. 821904 d. Work Unit No. 029	9b. OTHER REPORT NO(S) (Any other numbers that may be assigned this report) AFFDL-TR-71-162

10. DISTRIBUTION STATEMENT

Approved for public release; distribution unlimited.

11. SUPPLEMENTARY NOTES	12. SPONSORING MILITARY ACTIVITY
	Air Force Systems Command Air Force Flight Dynamics Laboratory WPAFB, Ohio 45433

13. ABSTRACT

A method for predicting tracking performance of Class IV airplanes in turbulence has been validated through a moving-base simulation of 16 F-5 and A-7 configurations on the Northrop Large Amplitude Flight Simulator. The method is based on pilot model theory and predicts root mean square tracking errors for piloted tasks in turbulence. Both lateral and longitudinal dynamics are considered, and the accuracy of the method is assessed. Specification design criteria are evolved from the simulation data for bank angle and pitch angle attitude hold tasks in turbulence. Digital programs that perform the prediction calculations accept arbitrary equations of motion and are available on request from the United States Air Force; a user's guide is included in the report, along with complete tracking error, gust level, and pilot rating data from the simulation.

DD FORM 1 NOV 65 1473

Unclassified
Security Classification

14 KEY WORDS	LINK A		LINK B		LINK C	
	ROLE	WT	ROLE	WT	ROLE	WT
Pilot Model Theory						
Multiloop Analysis						
Turbulence						
Pilot-Vehicle Performance						
Turbulence Simulation						
Performance Prediction Methods						
Flying Qualities						
Specification Criteria						

☆U.S.Government Printing Office: 1972 — 759-485/053